STUDY ON STRUCTURAL BEHAVIOUR OF HIGH STRENGTH STEEL S690 WELDED H- AND I-SECTIONS

KAI WANG

PhD

The Hong Kong Polytechnic University

2018

THE HONG KONG POLYTECHNIC UNIVERSITY

DEPARTMENT OF CIVIL AND ENVIRONMENTAL ENGINEERING

STUDY ON STRUCTURAL BEHAVIOUR OF HIGH STRENGTH STEEL S690 WELDED H- AND I-SECTIONS

Kai WANG

A thesis submitted in partial fulfillment of the requirements
for the Degree of Doctor of Philosophy

January 2018

CERTIFICATE OF ORIGINALITY

I hereby declare that this thesis is my own work and that, to the best of my knowledge and belief, it reproduces no material previously published or written, nor material that has been accepted for the award of any other degree or diploma, except where due acknowledgement has been made in the text.

____ (Signed)

WANG Kai (Name of student)

ABSTRACT

Motivation

High strength S690 steel material possesses a yield strength of 690 N/mm^2 which are double or triple to those of normal strength steel materials, i.e. S235 and S355 steel materials. In recent years, massive production of these high strength steel (HSS) materials was realized in modern steel mills, and many successful applications of HSS in machinery, equipment and structures have been reported. Hence, advantages of excellent strength-to-self-weight ratios and high levels of economy of HSS have been widely recognized by researchers and engineers. It is also realized that drawbacks such as reduced ductility, stringent welding requirements as well as insufficient design guidance should be overcome. Up to the presence, wide application of HSS is hindered, particularly for building construction. Hence, it is highly desirable to experimentally understand structural behaviour of S690 welded sections. Moreover, suitable design methods should be developed to facilitate safe and efficient design for HSS structures.

Objectives and scope of work

In this research project, a systematic experimental and numerical investigation into structural behaviour of S690 welded H- and I-sections is conducted. This research project is comprehensive in which material properties of S690 steel material and its residual stress patterns induced by welding were accurately measured, and structural behaviour of these S690 welded H- and I-sections is examined experimentally and numerically. The scope of work covers the following tasks:

- **Task 1: Stocky columns of S690 welded H-sections under compression**

  To examine section resistances of stocky columns of S690 welded H-sections through experimental and numerical studies.

- **Task 2: Slender columns of S690 welded H-sections**

To carry out a numerical investigation into overall buckling behaviour of slender columns of S690 welded H-sections.

- **Task 3: Restrained beams of S690 welded I-sections**
  To examine local buckling behaviour of restrained beams of S690 welded I-sections with various section compactness through experimental and numerical studies.
- **Task 4: Partially restrained beams of S690 welded I-sections**
  To examine lateral torsional buckling behaviour of partially restrained beams of S690 welded I-sections through experimental and numerical studies.

The areas of interest include:

- Deformation characteristics of HSS S690 welded H- and I-sections under i) compression and ii) combined compression and bending;
- Comparison of welding-induced residual stresses in S690 and S355 welded H- and I-sections, and effects of residual stresses on structural behaviour of S690 welded sections;
- Establishing a double Y-shaped finite element model which employs shell elements to facilitate accurate predictions on structural behaviour of welded H- and I-sections;
- Applicability of current design rules in EN 1993-1-1 by comparing design resistances with measured and predicted resistances of S690 welded sections.

It should be noted that four different cross-sections of welded H-sections, namely Sections C1 to C4, and six different cross-sections of welded I-sections, namely Sections B1 to B6 are fabricated with S690 steel plates of 6, 10 and 16 mm thickness. Moreover, plate thicknesses up to 40 mm are incorporated into numerical studies in order to cover a wide range of practical applications. Within this research framework, advantages of S690 steel materials and their wide application are elaborated systematically.

Research methodology and key findings

Based on a series of experimental and numerical investigations, all the four tasks have been successfully completed. It should be noted that:

- **Task 1: Stocky columns of S690 welded H-sections**

A total of 20 stocky columns of S690 welded H-sections were fabricated, and they were tested as follows: i) 12 stocky columns under compression, and ii) 8 stocky columns under combined compression and bending. Section resistances and deformation characteristics of the test specimens were successfully obtained. It was shown that predicted section resistances based on EN 1993-1-1 could be readily attained by all 20 test specimens. Large deformation capacity ratios as well as significant strength enhancement were obtained in S690 welded H-sections with high section compactness.

Verified residual stress patterns of S690 welded H-sections are incorporated into structural finite element models of stocky columns. Generally, entire load-shortening curves of stocky columns were accurately predicted with calibrated models. Moreover, enhancement of section resistances which was highly dependent on material properties and plate local buckling was closely examined.

The design rules given in EN 1993-1-1 are shown to be applicable to evaluate cross-section resistances of those stocky columns of S690 welded H-sections. In addition, it is also found that certain conservatism is embedded in interactive design curves for H-sections under combined compression and bending.

- **Task 2: Slender columns of S690 welded H-sections**

Calibrated double Y-shaped model is employed to predict overall buckling resistances of slender columns of S690 welded H-sections. Verification of the model is conducted against benchmark tests conducted by Wang et al. Through direct incorporation of residual stresses into H-sections, predicted load-shortening curves of these slender columns were found to compare very well with those of measured data.

In general, current design rules in EN 1993-1-1 and -12 were found to be applicable to predict member resistances of these slender columns of S690 welded H-sections. Owing to significantly reduced compressive residual stresses in those cross-sections comparing with those in S355 steel sections, buckling curve c should be replaced by possibly curve b or even curve a based on parametric studies. Therefore, an improved design efficiency is achieved.

- **Task 3: Restrained beams of S690 welded I-sections**

In order to determine section resistances of restrained beams of S690 welded I-sections, a total of 6 beams under single-point loads were tested. Local buckling in the flange outstands was observed in all test specimens. With different cross-sectional compactness, steel sections generally attained full plastic section resistances against bending based on EN 1993-1-1. And various strength enhancement levels were obtained in steel beams, depending on section classification of these sections.

Extensive studies based on verified models were conducted, and it was found that section classification rules in EN 1993-1-1 were applicable to restrained beams of S690 welded I-sections. Moreover, in order to achieve improved structural efficiency, new design criteria and methods are proposed according to numerical results of the comprehensive parametric studies.

- **Task 4: Partially restrained beams of S690 welded I-sections**

In order to investigate lateral torsional buckling of partially restrained beams of S690 welded I-sections, a total of 12 beams under single-point loads were tested. Different failure modes, including lateral torsional buckling and plastic section failure were observed in the test specimens. It was shown that partially restrained beams are readily assessed with buckling curve b instead of curve d as suggested in EN 1993-1-1.

All numerical studies were carried out successfully incorporating effects of residual stresses. It is shown that partially restrained beams of small to moderate slendernesses tend to be significantly affected by residual stresses, when compared with those of high slendernesses. Moreover, a certain conservatism embedded in the current design method in adopting curve d was highlighted according to numerical results of the comprehensive parametric studies.

Key findings and their significances

The major academic merits of this research project are:

- A whole-process simulation on temperature distribution, residual stress distribution and structural behaviour of S690 welded sections was fully established and verified to enable effective use of S690 welded sections;
- Residual stresses in S690 welded H- and I-sections were systematically investigated, and their effects on structural behaviour of columns and beams of S690 welded sections have been identified;
- Current design rules in EN 1993-1-1 were justified for designing S690 welded sections according to both experimental and numerical results. Moreover, current design rules with suitably selected design parameters were proposed for improved structural design efficiency; and,
- Application of HSS S690 steel materials in columns and beams were fully validated through comprehensive experimental investigation, and they are technically ready for wide application in steel structures.

PUBLICATIONS

Conference Papers

- K. Wang, Y. F. Hu, T. K. Chan and K. F. Chung (2016) Compression tests on stocky welded H-sections made of Q690 steel materials. Proceeding of the Fourteenth East Asia-Pacific Conference, Ho Chi Minh City, January 2016, p552-568.

- K.F. Chung, G.Q. Li, K. Wang, T.Y. Ma and X. Liu (2016). Experimental investigation into high strength steel columns of Q690 welded H-sections. Proceeding of the Eleventh Pacific Structural Steel Conference, Shanghai, October 2016, p936-942.

- K. F. Chung， X. Liu and K. Wang (2016) Numerical modelling of fabricating and loading processes for high strength steel stub columns. Proceeding of the Eighth International Conference on Steel and Aluminium Structures. Hong Kong China, December 2016, p1475-1484.

- K. Wang, X. Liu and K. F. Chung (2017) Study on structural behaviour of high strength steel S690 welded H-sections under axial compression. Proceeding of the Fifteenth East Asia-Pacific Conference, Xi’ an, China, October 2017, p893-901.

- M. H. Shen, K. Wang, and K. F. Chung (2017) Numerical investigation into structural behaviour of long spanning composite beams with perforated I-sections. Proceeding of the Fifteenth East Asia-Pacific Conference, Xi’ an, China, October 2017, p934-941.

ACKNOWLEDGEMENTS

My sincerest appreciation is devoted to my supervisor, Professor K.F. Chung, for giving me an opportunity to start my PhD research project since 2014. During my PhD journey, he gave me unique guidance, critical advice as well as his generous support and patience which I am truly grateful for. With his kind help, I gained comprehensive understandings on not only technical details but advanced research methodology, communicative approach, and critical thinking. His knowledge and expertise are educative and inspirational.

I would like to express my gratitude to the Department of Civil and Environmental Engineering of The Hong Kong Polytechnic University. It provided me with fine working environment and a well-equipped structural laboratory. Technical support during my experimental investigations from experienced technicians, Mr. M.C. Ng and Mr. Y.H. Yiu, are also gratefully acknowledged. I would also like to thank Professor Y. J. Shi, Dr H. Y. Ban from Tsinghua University and Professor L. Gardner from London Imperial College. The ideas obtained from technical discussions with them substantially sparkled my inspiration and intuition on my research project.

The financial support from the Research Committee of The Hong Kong Polytechnic University has been a major blessing to me. Great thanks are given to both Dr H. C. Ho and Ms C. E. Ng of CNERC. With their help, I could focus on my research project.

My sincere thanks also go to my colleagues, seniors and friends. Dr. X. Liu and Dr T. Y. Ma provided important technical support to my research project. I also thank Mr. Y.F. Hu, Mr. M. Xiao, Mr. Y. C. Wang, Ms Y. B. Guo, Mr. J.Y. Zhu, and Mr. J.K. Zhou for their cordial help and spiritual encouragement to both my research and life development.

At last, I may like to express my most heartfelt thanks to my wife, Stephanie Shen, my parents and parents-in-law for their continuous support and love throughout the course of my research study.

TABLE OF CONTENTS

CHAPTER FIVE NUMERICAL MODELLING I: RESIDUAL STRESS PATTERNS OF WELDED H- AND I-SECTIONS

CHAPTER SIX NUMERICAL MODELLING II:

STRUCTURAL INSTABILITY OF S690 WELDED H- AND I-SECTIONS

CHAPTER SEVEN PARAMETRIC STUDIES: STRUCTURAL INSTABILITY OF S690 WELDED H- AND I-SECTIONS

CHAPTER EIGHT   CONCLUSIONS AND FUTURE PLAN

CHATER ONE

INTRODUCTION

1.0 Research Background

Structural steel sections are considered to be economic, environment-friendly and recyclable building materials, and they have been widely adopted in buildings, bridges and marine structures. In recent years, high strength steel (HSS) materials with a nominal yield strength equal to or larger than 460 N/mm^2 a feasible option for design and construction engineers. It is widely known that yield strengths of HSS materials are double or triple of those of normal strength steel material. Hence, HSS materials possess high strength to self-weight ratios, and they are able to provide effective structural forms to heavily loaded structures and long spanning structures.

However, wide adoption of HSS materials is hindered because of: i) Lack of understanding on mechanical properties of HSS welded sections, and ii) insufficient guidance on structural behavior and design. To deal with these issues, research works were carried out in many parts of the world.

i) Residual stresses

In general, most steel structures are fabricated with hot-rolling, welding and flame-cutting methods. It should be noted that during welding residual stresses are inevitably introduced during heating and cooling circles. Hence, residual stresses and their impact onto welded H- or I-sections should be examined thoroughly.

More specifically, adverse effects from residual stresses on section resistances, section rigidities, buckling behaviour of steel members should be quantified. And all these effects are currently considered either directly or indirectly in current codified design rules. Hence, these effects for S690 steel welded sections should be scientifically established in order to facilitate subsequent development of design rules.

Experimental and numerical investigations into residual stresses in S690 steel welded sections are considered to be important in the current research project. Hole-drilling method is a widely recommended method to acquire surface stresses of steel sections (Withers et al., 2008). Through an effective use of coupled thermo-mechanical analyses, a complete residual stress distribution in an entire cross-section of S690 steel welded sections is readily determined (Liu, 2017). These residual stress distributions will be simplified into residual stress patterns for direct incorporation into finite element models of beams and columns. They will be compared with those residual stress pattern of S235 to S460 welded sections.

ii) Structural behaviour

In EN1993-1-1, highly developed design rules for structural steelwork with S235 to S460 steel materials are provided. Similarly, design rules for steel materials with yield strengths up to 485 N/mm^2 are incorporated in AISC 360-2010, and that for steel materials with yield strength up to 420 N/mm^2 are given in GB 50017-2003. In order to cover HSS materials up to S700, supplementary requirements on material ductility are provided in EN 1993-1-12. In general, only very simple and conservative design rules are given, and hence, structural behaviour of HSS cannot be estimated based on these design codes. Effective design rules for S690 welded sections should be developed.

While design rules given in EN 1993-1-1 are generally considered to be readily applicable in design of S690 welded sections, specific values of relevant design parameters, such as residual stress ratios in flange and web plates of welded I- and H-sections and associated imperfection parameters for columns and beam buckling should be established.

1.2 Objectives and Scope of Work

The main objective of this research project is to understand structural behaviour of columns and beams of high strength steel welded sections and identify any parameters which govern any major difference in their structural behaviour, when compared with those of normal strength steel materials. This research project examines mechanical properties of S690 steel plates and residual stresses induced by welding are examined. Moreover, adverse effects of residual stresses onto structural behaviour of steel members are also examined experimentally and numerically. The scope of work is divided into four major tasks as follows:

- *Task 1: Stocky columns of S690 welded H-sections under compression*
  To examine section resistances of stocky columns of S690 welded H-sections through experimental and numerical studies;

- *Task 2: Slender columns of S690 welded H-sections*
  To carry out a numerical investigation into overall buckling behaviour of slender columns of S690 welded H-sections;

- *Task 3: Restrained beams of S690 welded I-sections*
  To examine local buckling behaviour of restrained beams of S690 welded I-sections with various section compactness through experimental and numerical studies;

- *Task 4: Partially restrained beams of S690 welded I-sections*
  To examine lateral torsional buckling behaviour of partially restrained beams of S690 welded I-sections with various section compactness through experimental and numerical studies.

The areas of interest of the research project are:

a) Comparison of welding-induced residual stresses in S690 and S355 welded H- and I-sections;

b) Effects of residual stresses on structural behaviour of S690 welded sections;

c) Deformation characteristics of S690 welded H-sections under i) compression and ii) combined compression and bending;

d) Deformation characteristic of S690 welded I-sections with different lateral restraints under lateral loads;

e) Finite element modelling using shell elements with direct incorporating of residual stresses for accurate prediction on structural behaviour of S690 welded H- and I-sections;

f) Applicability of current design rules in EN 1993-1-1 on local plate buckling ,column buckling and beam buckling to S690 welded sections with measured and predicted resistances of S690 welded sections.

It should be noted that four different cross-sections of welded H-sections, namely Sections C1 to C4, and six different cross-sections of welded I-sections, namely Sections B1 to B6 are fabricated with S690 steel plates of 6, 10 and 16 mm thickness. Moreover, welded sections with plate thicknesses up to 40 mm are incorporated into numerical parametric studies to cover a wide range of practical cases. Through the research project, advantages of S690 steel materials and welded sections will be clearly elaborated.

1.3 Research methodology

In this research project, experimental and numerical investigations into residual stress patterns in S690 welded H- and I-sections and structural behaviour of columns and beams of S690 welded sections are carried out. The investigations are performed in the following four tasks:

- *Task 1: Stocky columns of S690 welded H-sections*

  A total of 20 stocky columns of S690 welded H-sections are fabricated, and they are tested as follows: i) 12 stocky columns under compression, and ii) 8 stocky columns under combined compression and bending. Section resistances and deformation characteristics of the test specimens are successfully obtained. It is shown that predicted section resistances based on EN 1993-1-1 can be readily attained by all 20 test specimens. Large deformation capacity ratios as well as significant strength enhancement are obtained in S690 welded H-sections with high section compactness.

  Calibrated residual stress patterns of S690 welded H-sections are incorporated into structural finite element models of stocky columns. Generally, the entire load-shortening curves of stocky columns are accurately captured with calibrated models. Moreover, enhancement of section resistances which is highly dependent on material properties and plate local buckling is examined.

- *Task 2: Slender columns of S690 welded H-sections*

  Calibrated double Y-shaped models are employed to predict overall buckling resistances of slender columns of S690 welded H-sections. These models are calibrated against reference tests conducted by Wang et al (2016). Through direct incorporation of residual stresses into finite element models of shell elements of H-sections, predicted load-shortening curves of these slender columns are found to compare very well with those of measured data. Numerical results are compared with current design rules in EN 1993-1-1 and -12. Owing to significantly reduced compressive residual stresses in those cross-sections comparing with those commonly adopted in S235 to S355 steel sections, an improvement on design efficiency is established.

- *Task 3: Restrained beams of S690 welded I-sections*

  In order to investigate local plate buckling and section resistances of restrained beams of S690 welded I-sections, a total of 6 restrained beams under single-point loads are tested. Local buckling in the flange outstands was observed in all test specimens. With different cross-sectional compactness, these sections generally attain full plastic resistances against bending based on EN 1993-1-1. And various strength enhancement levels are obtained in these beams, depending on their section classification.

  Extensive numerical parametric studies based on calibrated models are also conducted, and it is found that current section classification rules in EN 1993-1-1 are readily applicable to restrained beams of S690 welded I-sections. Moreover, in order to achieve improved structural efficiency, new design parameters are proposed according to results of the parametric studies.

- *Task 4: Partially restrained beams of S690 welded I-sections*

  In order to investigate lateral torsional buckling of partially restrained beams of S690 welded I-sections, a total of 12 partially restrained beams under single-point loads are tested. Different failure modes, including lateral torsional buckling and plastic local plate buckling are observed in these test specimens. It is shown that current beam buckling rules in EN 1993-1-1 are readily applicable to these partially restrained beams of S690 welded I-sections.

  Moreover, in order to achieve improved structural efficiency, new design parameters are proposed to results of the parametric studies. All numerical studies are carried out with the proposed residual stresses specifically developed for S690 welded sections residual stresses. It is shown that partially restrained beams of small to moderate slendernesses tend to be affected significantly by residual stresses, when compared with those with high slendernesses. Moreover, conservatism embedded in the current design method by adopting buckling curve d is identified.

1.4 Significance of the Research Project

Currently, there is a lack on mechanical properties and structural behaviour of columns and beams of S690 welded sections. Hence, it is highly desirable to provide test data and design guidance on residual stresses in S690 welded H- and I-sections, and on structural behaviour of columns and beams of S690 welded sections. In this research project, extensive experimental and numerical investigation into S690 welded sections is successfully carried out and welded. And welded H- and I-sections with steel plate thicknesses from 6 mm to 40 mm are covered.

In order to obtain residual stress patterns in S690 welded H- and I-sections, a whole process simulation on temperature history, residual stress distribution and structural behaviour of S690 welded sections is established to enable an effective use of S690 welded sections. It should be noted that predicted data are calibrated with measured data obtained in various experimental works. Hence, finite element models with a high level of accuracy is developed. With these numerical models, a large database is established to generate the extensive numerical data to supplement test data for a scientific review on current design rules.

In EN 1993-1-1, design rules are developed for normal strength steel welded sections with S235 to S460 steel. Hence, applicability of these design rules to S690 steel welded sections should be examined according to both experimental and numerical results. Moreover, suitably selected design parameters are proposed for improved structural design efficiency.

With this research project, application of S690 steel materials in columns and beams is fully validated through systematic investigations. Engineers are strongly encouraged to take advantage of highly effective structural solutions offered by high strength steel S690 steel material and welded sections.

1.5 Outline of the Thesis

The outline of this thesis is summarized in the Figure, and details are presented as follows:

- *Chapter 2 – Literature*

  The following topics of previous researches are reviewed and discussed: i) current design rules of steel structures based on EN 1993-1-1; ii) mechanical properties of S690 welded H- and I-sections; iii) Previous experimental and numerical studies on stocky columns, slender columns, restrained beams and partially restrained beams.

- *Chapter 3 – Experimental Study I: Section Resistances of High Strength Steel S690 Welded H-sections under Compression*

  A total of 20 stocky columns of S690 welded H-sections under compression are tested. Among these sections, 12 sections are under compression, and 8 sections are under combined combined compression and bending. Material properties and welding parameters of these H-sections are examined for good understanding of section properties. Failure modes and load shortening curves are also measured and fully reported. Both section resistances and deformation characteristics of these sections are discussed for subsequent analyses.

- *Chapter 4 – Experimental Study II: Structural Behaviour of Fully and Partially Restrained Beams of S690 Welded I-sections*

  A total of 18 beams of S690 welded I-sections under single-point loads are tested. Among these sections, 12 sections are partially restrained at load points with two different test configurations, and 6 sections are fully restrained. Material properties and welding parameters of these S690 welded I-sections are examined. Additionally, residual stresses in 3 typical sections are measured using the hole-drilling method. Failure modes and load deflection curves are measured and fully reported. Both section resistances and deformation characteristics are discussed and reported for subsequent analyses.

- *Chapter 5 – Numerical Modelling I: Residual Stress Patterns of Welded H- and I-Sections*

Coupled thermo-mechanical modelling is established using the general finite element package ABAQUS 6.12 to predict residual stress patterns in S690 welded H- and I-sections. Measured material properties and welding parameters are incorporated into the coupled finite element models. It is demonstrated that this model is successfully calibrated against surface residual stresses measured in 3 typical I-sections. With these calibrated numerical models, extensive parametric studies are carried out to predict residual stresses in S690 welded H- and I-sections with up to 40 mm thick steel plates. In addition, comparison of residual stresses in S355 and S690 sections is carried out.

- *Chapter 6 – Numerical Modelling II: Structural Instability of S690 Welded H- and I-Sections*

  In this chapter, a double Y-shaped model is proposed to simulate structural behaviour of S690 sections. Residual stress patterns predicted in Chapter 5 is fully incorporated into these models. Calibration of these proposed numerical model is achieved through 5 different sets of test data. It should be noted that failure mode, section resistances and load deformation characteristics predicted by the proposed models are demonstrated to be compared well with test data. Hence, they are ready to be extensively employed to parametric studies.

- *Chapter 7 –Parametric Studies: Structural Instability of S690 Welded H- and I-Sections*

  Parametric studies are carried out to four different types of structural members, i.e. stocky columns, slender columns, restrained beams and partially restrained beams. Effects of section geometries and residual stresses onto structural behaviour are highlighted in this study. In addition, comparison between current design rules given in EN 1993-1-1 and numerical predictions obtained from the parametric studies is carried out. In order to improve design efficiency, improved design parameters are proposed for S690 welded sections.

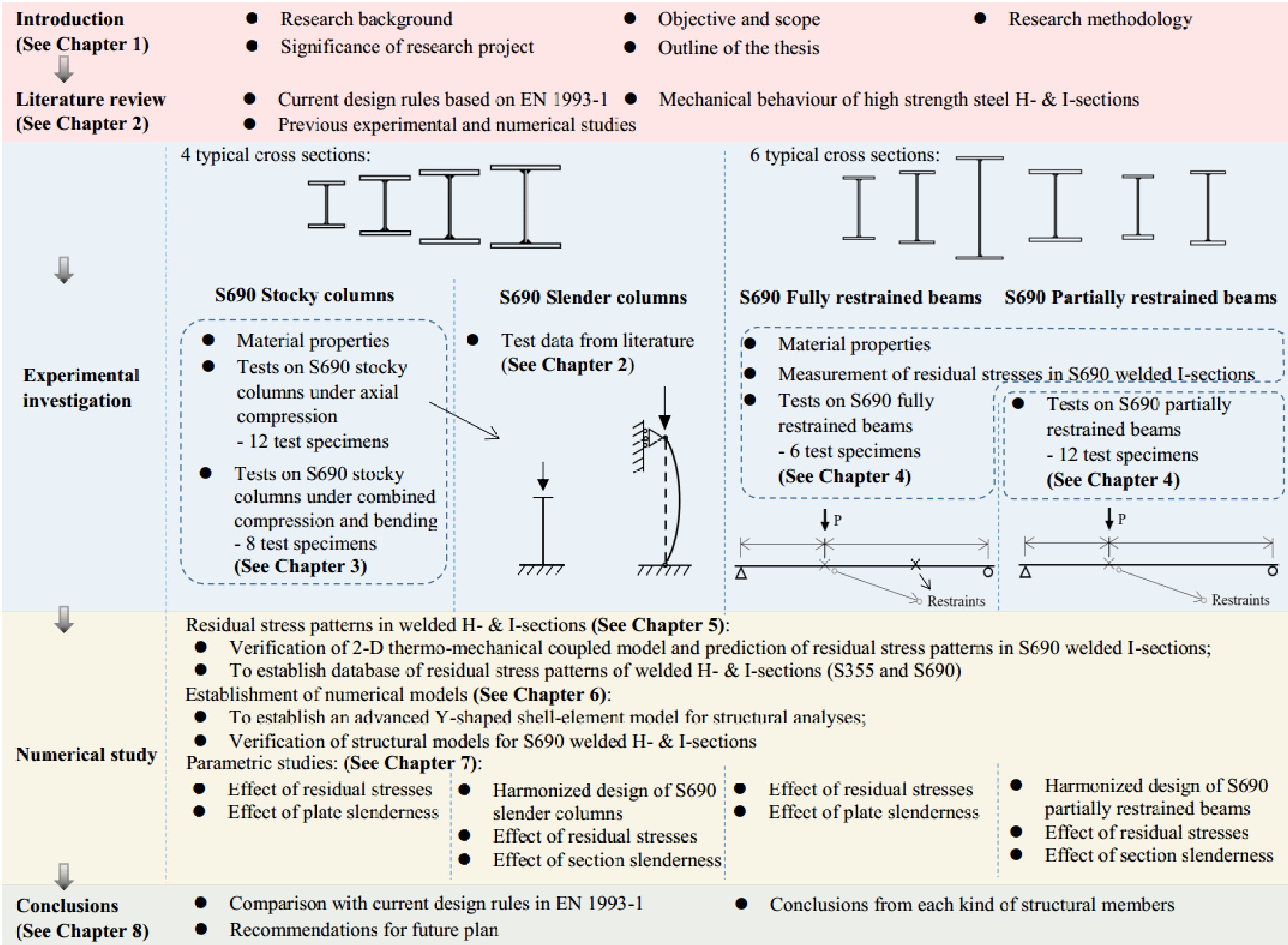

Figure: Flowchart of this research project

CHAPTER TWO

LITERATURE REVIEW

2.0 Introduction

This chapter presents a literature review on previous investigations into structural high strength steel (HSS) materials. Particularly, structural instability of high strength steel sections is focused with interest in experimental investigations and design rules of welded H- and I-sections. This review consists of the following parts:

i) Current design rules for HSS material properties and instability of steel sections specified in EN 1993-1-1 are reviewed. Schematic interpretation on these design rules is carried out. In addition, recent development of design methods consistent with EN 1993-1-1 is also covered.

ii) Mechanical properties of high strength steel are reviewed. Discussion of increased yield strengths comparing with conventional steel materials, and reduced residual stresses in welded sections would be covered.

iii) Previous experimental investigations into HSS columns and beams are reviewed. For each study, key parameters of test specimens, test setups and test results are reviewed. Most importantly, failure modes and buckling resistances of test specimens are summarized and compared with design values. Key conclusions are delivered based on these literatures.

iv) Structural models established by previous researchers were reviewed. The advantage of using shell elements is highlighted. In addition, a critical constraint of established models is also addressed.

2.1 Review of Current Design Rules

Design rules for instability of steel section are fully discussed in current EN 1993-1-1. Local buckling behavior of steel cross-sections were addressed through the design rules of section classifications. And consequently, full section resistances could be assessed. Based on full section resistances, buckling reduction factors owing to global buckling behaviour, i.e. overall buckling of slender columns and lateral torsional buckling of partially restrained beams, were presented in EN 1993-1-1. A harmonized buckling design method using buckling curves was utilized to estimate buckling resistances of slender sections.

In this section, a detailed review on EN 1993-1-1 design rules is carried out with following topics:

- Local buckling design of stocky columns under axial compression and combined compression and bending;
- Local buckling design of fully restrained beams;
- Overall buckling of slender columns; and,
- Lateral torsional buckling of partially restrained beams.

Additionally, various design methods were proposed to improve structural design efficiency based on EN 1993-1-1. As some of these researches are intuitive and fully validated through experimental investigations, they would also be covered in this section.

2.2.1 Design of local buckling of stocky columns based on Eurocode 3

2.2.1.1 Current design rules for stocky columns under axial compression

In EN 1993-1-1, local buckling behaviour of stocky columns under axial compression is estimated through cross-sectional dimensions, or namely the section classification method. This method simply determined whether material strengths could be fully mobilized and full section resistances could be attained. The distinctions amongst the structural behaviour of Class 1, 2 and 3 sections were not valid to stocky columns, as there is no stress redistribution in stocky column under axial compression (Davison et al, 2011). Hence, deformation characteristic of these structural members is not discussed in EN 1993-1-1.

For stocky columns with slender cross-sections, i.e. Class 4 sections, it is necessary to apply the design rules of EN 1993-1-5 which is provided for thin-walled steel structural members. Normalized slenderness of individual plate parts, i.e. $\bar{\lambda}_f$ of flanges and $\bar{\lambda}_w$ of webs, should be compared against design criteria of $\bar{\lambda}_{cr}$. Therefore, current design rules of section resistances for stocky columns under axial compression are summarized as illustration in Figure 2.1.

2.2.1.2 Current design rules for stocky columns under combined compression and bending

For stocky columns under combined compression and bending, local buckling behaviour is checked by applying section classification rules to respective steel plate element in a steel section. With this method, section resistances coming from different plate elements depend on cross-sectional dimensions, bending-to-compression ratios and material properties. Moreover, deformation characteristic of a stocky column could be implied by its section classification, as significant deformation capacities could be achieved by Class 1 sections.

In case of a welded H-section under combined major-axis bending and axial compression, local buckling may happen to external flanges or internal webs. It is necessary to check slenderness of each plate part. The flowchart to check the section classification of steel sections is illustrated in Figure 2.3. And for sections under combined minor-axis bending and compression, the design flowchart is similar and it is provided in parallel column.

To assess section resistances, interaction between bending and compression should be fully considered. Based on EN 1993-1, a bi-linear interaction curve is provided for Class 1 and Class 2 sections. Meanwhile, a more conservative linear interaction curve is applicable to Class 3 sections. These interaction curves are plotted in Figure 2.4 for reference.

2.2.1.3 Previous studies on existing design rules

For stocky columns under combined compression and major-axis bending, the flanges are under uniform compression and the webs in partial compression. Early research work on local buckling of these stocky columns proposed a bi-linear interactive design curve in 1950s (Driscoll and Beedle, 1957). In 1970s, a systematic research programme was launched to develop codified design rules in American and Canadian (Nash and Kulak, 1976; Perlynn and Kulak, 1974). Dawe and Kulak (1986) investigated local buckling behaviour of web plates in stocky columns under combined actions. It was followed by detailed experimental work and theoretical analysis (Dawe, 1980; Dawe and Kulak, 1984a). According to their research findings, interactive effect between adjacent flange and web was should be outlined and corresponding design consideration was proposed.

Dawe and Lee (1993) investigated local buckling behaviour of flange parts. In order to verify the Class 2 design criteria, an experimental programme incorporating eighteen test specimens were carried out. All stocky columns of H-section were loaded under eccentric compression. It was argued that the interactive effect between adjacent plates should not be pronounced. Moreover, comparing with design provision, a linear interactive curve was proposed to the design of Class 2 H-sections:

$$M_{Ed}/M_{pl.y,Rd} + N_{Ed}/\, N_{c,Rd} = 1 \qquad \text{(Eq. 2.1)}$$

Hancock and Rasmussen (1998) reported a comprehensive study on this topic for works completed in Australia. Three tests series were presented in their studies when detailed test information were presented by Chick and Rasmussen (1999a; b) and Hasham and Rasmussen (1998). H-sections under axial forces combined with major- and minor-axis bending were both incorporated into the tests. It was found that the interactive curve should be linear for welded H-sections under about major-axis bending, and be convex for those under minor-axis bending. More importantly, section resistances were found significantly underestimated for stocky columns under compression and minor-axis bending by major design codes.

In Liew and Gardner’s study (2015), an advanced design approach, namely Continuous Strength Method, was proposed to estimate the enhanced section resistances. In this method, deformation capacities were estimated with plate slenderness, and strength enhancement is calculated based on assessed strain levels. Consequently, section resistances can be achieved over full plastic resistances by most compact sections. With this design approach, continuous section resistances could be attained with variation of section compactness.

In order to facilitate easy comparison among the previous interactive design curves, resistances of H- and I-sections under combined axial and major-axis bending are plotted in

Figure 2.4(a). It is clearly demonstrated that Dawe and Lee's design curve is more conservative than Eurocode provision, while Liew and Gardner's design curve are most structurally efficient. For more information, the interaction curve of stocky columns of H- and I-sections under combined compression and minor-axis bending is given in Figure 2.4(b).

2.2.2 Design of local buckling of fully restrained beams based on Eurocode 3

2.2.2.1 Current design rules

In EN 1993-1-1, four different section classes are defined 0with distinctive behaviour for beams as following with an explanatory figure given in Figure 2.2 (CEN, 2005):

- Class 1: Plastic moment resistances can be attained with sufficient rotation capacity required from plastic analysis.
- Class 2: Plastic moment resistances can be attained with limited rotation capacity due to local buckling.
- Class 3: Elastic moment resistances can be attained with local buckling which prevents the development to plastic moment resistances.
- Class 4: Compression yield cannot be attained when local buckling governs the sectional failure.

According to EN 1993-1-1, Class 1 sections must be applied in plastic design of a steel frame structure. They are capable of maintaining full plastic moment resistances under a large degree of rotation capacity until a collapse mechanism forms. As explained by Commentary Document in American code AISC 360, a minimum rotation capacity over 3 is required for compact sections which is equivalent to Class 1 sections (AISC, 2010). Hence, plastic hinges should play a key role and moment redistribution should be fully developed these steel frames.

Typically, Class 2 sections are composed of Class 2 plate elements. The effective Class 2 sections are defined in EN 1993-1-1 which are fabricated with Class 3 webs and Class 1 or 2 flanges. In these cases, plastic moment resistance can be devised without accounting for some of the resistance contribution from web plates. Hence, plate slendernesses of outstanding flanges are more important, and they should be highlighted in practical design.

For all Class 3 sections, elastic moment resistances were defined as moment resistances when extreme fiber attains its first yield. This is generally a conservative approach to most Class 3 sections. Therefore, an interpolated moment resistance curve was proposed as shown in Figure 2.2 (Trahair and et. al., 2007). According to this proposal, section resistance is calculated with section slenderness and can reasonably lead to a higher structural efficiency.

2.2.2.2 Restraining requirement for fully restrained I-sections

In order to ensure the moment resistances of fully restrained beams, cross-sectional dimensions as well as lengths of unrestrained span should be limited. Adequate lateral torsional restraints should be installed to prevent lateral torsional buckling prior to full development of local buckling in beams. The corresponding design provisions are summarized in Table 2.1 for easy reference. In particular, design criteria for Class 1 sections are more restrict than others for other sections as high rotation capacities must be attained by Class 1 sections.

Moreover, according to recent studies, lateral torsional buckling has interactive effect with local buckling. The buckling resistance and rotation capacity could be dependent on this interactive effect (Kemp, 1996; Vayas, 2001). Thus, in study of the local buckling behaviour of steel sections, it is important to follow the design framework of current EN 1993-1-1 and control the lengths of restrained span.

2.2.2.3 Previous studies on existing design rules

As the interactive effect between local buckling and lateral torsional buckling was pronounced, some researchers proposed to design the buckling interaction with simplified methods (Hancock, 1977; Kemp, 1996; Vayas et al., 2001). In these methods, a comprehensive section slenderness is devised to assess reductions on sections resistances and rotation capacities. Typical design equations are presented as following:

Kemp, 1996: $$\lambda_R = K_f\, K_w\, K_d\, (L_{LT}/r_{yc})\varepsilon \qquad \text{(Eq. 2.2)}$$

where, K factors reflect the effect of flange and web slenderness and section type;

L_{LT}/r_{yc} is the lateral torsional buckling slenderness ratio.

Vayas et al., 2001: $\bar{\lambda}_M = \bar{\lambda}_{LT} \left(\frac{\lambda_f}{9}\right)^{1/3} \left(\frac{\lambda_w}{72}\right)^{1/5} \varepsilon$ (Eq. 2.3)

where, $\bar{\lambda}_{LT}$ is the normalized slenderness for lateral torsional buckling; and,

λ_f, λ_w is the plate slenderness for flange and web plate parts.

Kemp also investigated ductility of steel sections under combined compression and bending. It was found that rotation capacities of beams could be significantly reduced owing to the co-existed axial compression.

Shokouhian and Shi (2014) carried out a comprehensive study on rotation capacity of steel beams. Through a verified numerical model, data-based design equations were proposed to estimate moment resistance and rotation capacity. After that, an experimental investigation was conducted to high strength steel sections (Shokouhian and et al, 2015). Through test and numerical studies, it reported that the proposed design equations were also suitable to the design of high strength steel I-sections.

In current EN 1993-1-1, interactive effects are treated in a simple and conservative approach in which lateral torsional buckling resistances are factored based on moment design resistances, i.e. $M_{el,Rd}$ or $M_{pl,Rd}$. Hence, local and lateral torsional buckling behaviour are checked independently.

2.2.3 Design of overall buckling of slender columns based on EN 1993-1-1

Overall buckling of slender columns occurred before full section resistances are obtained. After buckled, flexure is developed in sections, and meanwhile, axial compression reduced sharply. The column buckling resistances are estimated with various buckling curves and section slenderness. Bjorhovde has incorporated 112 test data into his study, and proposed a column buckling curve in American steel code (Bjorhovde, 1971). Meanwhile, European Convention for Constructional Steelwork determined their column buckling curves through experimental and theoretical works (ECCS, 1976). Both residual stresses and material nonlinearity were considered into the research works.

Current design rules of overall buckling of slender columns is devised from these previous research outcomes. Amongst different design parameters, normalized slenderness ratio of slender columns is the most important one to determine section resistance. It is assessed with Euler buckling resistance as:

$$\bar{\lambda} = \sqrt{\frac{Af_y}{N_{cr}}} \qquad \text{(Eq. 2.4)}$$

With obtained column slenderness $\bar{\lambda}$, reduction factor can be simply obtained using the following equations as:

$$\chi = \frac{1}{\phi + \sqrt{\phi^2 - \bar{\lambda}^2}} \quad \text{but} \quad \chi \leq 1.0 \qquad \text{(Eq. 2.5)}$$

where,

$$\phi = 0.5\left[1 + \alpha\,(\bar{\lambda} - 0.2) + \bar{\lambda}^2\right] \qquad \text{(Eq. 2.6)}$$

It should be noted that a large variation of imperfection factor, i.e. α equal 0.13 to 0.76, is recommended in EN 1993-1-1 for different types of cross-sections. The different imperfection factors accounted for weld induced residual stress in steel sections. Moreover, EN 1993-1-1 has covered steel grade up to S460. Hence, it is highly necessary to determine an appropriate buckling curve for practical design of high strength steel columns in a reasonable basis.

2.2.4 Design of lateral torsional buckling of unrestrained beams based on EN 1993-1-1

2.2.4.1 Current design rules

Lateral torsional buckling is featured as a global buckling mode of unrestrained sections under moment and transverse loads. In this failure mode, full moment resistances could not be attained when section stiffness reduced sharply owing to out-of-plane displacement. For open sections like I-sections, this failure mode becomes more critical owing to their low torsional stiffness (Galambos and Fukumoto, 1963; Timoshenko and Gere, 1961).

Lateral torsional buckling behaviour of steel sections can be indicated with the elastic critical moment M_{cr}, or alternatively, the non-dimensional lateral torsional slenderness $\bar{\lambda}_{LT}$. These parameters were critical to partially restrained beams according to EN 1993-1-1, and details of design considerations are explained in non-contradictory complementary information (NCCI) publications. A most widely used expression for M_{cr} is stated in NCCI-SN003 as:

$$M_{cr} = C_1 \cdot \frac{\pi^2 EI_z}{L_E^2} \cdot \left\{ \sqrt{\frac{I_w}{I_z} + \frac{L_E^2 GI_t}{\pi^2 EI_z} + \left(C_2 z_g\right)^2} - C_2 z_g \right\} \quad \text{(Eq. 2.7)}$$

In this design equation, critical moment, namley M_{cr}, is assessed with various factors, such as effective length, moment distribution and load destabilization. While, some other sophisticated factors, like in-plane deformation prior to buckling are neglected. This may lead to a conservative estimation. Then, non-dimensional lateral torsional slenderness $\bar{\lambda}_{LT}$ can be readily obtained according to the follow equation:

$$\bar{\lambda}_{LT} = \sqrt{\frac{W_y f_y}{M_{cr}}} \quad \text{(Eq. 2.8)}$$

Alternatively, another expression derived from Eq. 2.7 and Eq. 2.8 can be directly used to estimate the non-dimensional slenderness as proposed in NCCI-SN002:

$$\bar{\lambda}_{LT} = \frac{1}{\sqrt{C_1}} UVD\bar{\lambda}_z \sqrt{\beta_w} \quad \text{(Eq. 2.9)}$$

With obtained $\bar{\lambda}_{LT}$, harmonized buckling design approach using buckling curves can be used to calculate buckling reduction factors, namely χ_{LT} The expression is as following:

$$\chi_{LT}=\frac{1}{\phi_{LT}+\sqrt{\phi_{LT}^2-\beta\bar{\lambda}_{LT}^2}} \qquad \text{but} \begin{cases}\chi_{LT}\leq 1.0\\ \chi_{LT}\leq 1/\bar{\lambda}_{LT}^2\end{cases} \qquad \text{(Eq. 2.10)}$$

where,

$$\phi_{LT}=0.5\left[1+\alpha_{LT}\left(\bar{\lambda}_{LT}-\bar{\lambda}_{LT,0}\right)+\beta\,\bar{\lambda}_{LT}^2\right] \qquad \text{(Eq. 2.11)}$$

For rolled I-sections and equivalent welded sections, $\bar{\lambda}_{LT,0}$ takes 0.4. In other general cases, $\bar{\lambda}_{LT,0}$ takes 0.2 which leads to a more conservative estimation. These two sets of lateral torsional buckling curves, i.e. from curve a to curve d, are illustrated in Figure 2.5 for direct comparison.

Amongst different design factors, it is important to note that the end and intermediate restraining conditions of beam sections have the most significant impact on lateral torsional buckling behaviour. These restraints must be clearly defined to determine effective lengths of partially restrained beams. Generally, it is necessary to check:

- If the section flanges have full, partial or free of restraints against in-plan rotation;
- If the support of cantilever has torsional or lateral restraints, or is just fully affixed;
- If the tip of cantilever has torsional or lateral restraint, or is just free;
- If the intermediate restraint is restrained on compressive flange or on the web; and,
- If the beam ends are notched.

The effective lengths of practical design cases are listed in NCCI document SN009. Moreover, explanatory guidelines can also be found in SCI publication P360 (Gardner, 2011).

2.2.4.2 Previous studies on existing design rules

For a continuous beam, interactive effect between adjacent beam segments was analytically investigated by Nethercot and Trahair (1976a). This effect is pronounced when flexural and torsional stiffness of a beam segment is significantly different from those of the adjacent segments owing to different span, moment profile or boundary conditions. Lateral torsional buckling of a beam segment should be induced or constrained by adjacent segments. Dux and Kitipornchai (1980, 1982) investigated this effect theoretically and provided elastic solution to this problem. Therefore, a simple design algorithm was proposed with the following conceptual equation as:

$$k = \text{Function } \{K, \beta, G_A, G_B\} \qquad \text{(Eq. 2.12)}$$

where, k is modified effective length for critical segment;

K is beam parameter, and equals $\sqrt{\pi^2 EI_\omega / GJL^2}$;

G_A, G_B are end restraint parameters at section ends A and B.

With this k factor, interactive effect could be accounted for, and it may lead to a highly accurate estimation of critical moment.

Moreover, Dux and Kitipornchai extended previous method to estimate nonlinear solutions to continuous beams (1984). And a similar design approach was proposed by Nethercot and Trahair (1976b; 1977) which was noted as direct strength method. While, these methods are not compatible with current EN 1993-1-1 design approaches which employ harmonized design approach with a variation of lateral torsional buckling curves.

2.3 Mechanical Properties of High Strength Steel H- and I-sections

In this section, a comprehensive review on mechanical properties of high strength steel materials and welded steel sections is carried out. Generally, high strength Grade S690 steel materials possess yield strengths over 690 N/mm^2, which is two to three times that of conventional Grade S235 or S355 steel materials. Hence, high strength steel sections are entitled with larger cross-sectional resistances and structural design efficiency. While, high strength steel sections are prone to buckle before section resistances fully mobilized due to increased yield strengths. Moreover, owing to different welding procedures, the residual stresses which is a key material imperfection induced by heating-and-cooling cycles has become different to those in conventional strength steel sections (Ban and et. al., 2013; Kin and et. al., 2014). Thus, in order to understand buckling behaviour of high strength welded H- and I-sections, it is highly necessary to clarify the mechanical properties of these sections (Chung and et. al., 2016).

2.3.1 Material properties

High strength steel materials, of which yield strengths are above 460 N/mm^2, possess doubled or tripled strengths of conventional steel materials. Hence, it is simple to achieve an efficient design with low self-weights and high strengths, and to fulfill aesthetic requirements from structure owners. In engineering practices, there have been successful applications of high strength steel materials up to Grade 1000 (N/mm^2) in modern structures (Shi, 2008; Pocock, 2006).

While, drawbacks of high strength steel materials are reported, such as low ductility and low tensile-to-yield ratios. And more importantly, buckling resistances of steel sections usually do not proportionally increase with material strengths. Therefore, for design purposes, a verification must be made before a wide application of high strength steels.

Previous researches reported material properties of high strength steels and ultra-high strength steels from standard tensile tests, as listed in Table 2.2 (Sun et. al, 2013; Ban et. al, 2013; Ban et. al, 2012; Earls, 2001; Wang et. al, 2016; Lee et. al, 2012; Green et. al, 2002;

Li et. al, 2015). Particularly, a comparison between measured material properties between requirements given in EN 1993-1 is conducted based on Eq 2.13 and Eq 2.14:

EN 1993-1-1 (for conventional strength steel):

$$f_u / f_y \geq 1.10 \qquad \varepsilon_u \geq 15\, \varepsilon_y \qquad \varepsilon_{eL} \geq 15\% \qquad \text{(Eq. 2.13)}$$

EN 1993-1-12 (for high strength steel):

$$f_u / f_y \geq 1.05 \qquad \varepsilon_u \geq 15\, \varepsilon_y \qquad \varepsilon_{eL} \geq 10\% \qquad \text{(Eq. 2.14)}$$

Bjorhovde has carried out a detailed investigation into high performance steel materials (Bjorhovde, 2004). Through these reported mechanical properties of high strength steel materials, it was found that excellent strength, ductility, toughness and weldability were provided by these materials. And consequently, structural demands could be well satisfied under various delivery and service conditions. Similar findings have also been supported by Shi (2008).

Ricles, and et. al (1998) studied material properties of high strength steel through a close examination on section resistances, rotation capacity and failure modes of 10 fully restrained beams. By comparing with structural behaviour of I-sections fabricated with both conventional and high strength steel materials, it was found that high strength steel materials facilitated a more efficient and economic design. It was also noted that increased Y/T ratios and plastic modulus of applied steel materials may lead to remarkable reduction on rotation capacity of beams. These evidences were consistent with those from other research outcomes (Green et. al, 1994; Kuhlmann, 1989).

Therefore, the use of high strength steel materials is based on optimized trade-off between structural efficiency and reliability. Mechanical properties of these materials should be examined carefully when existing experiences of designing conventional steel sections may not be valid to the design of high strength steel sections any more. Therefore, applications of high strength steel sections to various structural members should be thoroughly studied. Moreover, proper design rules should be developed to prevent unexpected failure of high strength steel structural members.

2.3.2 Residual stress distributions

The residual stress, which is induced by heating-and-cooling circles during the weld of steel sections, has negative impact on buckling resistances (ECCS, 1976). It may lead to early yielding of steel sections and reduce section rigidities. And hence, buckling resistance of steel sections and deformation capacities could be reasonably impaired. A typical residual stress pattern recommended by ECCS for welded conventional steel H-sections is presented in Figure 2.6 (a). This pattern was proposed with a polynomial shape which attained tensile strengths in tension and half of yield strengths in compression.

For high strength steel sections, the residual stress ratios are much smaller than their counterparts of conventional steels according to recent reports (Ban and et. al., 2012, 2013b; Chung and et. al., 2016; Li, and et. al., 2016). While, arguments were raised by contradictory measured results reported from different researches. It should be realized that appropriate measuring methods as well as fabrication procedures of parent metal and governing weld parameters are important to these studies. Most importantly, applicability and constraints of hole-drilling method and sectioning method must be well understood to interpret research outcomes. Liu obtained residual stress distributions for welded S690 H-sections through a comprehensive study with combined experimental and numerical methodology which well addressed this key issue (Liu, 2017).

A typical residual stress pattern for welded S690 H-section is provided by Liu as shown in Figure 2.7 (b). With a standard welding procedure, tensile residual stresses equal half of the yield strengths, and compressive stresses equaled 0.2 times the yield strengths. It should be noted that the obtained residual stress magnitudes are merely half of those of ECCS's pattern. According to Liu, the significant reduction in residual stress magnitude should be majorly attributed to increased yield strengths of steel materials. In addition, optimized welding procedures which decreased energy concentration, can also reduce magnitudes of residual stresses. Owing to this potential benefit, higher structural efficiency of welded S690 H-sections can be achieved.

2.3.3 Deformation capacity

The deformation capacity is usually used to define the capability of rotating or shortening for steel sections without significant reduction of section resistances (Kato, 1990, Ashraf and et. al., 2006). It is an essential factor to ensure structural performances of steel sections (Gioncu, 2000), and is also termed as rotation capacity for cases of beam and beam-column designs. As deformation capacity is highly dependent on plate slenderness of cross-sections. Hence reasonably, the deformation capacity could be used to differentiate section compactness between Class 1 and Class 2 based on EN 1993-1-1. Hence, it is important to examine the deformation capacities, or the section classification of steel sections in structural design.

For high strength steel sections, deformation capacities would become more critical owing to increased plate slenderness and reduced hardening modulus. Therefore, it is necessary to check structural adequacy of S690 compact sections according to EN 1993-1-1 design rules and examine the corresponding design criteria.

2.3.3.1 Definition of deformation capacity

Deformation capacity is defined in Equation 2.15 with symbols illustrated in Figure 2.7. It should be noted that there are different approaches to determine M' denoted in Figure 2.7 (Shokouhian et. al, 2014). According to Gioncu and Petcu (1997a), three widely used methods are as following:

$$R_\theta = \frac{\theta_2 - \theta_1}{\theta_1} \qquad \text{(Eq. 2.15)}$$

- Method 1: M' equals a certain ratio to moment resistances, e.g. 0.80 to 0.90 M_u;
- Method 2: M' equals full plastic moment M_{pl} or 0.9 × M_{pl} of the steel section;
- Method 3: Similar to Method 2, and additionally, the slope of descending part of the moment-rotation curve is linearized to intersect with M'.

Among those methods, the first method is rarely used, as the use of M_u could lead to large variations of rotation capacities (Nakashima, 1994). For the third method, curve fitting procedure for the descending part of moment-rotation curve is difficult to be determined and the application may lead to significant error (Axhag, 1995). Generally, the second method is more favorable. This approach has a reasonable technical background which leads to a reliable assessment and can be readily applied to any given cases. Meanwhile, it is also compatible with current practices adopted in Eurocode and AISC design codes. Therefore, comparisons among test and numerical results from different data sources would be readily facilitated.

For beam-columns, previous researchers used section-end rotation to represent deformation to estimate rotation capacity (Nakashima, 1992; Dawe and Kulak, 1986; Gioncu and Petcu, 1997b). This treatment is applicable to slender beam-columns when flexure governs the failure of steel sections. While, for stocky columns under combined compression and bending, it is not necessarily appropriate when shortening deformation is more critical than flexural deformation. In this sense, an alternative parameter, namely the axial shortening, could be utilized to illustrate the corresponding deformation capability.

2.3.3.2 Design consideration on deformation capacity

According to Lay (1965), a plastic hinge must be formed to compact sections after the redistribution of cross-sectional stresses. And after the development of plastic hinge, plastic local buckling happens and governs failure mode. In order to address the plastic local buckling resistances, plate slenderness of cross-sections was concerned and employed as the only design parameter. Lay also pointed out that rotation capacities of three should be applied as the criterion for plastic sections. This proposal was then applied in AISC (AISC, 2010).

Researches on steel beams were then conducted by Lukey et al. (1969), Kemp (1985, 1986) and Kuhlmann (1989). From these studies, a large test database incorporating different failure modes of steel sections was established. It was found that local buckling behaviour of plate parts had interactive responses with lateral torsional buckling. Hence, the implication is that slenderness of lateral torsional buckling should be fully considered in local buckling design of steel beams when interactive effect should have significant impact on it.

2.3.4 Summary

In this section, mechanical properties of high strength steel materials and structural behaviour of high strength steel sections are closely reviewed. The significances of investigation into S690 steel sections was outlined as these sections possess quite different properties from those of conventional steel sections. And they may introduce pronounced influence to mechanical behaviour Most importantly, recent studies has reported reduced residual stress magnitudes for welded high strength H-sections. These residual stress patterns must be incorporated into the following studies. Better structural performances of steel structures could be anticipated from this change. Moreover, definition of deformation capacity is clarified, and it will be then employed in study of Class 1 and Class 2 sections.

2.4 PREVIOUS RESEARCH STUDIES

2.4.1 Experimental investigations into local buckling of stocky columns

Researchers tended to study local buckling behaviour using stocky columns as overall buckling effect is eliminated due to section configurations. To identify different section classifications of H-and I-sections, compressive resistances are firstly concerned. With loading eccentricity, combined compression and bending actions determine the interactive resistances of H-sections. In addition to resistances, deformation capacities of H-sections are also studied. They may indicate the boundary between Class 1 and Class 2 for sections under moment gradient according to section classification method. Moreover, test rigs in previous test programme are also reviewed for references.

(a) Literature of high strength steel columns of H-sections under axial compression

Previous test studies on high strength steel stocky columns with non-slender cross-sections under axial compression are summarized here. Corresponding test data are listed in Table 2.3 and test results are listed in Table 2.4 for reference. Basically, a typical test setup was followed in which axial compression was implemented through end plates. According to the literature, length-to-width ratios of section plates should be larger than 3 to prevent over constraints, and careful alignment of geometric centers with loading axis must be ensured. From the test data, it is found that most specimens presented excessive capacity over their yielding level. This hardening behaviour is more evident when plate slenderness is smaller.

(b) Lay and Gimsing, 1965

Lay and Gimsing (1965) conducted a test programme including six stocky columns with four axially loaded and two eccentrically loaded. Two eccentrically loaded specimens were fabricated with high strength low alloy ASTM 441 steel, and they should be classified as Class 1 and Class 3 sections respectively. To realize free rotation at ends and eccentricity about major axis, a cylindrical surface was attached to section ends. Typical moment-curvature relation and test setup for beam-column test is shown in Figure 2.8.

From the moment curvature relation, beam-column resistance was found smaller than the corresponding plastic design value and it is identified as a Class 3 section. Moreover, good deformation capacity for the beam-column section is demonstrated when curvature achieved a high level before a significant decrease in section resistance.

(c) Perlynn and Kulak, 1974, and Nash and Kulak, 1976

In 1970s, a test programme incorporating 15 stocky columns was launched to develop the North American steel design code. The details of tests on nine compact (Class 1) sections and six non-compact (Class 2) sections were respectively addressed in two reports. In this test programme, Grade 275 steel was utilized to fabricate H-sections. During the tests, all specimens were loaded by imposing axial load first. After reaching the pre-determined load level, a uniform major-axis moment was applied through a pair of lever arms until local buckling failure. Typical local buckling waves were observed on flanges and webs with maximum deflections pointed out.

(d) Hasham and Rasmussen, 1998

To verify the applicability of linear interactive design curve for Class 3 sections, two test series were conducted on fabricated H-sections with eight specimens in each series. Different flange compactness was applied in two test series which included Class 1 for Series I and Class 3 for Series II. This was intended to examine the interactive supporting effect from webs to flange plates. Applied test rig is shown in Figure 2.9. Due to moderate lengths of test specimens, bracings were utilized at mid-span to prevent lateral torsional buckling and minor-axis flexure. During the tests, axial compression actions were applied first and moment actions were followed through lever arms.

From the test results, it was revealed that web-flange interaction was prominent when the section was under high level of moment, i.e. m larger than 0.8. This should be attributed to the stress redistribution of cross-sections and hardening effect of materials. Moreover, for Series I tests, section resistances obtained plastic design values based on Eurocode 3, in which flange compactness governed local buckling behaviour and enhanced deformation capacity for these sections.

(e) Kim et al., 2014

To verify the applicability of AISC local buckling criteria to Grade 800 steel, 4 identical H-sections were fabricated and loaded with different eccentricities. The H-sections were bent about major axis. The cross-section dimensions indicated Class 3 flanges and Class 1 webs. Comparing with AISC and EC3 design value, the ultimate resistances of the samples were significantly underestimated. This could be attributed to interactive effect between plates. Because the strength enhancement was more notable under larger load eccentricity in which cases webs were more compact. This implies that the conventional design rules are over conservative for high strength Class 3 beam-columns, especially when flanges are supported interactively by webs.

(f) Summary

There are various methods to realized combined actions according to the literature. It is important to quantify each action without introducing additional uncertainties. And both lever arms and loading eccentricity are reliable methods to implement combined compression and bending.

The reported test results are summarized in Figure 2.10. Comparing with design values based on Eurocode 3, all reference tests reached higher ultimate resistances. For Class 3 sections, many test results attained plastic resistances, especially when flanges are compact or non-compact. This improvement can be reflected by recognizing an effective Class 2 section as stated in Eurocode 3. Considering interaction between compression and bending, excessive resistances tend to be larger when large moment ratio is applied. The intuition is that material hardening can contribute excessive resistances to sections under large moment ratios.

2.4.2 Experimental investigations into overall buckling of slender columns

(a) Wang et al., 2017

A total of seven slender columns of S690 welded H-sections were tested under axial compression. Test setup was illustrated in Figure 2.11. Seven slender columns with various normalized slenderness were covered in this test programme with section heights of 1,610 mm and 2,410 mm. Thus, a practical column slenderness ranging from 0.62 to 1.41 was incorporated into this study. All of these seven slender columns failed in overall buckling about the minor axes. In general, these slender columns had failed with a sudden decrease of applied loads while lateral displacements at mid-height of columns developed quickly which implied a non-ductile failure mode. Comparing test results against buckling curves in EN 1993-1-1, it indicated that curve a should be applicable to design these columns instead of curve c as recommended by design rules. The improvement of buckling resistances should be mainly attributed to reduced residual stresses in welded S690 H-sections.

(b) Ban et al., 2012

Overall buckling behaviour of Q460 slender columns of Box-sections and H-sections were investigated experimentally and numerically in this comprehensive research programme. Five slender columns of Box-sections and six of H-sections were comprised in the test series. Based on test results, buckling resistances of welded Grade 460 slender columns were closely examined using numerical models fully verified. Measurements of residual stresses were also conducted using sectioning method to provide detail for direct comparison and numerical input (Ban et al., 2013a). The experimental and numerical results revealed that current buckling curve b is appropriate to design welded Q460 slender columns of H-sections.

Cylindrical hinges were applied to allow rotations of section ends. It should be noted that rotational friction was occurred at inception of overall buckling. Hence, experimental results were believed higher than theoretical values of columns setup in idealized conditions. This factor was reasonably considered in validation of numerical models, and parametric study was successfully conducted to provide reasonable predictions of section resistances.

(c) Wang and et al., 2012b

In this experimental investigation into Q460 slender columns of welded H-sections, six slender columns were included and buckled about minor axis. Material properties, residual stresses and geometric imperfections of test specimens were closely examined (Wang and et al., 2012a). During the loading process, axial shortening and strain readings at mid-height locations were measured to closely examine the deformation response of test specimens. Through test results and extensive parametric study, it was found that buckling curve c provided by EN 1993-1 was over conservative for high strength steel Q460 slender columns, and buckling curve b was suggested to obtain higher structural design efficiency. It should be noted that an idealized boundary condition was realized in this test arrangement.

(f) Summary

There were more previous experimental researches on overall buckling of high strengths steel slender columns (Ban et al., 2013; Shi et al., 2015; Shi et al., 2012; Rasmussen and Hancock, 1995; Li et al., 2016). Test results of previous researches were summarized in Figure 2.12 with reduction factors plotted against normalized slenderness. Basically, these solid test evidences indicated that current design rules were over conservative. The increased overall buckling resistances should be attributed to reduced residual stresses in welded high strength steel sections. While, most previous test studies did not consider various design parameters, especially the welding parameters. Therefore, it is necessary to conduct a comprehensive investigation to clarify the underlying failure mechanism of slender columns.

2.4.3 Experimental investigations into local buckling of fully restrained beams

(a) Ricles and et. al., 1998, and Green and et. al., 2002

In this research programme, a test series including 10 fully restrained beams under transverse loads was conducted. Both uniform moment and moment gradient were incorporated into the loading conditions. Among all test specimens, seven of them were fabricated with HSLA-80 steel which had a nominal yield strength of 552 N/mm^2, and the other three sections with

A36 steel. Out-of-plane restraints were installed at load points with intention to check the section compactness criteria for high strength steel beams. It was observed that 8 sections failed under local buckling mode and all sections underwent large deformation. Comparing with A36 sections with identical plate slenderness, high strength HSLA-80 sections possessed reduced rotation capacity, which should be attributed to increased yield strengths and Y/T ratios. As a conclusion, section compactness criteria of AISC should not be directly extended to differentiate plastic and compact sections. While, it was also noted that more research evidences should be obtained to clarify the effect of material plasticity on local buckling behaviour.

(b) Lee et. al., 2012

In this test study, welded I-sections fabricated with Grade 325 and Grade 690 steel materials were tested under one-point load and two-point load. A total number of 21 sections, which covered from Class 1 to Class 4, were incorporated in this test programme. The primary objective was to determine the effect of flange slenderness on local buckling and rotation capacity. Limiting unbraced lengths of sections were considered, and lateral bracings were provided to prevent overall buckling modes. According to test results, high strength steel specimens obtained expected strengths, but failed to reach designed rotation capacity according to design provision. It was attributed to large Y/T ratios and small plastic modulus. Moreover, brittle fracture was observed on test specimens with full-height transverse stiffeners and compact cross-sections. Therefore, better weld quality of high strength steel sections is required to achieve satisfying structural performances.

(c) Shokouhian and Shi, 2015

Bending tests on 3 hybrid I-sections and 3 homogeneous I-sections subjected to uniform moment were conducted. Total lengths of these specimens were laterally supported by bracings as shown in Figure 2.13. Hence, possible failure mode was limited to local buckling failure. Independent with overall failure modes, section classification limits were verified against test results. Measured moment capacity and rotational capacities implied that Class

1, 2 and 3 sections were all covered in this test programme. Moreover, through extensive study on test and numerical data, an interactive design rule to predict rotation capacity with any combination of local and global buckling slenderness was provided. It should be noted that a 3rd specimen had a small span-to-depth ratio below 5, which led to undesirable shear buckling failure. On the other hand, uniform lateral bracing is not a proper setup to justify local buckling criteria, as the allowance of free-span is indicated by design codes.

(d) Wilkinson and Hancock, 1998

A test programme including 44 welded RHS sections under two-point load was conducted to investigate limitation of plate slenderness for Class 1 sections. The steel sections are cold-formed welded RHS sections with thickness 1.6 mm to 6.0 mm fabricated with Grade 350 and 450 steel materials. In order to reflect ductility of these sections, end rotations were measured. Comparing with AS 1163 criteria, Class 1 sections were identified from these specimens. As different combination of flange and web slenderness was incorporated, local buckling interaction was clearly demonstrated. With measured data, a linear interactive equation was formulated for Class 1 limits of RHS.

(e) Summary

In general, the mechanic behaviour of beams depends on many variables. They can be different treatments on lateral support conditions, or fabrication methods in specimen perspective. In order to investigate local buckling, these variables should be closely examined and well controlled. From reported test data, contradictory conclusions were achieved and they should be attributed to different setting on variables. Therefore, sufficient information about test method and specimen details should be provided to reflect research objectives and make easily understood.

2.4.4 Experimental investigation into lateral torsional buckling of unrestrained beams

Early researches revealed that behaviour of lateral torsional buckling is sensitive to various factors including boundary conditions, loading conditions, and lateral torsional restraints. Owing to the complexity of lateral torsional buckling of steel beams under transverse loads, theoretical buckling solutions were closely verified against test data for conventional steel sections. Hence, a large test database incorporating 159 rolled I-sections was established to justify the practical design methods in BS code (Trahair and et al., 2007).

In this study, great efforts were spent on identifying governing factors of lateral torsional buckling and controlling them through appropriate testing rigs. Therefore, in this sub-section, attention is focused on test setup applied by previous studies. In general, these previous test setups were intuitive examples for design of current test programme on unrestrained high strength steel beams of I-sections subjected to lateral torsional buckling. In addition, key factors which have significant influences on buckling resistances are also reviewed.

(a) Dibley, 1969

In order to investigate the lateral torsional buckling under uniform bending moment, a test series including 30 Grade 55 rolled I-sections under two-point loads was carried out. All specimens had a span from 1 to 5 meters. Downward loadings were imposed at section ends and the supporting seats were located between the loading sections as presented in Figure 2.14. With this seating rig, lateral and rotational movement on beam supports was rigorously restrained. At middle of span, lateral deflection and rotation of beams were measured by two dial gauges to reflect buckling behaviour when lateral torsional buckling was expected to occur on the uniformly flexural segment.

All beam sections failed in lateral torsional buckling with resistances higher than predictions. The increased resistances were attributable mainly to application of high strength grade 55 steel material whose yield strengths were beyond 448 N/mm^2. Moreover, extensive numerical study was recently reported by Bradford and Liu based on Dibley's work (2016). Through parametric studies on applied material strengths and residual stresses, it was found that lateral torsional buckling strengths could be higher for S690 to S960 sections comparing with S355 counterparts owing to less severe residual stresses.

(b)Bose, 1982

In this test study, requirement at supports were investigated for beams subject to out-of-plane instability. A test programme including 7 rolled Grade 43A I-section specimens was carried out under one-point load. Lengths from 3 to 7 meters were selected to accommodate predetermined beam slenderness ratios, L/r_y from 100 to 300. Torsional stiffness was provided at section ends for the allowance of distortion on top flanges as illustrated test rigs in Figure 2.15. On loading sections, a special device was facilitated to impose point load.

According to test results, the torsional stiffness was found influential to lateral torsional buckling resistances, especially for sections with medium slenderness of $\bar{\lambda}_{LT}$ smaller than 1.0. A reduction was found for the existence with insufficient torsional restraints comparing with predictions from BS design code. Moreover, test results also indicted that requirement for restraint stiffness was adequate. Therefore, it is necessary to fully consider this factor in practical design of steel beam elements.

(c) Law and Gardner, 2012

Law and Gardner (2012) conducted a test programme including eight laterally unrestrained elliptical hollow sections (EHS) which were subject to lateral instability. Owing to the application of hollow sections, full span lengths of the specimens ranged from 4 to 11 meters. The elliptical sections had a constant aspect ratio of 2, and were tested in one-point loading. According to EN 1993-1-1 design rules, the non-dimensional slenderness of beam specimens ranged from 0.29 to 0.48. The normalized resistances to plastic moment capacity exceeded 1.0 for all sections. Hence, design provision of EN 1993-1-1 should be over-conservative to EHS sections.

The test rig for this experimental investigation is shown in Figure 2.16. It should be noted that at mid-span, a circular bearing was installed to allow free rotation and lateral move of test specimens. In this context, a regular boundary condition for one-point load simply supported beam was established. Comparison between test data and design values can be facilitated.

(d) Summary

In reported tests, well defined supporting and bracing conditions were implemented, and transverse loads were imposed in line with vertical direction. From these application, the test specimens can be analyzed accurately and comparisons between other test series can be facilitated. In respect of measured resistances, most are 10% to 20% higher than design values. This safe margin is considered necessary for lateral torsional buckling as this failure mode is not ductile.

2.4.5 Numerical studies into local and global buckling

As it is timely and costly to acquire sufficient data points through test method, researchers developed and validated finite element models against existing test data and extend them to obtain modelling results. For studies on structural behaviour of I- or H-sections, shell-element model was most widely utilized in previous studies. Successful applications can be found in:

- FE study on stocky columns by Shi et al. (2014), Chou et al. (2000), Yang and Hancock (2006), and Gao et al. (2009);
- FE study on beam-column members by Dawe and Kulak (1984b), Gardner, and Nethercot (2004) and Greiner and Kettler (2008);
- FE study on beam sections by Pi and Trahair (1994), Beg and Hladnik (1996), Earls (1999), and Shokouhian and Shi (2015).

With intention to capture local buckling and overall buckling responses, effect of material and geometric non-linearity should be taken into the numerical algorithms. In addition, residual stress distribution and initial geometric imperfection are also important to structural models when they are critical to mechanical behaviour of steel sections. With these features, high level of modelling accuracy could be achieved. Moreover, with numerical results, extensive interpretation on deformation behaviour of structural members can be achieved when load-deformation relations and strain history models can be tracked. This may help to deepen the understandings of local and global buckling mechanism.

A typical shell-element model for I- or H-section is given in Figure 2.17. It should be noted that for each shell element, nominal thickness is assigned to represent real parts of steel plates. Generally, five or sometimes more layers of Simpson integration points are assigned to simulate through-thickness behaviour of shell elements (Systemes, 2009). Hence, they are applicable to deal with any in-plane or out-of-plane flexure deformation. Comparatively, solid elements may not be good to model I- or H-sections, because it is too computational intense to achieve satisfactory accuracy level.

It is noted that widely applied shell-element model has a simple treatment on junction region of cross-sections. It may misrepresent the actual width-to-thickness ratios of section plate parts. In order to capture accurate local buckling behaviour of plate parts, weld root and exact plate width as illustrated in Figure 2.17 (a) should be incorporated into the numerical model. Hence, this technical problem will be addressed in following chapters.

2.5 Conclusions

In this chapter, requirements on material properties of high strength steel materials was reviewed. It was denoted that high strength steel materials up to Grade 700 should be applicable to be employed in structural design based on EN 1993-1-12. As high strength steel materials possess some distinctive characteristics from its normal strength steel counterparts, structural design rules were also closely reviewed. Basically, they could be extensively applied to high strength steel structures. While, more test evidences would be necessary to achieve better structural performance and economic efficiency.

Recent experimental works on high strength steel columns and beams were reviewed. They generally indicated appropriate application of high strength steel sections based on current design rules. Moreover, owing to the lack of systematic research programme on high strength steel sections, the following topics are proposed for further investigations which would lead to deepened understandings to welded S690 sections:

- To justify the adequacy of material ductility for application of welded S690 sections in steel structure;
- To learn the influences of weld induced residual stresses to structural behaviour of high strength welded S690 sections, especially the local and global buckling behaviour;
- To examine the suitability of current EN 1993-1-1 design rules of section classifications to S690 stocky columns and fully restrained beams;
- To study the overall buckling behaviour of slender columns of welded S690 H-sections; and,
- To study structural behaviour of partially restrained beams of welded S690 I-sections subject to lateral torsional buckling.

According to EN 1993-1-12, current buckling design rules of local and global instability are applicable to extensive application on high strength steel sections. While, they were barely supported by adequate research evidences. Moreover, influences of residual stresses in welded S690 sections should be quite different from those in S355 sections.

Hence, a systematic research programme on columns or beams of welded S690 I- or H-sections is required to support a safe and efficient design of high strength steel structures. And, verification of existing design rules in EN 1993-1-1 would be covered by this research programme in following chapters.

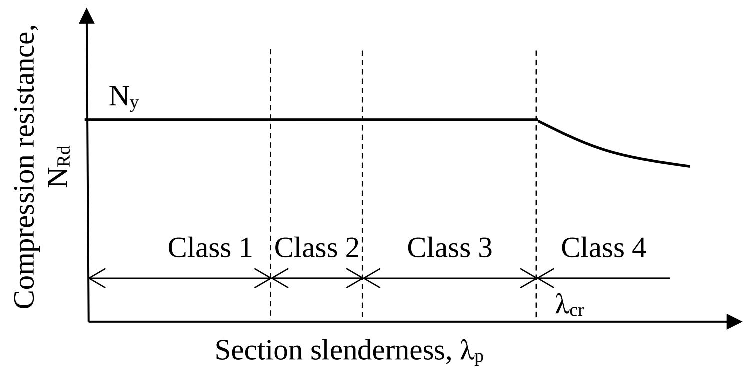

Figure 2.1: Design rule of section resistances for stocky columns under axial compression

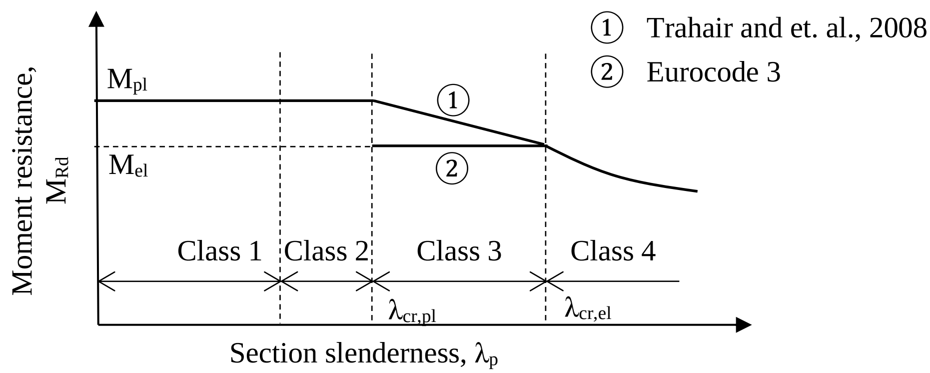

Figure 2.2: Section classification rule for beam sections

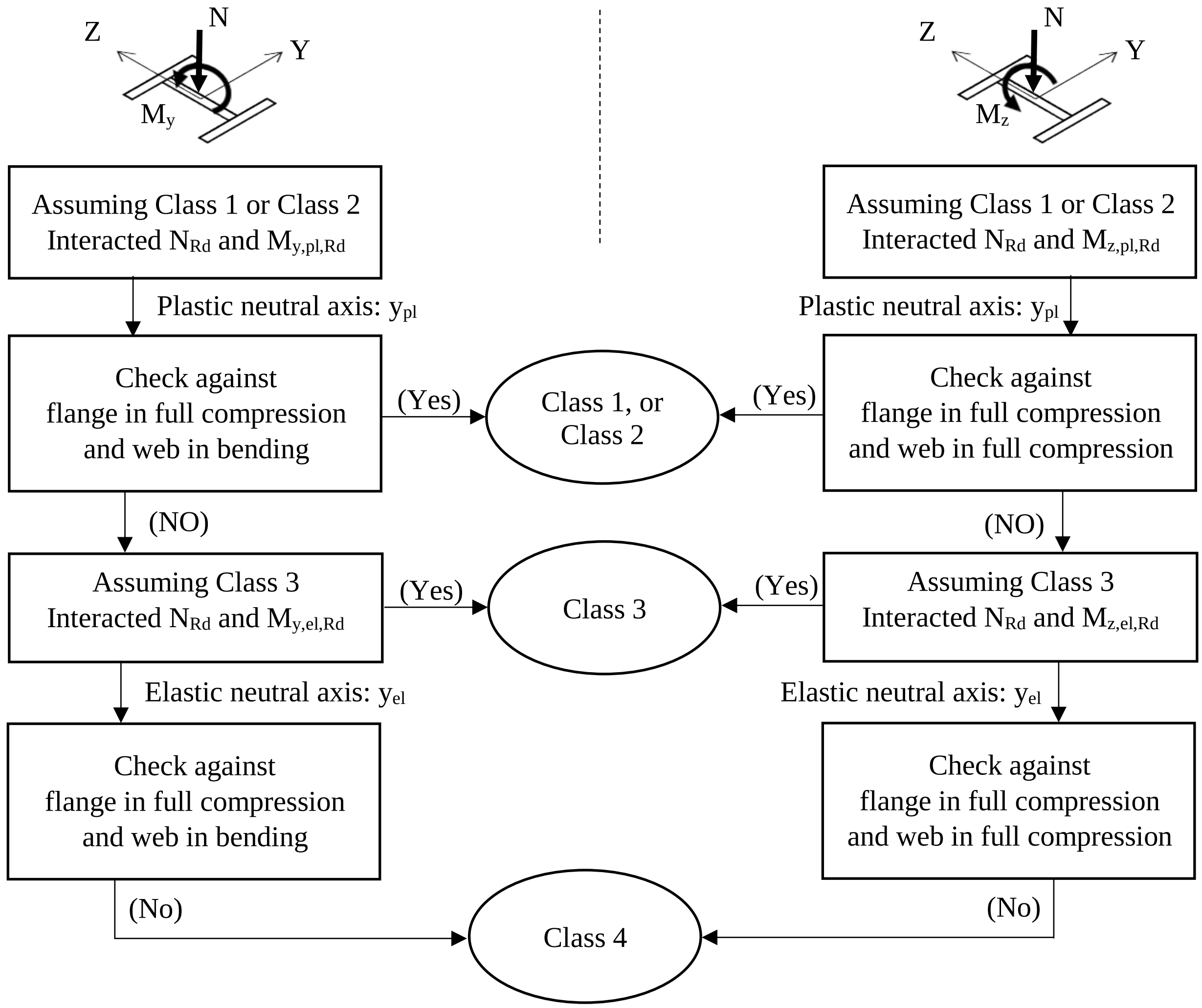

Figure 2.3: Design flowchart of local buckling for H-sections under combined actions

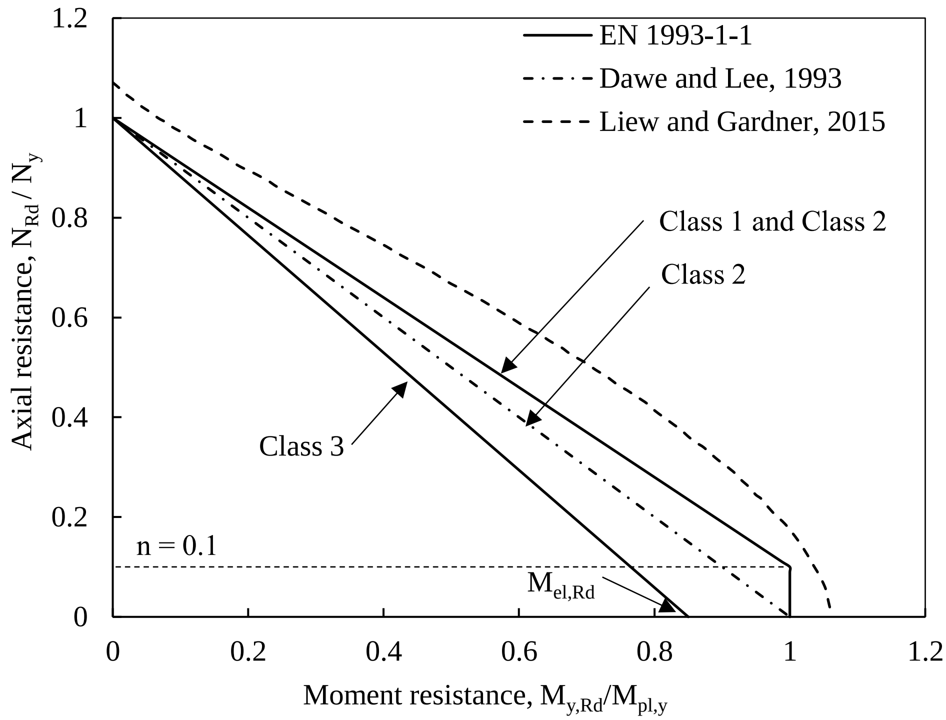

(a) H- or I-sections under combined compression and major-axis bending

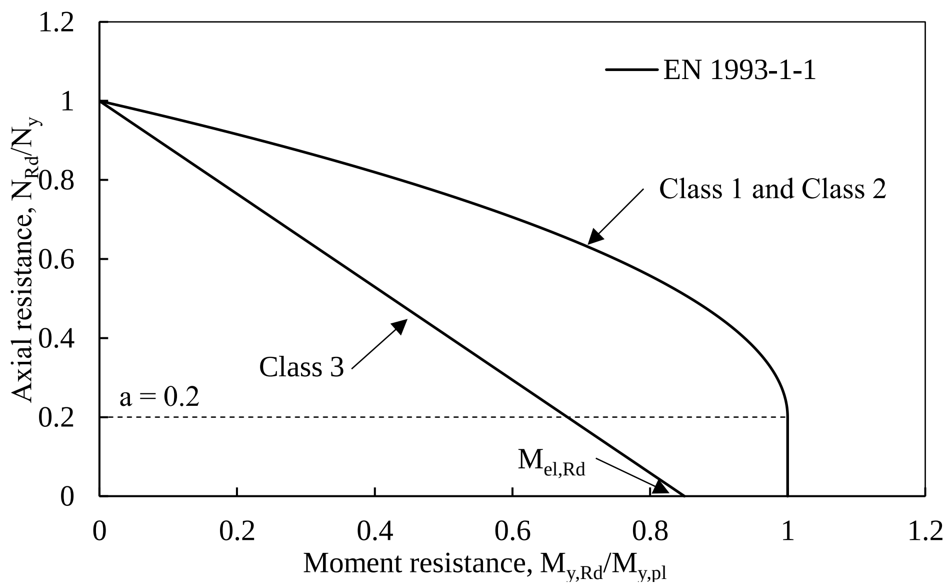

(b) H- or I-sections under combined compression and minor-axis bending

Figure 2.4: Interactive resistances for H- and I-sections under combined compression and bending

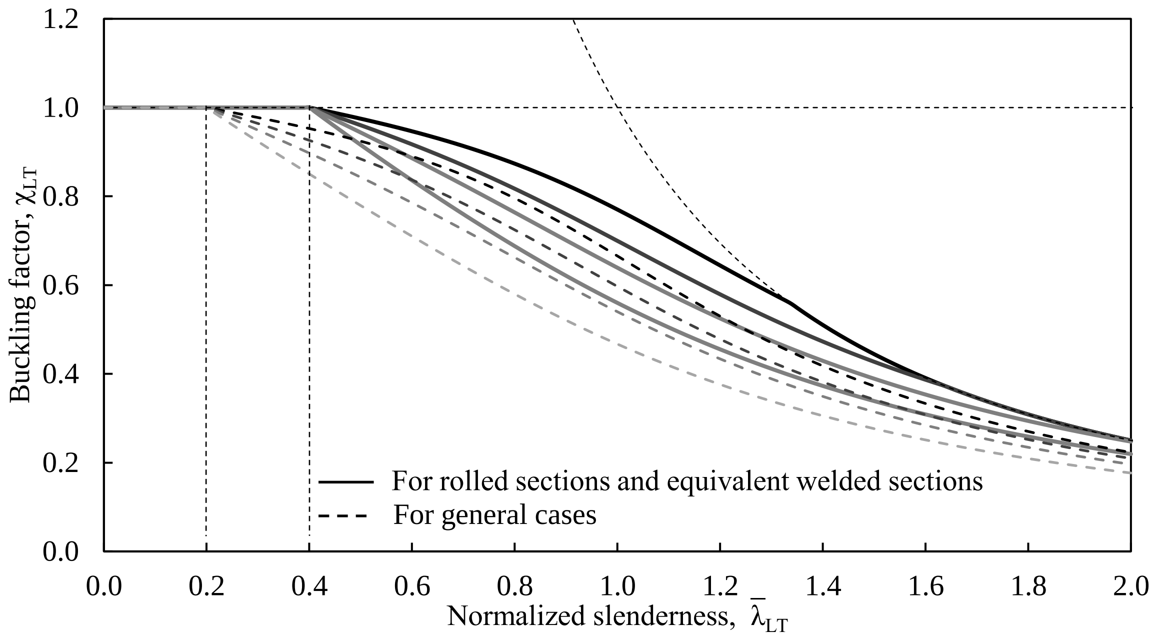

Figure 2.5: Lateral torsional buckling curves for two design cases

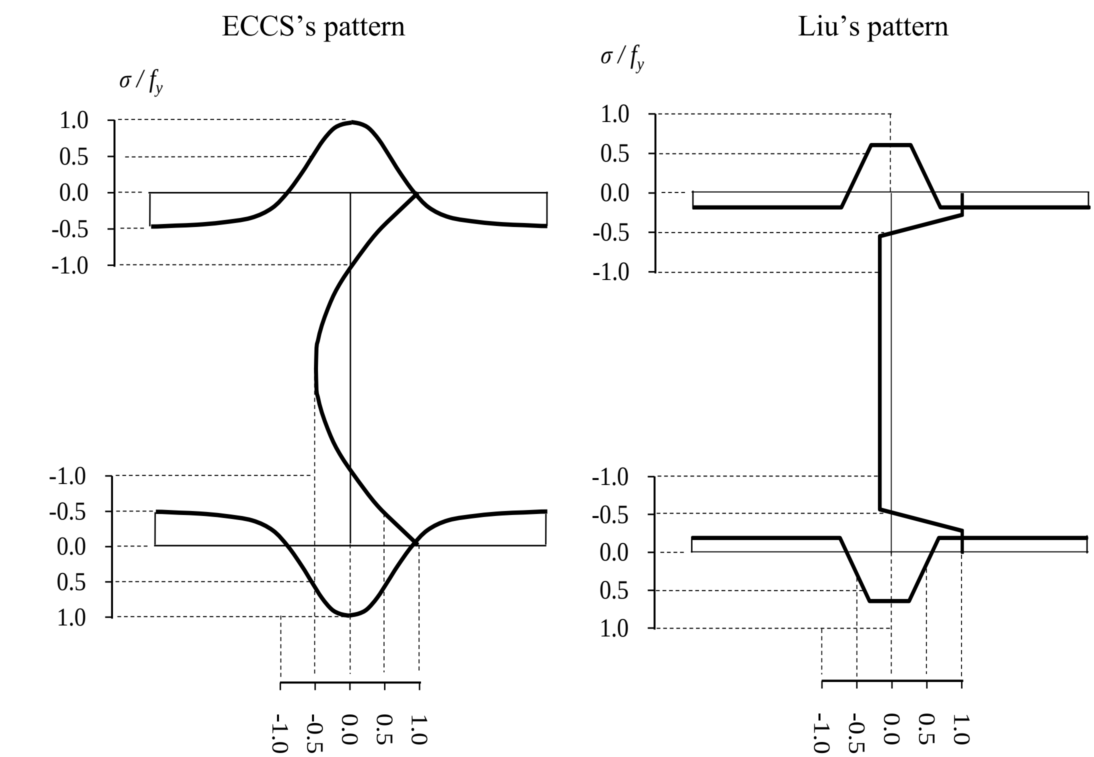

(a) Residual stress pattern for conventional strength steel sections

(b) Residual stress pattern for high strength steel sections

Figure 2.6: Comparison between typical residual stress patterns

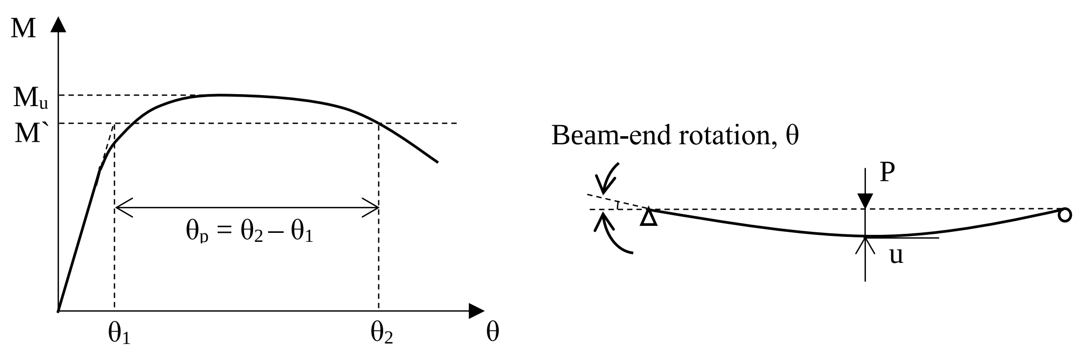

Figure 2.7: Definition of rotation capacity

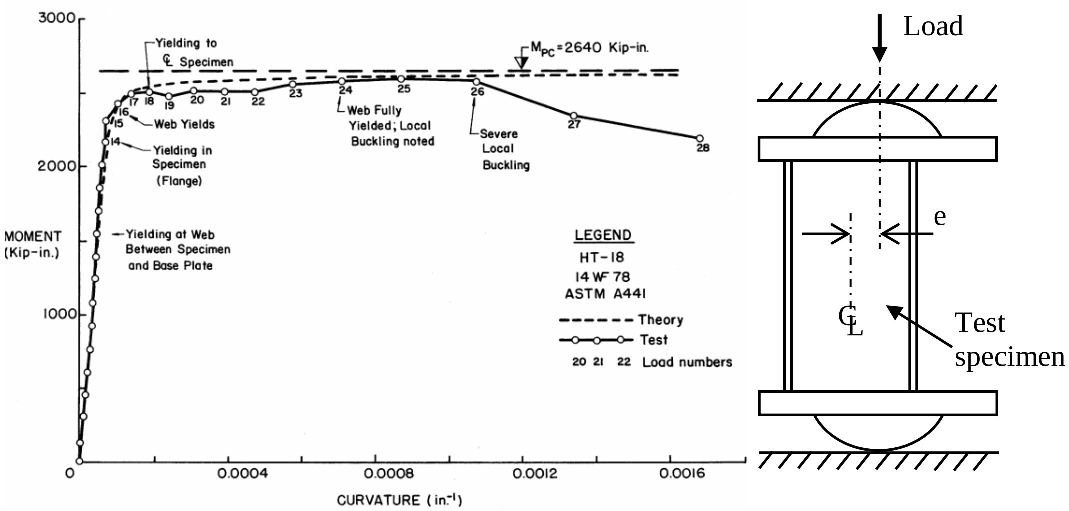

(a) Moment curvature response of test specimen (b) Test setup

Figure 2.8: Experimental work on stocky columns under combined actions (Lay and Gimsing, 1965)

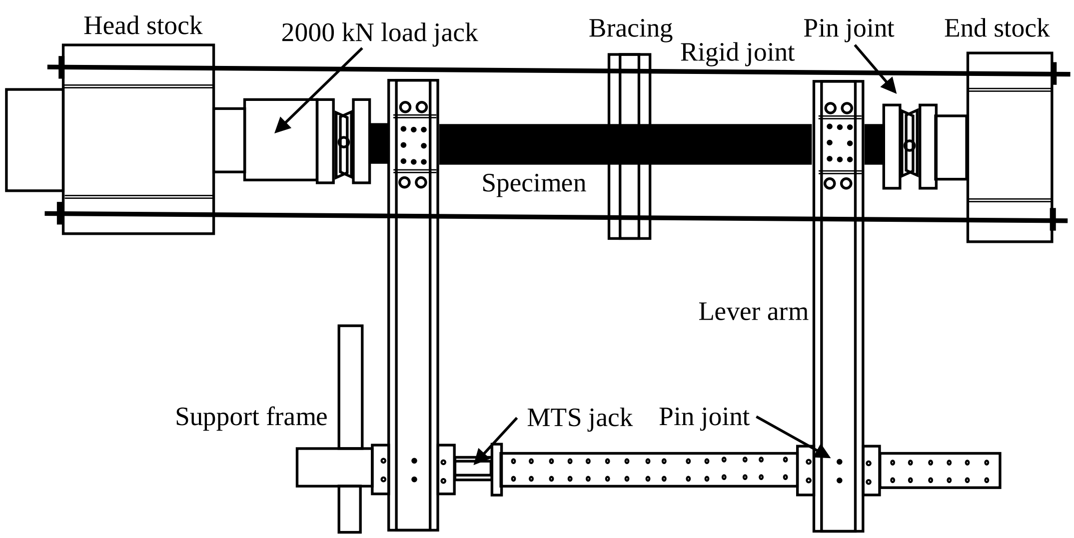

Figure 2.9: Applied test setup for stocky columns under combined compression and bending (Hasham and Rasmussen, 1998)

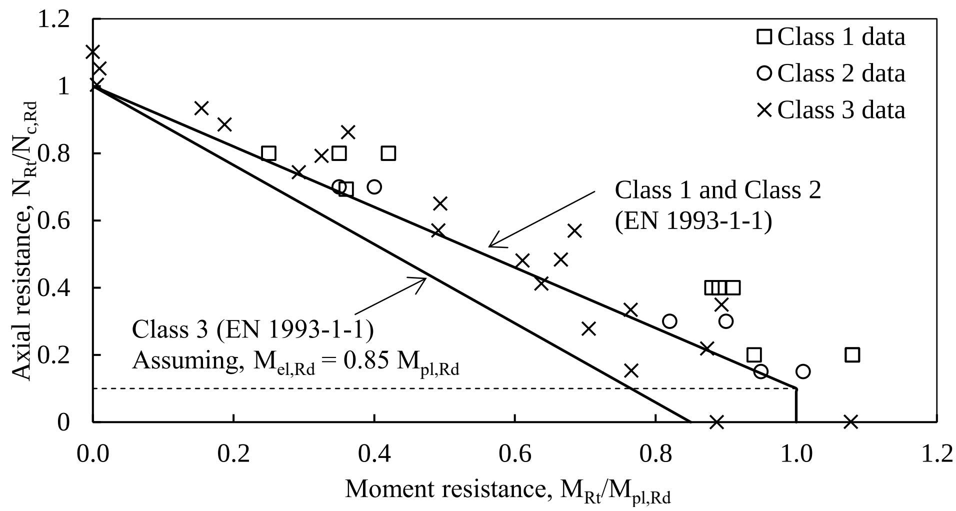

Figure 2.10: Summary of measured resistances for stocky columns under combined compression and major-axis bending

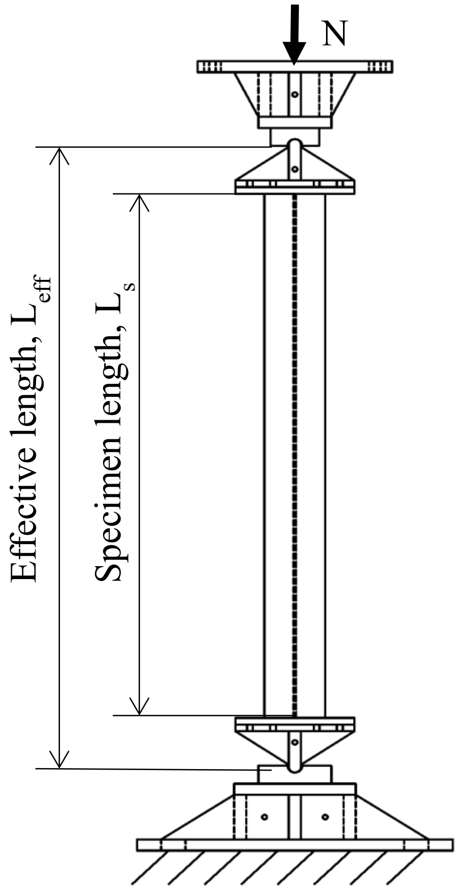

Figure 2.11: Test setup of slender columns under concentric load (Wang et al., 2017)

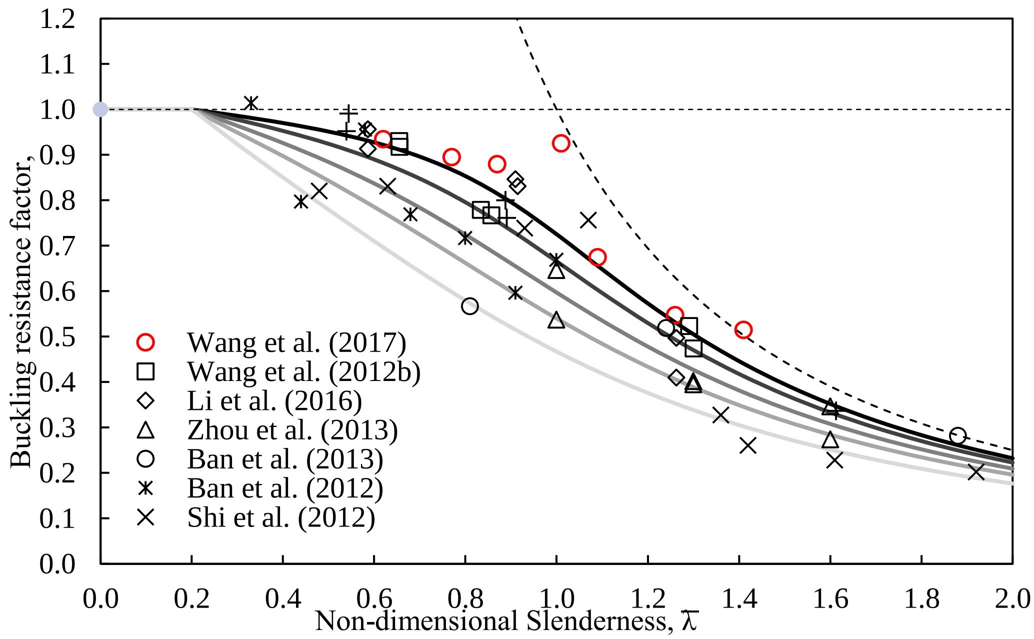

Figure 2.12: Summary of measure overall buckling resistances of high strength steel slender columns

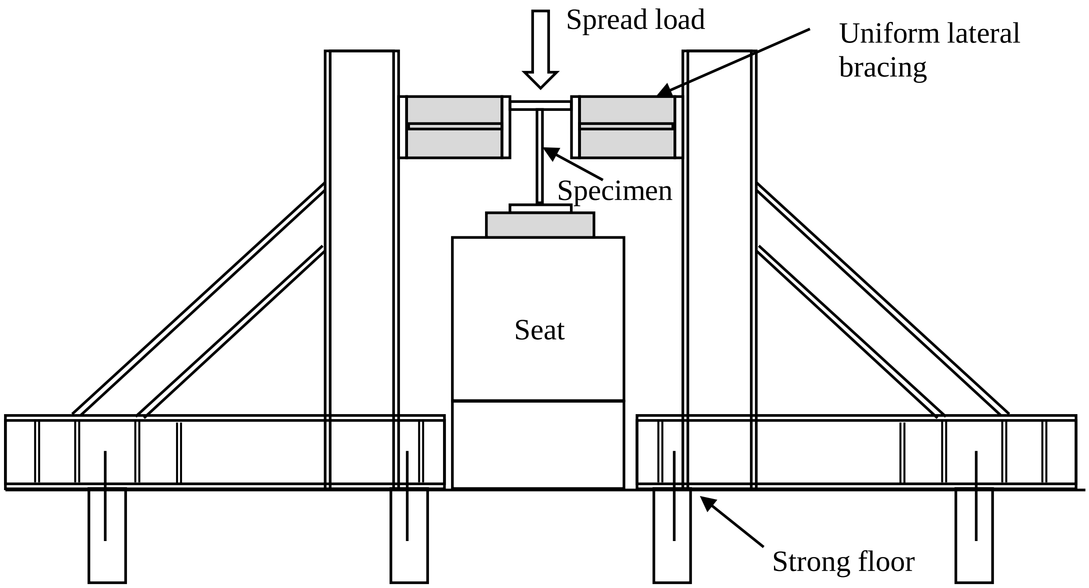

Figure 2.13: Applied test setup to partially restrained beams (Shokouhian and Shi, 2015)

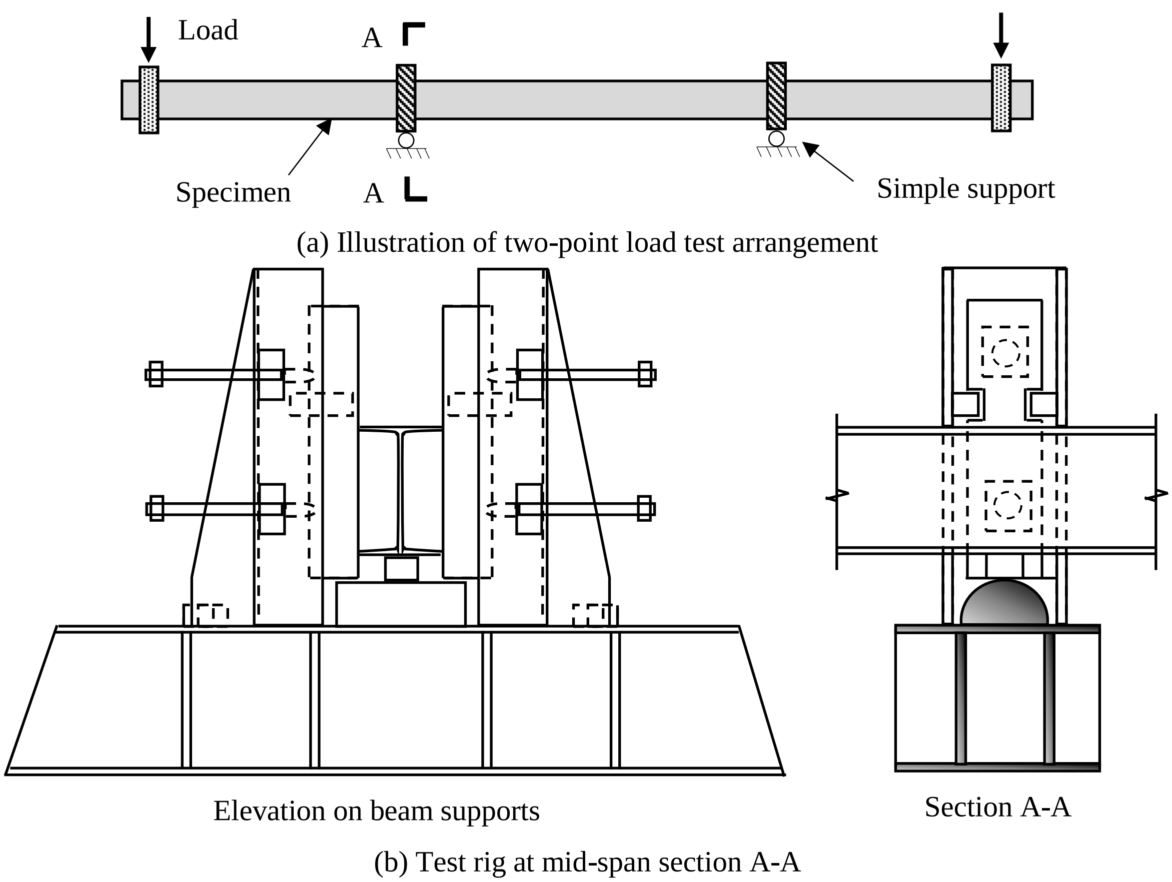

Figure 2.14. Test rig for two-point load on beam of H-section (Dibley, 1969)

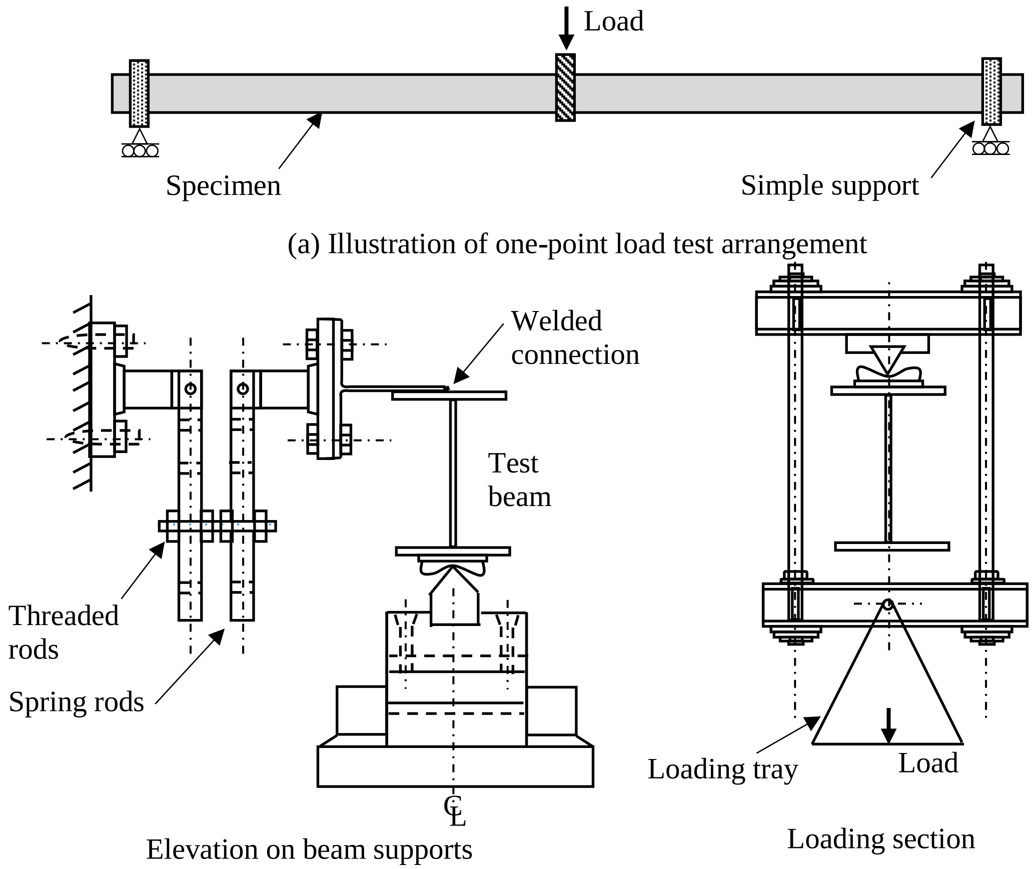

(a) Illustration of one-point load test arrangement

(b) Details on beam supports and loaded section

Figure 2.15: Test rig of simply supported I-section with partial restraints on beam ends (Bose, 1982)

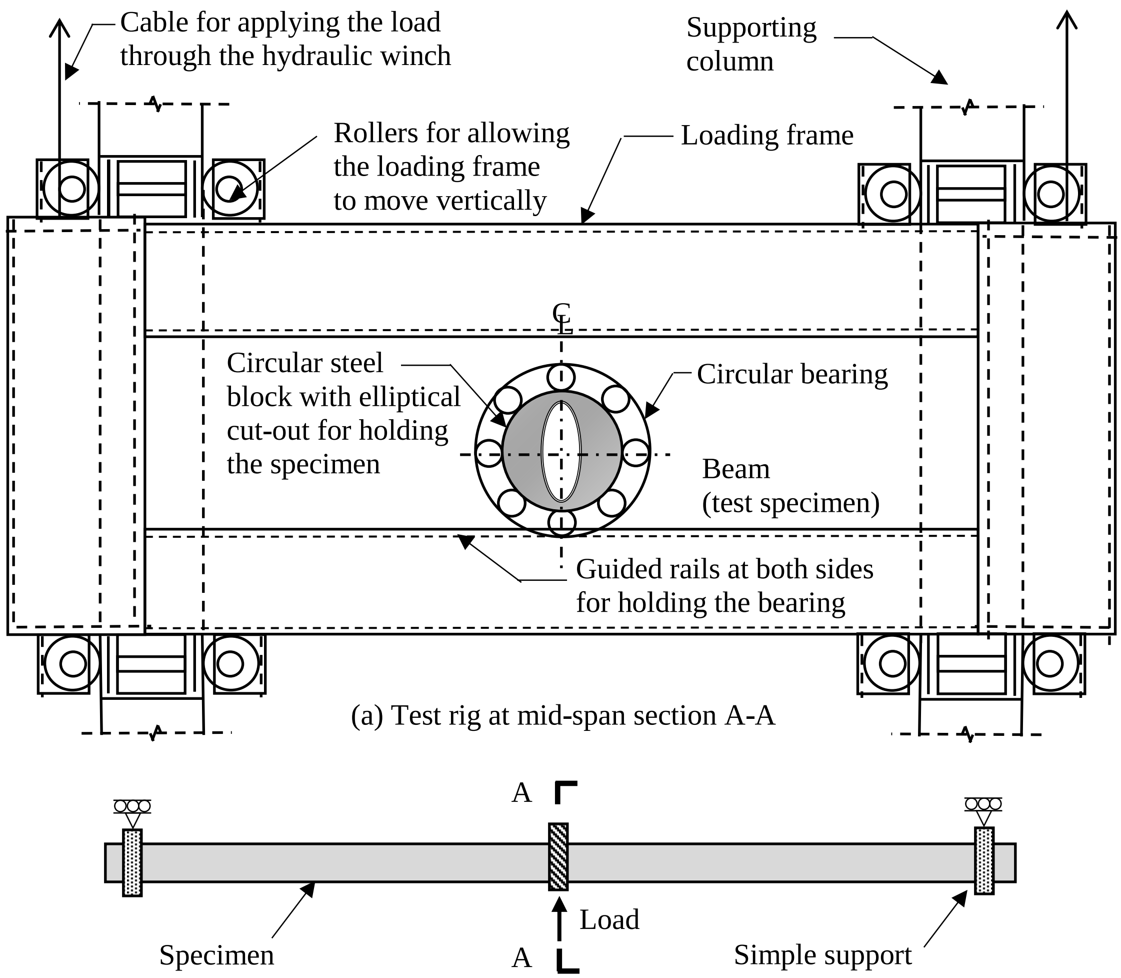

(a) Test rig at mid-span section A-A

(b) Illustration of one-point load test arrangement

Figure 2.16: Test rig for one-point load on beams of elliptical hollow section (2012)

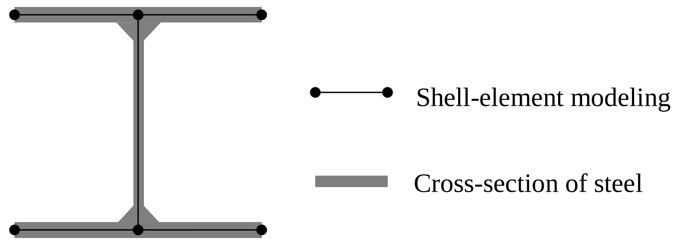

(a) Cross-sectional equivalence using thin-shell element modelling

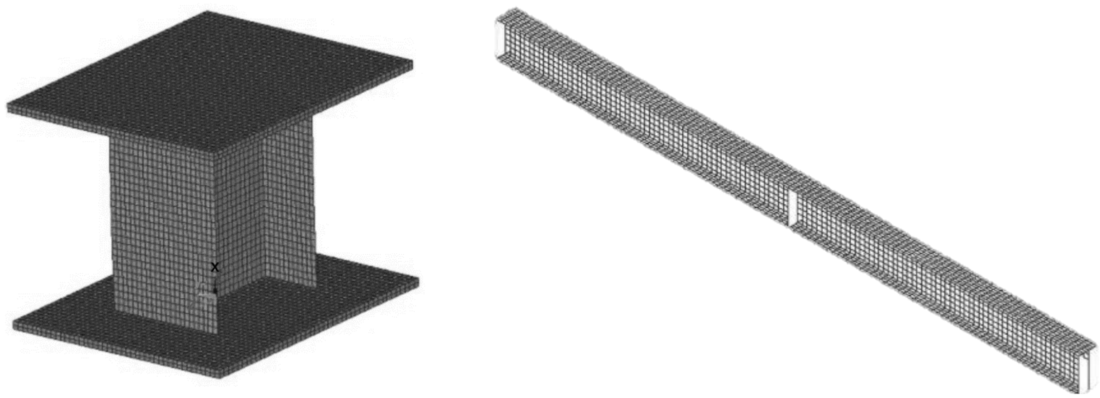

(b) Typical meshing network of steel sections using shell elements (Shi et al., 2014; Earls, 1999)

Figure 2.17: Modelling of beam and column sections with shell elements

Table 2.1: Restraining requirements for fully restrained beams based on EN 1993-1-1

Scope		**Specific design rules**	**Reference to the Clauses**
Class 1		At each rotated plastic hinge location, the cross section should have an effective lateral and torsional restraint with appropriate resistances to lateral forces and …	Cl. 6.3.5.2 Restraints at rotated plastic hinges
		$L_{stable} = 35\,\varepsilon\, i_z$, for $0.625 \leq \Psi \leq 1.0$, or $L_{stable} = (60 - 40\Psi)\,\varepsilon\, i_z$, for $-1.0 \leq \Psi \leq 0.625$	Cl. 6.3.5.3 Verification of stable length of segment
		$L_m = 38 i_z \Big/ \sqrt{\frac{1}{57.4}\left(\frac{N_{Ed}}{A}\right) + \frac{1}{756 C_1^2}\left(\frac{W_{pl,y}^2}{A I_t}\right)\left(\frac{f_y}{235}\right)^2}$	BB. 3.1.1 Stable lengths between adjacent lateral restraints
		$L_k = \left(5.4 + \frac{600 f_y}{E}\right)\left(\frac{h}{t_f}\right) i_z \Big/ \sqrt{5.4\left(\frac{f_y}{E}\right)\left(\frac{h}{t_f}\right)^2 - 1}$	BB. 3.1.2 Stable lengths between adjacent torsional restraints
	Class 2 to 4	$\bar{\lambda}_f = k_c L_c / i_{f,z} \lambda_1 \leq \bar{\lambda}_{c,0} M_{c,Rd} / M_{y,Ed}$ where, for full resistance design, $\bar{\lambda}_{c,0} = 0.5$	Cl. 6.3.2.4 Simplified assessment methods for beams with restraints
		For $\bar{\lambda}_{LT} \leq 0.4$ or for $M_{Ed}/M_{cr} \leq 0.16$, lateral torsional buckling effects may be ignored and only cross sectional checks apply.	Cl. 6.3.2.2 (4) Lateral torsional buckling curves – General case

Table 2.2: Measured material properties of high strength steel materials

Steel Grade	**Thickness t (mm)**	**Yield strength f_y (N/mm^2)**	**T/Y ratio f_u/f_y**	**Fracture elongation A (%)**	**Ultimate strain ε_u, (%)**	**Yield plateau -**
Grade 460	6	498	1.41	26.3	13.3	Yes
	11	506	1.18	23.7	6.5	No
	21	464	1.27	30.4	14.2	Yes
	10	532	1.23	26.7	14.0	Yes
	12	493	1.30	23.8	14.2	Yes
	14	492	1.27	28.6	14.9	Yes
Grade 483	10	539	1.19	-	11.8	Yes
Grade 552	10	586	1.14	-	4.7	No
	10*	576	1.10	20.5	9.7	No
	10*	609	1.14	14.7	7.3	No
	10	596	1.14	15.0	7.3	No
Grade 690	6#	799	1.03	19.0	7.1	Yes
	6#	774	1.02	19.0	7.4	Yes
	6#	777	1.02	18.8	7.4	Yes
	10*	750	1.08	16.7	8.0	No
	16*	772	1.08	21.0	6.1	Yes
Grade 800	15#	956	1.09	25.5	5.7	No
	18#	991	1.04	18.7	6.3	No
	18#	937	1.11	27.8	5.8	No
	20*	903	1.06	30.2	7.2	No
	21#	879	1.05	19.5	5.7	No
Grade 960	14#	964	1.09	12.4	1.5	No
	14#	984	1.08	12.6	2.5	No
	14#	973	1.09	12.4	1.9	No

Note:
* Sample ductility fulfilled requirement from EN 1993-1-12, but did not satisfied with EN 1993-1-1;
# Sample ductility didn't fulfil the requirement of EN 1993-1-12 and EN 1993-1-1.

Table 2.3: Previous test study of high strength steel H-sections under concentric compression

I-section

Literature	Sample	f_y N/mm^2	L mm	h mm	b mm	t mm	r mm	c_w mm	c_f mm	$c_f/t_f\,\varepsilon$ -	$c_w/t_w\,\varepsilon$ -	Classification -
She et al., 2014	I-960-1	973	400	212.3	210.0	13.9	6.0	92.1	172.4	13.4	25.3	Class 3
Y. Bing, 1997	480-1	590	300	96.9	84.1	6.4	6.4	32.5	84.1	8.0	20.8	Class 1
	480-2	590	300	96.9	84.1	6.4	6.4	32.5	84.1	8.0	20.8	Class 1
	480-3	590	300	96.9	84.1	6.4	6.4	32.5	84.1	8.0	20.8	Class 1
	700-1	711	280	82.4	69.6	6.4	6.4	25.2	69.6	6.8	18.9	Class 1
	700-2	711	280	82.4	69.6	6.4	6.4	25.2	69.6	6.8	18.9	Class 1
	700-3	711	280	82.4	69.6	6.4	6.4	25.2	69.6	6.8	18.9	Class 1
Rasmussen, 1992	I1SC1	725	350	133.9	95.1	6.0	5.4	39.2	111.2	11.5	32.8	Class 3

Box-section

Literature	Sample	Section type	f_y N/mm^2	L mm	h mm	b mm	t mm	c_w mm	c_f mm	$c/t\,\varepsilon$ -	Classification -
She et al., 2014	B-960-1	Type 2	973	150	139.6	139.6	13.9	111.8	111.8	16.4	Class 1
	B-960-2	Type 2	973	250	209.4	209.4	14.0	181.4	181.4	26.3	Class 1
Rasmussen, 1992	B1SC1	Type 1	670	300	89.5	89.5	4.96	79.6	79.6	27.1	Class 1

Table 2.4: Measured resistances comparing with design values

I-section

Literature	Sample	Design value N_y (kN)	Test resistance N_{Test} (kN)	N_{Test}/N_Y
She et al., 2014	I-960-1	8255.6	8389.4	1.02
Y. Bing, 1997	480-1	1001.0	1125.8	1.12
	480-2	1001.0	1135.0	1.13
	480-3	1001.0	1133.3	1.13
	700-1	1008.4	1000.3	0.99
	700-2	1008.4	1021.5	1.01
	700-3	1008.4	1035.6	1.03
Rasmussen, 1992	I1SC1	1391.2	1377.0	0.99

Box-section

Literature	Sample	Design value N_y (kN)	Test resistance N_{Test} (kN)	N_{Test}/N_Y
She et al., 2014	B-960-1	6797.5	7172.5	1.06
	B-960-2	10656.6	11522.2	1.08
Rasmussen, 1992	B1SC1	1124.0	1146.0	1.02

CHATER THREE

EXPERIMENTAL STUDY I: SECTION RESISTANCES OF HIGH STRENGTH STEEL S690 WELDED H-SECTIONS UNDER COMPRESSION

3.0 INTRODUCTION

In order to understand structural behaviour of stocky columns of welded S690 H-sections, a systematic experimental investigation into stocky columns under concentric and eccentric loads was conducted and presented in this chapter. A total of two test programmes were carried out to examine deformation characteristics of S690 stocky columns of welded H-sections. Four typical cross-sections, i.e. Sections C1 to C4, are employed into this study and dimensions of these four sections are shown in Figure 3.1.

A description on fabrication process of S690 welded H-sections was introduced to provide background information of residual stresses. Table 3.1 summarizes various welding parameters adopted during the fabrication of these welded sections. It should be noted that measured and predicted residual stress patterns reported by Liu and Chung (2016) were presented for easy reference. Standard tensile tests were also conducted on S690 steel materials to report material properties of S690 steel.

A total of twenty columns were tested in this study, as:

- 12 stocky columns of S690 welded H-sections under axial compression; and,
- 8 stocky columns of S690 welded H-sections under combined compression and bending.

For each test programme, test setup, instrumentation and loading conditions are described, and test results such as observed failure modes and measured load shortening curves are presented. It should be noted that all the test results are closely interpreted and compared with design rules of section classification given in EN 1993-1-1. Suitability of these design rules is discussed according to these test results.

3.1 OBJECTIVES

In order to understand structural behaviour of S690 stocky columns of welded H-sections, a systematic experimental investigation into 20 stocky columns under concentric and eccentric loads were conducted. Main objectives of these tests are:

- To understand mobilization of section resistances of these S690 stocky columns under i) compression, and ii) under combined compression and bending, in particular, local buckling of the flange outstands; and,
- To assess suitability of current design rules on section classification given in EN 1993-1-1 to S690 stocky columns

The areas of interest include:

1. Deformation characteristics and failure modes of S690 stocky columns with different section geometries;
2. Load shortening curves and strain history of stocky columns for detailed analyses;
3. Deformation capacities of stocky columns with various plate slenderness in internal webs and flange outstands; and,
4. Effects of material properties and residual stresses on structural behaviour of stocky columns.

3.2 MATERIAL PROPERTIES

3.2.1 Standard tensile tests on S690 steel materials

In order to determine stress-strain curves of S690 steel materials, standard tensile tests were conducted on standardized coupons according to EN-6892-1 (CEN, 2009). To measure their material properties in longitudinal direction of the steel plates, a total of 15 standard coupons cut from 5 different steel plates were tested.

Nominal dimensions of coupons are given in Figure 3.2, and the gauge lengths of these coupons are 20 mm or 30 mm according to the following relationship:

$$L_0 \quad = \quad 5.65\sqrt{S_0} \qquad \text{(Eq. 3.1)}$$

where S_0 is the original cross-section area of the coupon; and,
L_0 is the gauge length which is dependent on S_0.

Stain gauges were mounted onto both sides of the coupon to measure local strains, and they were effective up to 5% strains. Beyond that strain level, a simple digital photo method was adopted to capture large strain readings.

The standard tensile tests were conducted using a MTS 50kN Testing System. An initial loading rate was taken as 0.3 mm/min under displacement control. Up till yielding in the coupon, a reduced displacement rate at 0.02 mm/min was applied. After yielding, loading was paused for every 30 seconds to obtain a lower bound of the yield strengths. When local strains exceeded 5%, a displacement control at a rate of 0.4 mm/min was used until fracture. Typical stress-strain relationships are shown in Figure 3.3 and key results of each series are given in Table 3.2.

It should be noted that in EN 1993-1-12, the following three criteria are specified for S460 to S700 steel materals:

i) $f_u / f_y \geq 1.05$, ii) $\varepsilon_u \geq 15\varepsilon_y$, and iii) $\varepsilon_L \geq 10\%$.

where, f_y is the yield strength; ε_y is the yield strain;

f_u is the tensile strength; ε_L is the strain at fracture; and,

ε_u is the strain corresponding to the tensile strength f_u.

Comparing measrued data to these criteria, all S690 steel materials are demonstrated to be able to meet these requirements. Therefore, these S690 steel materials can be applied in steel construction in accordance with EN 1993-1-12.

3.2.2 Fabrication process and residual stress patterns

Welding has complex influences on welded H-sections, especially in high strength steel plates. Differential cooling in flange-web junctions always introduces highly localized tension stresses in junction regions, while moderate to low compression stresses are generated on other parts of the flanges and the webs. Variations of residual stresses can be large due to usage of different welding procedures. In this study, influences from fabrication process is considered to be very important, and key parameters are quantified to determine effects of fabrication process on those welded S690 H-sections under investigation.

It should be noted that all S690 plate parts were cut by underwater wire-cutting method to limit heat energy input. Preheating treatment was applied to these steel plates before welding, and temperature was rigorously controlled below 200 °C as well as monitored with an infrared thermometer. Before processing, welding parameters were selected, and heat energy inputs were controlled to be between 1.0 kJ/mm and 3.0 kJ/mm. Other key welding parameters are summarized in Table 3.1. With this welding scheme, material deterioration and cracks on weldments were prevented successfully (Schroter et al, 2005).

Liu and Chung (2016) closely examined residual stresses in Sections C1 to C4 which were fabricated using the same procedure. They obtained accurate residual stress patterns through a comprehensive experimental and numerical investigation. The proposed patterns are provided in Chapter 5 for easy reference.

3.3 Tests on S690 Stocky Columns under Compression

3.3.1 Test programme

In this test programme, 4 different cross-sections were devised, namely Section C1 to Section C4 as shown in Figure 3.1. For each cross-section, there were three test specimens of nominally identical sections. Hence, a total of 12 stocky columns were tested under axial compression. Measured dimensions and plate slenderness ratios of these test specimens are presented in Table 3.3. Nominal lengths of these stocky columns are larger than 3 times of their web depths so that local buckling might be readily developed in the plates without constraints. It should be noted that the column lengths of those stocky columns should be small enough to prevent overall buckling.

Based on section dimensions and plate slenderness ratios given in Table 3.3, it is shown that these test specimens are at least compact sections according to the criteria provided for section classifications given in EN 1993-1-1. These section classification rules indicate that Series C2S and Series C4S are Class 3 sections, while Series C1S and Series C3S are respectively Class 1 and Class 2 sections. Hence, all 12 sections are expected to be able to mobilize their respective full section resistances. Through this study, distinctive local buckling behaviour in S690 stocky columns with various section classifications is examined in details.

3.3.2 Test setup

Two different testing systems were employed to apply axial compression forces to provide different levels of loading according to the sizes of these stocky columns. The testing systems are shown in Figure 3.4. Series C3S and Series C4S were tested by a Hydraulic Servo Control Testing System with a 10,000 kN capacity. And Series C1S and C2S were tested by a Hydraulic MTS Testing System with a 3,500 kN capacity. Both ends of the H-sections were welded with thick end plates, and thus, these stocky columns were loaded with a fixed end condition.

Instrumentation of the test specimens is illustrated in Figure 3.5. Four strain gauges were mounted on flange tips at mid-height of the columns to measure local strains. It should be noted that these readings from strain gauges might include strains due to compression and strains due to bending because of plate local buckling. Four LVDTs were also installed to record axial shortenings of the test specimens. The probes of LVDTs were positioned to touch the top end plates while their seats were placed on the bottom end plates. By employing this arrangement, relative shortenings between the two end plates could be obtained.

During the tests, a predetermined loading scheme was followed as:

- To load to 30% of the predicted section resistances, $N_{c,Rd}$, and then unload back to zero at a loading rate of 300 kN/min;
- To apply a compression force up to 0.8 $N_{c,Rd}$ at a loading rate of 200 kN/min;
- To continue the loading through displacement control at a rate of 0.5 mm/min; and,
- To terminate testing when the applied load was reduced by more than 20% of its measured ultimate resistances.

It should be noted that unintended eccentricities of load application should be eliminated with careful alignment of the test specimens, and such eccentricities should be carefully detected during preloading. Moreover, the applied loading rate was controlled to be very low in order to prevent dynamic effects.

3.3.3 Test results

3.3.3.1 Failure modes

Typical failure modes of these stocky columns are illustrated in Figure 3.6. It should be noted that, in all cases, local buckling appeared in both flanges of these welded H-sections in a symmetrical manner. Corresponding local buckling was also found in the web plates. Hence, the governing failure mode of these stocky columns is local buckling with significant yielding.

3.3.3.2 Section resistances

Table 3.4 presents measured resistances of high strength S690 steel welded H-sections, i.e. $N_{c,Rt}$, together with the design resistances, $N_{c,Rd}$ and the enhanced design resistances $N_{cu,Rd}$ predicted with measured material properties as:

$$N_{c,Rd} = 2f_{y,f} \cdot bt_f + f_{y,w} \cdot dt_w \quad \text{(Eq. 3.2)}$$

$$N_{cu,Rd} = 2f_{u,f} \cdot bt_f + f_{u,w} \cdot dt_w \quad \text{(Eq. 3.3)}$$

It is shown that the design resistances are always smaller than the measured resistances, and hence, the current design rules given in EN 1993-1-1 are able to predict compressive resistances of stocky columns of S690 welded H-sections successfully. Moreover, strength enhancement is observed in some of these sections. For Series C1S and Series C3S, the stocky columns have attained a strength enhancement at 7% to 8% of the design resistances. While, a strength enhancement at 3% for Series C2S and merely at 1% for Series C4S were also attained. Therefore, a strength enhancement is generally attained in sections with these welded H-stocky plate elements.

3.3.3.3 Load shortening behaviour

All the load shortening curves of these stocky columns are presented in Figure 3.7. It should be noted that axial shortenings, i.e. Δ, is taken as the average values of four LVDT readings. Axial compression was found to increase elastically up to 80% to 90% of the section resistances of these stocky columns. Then, gradients of the load shortening curves were reduced gradually. This should be attributed to the presence of residual stresses which caused gradual yielding the steel plates. At failure, all the stocky columns in Series

C1S and C3S attained significant strength enhancement over their design resistances. For these stocky columns in Series C2S and C4S, section resistances were reached, but limited ductility were achieved. Consequently, it is shown that Class 1 and Class 2 sections possess good deformation capacities while Class 3 sections have little. These responses are found to be consistent with structural behaviour implied in the section classifications of these stocky columns.

In Table 3.5, shortening parameters are provided to reflect shortening behaviour of the test specimens. In this table, ultimate shortening, i.e. Δ_u is defined as the measured shortening when the ultimate resistances are attained. And, the corresponding strain is given by Δ_u/L. It is shown that the compressive resistance with significant strength enhancement may be readily attained in Class 1 and Class 2 sections with large shortening compressive strains at 1.0% to 1.3%. It is argued that it may not be a good practice to incorporate any strength enhancement into practical structural design of stocky columns as large axial shortening is needed to mobilize these enhanced resistances.

A definition of deformation capacity for stocky columns is illustrated in Figure 3.9. As discussed in Chapter 2, this factor may be utilized to quantify deformation capability of stocky columns, and it is an analogy of a rotational ductility of beams. It is given by:

$$\Phi = \frac{\Delta_c - \Delta_{c1}}{\Delta_c}$$

where, Δ_{c1} is the measured shortening of a stocky column when its resistance is reduced to be below the design resistance.

According to test results, Class 1 sections possess a high level of deformation capacities at least equal to 3.74, and Class 2 sections possess an intermediate level of deformation capacities with ϕ ranging from 2.63 to 2.86. Class 3 sections possess a low level of deformation capacities smaller than 1.5. In such a case, no strength enhancement can be mobilized. These test results confirm that compact sections are able to achieve a high level of deformation capacities.

3.3.3.4 Measured strains

Typical measured load strain curves are presented in Figure 3.8. Initially, measured strains increase linearly with the applied loads. However, after reaching 80% to 90% of the design section resistances, the slopes of these load strain curves are reduced gradually owing to partial yielding within the cross-sections. Once the ultimate resistances of these stocky columns have been obtained, tensile stresses are measured in some of the strain gauges because of local buckling of steel plates. After that, these stocky columns are unable to sustain any additional load, and unloading takes place.

It should be noted that the maximum strains measured in stocky columns of Series C1S and C3S reach at least 1.5% at failure, while, the maximum strains measured in stocky columns of Series C2S and C4S are found to be smaller than 1.0%. Therefore, a large strain might be attained in sections with stocky plate elements. Moreover, the maximum strain measured among all columns is found to be about 5%. This compares well with the ductility requirements stipulated in EN 1993-1-12 for S690 steel materials.

In Table 3.5, the averaged strain readings measured from four tips of the flange outstands of the stocky columns are listed for reference. They represent average strains in different conditions: i) ε_1 when local buckling was fully developed, and ii) ε_2 when failure was attained. According to section classifications of these test specimens, it is revealed that high levels of strains are readily attained in stocky plate elements. Moreover, ε_1 and ε_2 were generally close in values in most cases.

3.3.4 Summary

A total of 12 stocky columns of S690 welded H-sections under compression were successfully conducted. All of these sections were found to be failed in local buckling, and attained full section resistances. Moreover, different levels of strength enhancement and deformation capacities were observed, depending on slenderness of plate elements of the sections. Based on these test results, the following key findings are obtained:

- For Class 1, 2 and 3 sections, full section resistances with a range of deformation capacities are achieved;
- Owing to strain hardening in these high strength S690 steel plates, significant strength enhancement over 5% of section resistances is readily attained in Class 1 and 2 sections together with large axial shortening; and,
- Ultimate resistances of the stocky columns have been fully mobilized before plastic local buckling in plate elements of the sections occurs.

It should be noted that full section resistances with different levels of deformation capacities were attained by high strength S690 welded steel sections. Strength enhancement is shown to be directly related to the deformation capacity ratios ranging from 1 to 3 as shown in the load-shortening curves of the stocky columns.

Hence, current design rules of section classifications in EN 1993-1-1 are shown to be applicable to design stocky columns of S690 welded H-sections. Detailed analysis assisted with numerical modelling will be conducted in Chapter 6. Effects of residual stresses on structural behaviour of stocky columns of high strength S690 welded H-sections will be addressed in Chapter 7.

3.4 Tests on S690 Stocky Columns under Combined Compression and Bending

3.4.1 Test programme

In this test programme, a total of eight stocky columns were tested under eccentric loads to investigate local buckling behaviour of high strength S690 stocky columns under combined compression and bending. Two different cross-sections, i.e. Section C3 and Section C4 as shown in Figure 3.1 were adopted. With different combinations of cross-sections and bending directions, four test series, namely Series C3SY, C4SY, C3SZ and C4SZ were devised. In each test series, two geometrically identical test specimens were tested under different loading eccentricities. Measured dimensions of these sections together with measured eccentricities of the tests are presented in Table 3.6.

In order to examine local buckling in these sections, their nominal heights were rigorously controlled to prevent overall column buckling. Due to limited heights of these sections under combined compression and minor-axis bending, restrains from the welded end plates acting onto the plate elements of the sections are inevitable.

As provided in Table 3.7, section classifications of these sections are determined according to EN 1993-1-1. Depending on various dimensional ratios of the flange and the web plate elements of the sections and locations of neutral axes, these sections were respectively classified as Class 2 and Class 3 sections. Therefore, it could be anticipated that Series C3SY and C3SZ sections should fail with resistances larger than predicted section resistances, and Series C4SY and C4SZ sections should fail merely with resistances close to predicted section resistances. Moreover, local buckling on the two flange outstands and the internal webs under compression was predicted as typical failure modes in these sections.

3.4.2 Test setup

In this test programme, a Hydraulic Servo Control Testing System with a 10,000 kN capacity was used to conduct the tests. The test setup is illustrated in Figure 3.10. In order to impose co-existed compression and bending, specially designed attachments are employed to introduce eccentric loads to these sections. Hence, free rotation about major or minor axis of the cross-sections of these stocky columns was allowed at both ends.

Instrumentation of test specimens under combined compression and major-axis bending is illustrated in Figure 3.11. Relative shortening between load points was measured through two LVDTs installed on both ends of the stocky columns. In addition, a third LVDT was placed on mid-height of the stocky columns to record displacements. Strain gauges were mounted at mid-heights of the stocky columns to record strains. They were used to monitor development of section plasticity during testing. Similarly, instrumentation for test specimens under combined compression and minor-axis bending is illustrated in Figure 3.12.

During the test, a pre-determined loading scheme was followed as:

- To load to 30% of the predicted section resistances, i.e. $N_{pl,Rd}$, and then unload back to zero at a rate of 300 kN/mm^2;
- To apply a compression force up to 0.8 $N_{pl,Rd}$ at a loading rate of 200 kN/min;
- To continue the loading through displacement control at a rate of 0.4 mm/min; and,
- To terminate testing when the applied load was reduced by more than 20% of its measured ultimate resistances.

3.4.3 Test results

3.4.3.1 Failure mode

Failure modes of stocky columns in Series C3SY and C4SY are shown in Figure 3.13. It should be noted that local buckling was observed on two flange outstands at mid-heights of the welded H-sections. Therefore, the governing failure mode of the sections in Series C3SY and C4SY is local buckling on the flange outstands.

For those sections of Series C3SZ and C4SZ, local buckling was also observed in the flange outstands under combined compression and moment gradient as shown in Figure 3.14. Restraints from the end plates onto the flanges were also evident.

3.4.3.2 Section resistances

Table 3.7 summarized data analysis on the test data and results of the programme. It is shown that full section resistances were attained in all these eight test specimens together with different levels of strength enhancement. Generally, plate elements in stocky columns of Series C3SY and C3SZ have lower plate slenderness ratios, and they have attained higher strength enhancement than those in Series C4SY and C4SZ. Hence, strength enhancement over full section resistances can be readily attained in sections with compact cross-sections.

For sections with minor-axis bending, they have acquired higher strength enhancement than their counterparts under major-axis bending. This may be attributed to restraining effects on local buckling offered by attachments in stocky columns of Series C3SZ and C4SZ.

Comparison between the test results and the design results according to EN 1993-1-1 is illustrated in Figure 3.21. It is found that section resistances of stocky columns of S690 welded H-sections under combined compression and bending are successfully predicted with these design rules. Moreover, stocky columns of Series C4SY and C4SZ are fully capable of mobilizing their plastic resistances, even though they are classified merely as Class 3 sections.

3.4.3.3 Load shortening curves

Load shortening curves of stocky columns under combined compression and bending are plotted against their section resistances, i.e. $N_{pl,Rd}$ as shown in Figure 3.15 and Figure 3.16. These curves have initially a linear elastic slope. Then, they become nonlinear, inelastic and yet highly ductile responses after 60% design resistances are reached. It should be noted that full section resistances have been attained in all eight test specimens. Comparing Section C3 with Section C4, it is found that Section C3 is able to deform in a more ductile manner owing to good compactness of their plate elements.

The deformation capacity ratios of the stocky columns, Φ_u are listed in Table 3.8, and therefore are determined according to their load shortening curves. The definition of Φ_u is illustrated in Figure 3.9.

Sections C3 exhibit high levels of deformation capacities with a ratio larger than 3.0, which fully satisfy the requirements stipulated to Class 1 sections. And all Sections C4 are demonstrated to have moderate deformation capacities with a ratio over 1.0. Hence, they generally meet with the requirements for Class 2 sections. Therefore, test observations were found consistent with section classification rules given in EN 1993-1-1 with embedded conservatism.

The load displacement curves of all the stocky columns under compression and bending are presented in Figure 3.17 and Figure 3.18. In general, they reflect flexural behaviour of the columns under combined actions.

3.4.3.3 Measured Strains

Measured strains of all the eight stocky columns are plotted in Figure 3.19 and Figure 3.20. Gradients of load strain curves began to reduce gradually owing to partial plasticity. After maximum resistances obtained, compression strains could change more sharply. Moreover, when sections resistances were fully mobilized, the maximum compressive strains could reach up to 5%. Hence, this agrees well with requirements provided in EN 1993-1-12 for high strength S690 steel materials.

3.4.4 Summary

A total of 8 stocky columns of S690 welded H-sections under combined compression and bending were successfully conducted. All of these sections were found to be failed in local buckling, and they have obtained full section resistances at failure. Moreover, different levels of strength enhancement and deformation capacities were observed, depending on slenderness of plate elements of the sections. Based on these test measurements, the following key findings are obtained:

- Owing to strain hardening in these high strength S690 steel plates, significant strength enhancement larger than 5% of full resistances is readily attained in Class 1 and 2 sections;

- Comparing with the stocky columns under axial compression, those counterparts under combined actions can achieve higher levels of strength enhancement and deformation capacities; and,
- Ultimate resistances of the stocky columns under combined actions have been fully mobilized before local buckling in plate elements of the sections occurs.

Predictions on basis of EN1993-1-1 are also reviewed. It is evident that full section resistances together with large deformation capacities are readily attained in all the 8 stocky columns. Hence, EN 1993-1-1 design rules are shown to be readily applicable to assess section classifications as well as section resistances of these stocky columns of S690 welded H-sections under combined actions.

3.5 CONCLUSIONS

This chapter reports an experimental investigation into local buckling behavior of high strength S690 stocky columns of welded H-section was successfully conducted on twenty test specimens. Key conclusions of the investigation are presented as follows:

- Based on experimental investigation, all the stocky columns of S690 welded H-sections are able to readily mobilize their full section resistances with various degrees of strength enhancement for Class 1, 2 and 3 sections;
- Significant strength enhancement at typically 5% for sections under compression, and at typically 5% to 10% for sections under combined compression and bending are evident; and,
- Design rules given in EN 1993-1-1 on section classification, section resistances under compression and under combined compression and bending are demonstrated to be applicable.

Moreover, design rules given in EN 1993-1-1 are found applicable to design of high strength S690 stocky columns of welded H-sections. While, 20 data points from tests were just insufficient to reach a solid conclusion. In order to address this problem, numerical tools will be established in Chapter 6, and parametric study will be conducted with validated numerical models in Chapter 7.

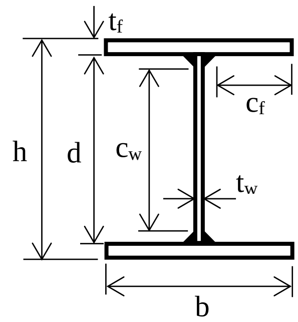

(a) Symbols of cross-sectional dimensions

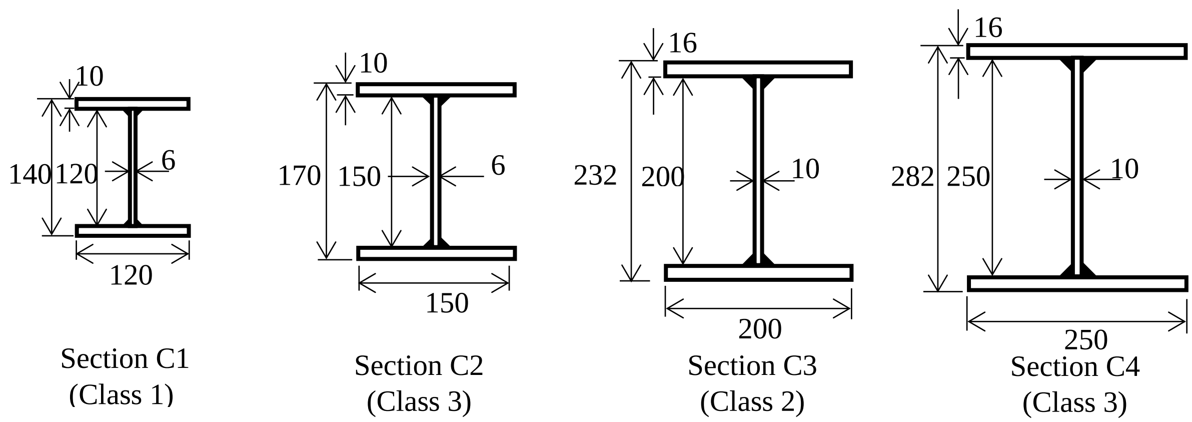

(b) Nominal cross-sectional dimensions of Section C1 to Section C4

Figure 3.1: Cross-sectional dimensions of high strength S690 welded H-sections

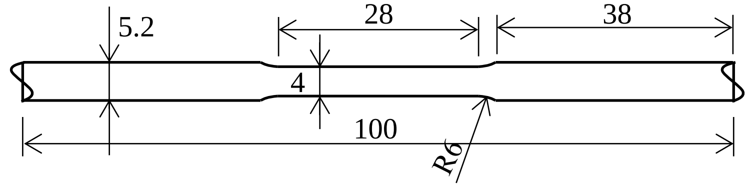

(a) Standard coupon from 6 mm thick steel plates

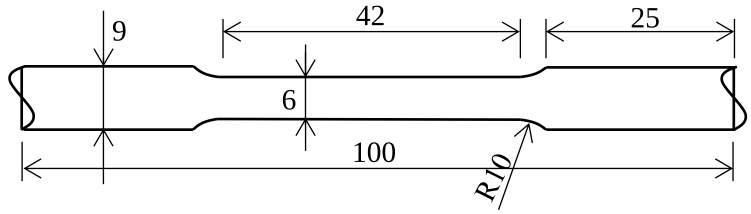

(b) Standard coupon from 10 mm and 16 mm thick steel

Figure 3.2: Dimensions of tensile coupons

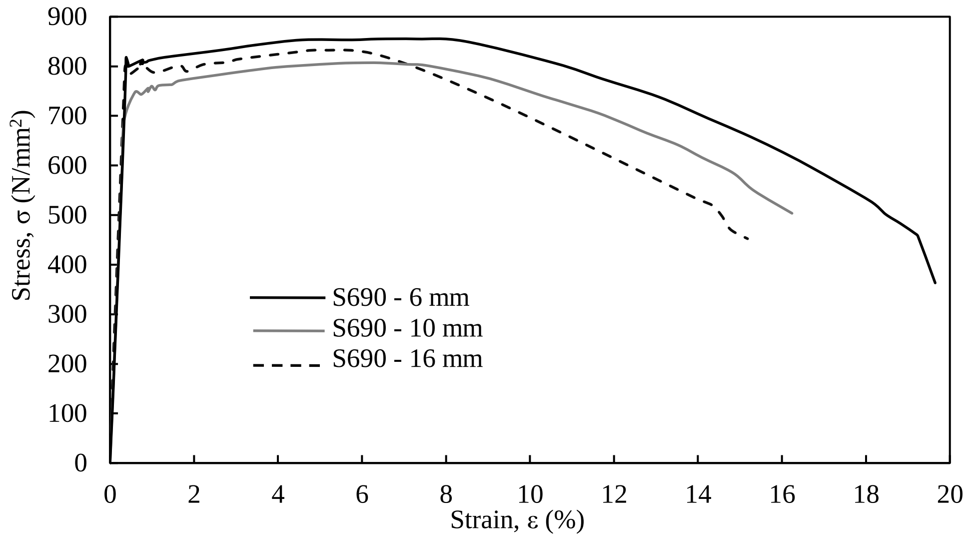

(a) Steel materials for S690 stocky columns under axial compression

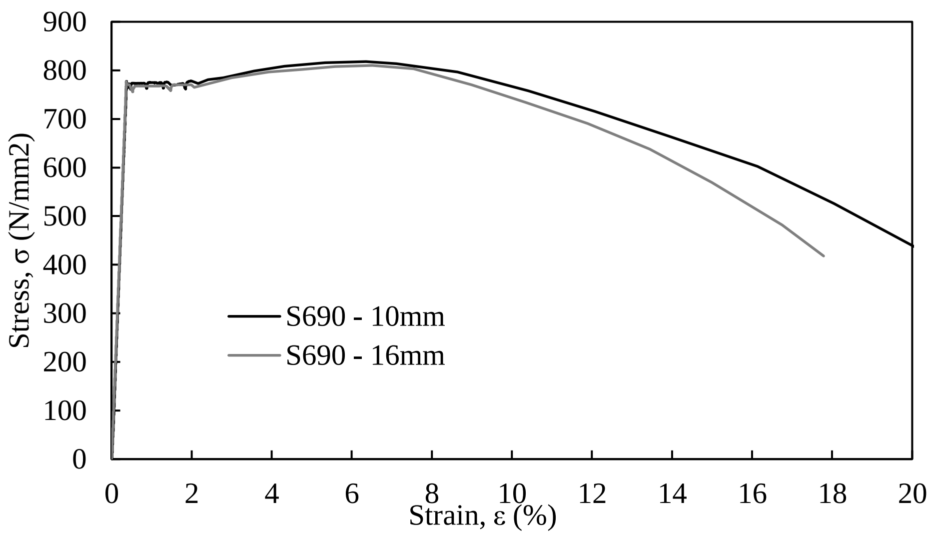

(b) Steel materials for S690 stocky columns under combined compression and bending

Figure 3.3: Typical measured stress strain curves of Q690 steel materials

(a) MTS Testing System
(Applied to C1S and C2S sections)

(b) 1000 tons Hydraulic Servo Control Testing System
(Applied to C3S and C4S section)

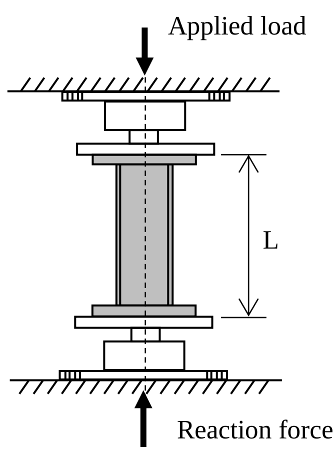

(c) Schematic test setup

Figure 3.4: Test setup for stocky columns under axial compression

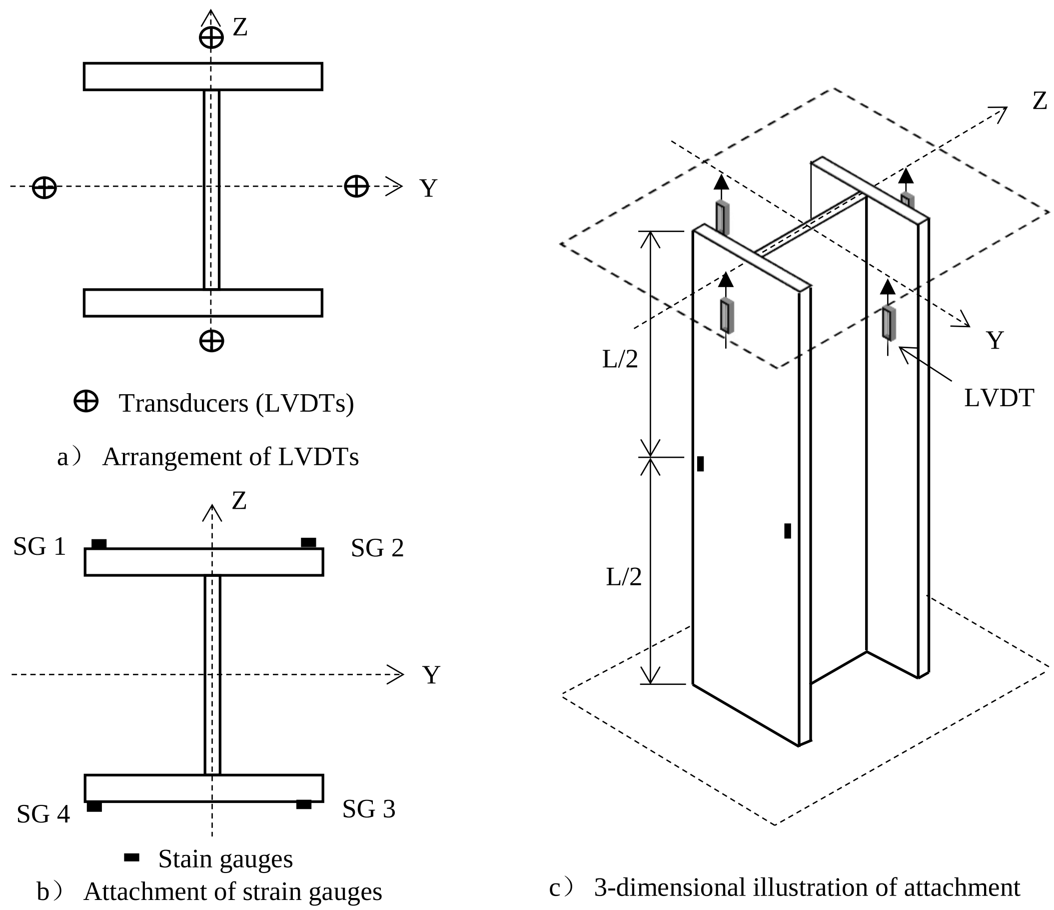

Figure 3.5: Instrumentation on stocky columns under axial compression

Section C1S-a

Section C1S-b

Section C1S-c

(a) Series C1S

Section C2S-a

Section C2S-b

Section C2S-c

(b) Series C2S

Figure 3.6: Failure modes of S690 stocky columns under axial compression

Section C3S-a

Section C3S-b

Section C3S-c

(c) Series C3S

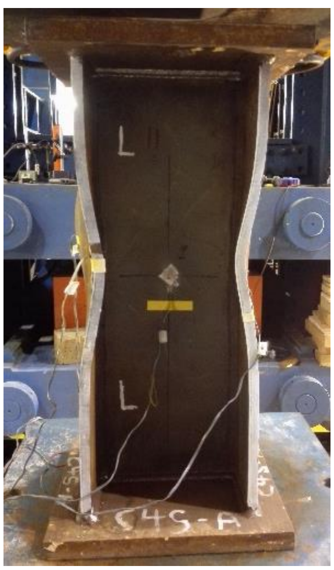

Section C4S-a

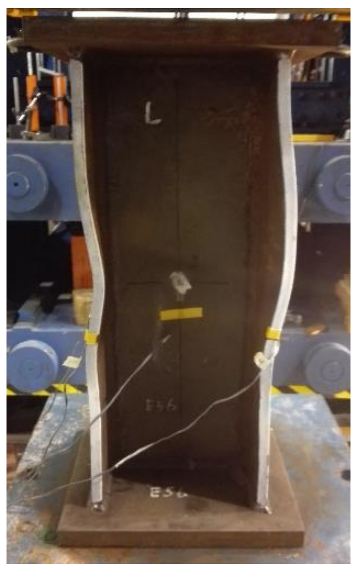

Section C4S-b

Section C4S-c

(d) Series C4S

Figure 3.6: Failure modes of S690 stocky columns under axial compression (Continued)

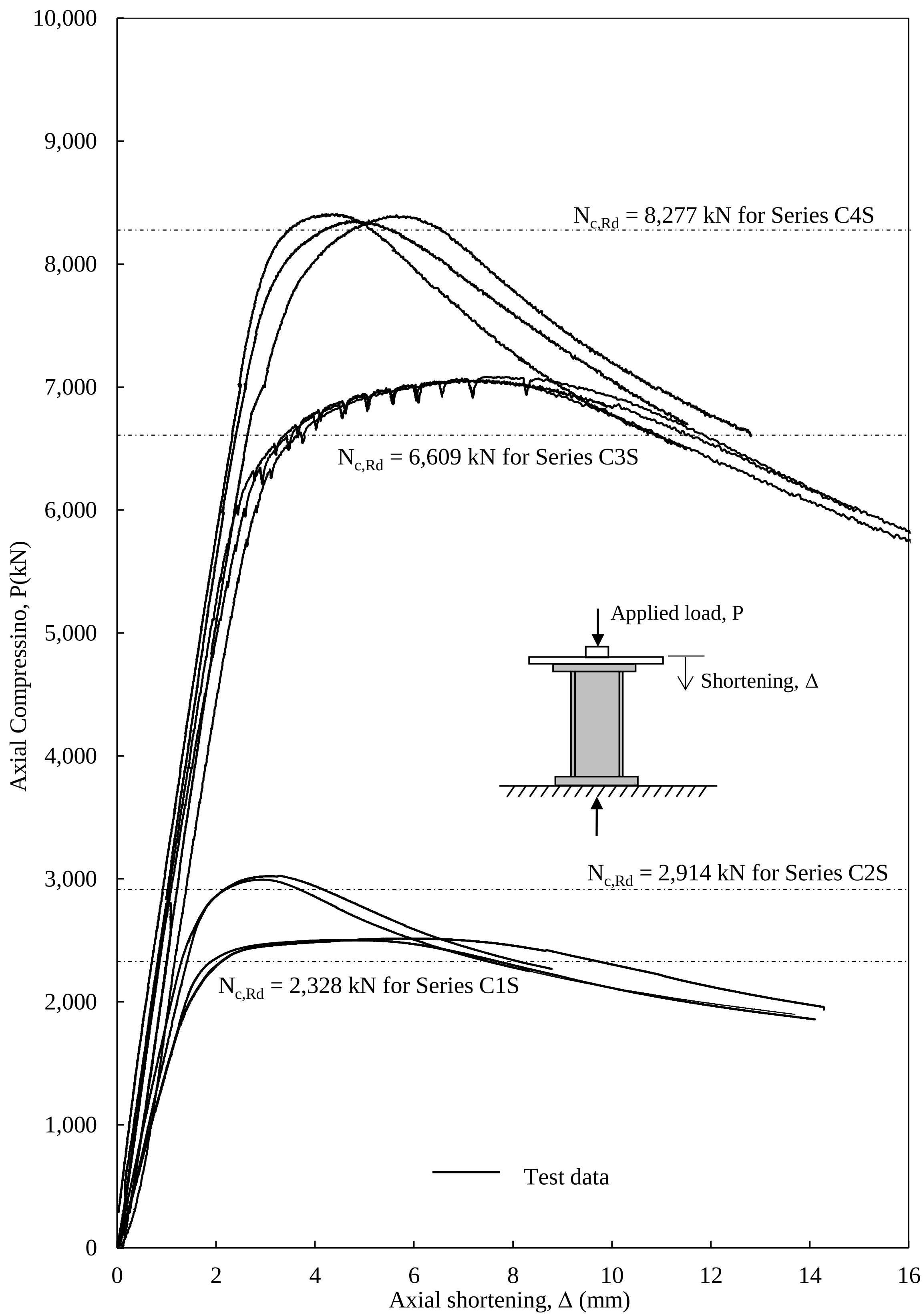

Figure 3.7: Load shortening curves of stocky columns under axial compression

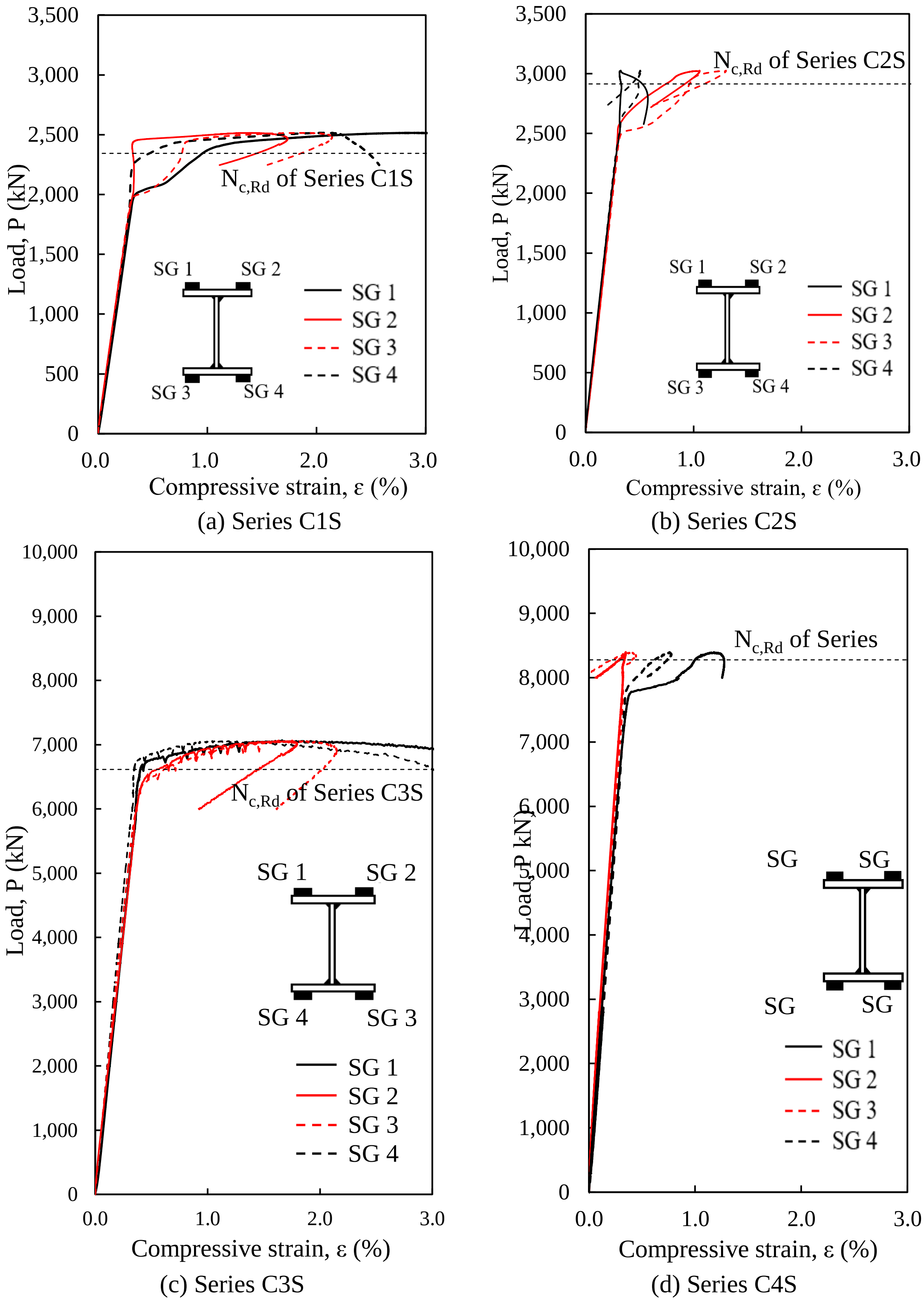

Figure 3.8: Typical load stain curves of stocky columns

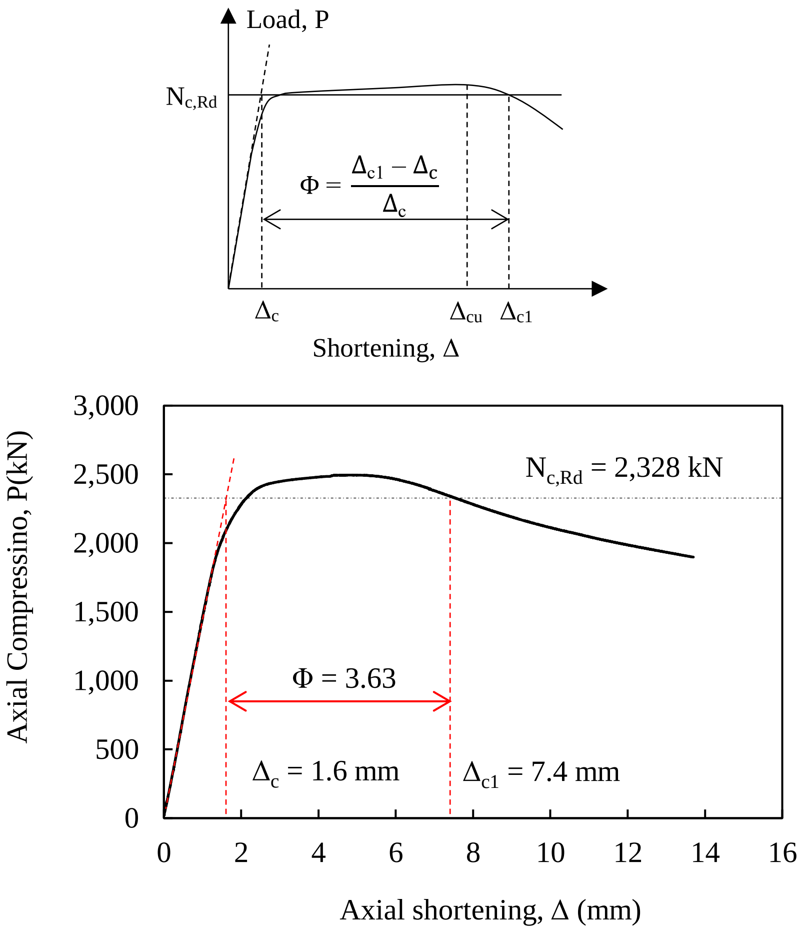

Figure 3.9: Definition of deformation capacity ratio for stocky columns

(a) Test setup with a 1000 tons hydraulic testing machine

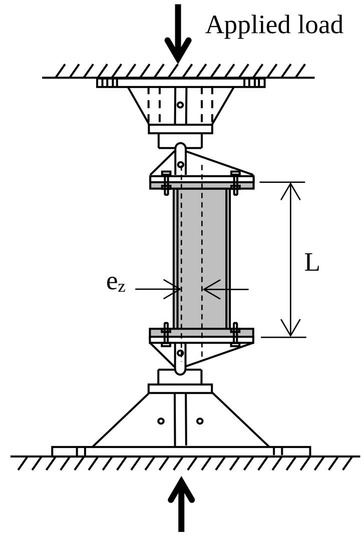

(b) Schematic illustration

Figure 3.10: Test setup of stocky columns under combined compression and bending

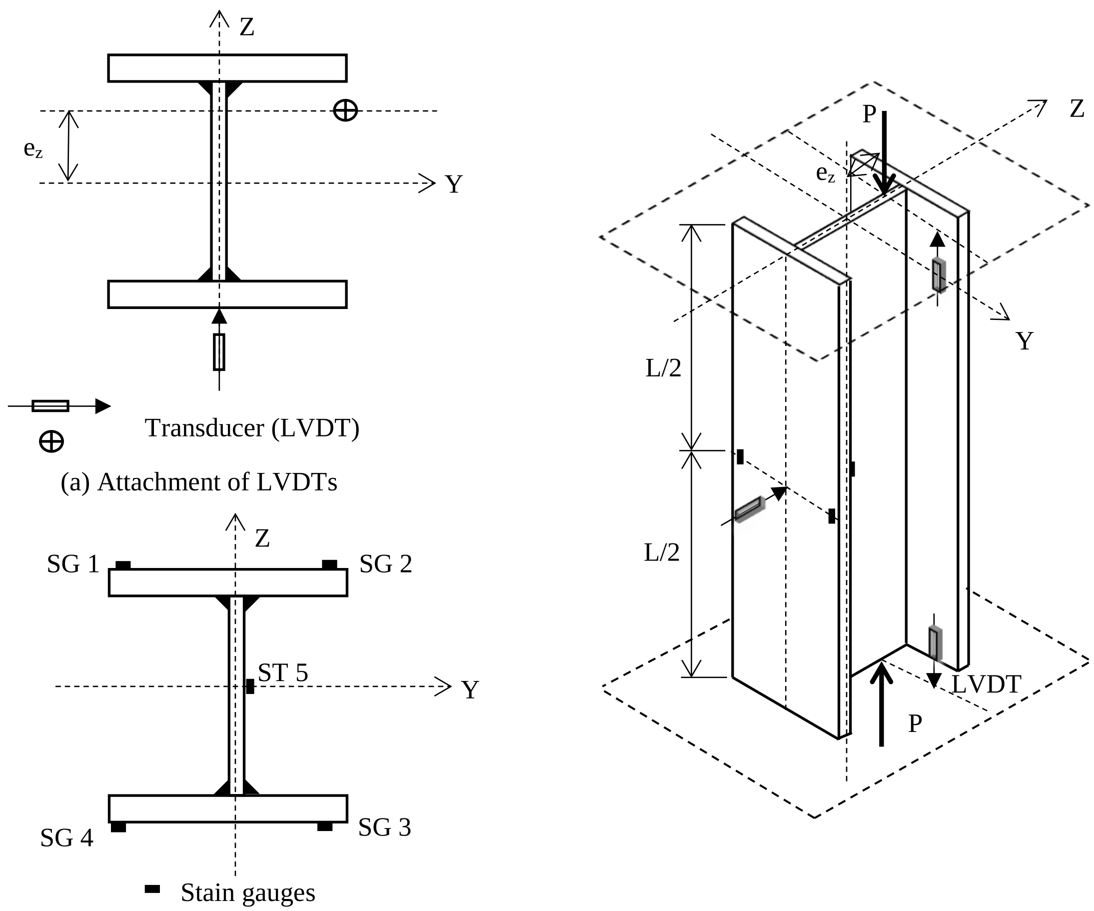

(a) Attachment of LVDTs

(b) Attachment of strain gauges

(c) 3-dimensional presentation of instrumentation

Figure 3.11: Instrumentation of stocky columns under combined compression and major-axis bending

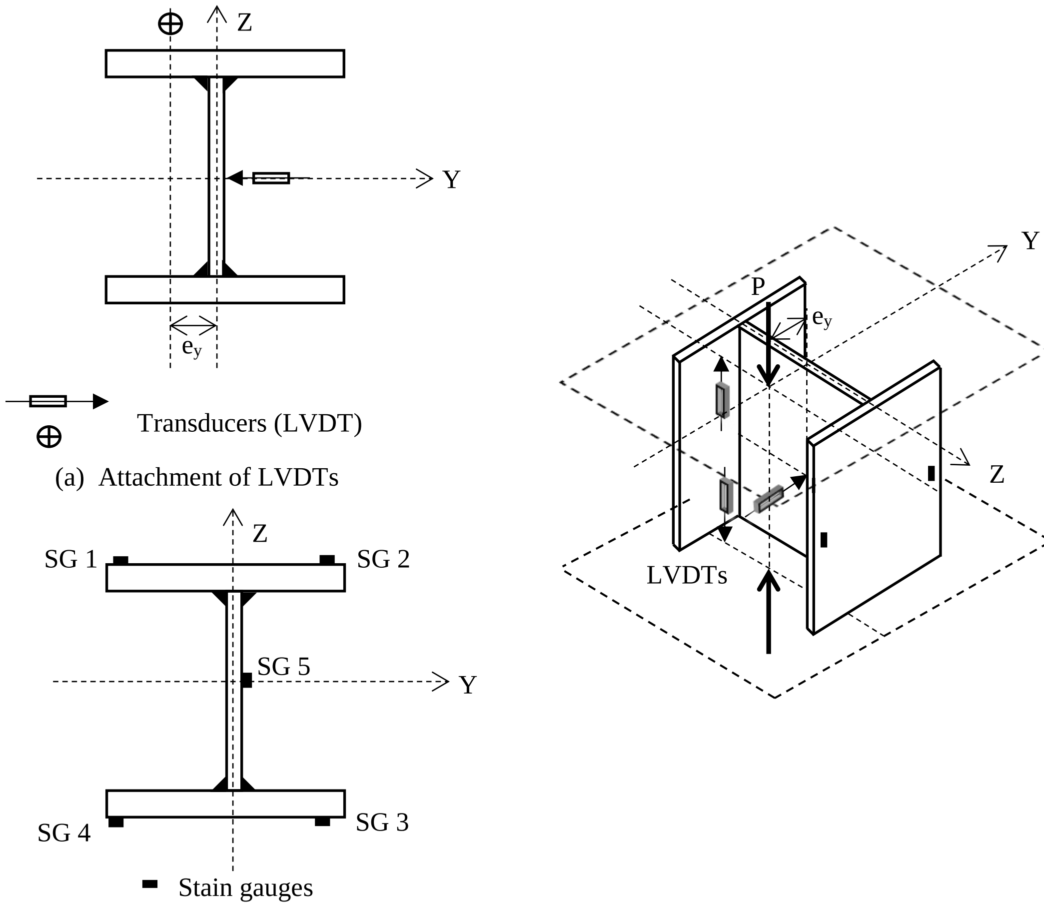

(b) Attachment of strain gauges

(c) 3-dimensional illustration of attachment

Figure 3.12: Instrumentation of stocky columns under combined compression and minor-axis bending

Section C3SY-d

Section C3SY-e

(a) Series C3SY

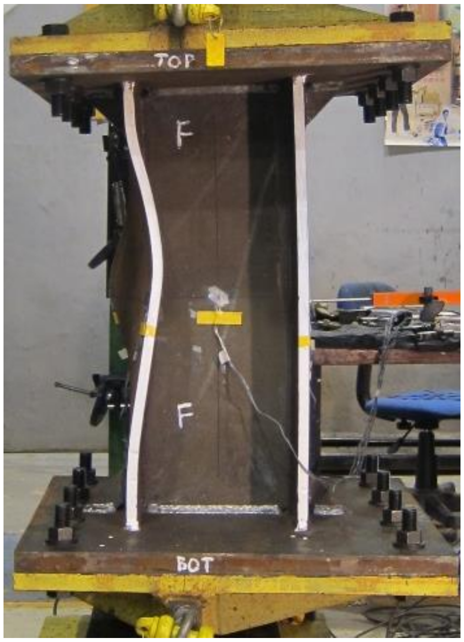

Section C4SY-d

Section C4SY-e

(b) Series C4SY

Figure 3.13: Failure modes of stocky columns under combined compression and major-axis bending

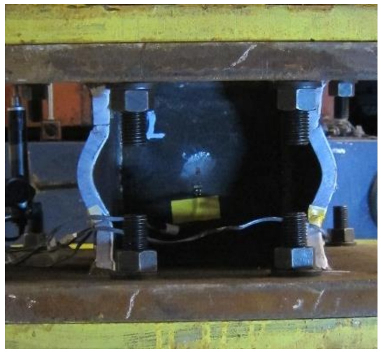

C3SZ-f

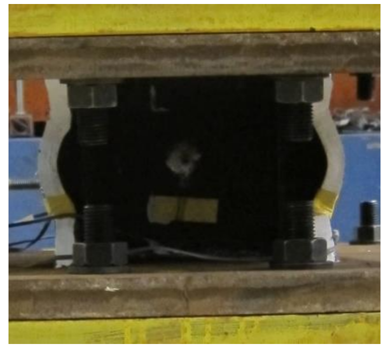

C3SZ-g

(c) Series C3SZ

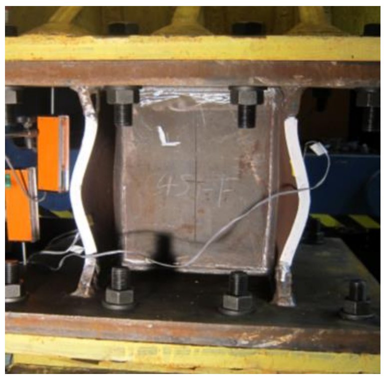

C4SZ-f

C4SZ-g

(d) Series C4SZ

Figure 3.14: Failure modes of stocky columns under combined compression and minor-axis bending

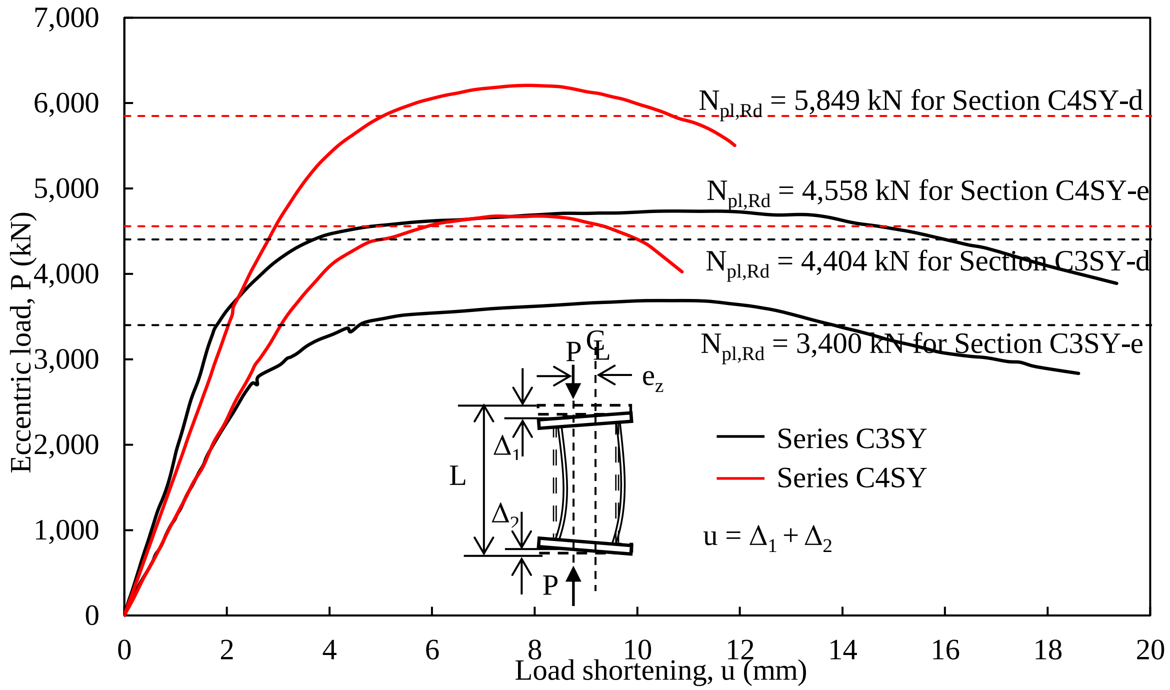

Figure 3.15: Load shortening curves of stocky columns under combined compression and major-axis bending

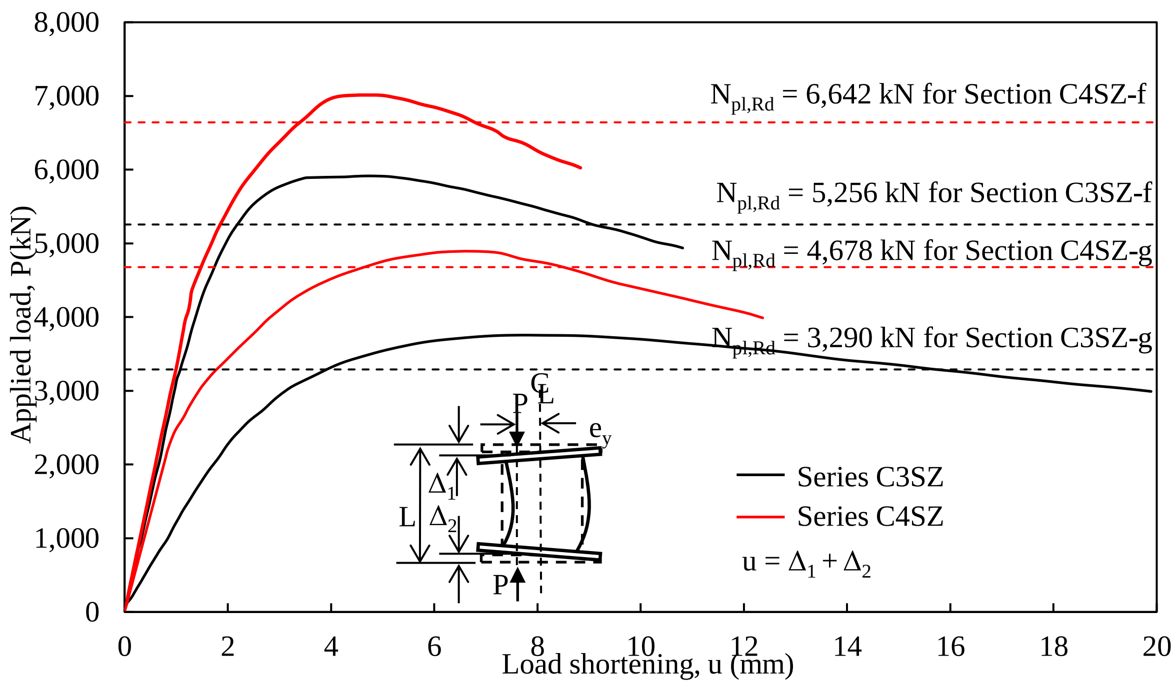

Figure 3.16: Load shortening curves of stocky columns under combined compression and minor-axis bending

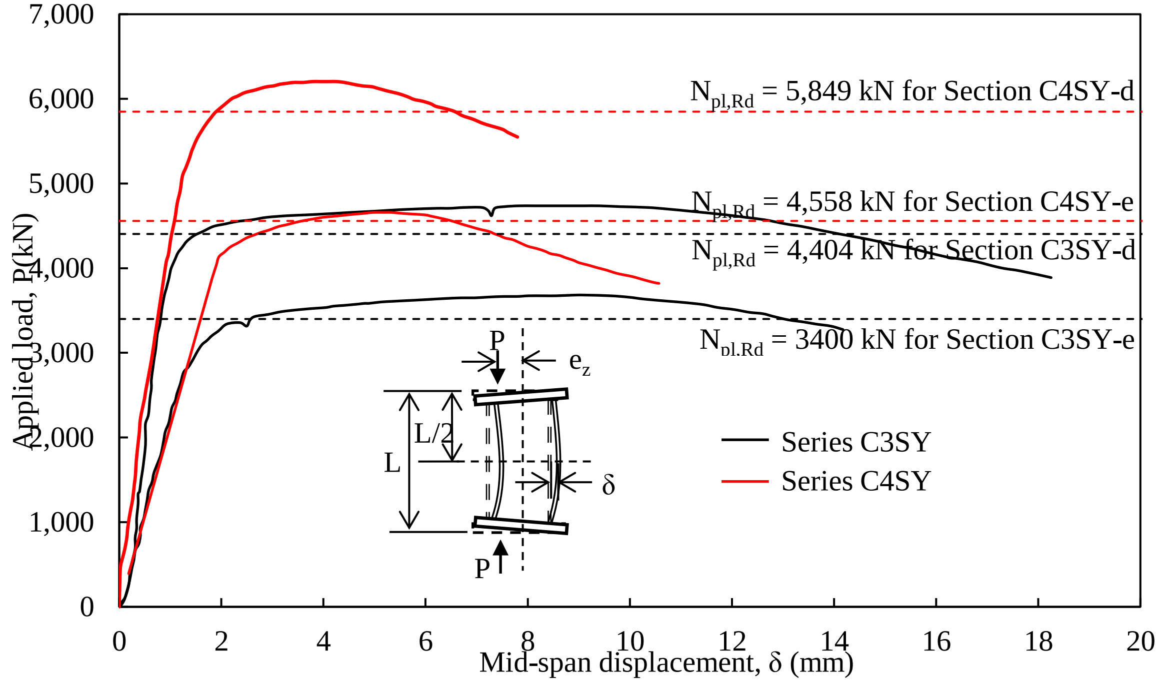

Figure 3.17: Load displacement curves of stocky columns under combined compression and major-axis bending

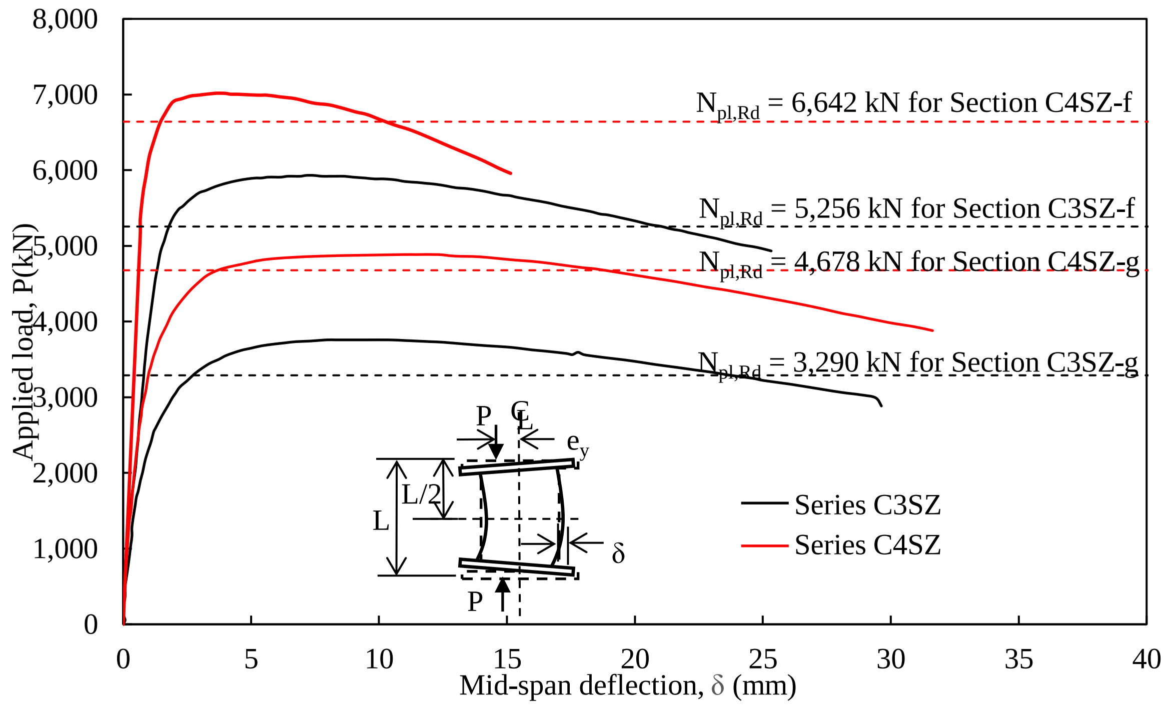

Figure 3.18: Load displacement curves of stocky columns under combined compression and major-axis bending

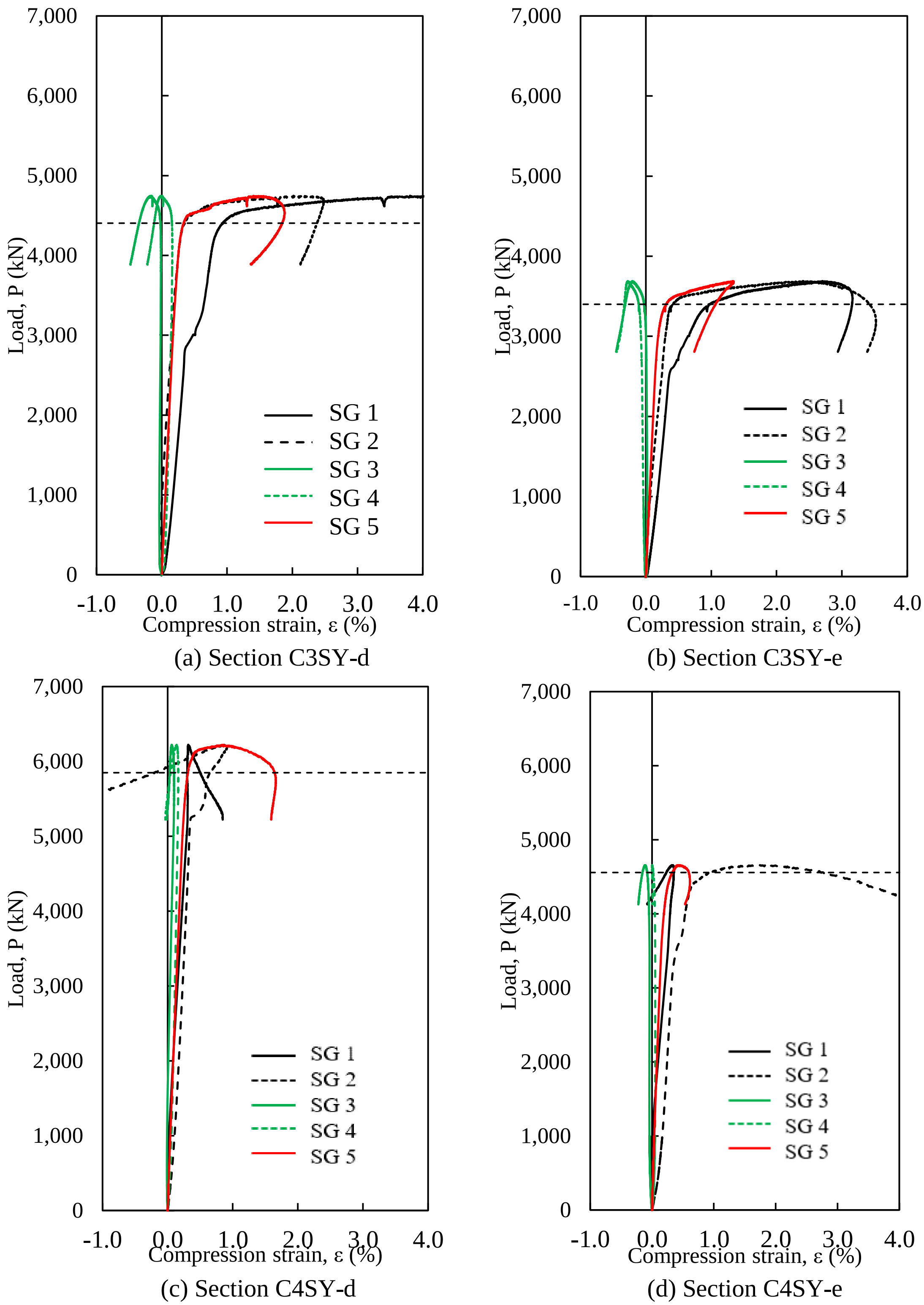

Figure 3.19: Measured strains of stocky columns under combined compression and major-axis bending

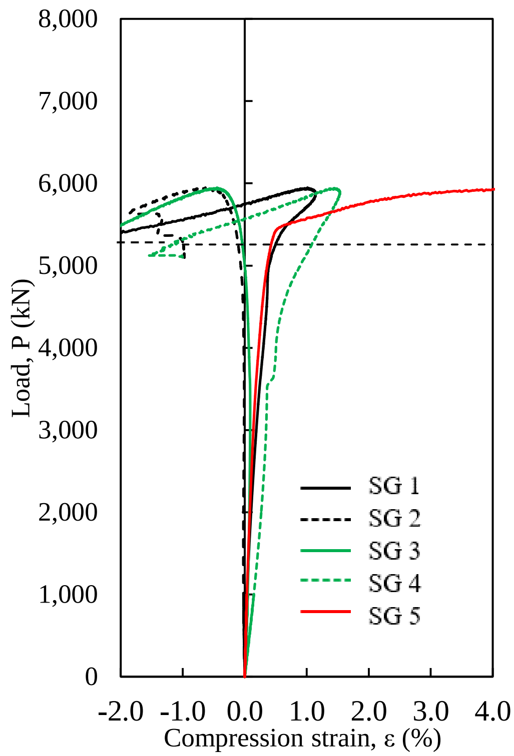

(a) Section C3SZ-f

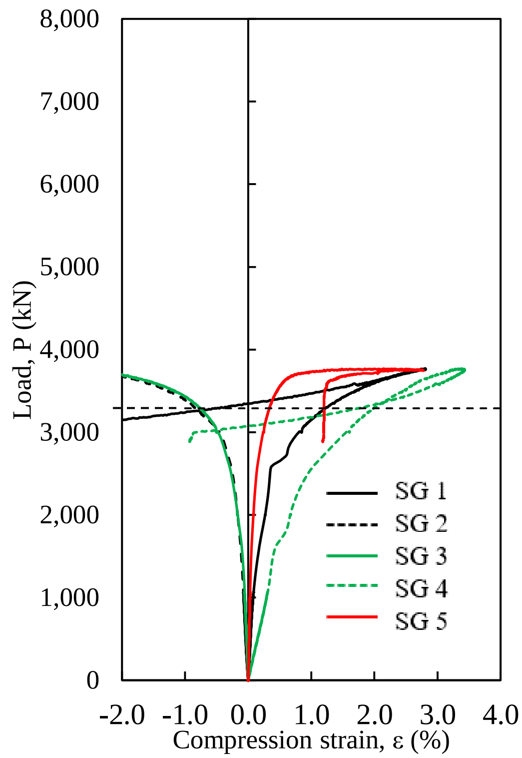

(b) Section C3SZ-g

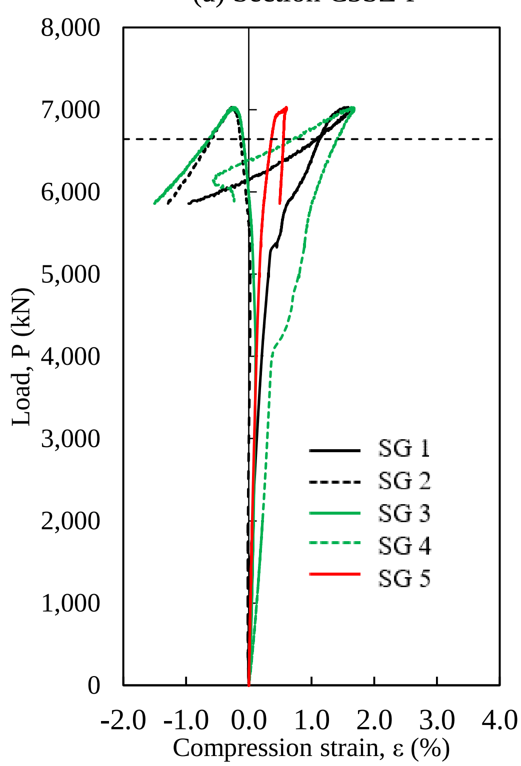

c) Section C4SZ-f

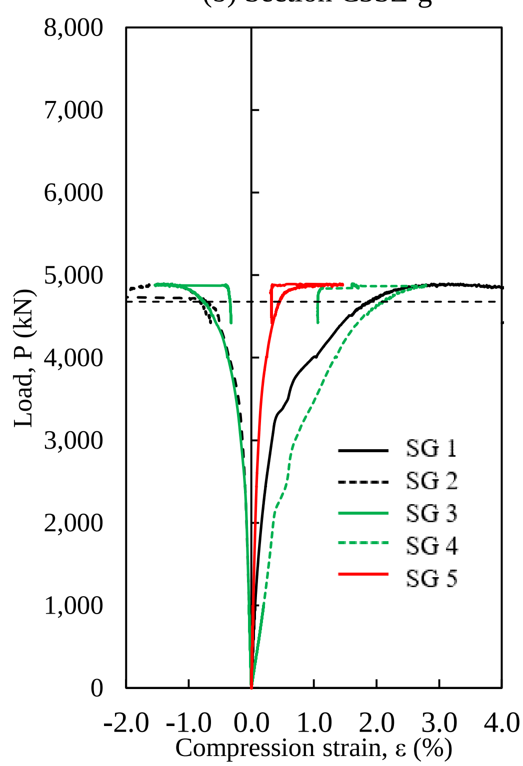

d) Section C4SZ-g

Figure 3.20: Measured strains of stocky columns under combined compression and minor-axis bending

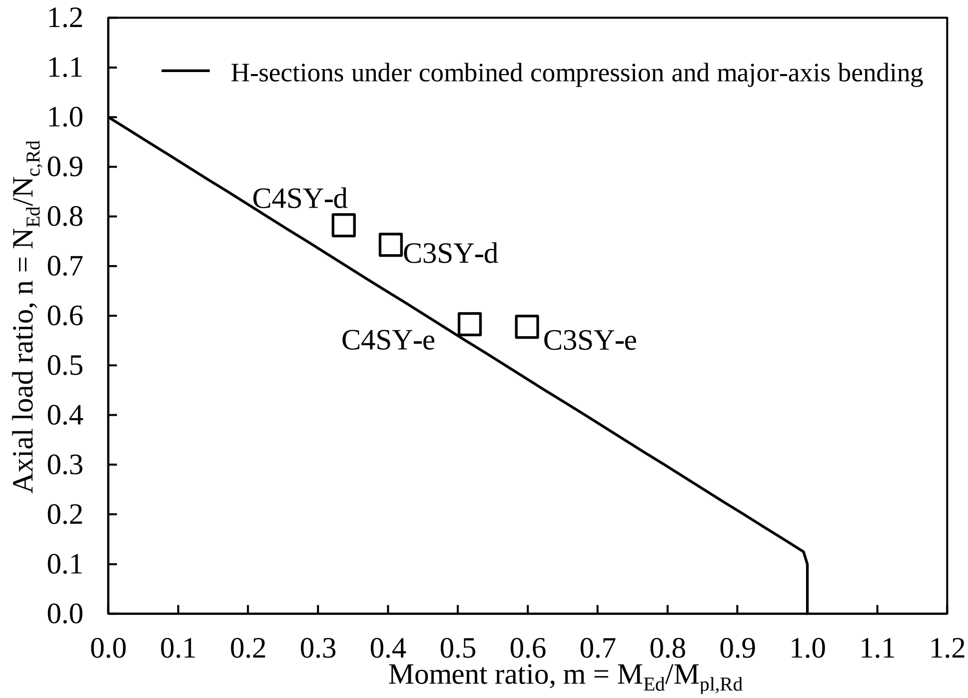

(a) Sections under combined compression and major-axis bending

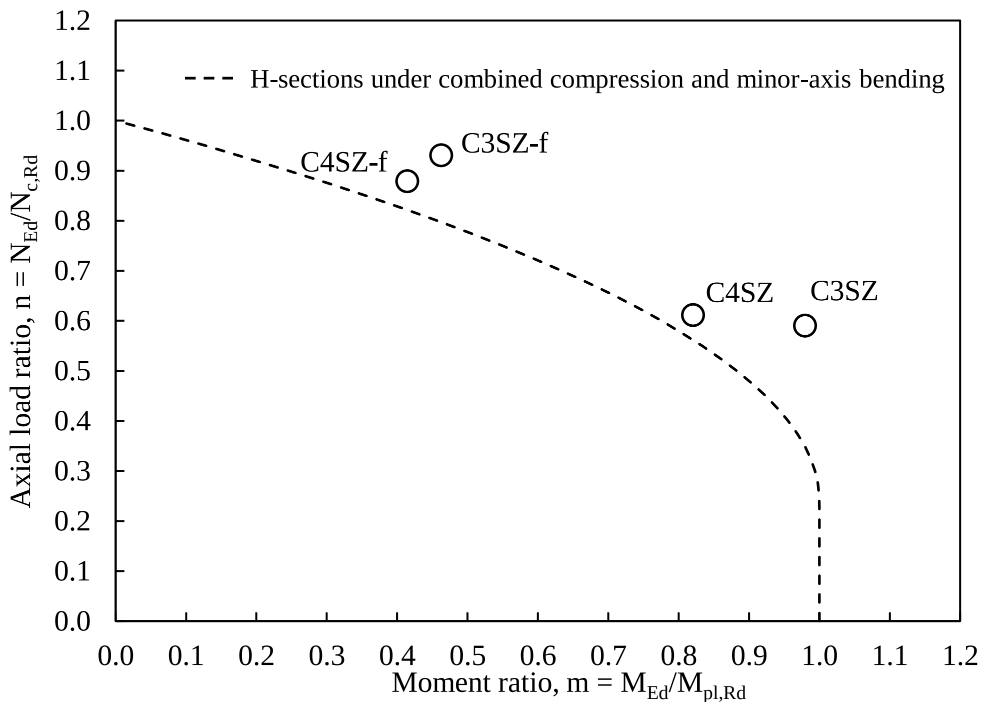

(b) Sections under combined compression and minor-axis bending

Figure 3.21: Comparison between test results and design curves for S690 welded H-sections under combined compression and bending

Table 3.1: Welding parameters

Specimens	Welding method	Electrode	Welding parameters: Voltage U (V)	Current A (I)	Speed v (mm/s)	Energy input W (kW/mm)
Stocky columns under compression:						
C1S, C2S	GMAW	CHW-80C1	30	240	4.0	1.8
C3S, C4S	SAW	CHW-S80	36	430	5.8	2.7
Stocky columns under combined compression and bending:						
C3S, C4S	SAW	CHW-S80	36	430	5.8	2.7

Table 3.2: Key results of standard tensile coupon tests

Plate thickness (mm)		Yield strength f_y (N/mm^2)	Tensile strength f_u (N/mm^2)	Young's modulus E (kN/mm^2)	Strain at tensile strength ε_u (%)	Elongation at fracture ε_L (%)
Stocky columns under compression	**6**	780	833	215	5.06	19.7
	10	754	807	208	5.85	16.2
	16	799	855	208	7.53	15.2
Stocky columns under combined compression and bending	**10**	761	821	212	6.35	20.6
	16	756	813	216	6.52	18.1

Table 3.3: Measured dimensions of S690 stocky columns under compression

Specimens		Measured dimensions						Slenderness ratios				Area
		L (mm)	h (mm)	b (mm)	t_f (mm)	t_w (mm)	r (mm)	$\frac{c_f}{t_f}$	$\frac{c_w}{t_w}$	$\bar{\lambda}_f$	$\bar{\lambda}_w$	A (mm^2)
C1S	-a	460	137.3	119.6	9.95	6.00	8.0	5.0	16.9	0.48	0.54	3084.4
	-b		137.1	119.1	9.97	6.00	8.0	5.0	16.9	0.48	0.54	3077.8
	-c		138.3	119.2	9.96	5.98	8.0	5.0	17.1	0.48	0.54	3084.7
C2S	-a	460	166.7	149.3	9.95	6.02	8.0	6.5	21.8	0.63	0.70	3851.9
	-b		166.2	149.4	10.00	6.00	8.0	6.5	21.7	0.63	0.70	3865.2
	-c		167.1	149.3	9.93	6.00	8.0	6.5	21.9	0.63	0.70	3848.5
C3S	-a	610	228.3	199.5	16.02	9.97	9.0	5.3	17.9	0.53	0.56	8348.7
	-b		230.9	200.2	16.03	9.97	9.0	5.3	18.1	0.53	0.57	8400.8
	-c		229.8	200.4	16.03	9.97	9.0	5.3	18.0	0.53	0.57	8396.3
C4S	-a	760	283.2	249.9	16.03	9.97	9.0	6.9	23.4	0.69	0.74	10515.7
	-b		282.8	250.1	15.95	9.97	9.0	6.9	23.4	0.69	0.74	10479.7
	-c		282.9	250	15.95	9.97	9.0	6.9	23.4	0.69	0.74	10477.5

Table 3.4: Section resistances of S690 stocky columns under compression

Specimens		Design resistances				Measured resistances		
		Section height L (mm)	Section classification	Section resistance $N_{c,Rd}$ (kN)	Enhanced section resistance $N_{cu,Rd}$ (kN)	Measured resistance $N_{c,Rt}$ (kN)	$\frac{N_{c,Rt}}{N_{c,Rd}}$	$\frac{N_{c,Rt}}{N_{cu,Rd}}$
C1S	-a	460	Class 1	2330	2507	2515	1.08	1.00
	-b			2324	2502	2495	1.07	1.00
	-c			2330	2508	2504	1.07	1.00
C2S	-a	460	Class 3	2912	3131	2998	1.03	0.96
	-b			2920	3142	3029	1.04	0.96
	-c			2910	3129	2994	1.03	0.96
C3S	-a	610	Class 2	6585	7044	7055	1.07	1.00
	-b			6622	7088	7084	1.07	1.00
	-c			6620	7084	7066	1.07	1.00
C4S	-a	760	Class 3	8297	8871	8384	1.01	0.95
	-b			8268	8840	8351	1.01	0.94
	-c			8266	8838	8392	1.02	0.95

Table 3.5: Deformation characteristics of S690 stocky columns under compression

Specimens		Section properties: Section height L (mm)	Section properties: Section classification	Shortening parameters: Shortening ratio Δ_u / L (%)	Shortening parameters: Deformation capacity ratio Φ	Average strain: Strain at local buckling ε_1 (%)	Average strain: Strain at failure ε_2 (%)
C1S	**-a**	460	Class 1	1.28	5.00	2.39	2.05
	-b			1.11	3.74	3.52	2.93
	-c			1.04	3.80	1.83	1.57
C2S	**-a**	460	Class 3	--	--	1.37	0.76
	-b			0.71	1.22	0.80	0.79
	-c			0.65	1.46	0.60	0.59
C3S	**-a**	610	Class 2	1.23	2.63	1.06	1.47
	-b			1.26	2.86	1.46	1.38
	-c			1.15	2.75	1.63	1.53
C4S	**-a**	760	Class 3	0.52	0.76	0.76	0.51
	-b			0.63	0.85	0.43	0.52
	-c			0.67	0.97	0.52	0.58

Table 3.6: Measured dimensions of S690 stocky columns under combined compression and bending

Specimens		Measured dimensions								Geometrical ratios		Area
		L (mm)	h (mm)	b (mm)	t_f (mm)	t_w (mm)	r (mm)	Eccentricities e_y (mm)	Eccentricities e_z (mm)	$\frac{c_f}{t_f}$	$\frac{c_w}{t_w}$	A (mm^2)
C3SY	**-d**	610	231.0	200.9	16.09	10.0	9.0	0	51.0	5.4	18.1	8453.2
	-e		231.5	200.4	16.09	10.0	9.0	0	97.5	5.4	18.1	8442.1
C4SY	**-d**	760	282.0	250.5	16.01	10.0	9.0	0	50.0	7.0	23.2	10519.1
	-e		282.0	251.3	16.05	10.0	9.0	0	103.0	7.0	23.2	10562.4
C3SZ	**-f**	300	232.5	200.5	16.09	10.0	9.0	19.3	0	5.4	18.2	8455.3
	-g		232.0	200.2	16.09	10.0	9.0	64.3	0	5.4	18.2	8440.6
C4SZ	**-f**	330	282.0	250.8	16.09	10.0	9.0	22.8	0	6.9	23.2	10567.6
	-g		282.0	251.0	16.10	10.0	9.0	65.0	0	6.9	23.2	10578.8

Table 3.7: Test results of S690 stocky columns under combined compression and bending

Specimens		Section properties						Resistance		
		Slenderness ratios Flange $\bar{\lambda}_f$	Slenderness ratios Web $\bar{\lambda}_w$	Section classification	Section resistance $N_{c,Rd}$ (kN)	Section resistance $M_{pl,Rd}$ (kNm)	Neutral axis y (mm)	Design resistance $N_{pl,Rd}$ (kN)	Measured resistance N_{Rt} (kN)	$\frac{N_{Rt}}{N_{pl,Rd}}$
C3SY	**-d**	0.52	0.57	Class 2	6400.5	600.4	6.6	4,404	4,747	1.08
	-e	0.52	0.57		6392.2	600.7	9.9	3,400	3,690	1.09
C4SY	**-d**	0.67	0.53	Class 3	7965.0	925.2	5.6	5,849	6,222	1.06
	-e	0.67	0.53		7997.7	929.4	9.1	4,558	4,657	1.02
C3SZ	**-f**	0.52	0.58	Class 2	6402.2	248.3	23.6	5,256	5,948	1.13
	-g	0.52	0.58		6391.1	247.6	63.7	3,290	3,770	1.15
C4SZ	**-f**	0.60	0.73	Class 3	8001.6	387.2	27.9	6,642	7,030	1.06
	-g	0.60	0.73		8010.0	388.1	68.4	4,678	4,897	1.05

Table 3.8: Deformation behaviour of S690 stocky columns under combined compression and bending

Specimens		Slenderness ratios: Flange $\bar{\lambda}_f$	Slenderness ratios: Web $\bar{\lambda}_w$	Section classification	Deformation capacity ratio Φ
C3SY	**-d**	0.52	0.57	Class 2	6.1
	-e	0.52	0.57		3.8
C4SY	**-d**	0.67	0.53	Class 3	2.0
	-e	0.67	0.53		1.3
C3SZ	**-f**	0.52	0.58	Class 2	4.6
	-g	0.52	0.58		4.9
C4SZ	**-f**	0.60	0.73	Class 3	2.5
	-g	0.60	0.73		3.5

CHATER FOUR

EXPERIMENTAL STUDY II: STRUCTURAL BEHAVIOUR OF FULLY AND PARTIALLY RESTRAINED BEAMS OF S690 WELDED I-SECTIONS

4.0 Introduction

In order to study structural instability of fully and partially restrained beams of S690 welded I-sections, a systematic experimental investigation into these beams was conducted and presented in this chapter. A total of 18 high strength steel S690 welded I-sections which included six different cross-sections were devised in this test programme. Dimensions of these six sections are shown in Figure 4.1.

Section resistances of S690 welded I-sections were examined through standard tensile tests and measurement of residual stresses. Influences from these section resistances to structural behaviour of S690 beams were critically studied.

Two different test programmes are presented in this chapter:

- Tests on 6 fully restrained beams of S690 welded-I-sections which are denoted as Series LT0;
- Tests on 12 partially restrained beams of S690 welded-I-sections which are denoted as Series LT1 and Series LT2.

In each test series, six beams with different cross-sections as shown in Figure 4.1 were tested. Difference among these three different test series are illustrated in Figure 4.2. In this experimental investigation, structural behaviour of S690 fully restrained beams and partially restrained beams were closely examined, compared and interpreted. A comparison between measured and predicted resistances based on EN 1993-1-1 is also presented.

4.1 Objectives

In order to understand structural behaviour of beams of S690 welded I-sections, a systematic experimental investigation into structural behaviour of 6 fully restrained beams and 12 partially restrained beams were carried out. Main objectives of these tests are:

- To understand mobilization of section resistances of fully restrained beams of S690 welded I-sections;
- To study lateral torsional buckling behaviour of partially restrained beams of S690 welded I-sections; and,
- To assess suitability of current design rules on section classification and lateral torsional buckling given in EN 1993-1-1 to high strength S690 welded I-sections.

The following areas of interest are addressed:

1. Mechanical properties of S690 steel material, and residual stresses of S690 welded I-sections;
2. Failure modes and section resistances of fully restrained beams with different cross-sectional dimensions;
3. Failure modes, buckling resistances, and deformation characteristics of partially restrained beams against different member slendernesses;
4. Comparison between Series LT0 and LT1 to reveal effects of lateral torsional buckling to failure modes and section resistances of S690 welded I-sections; and,
5. Comparison between Series LT1 and LT2 to reveal effects of member slenderness to failure modes and member resistances of S690 welded I-sections.

4.2 Section Properties

4.2.1 Standard coupon tests on S690 steel materials

According to BS EN ISO 6892-1, standard tensile tests were conducted to determine the stress-strain curves of S690 steel materials. A total of 12 standard coupons were tested as a total of four different S690 steel plates were utilized to fabricate welded I-sections.

Details of coupons and coupon tests, including coupon sizes, gauge lengths and instrumentation, as well as testing procedures may be found in Section 3.2.1. Typical measured stress-strain curves are plotted in Figure 4.3 with key parameters of material properties listed in Table 4.1. True stress-strain curves are also plotted in Figure 4.3 for easy reference. Comparing with measured mechanical properties with various criteria given in EN 1993-1-12, it is shown that these steel materials generally meet the requirements for structural design. Therefore, it is evident that quality S690 steel materials are directly applicable in steel construction according to EN 1993-1.

4.2.2 Welding parameters

A total of eighteen high strength steel S690 welded I-sections were fabricated in a steel fabricator. In order to mitigate adverse heating effect, steel plates were cut from four S690 steel plates using a wire-cutting method. Hence, limited heat energy input was introduced during the welding process. Then, all these plates were welded up using a matching electrode of GM110. A gas metal arch welding approach, i.e. GMAW approach, was employed with single-pass runs on each T-joint to fabricate these I-sections. Optimized welding parameters were adopted after trials as follows:

- Welding voltage: 28.0V;
- Welding current: 225A; and,
- Welding speed: 5 mm/s .

Based on these welding parameters, a heat energy input rate ranging from 1.0 to 1.3 kJ/mm was provided as shown in Table 4.2. With this energy input level, adverse effects onto mechanical properties of S690 steel plates at junction regions were kept being minimal (Liu, 2017).

4.3 Measurements of Residual Stresses in S690 Welded I-sections

It was important to obtain residual stresses in S690 welded I-sections and they were measured with the ASTM hole-drilling method. Three different cross-sections, i.e. Sections B2, B4 and B6 were utilized. In this section, test setup, instrumentation and measured data are described. Moreover, a schematic interpretation of measured data and a comparison with residual stress patterns given by ECCS are also presented.

4.3.1 Test setup and instrumentation

The test programme of residual stress measurement of S690 welded I-sections is summarized in Figure 4.4. As an ASTM hole-drilling method was adopted in this study, the arrangement of strain gauge rosettes in various locations of a steel beam is illustrated. It should be noted that the rosettes were mounted onto cross-sections away from vertical stiffeners, so that disturbance to residual stresses induced during welding of stiffeners was avoided.

It should be noted that ten strain gauge rosettes were mounted onto each welded I-section. According to the requirements of ASTM 1837-E, the rosettes were placed at least 10 mm away from the flange tips, and a spacing of at least 25 mm from each other should be provided. Hence, the rosettes are staggered on the flanges of the steel beam as shown in Figure 4.5.

As a high-speed RS-200 milling guide was employed to conduct hole-drilling tests, typical test setup is presented in Figure 4.5. Moreover, two sprit levels were used to ensure the horizontal state of outer surfaces and the perpendicular relationship between the drill bits and the outer surfaces. It should be noted that any error of alignment was rigorously controlled to be within ±0.026mm to meet the requirements given in ASTM 1837-E (ASTM, 2013).

4.3.2 Test results

It should be noted that the strain gauge rosettes were attached onto two different surfaces in the cross-sections of the I-sections, i.e. i) the outer surface of the top flange (TF), and ii) the left surface of the web (LW). During the hole drilling process, various direct and shear residual strains were relieved and measured by the rosettes. Then, residual stress components were calculated from the measured strains.

Measured residual stresses of S690 welded I-sections are summarized in Table 4.4. In these tables, σ_1 and σ_3 are the residual stresses in the longitudinal and the transverse directions, and τ_{13} represents the in-plane shear residual stress. In general, the longitudinal residual stresses are found to be larger than both the transverse and the shear stresses. Hence, only the longitudinal residual stress component is presented in detail. Stress ratios of the longitudinal stresses to the yield strengths of steel materials are presented in Table 4.5.

For easy reference, cross-sectional distributions of longitudinal residual stresses in three different S690 welded I-sections are plotted in Figure 4.5. The tensile residual stresses were measured as 400, 111 and 453 N/mm^2, and the corresponding $\sigma_{rs,f}$-to-f_y ratios were 0.51, 0.15 and 0.58. The maximum compressive residual stresses on the flanges were found to be -191, -102 and -197 N/mm^2 and those on the webs were found to be -168, -83 and -195 N/mm^2. The corresponding σ_{rs}-to-f_y ratios on the flanges were -0.24, -0.14, and -0.25, while on those the webs were -0.23, -0.12 and -0.27. Hence, the values of tensile residual stresses on the flange-web junctions are generally higher than those of the compressive residual stresses on the steel plates.

4.3.3 Summary

In this section, residual stresses in S690 welded I-sections induced by heating and cooling cycles from welding process were successfully measured. It should be noted that large tensile residual stresses were found to be highly concentrated on the flange-web junctions while small compressive residual stresses were measured in the plate elements.

A comparison between the measured residual stresses and the suggested residual stress patterns of welded I-sections given in ECCS (1976) is presented in Table 4.6. It should be noted that all measured residual stress ratios are significantly smaller than values suggested in ECCS. Hence, the residual stresses originally proposed for S355 welded I-sections are found to be too high for S690 welded I-sections. Therefore, residual stress patterns from ECCS are not applicable to high strength steel S690 welded I-sections. Measured residual stress patterns for S690 welded I-sections obtained with the hole-drilling method should be used.

4.4 Tests on Fully Restrained Beams

4.4.1 Test Programme

In this test series, a single-point transverse load was imposed to simply supported beams. These beams were fully restrained according to requirements given in EN 1993-1-1. A total of six beams of different cross-sections were devised in this test programme with the following characteristics:

- Sections B1 to B3: Three doubly symmetrical I-sections with class 1, 2 and 3 cross-sections respectively;
- Section B4: A doubly symmetrical I-section with 16 mm thick flanges; and,
- Sections B5 to B6: Two singly symmetrical I-sections with at least Class 2 flanges and Class 3 web elements.

Measured dimensions and section parameters of the six beam sections are summarized in Table 4.7. The total spans of these beams range from 1.9 m to 4.5 m. Based on section classification design rules in EN 1993-1-1, these I-sections are comprised of class 1 to class 3 flanges and webs. Through this test series, local buckling in these six fully restrained beams with various plate slendernesses and mobilization of moment resistances are examined in details.

4.4.2 Test setup

In order to present any out-of-plane displacement of the I-sections, a strong restraining system was provided as shown in Figure 4.7. A typical test setup for a simply supported beam adopted in this test programme is shown in Figure 4.8. It should be noted that the restraining system included two Channel sections, and I-sections were positioned in between these two Channel sections. For each I-section, two points along the section were restrained as shown in Figure 4.8. Teflon membranes were attached onto touching surfaces of both the Channel Sections and the T-stiffeners with greases to minimize sliding friction. Therefore, the strong restraining system was able to provide efficient lateral and torsional restraints to the I-sections during loading application.

A hydraulic jack with a 2,000 kN capacity was employed in the tests. The applied load was measured by a load cell with a 1,500 kN capacity. In order to impose static loads, the loading rate was controlled at a rate of 0.2 kN/s in the elastic range. After attaining full moment resistances of the I-sections, a displacement control at a rate of 1 mm/min was adopted.

Instrumentation of this test series is illustrated in Figure 4.9. Ten strain gauges, denoted as SG1 to SG10, were mounted onto a cross-section 100 mm from the loaded points. These strain gauges were used: i) to observe development of plasticity across section depth, and ii) to monitor local buckling of a cross-section. Seven LVDTs were installed to record vertical deflections at the loaded points and rotations at section ends as follows:

- LVDT 1 and 2: To measure rotations at a section end;
- LVDT 3 and 4: To measure deflections at the loaded point;
- LVDT 5 and 6: To measure rotations at another section end; and,
- LVDT 7: To monitor movement of the restraining system (not shown in Figure 4.9 for simplicity)

4.4.3 Test results

4.4.3.1 Failure modes

Failure modes of all six fully restrained beams are illustrated in Figure 4.10. Generally, local buckling was observed in top (compression) flanges of Sections B1 to B5. It should be noted that local buckling occurred on both flanges and webs of Sections B1 to B4 simultaneously as plate slendernesses of both the flange and web plates were identical in each of these sections. In Section B5, local buckling was only observed in the web plate because a Class 3 web plate and Class 1 flanges were adopted in this section; hence, local buckling was only developed in the web plate. For Section B6, it failed in lateral torsional buckling. This failure mode was unexpected, owing to a failure of bottom plates of the restraining system, and a lateral drift of the restraining system was detected by LVDT7.

According to strain measurements of SG1 and SG3, moment resistances of these I-sections were attained when local buckling began to develop. At that time, the values of measured strains SG1 and SG3 would have significant difference as shown in Figure 4.11. It should be noted that local buckling developed quickly, and deformed shape of local buckling was apparent in flanges of the I-sections.

4.4.3.2 Moment resistances

Measured moment resistances of fully restrained beams of high strength S690 welded I-sections, i.e. M_{Rt}, together with the plastic moment resistances calculated with measured material properties, i.e. $M_{pl,Rd}$, are summarized in Table 4.8 for direct comparison. It is shown that Class 1 and 2 I-sections were able to attain plastic moment resistances. For Section B3 with a Class 3 cross-section, elastic moment resistance was achieved. Hence, the current section classification rules given in EN 1993-1-1 are able to predict moment resistances of these S690 welded I-sections satisfactorily.

It should be noted that strength enhancement on the moment resistances of these I-sections was evident in some of them with Class 1 and Class 2 sections. For Sections B1, B2 and B4, these I-sections attained a strength enhancement at 5% over the predicted moment resistances. Hence, a significant strength enhancement may be mobilized in I-sections with compact plate elements. It should also be noted that strength enhancement generally increases inversely with slenderness ratios of the steel plate elements in an I-section.

Moreover, shear forces at ULS are compared with shear capacity of S690 welded I-sections as listed in Table 4.10. Only in Sections B1 and B4, shear ratios are found to be slightly higher than 0.50. Based on measured moment resistances, strength enhancement was not influenced by shear forces applied onto these web plates. And shear buckling mode was not observed in webs of these sections. Hence, failure of these beams was governed only by moment resistances.

4.4.3.3 Load deformation behaviour

Measured deformation parameters at ULS are listed in Table 4.9, and load deflection curves of fully restrained beams are presented in Figure 4.10. It should be noted that deflection at loaded point, Δ, is taken as the average of measured readings from LVDTs 3 and 4. The load deflection curves were found to increase elastically up to 80% to 90% of predicted resistances. After significant yielding in the cross-sections, gradients of these load deflection curves were found to be reduced gradually. At failure, large deflections together with enhanced moment resistances were attained in beams with Class 1 sections. Specifically, span multiple of 60 was achieved by Section B4 owing to its small depth-to-width ratio of 1.6.

It is noted that Section B1 with Class 1 section is shown to attain a rotational capacity of 2.36. This is smaller than the required capacity of 3.00 suggested in AISC 360 (AISC, 2010). This may be explained by the failure of restraining system after ULS of Section B1. Owing to this reason, significant yielding reduced section rigidity and introduced unexpected plastic lateral torsional buckling.

4.4.4 Summary

A total of 6 fully restrained beams of S690 welded I-sections under single point load were carried out. Five of these sections were found to be failed in section failure primarily under large bending moment. Plastic local buckling in the flange outstands of these sections was apparent. Different levels of strength enhancement and deformation capacities were observed, depending on slenderness of plate elements of the sections. Based on these test results, the following key findings are obtained:

- For fully restrained beams with welded I-sections with Class 1 and 2 sections, plastic section resistances were attained with a significant strength enhancement at 5% above their design plastic moment resistances;
- For Section B3 with Class 3 section, an elastic moment resistance was attained with limited yielding developed in the sections; and,
- Full resistances of fully restrained beams have been mobilized before occurrence of plastic local buckling in plate elements of the sections

It should be noted that plastic moment resistances with different levels of rotational capacities were attained in these welded I-sections. Strength enhancement in these sections is found to be proportional to their rotational capacities according to the load end-rotation curves of the beams.

Hence, current design rules of section classifications in EN 1993-1-1 is applicable to design fully restrained beams of S690 welded I-sections. It is also noted that the criteria of Class 3 section may be overconservative in the presence of reduced residual stresses in S690 welded I-sections.

4.5 Tests on Partially Restrained Beams

4.5.1 Test programme

In order to investigate lateral torsional buckling of partially restrained beams of S690 welded I-sections, a single-point transverse load was applied to each of the 12 simply supported beams in this test programme with two test series, i.e. Series LT1 and Series LT2. It should be noted that there are 6 beams with different cross-sections in each series, as shown in Figure 4.1. Measured dimensions of the cross-sections in two test series are presented in Tables 4.11 and 4.14. The total spans of these beams range from 1.9 m to 4.5 m which lead to a wide range of normalized slenderness $\bar{\lambda}_{LT}$. Moreover, section classifications of partially restrained beams range from Class 1 to Class 3 sections based on section classification rules of EN 1993-1-1.

Differences between configurations of beam sections were as followings:

- Sections of Series LT1 possess a critical span L_1 smaller than those of sections of Series LT2; and,
- Vertical stiffeners were not installed at the supported end of critical spans in sections of Series LT2.

It should be noted that vertical stiffeners at section ends can be removed in practice when obstruction to passage of important facility should be avoided at the section ends. In some cases, stiffeners may entirely fail due to fatigue crack and corrosion (Spadea and Frank, 2002, DeLong and Bowman, 2010). Consequently, sections of Series LT1 possess small to moderate section slendernesses ranging from 0.39 to 0.77. The corresponding sections of Series LT2 have increased section slendernesses which range from 0.52 to 1.23. Through this study, lateral torsional buckling in partially restrained beams of S690 welded I-sections with various section slendernesses are examined in detail.

4.5.2 Test setup

Basically, simply supported beams were loaded under a moment gradients as shown in Figures 4.12 and 4.14. A strong restraining system presented in Figure 4.7 is also applied in this test programme. The restraining system provides effective lateral and torsional restraints to the beam sections at loaded points. Hence, a destabilizing effect of the load imposed on the top flange is well prevented. And, it is ensured that the applied load can always pass through the shear centre of each of the I-sections during the tests. With this test setup, both the loading condition and effective restraints are clearly defined in this test programme.

A hydraulic jack with a 2,000 kN capacity was employed in the tests. The applied load was measured by a load cell with a 1,500 kN capacity. In order to impose static loadings, the loading rate was controlled at 0.2 kN/s in the elastic range. After attaining full moment resistances of the I-sections, a displacement control at a rate of 1 mm/min was adopted.

Instrumentations of these two test series are illustrated in Figures 4.13 and 4.15. Ten strain gauges, denoted as SG1 to SG10, were mounted onto the test specimens. It should be noted that eight of these strain gauges were attached across section depths. These strain gauges are located at mid-span for sections of Series LT1, and 600 or 900 mm away from loaded points for sections of Series LT2. Other two strain gauges were mounted on top flanges 300 mm or 450 mm away. All these strain gauges are used: i) to measure yielding across the section depths, and ii) to monitor any minor-axis bending of the section over the critical span against lateral torsional buckling.

Eight LVDTs were installed to record vertical deflections and lateral displacements of the sections at the loaded points and rotations at section ends, as shown in Figures 4.13 and 4.15 as follows:

- LVDT 1 and 2: To measure rotations at a section end;
- LVDT 3 and 4: To measure deflections at the loaded point;
- LVDT 5: To record lateral displacements induced by lateral torsional buckling;
- LVDT 6 and 7: To measure rotations at another section end;
- LVDT 8: To record lateral displacements at section ends; and,

- LVDT 9: To monitor movement of the restraining system. (not shown in Figures 4.13 and 4.15 for simplicity)

4.5.3 Test Results

4.5.3.1 Failure modes

In order to examine observed structural behaviour of partially restrained beams, load-deflection curves and load-displacement curves of the six welded I-sections are presented together with failure modes shown in Figures 4.16 and 4.17. Measured moment resistances of these beams are listed in Tables 4.11 and 4.14 design values for direct comparison with

- Test specimens of Series LT1:

  According to observed deformed shapes and test measurements, section failure is found to occur in Sections B1, B2 and B4 as full moment resistances were obtained by these sections. It should be noted that these three beams possess small slenderness ratios at 0.39, 0.54 and 0.47 respectively. Hence, plasticity was fully developed in these three sections before lateral torsional buckling was fully developed. Lateral torsional buckling is found to occur in Sections B2, B3, B5 and B6 as large out-of-plane displacements were found at mid of the critical spans at failure. For Section B3, local buckling was also observed together with lateral torsional buckling as shown in Figure 4.20. Therefore, the interaction between lateral torsional buckling and local buckling is found to occur in this section. Comparing with measured full moment resistances of the beams in Series LT0, buckling resistances of the beams of Series LT1 are generally smaller owing to increased slendernesses.

- Test specimens of Series LT2:

  As shown in Figure 4.17, lateral torsional buckling occurred in all six beams of Series LT2. More specifically, the beams buckling with gross deformation over their critical spans except for Section B5. This should be attributed to unstiffened section ends, and geometry of steel sections. Amongst all these beams, Sections B1 and B4 attained full moment resistances owing to their small slenderness ratios at 0.62 and 0.52 respectively. Comparing with measured moment resistances of the beams in Series LT0 and LT1, buckling resistances of the beams of Series LT2 are generally smaller owing to increased slendernesses.

4.5.3.2 Load deflection curves

According to the measured load deflection curves shown in Figure 4.16 and 4.17, moment resistances of partially restrained beams are found to reduce quickly after lateral torsional buckling. For sections which attained their full moment resistances, strength enhancement was smaller when comparing with those beams in Series LT0. Moreover, the moment resistances in these sections dropped off quickly at large deformation owing to reduced section stiffness. Hence, these observations indicated that Class 1 and Class 2 sections should be properly restrained to achieve designed moment resistances as well as rotational capacities.

Moreover, full moment resistances were attained in Sections with lateral torsional slenderness ratios, $\bar{\lambda}_{LT}$ from 0.39 to 0.62. They are larger than the threshold value for buckling check, i.e. $\bar{\lambda}_{LT,0}$ equal to 0.4, as proposed by EN 1993-1-1. Therefore, it may be more efficient to modify the design criteria for partially restrained beams of S690 welded I-sections.

4.5.3.3 Strain readings

A total of 8strain gauges, namely SG1 to SG8, were used to measure development yielding across the sections. And strain gauges SG9 and SG10 were mounted to detect any minor-axis bending of the top flanges owing to lateral torsional buckling. Measured strain readings across section depth at failure are plotted in Figures 4.18 and 4.19. Yield strain levels of the steel plates are marked against the strain readings for easy reference. Moreover, key strain parameters calculated from direct measurements are listed in Tables 4.13 and 4.16 with their definitions as followings:

- $\varepsilon_{u.tf}$: denotes average compressive strains on top flanges which are the averaged strains of the readings of SG1 and SG2;

- $\varepsilon_{u.bf}$: denotes averaged tensile strains on bottom flanges which are the averaged strains of the readings of SG7 and SG8;
- ϕ_{mz} : $\phi_{mz} = |\varepsilon_9 - \varepsilon_{10}| / (b - 20)$ (Eq. 4.1)

  denotes minor-axis bending curvature, which is the absolute difference between SG9 and SG10 over the distance between mounted strain gauges.

For Series LT1, plasticity was generally detected in top flanges of all six sections according to $\varepsilon_{u,tf}$. For sections which attained full moment resistances, absolute differences between $\varepsilon_{u,tf}$ and $\varepsilon_{u,bf}$ should be larger than ($2\varepsilon_y$) which is about 0.7%. Similar behaviour was also observed in Series LT2. Therefore, it is realized that development of section plasticity is limited in partially restrained beams which fail prematurely owing to lateral torsional buckling.

Minor-axis bending curvature ϕ_{mz} was utilized by previous researchers to indicate occurrence of lateral torsional buckling (Kubo and Fukumoto, 1988). Through a study on all the beams in Series LT1, it is revealed that ϕ_{mz} is significantly larger when compared with those sections which cannot attain full moment resistances due to lateral torsional buckling.

4.5.4 Summary

4.5.4.1 Comparison among tests of Series LT0, LT1 and LT2

Comparison on moment resistances of all the beams of welded I-sections in three different test series is presented in Table 4.17. Full moment resistances of these beams with six different cross-sections were also provided for direct comparison with measured moment resistances. Obviously, for each cross-section, moment resistances of the beams in Series LT0 is the highest, and those from Series LT2 is the lowest among these series.

As those beams in Series LT0 have one more restrained point than those beams in Series LT1, their moment resistances are reasonably higher than sections of Series LT1. The differences of the moment resistances were observed to range from 0 to 15%, which increases with an increment in the lateral torsional slendernesses of partially restrained beams in Series LT1. Typically, Section B1-LT0 possess an identical moment resistance to that of Section B1-LT1, because lateral torsional buckling occurred only after full moment resistance in the beam was attained. Moreover, when lateral torsional slendernesses exceeds 0.5, full moment resistances may not be achieved because of lateral torsional buckling.

Measured moment resistance ratios, M_{Rt} / $M_{pl,Rd}$, of partially restrained beams in Series LT1 are generally larger than those from Series LT2. This should be attributed to longer critical spans and a removal of vertical stiffeners at section end. These stiffeners increase effective lengths of the critical spans significantly. It is also found that differences between moment resistance ratios may increase with differences between lateral torsional slendernesses of each section. Therefore, the effect of small to large lateral torsional slendernesses on moment resistances of high strength S690 partially restrained beams is clarified. It is realized that presence of lateral restraints and vertical stiffeners are very critical to beams under heavy loads.

4.5.5.1 Design of moment resistances based on section classification rule in EN1993-1-1

In general, the moment resistances of fully restrained beams of S690 welded I-sections can be successfully assessed using the section classification rules stipulated in EN 1993-1-1. More specifically, full moment resistances are readily obtained in Class 1 and Class 2 sections while elastic moment resistances are attained in a Class 3 Section. Rotational capacities of fully restrained beams are also found to be increased with reduced plate slenderness ratios. Hence, the section classification rules in EN 1993-1-1 are applicable to fully restrained beams of S690 welded I-sections.

4.5.5.3 Design of lateral torsional buckling based on buckling curves in EN1993-1-1

According to EN 1993-1-1, partially restrained beams are expected to fail with buckling reduction factors which are higher than those given in curve d. In Figure 4.20, lateral torsional buckling curves given in EN 1993-1-1 are plotted against measured moment resistances of partially restrained beams of both Series LT1 and LT2. Through a direct comparison between measured and designed moment resistances, it is easy to find that curve d is applicable to assess lateral torsional buckling resistances of partially restrained beams of S690 welded I-sections. It should be noted that there is a significant safety margin of the measured buckling resistances of the beams when compared with those design values. This should be attributed to smaller residual stresses in S690 welded I-sections, when compared with those in S355 welded I-sections. Owing to smaller residual stress ratios, section rigidities of these I-sections can be more persistent under heavy loads. Consequently, lateral torsional buckling resistances in S690 welded I-sections are reasonably increased.

4.6 CONCLUSIONS

In this chapter, a systematic experimental investigation into structural behaviour of both fully and partially restrained beams of S690 welded I-sections was successfully conducted, and a total of 18 beams with different loading and support conditions were tested. Residual stresses in these welded I-sections were measured using the ASTM hole-drilling method for subsequent analysis and numerical calibration. Key conclusions from the tests are presented as follows:

- *Measurement of residual stresses in S690 welded I-sections*

Through the hole-drilling method, residual stresses in S690 welded I-sections were successfully measured. High tensile residual stresses were measured on flange-web junctions while small compressive residual stresses were measured on the flange and web plates. Comparison between residual stresses given in ECCS and measured values in the tests was carried out. It was found that recommended residual stress values are much higher. Hence, direct application of the ECCS patterns to S690 welded I-sections is not applicable as the adverse effect from residual stresses to structural behaviour of high strength S690 beams can be over-estimated.

- *Fully restrained beams of S690 welded I-section*

In order to study local buckling in fully restrained beams of S690 welded I-sections, a test programme with six beams were successfully conducted. Key conclusions of the experimental investigation are presented as follows:

1. Based on measured moment resistances, fully restrained beams of S690 welded I-sections with Class 1 and Class 2 sections are able to mobilize their full moment resistances while fully restrained beams of S690 welded I-sections with Class 3 sections are able to mobilize their elastic moment resistances.
2. Strength enhancement at over 5% of the full moment resistances was attained in Class 1 and Class 2 sections, and it increases with reduced slendernesses of plate elements.

3. Section classification rules given in EN 1993-1-1 are applicable to assess moment resistances of fully restrained beams of S690 welded I-sections.

- *Partially restrained beams of S690 welded I-sections*

In order to study lateral torsional buckling of partially restrained beams of S690 welded I-sections, a test programme with two test series of twelve beams were successfully conducted. Based on these tests, it is concluded that:

1. Lateral torsional buckling occurs in those beams without sufficient lateral restraints, and buckling resistances are found to increase with reduced lateral torsional slendernesses.
2. Full moment resistances can only be attained in those partially restrained beams which possess sufficiently small lateral torsional slendernesses.
3. Lateral torsional buckling curve d given in EN 1993-1-1 is applicable to assess lateral torsional buckling resistances of beams of high strength S690 welded I-sections.

It should be noted that a significant margin between measured buckling resistances and design values is found through a direct comparison on the test results. Hence, a higher lateral torsional buckling curve may be used in design to achieve an improved structural efficiency for S690 partially restrained beams. This should be attributed to reduced residual stress ratios in S690 welded I-sections, when compared with conventional S355 welded I-sections.

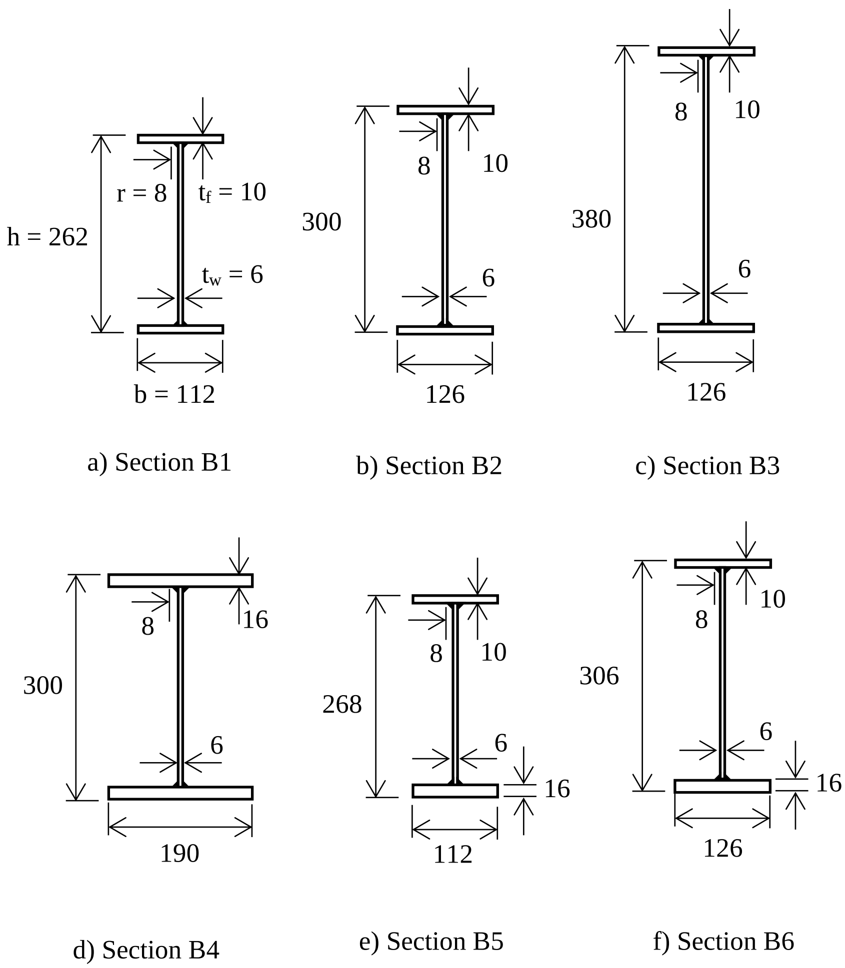

Figure 4.1: Cross-sectional dimensions of high strength S690 welded I-sections

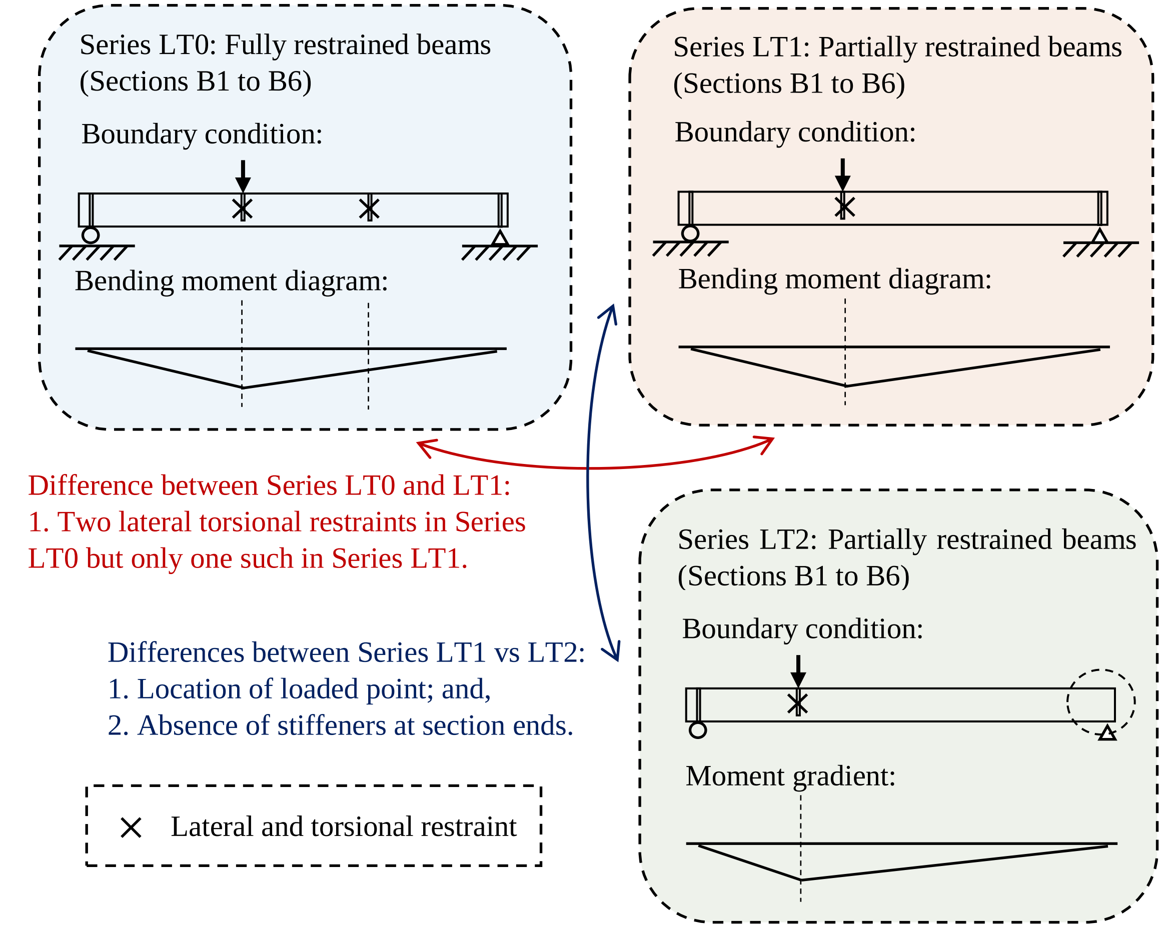

Figure 4.2: Differences among test series of beams of S690 welded I-sections

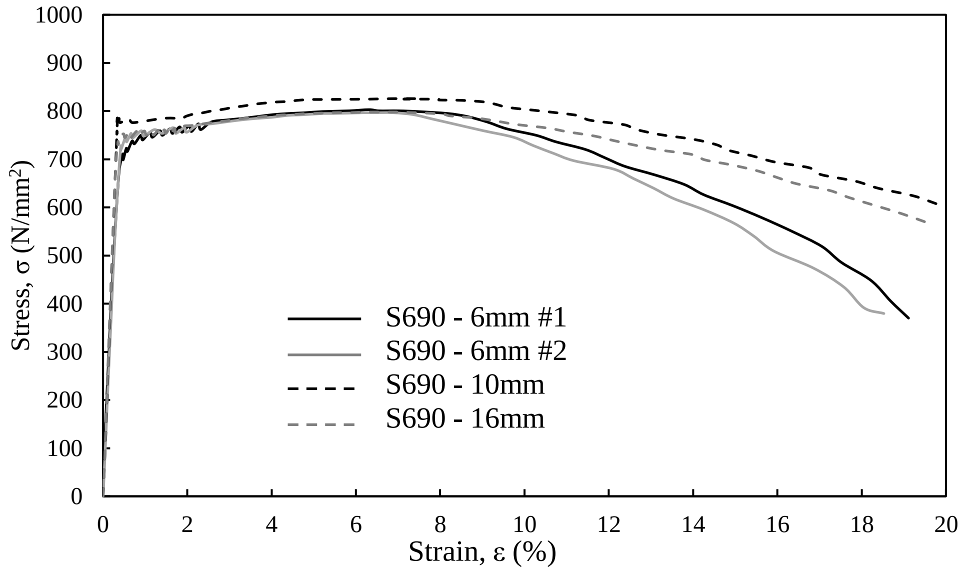

(a) Engineering stress strain curves

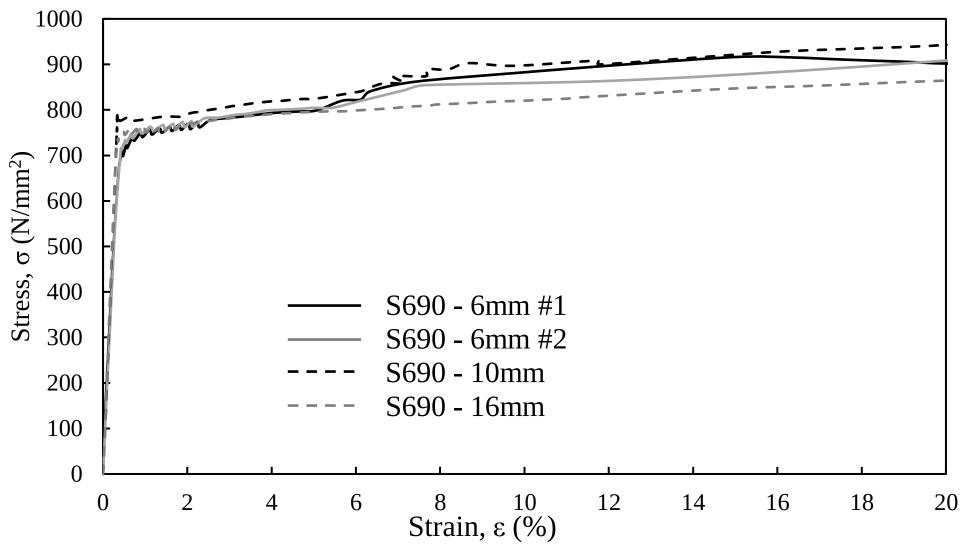

(b) True stress strain curves

Figure 4.3: Typically measured stress strain relationship of S690 steel

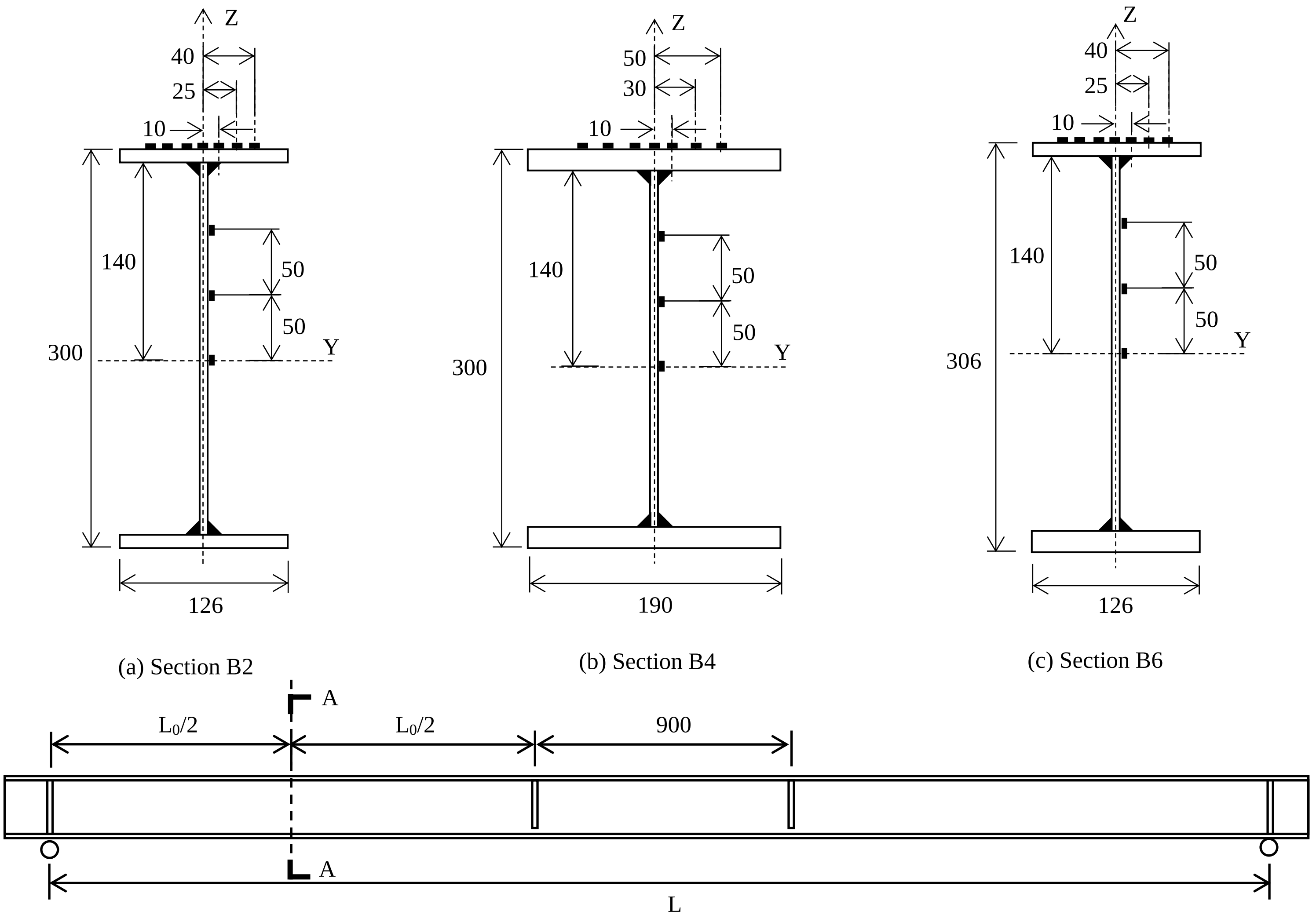

(a) Section B2

(b) Section B4

(c) Section B6

(d) Typical section A-A for residual stress measurement

Figure 4.4: Test programme of residual stress measurement on S690 welded I-sections

(a) Installation of a high-speed RS-200 milling guide

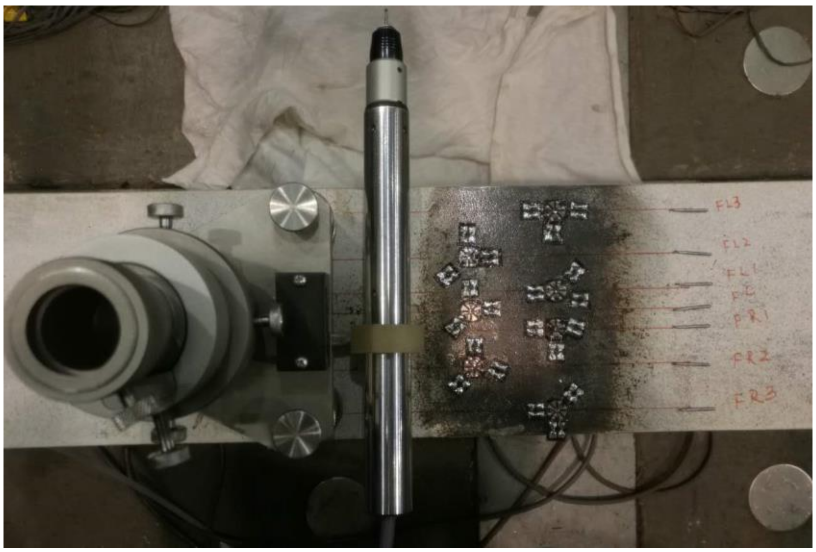

(b) Hole-drilling apparatus, staggered rosettes and used drill bits

Figure 4.5: Test setup for residual stress measurement of S690 welded I-sections

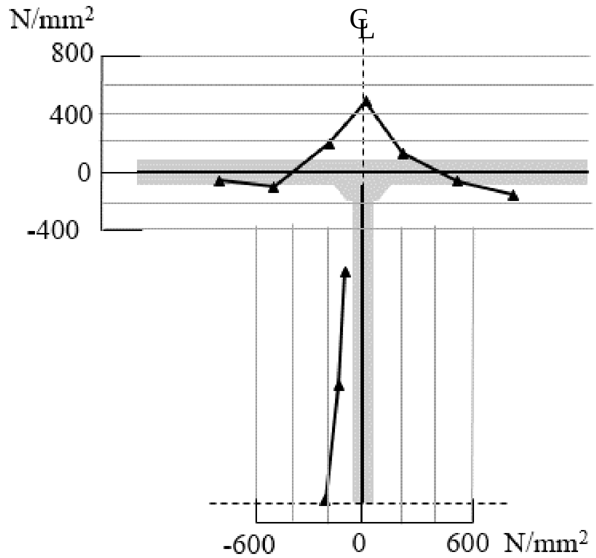

(a) Section B2

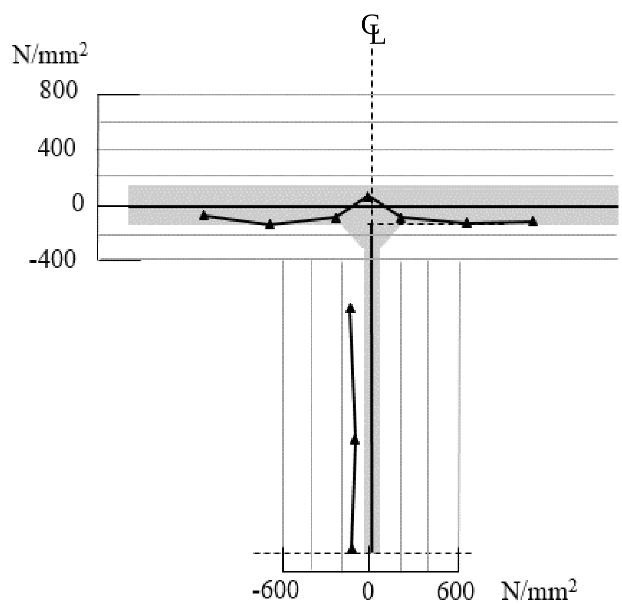

(b) Section B4

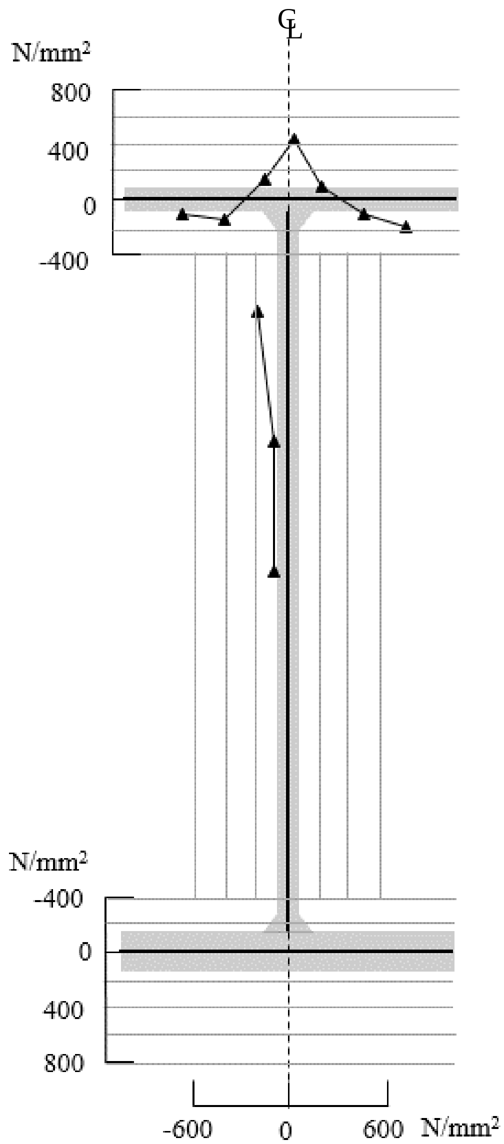

(c) Section B6

Figure 4.6: Measured residual stress patterns of welded I-sections

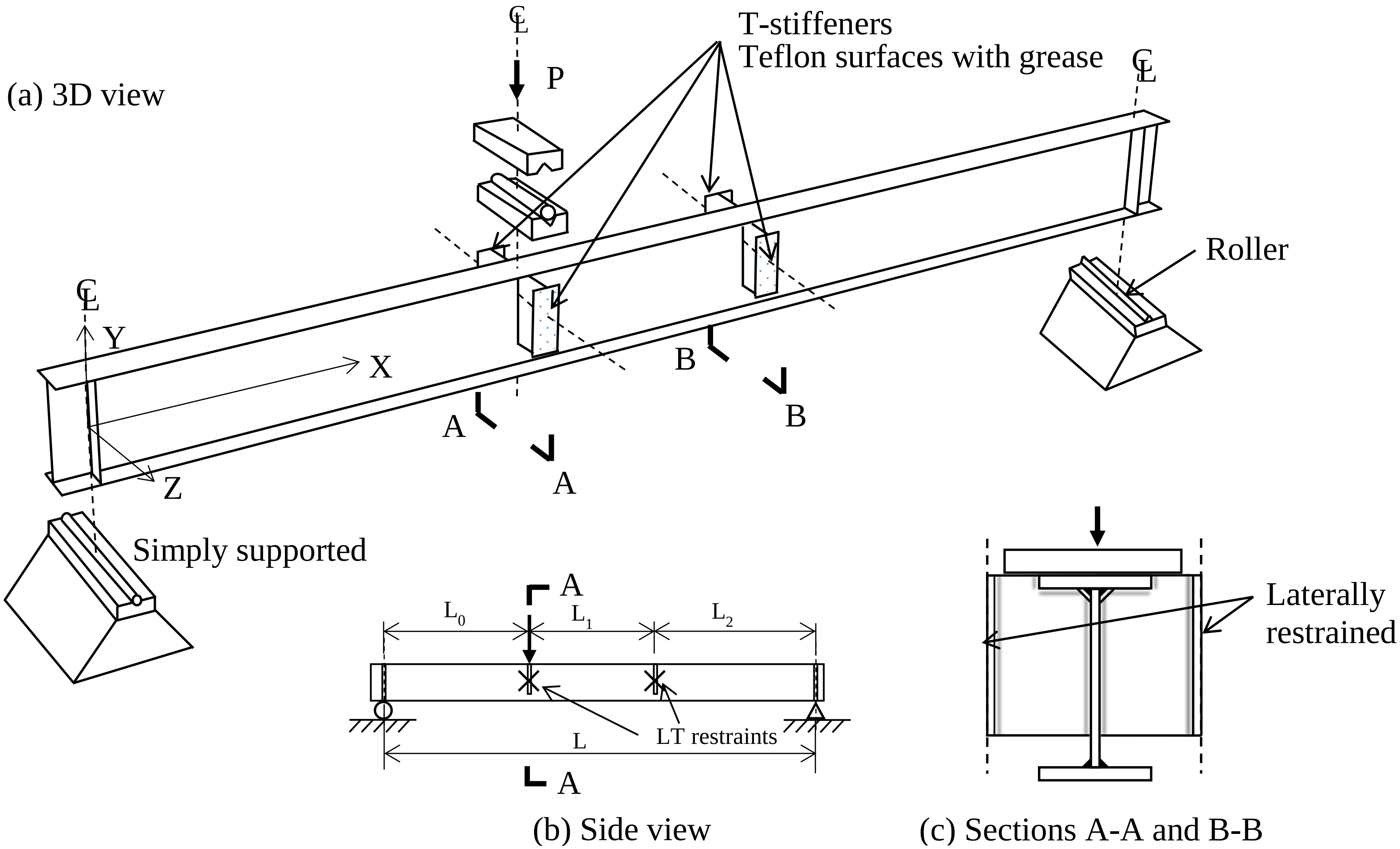

Figure 4.7: Loading and support conditions of fully restrained beams of Series LT0

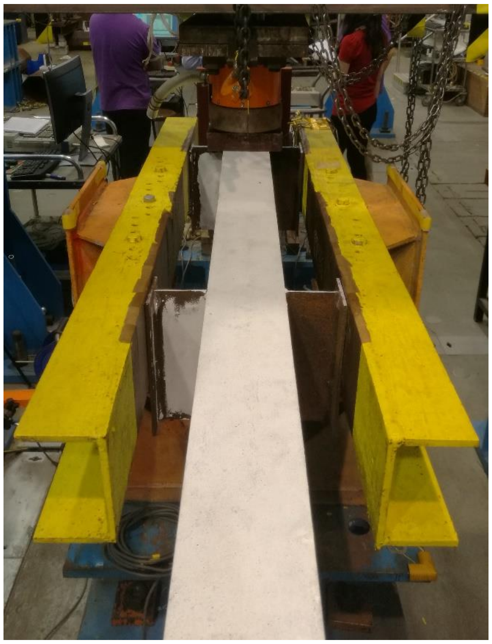

(a) Longitudinal view

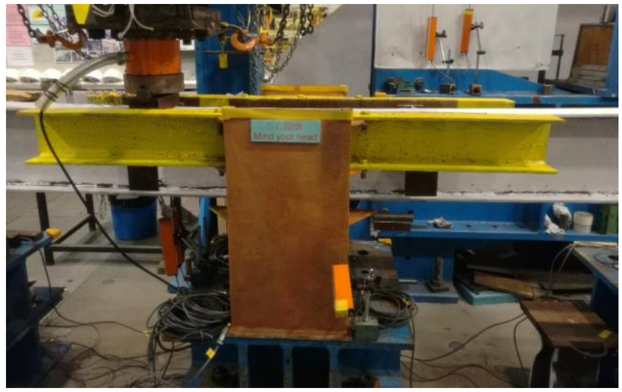

(b) Side view

(c) 3-D view

Figure 4.8: A restraining system to provide effective lateral and torsional restraints

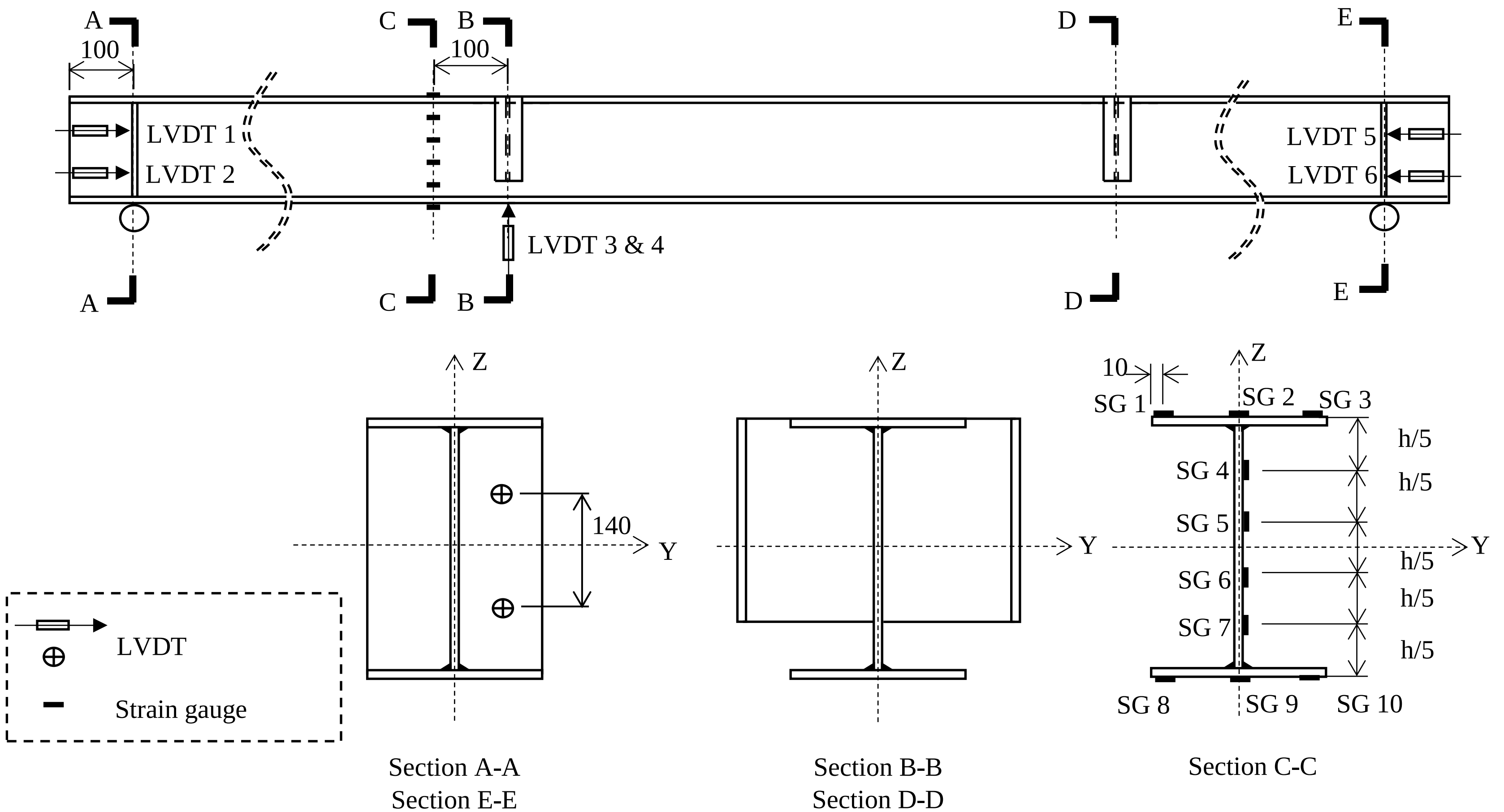

Figure 4.9: Instrumentation in fully restrained beams of Series LT0

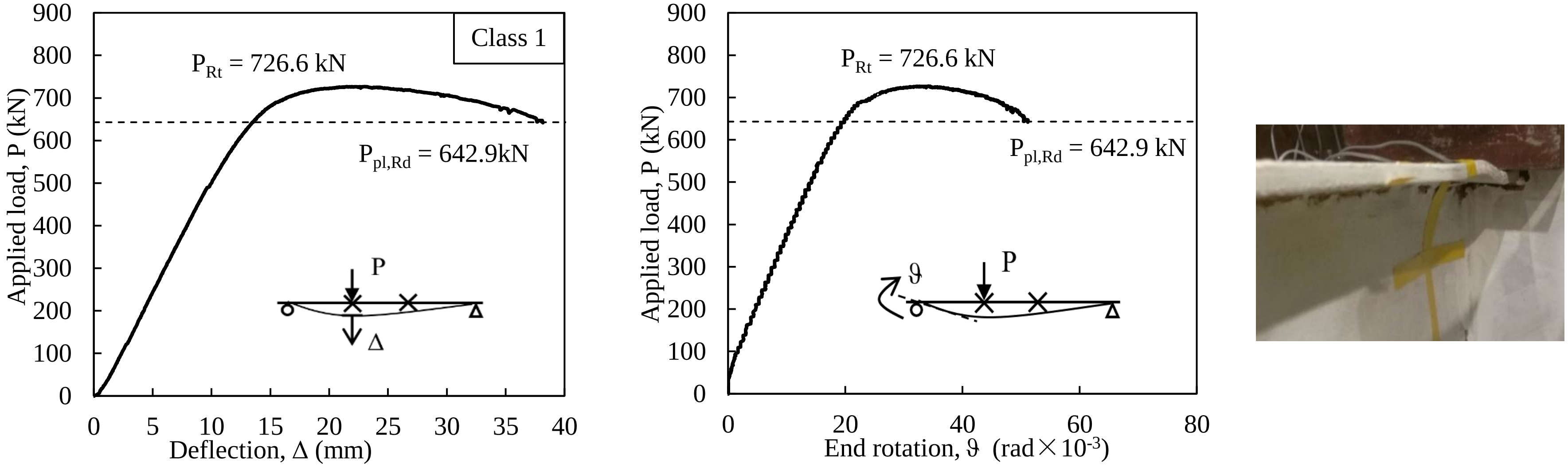

(a) Beam B1-LT0

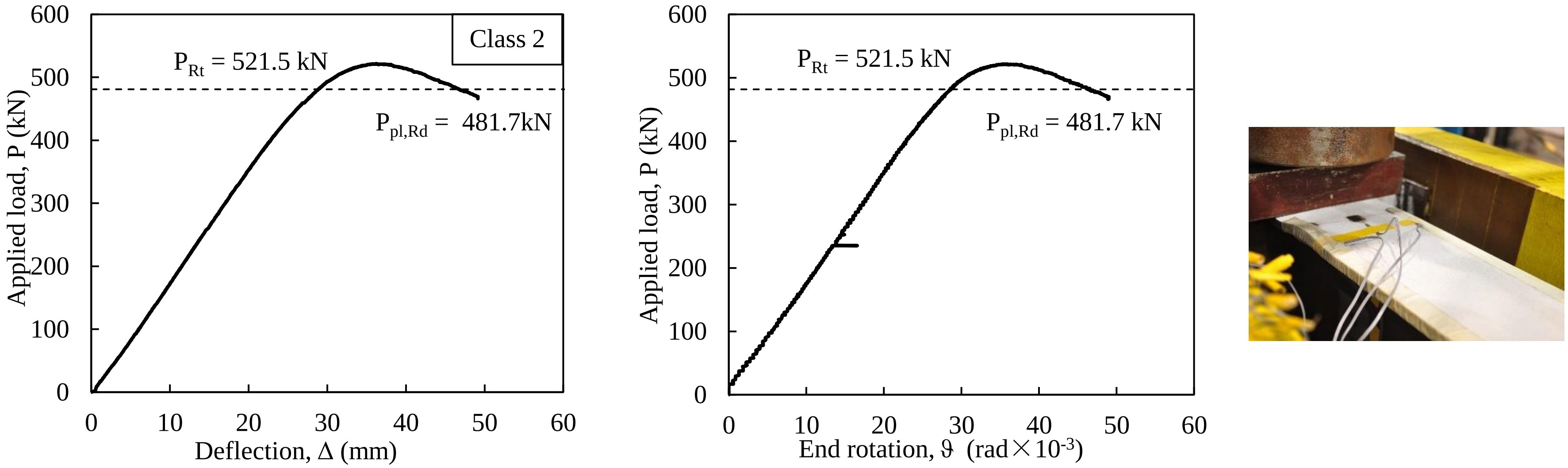

(b) Beam B2-LT0

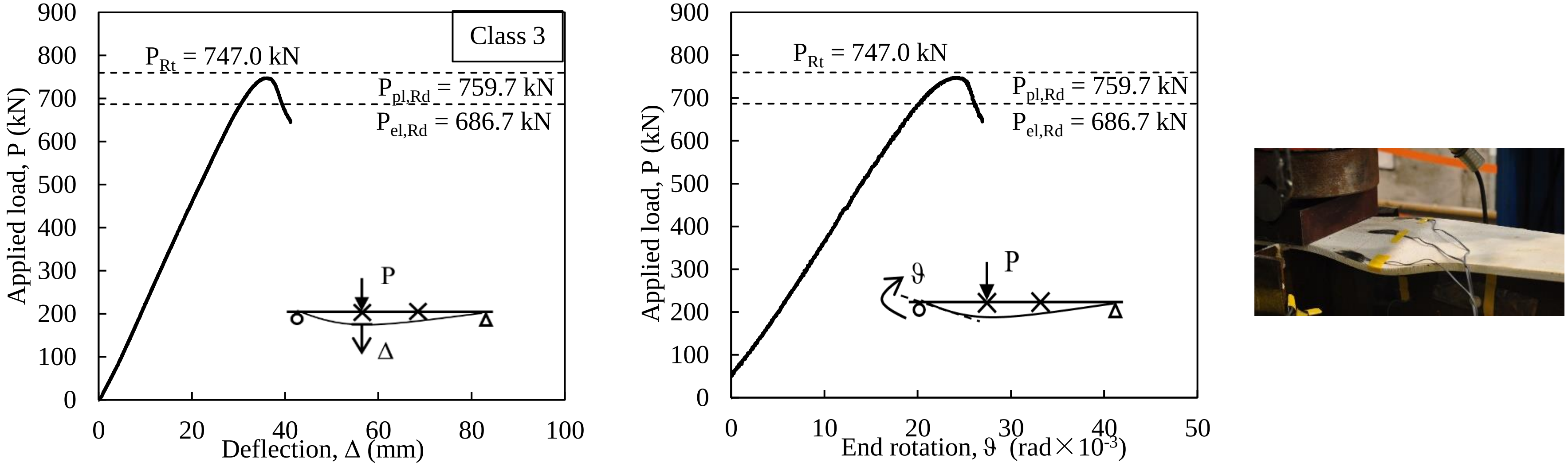

(c) Beam B3-LT0

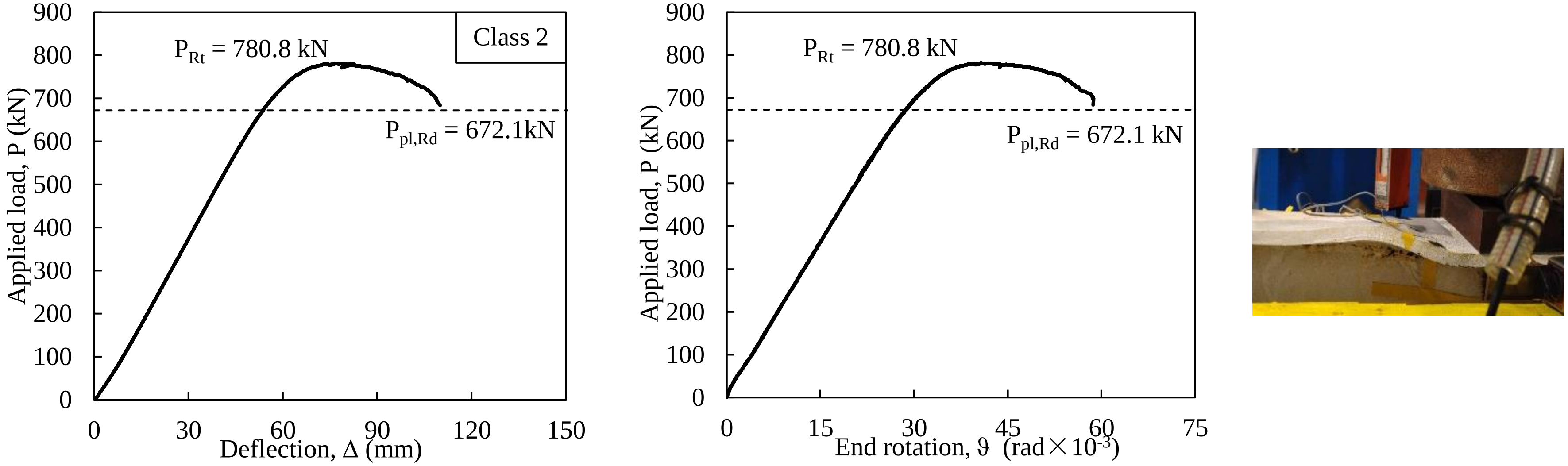

(d) Beam B4-LT0

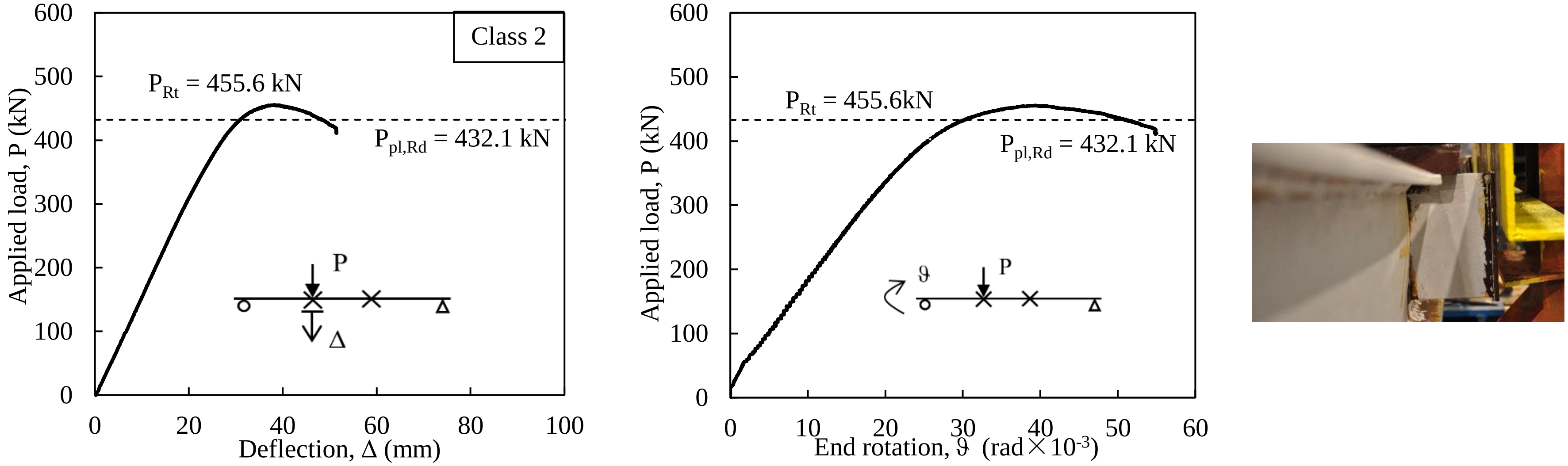

(e) Beam B5-LT0

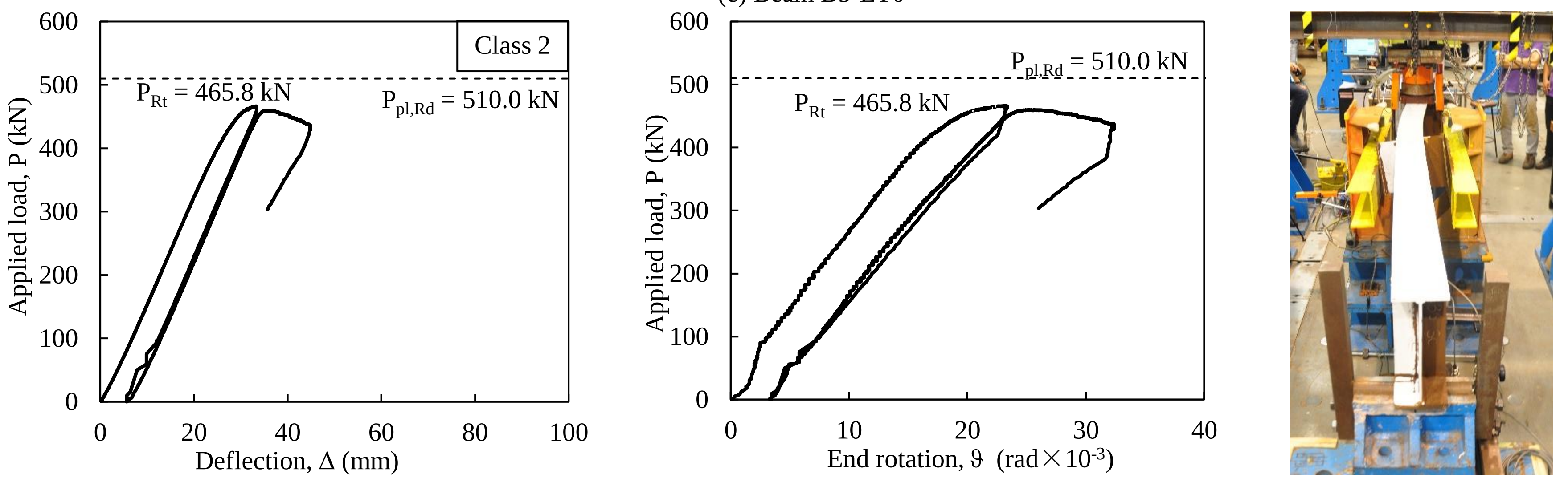

(f) Beam B6-LT0

Figure 4.10: Load deformation curves of fully restrained beams of S690 welded I-sections - Series LT0

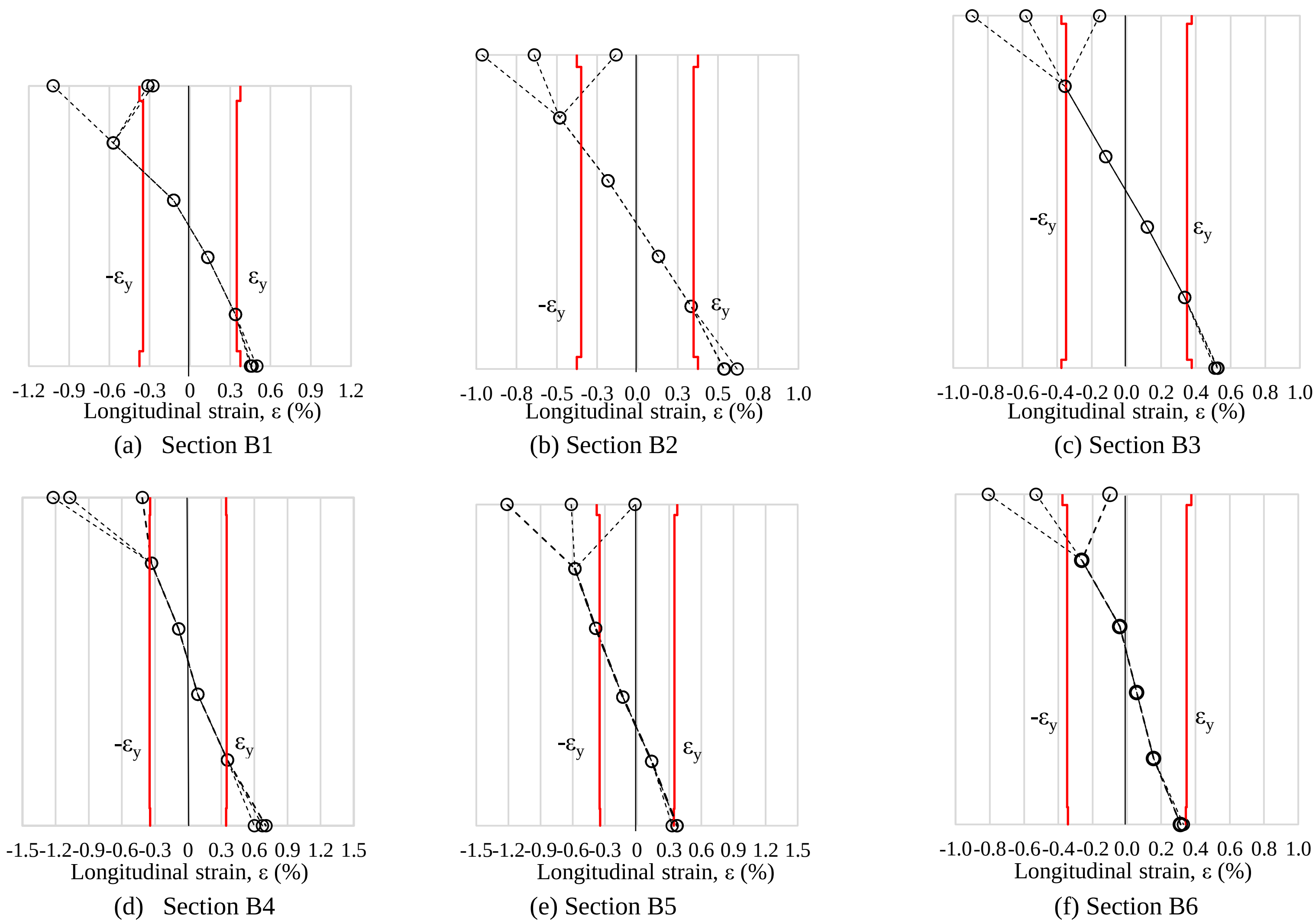

Figure 4.11: Cross-sectional strains measured at failure across section depth in Series LT0

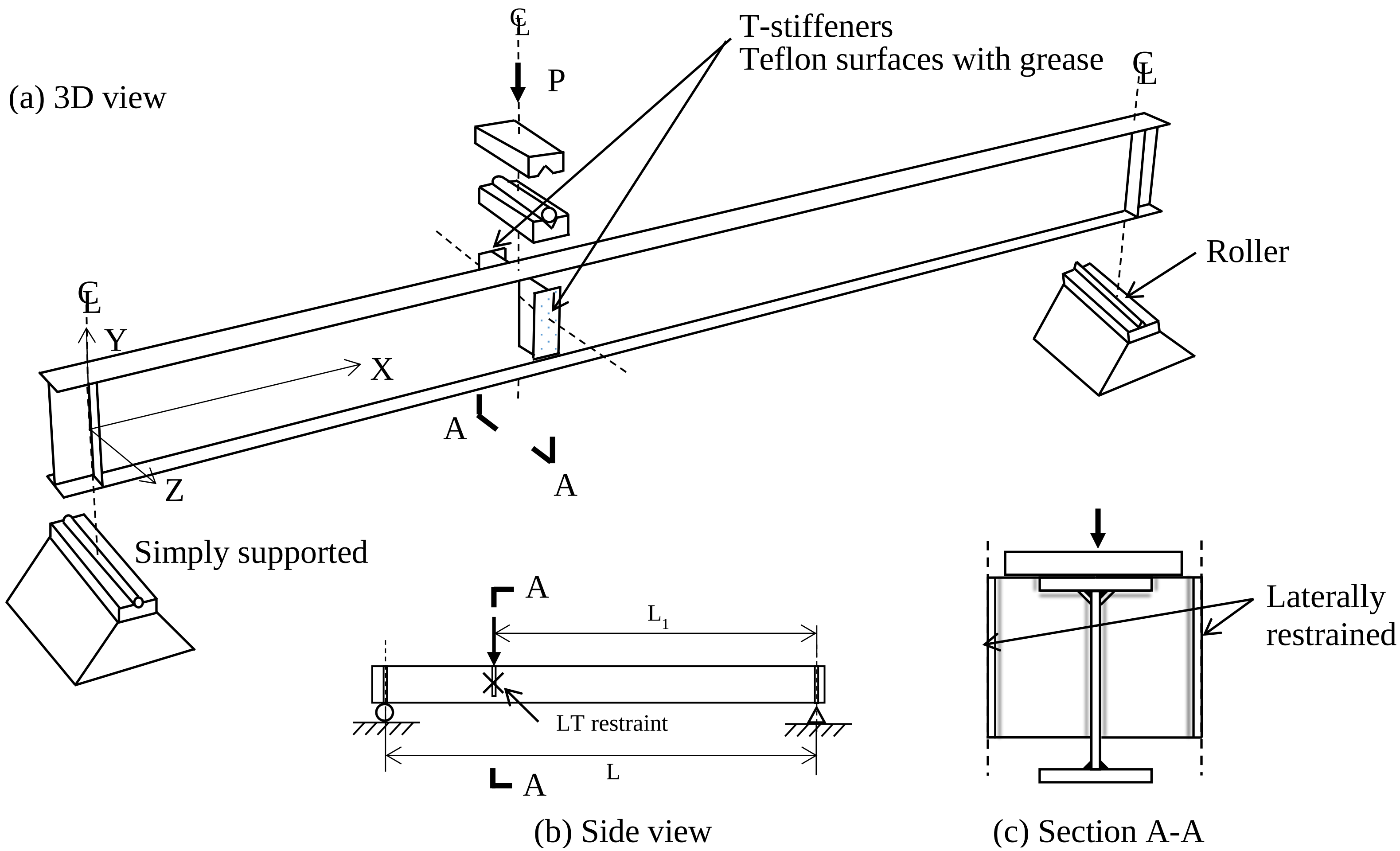

Figure 4.12: Loading and support conditions of partially restrained beams of Series LT1

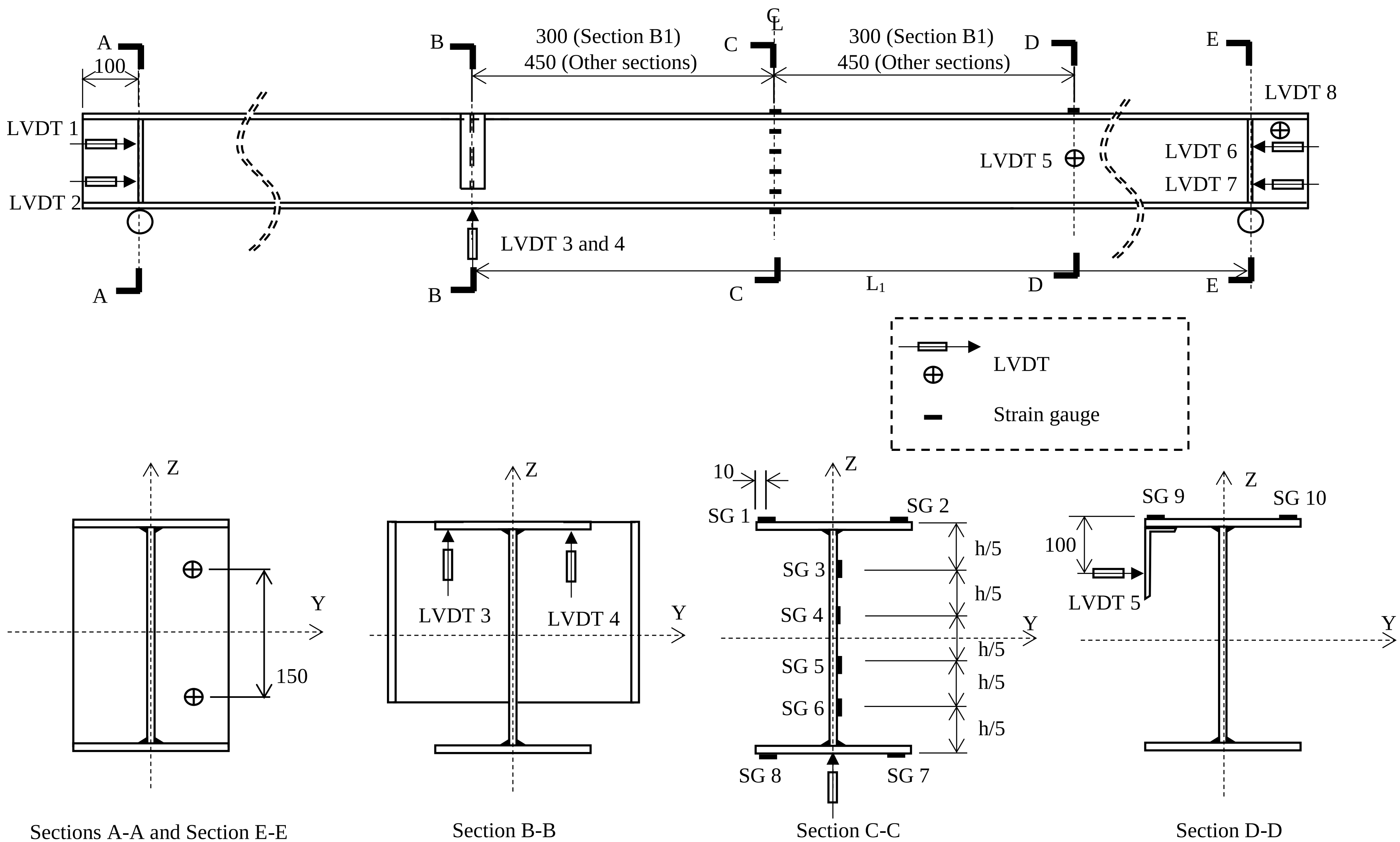

Figure 4.13: Instrumentation in partially restrained beams of Series LT1

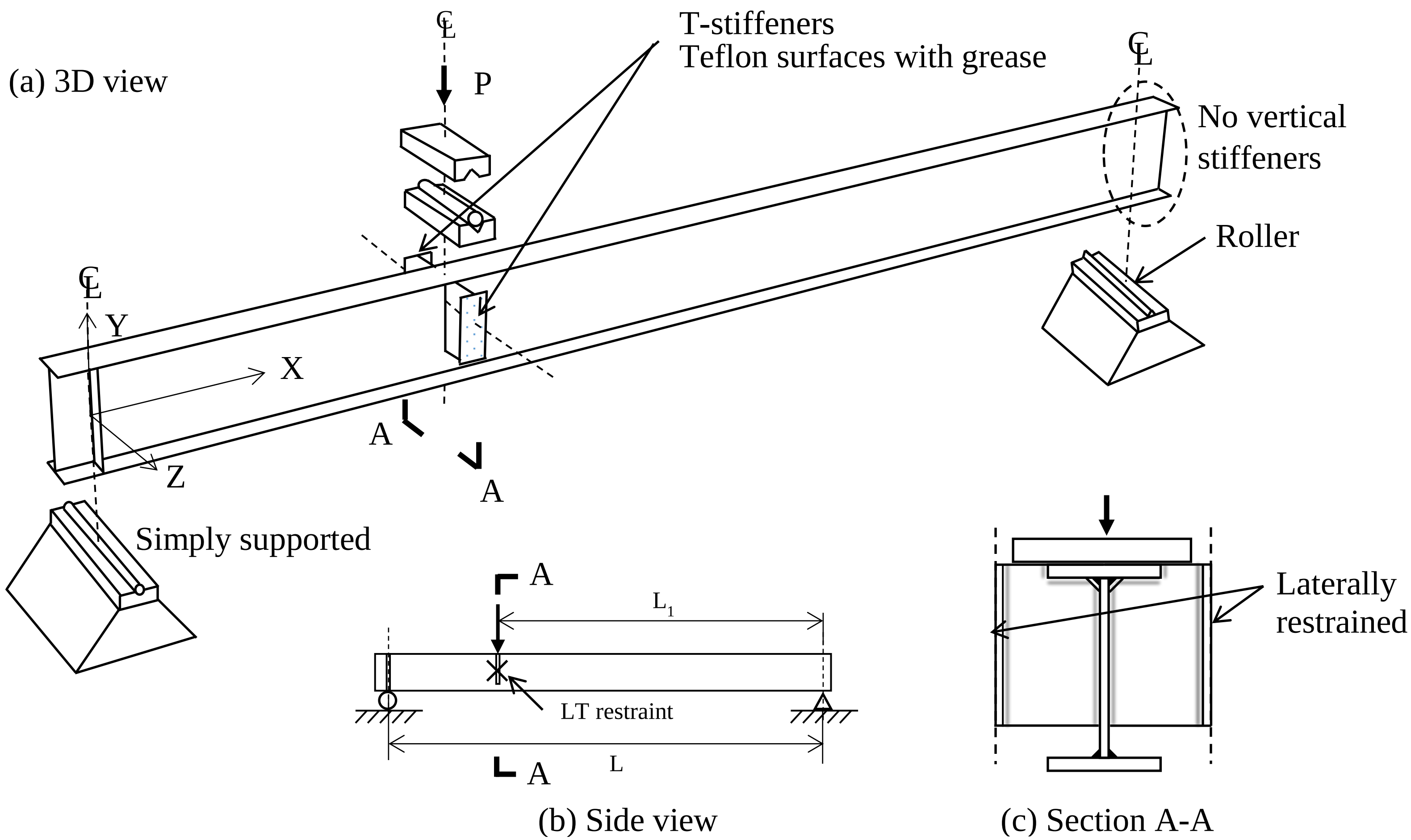

Figure 4.14: Loading and support conditions of partially restrained beams of Series LT

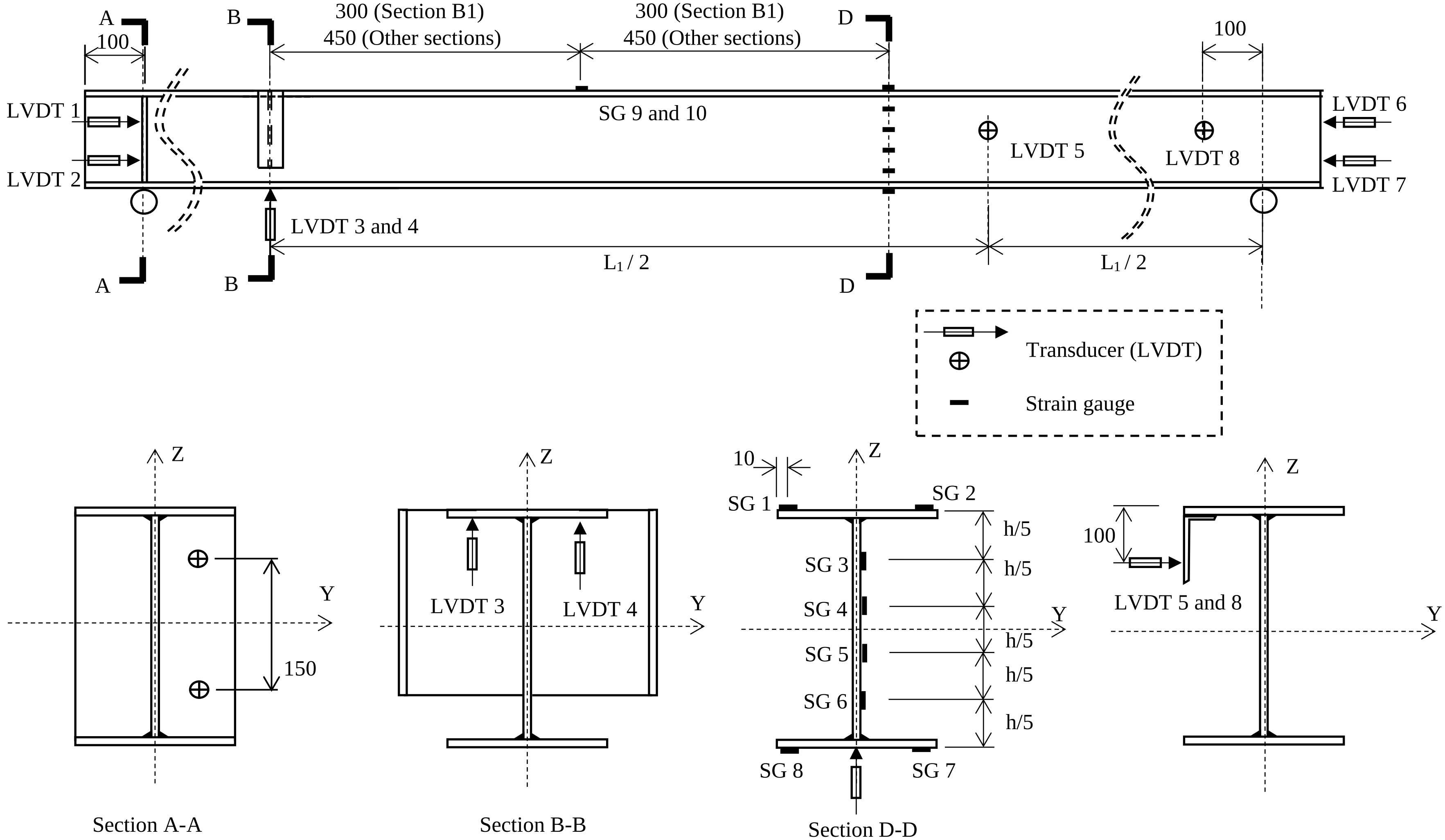

Figure 4.15: Instrumentation of partially restrained beams of Series LT2

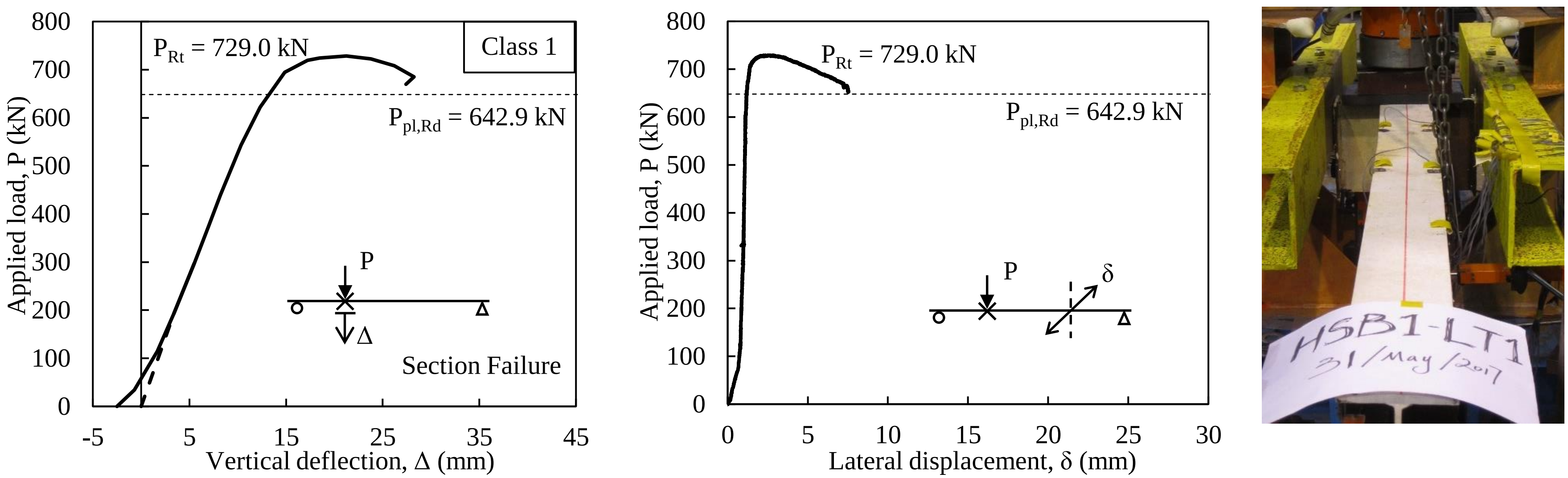

(a) Beam B1-LT1 ($\bar{\lambda}_{LT} = 0.39$)

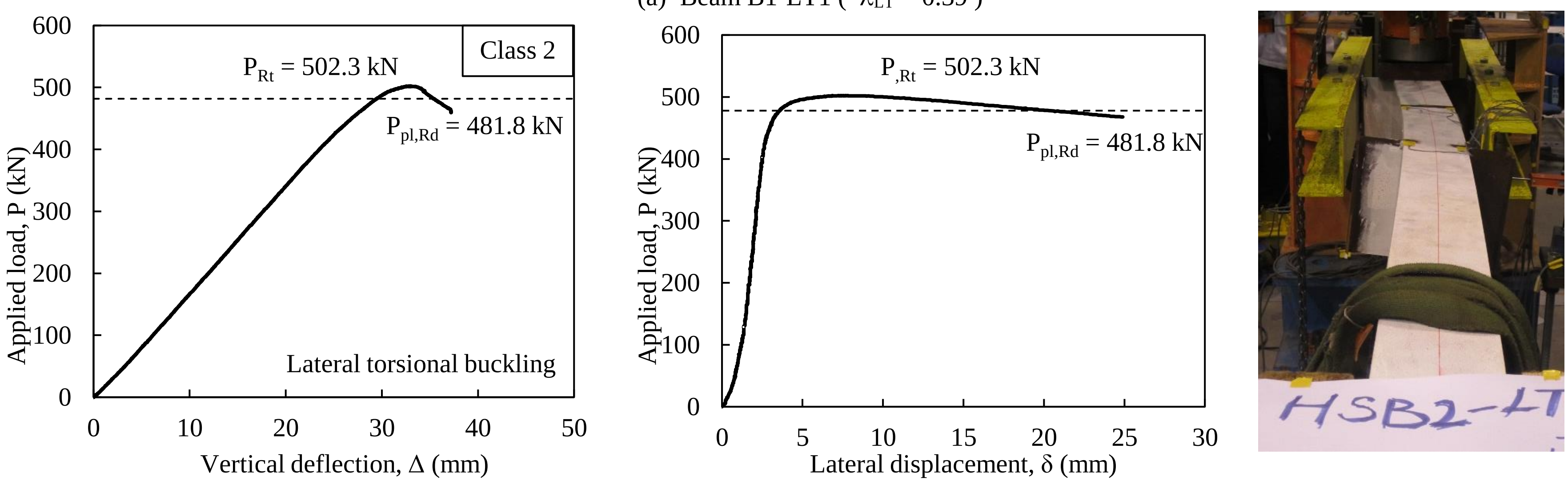

(b) Beam B2-LT1 ($\bar{\lambda}_{LT} = 0.54$)

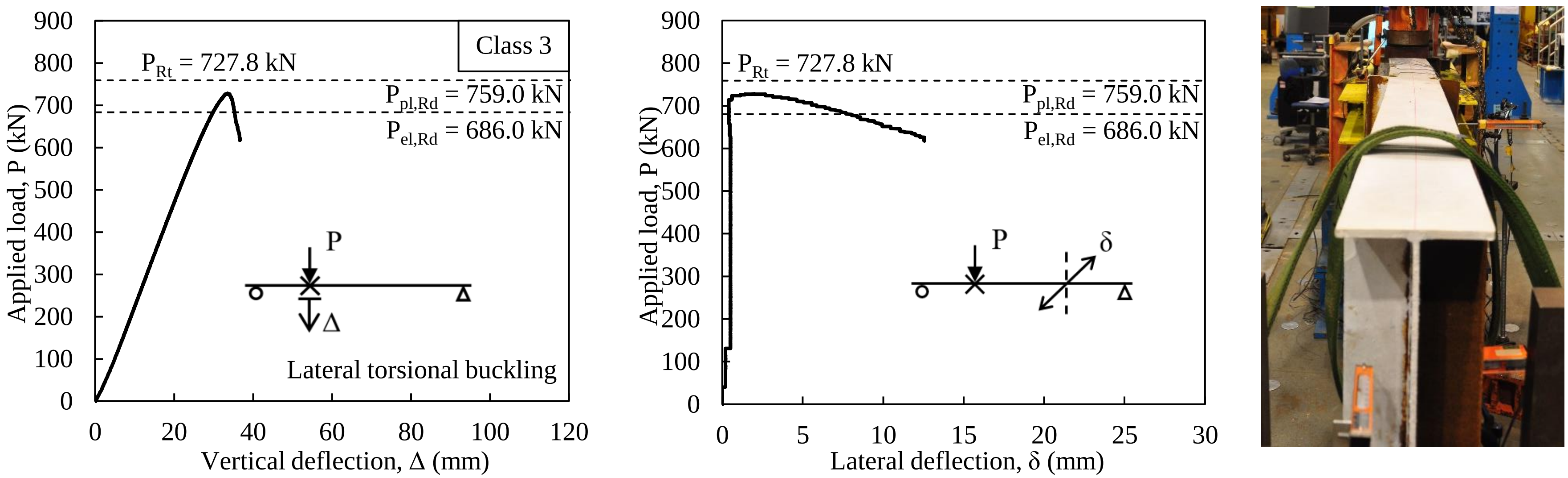

(c) Beam B3-LT1 ($\bar{\lambda}_{LT}$ = 0.66)

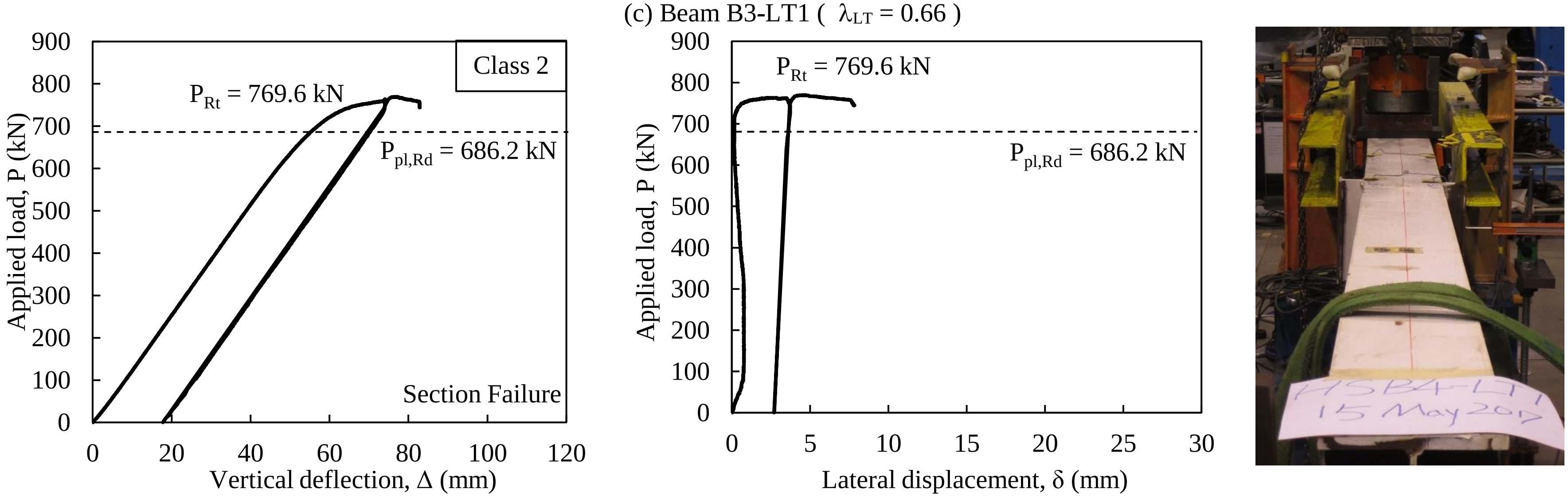

(d) Beam B4-LT1 ($\bar{\lambda}_{LT}$ = 0.47)

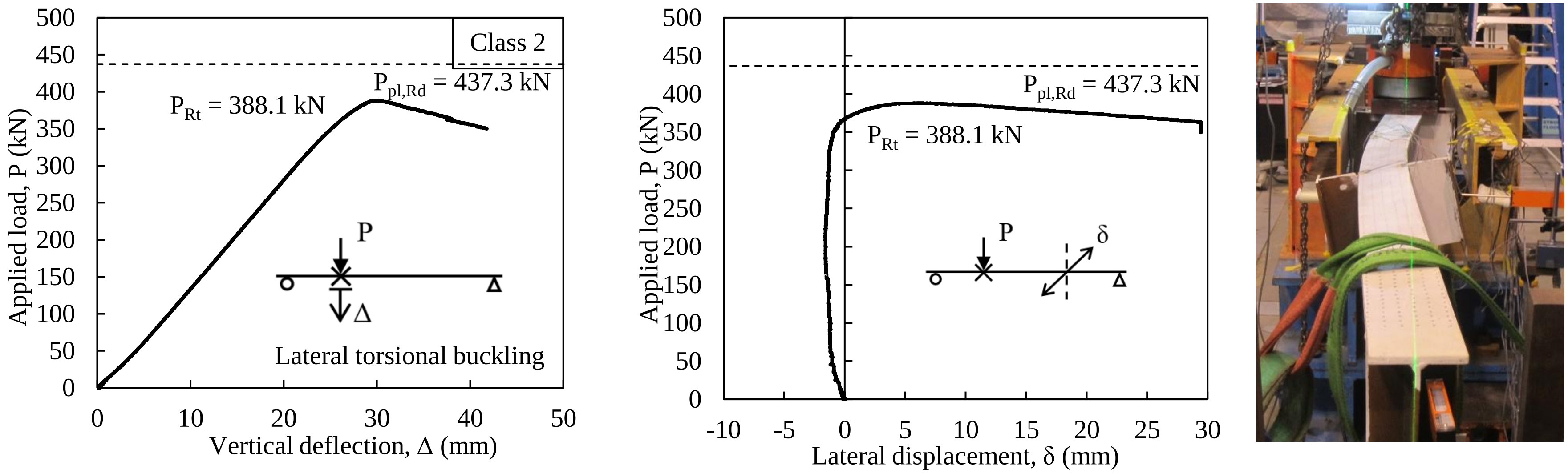

(e) Beam B5-LT1 ($\bar{\lambda}_{LT} = 0.77$)

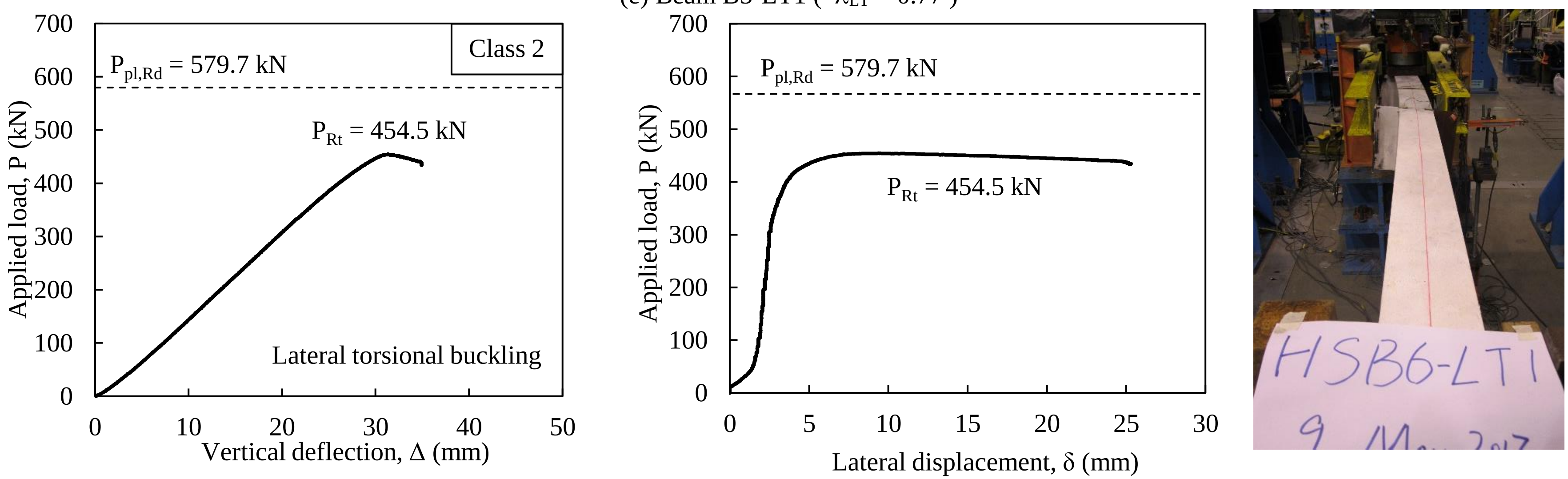

(f) Beam B6-LT1 ($\bar{\lambda}_{LT} = 0.75$)

Figure 4.16: Load deformation curves of Series LT1

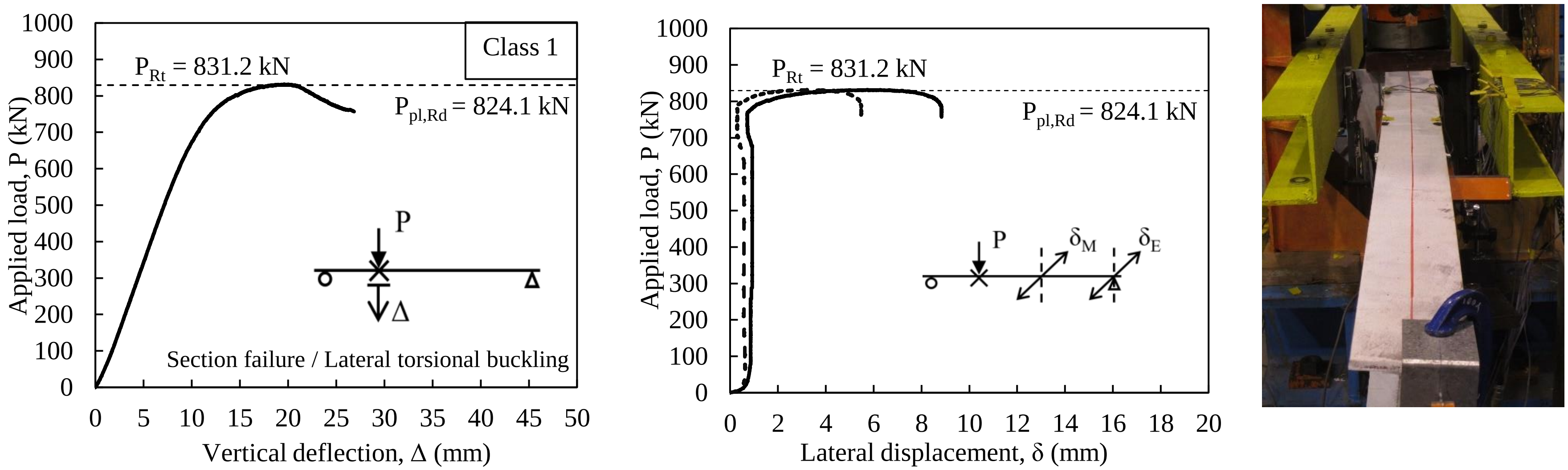

(a) Beam B1-LT2 ($\bar{\lambda}_{LT}$ = 0.62)

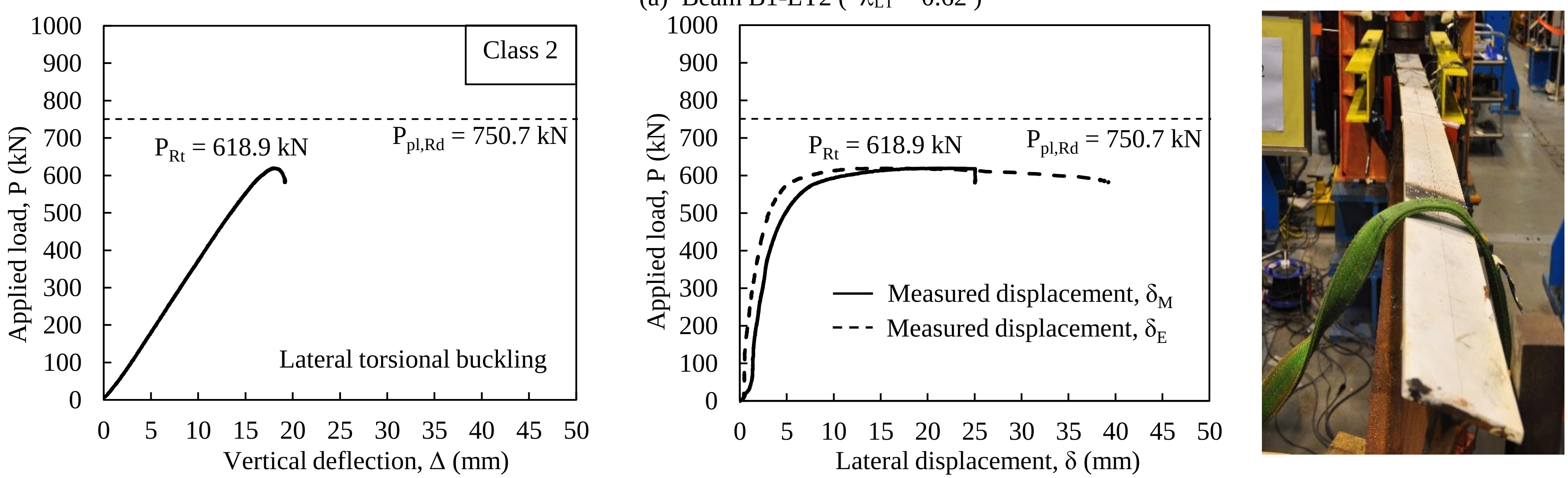

(b) Beam B2-LT2 ($\bar{\lambda}_{LT}$ = 0.62)

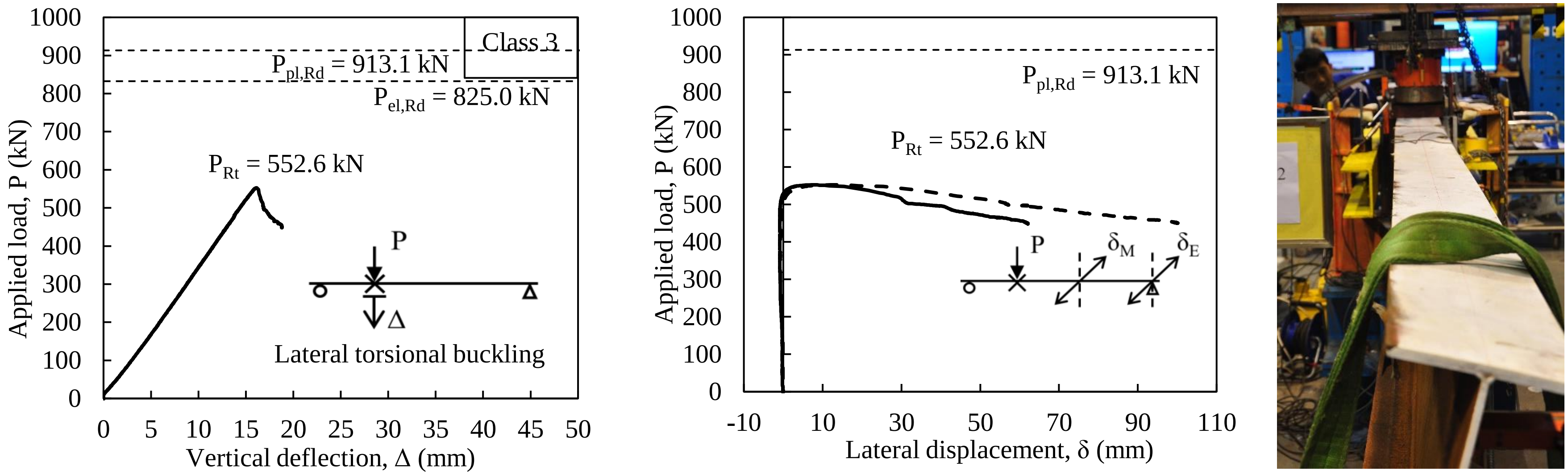

(c) Beam B3-LT2 ($\bar{\lambda}_{LT}$ = 1.23)

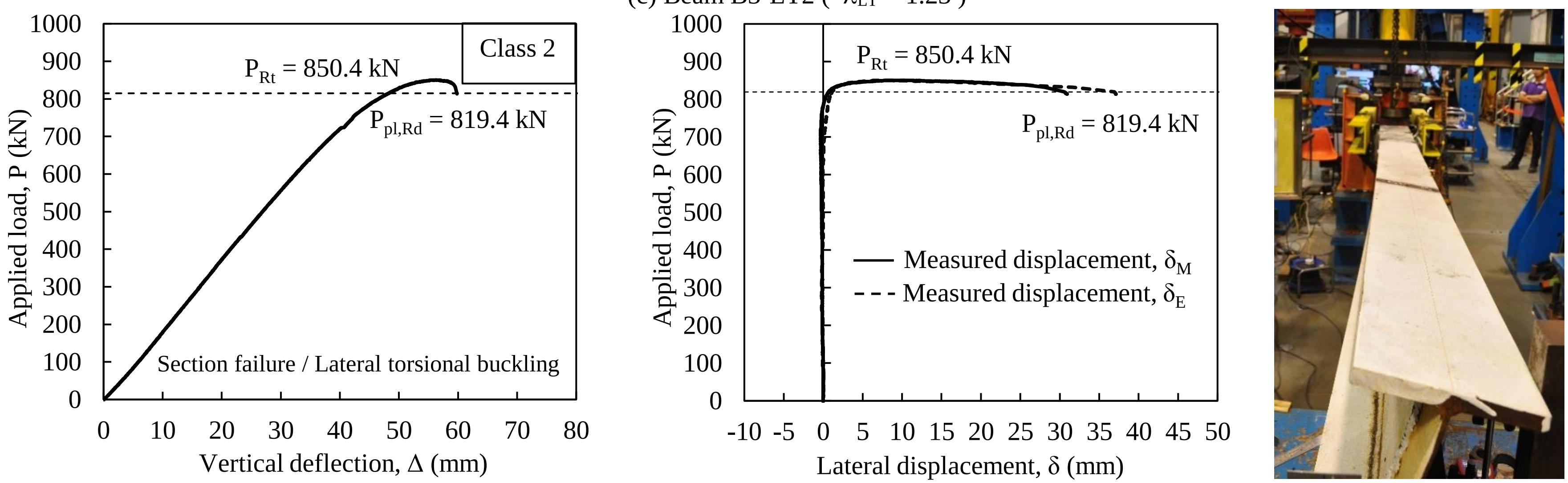

(d) Beam B4-LT2 ($\bar{\lambda}_{LT}$ = 0.52)

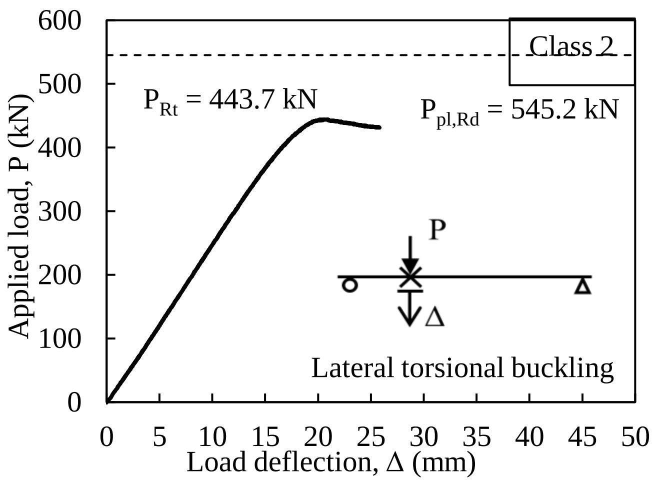

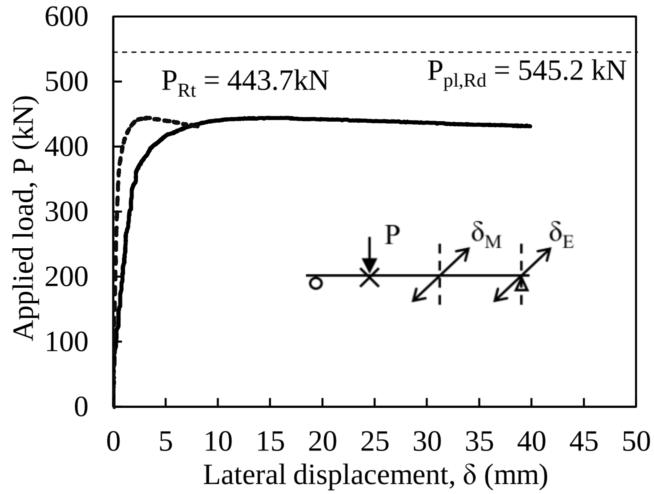

(e) Beam B5-LT2 ($\bar{\lambda}_{LT} = 0.89$)

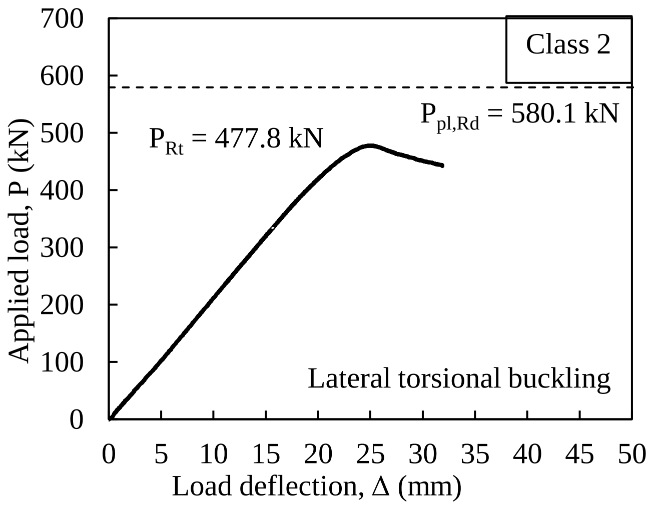

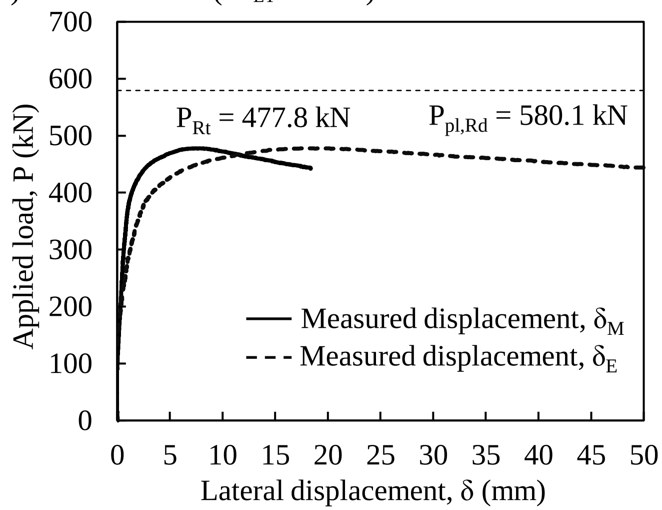

(f) Beam B6-LT2 ($\bar{\lambda}_{LT} = 0.97$)

Figure 4.17: Load deformation curves of Series LT2

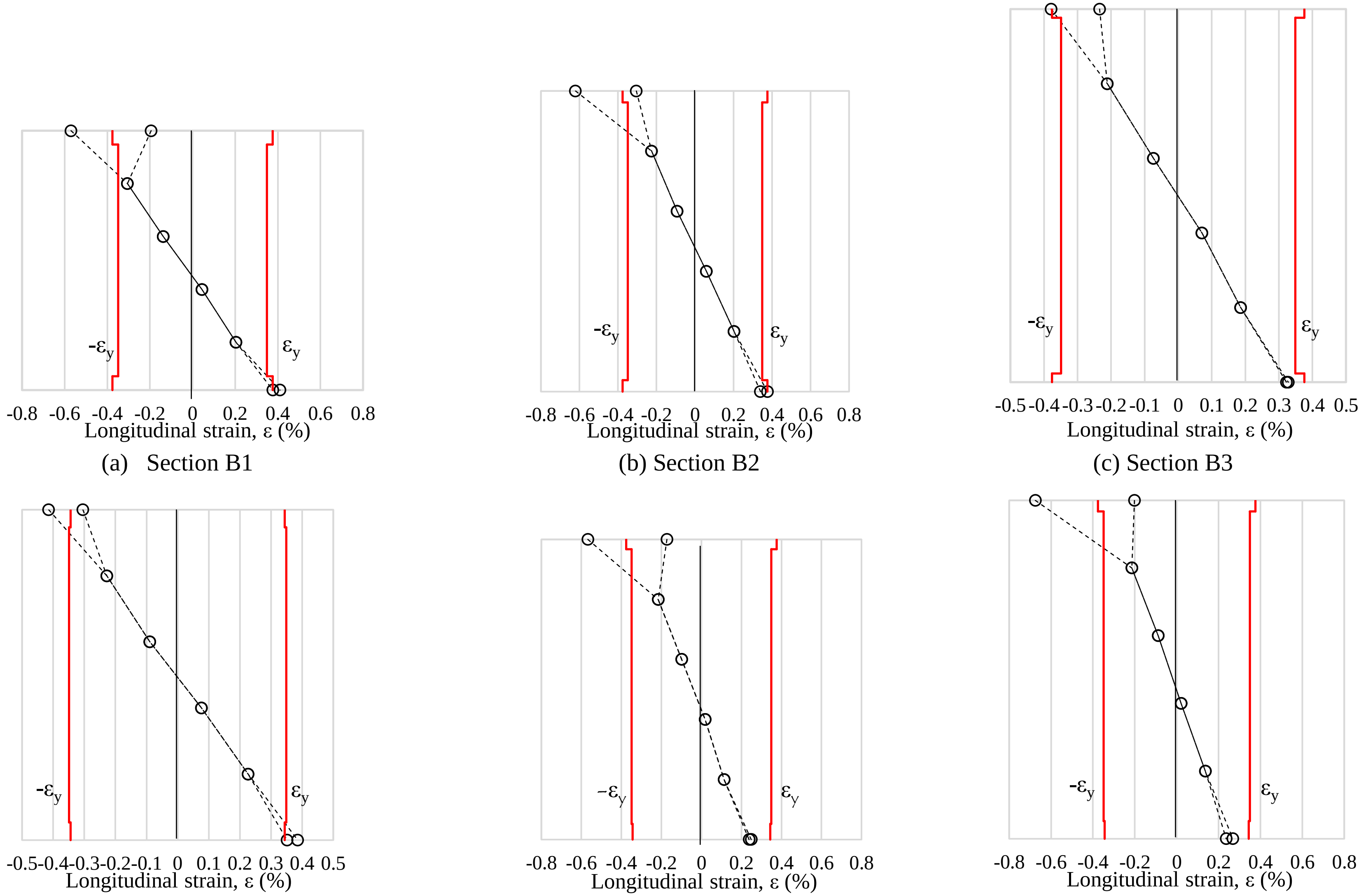

(a) Section B1 (b) Section B2 (c) Section B3

(d) Section B4 (e) Section B5 (f) Section B6

Figure 4.18: Cross-sectional strains measured at failure across section depth in sections of Series LT1

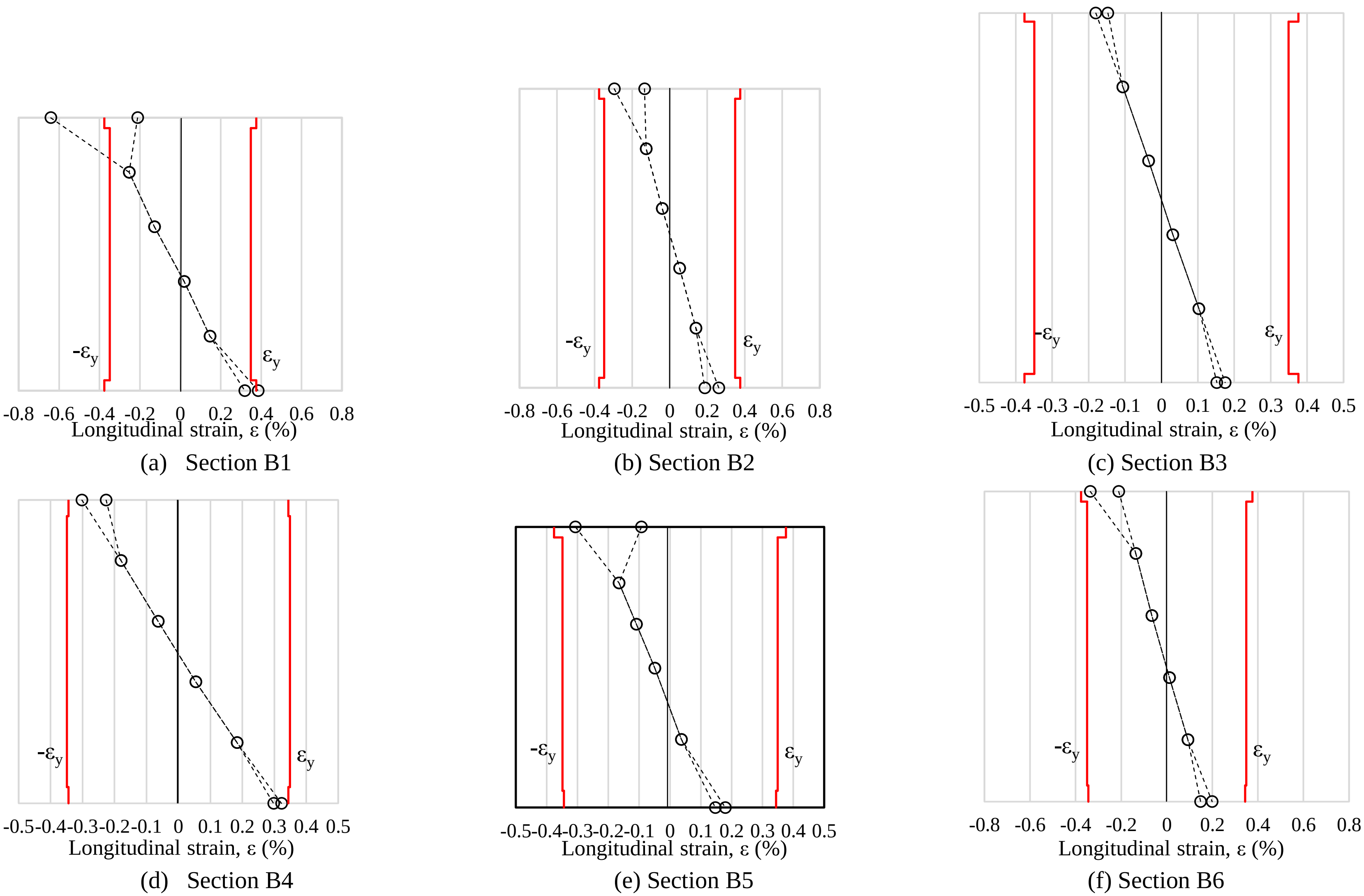

Figure 4.19: Cross-sectional strains measured at failure across section depth in sections of Series LT2

Figure 4.20: Observed local buckling in top flange of Section B3 of Series LT1

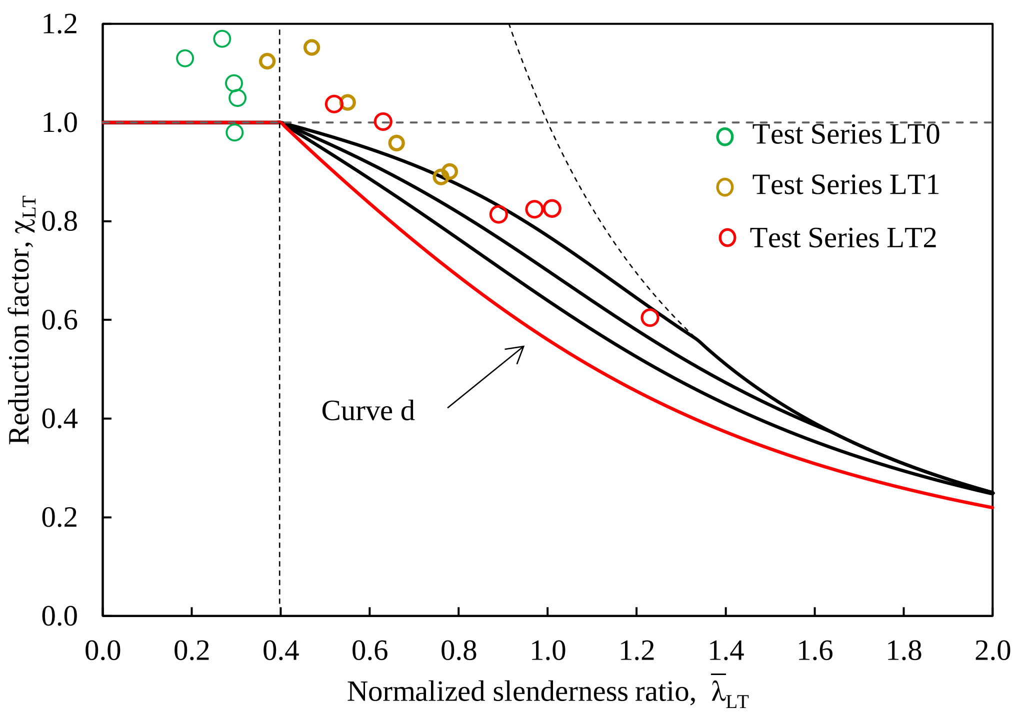

Figure 4.21: Reduction factors for beam buckling in EN 1993-1-1

Table 4.1: Key parameters of coupon test results

Plate thickness		Yield Strength f_y (N/mm^2)	Tensile strength f_u (N/mm^2)	Young's modulus E (kN/mm^2)	Strain at tensile strength ε_u (%)	Elongation at fracture ε_L (%)
Beams	**6 mm#1**	723	850	207	6.31	18.5
	6 mm#2	720	843	211	6.41	19.1
	10 mm	784	874	206	7.42	19.8
	16 mm	745	832	216	6.62	19.6

Table 4.2: Measured welded parameters

Specimens		Welding method	Electrode	Welding parameters			
				Voltage U (V)	Current A (I)	Speed v (mm/s)	Line heat energy input* q (kJ/mm)
Beams	**6mm – 10mm T-joints**	GMAW	GM110	28	225	5.3	1.01
	6mm – 16mm T-joints	GMAW	GM110	28	225	4.2	1.28
	10mm – 16mm T-joints	GMAW	GM110	28	225	4.8	1.12

*** Note:**
Since GMAW welding method was adopted in section fabrication, line heat energy is factored with welding efficiency η which equals 0.85 (Pépe et al., 2011).

Table 4.3: Test programme of residual stress measurements

Specimens	Dimensions						Welding parameters		
	h (mm)	b (mm)	t_f (mm)	t_w (mm)	L (mm)	L_{rs} (mm)	Welding method	Pass number	Heat input Energy E (kJ/mm)
B2	300	126	10	6	3300	600	GMAW	One	1.2
B4	300	190	16	6	4500	900	GMAW	One	1.2
B6	306	126	TF: 10 BF: 16	6	3600	675	GMAW	One	Top: 1.2 Bottom: 1.5

Table 4.4. Measured residual stresses of S690 welded I-sections

Section	Residual stress	Top flange: Left --------------------------> Right							Web: Mid -----> Top		
Section B2	Longitudinal stress $f_{1,rs}$ (N/mm^2)	-159	-191	145	400	235	-148	-129	-168	-106	-74
	Transverse stress $f_{3,rs,FE}$ (N/mm^2)	-87	-62	57	-158	-22	-57	-73	-183	-87	-88
	Shear stress $\tau_{rs,FE}$ (N/mm^2)	-15	-5	6	-23	15	9	-1	1	5	7
Section B4	Longitudinal stress $f_{1,rs}$ (N/mm^2)	-35	-102	-52	111	-48	-88	-77	-73	-48	-83
	Transverse stress $f_{3,rs,FE}$ (N/mm^2)	-21	-36	-14	-40	-23	-22	-44	-56	-35	-70
	Shear stress $\tau_{rs,FE}$ (N/mm^2)	-3	10	-1	9	11	-10	-8	2	-4	-9
Section B6	Longitudinal stress $f_{1,rs}$ (N/mm^2)	-101	-146	156	453	92	-106	-197	-88	-94	-195
	Transverse stress $f_{3,rs,FE}$ (N/mm^2)	-64	-47	-56	78	42	-44	-84	-36	-47	-88
	Shear stress $\tau_{rs,FE}$ (N/mm^2)	-5	11	-4	-17	-1	-8	9	6	7	-3

Table 4.5. Measured residual stress and stress ratios in S690 welded I-sections

Section	Residual stress	Top flange: Left --------------------------> Right							Web: Mid -----> Top		
Section B2	Measured value f_{rs} (N/mm^2)	-159	-191	145	400	235	-148	-129	-168	-106	-74
	Stress ratio f_{rs} / f_y	-0.20	-0.24	0.18	0.51	0.30	-0.19	-0.16	-0.23	-0.15	-0.10
Section B4	Measured value f_{rs} (N/mm^2)	-35	-102	-52	111	-48	-88	-77	-73	-48	-83
	Stress ratio f_{rs} / f_y	-0.05	-0.14	-0.07	0.15	-0.06	-0.12	-0.10	-0.10	-0.07	-0.12
Section B6	Measured value f_{rs} (N/mm^2)	-101	-146	156	453	92	-106	-197	-88	-94	-195
	Stress ratio f_{rs} / f_y	-0.13	-0.19	0.20	0.58	0.12	-0.14	-0.25	-0.12	-0.13	-0.27

Table 4.6: Maximum residual stress values and critical ratios

Section	Residual stress	Top flange $f_{t,rs,f} / f_y$ Test	Top flange $f_{t,rs,f} / f_y$ ECCS	Top flange $f_{c,rs,f} / f_y$ Test	Top flange $f_{c,rs,f} / f_y$ ECCS	Web $f_{t,rs,w} / f_y$ Test	Web $f_{c,rs,w} / f_y$ ECCS
Section B2	Measured value f_{rs} (N/mm^2)	400	784	-191	-392	-168	-392
	Stress ratio f_{rs} / f_y	0.51	1.00	-0.24	-0.50	-0.23	-0.50
Section B4	Measured value f_{rs} (N/mm^2)	111	745	-102	-373	-83	-373
	Stress ratio f_{rs} / f_y	0.15	1.00	-0.14	-0.5	-0.12	-0.50
Section B6	Measured value f_{rs} (N/mm^2)	453	784	-197	-392	-195	-392
	Stress ratio f_{rs} / f_y	0.58	1.00	-0.25	-0.50	-0.27	-0.50

Table 4.7: Test programme of fully restrained beams of S690 welded I-sections: Series LT0

Section	Measured dimensions: Total span L (mm)	Span length L_0 (mm)	h (mm)	b (mm)	t_f (mm)	t_w (mm)	Section parameters: $M_{pl,Rd}$ (kNm)	Section classification: Flange	Web
B1	1,940	670	262	112	10.0	6.0	284.4	Class 1	Class 1
B2	3,300	1,200	300	126	10.0	6.0	368.4	Class 2	Class 2
B3	4,100	1,600	380	170	10.1	6.0	741.1	Class 3	Class 3
B4	4,500	1,800	300	190	16. 1	6.0	725.9	Class 2	Class 2
B5	3,300	1,200	268	112	TF: 10.0 BF: 16.0	6.0	330.0	Class 1	Class 3
B6	3,600	1,350	306	126	TF: 10.0 BF: 16.0	6.0	430.9	Class 2	Class 3

Nominal dimensions

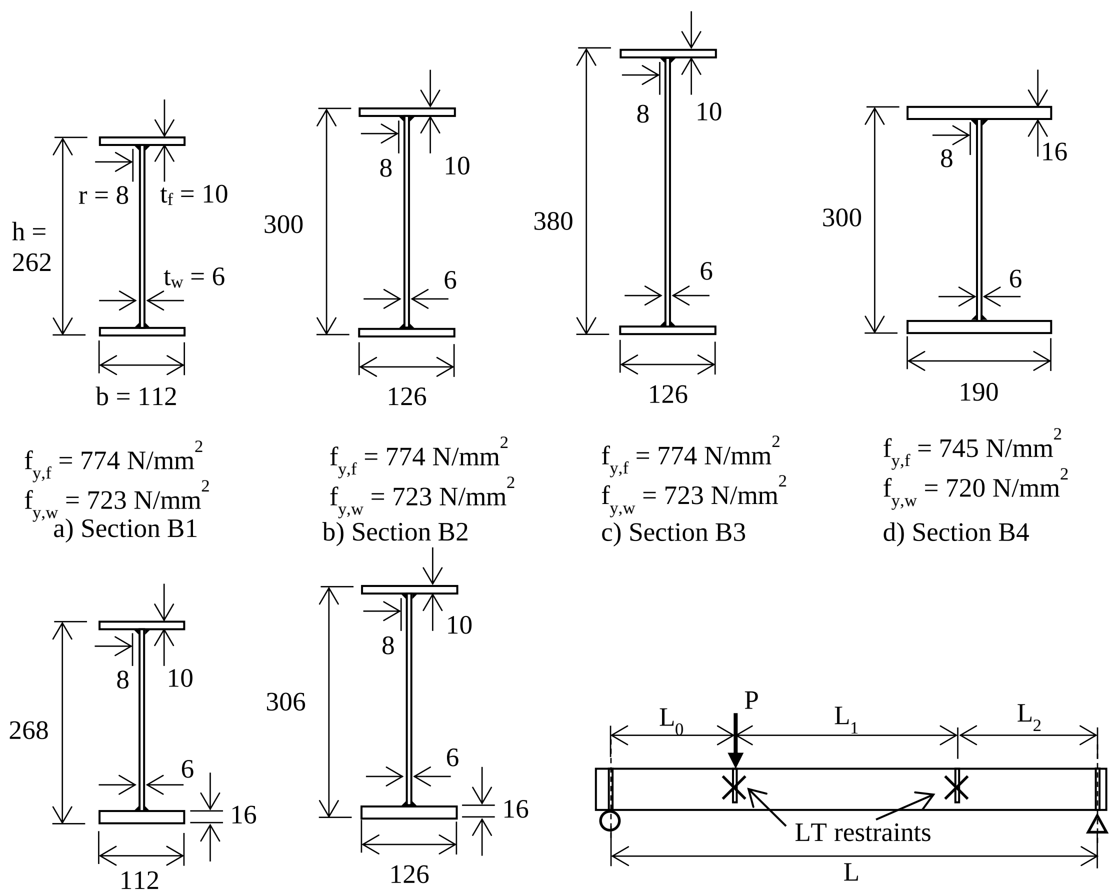

$f_{y,f}$ = 774 N/mm^2
$f_{y,w}$ = 723 N/mm^2
a) Section B1

$f_{y,f}$ = 774 N/mm^2
$f_{y,w}$ = 723 N/mm^2
b) Section B2

$f_{y,f}$ = 774 N/mm^2
$f_{y,w}$ = 723 N/mm^2
c) Section B3

$f_{y,f}$ = 745 N/mm^2
$f_{y,w}$ = 720 N/mm^2
d) Section B4

$f_{y,tf}$ = 774 N/mm^2
$f_{y,bf}$ = 745 N/mm^2
$f_{y,w}$ = 720 N/mm^2
e) Section B5

$f_{v,tf}$ = 774 N/mm^2
$f_{y,bf}$ = 745 N/mm^2
$f_{y,w}$ = 723 N/mm^2
f) Section B6

g) Test setup

a) to f): Cross-sectional dimensions for S690 welded I-sections
g): Test setup for simply supported beams

Table 4.8: Test results of fully restrained beams of S690 welded I-sections: Series LT0

Section	Section properties: Total span L (mm)	Span length L_0 (mm)	Slenderness ratios $\bar{\lambda}_f$	$\bar{\lambda}_w$	Section classification	Predicted Resistance $M_{pl,Rd}$ (kNm)	P_{Rd} (kN)	Test data: Measured resistance M_{Rt} (kNm)	P_{Rt} (kN)	$\frac{M_{Rt}}{M_{pl,Rd}}$
B1	1,940	670	0.47	0.48	Class 1	282.0	642.9	318.7	726.6	1.13
B2	3,300	1,200	0.53	0.56	Class 2	367.8	481.7	398.2	521.5	1.08
B3	4,100	1,600	0.75	0.72	Class 3	741.1	759.7(1)	728.8	747.0	0.98
B4	4,500	1,800	0.52	0.53	Class 2	720.8	672.1	843.3	780.8	1.17
B5	3,300	1,200	0.47	0.71	Class 2(2)	330.0	432.1	347.9	455.6	1.05
B6	3,600	1,350	0.53	0.82	Class 2(2)	430.8	510.5	393.0	465.8	0.91

Note:
(1): The plastic moment resistance $M_{pl,Rd}$ is taken as the predicted moment resistance of Section B3, although this beam section is Class 3 based on EN 1993-1-1; and,
(2): Based on Clause 6.2.2.4 in EN 1993-1-1, Sections B5 and B6 should be classified as effective class 2 sections.

Table 4.9: Measured deformation parameters at ultimate limit states: Series LT0

Section	Deformation characteristics: Measured value Δ_u (mm)	Span multiple L / Δ_u	Rotational capacity Φ_{Rt}	Strain parameters*: Top flange $\varepsilon_{u,tf}$ (%)	Bottom flange $\varepsilon_{u,bf}$ (%)	Plastic moment resistance obtained Yes / No
B1	22.6	90	2.36	-0.31	0.36	Yes
B2	35.8	90	0.67	-0.64	0.53	Yes
B3	35.9	110	N.A.	-0.58	0.52	No
B4	78.1	60	1.02	-1.07	0.67	Yes
B5	38.2	90	0.99	-0.61	0.37	Yes
B6	32.7	110	N.A.	-0.53	0.33	No

***Note**: The strains read from strain gauges SG2 and SG9 are taken.

Table 4.10: Check of critical shear forces in S690 welded I-sections

Section	Critical shear forces		
	Shear force V_{Rt} (kN)	Shear resistance V_{Rd} (kN)	Shear ratio $\frac{V_{Rt}}{V_{Rd}}$
B1	420.9	787.4	0.53
B2	331.9	901.7	0.37
B3	455.5	1142.0	0.40
B4	468.5	897.8	0.52
B5	289.9	802.1	0.36
B6	291.1	919.7	0.32

Table 4.11: Test programme of partially restrained beams of S690 welded I-sections: Series LT1

Section	Measured dimensions						Section parameters		
								Section classification	
	Total span L (mm)	Span length L_1 (mm)	h (mm)	b (mm)	t_f (mm)	t_w (mm)	$M_{pl,Rd}$ (kNm)	Flange	Web
B1	1,940	1,270	262.0	112.2	10.1	6.0	284.4	Class 1	Class 1
B2	3,300	2,100	300.0	126.3	10.0	6.0	368.4	Class 2	Class 2
B3	4,100	2,500	430.0	170.1	10.1	6.0	740.5	Class 3	Class 3
B4	4,500	2,700	300.0	190.1	16.0	6.0	721.1	Class 2	Class 2
B5	3,300	2,100	268.0	111.9	TF: 9.9 BF: 16.0	6.0	330.6	Class 1	Class 3
B6	3,600	2,250	306.0	125.9	TF: 10.0 BF: 16.0	6.0	430.9	Class 2	Class 3

Nominal dimensions

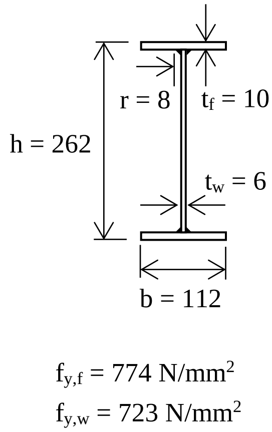

a) Section B1

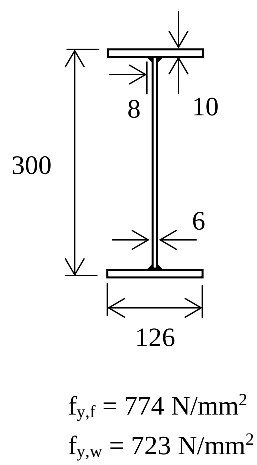

b) Section B2

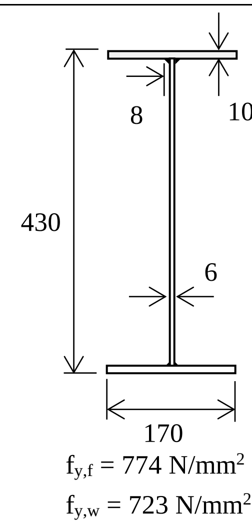

c) Section B3

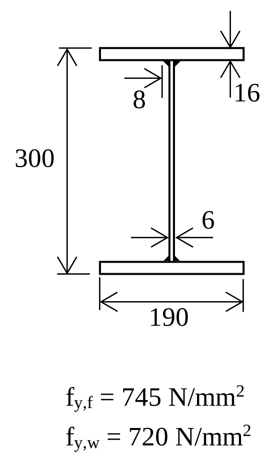

d) Section B4

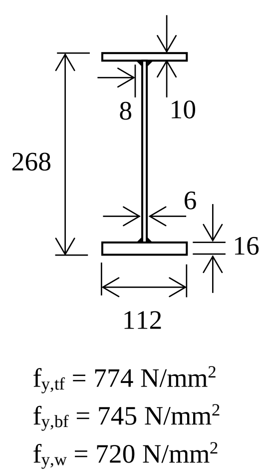

e) Section B5

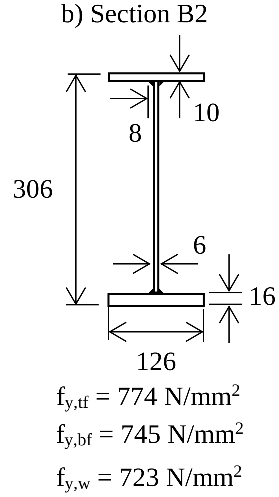

f) Section B6

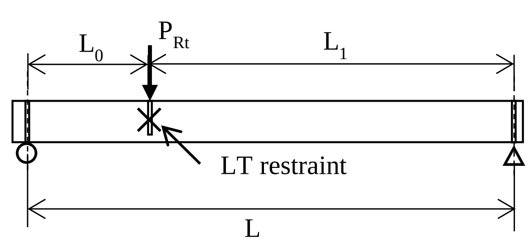

g) Test setup

a) to f): Nominal values of cross-sectional dimensions for S690 welded I-sections
g): Test setup for simply supported beams

Table 4.12: Test results of partially restrained beams of S690 welded I-sections: Series LT1

Section	Critical lengths		Lateral torsional buckling design parameters				Test data			
	L (mm)	L_1 (mm)	$M_{pl,Rd}$ (kNm)	$\bar{\lambda}_{LT}$	χ_{LT}	$M_{b,Rd}^*$ (kNm)	P_{Rt} (kN)	M_{Rt} (kNm)	$\frac{M_{Rt}}{M_{b,Rd}}$	$\frac{M_{Rt}}{M_{pl,Rd}}$
B1	1,940	1,270	284.4	0.39	1.000	284.4	729.0	319.8	1.12	1.12
B2	3,300	2,100	368.5	0.54	0.883	325.4	502.3	383.5	1.18	1.04
B3	4,100	2,500	740.5	0.66	0.790	584.8	727.8	710.0	1.21	0.96
B4	4,500	2,700	721.1	0.47	0.945	681.3	769.9	831.4	1.22	1.15
B5	3,300	2,100	328.9	0.77	0.705	231.9	388.1	296.4	1.28	0.90
B6	3,600	2,250	430.9	0.75	0.716	308.5	454.5	383.5	1.24	0.89

*** Note**: Design resistance of beam buckling, i.e. $M_{b,Rd}$ is based on 'curve d' as suggested by EN1993-1-1.

Table 4.13: Measured deformation parameters at ultimate limit states: Series LT1

Section	Ultimate deflection		Ultimate lateral displacement	Strain parameters			Failure mode (2)
	Measured value	Span multiple		Top flange (1)	Bottom flange (1)	Minor-axis bending curvature	
	Δ_u (mm)	L / Δ_u	δ_u (mm)	$\varepsilon_{u,tf}$ (%)	$\varepsilon_{u,bf}$ (%)	ϕ_{mz} ($10^{-6}mm^{-1}$)	
B1	23.7	80	2.6	-0.39	0.38	5.4	SF
B2	32.9	100	7.5	-0.37	0.37	22.5	SF / LTB
B3	33.4	120	2.2	-0.32	0.31	26.0	LTB
B4	77.0	60	4.4	-0.44	0.44	3.2	SF
B5	29.9	110	6.7	-0.37	0.23	31.6	LTB
B6	33.3	110	9.4	-0.44	0.24	39.7	LTB

*** Note**:

(1): Averaged strains measured; and,

(2): SF denotes section failure, and LTB denotes lateral torsional buckling

Table 4.14: Test programme of partially restrained beams of S690 welded I-sections: Series LT2

Section	Measured Dimensions						Section parameters		
	Total span L (mm)	Span length L_1 (mm)	h (mm)	b (mm)	t_f (mm)	t_w (mm)	$M_{pl,Rd}$ (kNm)	Section classification: Flange	Section classification: Web
B1	1,940	1,500	262.0	112.2	9.9	6.0	280.4	Class 1	Class 1
B2	3,300	2,700	300.0	126.1	10.0	6.0	368.1	Class 2	Class 2
B3	4,100	3,000	430.0	170.1	10.0	6.0	735.3	Class 3	Class 3
B4	4,500	3,300	300.0	190.1	16.0	6.0	721.1	Class 2	Class 2
B5	3,300	2,500	268.0	111.9	TF: 10.0 BF: 16.0	6.0	330.4	Class 1	Class 3
B6	3,600	2,550	306.0	126.1	TF: 10.0 BF: 16.0	6.0	431.4	Class 2	Class 3

Nominal dimensions

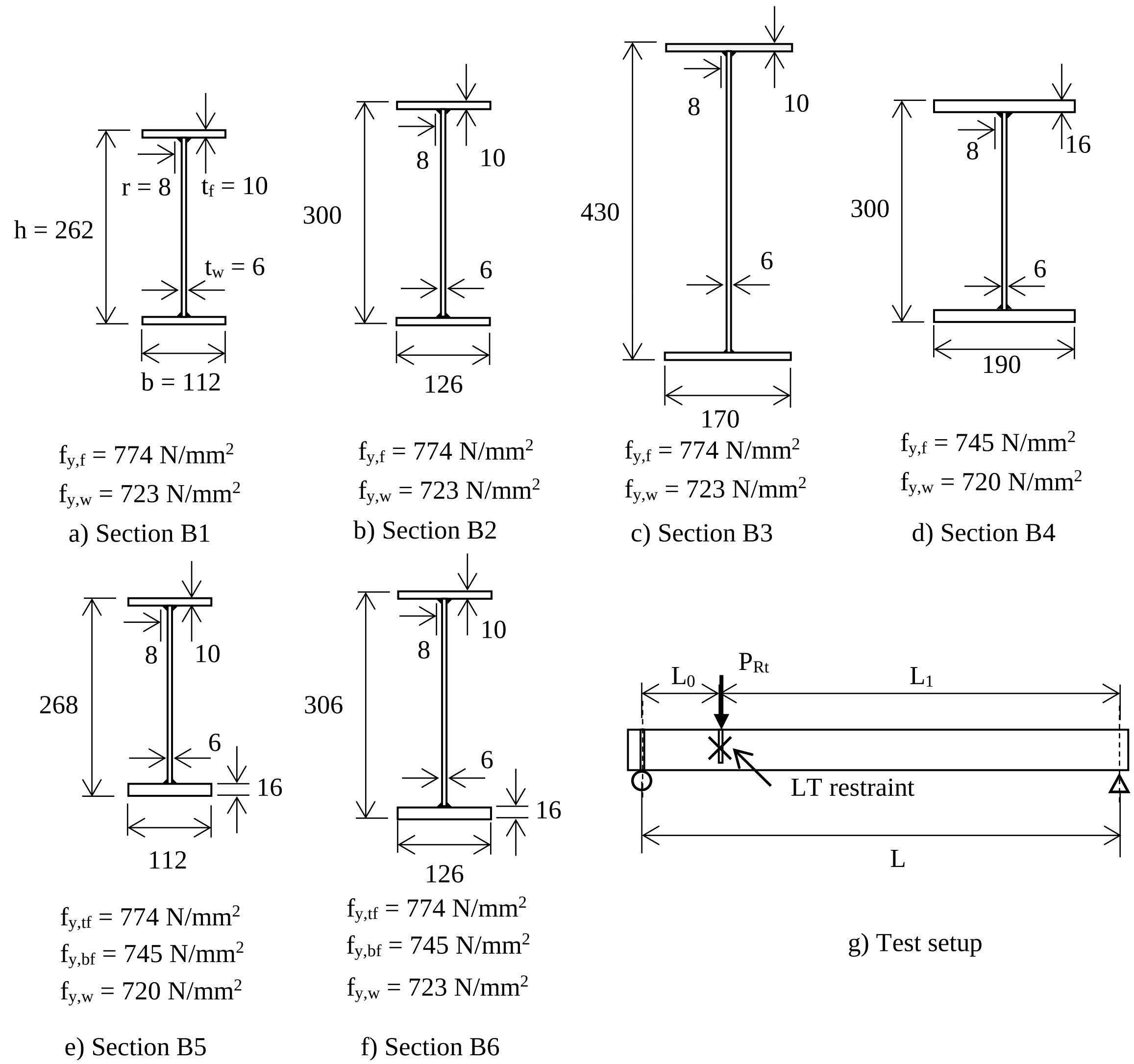

a) to f): Nominal values of cross-sectional dimensions for Q690 beam specimens (1:100)
g): Illustrative setup for simply supported beam test

Table 4.15: Test results of partially restrained beams of S690 welded I-sections: Series LT2

Section	Critical lengths		Lateral torsional buckling design parameters				Test data			
	L (mm)	L_1 (mm)	$M_{pl,Rd}$ (kNm)	$\bar{\lambda}_{LT}$	χ_{LT}	$M_{b,Rd}$* (kNm)	P_{Rt} (kN)	M_{Rt} (kNm)	$\frac{M_{Rt}}{M_{b,Rd}}$	$\frac{M_{Rt}}{M_{pl,Rd}}$
B1	1,940	1,500	280.4	0.62	0.822	230.5	831.2	282.8	1.23	1.01
B2	3,300	2,700	368.1	1.01	0.555	204.3	618.9	303.8	1.49	0.83
B3	4,100	3,000	735.3	1.23	0.443	325.4	552.6	444.8	1.37	0.60
B4	4,500	3,300	721.1	0.52	0.934	673.3	850.4	748.4	1.11	1.04
B5	3,300	2,500	330.4	0.89	0.625	206.4	443.7	268.9	1.30	0.81
B6	3,600	2,550	431.4	0.97	0.577	249.1	477.8	355.4	1.43	0.82

*** Note**: Design resistance of beam buckling, i.e. $M_{b,Rd}$ is based on 'curve d' as suggested by EN1993-1-1.

Table 4.16: Measured deformation parameters at ultimate limit states: Series LT2

Section	Ultimate deflection		Ultimate lateral displacement (1)	Strain parameters			Plastic moment resistance obtained (4)
	Measured value	Span multiple		Top flange (2)	Bottom flange (2)	Minor-axis bending curvature	
	Δ_u (mm)	L / Δ_u	δ_u (mm)	$\varepsilon_{u,tf}$ (%)	$\varepsilon_{u,bf}$ (%)	ϕ_{mz} ($10^{-6}mm^{-1}$)	Yes / No
B1	20.4	100	M: 6.7	-0.43	0.43	13.9	SF / LTB
B2	17.9	180	E: 19.6	-0.22	0.22	4.1	LTB
B3	16.1	250	E: 12.0	-0.16	0.16	3.3	LTB
B4	56.3	80	E: 10.2	-0.31	0.31	7.1	SF / LTB
B5	20.6	160	M: 15.0	-0.20	0.15	43.5	LTB
B6	24.8	140	E: 17.6	-0.27	0.18	N.A.(3)	LTB

Note:

(1): "E" represents displacement measured at section end which is more critical;
"M" represents displacement measured at middle of free-span segments which is more critical;

(2): Strain readings of strain gauges mounted on top and bottom flanges are averaged;

(3): Data was not available owing to stain gauges detached from beam specimen during the test; and,

(4): SF denotes section failure, and LTB denotes lateral torsional buckling.

Table 4.17: Comparison amongst measured moment resistances among three test series

Section	Section classification	Plastic moment resistance $M_{pl,Rd}$* (kNm)	Measured moment resistances: Series LT0 M_{Rt} (kNm)	Series LT0 $\frac{M_{Rt}}{M_{pl,Rd}}$	Series LT1 M_{Rt} (kNm)	Series LT1 $\frac{M_{Rt}}{M_{pl,Rd}}$	Series LT2 M_{Rt} (kNm)	Series LT2 $\frac{M_{Rt}}{M_{pl,Rd}}$
B1	Class 1	282.0	318.7	1.13	319.8	1.13	282.8	1.00
B2	Class 2	367.8	398.2	1.08	383.5	1.04	303.8	0.83
B3	Class 3	734.9	728.8	0.98	710.0	0.97	444.8	0.61
B4	Class 2	720.8	843.3	1.17	831.4	1.15	748.4	1.04
B5	Class 2	330.6	347.9	1.05	296.4	0.90	268.9	0.81
B6	Class 2	430.8	393.0	0.91	383.5	0.89	355.4	0.82

* **Note**: Plastic moment resistances are calculated with nominal dimensions of steel sections

CHAPTER FIVE

NUMERICAL MODELLING I: RESIDUAL STRESS PATTERNS OF WELDED H- AND I-SECTIONS

5.0 Introduction

In this Chapter, a systematic numerical investigation into residual stress patterns in welded H- and I-sections of a wide range of section sizes and plate thicknesses is presented. A finite element package ABAQUS (Dassault Systemes Simulia Corp., 2010) was adopted to conduct thermo-mechanical coupled analyses. An introduction to practical welding parameters and two-dimensional thermo-mechanical coupled models are presented. The numerical models were then verified and calculated against measured residual stresses of S690 welded I-sections presented in Chapter 4.

With calibrated thermo-mechanical coupled models, the following parametric studies on residual stress patterns are conducted.

- Task 1: Sections C1 to C4 of S690 and S355 welded H-sections;
- Task 2: Sections B1 to B6 of S690 and S355 welded I-sections;
- Task 3: Sections C1 to C8 of S690 welded H-sections fabricated with high-energy and low-energy welding procedures; and,
- Task 4: Sections B1 to B8 of S690 welded H-sections fabricated with high-energy and low-energy welding procedures.

In general, the residual stresses of S690 welded sections when compared with their respective yield strengths are found to be significantly smaller than the corresponding values of those S355 welded sections, especially for those welded sections with thick steel plates and fabricated with low-energy welding procedures.

5.1 Objectives

In order to understand effects of welding in S690 welded sections, a systematic numerical investigation is carried out to assess residual stress patterns of welded H- and I-sections. The main objectives of the numerical investigation are:

- To determine the residual stress patterns in high strength S690 welded H- and I-sections; and,
- To highlight differences of residual stress patterns in welded H- and I-sections with different steel grades, weld procedures and section sizes.

The following areas of interest in the numerical investigation are:

1. Accuracy of the thermo-mechanical coupled model as calibrated against measured residual stresses in S690 welded H- and I-sections;
2. Typical residual stress patterns of S690 welded H- and I-sections; and,
3. Comparison between predicted residual stress patterns of S690 welded sections and recommended residual stress patterns of S355 welded section given in ECCS (1976).
4. Comparison between predicted residual stress patterns of S690 welded sections and estimated residual stresses for S690 welded section proposed by Liu (2017).

5.2 Establishment of two-dimensional thermo-mechanical coupled model

5.2.1 Overview of the thermo-mechanical coupled analysis

With recent development of numerical modelling of heat transfer, finite element method is readily employed to calculate welding-induced temperature and stress distributions in steel sections (Liu and Chung, 2016). In general, the finite element package ABAQUS 6.12 is adopted to conduct thermo-mechanical coupled analyses to determine residual stresses in welded H- and I-sections.

In order to develop two-dimensional models, a 4-noded plane strain thermally coupled element, namely Shell Element CPEG4T, is adopted to perform coupled analyses. A typical gradient mesh of the thermo-mechanical coupled model is given in Figure 5.1. It should be noted that in Element CPEG4T, there are four integration points which guarantee a high numerical accuracy. Moreover, this element is capable of capturing out-of-plane expansion or contraction, and hence, it is suitable to compute welding-induced residual stresses in steel sections. The “Birth and Death” technique is applied to weldments as a means to simulate a welding sequence satisfactorily.

5.2.2 Material properties

An idealized bi-linear stress-strain curve as shown in Figure 5.2 was applied to both S355 and S690 steel materials. A bi-linear stress-strain relation is applied as it is found to match well with measured true stress-strain curves shown in Figure 4.3. Reduction factors at elevated temperatures provided by ASM handbook (ASM,1990) is adopted to allow for reduction in yield strengths of steel materials. According to Chiew et. al. (2014), this material model has been satisfactorily against test data. Temperature-dependent coefficients, namely thermal conductivity, heat specific and thermal expansion coefficient provided by EN 1993-1-2 are used (CEN, 2005). Moreover, it should be noted that measured material properties are adopted in Tasks 1 and 2 for S690 welded sections.

5.2.3 Boundary conditions

Boundary conditions of the numerical model is presented in Figure 5.1. It should be noted that during welding, the bottom steel plate is fully fixed while the top flange is partially fixed as thermal expansion of steel plates is allowed. Hence, boundary conditions adopted in the model can generally reflect the test setup of the welding process.

5.2.4 Ramp model of heat source

A heat source in the form of a ramp model is adopted to simulate a welding torch moving through the thickness of the model as shown in Figure 5.3. Through this model, the applied heat energy history is represented consistently with the movement of the welding torch. Different stages of heat energy input are defined as follows:

- Stage 1: The brink of the heat source entering the regime of 2D thermal shell elements with $t_1 = 0$ and $q_1 = 0$;
- Stage 2: The centre of the heat source reaching the edge of 2D thermal shell elements with $t_2 = 0.5$ second and $q_2 = q$ which is defined in Equation 5.1;
- Stage 3: The centre of the heat source leaving the edge of 2D thermal shell elements with $t_3 = 1.0$ second and $q_3 = q$; and,
- Stage 4: The brink of the heat source leaving the regime of 2D thermal shell elements with $t_4 = 1.5$ second and $q_4 = 0$.

It should be noted that the input heat energy from the welding torch, q, given by Liu (2017) is defined as follows:

$$q = \frac{\eta \cdot U \cdot I}{A \cdot a} \qquad \text{(Eq. 5.1)}$$

where A is the cross-sectional area of the heat source; and,

a is the longitudinal length of the heat source, and it is taken to be 8 mm in this study for simplicity.

5.2.5 Welding parameters

In this study, measured residual stresses are verified against thermo-mechanical coupled numerical model. Heat energy input, which is a key input parameter in numerical model, is measured during the welding process, and it is incorporated into the coupled numerical model as shown in Table 5.1. It should be noted that two different line heat energy inputs are introduced into the models as there are two different combinations of plate thicknesses.

In the proposed parametric study, a total of four different combinations of plates thicknesses are used to form different H- and I-sections of a wide range of section sizes and plate thicknesses as shown in Table 5.1. The plate thicknesses range from 6 mm to 40 mm.

In order to follow practical welding of these steel plates, a list of welding parameters are summarized in Table 5.1. They are selected according to established practice recommended by the American Welding Society (AWS, 2006). It should be noted that these welding parameters have been successfully employed in fabrication of the test specimens in this research project. These welding parameters are adopted in subsequent analyses of the welded sections.

5.3 Verification and results of numerical models

It should be noted that Liu has successfully calibrated a number of three dimensional thermo-mechanical coupled models against measured residual stresses of S690 welded H-sections, namely Sections C1 to C4 (2017). In this section, a two-dimensional thermo-mechanical coupled model is calibrated against measured residual stress distributions of S690 welded I-sections presented in Chapter 4. It should be noted that all the measured welding parameters given in Chapter 4 are adopted in the numerical models.

5.3.1 Comparison of residual stresses

A direct comparison between measured and predicted residual stresses of three S690 welded I-sections are illustrated. It is shown that predicted residual stresses from outer surfaces of the top flanges of these I-sections agree well with measured data. A quantitative comparison between measured and predicted residual stresses is presented in Table 5.2. Only the residual stresses obtained from outer surfaces of flanges and webs of the I-sections are listed. It is shown that relative errors of the residual stresses range from 1.0% to 16.3% with an average value at 4.4%. Hence, the proposed numerical model is considered to be able to predict residual stresses satisfactorily.

It should be noted that as shown in the predicted residual stress distributions, through-thickness gradient is quite large in the flange-web junctions. Measured compressive residual stresses should not be taken as the residual stresses of the sections. Otherwise, effect of residual stresses is significantly underestimated.

5.3.2 Contour plots of residual stresses in welded I-sections

Color contour plots of residual stresses in welded I-sections are illustrated in Figure 5.6. It is shown that residual stresses are highly localized within the plate thicknesses adjacent to the flange-web junctions. Tensile residual stresses are highly concentrated in these locations. Moreover, tensile yielding is observed in those locations in direct contract with the weldments. It should be noted that average values of the residual stresses across plate thicknesses will be very different from those of the surface residual stresses.

It is also noted that predicted residual stress distributions are not strictly symmetrical about the minor axes of the cross-sections. This is attributed to tempering effect on the flange-web junctions owing to line heat input energy released in subsequent welding runs. Hence, tensile residual stresses are slightly smaller than those welding runs completed earlier.

5.4 Parametric studies on residual stress patterns

This section presents predicted residual stress patterns of I-sections with different section sizes and plate thicknesses. Key values of residual stress patterns are compared with establish a typical simplified pattern. It should be noted that in each task, only the residual stresses in the longitudinal direction averaged within a plate thickness are plotted for simplicity. Section dimensions, residual stress patterns and key residual stress parameters for welded H- and I-sections are listed as follows for easy reference.

	Section Dimensions	**Residual stress patterns**	**Key residual stress parameters**
Task 1	Figure 5.7	Figures 5.8 to 5.9	Table 5.3
Task 2	Figure 5.10	Figures 5.11 to 5.12	Table 5.4
Task 3	Figure 5.13	Figure 5.14	Table 5.6
Task 4	Figure 5.15	Figure 5.16	Table 5.7

5.4.1 Effect of steel grades

Task 1: Sections C1 to C4 of S690 and S355 welded H-sections

Task 2: Sections B1 to B6 of S690 and S355 welded I-sections

As shown in Figures 5.8, 5.9, 5.11 and 5.12, a comparison on residual stress patterns of S690 and S355 welded sections with identical cross-sectional dimensions is conducted. The residual stress patterns are found to be similar in shape, but with quite different magnitudes. Tensile yielding is generally found in the flange-web junctions in S355 welded H- and I-sections, though only small portions of the internal webs of S690 welded H- and I-sections are yielded. Moreover, compressive stresses are comparatively smaller, and they generally exist in the flange and the web plates.

In Tables 5.3 and 5.4, residual stress magnitudes are presented together with their ratios to yield strengths. In S690 welded H-sections, tensile residual stresses are shown to be significantly smaller than their yield strengths. And they are generally reduced with increasing plate widths and thicknesses. This trend is also found to be valid to magnitudes of compressive residual stresses in S690 and S355 welded sections. Since the yield strengths of S690 steel plates are double to those of S355 steel plates, residual stresses in S690 welded H- and I-sections are found to be proportionally less pronounced when compared with S355 welded sections of similar dimensions. Therefore, S690 welded sections are expected to behave structurally superior to those of S355 welded sections in terms of section strength and rigidity.

In Table 5.5, all predicted force components owing to residual stresses are summarized. In general, force equilibrium is justified in all 12 sections including both S355 and S690 welded I-sections as maximum out-of-balance forces for numerical results is only 5kN. The out-of-balance forces in 12 sections are found to be smaller than 1% of total section resistances. Therefore, the proposed numerical models are considered to be effective as force equilibrium conditions are satisfied.

5.4.2 Effects of welding procedure and plate thickness

Task 3: Sections C1 to C8 of S690 welded H-sections fabricated with different welding procedures
Task 4: Sections B1 to B8 of S690 welded I-sections fabricated with different welding procedures

The effects of two different welding procedures, i.e. high-energy welding and low-energy welding, are compared in a numerical study. They are differentiated by numbers of weld runs and line heat energy input in each run. As shown in Table 5.1, the line heat energy input for a high-energy welding is three times of that in a low-energy welding. Hence, the temperature at flange-web junctions with a high-energy welding will be significantly higher than those temperatures with a low-energy welding. Hence, residual stresses induced by heating and cooling circles will be correspondingly large.

In Figures 5.14 and 5.16, residual stress patterns of S690 welded H- and I-sections with different welding procedures are presented for a direct comparison. Generally, residual stress magnitudes are found to be significantly larger in welded sections with a high-energy welding procedure. Compressive residual stresses in high-energy welding are found to be double to those sections with low-energy welding procedures. Therefore, welded sections with high-energy welding procedure are expected to have large residual stresses. It should be noted that effects of welding procedures to structural behaviour of S690 welded sections will be presented in Chapter 7.

In the current study, a wide range of plate thickness from 6 mm to 40 mm is considered. Obviously, there is a pronounced reduction in both tensile and compressive residual stresses with the increasing plate thicknesses as shown in Table 5.7. In particular, compressive residual stresses of Sections B1 and B2 are triple to those corresponding values in Sections B7 and B8. This trend is also found to be valid to I-sections fabricated with both high-energy and low-energy welding procedures. Moreover, compressive residual stresses in Sections B5 to B8 are generally 10% smaller than of yield strengths of the steel materials. Hence, early reduction of section rigidity will not be as critical as it is in thin-plate S690 welded I-sections.

5.4.3 Comparison with recommended residual stress patterns

Recommended residual stress pattern given in a ECCS document entitled “Manual on stability of steel structures” is compared with validated numerical results in Table 5.8. It should be noted that the ECCS pattern is proposed for S235 and S355 welded sections. It is shown that the tensile stresses in flanges of S690 welded I-sections, i.e. $f_{rs,t,f}$ is significantly smaller than the corresponding value in the ECCS pattern. The corresponding stress ratios are found to be generally smaller than 0.80. For compressive residual stresses, the predicted residual stresses are smaller than half of the recommended values. Moreover, the tendency of reduced residual stresses with increasing section sizes and plate thickness is not reflected in the ECCS pattern. As a whole, the ECCS pattern is shown to give highly over-estimated residual stresses if directly adopted in S690 welded I-sections.

A simplified model to predict residual stress distributions and magnitudes in S690 welded H-sections with different line heat input energies and plate thicknesses is proposed and verified (Liu, 2017). The expressions of Liu's model are presented in Table 5.9. Comparison between estimated and predicted residual stresses in S690 welded I-sections is carried out. It is noted that an average discrepancy of $0.07f_y$ is observed between predicted and estimated residual stresses. Moreover, Liu's model is considered to be highly effective because of:

- applicability to a range of steel grades, plate thickness and welding procedures;
- widths of tensile and compressive residual stresses are defined; and,
- self-equilibrium of residual stresses within cross-sections is satisfied.

Therefore, residual stresses in S690 welded I-sections based on Liu's model is considered to be highly acceptable.

5.5 Conclusions

- *Verification against test measurement*

An advanced thermo-mechanical coupled model is successfully established with finite element package ABAQUS to predict welding induced residual stresses in welded H- and I-sections. A coupled 2D 4-noded plane strain element, i.e. Shell Element CPEG4T, is adopted in this model. It is found that predicted surface residual stresses in S690 welded I-sections of different section sizes and plate thicknesses compare well with measured values. Hence, this model is readily applied to welded H- and I-sections with different cross-sectional dimensions. Moreover, tensile residual stresses with large through-thickness gradients are found in flange-web junctions of these sections. Hence, it is necessary to determine averaged residual stresses instead of simply adopting the measured surface residual stresses in establishing representative residual stress patterns of S690 welded sections.

- *Parametric studies on residual stress patterns*

A number of systematic parametric studies on residual stress patterns are carried out. Welded sections of identical cross-sectional dimensions with S355 and S690 steel plates are investigated to predict residual stresses in welded sections of different yield strengths. Effects of welding procedures and plate thicknesses are also examined. It is found that residual stresses in welded H- and I-sections with the following features are significantly reduced:

- To be welded with high strength steel plates;
- To use thick steel plates;
- To adopt low-energy welding procedure with multiple weld runs.

Comparing with residual stress patterns recommended in the ECCS document reveals that recommended residual stresses for S355 welded sections are not applicable to S690 welded sections. A direct application of the pattern to S690 welded sections will lead to significant overestimation on residual stresses, and their effects on structural behaviour of the welded sections.

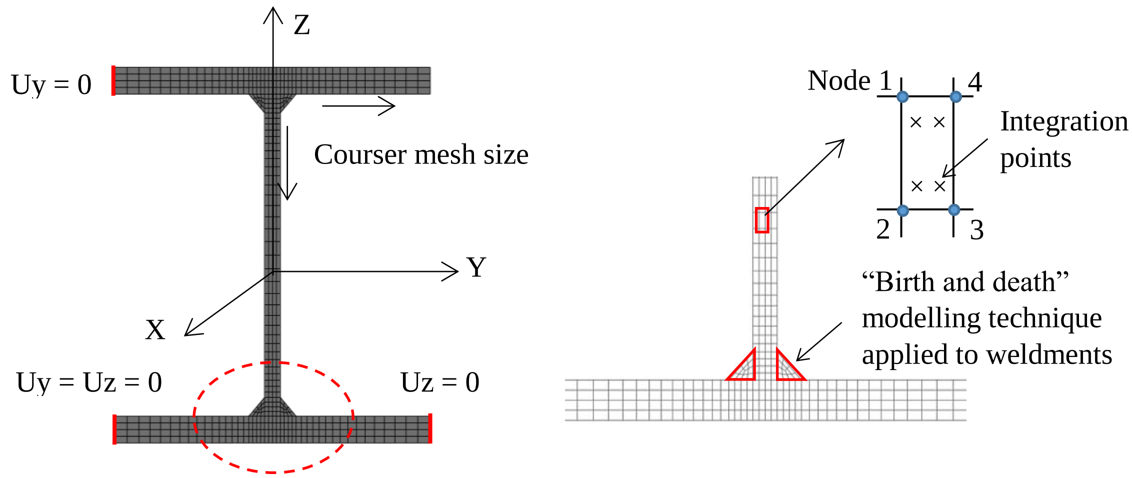

Figure 5.1: Two-dimensional thermo-mechanical coupled model

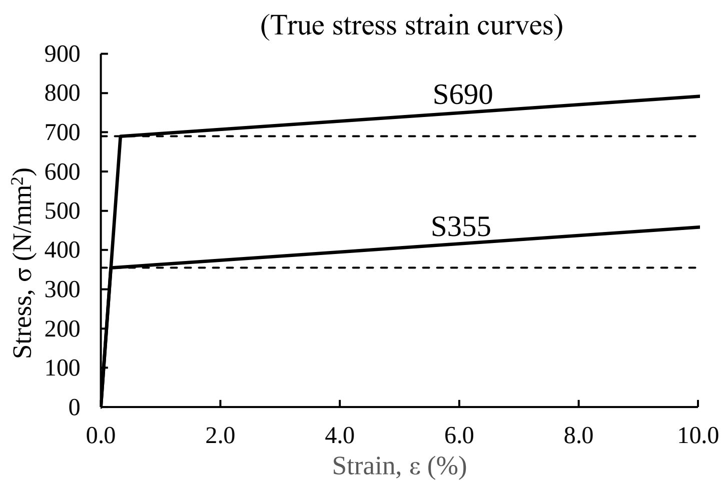

Figure 5.2: Bi-linear material model for S355 and S690 steel materials

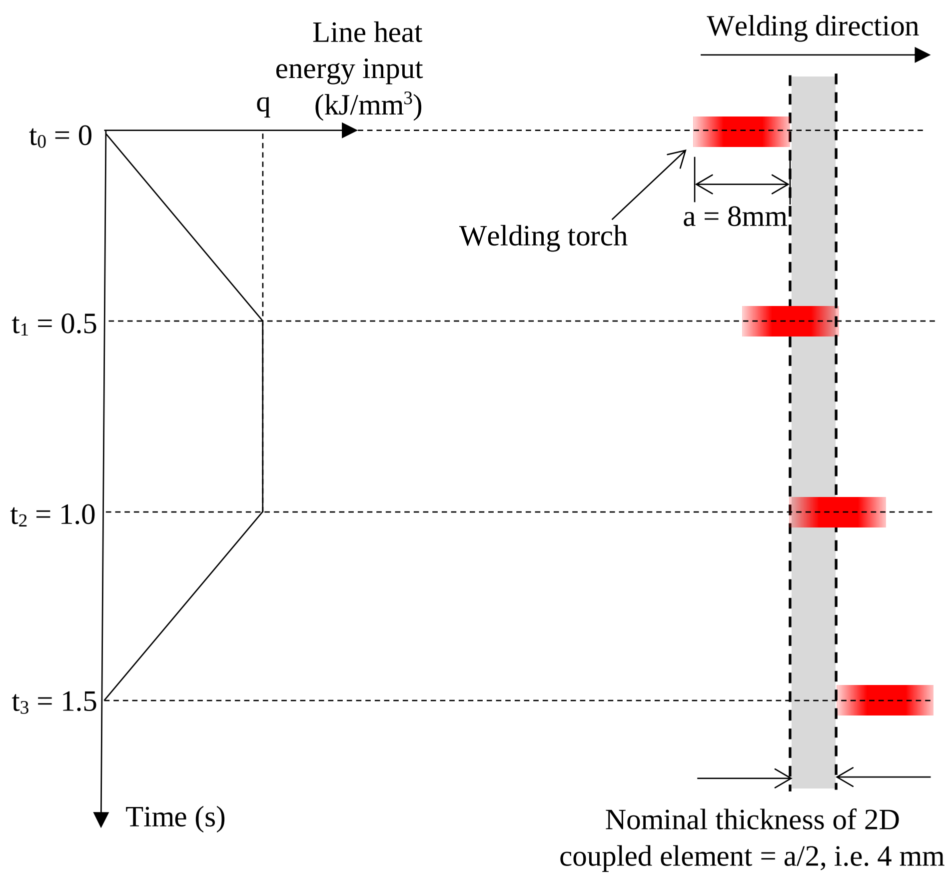

Figure 5.3: Heat source model in 2D models

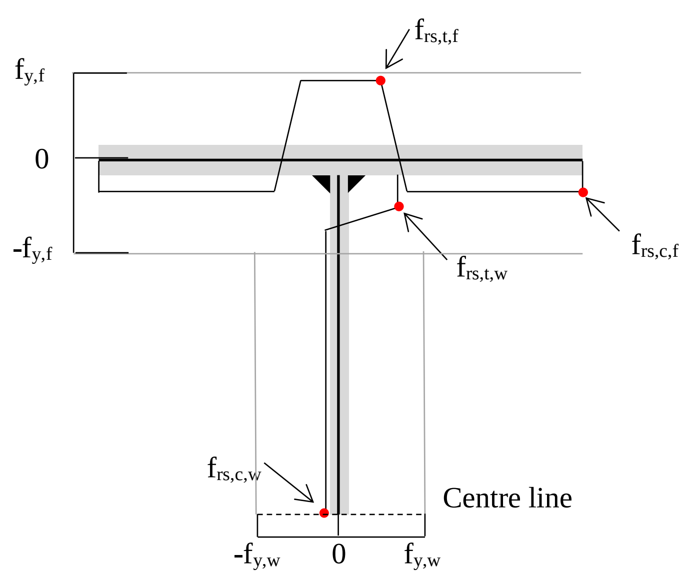

Figure 5.4: Schematic residual stress distribution in a welded I-section

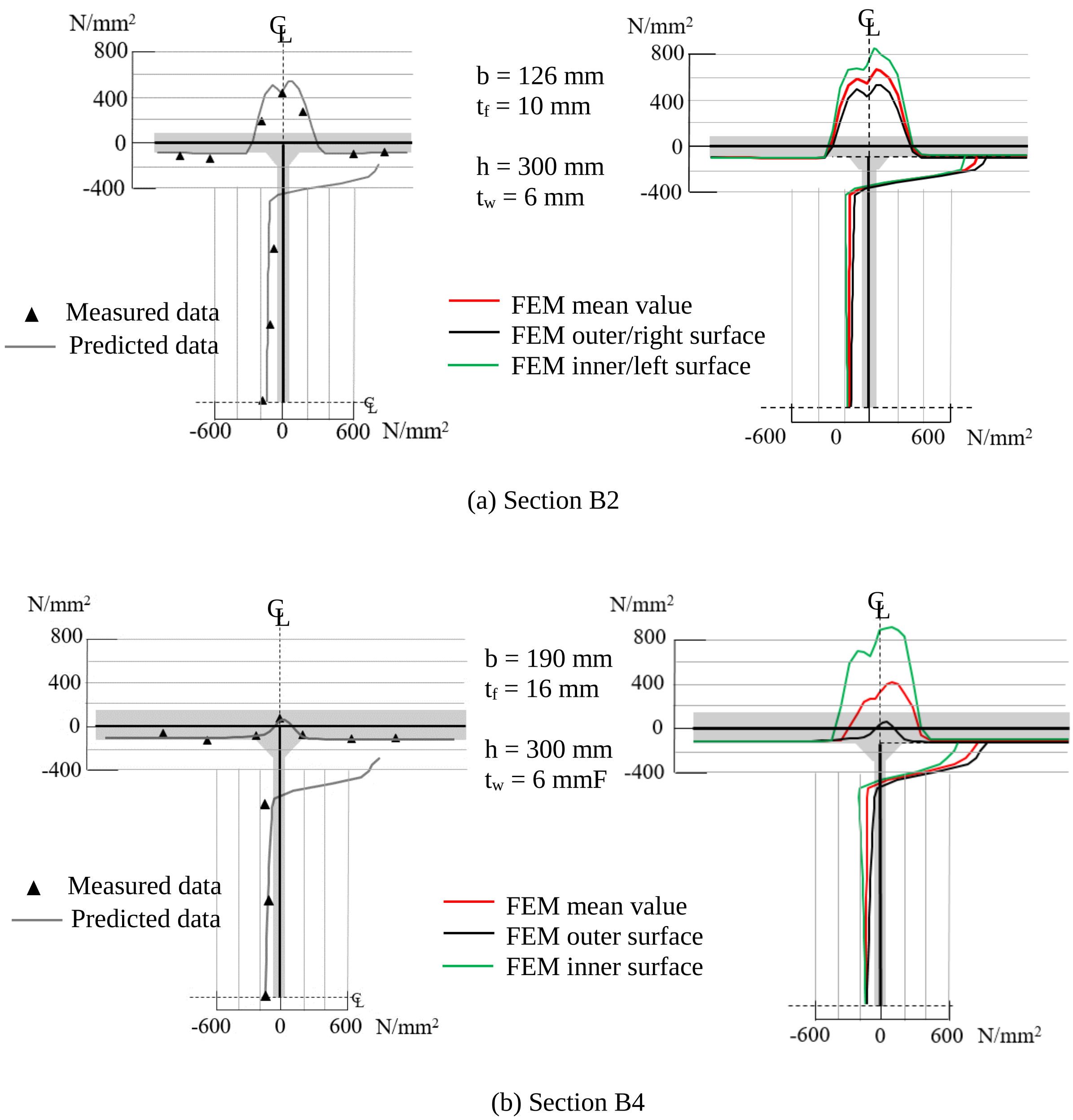

Figure 5.5: Comparison of measured and predicted residual stresses in S690 welded I-sections

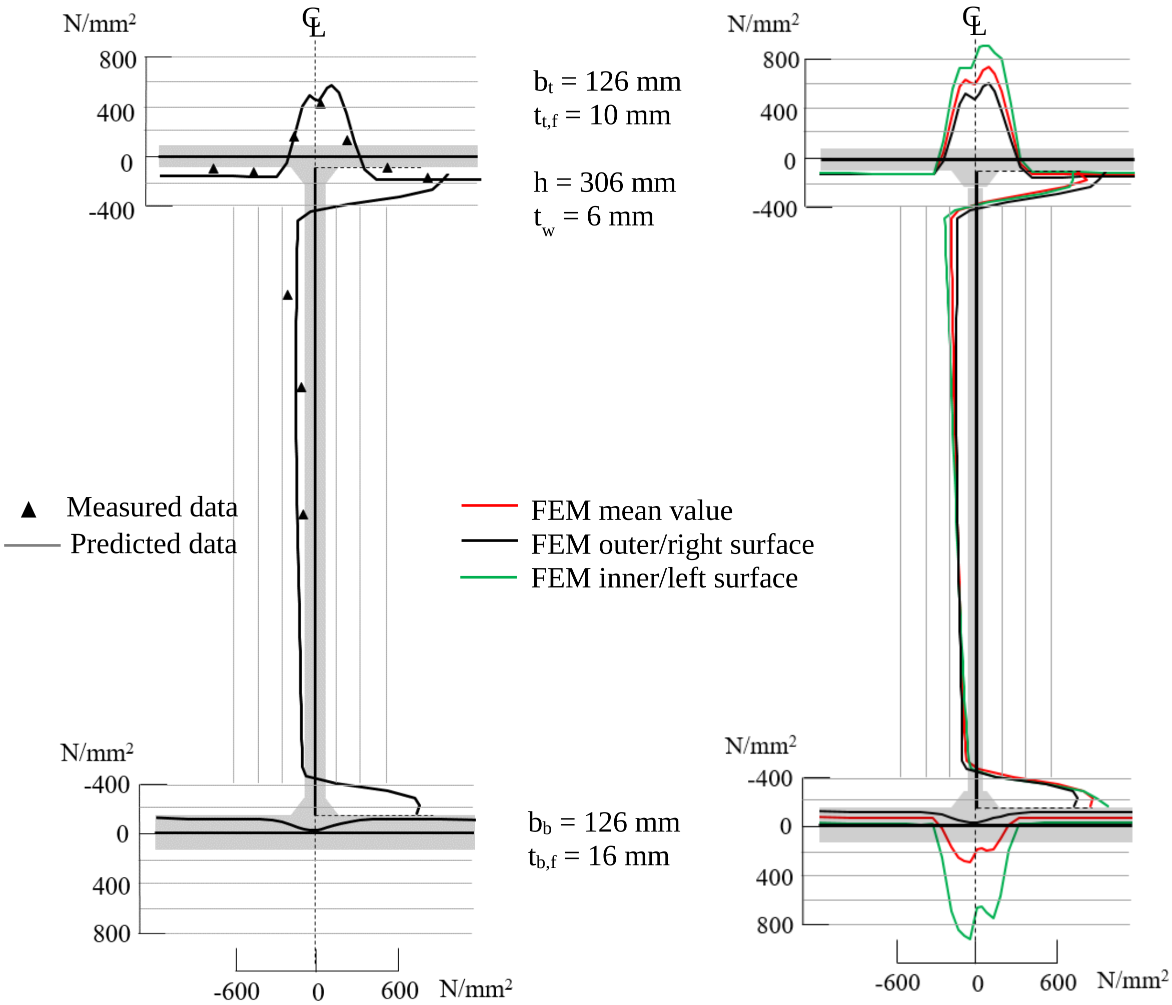

(c) Section B6

Figure 5.5: Comparison of measured and predicted residual stresses in S690 welded I-sections (Continued)

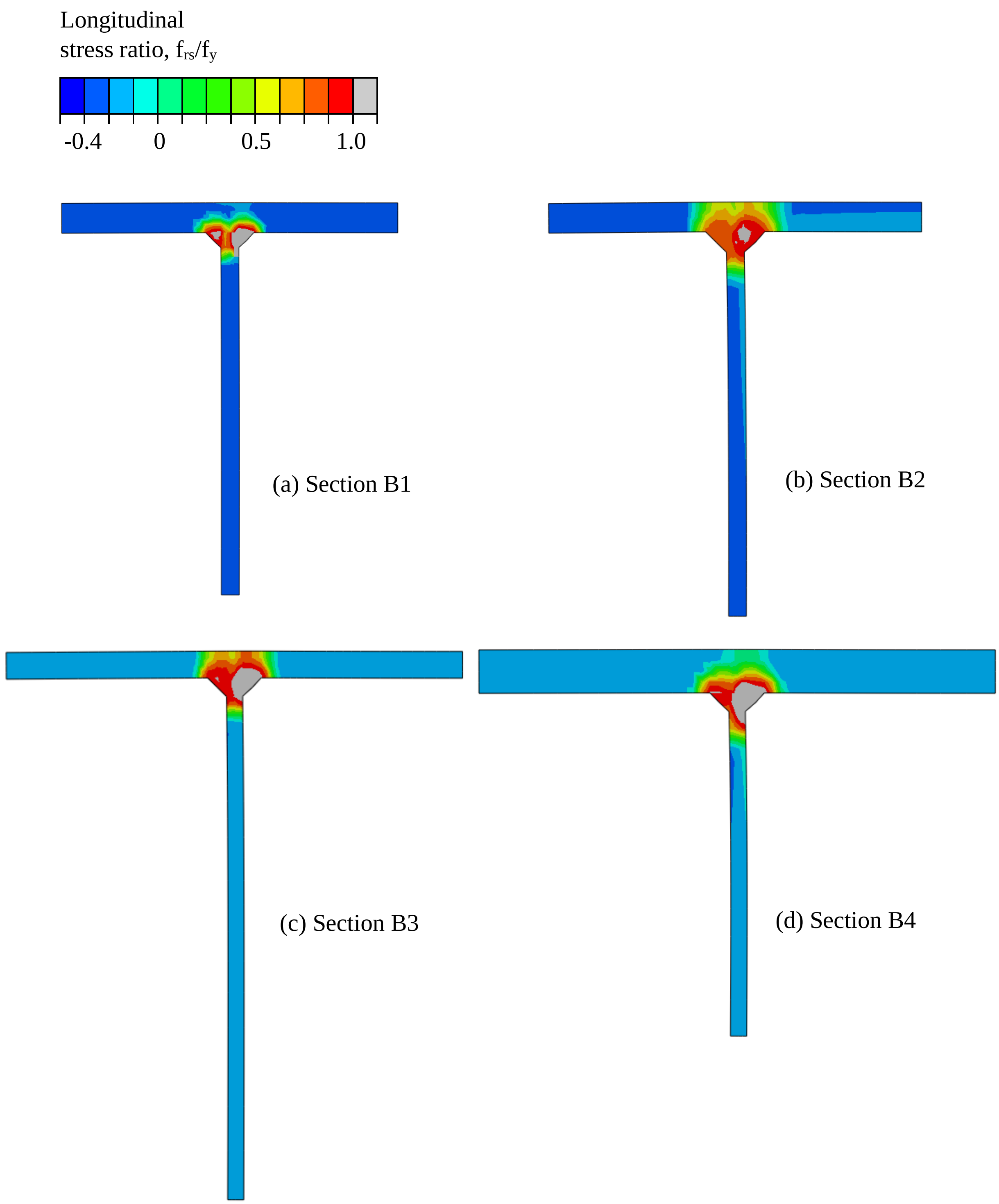

Figure 5.6: Contour plots of residual stresses in welded S690 I-sections

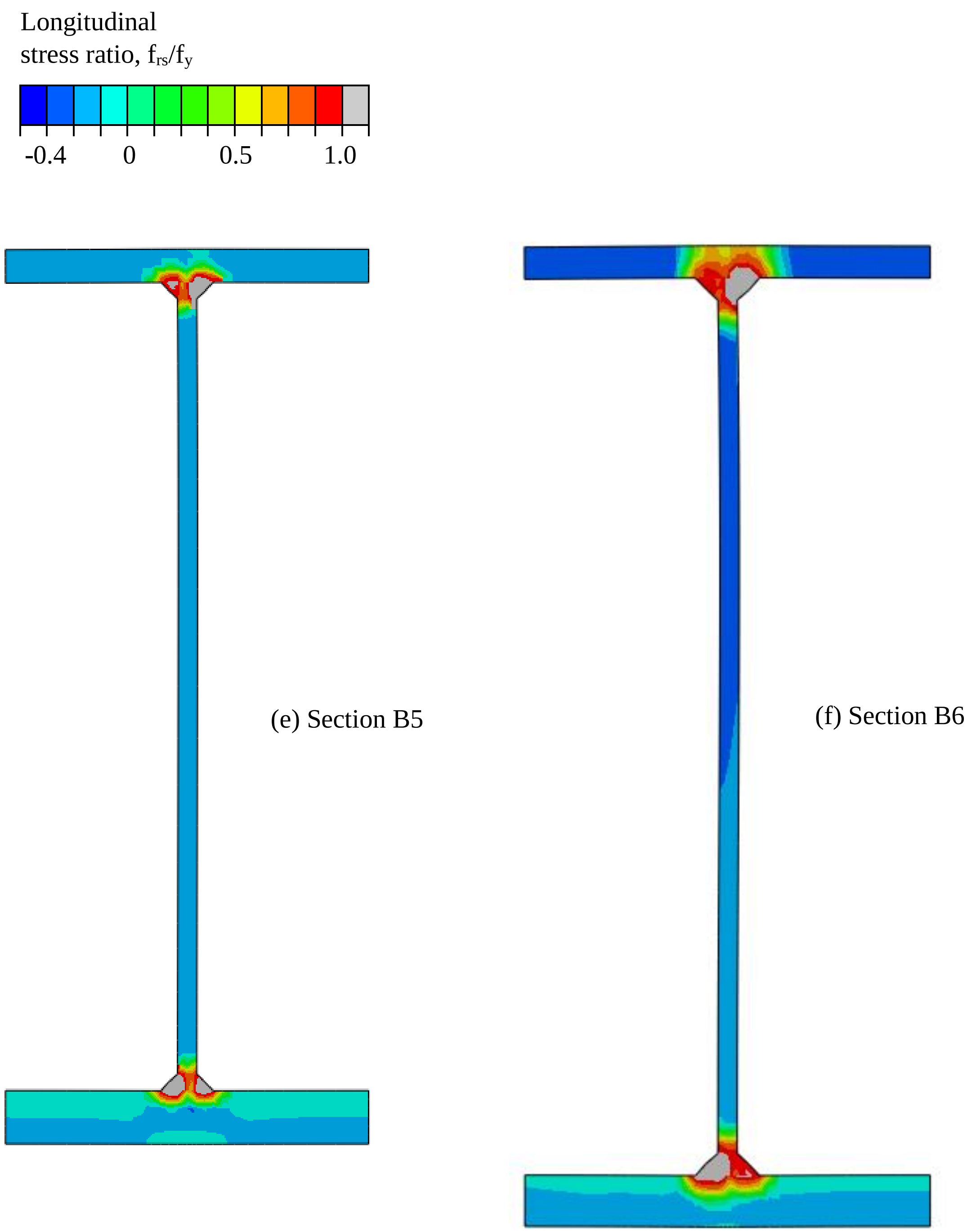

Figure 5.6: Calculated contour of residual stresses in welded S690 I-sections (Continued)

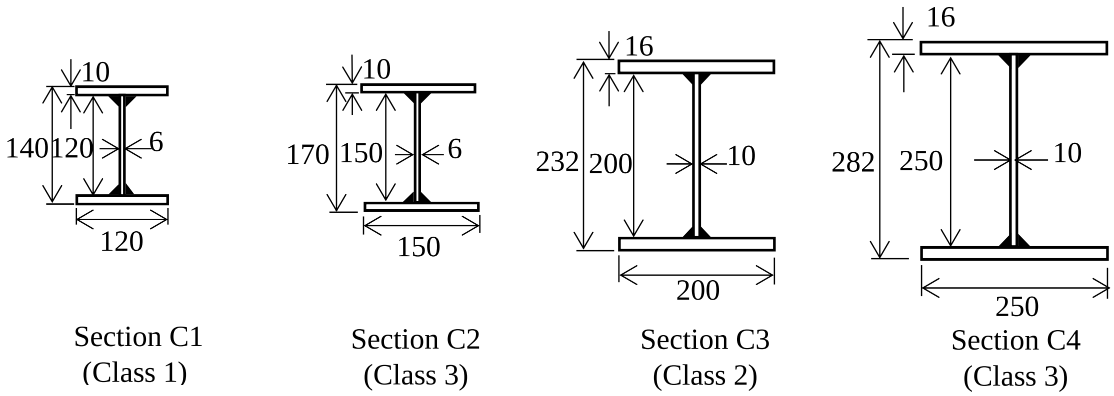

Figure 5.7: Dimensions of welded S690 H-sections applied in numerical study

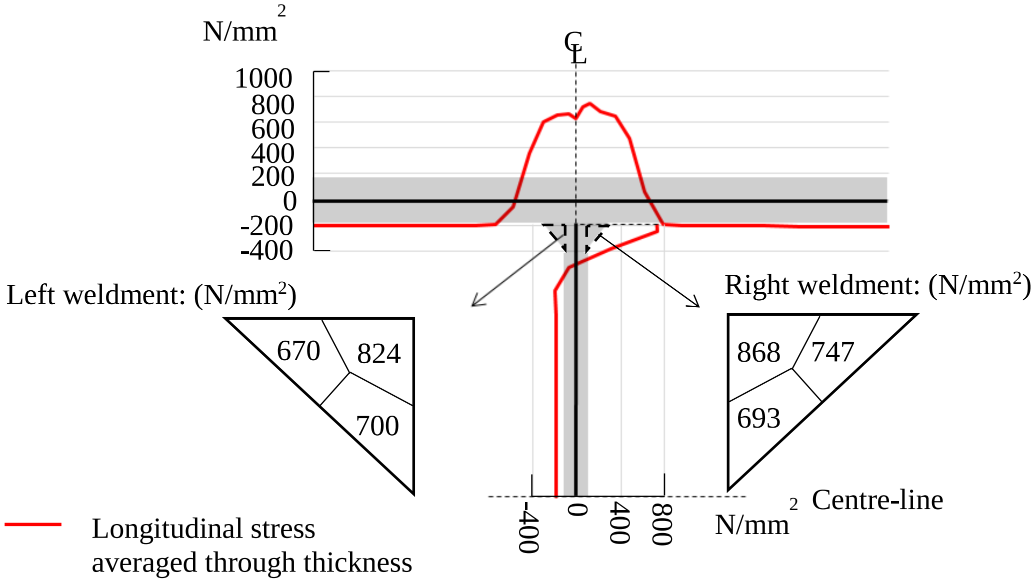

(a) Section C1

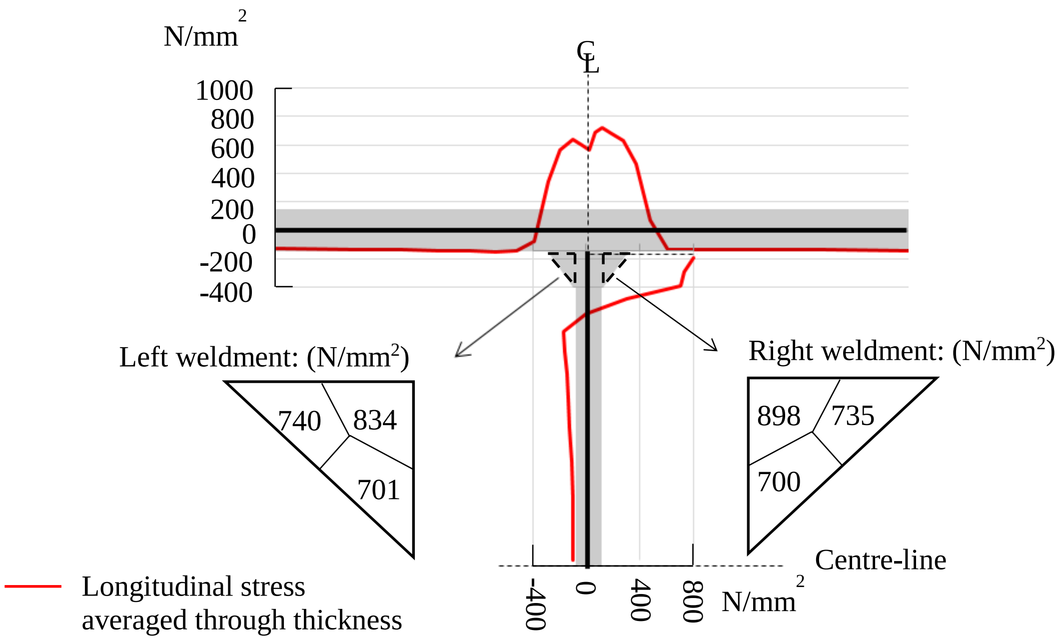

(b) Section C2

Figure 5.8: Predicted residual stress patterns for welded S690 H-sections

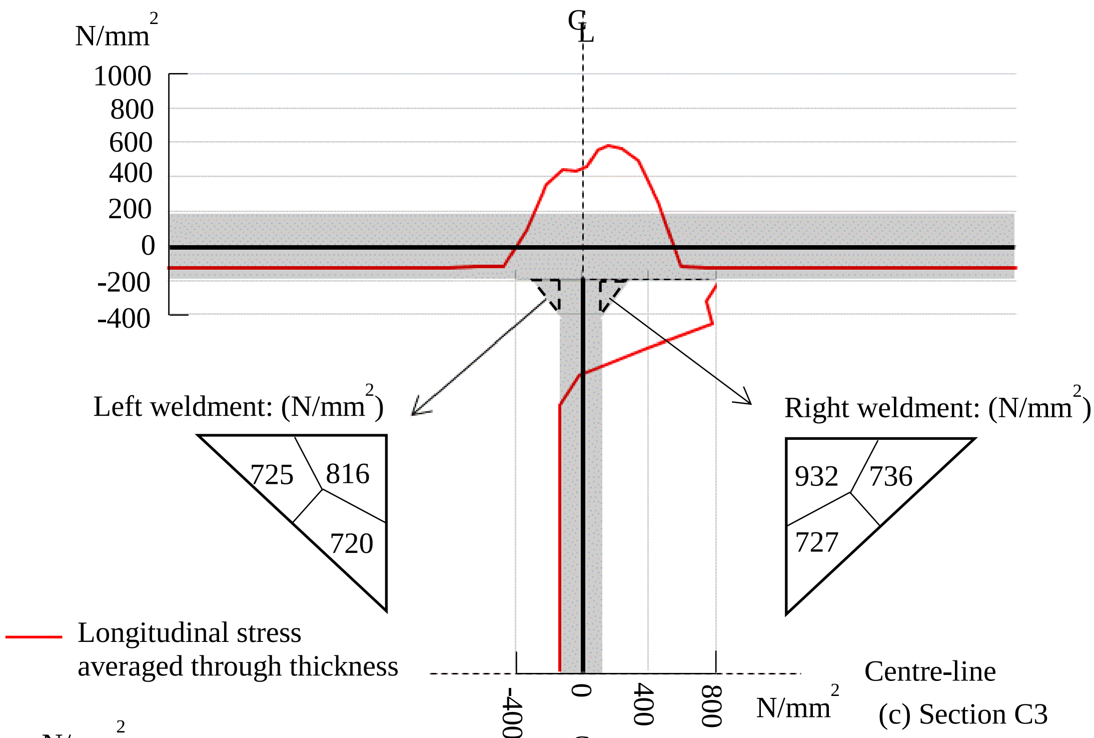

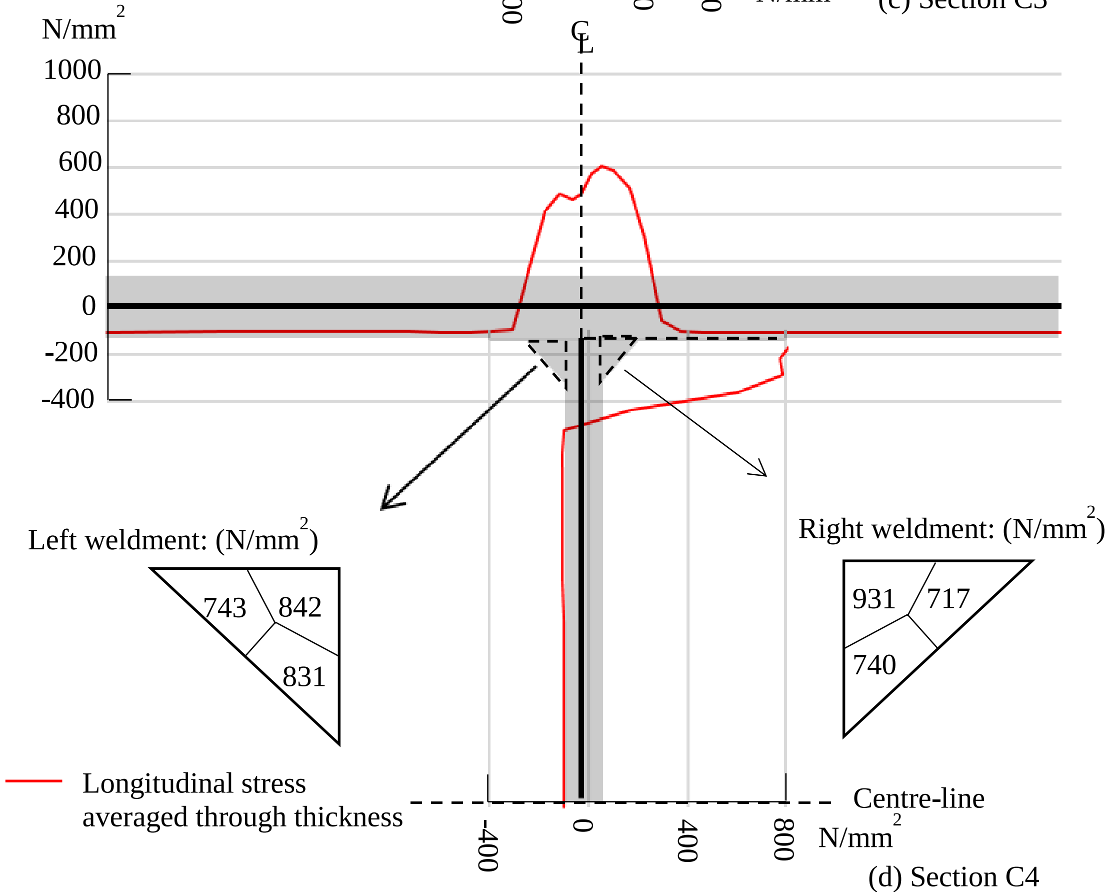

Figure 5.8: Predicted residual stress patterns for welded S690 H-sections (Continued)

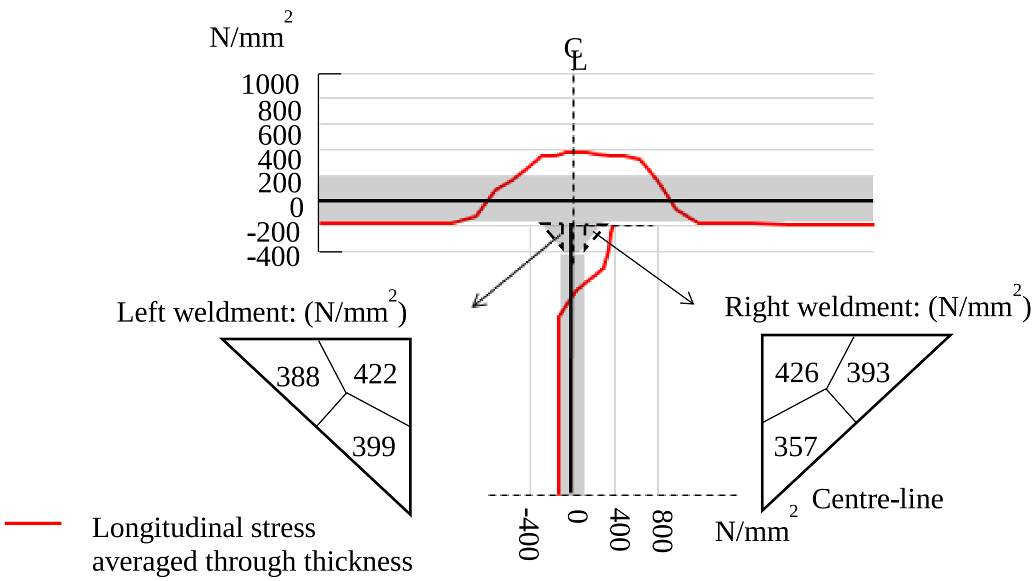

(a) Section C1

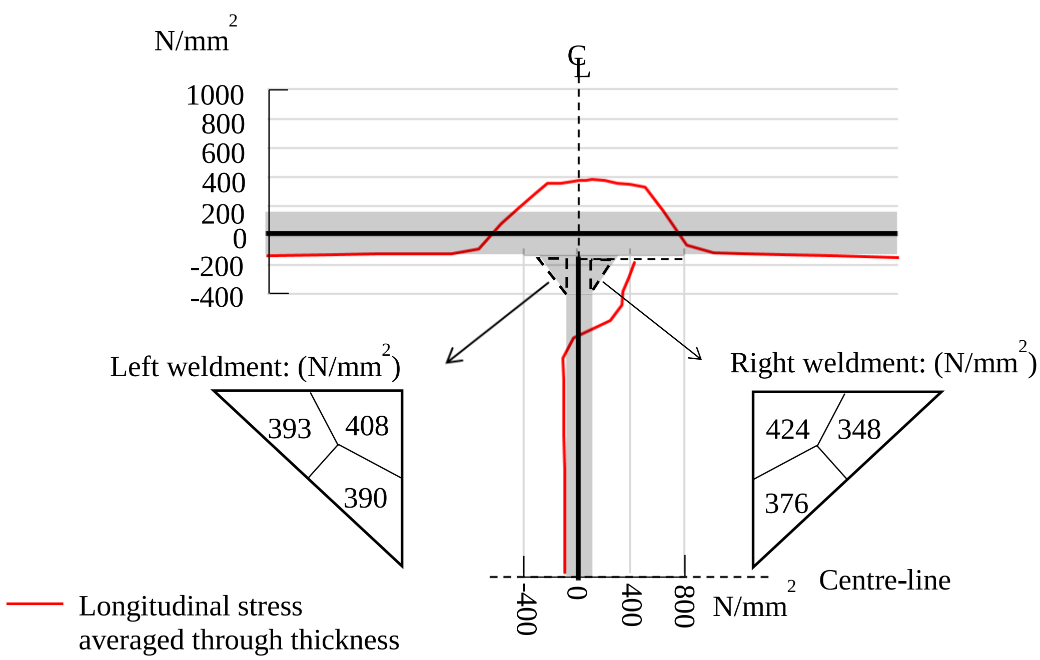

(b) Section C2

Figure 5.9: Predicted residual stress patterns for welded S355 H-sections

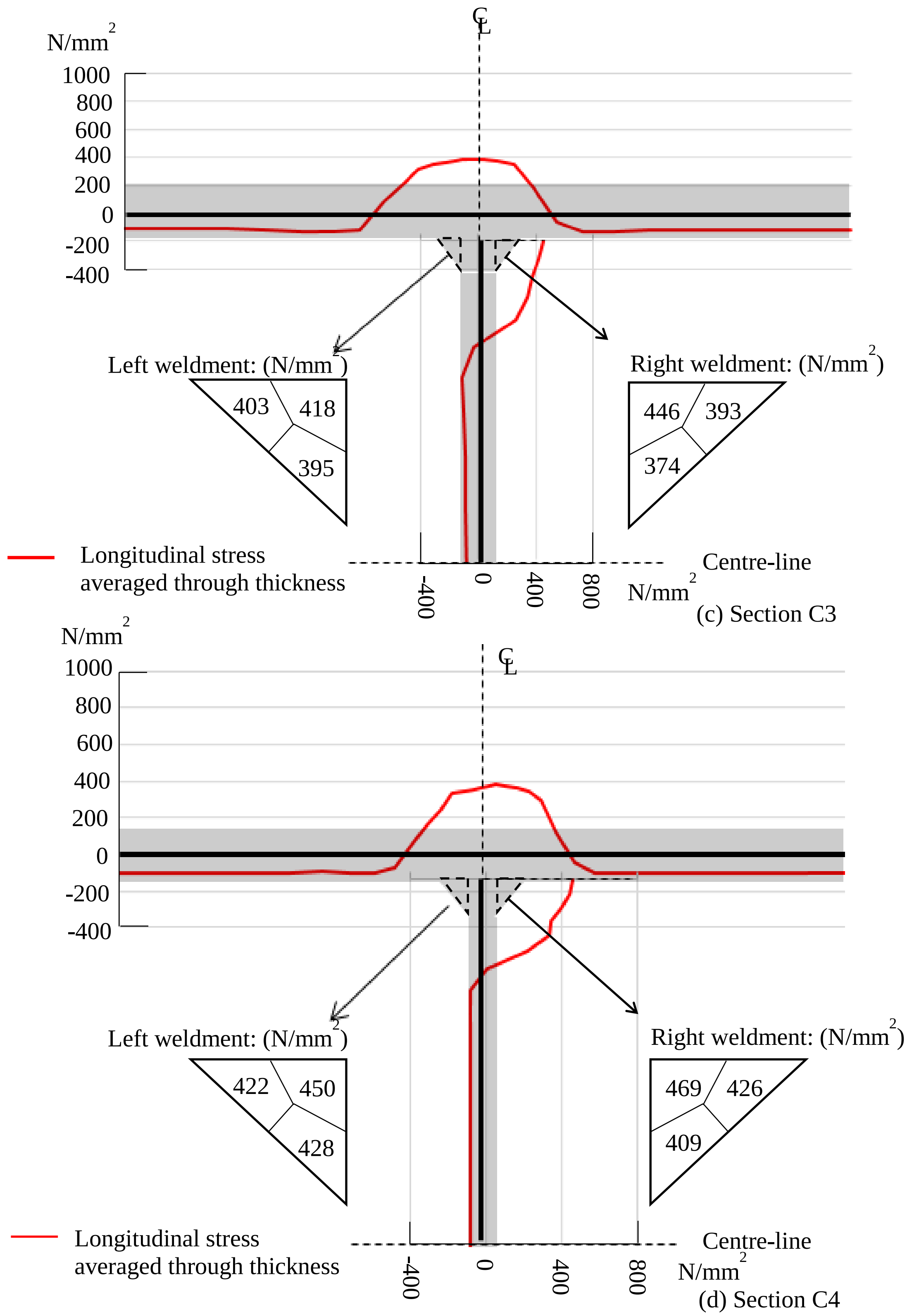

Figure 5.9: Predicted residual stress patterns for welded S355 H-sections (Continued)

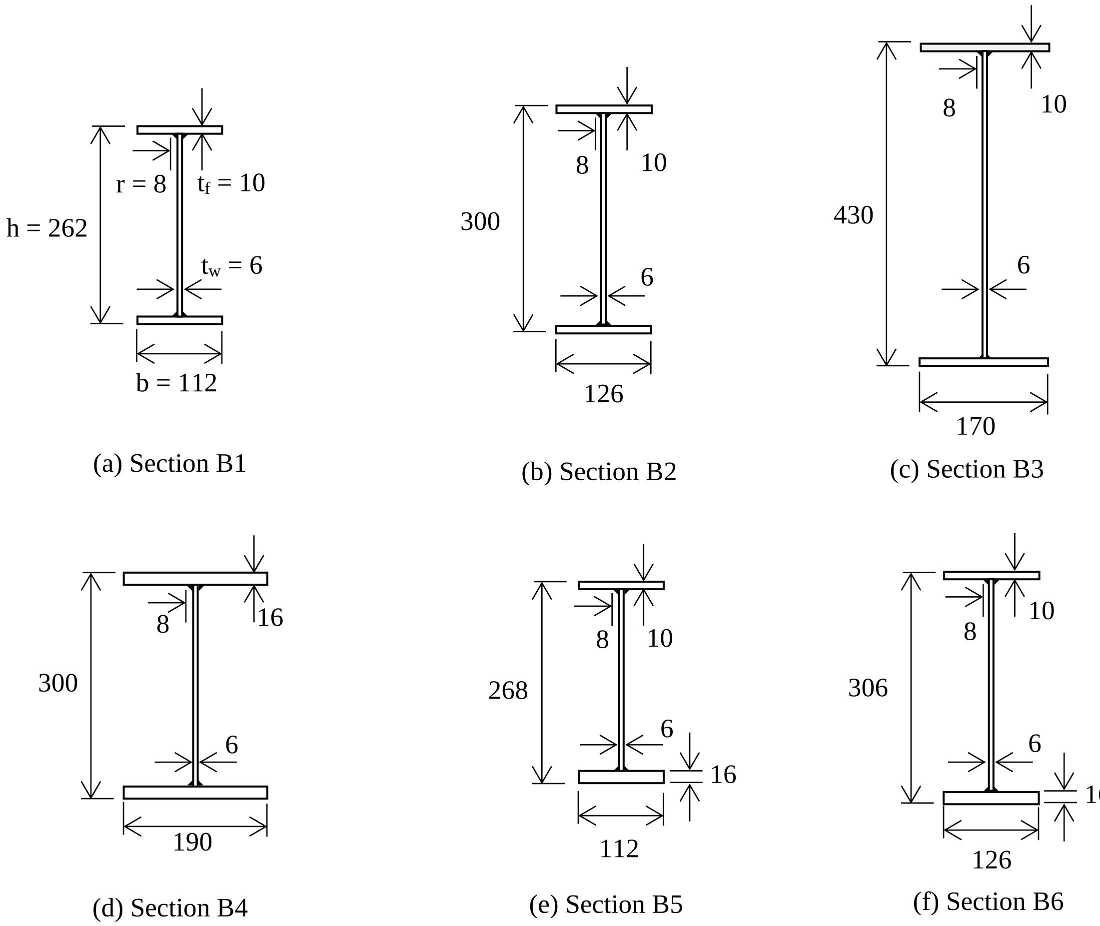

Figure 5.10: Dimensions of S690 welded I-sections applied in numerical study

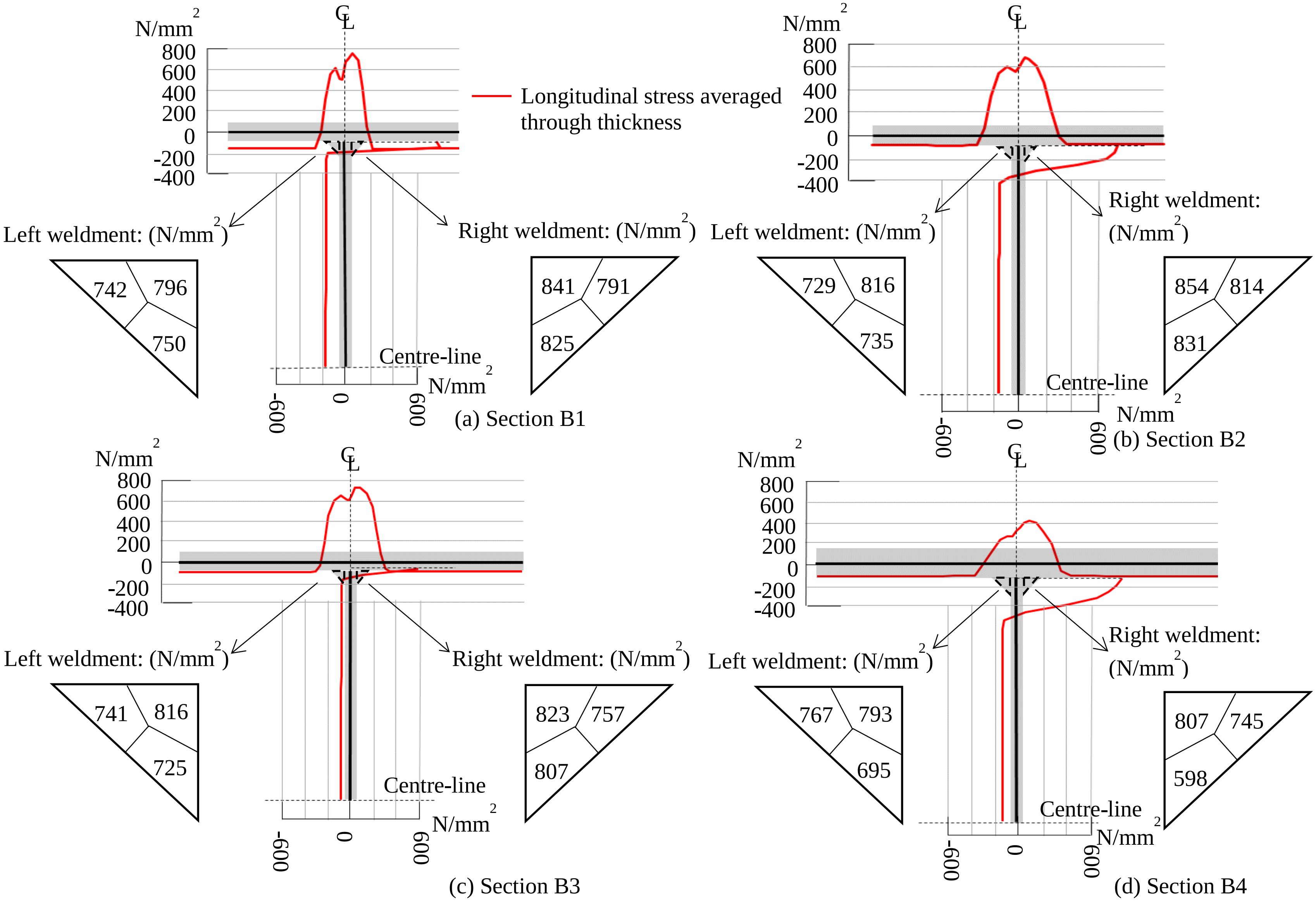

Figure 5.11: Predicted residual stress patterns for welded S690 I-sections

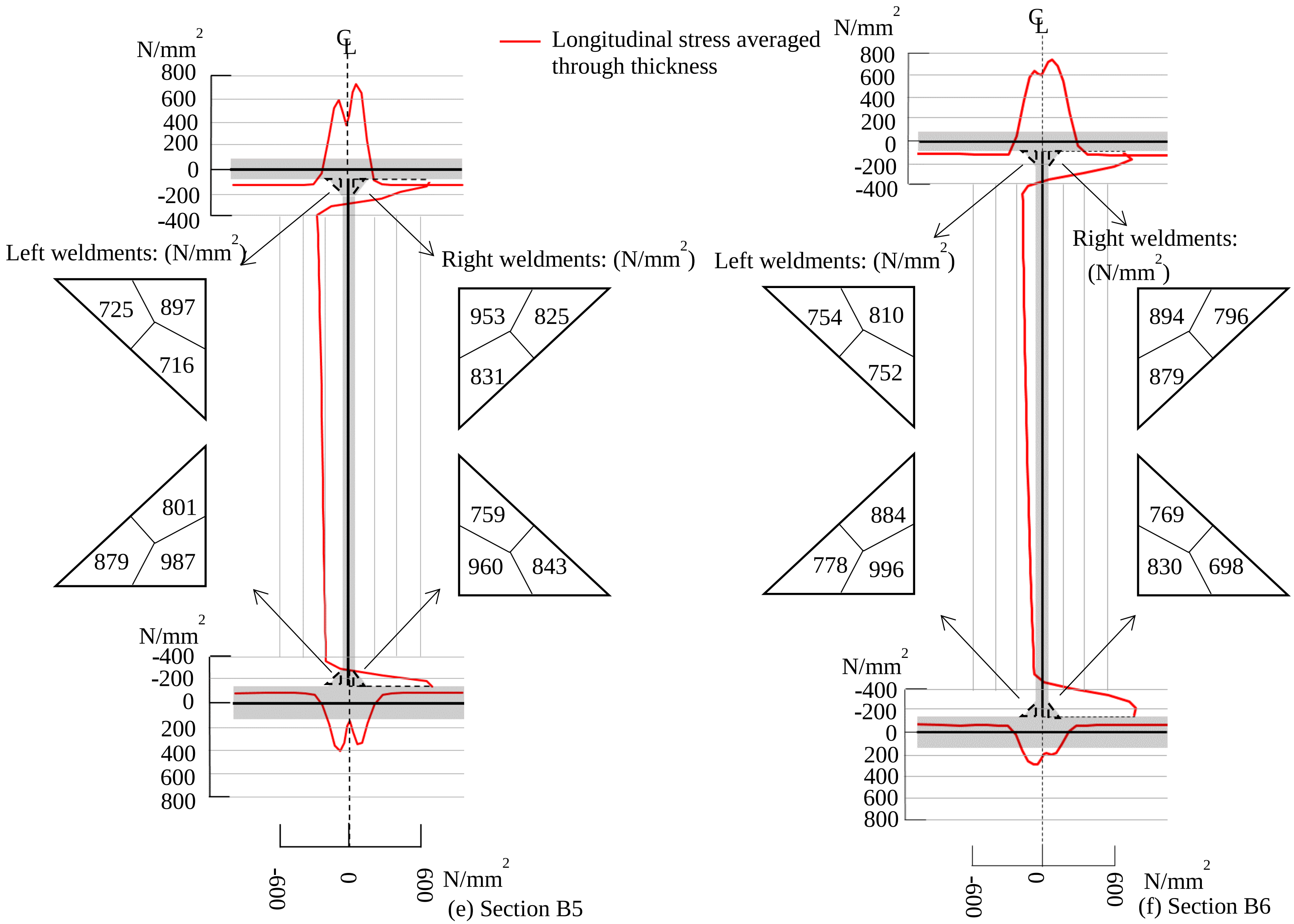

Figure 5.11: Predicted residual stress patterns for welded S690 I-sections (Continued)

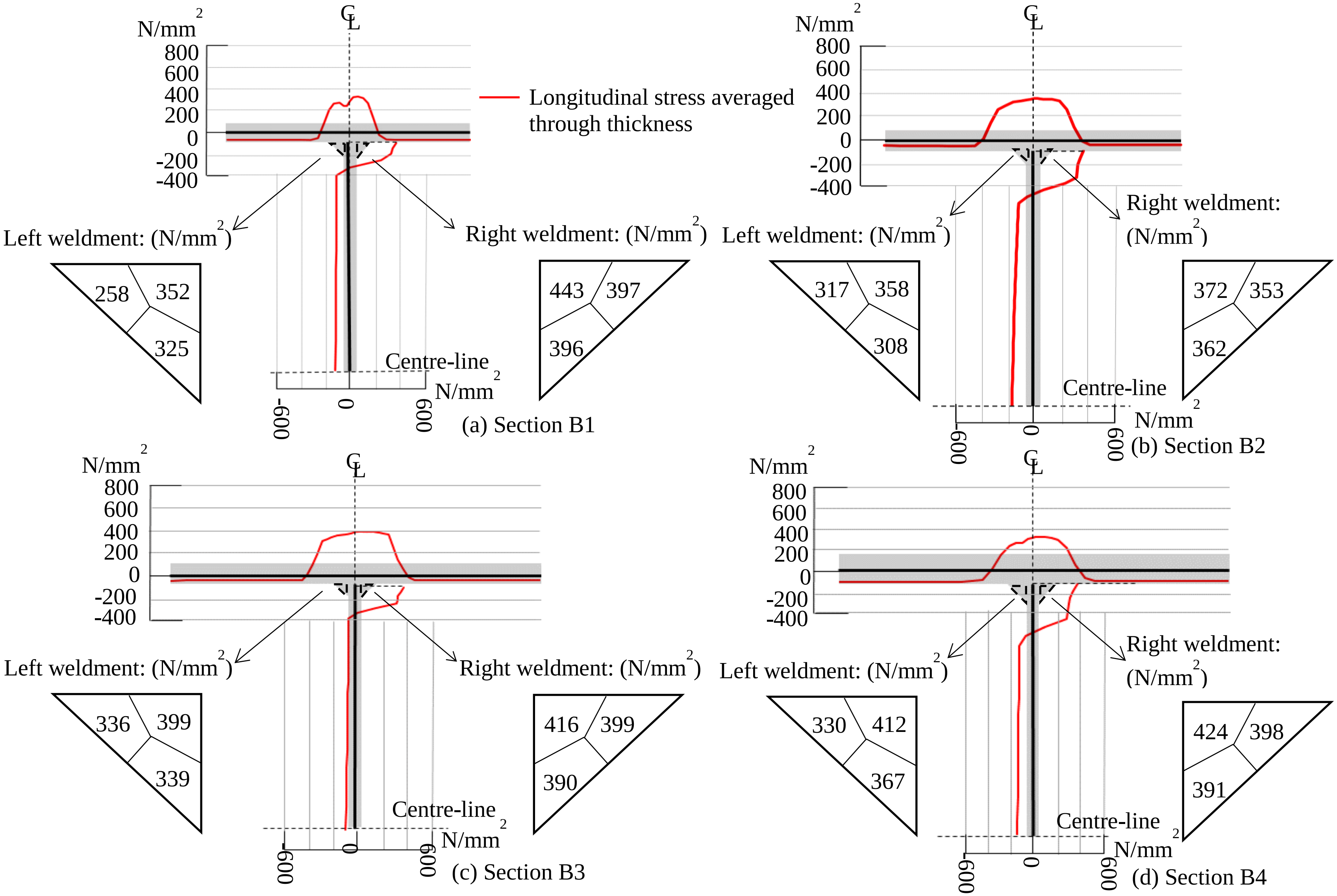

Figure 5.12: Calculated residual stress pattern for welded S355 I-sections

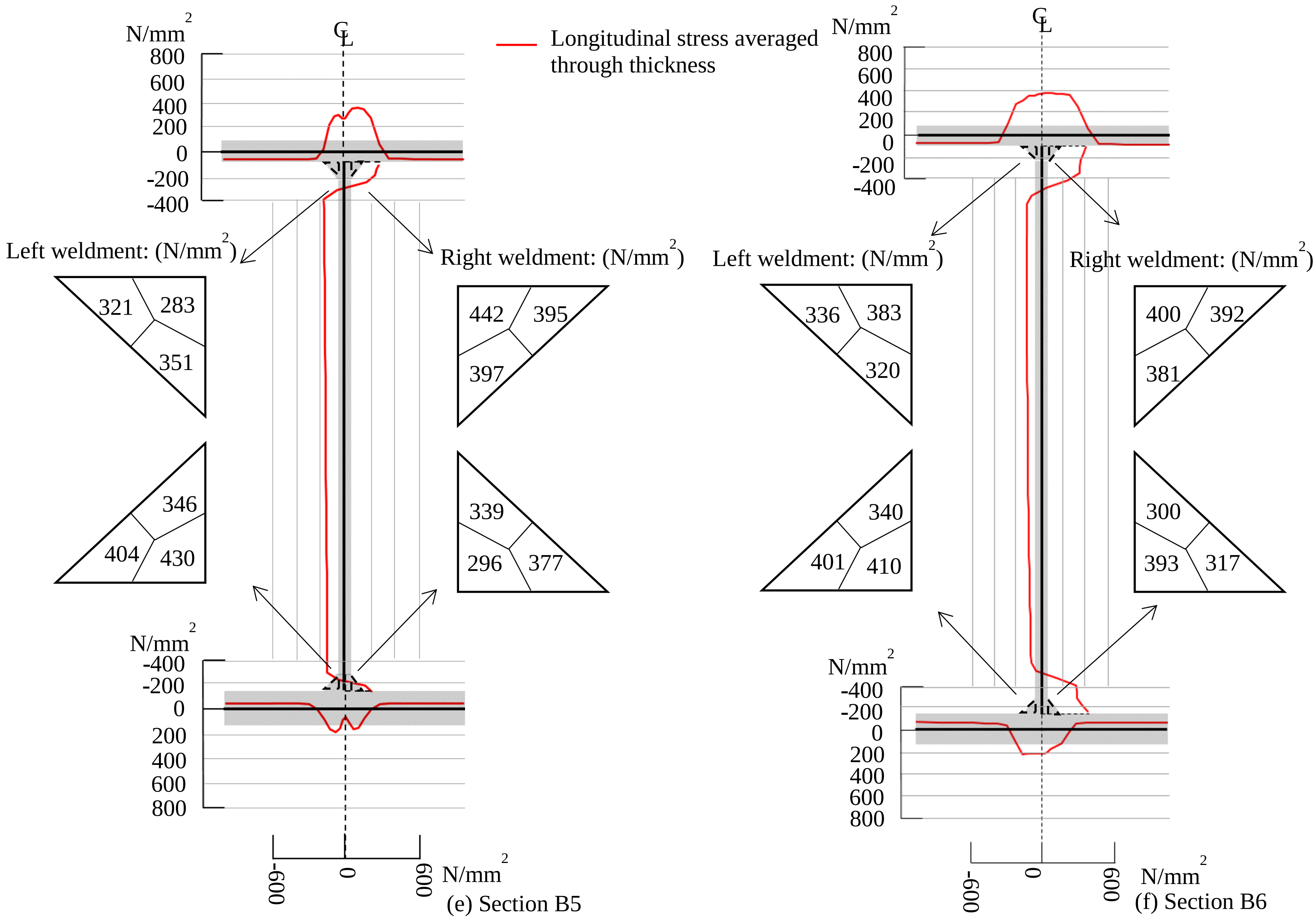

Figure 5.12: Calculated residual stress patterns for welded S355 I-sections (Continued)

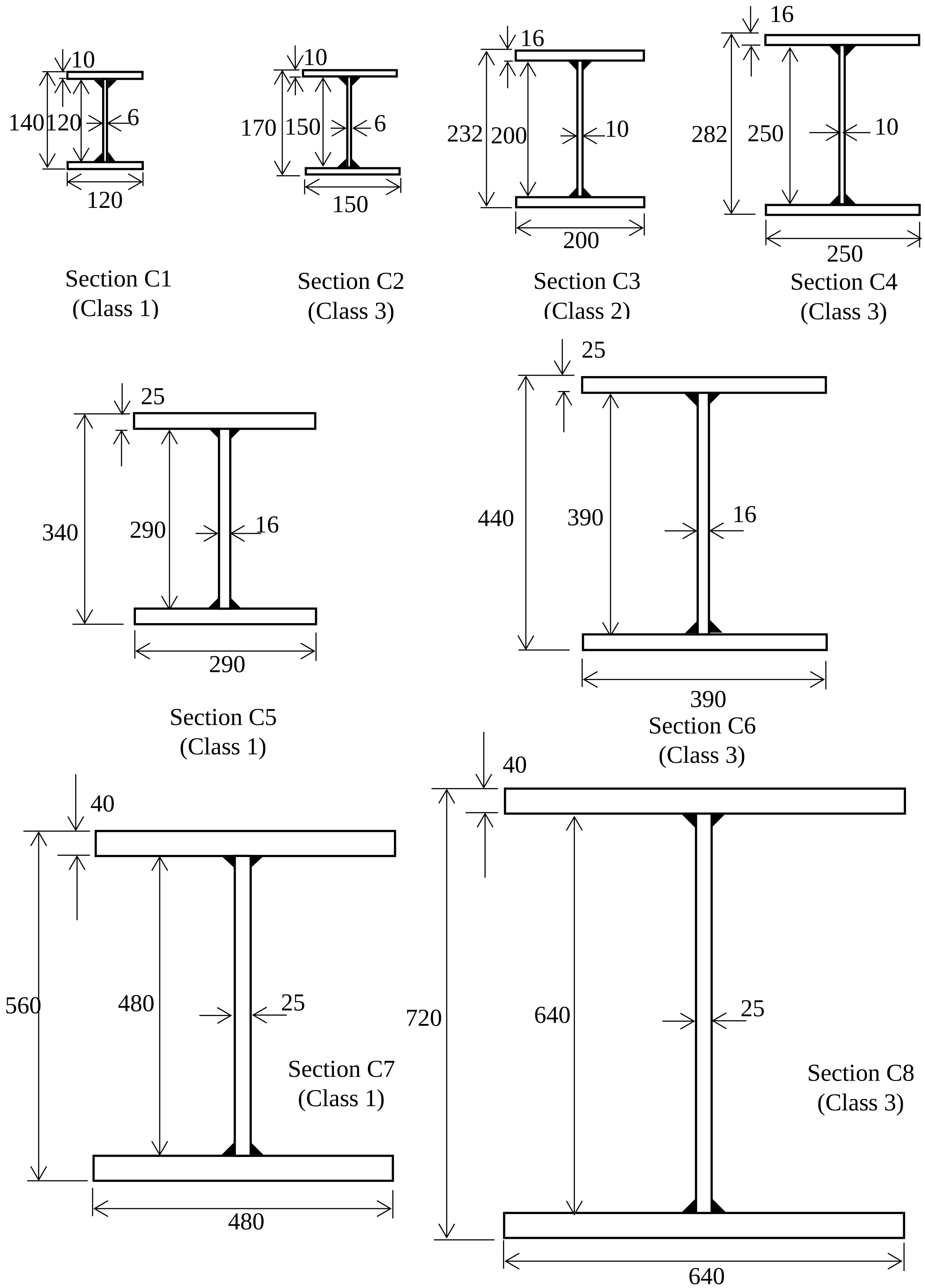

Figure 5.13: Dimensions of welded S690 H-sections including plates up to 40mm thickness

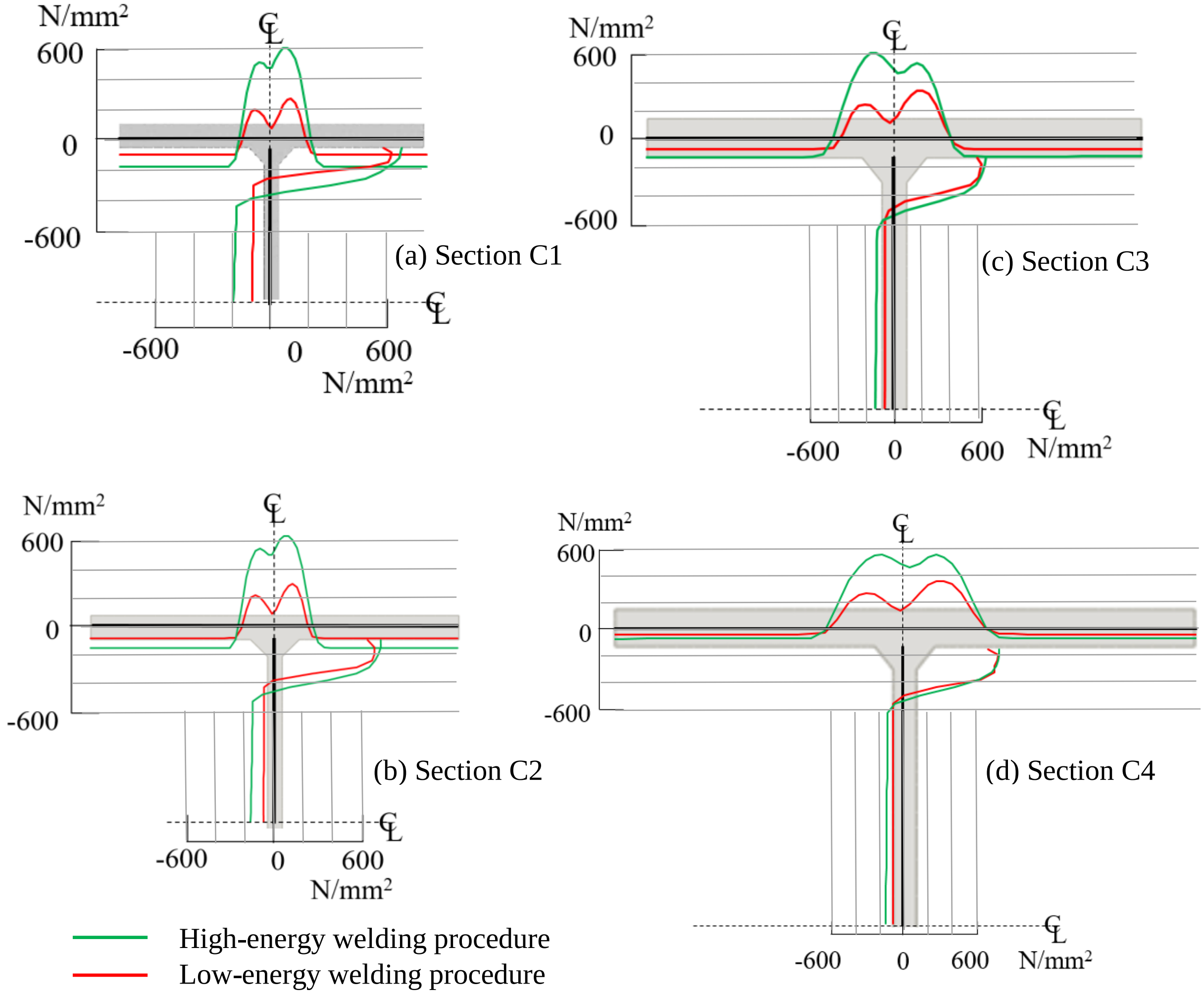

Figure 5.14: Residual stress patterns of welded S690 H-sections with different welding procedures (Sections C1 to C4)

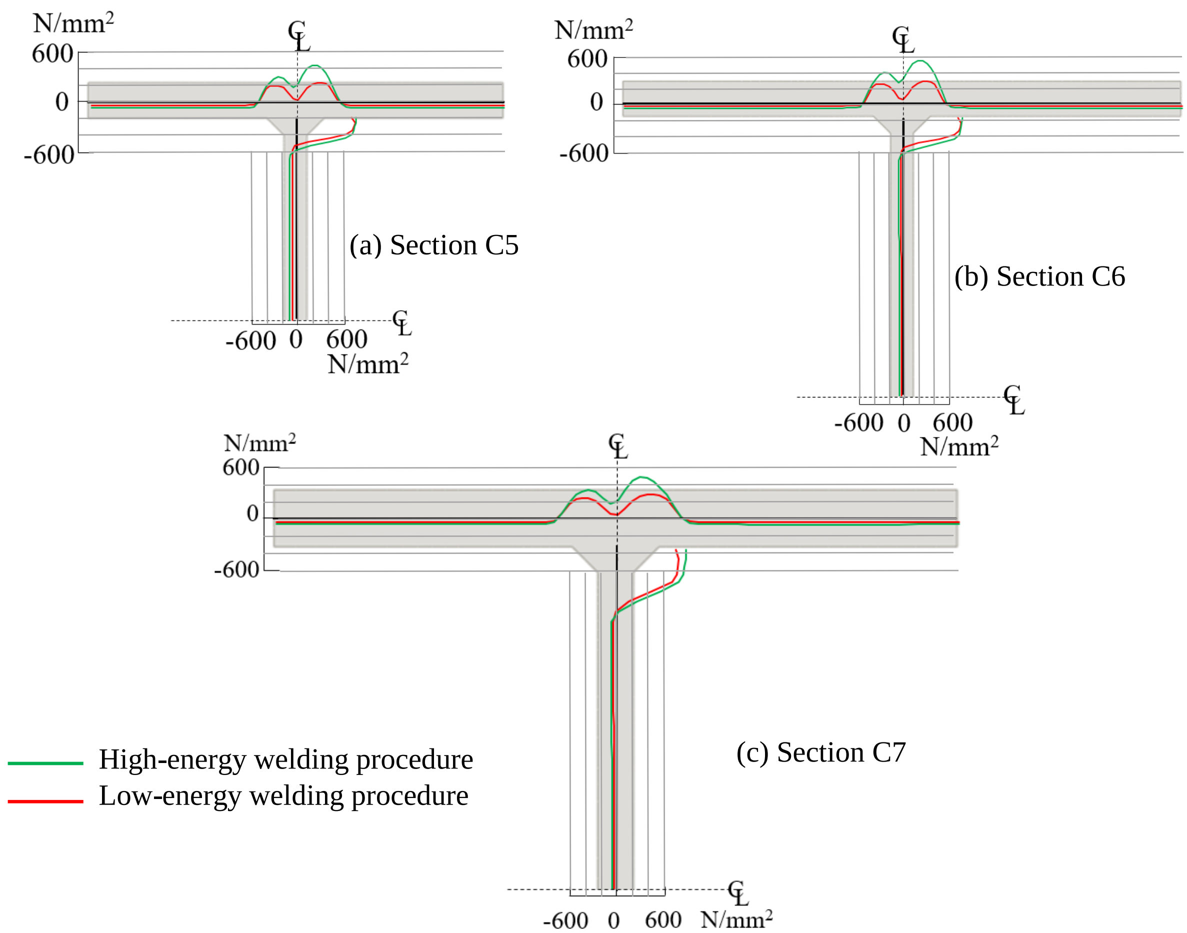

Figure 5.14: Residual stress patterns of S690 welded sections using different welding procedures (Sections C5 to C7)

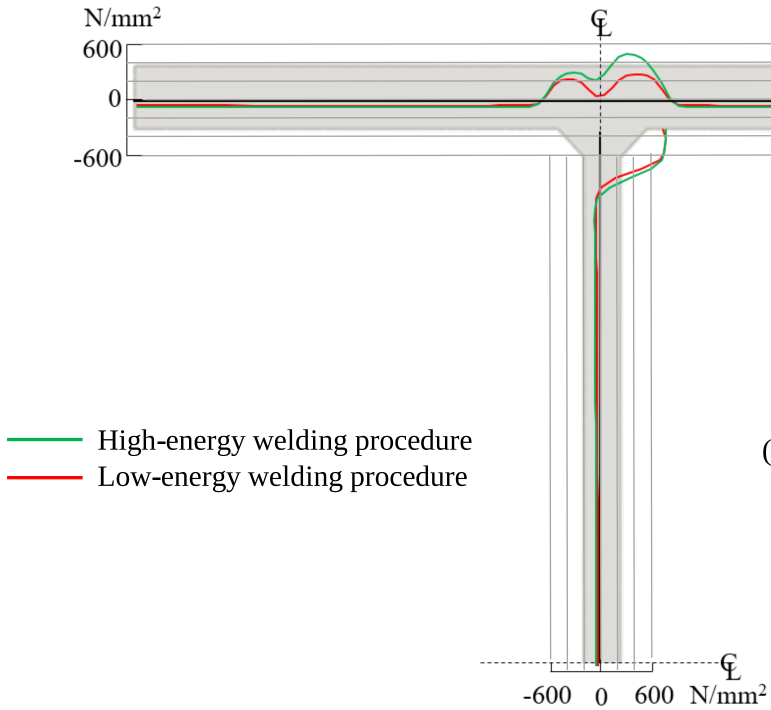

Figure 5.14: Residual stress patterns of S690 welded sections using different welding procedures (Section C8)

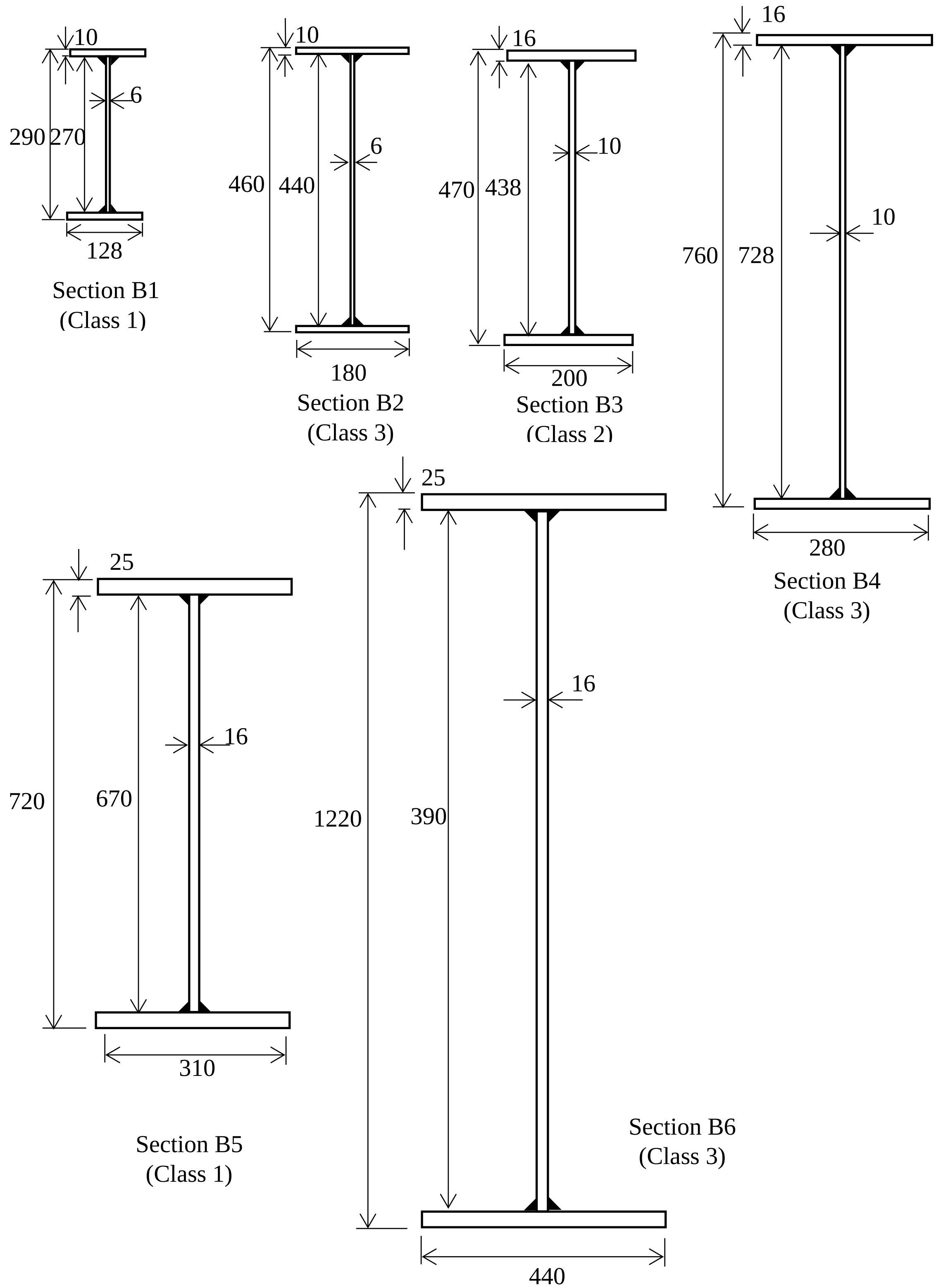

Figure 5.15: Dimensions of welded S690 I-sections including plates up to 40mm thickness

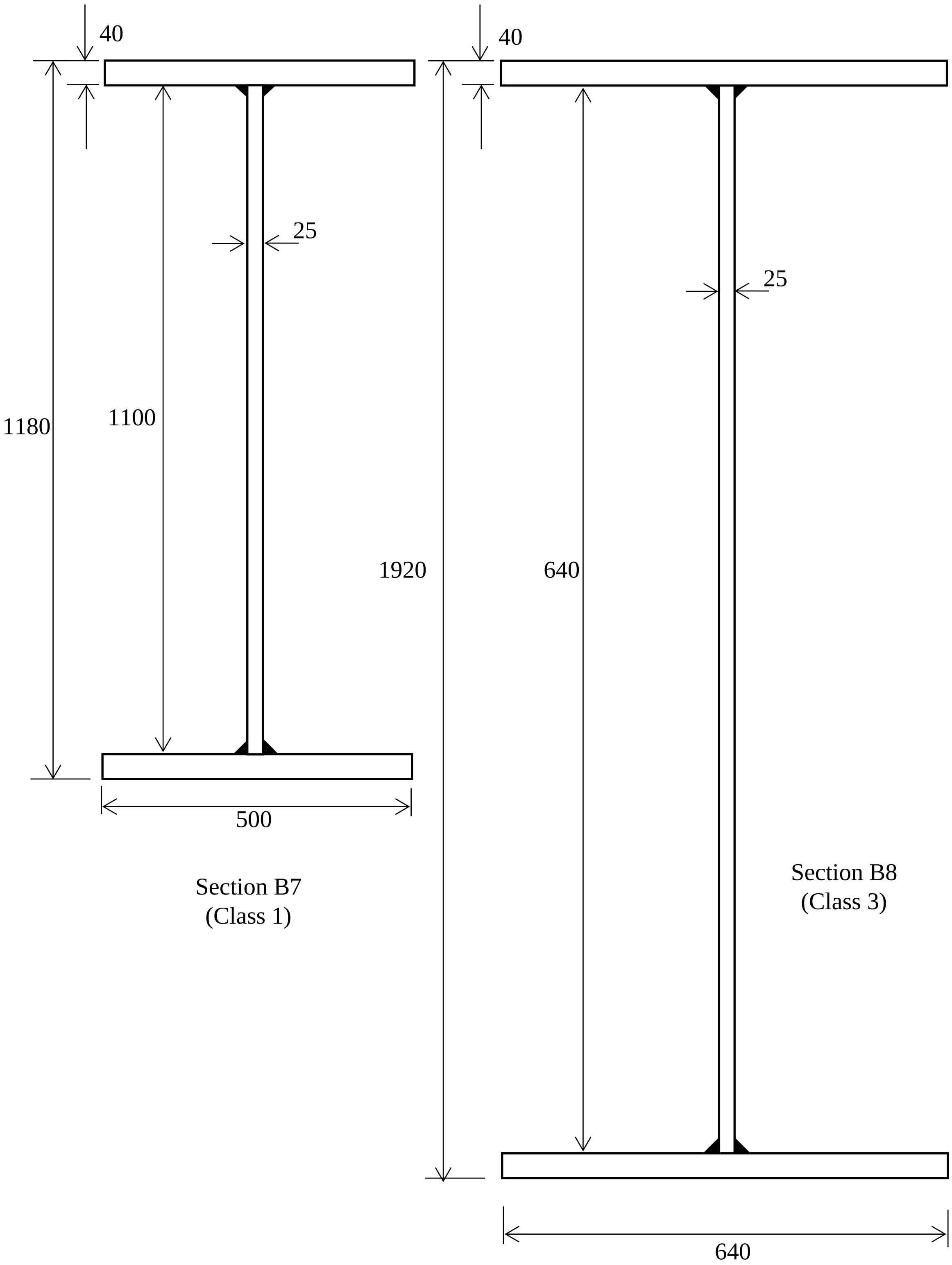

Figure 5.15: Dimensions of welded S690 I-sections including plates up to 40mm thickness (Continued)

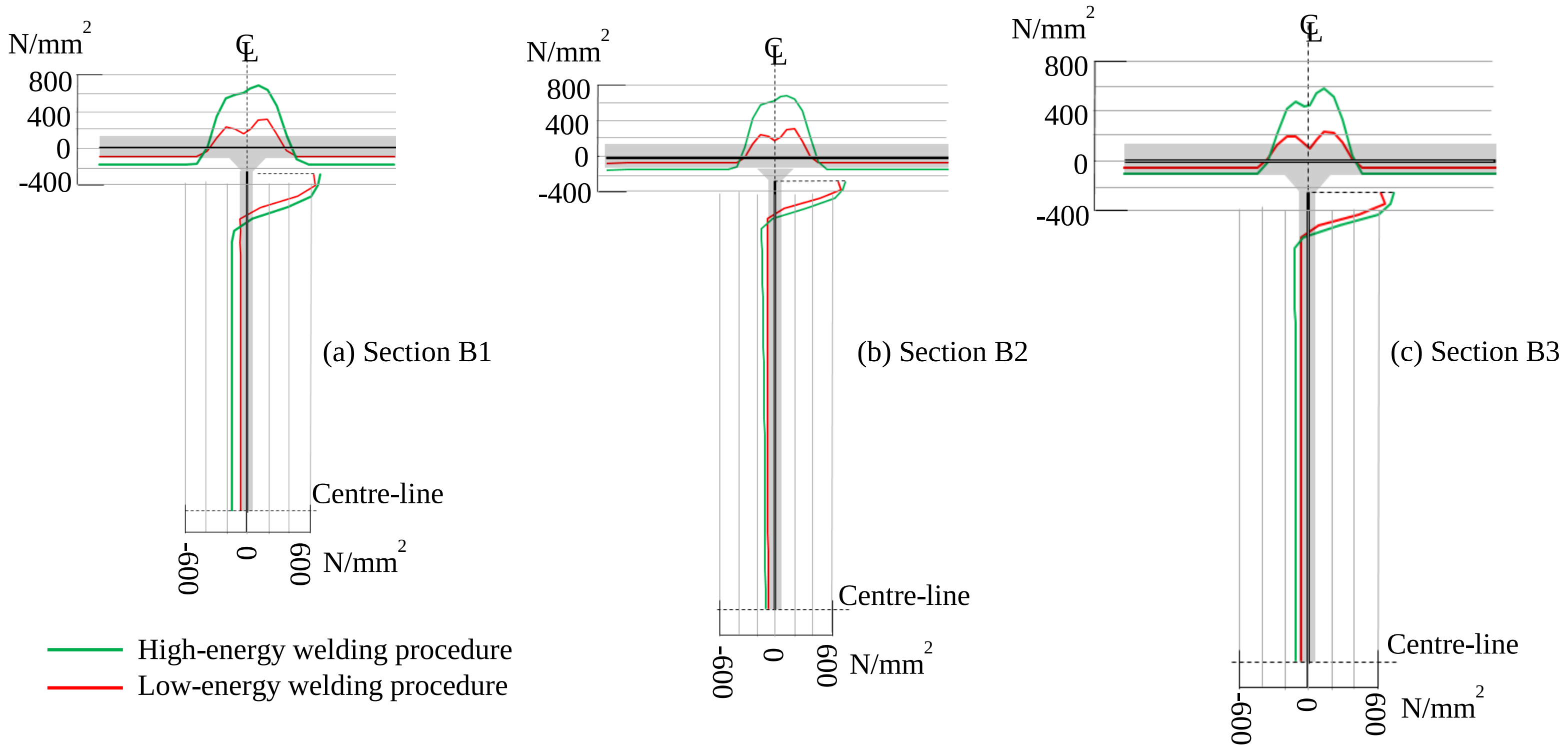

Figure 5.16: Residual stress patterns of S690 welded I-sections using different welding procedures (Sections B1 to B4)

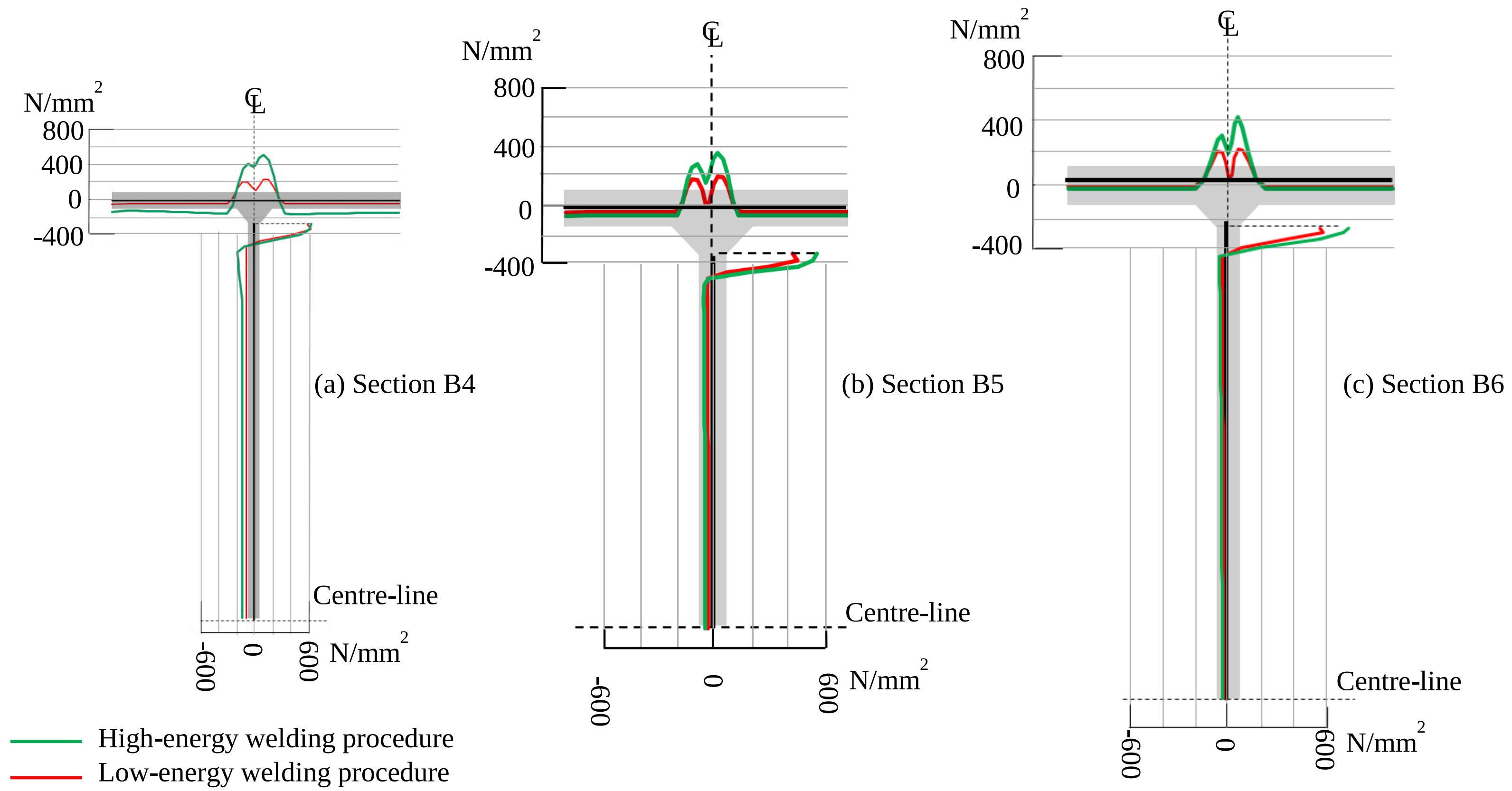

Figure 5.16: Residual stress patterns of S690 welded I-sections using different welding procedures (Sections B4 to B6)

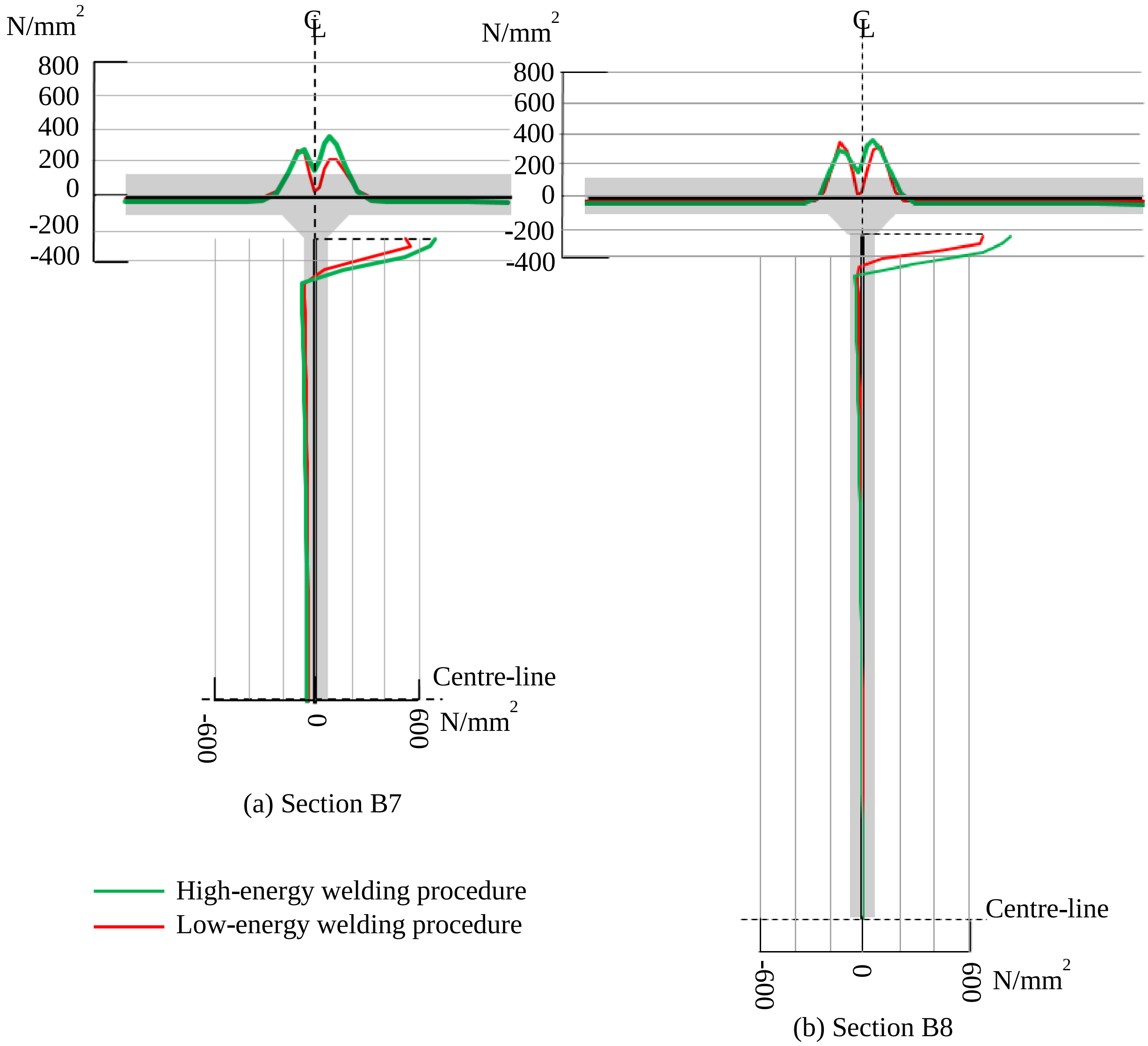

Figure 5.16: Residual stress patterns of S690 welded I-sections using different welding procedures (Sections B7 and B8)

Table 5.1: Welding parameters of S690 welded H- and I-sections applied in numerical models

Welding procedures	Thickness of combined steel plates			Welding parameters					Cross-sectional area per run A_{weld} (mm^2)	heat flux per unit volume Q (kJ/mm^3)	Line heat energy input for a single run q (kJ/mm)
	t_f (mm)	t_w (mm)	r (mm)	Voltage U (V)	Current I (A)	Velocity v (mm/s)	Pass No.	Welding efficiency η			
High-energy welding (Measured)	10	6	8	28.0	225	5.3	1	0.85	18	0.056	1.01
	16	6	8	28.0	225	4.2	1	0.85	18	0.071	1.28
	16	10	8	28.0	225	4.8	1	0.85	18	0.062	1.12
High-energy welding	10	6	8	30.5	260	6.3	1	0.85	18	0.059	1.07
	16	10	8	34.0	450	5.4	1	0.95	50	0.054	2.69
	25	16	12	36.0	545	4.8	1	0.95	72	0.054	3.88
	40	25	18	34.0	450	1.7	1	0.95	162	0.053	8.55
Low-energy welding	10	6	8	30.5	260	18.9	3	0.85	6	0.059	0.36
	16	10	8	34.0	450	16.2	3	0.95	17	0.053	0.90
	25	16	12	36.0	545	14.4	3	0.95	24	0.054	1.29
	40	25	18	34.0	450	5.0	3	0.95	54	0.054	2.91

Table 5.2: Comparison between measured and predicted residual stresses

Section	Residual stress	Top flange: Left ---------------------------> Right							Web: Mid -----> Top		
Section B2	Measured value f_{rs} (N/mm^2)	-159	-191	145	400	235	-148	-129	-168	-106	-74
	Predicted value $f_{rs,FE}$ (N/mm^2)	-137	-137	273	438	297	-138	-137	-137	-130	-117
	Relative error $\lvert f_{rs,FE} - f_{rs}\rvert / f_y$ (%)	2.8	6.9	16.3	4.8	7.9	1.3	1.0	4.3	3.3	5.9
Section B4	Measured value f_{rs} (N/mm^2)	-35	-102	-52	111	-48	-88	-77	-73	-48	-83
	Predicted value $f_{rs,FE}$ (N/mm^2)	-80	-78	-54	96	-61	-93	-93	-80	-61	-24
	Relative error $\lvert f_{rs,FE} - f_{rs}\rvert / f_y$ (%)	6.0	3.2	0.3	2.0	1.7	0.7	2.1	1.0	1.8	8.2
Section B6	Measured value f_{rs} (N/mm^2)	-101	-146	156	453	92	-106	-197	-88	-94	-195
	Predicted value $f_{rs,FE}$ (N/mm^2)	-161	-163	189	478	182	-175	-188	-127	-132	-205
	Relative error $\lvert f_{rs,FE} - f_{rs}\rvert / f_y$ (%)	7.7	2.2	4.2	3.2	11.5	8.8	1.1	5.4	5.3	1.4

Table 5.3: Key residual stress parameters for welded S690 and S355 H-sections

Section type	Section	Section Dimensions h (mm)	b (mm)	t_f (mm)	t_w (mm)	r (mm)	Flange $f_{rs,t,f}$ (N/mm^2)	$\frac{f_{rs,t,f}}{f_{y,f}}$	$f_{rs,c,f}$ (N/mm^2)	$\frac{f_{rs,c,f}}{f_{y,f}}$	Web $f_{rs,t,w}$ (N/mm^2)	$\frac{f_{rs,t,w}}{f_{y,w}}$	$f_{rs,c,w}$ (N/mm^2)	$\frac{f_{rs,c,w}}{f_{y,w}}$
S690 welded H-sections	C1S	140	120	10	6	8	678	0.90	-201	-0.27	773	0.99	-192	-0.25
	C2S	170	150	10	6	8	650	0.86	-137	-0.18	763	0.98	-130	-0.17
	C3S	232	200	16	10	8	505	0.65	-129	-0.17	786	1.04	-128	-0.17
	C4S	282	250	16	10	8	605	0.78	-103	-0.13	802	1.06	-103	-0.14
S355 welded H-sections	C1S	140	120	10	6	8	374	1.05	-176	-0.50	373	1.05	-136	-0.38
	C2S	170	150	10	6	8	370	1.04	-127	-0.36	381	1.07	-87	-0.25
	C3S	232	200	16	10	8	364	1.03	-117	-0.33	391	1.10	-96	-0.27
	C4S	282	250	16	10	8	361	1.02	-101	-0.28	395	1.11	-85	-0.24

Table 5.4: Key residual stress parameters for welded S690 and S355 I-sections

Section type	Section	Section dimensions					Flange				Web			
		h (mm)	b (mm)	t_f (mm)	t_w (mm)	r (mm)	$f_{rs,t,f}$ (N/mm^2)	$\frac{f_{rs,t,f}}{f_{y,f}}$	$f_{rs,c,f}$ (N/mm^2)	$\frac{f_{rs,c,f}}{f_{y,f}}$	$f_{rs,t,w}$ (N/mm^2)	$\frac{f_{rs,t,w}}{f_{y,w}}$	$f_{rs,c,w}$ (N/mm^2)	$\frac{f_{rs,c,w}}{f_{y,w}}$
S690 welded I-sections	B1	262	112	10	6	8	640	0.83	-152	-0.20	763	1.05	-153	-0.21
	B2	300	126	10	6	8	539	0.70	-137	-0.18	713	0.99	-142	-0.20
	B3	430	170	10	6	8	596	0.77	-99	-0.13	809	1.12	-102	-0.14
	B4	300	190	16	10	8	385	0.52	-78	-0.10	842	1.17	-77	-0.11
	B5	268	112	TF: 10 BF: 16	6	8	TF: 555 BF: 276	TF: 0.72 BF: 0.37	-69	-0.09	734	1.02	-63	-0.09
	B6	306	126	TF: 10 BF: 16	6	8	TF: 591 BF: 226	TF: 0.76 BF: 0.30	-168	-0.22	731	1.01	-126	-0.17
S355 welded I-sections	B1	262	112	10	6	8	306	0.86	-63	-0.18	367	1.03	-70	-0.20
	B2	300	126	10	6	8	321	0.90	-86	-0.24	354	1.00	-125	-0.35
	B3	430	170	10	6	8	345	0.97	-69	-0.19	382	1.08	-90	-0.25
	B4	300	190	16	10	8	333	0.94	-75	-0.21	375	1.06	-94	-0.26
	B5	268	112	TF: 10 BF: 16	6	8	TF: 315 BF: 156	TF: 0.89 BF: 0.44	-73	-0.21	365	1.03	-62	-0.17
	B6	306	126	TF: 10 BF: 16	6	8	TF: 336 BF: 216	TF: 0.94 BF: 0.61	-124	-0.35	376	1.06	-116	-0.33

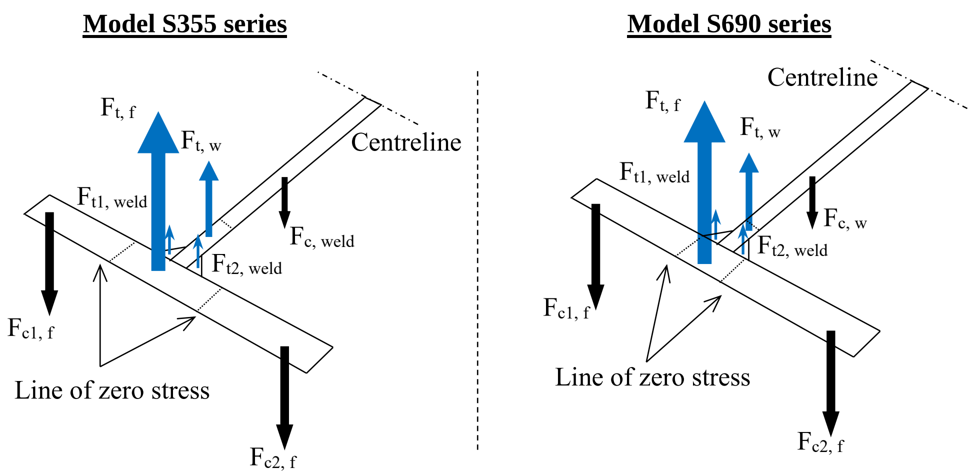

Table 5.5 (a): Force equilibrium in single-pass S355 welded H-sections (kN)

Section	Flange			Flange-web junction		Web		Out-of-balance force		
	$F_{t,f}$	$F_{c1,f}$	$F_{c2,f}$	$F_{t1,weld}$	$F_{t2,weld}$	$F_{t,w}$	$F_{c,w}$	Tension	Compression	Total
B1	62	-27	-26	8	9	21	-45	+100	-98	+2
B2	107	-33	-36	8	9	37	-96	+161	-165	-4
B3	125	-43	-41	9	10	40	-99	+184	-183	+1
B4	152	-80	-73	10	11	77	-99	+250	-252	-2
B5*	69	-33	-27	7	10	23	-39	+165	-164	+1
	30	-16	-16	9	8	9	-33			
B6*	116	-46	-42	9	10	34	-76	+306	-304	+2
	85	-34	-34	9	8	35	-72			

*** Note:**
Sections B5 and B6 are singly symmetrical sections, hence longitudinal forces obtained from both top and bottom half T-sections are presented.

Table 5.5 (b): Force equilibrium in single-pass S690 welded H-sections (kN)

Section	Flange			Flange-web junction		Web		Out-of-balance force		
	$F_{t,f}$	$F_{c1,f}$	$F_{c2,f}$	$F_{t1,weld}$	$F_{t2,weld}$	$F_{t,w}$	$F_{c,w}$	Tension	Compression	Total
B1	140	-60	-60	25	23	25	-95	+213	-215	-2
B2	142	-64	-56	19	20	51	-107	+232	-227	+5
B3	164	-70	-66	19	19	59	-127	+261	-263	-2
B4	151	-95	-92	18	19	113	-112	+301	-299	+2
B5*	112	-54	-52	18	19	41	-85	+326	-327	-1
	63	-35	-34	21	20	32	-67			
B6*	136	-76	-75	19	22	52	-102	+414	-416	-2
	79	-45	-45	22	19	65	-73			

*** Note:**
Sections B5 and B6 are singly symmetrical sections, hence longitudinal forces obtained from both top and bottom half T-sections are presented.

Table 5.6: Key residual stress parameters for welded S690 H-sections using different welding procedures

Welding procedures	Section	Dimensions h (mm)	b (mm)	t_f (mm)	t_w (mm)	r (mm)	Flange $f_{rs,t,f}$ (N/mm^2)	$\frac{f_{rs,t,f}}{f_{y,f}}$	$f_{rs,c,f}$ (N/mm^2)	$\frac{f_{rs,c,f}}{f_{y,f}}$	Web $f_{rs,t,w}$ (N/mm^2)	$\frac{f_{rs,t,w}}{f_{y,w}}$	$f_{rs,c,w}$ (N/mm^2)	$\frac{f_{rs,c,w}}{f_{y,w}}$
High-energy welding	C1S-SP	140	120	10	6	8	547	0.79	-169	-0.24	732	1.06	-197	-0.29
	C2S-SP	170	150	10	6	8	583	0.84	-143	-0.21	663	0.96	-163	-0.24
	C3S-SP	232	200	16	10	8	546	0.79	-139	-0.20	762	1.10	-143	-0.21
	C4S-SP	282	250	16	10	8	523	0.76	-103	-0.15	785	1.14	-124	-0.18
	C5S-SP	312	290	25	16	12	415	0.60	-88	-0.13	805	1.17	-88	-0.13
	C6S-SP	412	390	25	16	12	423	0.61	-70	-0.10	792	1.15	-67	-0.10
	C7S-SP	530	480	40	25	18	372	0.54	-81	-0.12	835	1.21	-73	-0.11
	C8S-SP	690	640	40	25	18	358	0.52	-64	-0.09	783	1.13	-57	-0.08
Low-energy welding	C1S-MP	140	120	10	6	8	186	0.27	-86	-0.12	632	0.92	-91	-0.13
	C2S-MP	170	150	10	6	8	203	0.29	-73	-0.90	621	0.90	-73	-0.11
	C3S-MP	232	200	16	10	8	222	0.32	-79	-0.11	736	1.07	-82	-0.12
	C4S-MP	282	250	16	10	8	215	0.31	-66	-0.10	753	1.09	-66	-0.10
	C5S-MP	312	290	25	16	12	155	0.22	-57	-0.08	777	1.13	-54	-0.08
	C6S-MP	412	390	25	16	12	182	0.26	-44	-0.06	769	1.11	-41	-0.06
	C7S-MP	530	480	40	25	18	209	0.30	-58	-0.08	763	1.11	-50	-0.07
	C8S-MP	690	640	40	25	18	188	0.27	-48	-0.07	759	1.10	-39	-0.06

Table 5.6: Key residual stress parameters for welded S690 I-sections using different welding procedures

Welding procedures	Section	Dimensions					Flange				Web			
		h (mm)	b (mm)	t_f (mm)	t_w (mm)	r (mm)	$f_{rs,t,f}$ (N/mm^2)	$\frac{f_{rs,t,f}}{f_{y,f}}$	$f_{rs,c,f}$ (N/mm^2)	$\frac{f_{rs,c,f}}{f_{y,f}}$	$f_{rs,t,w}$ (N/mm^2)	$\frac{f_{rs,t,w}}{f_{y,w}}$	$f_{rs,c,w}$ (N/mm^2)	$\frac{f_{rs,c,w}}{f_{y,w}}$
High-energy welding	B1-SP	290	128	10	6	8	637	0.92	-181	-0.26	686	0.99	-176	-0.26
	B2-SP	460	180	10	6	8	616	0.89	-143	-0.21	717	1.04	-126	-0.18
	B3-SP	470	200	16	10	8	527	0.76	-108	-0.16	693	1.00	-103	-0.15
	B4-SP	760	280	16	10	8	429	0.62	-152	-0.22	610	0.88	-128	-0.19
	B5-SP	720	310	25	16	12	284	0.41	-59	-0.09	524	0.76	-52	-0.08
	B6-SP	1,220	440	25	16	12	263	0.38	-46	-0.07	701	1.02	-40	-0.06
	B7-SP	1,180	500	40	25	18	186	0.27	-66	-0.10	625	0.91	-50	-0.07
	B8-SP	1,920	640	40	25	18	218	0.32	-51	-0.07	715	1.04	-43	-0.06
Low-energy welding	B1-MP	290	128	10	6	8	225	0.33	-92	-0.13	660	0.96	-96	-0.14
	B2-MP	460	180	10	6	8	245	0.36	-60	-0.09	655	0.95	-61	-0.09
	B3-MP	470	200	16	10	8	228	0.33	-56	-0.08	626	0.91	-60	-0.09
	B4-MP	760	280	16	10	8	239	0.35	-38	-0.06	592	0.86	-35	-0.05
	B5-MP	720	310	25	16	12	163	0.24	-36	-0.05	426	0.62	-31	-0.04
	B6-MP	1,220	440	25	16	12	157	0.23	-28	-0.04	482	0.70	-24	-0.03
	B7-MP	1,180	500	40	25	18	132	0.19	-44	-0.06	554	0.80	-33	-0.05
	B8-MP	1,920	640	40	25	18	118	0.17	-33	-0.05	649	0.94	-28	-0.04

Table 5.7: Comparison on predicted residual stresses and estimation from ECCS

Sections		Flange				Web			
		$f_{rs,t,f}$ / $f_{y,f}$		$f_{rs,c,f}$ / $f_{y,f}$		$f_{rs,t,w}$ / $f_{y,f}$		$f_{rs,c,w}$ / $f_{y,f}$	
		FEM	**ECCS**	**FEM**	**ECCS**	**FEM**	**ECCS**	**FEM**	**ECCS**
S690 Welded I-sections	**B1**	0.83	1.00	-0.20	-0.50	1.05	1.00	-0.21	-0.50
	B2	0.70	1.00	-0.18	-0.50	0.99	1.00	-0.20	-0.50
	B3	0.77	1.00	-0.13	-0.50	1.12	1.00	-0.14	-0.50
	B4	0.52	1.00	-0.10	-0.50	1.17	1.00	-0.11	-0.50
	B5	TF: 0.72 BF: 0.37	1.00	-0.09	-0.50	1.02	1.00	-0.09	-0.50
	B6	TF: 0.76 BF: 0.30	1.00	-0.22	-0.50	1.01	1.00	-0.17	-0.50

Table 5.8: Simplified model to estimate residual stresses in S690 welded sections

Location of residual stresses		High-energy weld	Low-energy weld
Flange	Tension, $f_{rs,t,f}$ / $f_{y,f}$	-0.17 ln(t_f) + 1.14	-0.02 ln(t_f) + 0.35
	Compression, $f_{rs,c,f}$ / $f_{y,f}$	0.067 ln(t_f) – 0.36	0.025 ln(t_f) – 0.17
Web	Tension, $f_{rs,t,w}$ / $f_{y,f}$	1.00	0.92
	Compression, $f_{rs,c,w}$ / $f_{y,f}$	0.067 ln(t_f) – 0.36	0.025 ln(t_f) – 0.17

Table 5.9: Comparison on residual stress ratios from numerical models and Liu's simplified model

Sections		Flange				Web			
		$f_{rs,t,f}$ / $f_{y,f}$		$f_{rs,c,f}$ / $f_{y,f}$		$f_{rs,t,w}$ / $f_{y,f}$		$f_{rs,c,w}$ / $f_{y,f}$	
		FEM	Liu	FEM	Liu	FEM	Liu	FEM	Liu
High-energy welding	B1-SP	0.92	0.75	-0.26	-0.21	0.99	1.00	-0.26	-0.21
	B2-SP	0.89	0.75	-0.21	-0.21	1.04	1.00	-0.18	-0.21
	B3-SP	0.76	0.67	-0.16	-0.17	1.00	1.00	-0.15	-0.17
	B4-SP	0.62	0.67	-0.22	-0.17	0.88	1.00	-0.19	-0.17
	B5-SP	0.41	0.59	-0.09	-0.14	0.76	1.00	-0.08	-0.14
	B6-SP	0.38	0.59	-0.07	-0.14	1.02	1.00	-0.06	-0.14
	B7-SP	0.27	0.51	-0.10	-0.11	0.91	1.00	-0.07	-0.11
	B8-SP	0.32	0.51	-0.07	-0.11	1.04	1.00	-0.06	-0.11
Low-energy welding	B1-MP	0.33	0.30	-0.13	-0.11	0.96	0.92	-0.14	-0.11
	B2-MP	0.36	0.30	-0.09	-0.11	0.95	0.92	-0.09	-0.11
	B3-MP	0.33	0.29	-0.08	-0.10	0.91	0.92	-0.09	-0.10
	B4-MP	0.35	0.29	-0.06	-0.10	0.86	0.92	-0.05	-0.10
	B5-MP	0.24	0.29	-0.05	-0.09	0.62	0.92	-0.04	-0.09
	B6-MP	0.23	0.29	-0.04	-0.09	0.70	0.92	-0.03	-0.09
	B7-MP	0.19	0.28	-0.06	-0.08	0.80	0.92	-0.05	-0.08
	B8-MP	0.17	0.28	-0.05	-0.08	0.94	0.92	-0.04	-0.08

CHAPTER SIX
NUMERICAL MODELLING II: STRUCTURAL INSTABILITY OF S690 WELDED H- AND I-SECTIONS

6.0 Introduction

In order to study the structural behaviour of high strength steel S690 columns and beams, a systematic numerical investigation is carried out in this chapter with advanced modeling technology. Finite element package ABAQUS 6.12 was adopted to carry out material and geometrical nonlinear analyses on finite element models containing both weld-induced residual stresses and scaled eigen modes as initial imperfections. An advanced double Y-shaped finite element model for welded H- and I-sections using 3D shell elements is proposed. Details of the proposed numerical models are presented, including mesh configurations, material models and boundary conditions etc. Convergence studies on various mesh configurations of the numerical models were also conducted.

Five different types of high strength S690 welded sections were modelled carefully, and all of them have been verified against test results as follows:

- Stocky columns of S690 welded H-sections under compression;
- Stocky columns of S690 welded H-sections under combined compression and bending;
- Slender columns of S690 welded H-sections under compression;
- Fully restrained beams of S690 welded I-sections under moment gradient;
- Partially restrained beams of S690 welded I-sections under moment gradient.

Verification of the numerical models is carried out against test results through comparing failure modes, measured resistances and full range deformation characteristics. Interpretation of the numerical results is presented to examine structural behaviour of high strength steel S690 columns and beams.

6.1 Establishment of Numerical Models

In this study, a finite element package ABAQUS 6.12 is employed to carry out material and geometrical nonlinear analyses of S690 welded sections. It should be noted that this numerical tool is capable of simulating structural behaviour of welded sections under different boundary conditions (Systemes, 2009). Hence, comprehensive structural models incorporating material and geometrical nonlinearity are established.

In this section, an innovative model, i.e. a double Y-shaped model, for welded H- and I-sections is proposed. Details of the model are introduced.

6.1.1 Proposed model

An illustration of the proposed double advanced Y-shaped model is given in Figure 6.1. A comparison of I-shaped model. In both models, four-node shell element S4R is employed to comprise an H-section is shown in Figure 6.2. It should be noted that in the double Y-shaped model, a special element connectivity is adopted to model as shown in Figure 6.2. The proposed model is more advantageous as various cross-sectional properties, such as cross-sectional area, and width-to-thickness ratios of plate elements, can be precisely defined.

It should be noted that a cross-section may be divided into three parts, namely flanges, webs and junctions as shown in Figure 6.1. Plate thicknesses of the flanges and the web are directly specified in corresponding elements while the thickness of the linking shell elements in the junction regions, t_j is given as:

$$t_j = \frac{r \times (t_w + r)}{2\sqrt{(r + t_w/2)^2 + (r + t_f/2)^2}} \qquad \text{(Eq. 6.1)}$$

Hence, local buckling behaviour in both the flange outstands and the web plates of H- and I-sections can precisely be predicted corresponding to the actual dimensions of the welded sections. Moreover, overall failure of welded sections can also be accurately assessed when cross-sectional geometry and dimensions are well represented in the numerical model.

6.1.2 Material properties

Measured mechanical properties of high strength S690 steel plates obtained from tensile tests are summarized in Table 6.1, and they are simplified into a tri-linear model as shown in Figure 6.3 (a) for direct adoption into the proposed models.

It should be noted that the Von Mises yielding criteria is also adopted to allow for plasticity in the shell elements. Since dynamic effect was not included in this study, isotropic hardening rule is utilized in the numerical models. A typical tri-linear yielding surface of the S690 steel plates is given in Figure 6.3; Poisson's ratio is taken as 0.3 in these analyses.

6.1.3 Initial imperfections

In this study, two distinctive types of initial imperfections are incorporated into the models, namely i) welding-induced residual stresses, and ii) initial geometric imperfections.

(a) Welding-induced residual stresses

Structural behaviour of welded steel sections are influenced by the presence of welding-induced residual stresses. In Chapter 5, residual stress of these S690 welded sections are readily determined with 2D thermo-mechanical coupled models. These residual stresses are readily adopted element-by-element in proposed models. With this approach, effects of residual stresses are fully incorporated into this numerical study. It should be noted that through-thickness residual stresses in steel plates are have significant variations in their magnitudes, and they are averaged before incorporating into the mid-line of the shell elements of the previous model. Only longitudinal components of the residual stresses are input into the numerical models as they are critical to structural behaviour of the welded sections.

(b) Initial geometrical imperfection

Initial geometrical imperfection, which is another form of initial imperfection in welded sections will impose adverse effects on their structural behaviour. Hence, it is also introduced into the proposed models in the numerical study. In general, the first eigen buckling mode shape is adopted as an initial geometrical imperfection while its maximum magnitude may be taken as one of the following values according to measured data in various experimental studies:

- 1/500 of flange width in stocky columns of S690 welded H-sections;
- 1/500 of flange width in fully restrained beams of S690 welded I-sections;
- 1/2000 of total height for slender columns of S690 welded H-sections; and,
- 1/2000 of total span for partially restrained beams of S690 welded I-sections.

6.2 Modelling of S690 Stocky Columns under Compression

In this section, advanced numerical modelling using the proposed double Y-shaped models are established to simulate structural behaviour of stocky columns of high strength S690 welded H-sections under compression. Details of the compression tests on stocky columns are presented in Chapter 3. A convergence study on the mesh configuration of the proposed models and verification on their adequacy are also carried out and presented. Moreover, structural behaviour of these stocky columns are fully presented and elaborated.

6.2.1 Establishment of numerical model

A total of four double Y-shaped models were established to simulate stocky columns of S690 welded H-sections as shown in Figure 6.4(a). Each model is comprised of an H-section and two end plates which are affixed to section ends. Two reference points are introduced into the model, and each of them is fully coupled with an end plate. They are aligned with the geometric centre of the welded H-sections. Then, all six degrees of freedom of the end plates could be made consistent with those of the reference points. Loading and boundary conditions of the proposed model is illustrated in Figure 6.4 (c). Onto the top reference point, axial shortening is imposed whilst other five degrees of freedom of the proposed model are fully restrained. All six degrees of freedom of the bottom plate are restrained to the bottom reference point.

Initial geometric imperfections are incorporated into the proposed models. Eigen buckling modes with the lowest eigenvalues are adopted. Welding-induced residual stresses are also incorporated into these models. It should be noted that measured welding parameters were used in coupled thermo-mechanical analyses as described in Chapter 5 to calculate all the residual stresses. The adopted residual stress patterns of Sections C1 to C4 are illustrated in Figure 5.8.

6.2.2 Convergence studies on mesh configurations

A convergence study on mesh configurations of stocky columns was conducted to four mesh configurations with various element sizes. Test data of S690 stocky columns of Sections C1 and C3 were adopted in this convergence study. Table 6.2 presents details of the element sizes, namely Meshes M1 to M4 of these models.

Predicted load-shortening curves of the proposed models of Sections C1S and C3S are plotted in Figure 6.5. Generally, local buckling of the flange and the web plates were observed in all these models. It should be noted that the predicted load shortening curves of Meshes M3 and M4 agreed well with the measured curves. Moreover, discrepancies between the predicted resistances are found to be smaller than 1% for both Meshes M3 and M4. Therefore, Mesh M3 with mesh sizes ranging from 3 to 10 mm are adopted in subsequent numerical investigations into stocky and slender columns owing to its balanced computational efficiency and accuracy.

6.2.3 Verification of numerical models against test data

6.2.3.1 Failure modes

Predicted failure modes of the stocky columns of welded H-sections under compression are presented in Figure 6.6 after full development of local buckling in both flanges and webs. It should be noted that flange plates are found to deform in an anti-symmetrical shape about the web plates, and this agrees well with observed failure modes of the stocky columns after testing. Hence, the failure modes of stocky columns of high strength S690 welded H-sections were successfully captured in the proposed models.

6.2.3.2 Load shortening behaviour

Predicted and measured load shortening curves are presented together in Figure 6.7 for direct comparison. In addition, design resistances of these stocky columns, i.e. $N_{c,Rd}$, are also given in this figure for direct comparison.

It is shown that the predicted load shortening curves follow closely with the measured curves. The compression loads were found to increase elastically up to about 80% to 90% of the full design resistances. Then, the curves became non-linear due to gradual reduction in their section rigidities because of the presence of residual stresses. All these curves were found to exceed the design section resistances of the stocky columns. Consequently, it is shown that the proposed model is successfully calibrated against test data. Moreover, both welding-induced residual stresses and initial geometrical imperfections were properly incorporated into the proposed models.

Table 6.3 presents both predicted and measured section resistances of the stocky columns. It is shown that the ratios between the measured and predicted resistances of all the stocky columns range from 0.99 to 1.02 with an average of 1.00. Therefore, the section resistances of the stocky columns of S690 welded H-sections are accurately predicted with the proposed models.

Moreover, the predicted deformation capacities of the stocky columns, i.e. $\Phi_{R,FE}$ are presented in Table 6.3 together with those capacities corresponding to the measured values. A comparison between the predicted and the measured values show that the ratios range from 0.61 to 0.97 with an average of 0.83 and a standard deviation of 0.12. These comparisons are considered to be acceptable, and hence, deformation capacities of S690 stocky columns are also readily assessed with the proposed models.

6.2.3.3 Predicted deformations

Predicted load-strain curves history in stocky columns are illustrated in Figure 6.8. Details of the locations of four strain gauges are all shown in Figure 3.5. Generally, local buckling takes place when axial strains in the steel flanges deviate sharply from each other. The predicted strains at section failure also found to agree well with the measured values plotted in Figure 3.8; the measured values are listed in Table 3.5.

When the stocky columns obtain maximum resistances, compressive strains on the flange tips reached 3.0%, 2.5% and 2.0% for Class 1, 2 and 3 sections respectively. At section failure, the applied loads reduced the section resistances of the stocky columns, and their compressive strains reach at most 9.0% at the location of a fully buckled flange on buckling waves. Hence, the attained strain level is found to compare well with the ductility requirements stipulated in EN 1993-1-12 for high strength S690 steel materials.

6.2.3.4 Out-of-plane displacements

Predicted load versus out-of-plane displacements of the flange plates are plotted in Figure 6.8. The displacement is either taken from the flange tips or the center-line of the webs. It should be noted that both the flange and the web plates had similar out-of-plane displacement characteristic.

6.2.3.5 Development of longitudinal stresses

Predicted longitudinal stresses of all four welded H-sections are illustrated in Figures 6.9 to 6.12. The stress values are averaged from predicted stresses over all 5 layers of the steel plates from double Y-shaped models. In order to demonstrate development of those axial stresses, three critical states are defined as follows:

- Stage 0 is the initial stage in which both two-dimensional and three-dimensional illustrations of the residual stress patterns are provided;
- Stage 1 is the yielding stage when full design resistances are just attained, i.e. small axial deformation; and,
- Stage 2 is the ultimate stage when maximum section resistances are obtained.

It should be noted that:

In Stage 1, both the flange and web plates were in compressive yielding, and the residual stresses over the junction regions amounted to 15% to 20% of the total cross-sectional area of H-sections were generally in small compressive stresses. This can be explained by large tensile residual stresses in the junction regions which were not entirely offset by the compressive deformation. It is also evident that the cross-sections are in partial yielding when full design resistances are firstly obtained by stocky columns.

In Stage 2, the compressive yielding is attained by the entire cross-sections, and tensile residual stresses are found to be offset in junction regions. Consequently, full design resistances of stocky columns are not reduced owing to compressive residual stresses when H-sections are compact enough to resist early local buckling. Moreover, local buckling is found to be evident in Stage 2 when stress softening is obvious in plate elements. Hence, maximum section resistances of stocky columns are acquired when local buckling begins to govern.

6.2.4 Summary

In this section, double Y-shaped models are established for modelling of stocky columns of S690 welded H-sections. Based on a comparison between measured and predicted results, calibration of the proposed models was successfully conducted. Key findings are obtained as follows:

- High strength S690 steel materials are demonstrated to fully satisfy all ductility requirements stipulated in EN 1993-1-1 and 1-12, and they are readily employed as stocky columns to carry heavy loads.
- Failure modes, compressive section resistances and deformation capacities of stocky columns of S690 welded H-sections are demonstrated to be predicted accurately with the proposed models.
- Owing to high deformation capacities, influences from compressive and tensile residual stresses of S690 welded H-sections are found to be not critical to maximum section resistances of stocky columns.

6.3 Modelling of S690 Stocky Columns under Combined Compression and Bending

In this section, advanced numerical modelling using the proposed double Y-shaped models are established to simulate structural behaviour stocky columns of high strength S690 welded H-sections under combined compression and bending. Details of the compression tests on 8 stocky columns are presented in Chapter 3. With predicted results, verification on proposed model is carried out. Moreover, structural behaviour of these stocky columns are also closely elaborated and investigated.

6.3.1 Establishment of numerical model

Sections C3 and C4 are established to simulate the stocky columns as shown in Figure 6.13. End plates are introduced into these models and two reference points are fully coupled with them. It should be noted that reference points were deviated from the center line of H-sections, and measured eccentricities was employed in these models. The boundary conditions of proposed models are also presented in Figure 6.13. Onto the top reference point, shortening is imposed whilst only rotations about major or minor axis are unrestrained.

Initial geometric imperfections are incorporated into the proposed models. Eigen buckling modes with the lowest eigenvalues are adopted. Welding-induced residual stresses are also incorporated into these models. It should be noted that measured welding parameters were used in coupled thermo-mechanical analyses as described in Chapter 5 to calculate all the residual stresses. The adopted residual stress patterns of Sections C3 to C4 are illustrated in Figure 5.8.

6.3.2 Verification of numerical models against test data

6.3.2.1 Failure mode

A direct comparison between measured and predicted failure modes are presented in Figure 6.14 and Figure 6.15. Moreover, predicted failure modes of all 8 sections are also presented in Figure 6.16 after full development of local buckling in both flanges and webs. It should be noted that flanges under large compression forces deformed in an anti-symmetrical shape about the web plates for sections under combined compression and major-axis bending. On the other hand, symmetrical local buckling shape was found to sections under combined compression and minor-axis bending. Hence, the failure modes of stocky columns of S690 welded H-sections were successfully captured in the proposed models.

6.3.2.2 Load deformation behaviour

Predicted load displacement curves, i.e. P-δ curves, of all eight stocky columns are presented with measured data in Figure 6.16 and Figure 6.17. In addition, full design resistances of these stocky columns, i.e. $N_{pl,Rd}$, are also given in this figure for direct comparison.

In general, it is shown that predicted load displacement curves follow closely with measured curves. The compression loads were found to increase elastically up to 60% to 80% of the full design resistances. Then, curves became nonlinear due to partial plasticity and reduced section rigidity. All these curves were found to exceed the design section resistances of the stocky columns. Consequently, it is shown that the proposed model is successfully calibrated against test data. Moreover, both welding-induced residual stresses and initial geometrical imperfections were properly incorporated into the proposed models.

Table 6.4 presents both predicted and measured section resistances of the stocky columns. It is shown that the ratios between the measured and predicted resistances of all stocky columns range from 0.99 to 1.04 with an average of 1.01. Therefore, the section resistances of the stocky columns of S690 welded H-sections are accurately predicted with the proposed models.

6.3.2.3 Development of longitudinal stresses

Predicted longitudinal stresses of four typical welded H-sections are illustrated in Figure 6.21 to Figure 6.24. The stress values are averaged from predicted stresses over all 5 layers of the steel plates from the double Y-shaped models. In order to demonstrate development of those axial stresses, three critical states are defined as follows:

- Stage 0 is the initial stage in which both two-dimensional and three-dimensional illustrations of the residual stress patterns are provided;
- Stage 1 is the yielding stage when full design resistances are just attained, i.e. small axial deformation; and,
- Stage 2 is the ultimate stage when maximum section resistances are obtained.

It should be noted that:

In stage 1, compressive yielding is found in the flange and web plates in H-sections under combined compression and bending. Tensile residual stresses in these regions were just partially offset by large compression. This can be explained by large tensile residual stresses in the junction regions which were not offset by compression and bending deformations. It is also evident that the cross-sections are in partial yielding due to compression, and tensile yielding due to bending were not obtained by stocky columns.

In stage 2, compressive yielding is attained by the entire cross-sections and tensile residual stresses are found to be entirely offset in junction regions under large compression. Consequently, full design resistances of stocky columns are not reduced owing to compressive residual stresses when H-section are compact enough to resist early local buckling. Moreover, local buckling is found to be evident in Stage 2 when stress softening is obvious in the flange tips and the mid of webs. Hence, maximum resistances of stocky columns are acquired when local buckling begins to govern.

6.3.3 Summary

In this section, double Y-shaped models are established for modelling of stocky columns of S690 welded H-sections under combined compression and bending. Based on a comparison between measured and predicted results, calibration of the proposed models was successfully conducted. Key findings are obtained as follows:

- High strength S690 steel materials are demonstrated with full satisfaction with all ductility requirement in EN 1993-1-1 and 1-12, and they can be readily employed in stocky columns under heavy combined compression and bending loads.
- Failure modes, compressive section resistances and deformation capacities of stocky columns of S690 welded H-sections are demonstrated to be predicted accurately with proposed models.
- Owing to high ductility, influences from compressive and tensile residual stresses of S690 welded H-sections are found to be not critical to maximum section resistances of stocky columns.

6.4 Modelling of S690 Slender Columns under Compression

In this section, double Y-shaped model is employed to simulate axial compression tests on 7 slender columns of high strength S690 welded H-sections. Details of the compression tests can be founded in Ma and et al (2016). With predicted results, verification on proposed model is carried out. Moreover, structural behaviour of these slender columns of S690 H-sections are also closely examined.

It should be noted that all column sections were welded with S690 high strength steel plates. Among the 7 slender columns, four different sections, namely Sections C1 to C4, were adopted. Two different column heights, i.e. 1,610 mm and 2,410 mm were included to cover a variety of overall slendernesses which range from 0.62 to 1.41. The test programme is listed in Table 6.5 for easy reference.

This test programme of slender columns is chosen for the following reasons:

- Technical background of these benchmark tests which is necessary to facilitate a high-quality numerical study was fully disclosed;
- A practical scope of buckling slendernesses was covered by this test programme;
- Corresponding test data on the stocky columns with Sections C1 to C4 are available and comparable; and,
- Predicted residual stress patterns in S690 welded H-sections of Sections C1 to C4 are readily available as given in Chapter 5.

6.4.1 Establishment of numerical model

Double Y-shaped models of slender columns of S690 H-sections are illustrated in Figure 6.25. A typical mesh configurations which are employed to stocky columns of H-sections are adopted in this numerical study as they have identical cross-sectional dimensions. An H-section together with two end plates affixed to section ends is incorporated into section models. Two reference points are introduced into the models, and coupled with end plates. Loading and boundary conditions of slender columns are presented in Figure 6.25.

Initial geometric imperfections are incorporated into the proposed models. Eigen buckling modes with the lowest eigenvalues are adopted. Welding-induced residual stresses are also incorporated into these models. It should be noted that measured welding parameters were used in coupled thermo-mechanical analyses as described in Chapter 5 to calculate all the residual stresses. The adopted residual stress patterns of Sections C1 to C4 are illustrated in Figure 5.8.

6.4.2 Verification of numerical models against test data

6.4.2.1 Failure modes

Typical failure modes of slender columns, together with load shortening curves and load displacement curves are obtained by section models and plotted in Figure 6.26 to Figure 6.28. A direct comparison can be facilitated as both measured and predicted data are provided in those figures. It should be noted that minor-axis buckling was successfully predicted by all seven slender columns, and this agrees well with observed failure modes of the slender columns after testing. Hence, the failure modes of slender columns of S690 welded H-sections were successfully captured in the proposed models.

6.4.2.2 Load deformation behaviour

Predicted and measured load shortening and load displacement curves are presented in Figures 6.26 to 6.29 for direct comparison. In addition, design resistances of slender columns, i.e. $N_{b,Rd}$, are also given in these figures for direct comparison.

It is shown that predicted load shortening curves follow closely with the measured curves. The compression loads are found to increase elastically up to the failure. Then, a sharp reduction of section resistance occurs due to overall buckling. All these curves were found to exceed the design buckling resistances of the slender columns. Therefore, the load deformation behaviour of slender columns are successfully calibrated against test data.

Moreover, both welding-induced residual stresses and initial geometrical imperfections were properly incorporated into the proposed models.

6.4.2.3 Buckling resistances

Both measured and predicted buckling resistances of slender columns are presented in Table 6.6. For easy comparison, design resistances, i.e. $N_{b,Rd}$, based on buckling curve c in EN 1993-1-1 are also presented. It should be noted that resistance ratios, namely $N_{b,Rt}$ / $N_{b,FE}$, range from 1.00 to 1.07 except for Section C2M which attained extremely high resistance from the testing. Hence, proposed models are conservative and accurate.

In Figure 6.30, measured buckling resistances and calculated buckling resistances are plotted comparing with the column buckling curve c. It should be noted that curves c is the design curve suggested in EN 1993-1-1 for slender columns of high strength steel welded H-sections. It is clearly demonstrated that current buckling curve c is applicable to design these column sections.

Moreover, it is reflected by Figure 6.30 that buckling curves are most critical to slender columns with small to medium section slendernesses, i.e. $\bar{\lambda}_z$ from 0.4 to 0.8. Hence, effects of compressive residual stresses become critical, as section rigidities may reduce under large compression forces. Owing to smaller residual stress ratios in S690 welded H-sections than those in S355 H-sections, it is reasonable to propose a more structurally efficient buckling curve for slender columns of S690 welded H-sections.

6.4.3 Summary

In this section, double Y-shaped models are established for modelling of slender columns of S690 welded H-sections. Based on a comparison between measured and predicted results, calibration of the proposed models was successfully carried out against a benchmark test programme including 7 sections. Through interpretation on numerical data, key findings are obtained as follows:

- Design provisions in current EN 1993-1-1 is applicable to design slender columns of S690 welded H-sections buckling about their minor axes;
- Influences of residual stresses are most critical to slender columns of S690 sections with small to medium section slendernesses; and,
- Owing to smaller residual stress ratios in S690 welded H-sections than those in S355 welded H-sections, it is reasonable to propose a more structurally efficient buckling curve for slender columns of S690 welded H-sections.

6.5 Modelling of Fully Restrained Beams of S690 Welded I-sections

In order to study the structural behaviour of fully restrained beams of high strength steel S690 welded I-sections, double Y-shaped model is used to simulate the bending tests on fully restrained beams. Details of the bending tests on 6 fully restrained beams are introduced in Chapter 4. A convergence study on the mesh configuration of the proposed models and verification on their adequacy are also carried out and presented. Moreover, structural behaviour of these fully restrained beams are presented and elaborated.

6.5.1 Establishment of numerical model

A total of six double Y-shaped models were established to simulate fully restrained beams of S690 welded I-sections as shown in Figure 6.31. A gradient mesh is imposed onto these models. Welded I-sections together with vertical stiffeners are introduced into the section models. Loading and boundary conditions of the proposed models are illustrated in Figure 6.32. It should be noted that beams are simply supported in these models, and rotations are allowed at section ends. Loads and reactions are applied through the geometric centre of these welded I-sections. Lateral displacements of those vertical stiffeners are restrained in these models.

Initial geometric imperfections are incorporated into the proposed models. Eigen buckling modes with the lowest eigenvalues are adopted. Welding-induced residual stresses are also incorporated into these models. It should be noted that measured welding parameters were used in coupled thermo-mechanical analyses as described in Chapter 5 to calculate all the residual stresses. The adopted residual stress patterns of Sections B1 to B4 are illustrated in Figure 5.11.

6.5.2 Convergence studies on mesh configurations

A convergence study on mesh configurations of beams was conducted to four different mesh configurations with various element sizes. Test data of S690 fully restrained beams of Sections B1 and B3 were adopted in this convergence study. Table 6.7 presents details of the element sizes, namely Meshes M1 to M4 of these models.

Predicted load-deflection curves of the proposed models of Sections B1 and B3 are plotted in Figure 6.33. In general, local buckling of the flange and the web plates were observed in all these models. It should be noted that the predicted load deflection curves of Meshes M3 and M4 agreed well with the measured curves. Moreover, discrepancies between the predicted resistances are found to be small for both Meshes M3 and M4. Therefore, Mesh M3 with mesh sizes ranging from 3 to 10 mm are adopted in subsequent numerical investigations beams owing to its balanced computational efficiency and accuracy.

6.5.3 Verification of numerical models against test data

6.5.3.1 Failure modes

Predicted failure modes of fully restrained beams of welded H-sections under bending are illustrated in Figure 6.34 after full development of local buckling in both flanges and webs. It should be noted that local buckling was successfully predicted by the numerical models. On basis of both test observations and numerical prediction, local buckling is the governing failure mode as it becomes evident at failure. Hence, the failure modes of fully restrained beams of S690 welded I-sections were successfully captured in the proposed models.

6.5.3.2 Ultimate resistances and rotational capacity

Both predicted moment resistances and rotational capacity of S690 fully restrained beams are presented comparing with test measurements in Table 6.8. It should be noted that resistance ratios, namely M_{Rt} / $M_{R,FE}$, are either 1.00 or 1.01 except for Section B6 which failed in unexpected failure mode. Hence, proposed models are conservative and accurate.

Moreover, the predicted rotational capacities of the fully restrained beams, i.e. $\Phi_{R,FE}$, are presented based on load rotational curves shown in Figure 6.36. Ratios between measured and predicted rotational capacities are given in Table 6.8. It should be noted that these ratios range from 0.73 to 1.09 with an average of 0.95. Comparing with EN 1993-1-1, predicted rotational capacities well met the criteria for Class 1 to Class 3 cross-sections. Hence, extensive applications of section classification rules in EN 1993-1-1 to steel beams of S690 I-sections are found to be applicable. Moreover, it is appropriate to design beams with high rotational capacities and strength enhancement using high strength S690 steel materials.

6.5.3.3 Strain at maximum resistances

Strain contours of S690 welded I-sections at maximum load are presented in Figure 6.34. Plasticity in beams were found to be highly dependent on section classifications. Typically, compressive strain in Section B1 attained 6.9% at maximum load, whilst in Section B3, plastic strain was found to be small.

More specifically, maximum compressive strains of top flanges at loaded sections are presented in Table 6.9. For easy comparison, ratios between compressive strains and yielding strain, namely ($\varepsilon_{tf,FE}/\varepsilon_y$), are given to indicate local plasticity. It should be noted that strain ratios of Sections B1 and B4 exceeded 10.0, while it is merely 3.6 in Section B3 which is a Class 3 section. Hence, compressive strains of top flanges may increase with section compactness of fully restrained beams. Moreover, with higher attained strain ratios, strength enhancement over full moment resistances was found to increase significantly.

6.5.4 Summary

In this section, verification of double Y-shaped model was successfully carried out against a benchmark test programme of fully restrained beams introduced in Chapter 4. Key findings are obtained as follows:

- High strength S690 steel materials are demonstrated with sufficient ductility, and can be applied in beams requiring high rotational capacities.

- Failure mode, moment resistances and rotational capacities of fully restrained beams were accurately predicted by proposed models.
- In practical design, lateral torsional restraints must be adequate and strong enough to mobilize full moment resistances and high rotational capacities of fully restrained beams.

6.6 Modelling of Partially Restrained Beams of S690 Welded I-sections

In this section, double Y-shaped model is employed to simulate lateral torsional buckling behaviour of 12 partially restrained beams of high strength S690 welded I-sections. Details of the test programme are discussed in Chapter 4. It should be noted that eigen buckling analysis was carried out to determine failure modes and critical moment resistances of steel beams. And nonlinear analyses of structural models were then carried out and verified against test data. Moreover, structural behaviour of S690 partially restrained beams is also closely examined.

6.6.1 Mesh network and boundary condition

Double Y-shaped models of beams of welded I-sections illustrated in Figures 6.31(a) to 6.31(c) are also employed in this numerical study. Mesh configurations which are adopted to fully restrained beams of I-sections are applied in this study as these I-sections have identical cross-sectional dimensions. In each section model, it is composed of an I-section and 3 or 4 vertical stiffeners. It should be noted that lateral torsional restraints are introduced into the models at loaded points. Moreover, detailed loading and boundary conditions of partially restrained beams are presented in Figure 6.37.

Initial geometric imperfections are incorporated into the proposed models. Eigen buckling modes with the lowest eigenvalues are adopted. Welding-induced residual stresses are also incorporated into these models. It should be noted that measured welding parameters were used in coupled thermo-mechanical analyses as described in Chapter 5 to calculate all the residual stresses. The adopted residual stress patterns of Sections B1 to B6 are illustrated in Figure 5.11.

6.6.2 Eigen buckling mode of S690 welded I-sections

Eigen buckling modes of all 12 partially restrained beams are predicted with proposed beam models. This prediction was motivated by three objectives:

- To find out first eigen buckling mode of partially restrained beams;
- To determine lateral torsional slenderness with consideration of all factors; and,
- To provide patterns of initial geometrical imperfections for subsequent analyses.

Predicted eigen buckling modes of partially restrained beams of Series LT1 and LT2 are plotted in Figure 6.38. Maximum lateral displacements are observed at mid of span in sections of Series LT1. While, maximum lateral displacements are observed mostly at ends in most sections of Series LT2. Therefore, two distinctive eigen buckling modes were introduced into this test programme. According to a harmonized lateral torsional buckling design method in EN 1993-1-1, the following equation was utilized to assess the lateral torsional slenderness of partially restrained beams, as:

$$\bar{\lambda}_{LT} = \sqrt{\frac{M_{pl,Rd}}{M_{cr}}} \quad \text{(Eq. 6.2)}$$

In this equation, M_{cr} is the eigen buckling moment resistances of steel beams given in Figure 6.38. Hence, a wide range of normalized slenderness from 0.39 to 1.23 was incorporated into this test programme.

6.6.4 Verification of numerical models against test data

6.6.4.1 Failure modes

Typical failure modes of partially restrained beams predicted by section models are illustrated in Figures 6.39 and 6.40. Maximum lateral displacements are observed at mid of span in sections of Series LT1 and ends in most sections of Series LT2. Moreover, for Section B3-LT1 with a Class 3 cross-section, local buckling was observed in top flange which was successfully precited by proposed model as shown in Figure 6.41. Section failure of beams with low slendernesses are predicted by strain contours demonstrated in Figures 6.39 and 6.40. Hence, predicted failure modes are generally found to be consistent with test measurements displayed in Figures 4.16 and 4.17.

6.6.3.2 Moment resistances

In Table 6.10, a comparison between measured and calculated moment resistances of S690 partially restrained beams is presented. A maximum discrepancy of ±3% design resistances was achieved by proposed models. Hence, moment resistances of S690 partially restrained beams are successfully verified against benchmark tests.

Comparing with lateral torsional buckling curves provided by EN 1993-1-1, predicted lateral torsional buckling resistances are plotted in Figure 6.44 with measured resistances. It should be noted that buckling curve d suggested by EN 1993-1-1 is applicable to either test measurements and numerical results. Moreover, a significant safe margin was obtained by numerical predictions. Therefore, a more structurally efficient lateral torsional buckling design curve could be proposed to partially restrained beams of S690 welded I-sections based on extensive study using the established numerical model.

6.6.3.3 Strain development

In these Figures 6.39 and 6.40, strain contours of S690 welded I-sections at maximum loads are presented. Material yielding can be easily recognized as it is in gray scale. Section plasticity is found to develop in limited portion of I-sections which possess medium to large lateral torsional slendernesses. Therefore, effects of residual stresses are limited in those regions as section rigidities can be reduced owing to early development of section plasticity.

For beams with small to moderate lateral torsional slendernesses, namely Sections B1-LT1 etc., they attained full moment resistances with strength enhancement. Meanwhile, lateral torsional buckling is found to occur in those sections but with small deformation magnitudes. Hence, the governing failure mode in these sections is the section plasticity.

6.6.3.4 Load versus deflection and lateral displacement curves

Predicted and measured load versus deflection and displacement curves are shown in Figures 6.42 and 6.43 for direct comparison. In addition, full design resistances of beams, i.e. $N_{pl,Rd}$, are also given in these figures.

In general, the predicted load deflection and displacement curves closely follow measured curves. The transverse loads are found to increase elastically up to a sharp failure due to lateral torsional buckling in most cases. For sections with small to medium lateral torsional slendernesses, curves were found to exceed the full design resistances of beams. Hence, the load deformation behaviour of beams are successfully calibrated against test data. Moreover, effects of both welding-induced residual stresses and initial geometrical imperfections were properly incorporated into the proposed models.

6.6.4 Summary

In this section, double Y-shaped models are established for modelling of partially restrained beams of S690 welded I-sections. Based on a comparison between measured and predicted results, calibration of proposed models was successfully conducted. Through this study, key findings are obtained as follows:

- Failure modes of section plasticity, lateral torsional buckling and local buckling were observed from tests and predicted by the numerical models as well;
- Comparing with numerical results, it is found that curve d based on EN 1993-1-1 is applicable in design of lateral torsional buckling of S690 welded I-sections; and,
- Owing to reduced residual stresses in S690 welded I-sections comparing with those in S355 welded I-sections, higher structural efficiency can be achieved.
- Design rules can be improved by adopting lateral torsional buckling curve b or curve c, or by increasing the critical slenderness, i.e. $\bar{\lambda}_{LT,0}$.

6.7 CONCLUSIONS

In this chapter, a double Y-shaped model is proposed for welded I- and H-sections. In this proposed model, material nonlinearity, welding-induced residual stresses and geometrical imperfections were fully incorporated. In chapter 5, it was found that compressive residual stress ratios are much smaller in S690 welded H-sections than those in S355 sections. Hence, reduction of section rigidity is less pronounced when steel sections are under heavy loads. And buckling resistance ratios of S690 welded H- and I-sections are higher than those of S355 steel sections.

To five different kinds of columns and beams, calibration of double Y-shaped model is successfully conducted against benchmark tests. Ultimate resistances, failure modes and deformation characteristics of S690 H- and I-sections were accurately captured the proposed models. Key findings of these studies are as follows:

- Based on stress and strain readings from the numerical models, it is found that material properties of high strength S690 steel fully satisfied the requirements in EN 1993-1-12 and can be applied into column and beam elements.
- For stocky columns of S690 welded H-sections, full section resistances can be attained with various deformation capacities depending on slendernesses of steel plates;
- Comparing with buckling curves suggested by EN 1993-1-1, overall buckling resistances of S690 slender columns are much higher majorly owing to smaller compressive residual stresses in these steel sections;
- Section plasticity and strength enhancement were developed in Class 1 and Class 2 restrained beams of S690 welded I-sections, and moment resistance of a Class 3 section was found to be much higher than its elastic moment resistance; and,
- Comparing with buckling curves suggested by EN 1993-1-1, lateral torsional buckling resistances of S690 partially restrained beams are much higher and the critical lateral torsional slenderness of 0.40 is over conservative.

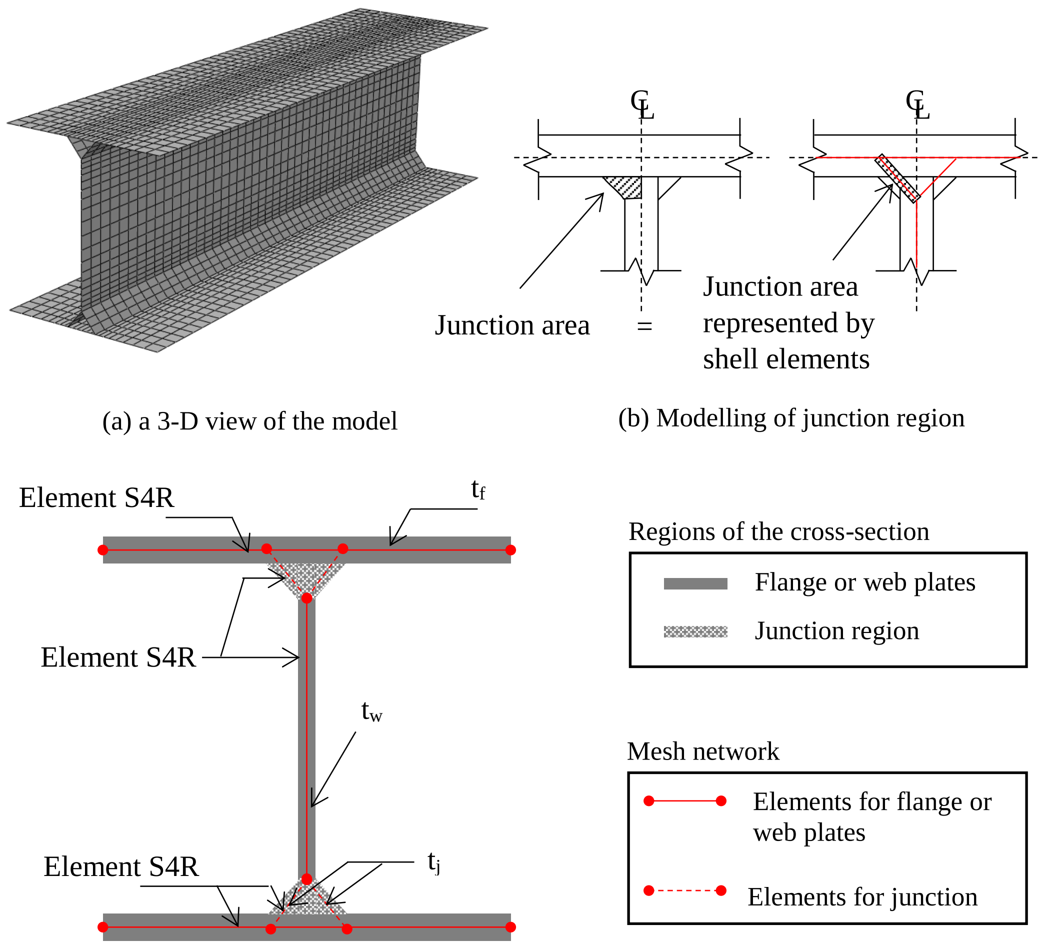

(a) a 3-D view of the model

(b) Modelling of junction region

(c) Mesh connectivity in the model

Figure 6.1: Proposed double Y-shaped model

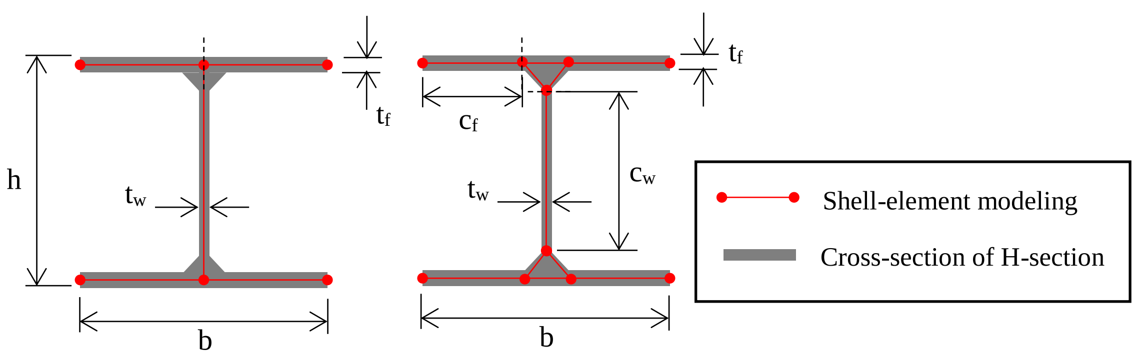

(a) Conventional model

(b) Proposed model

Figure 6.2: Comparison between conventional and proposed models

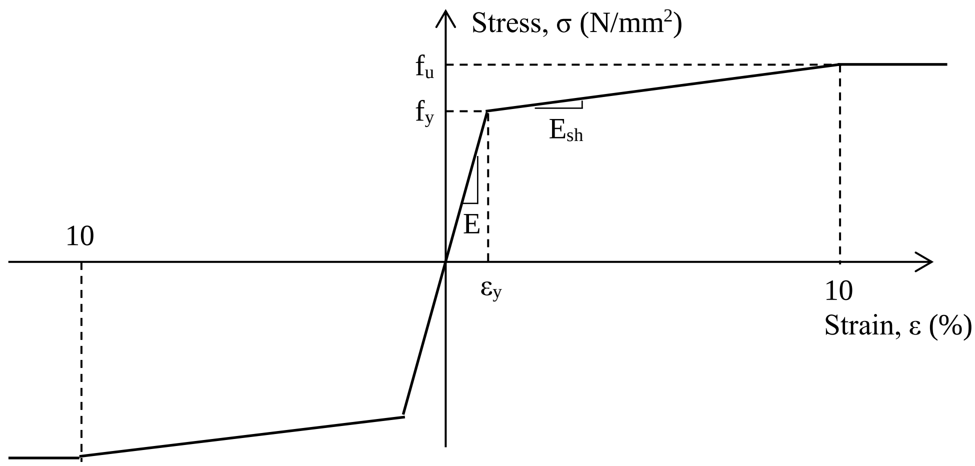

(a) Uni-axial stress-strain curve

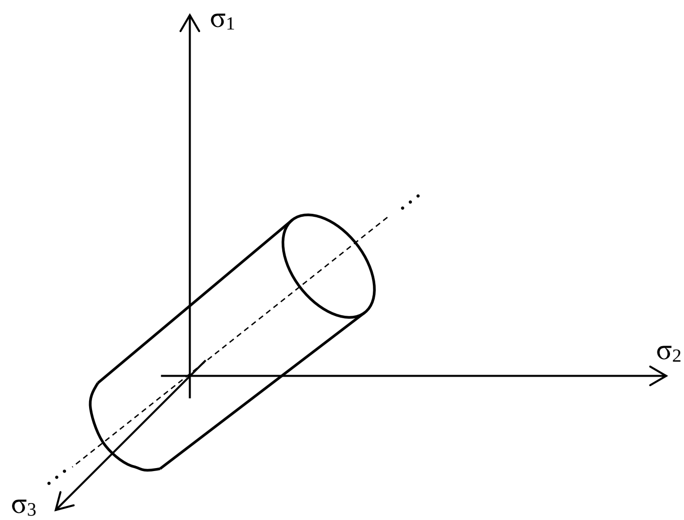

(b) Tri-linear yielding surface

Figure 6.3: Material model of S690 steel plates

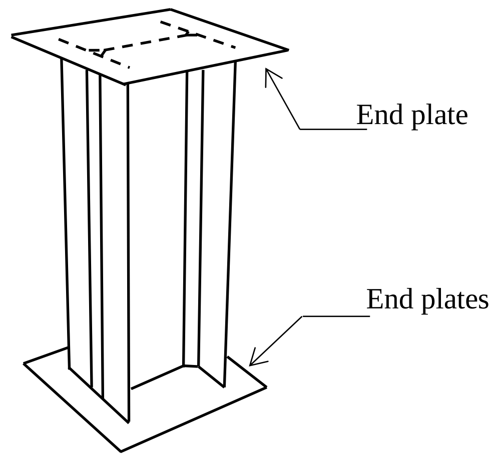

(a) 3D view of proposed model for stocky columns

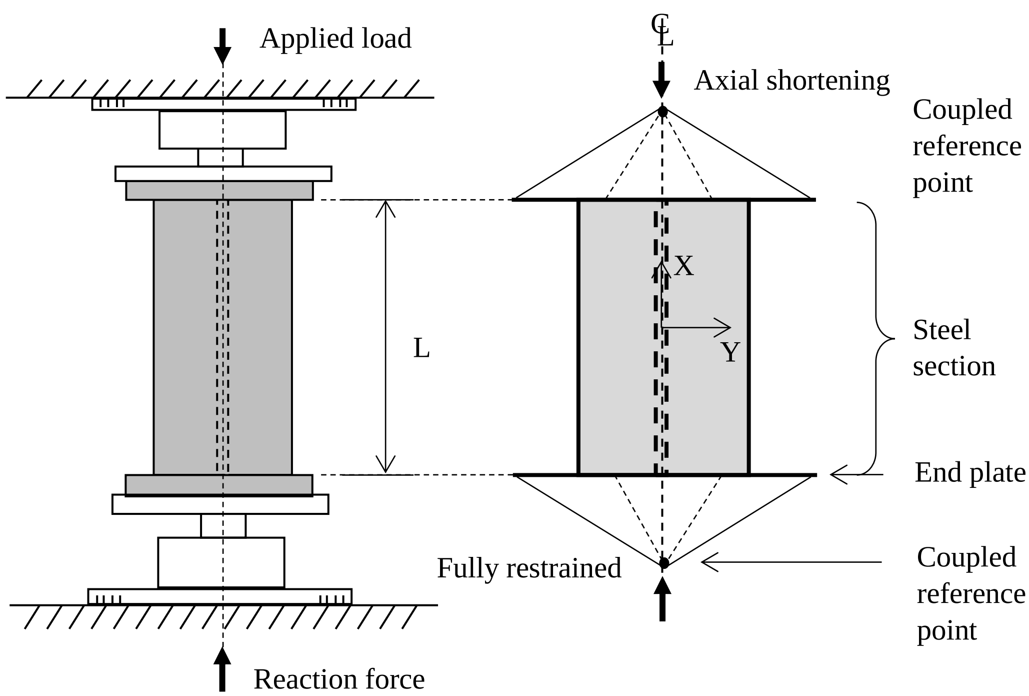

(b) Test setup (c) Boundary conditions

Figure 6.4: Loading and boundary conditions for stocky columns of H-sections under compression

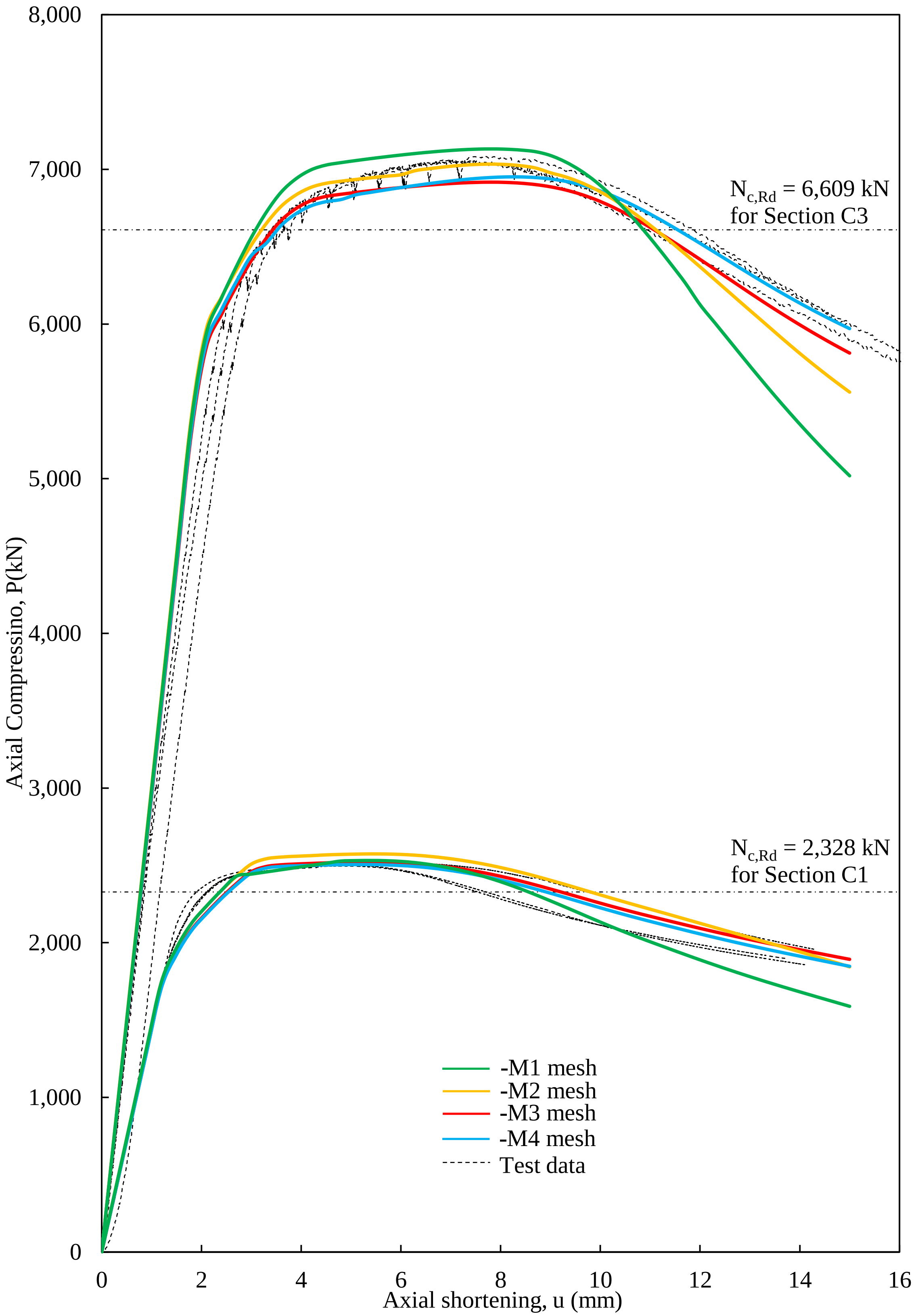

Figure 6.5: Load deflection curves of stocky columns for convergence study

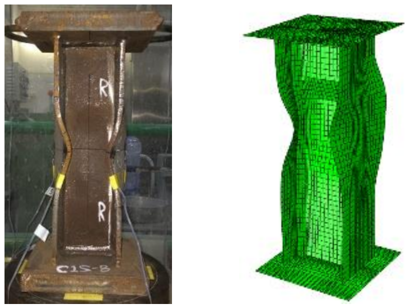

(a) Section C1S

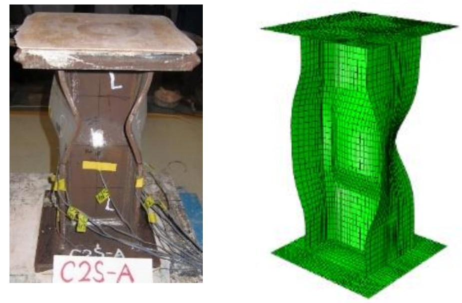

(b) Section C2S

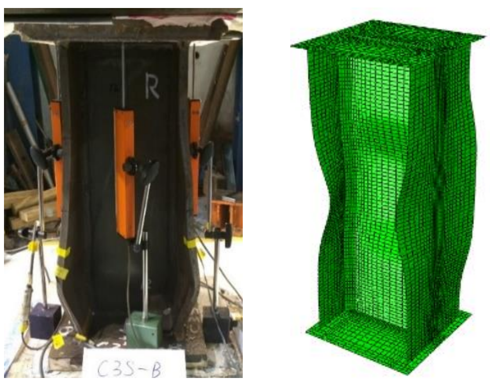

(c) Section C3S

(d) Section C4S

Figure 6.6: Failure modes of stocky columns of S690 welded H-sections under compression

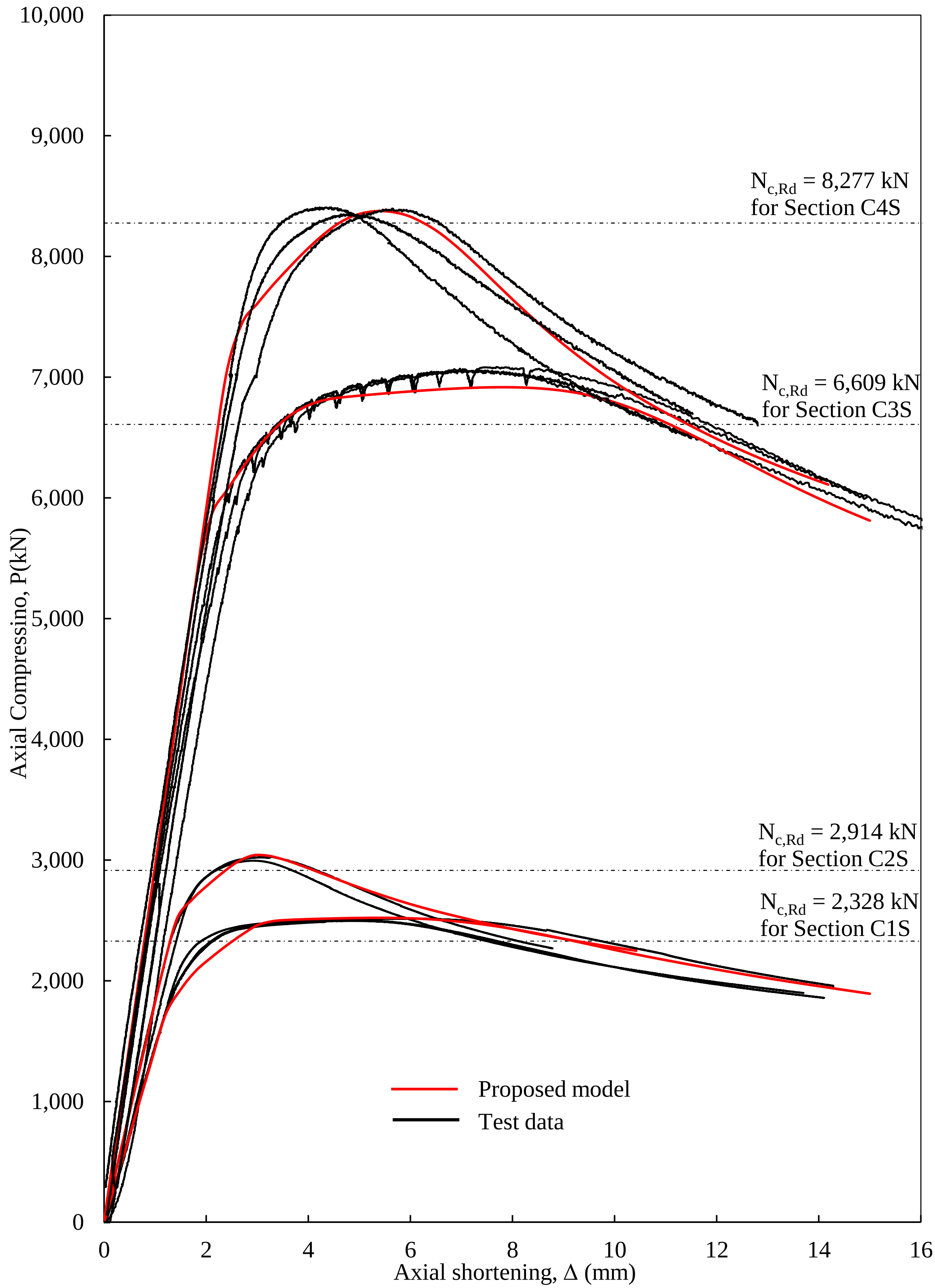

Figure 6.7: Load shortening curves of S690 welded H-sections

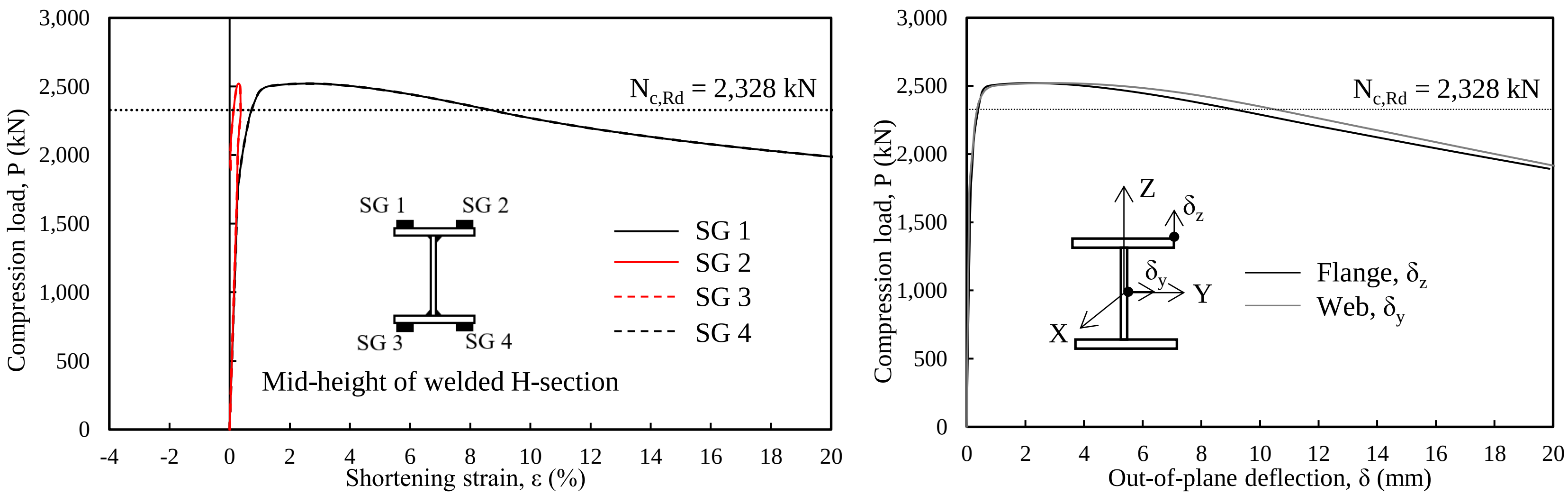

(a) Section C1S

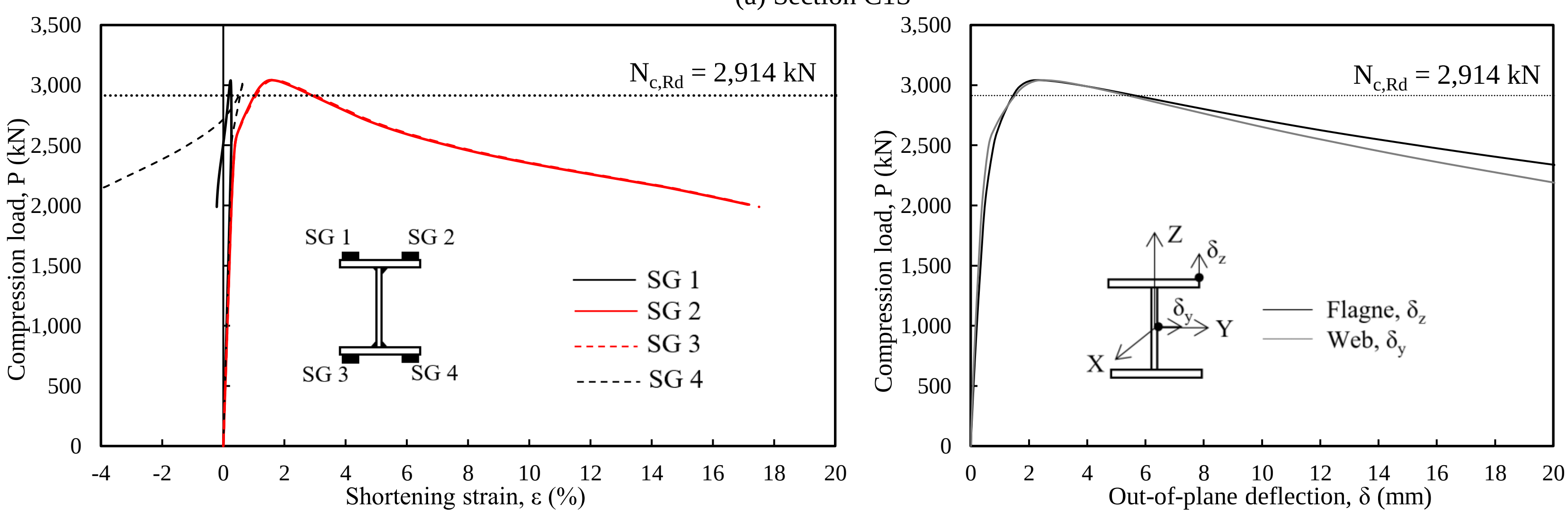

(b) Section C2S

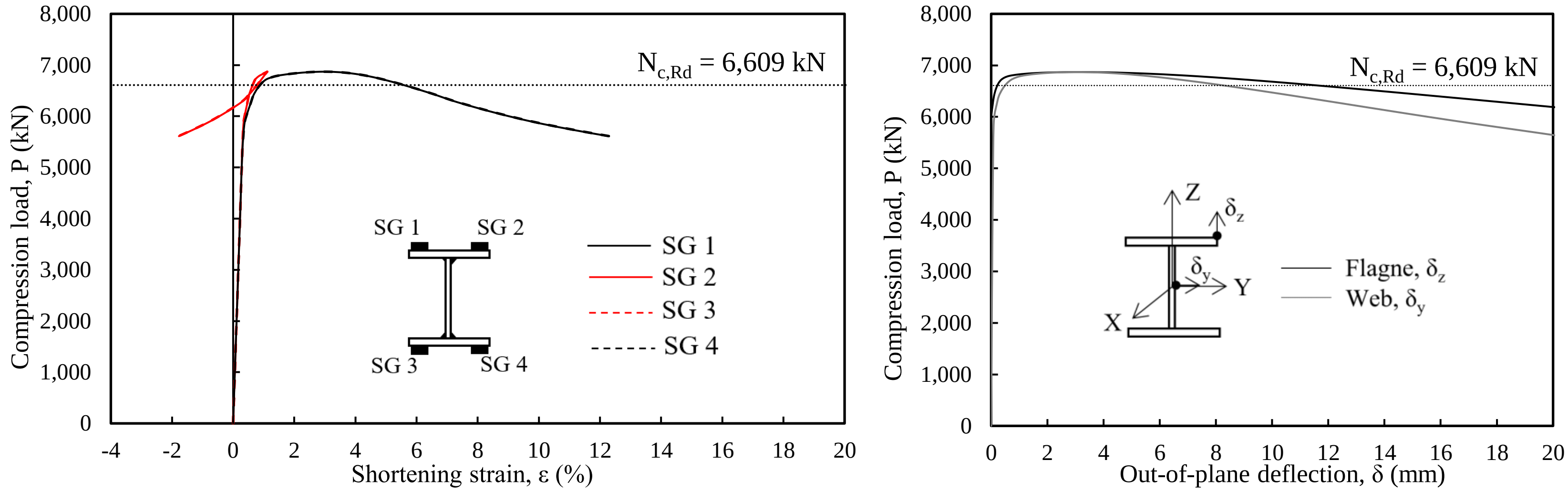

(c) Section C3S

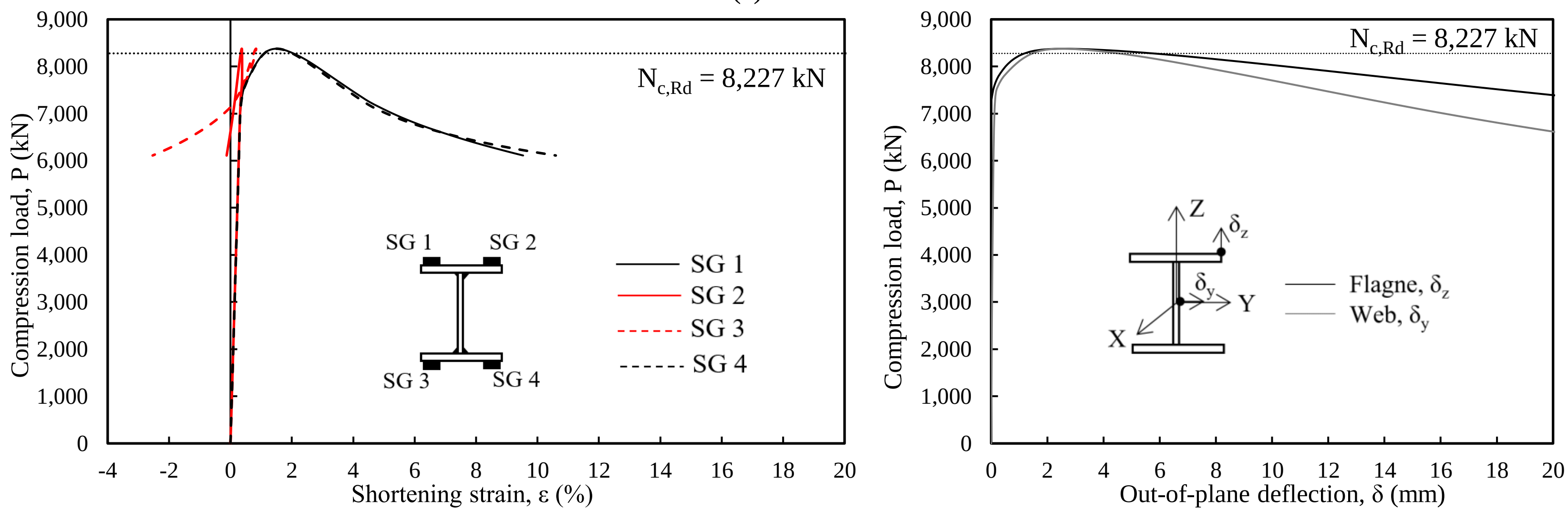

(d) Section C4S

Figure 6.8: Predicted shortening strains on flange tips and maximum out-of-plane deflections of plate parts

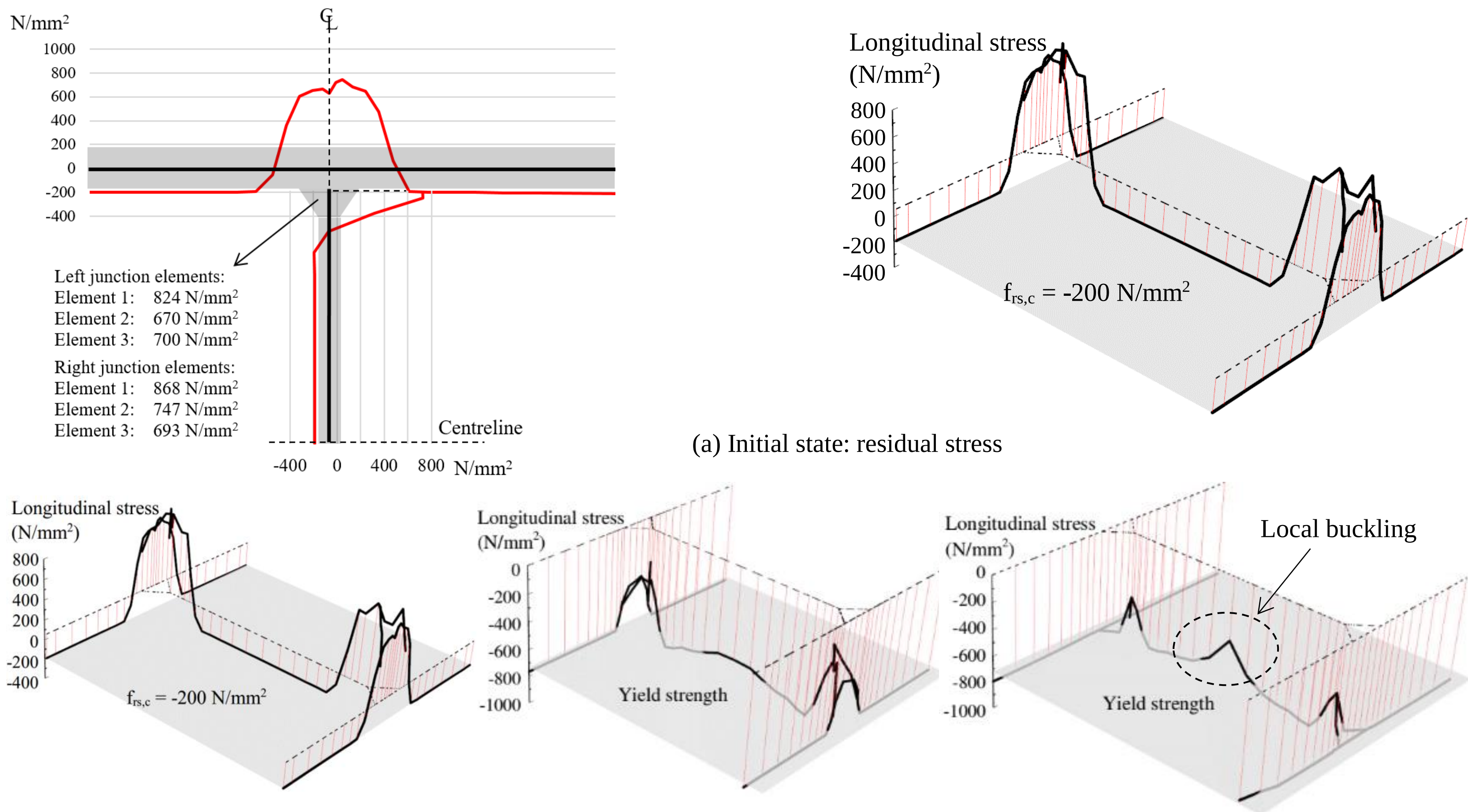

(a) Initial state: residual stress

(b) Stage 0: residual stresses

(c) Stage 1: first obtaining yielding resistance

(d) Stage 2: obtaining maximum resistance

Figure 6.9: Development of longitudinal stresses in Section C1S

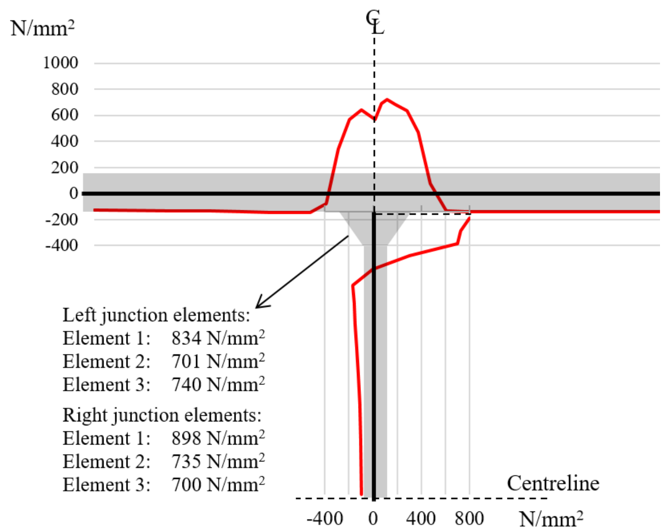

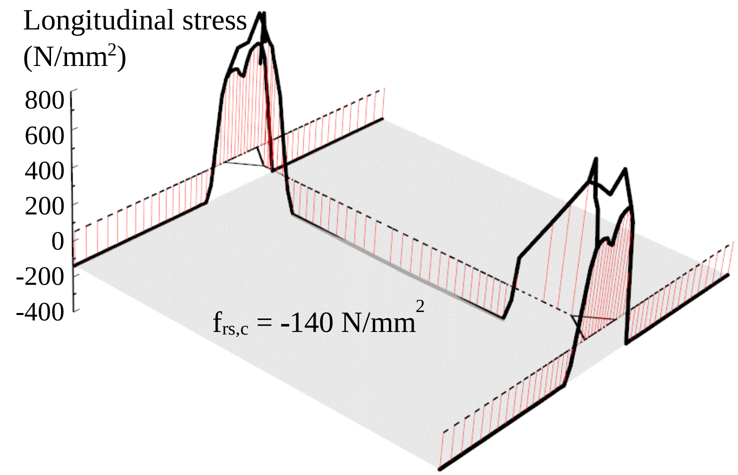

(a) Initial state: residual stress

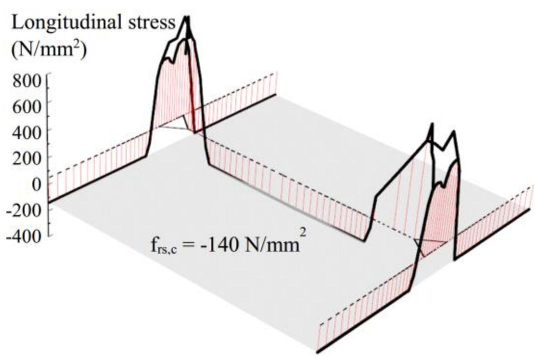

(b) Stage 0: residual stresses

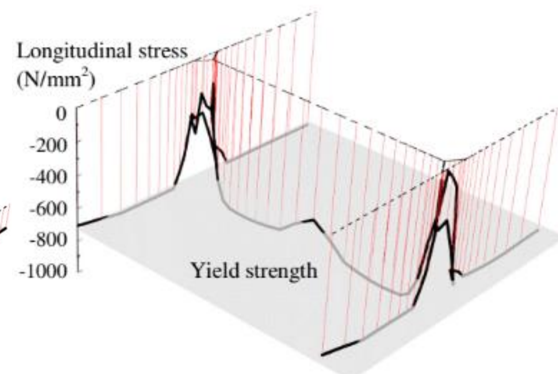

(c) Stage 1: first obtaining yielding resistance

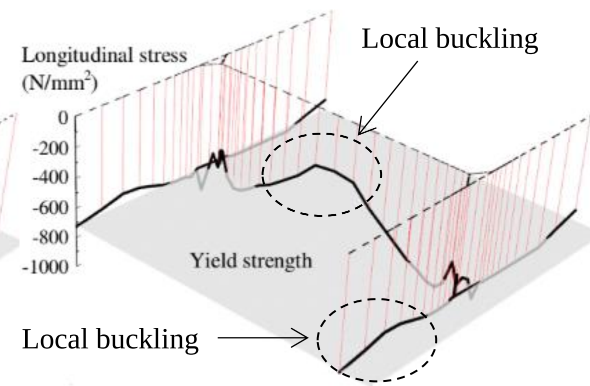

(d) Stage 2: obtaining maximum resistance

Figure 6.10: Development of longitudinal stresses in Section C2S

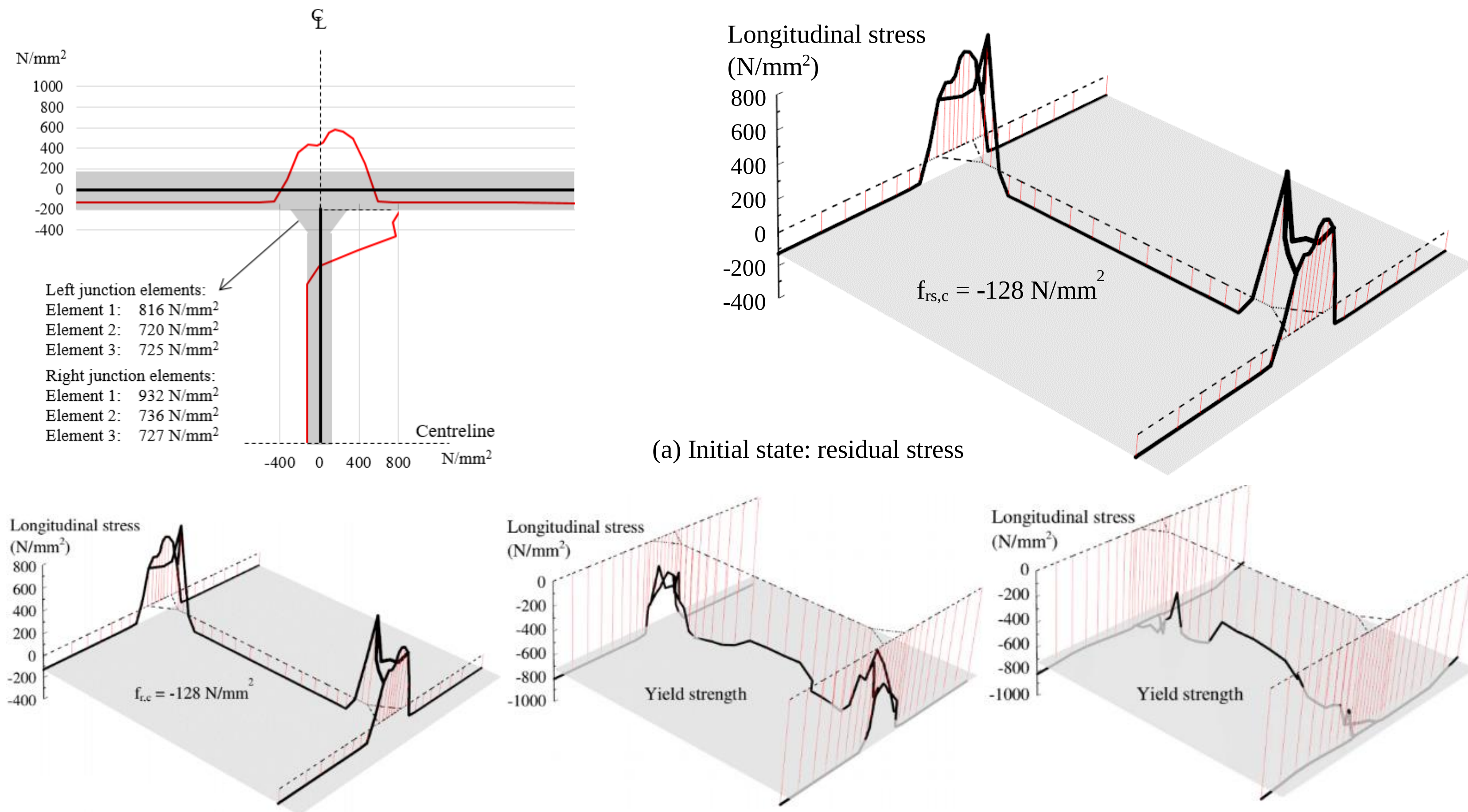

(a) Initial state: residual stress

(b) Stage 0: residual stresses

(c) Stage 1: first obtaining yielding resistance

(d) Stage 2: obtaining maximum resistance

Figure 6.11: Development of longitudinal stresses in Section C3S

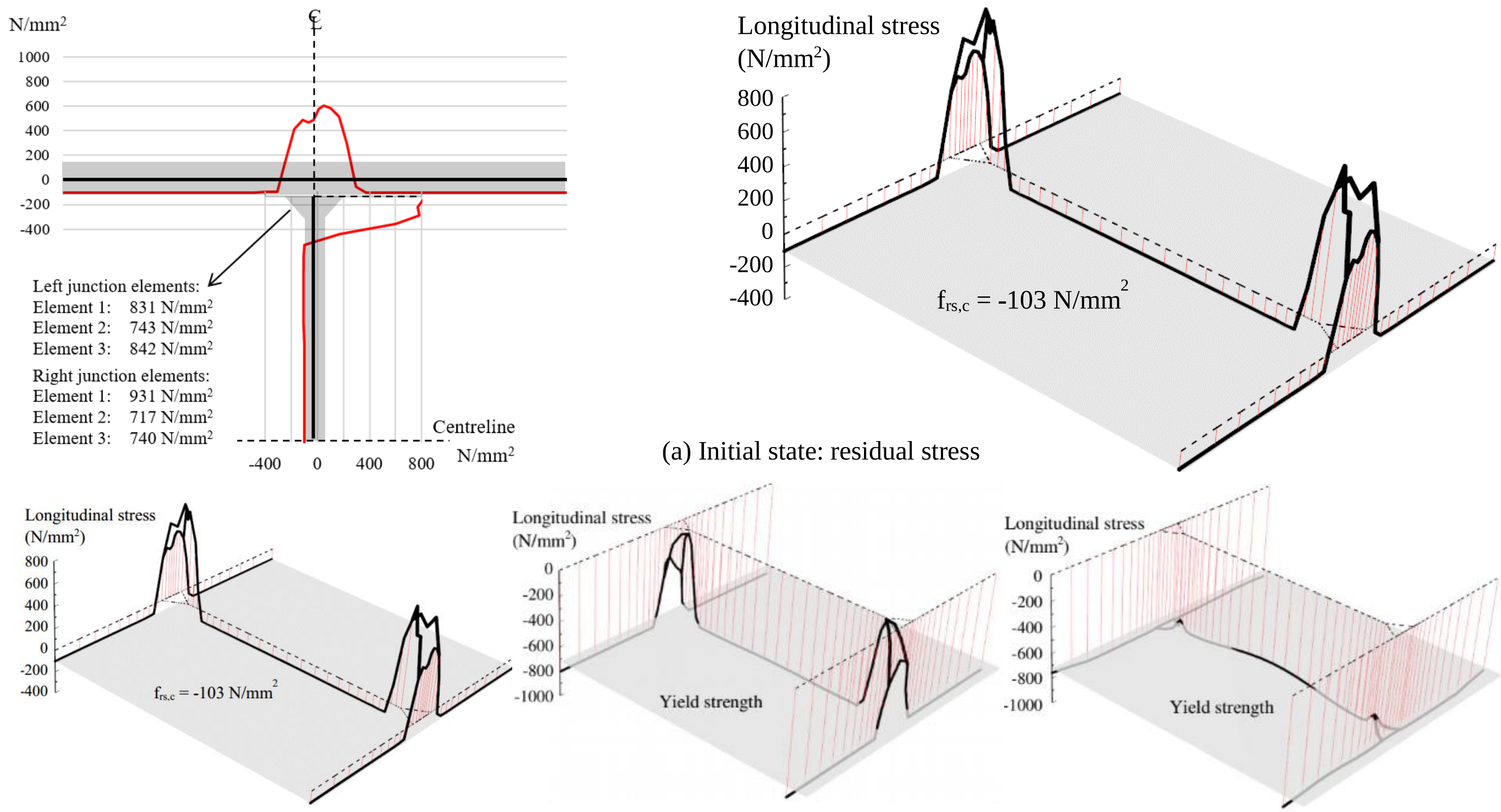

(a) Initial state: residual stress

(b) Stage 0: residual stresses

(c) Stage 1: first obtaining yielding resistance

(d) Stage 2: obtaining maximum resistance

Figure 6.12: Development of longitudial stresses in Section C4S

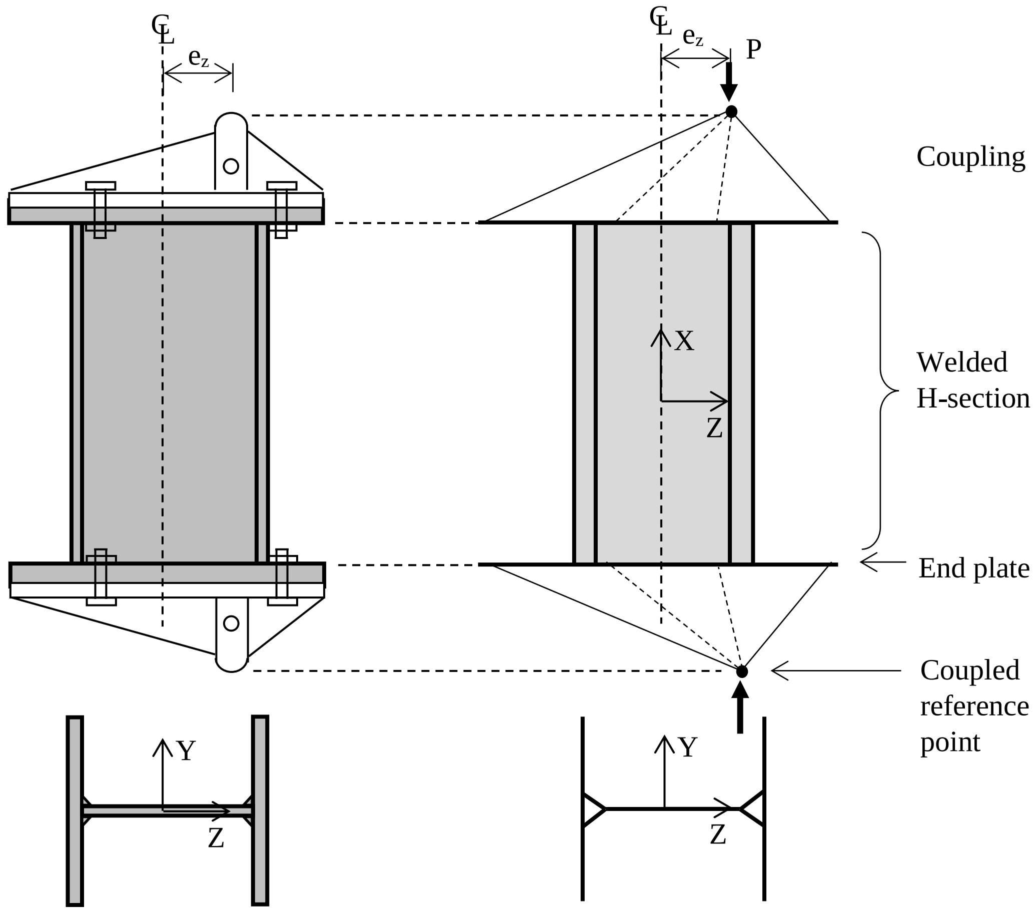

(a) Test setup (b) Modelling of stocky column

Boundary condition of reference points*:

	X	Y	Z
Translation	✓	✗	✗
Rotation	✗	✓	✗

*Note: ✗ denotes prohibited degree of freedom; and,
✓ denotes allowed degree of freedom.

Figure 6.13: Boundary conditions for stocky H-sections under combined compression and bending

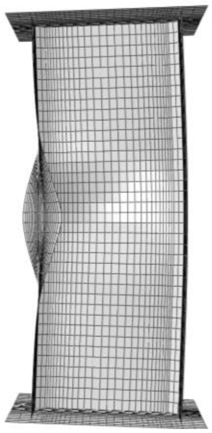

(a) Front view of FE model

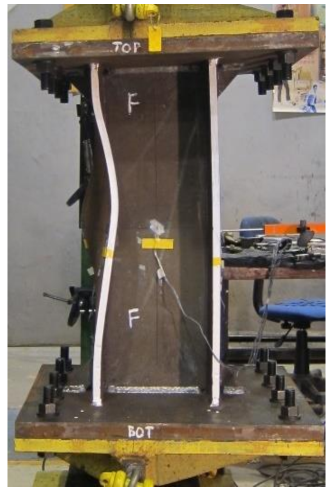

(b) Front view of test specimen

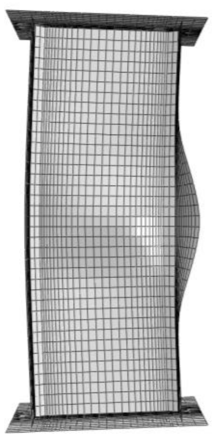

(c) Back view of FE model

(d) Back view of test specimen

Figure 6.14: Comparison between predicted and observed failure mode of Section C4SY-d

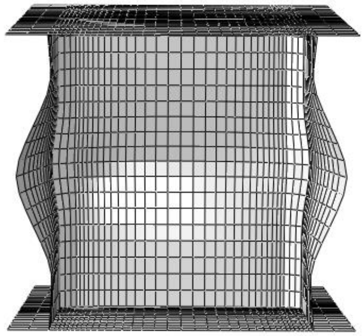

(a) Front view of FE model

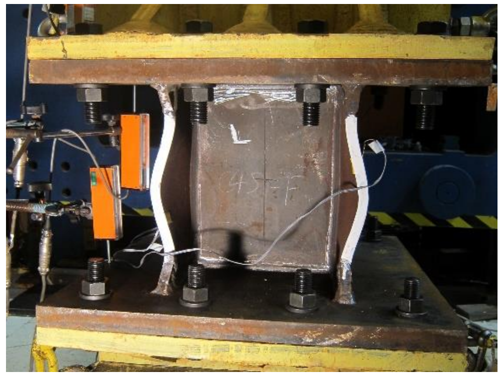

(b) Front view of test specimen

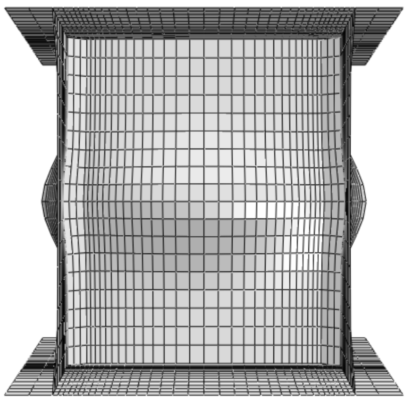

(c) Back view of FE model

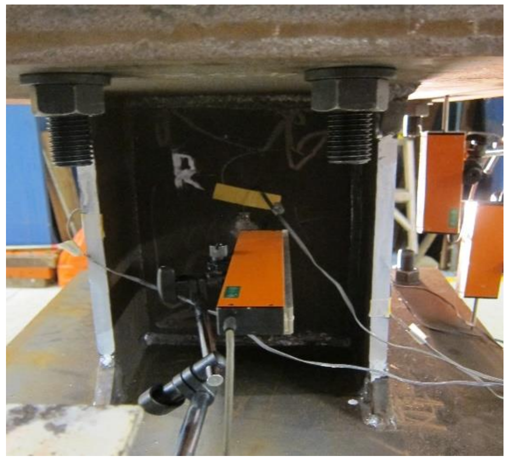

(d) Back view of test specimen

Figure 6.15: Comparison between predicted and observed failure mode of Section C4SZ-f

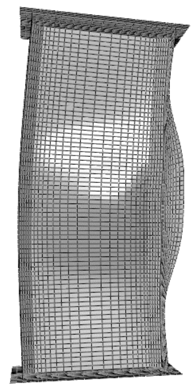
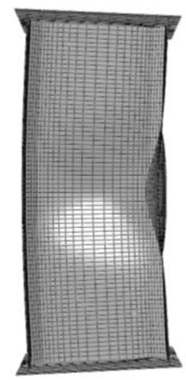

(a) Section C3SY-d

(b) Section C3SY-e

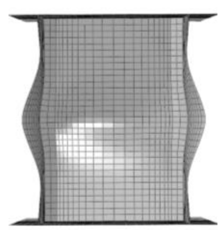
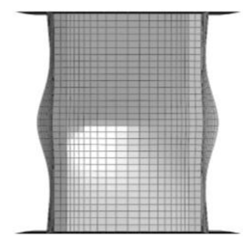

(c) Section C3SZ-f

(d) Section C3SZ-g

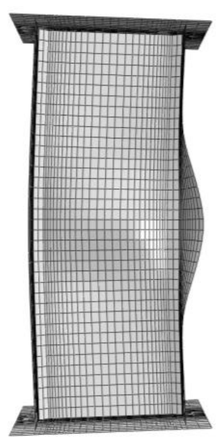
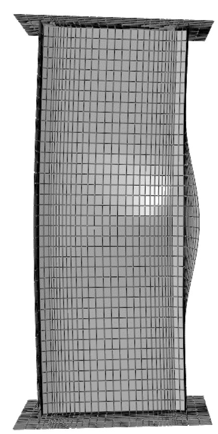

(g) Section C4SY-d

(h) Section C4SY-e

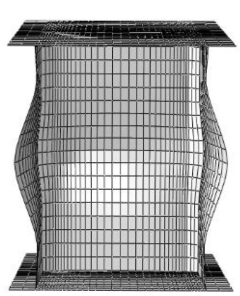
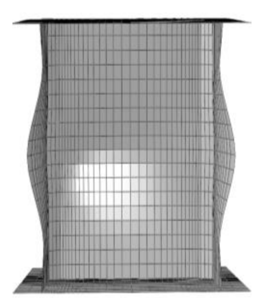

(g) Section C4SZ-f

(h) Section C4SZ-g

Figure 6.16: Predicted failure mode of all 8 stocky columns

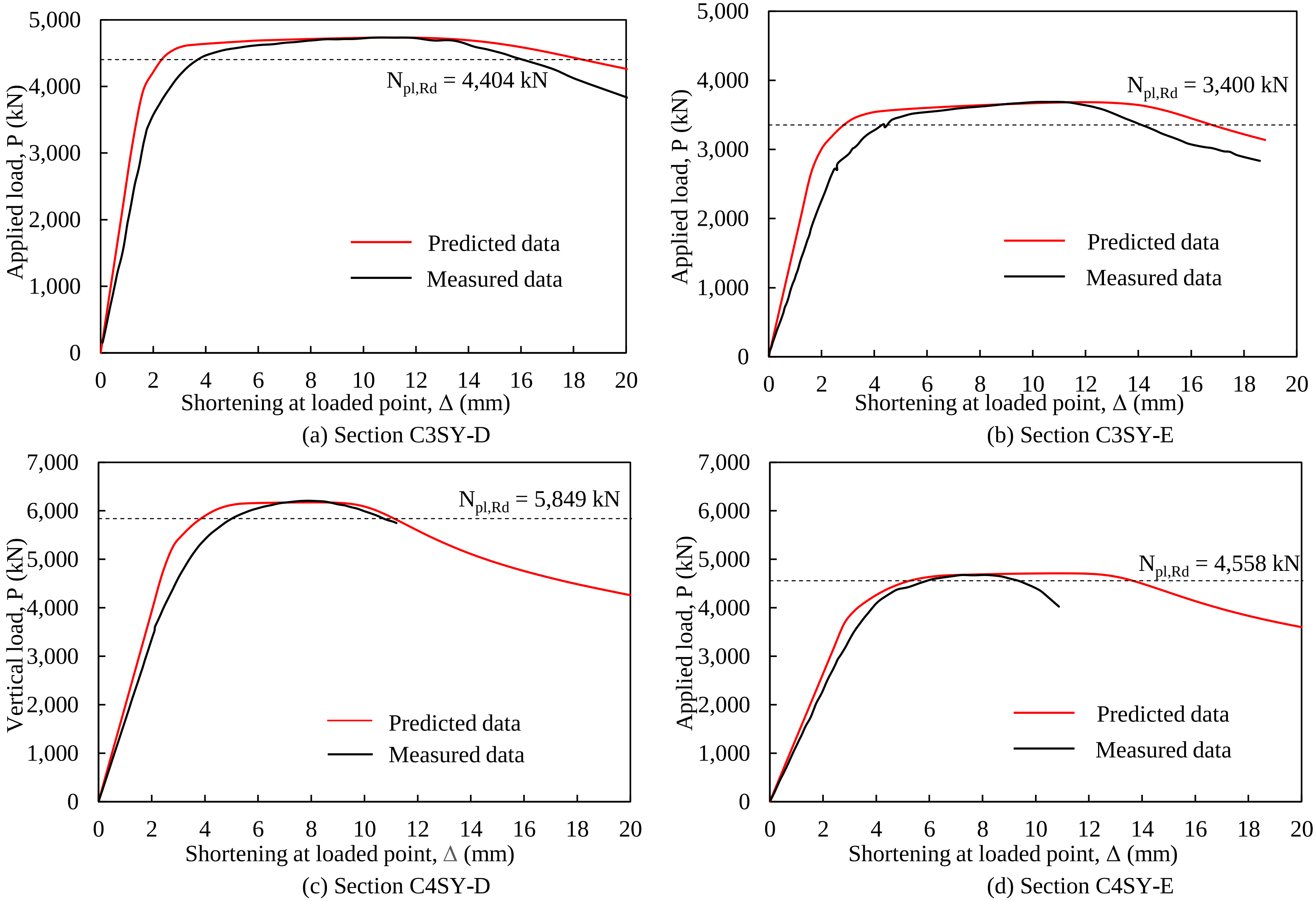

Figure 6.17: Load shortening curves of stocky columns under combined compression and major-axis bending

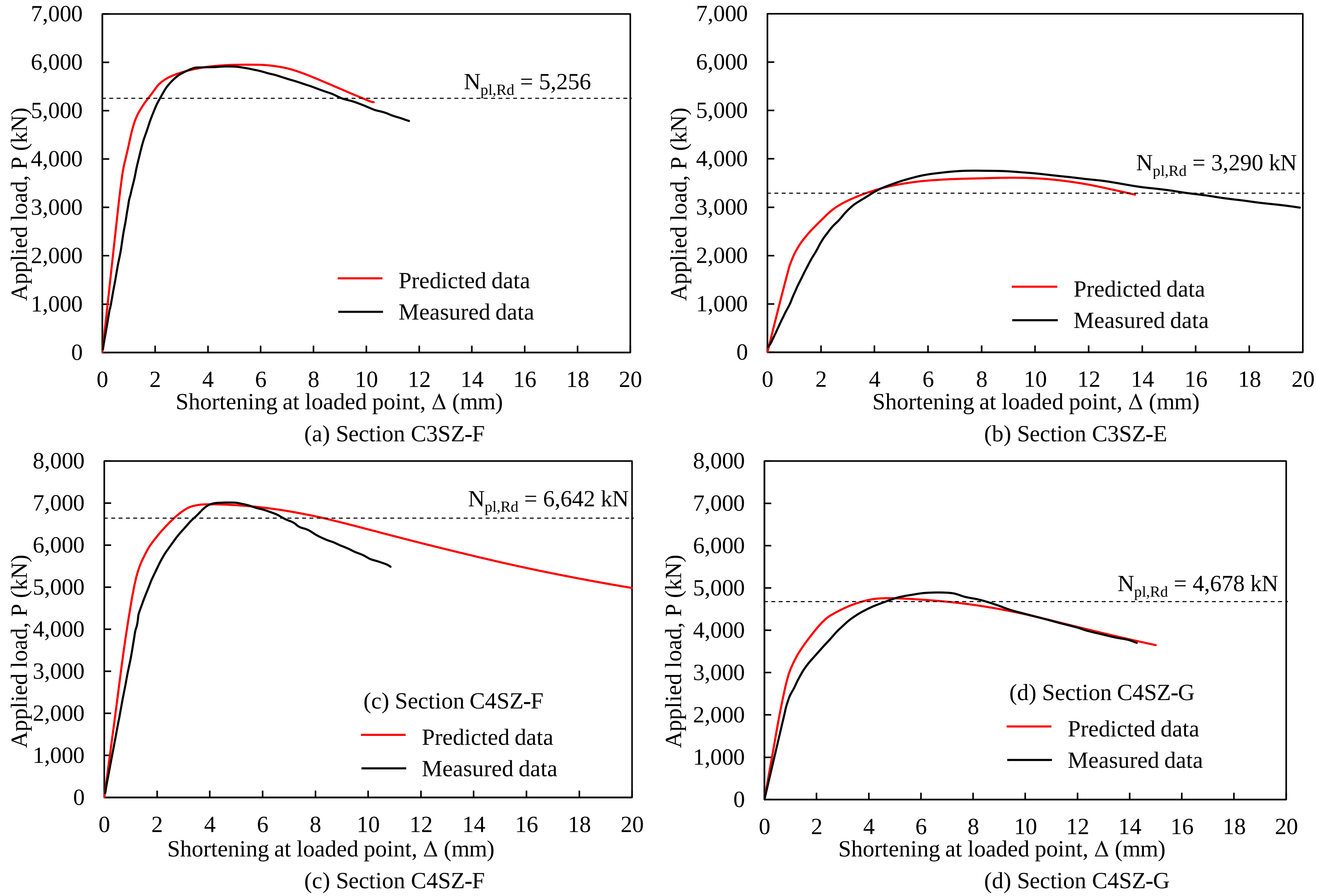

Figure 6.18: Load shortening curves of stocky columns under combined compression and minor-axis bending

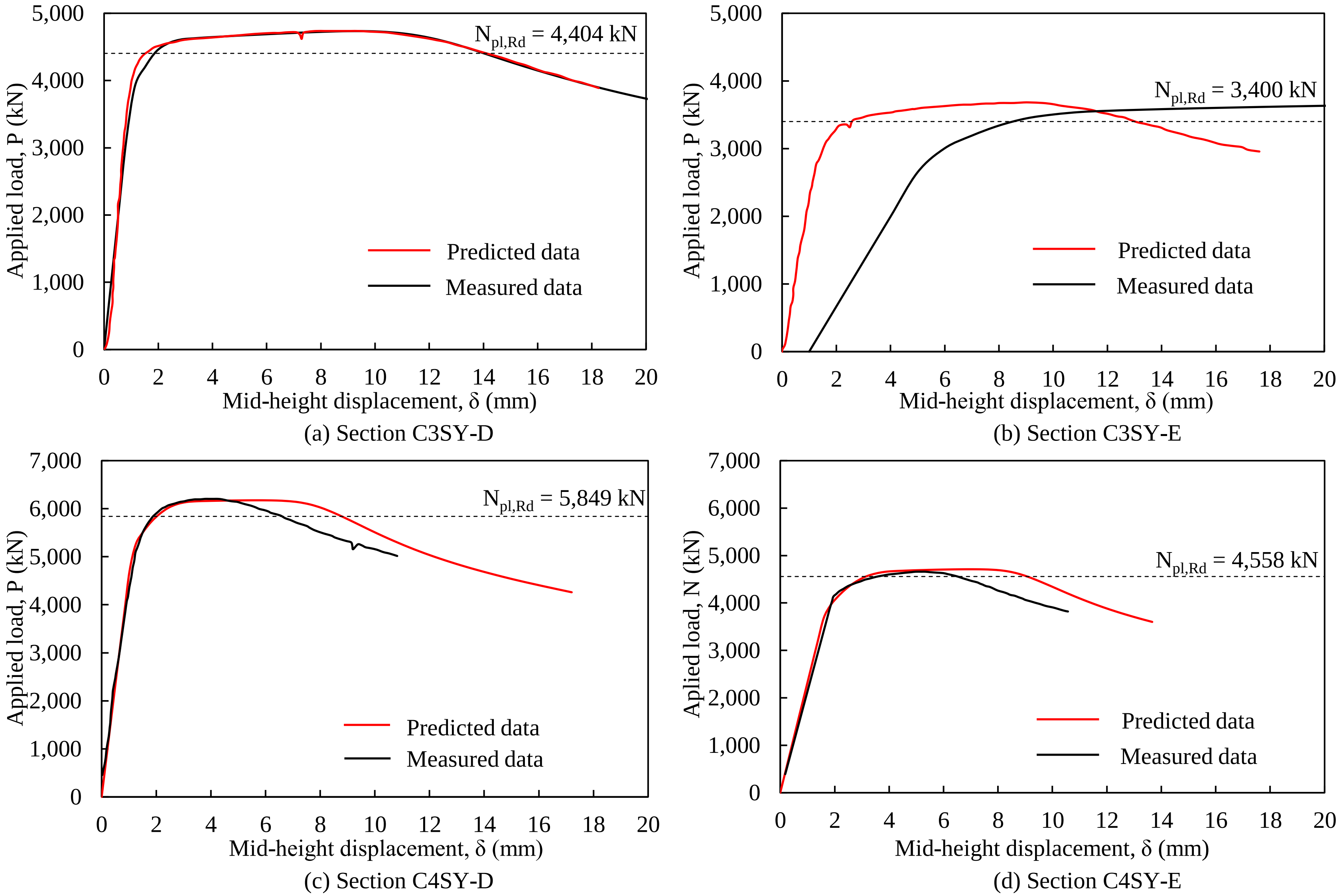

(a) Section C3SY-D

(b) Section C3SY-E

(c) Section C4SY-D

(d) Section C4SY-E

Figure 6.19: Load displacement curves of stocky columns under combined compression and major-axis bending

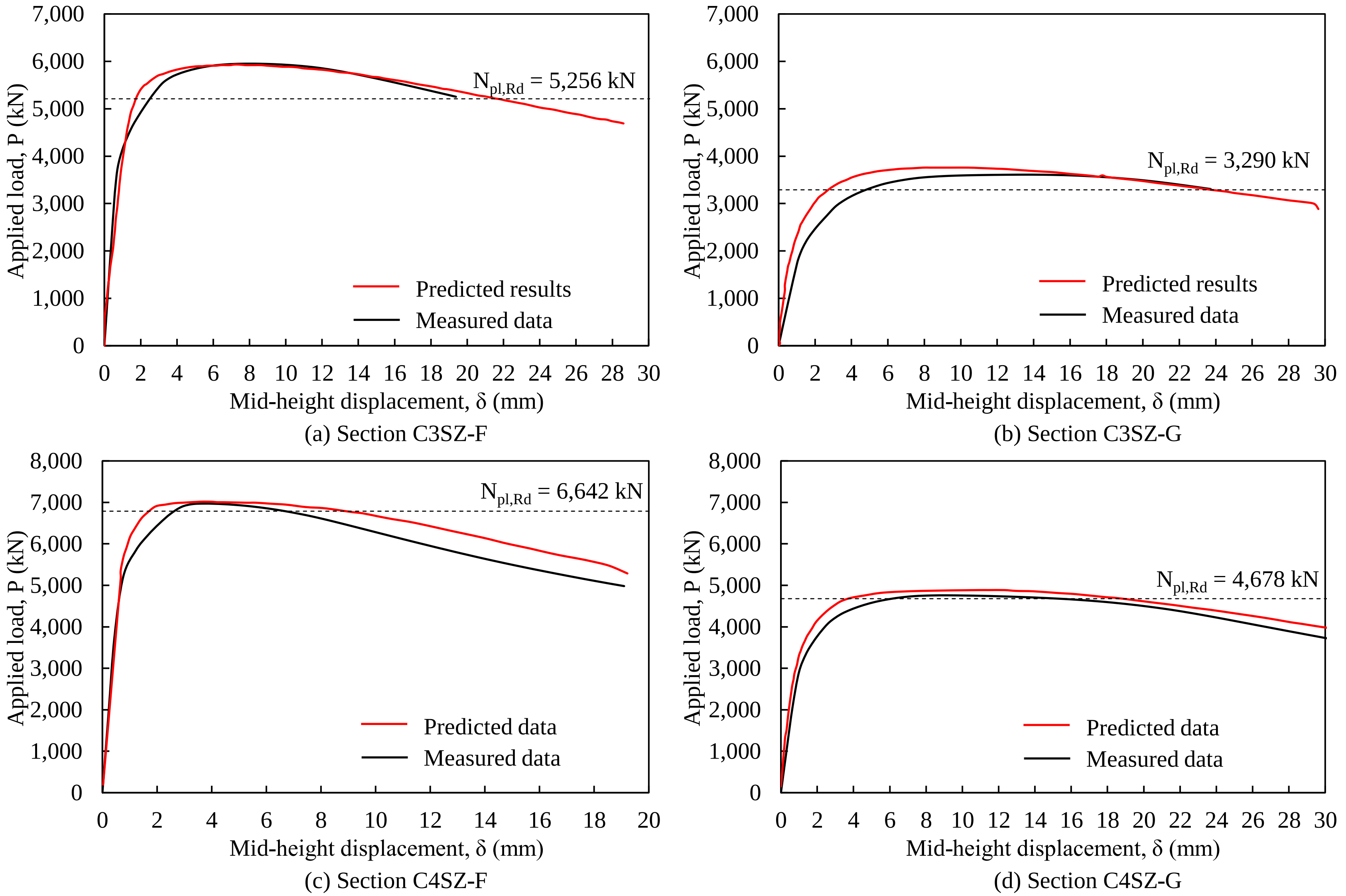

(a) Section C3SZ-F

(b) Section C3SZ-G

(c) Section C4SZ-F

(d) Section C4SZ-G

Figure 6.20: Load displacement curves of stocky columns under combined compression and minor-axis bending

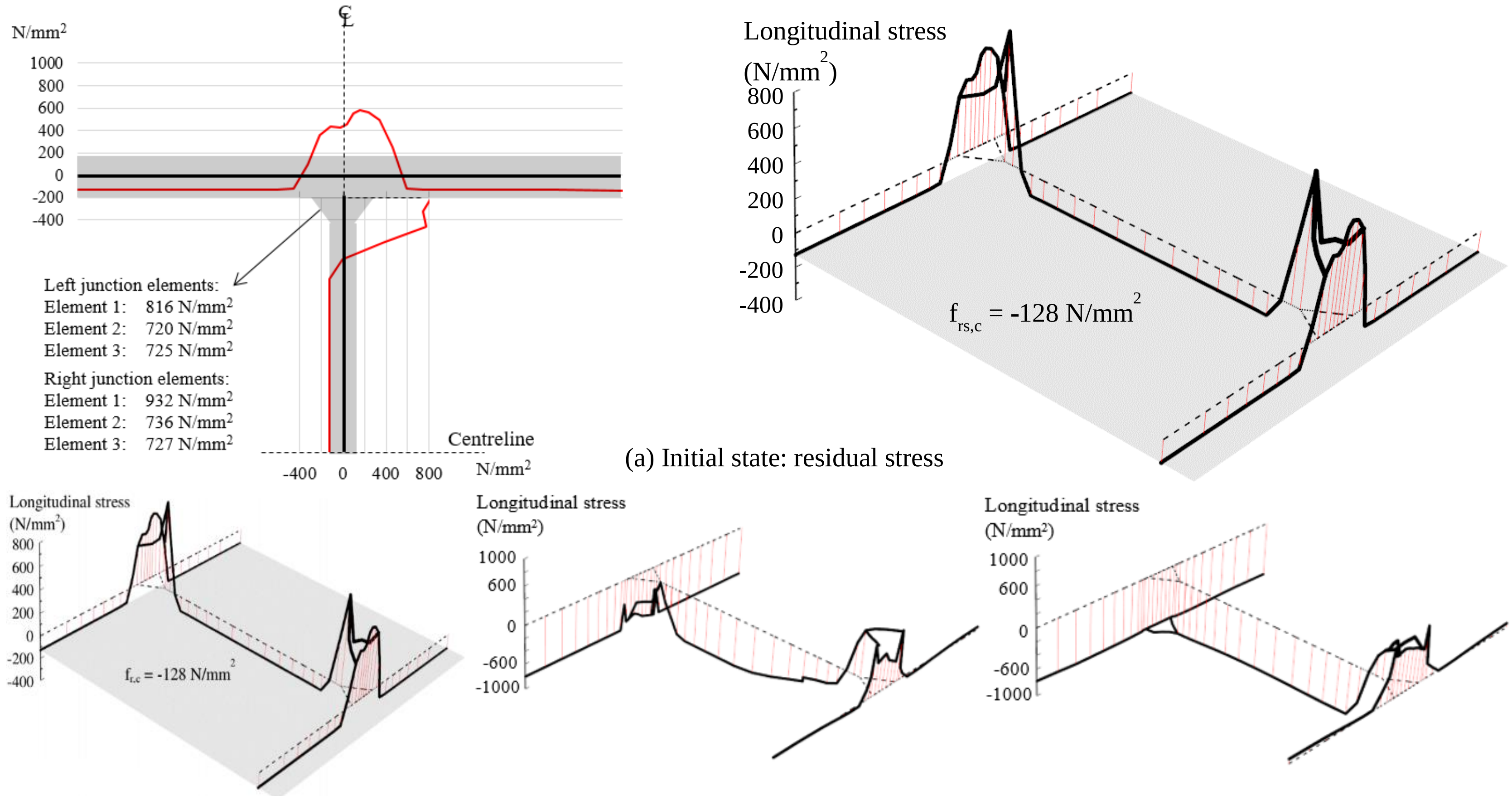

(b) State 0: residual stresses

(c) State 1: first obtaining yielding resistance

(d) Stage 2: obtaining maximum resistance

Figure 6.21: Development of longitudial stresses in Section C3SY-e

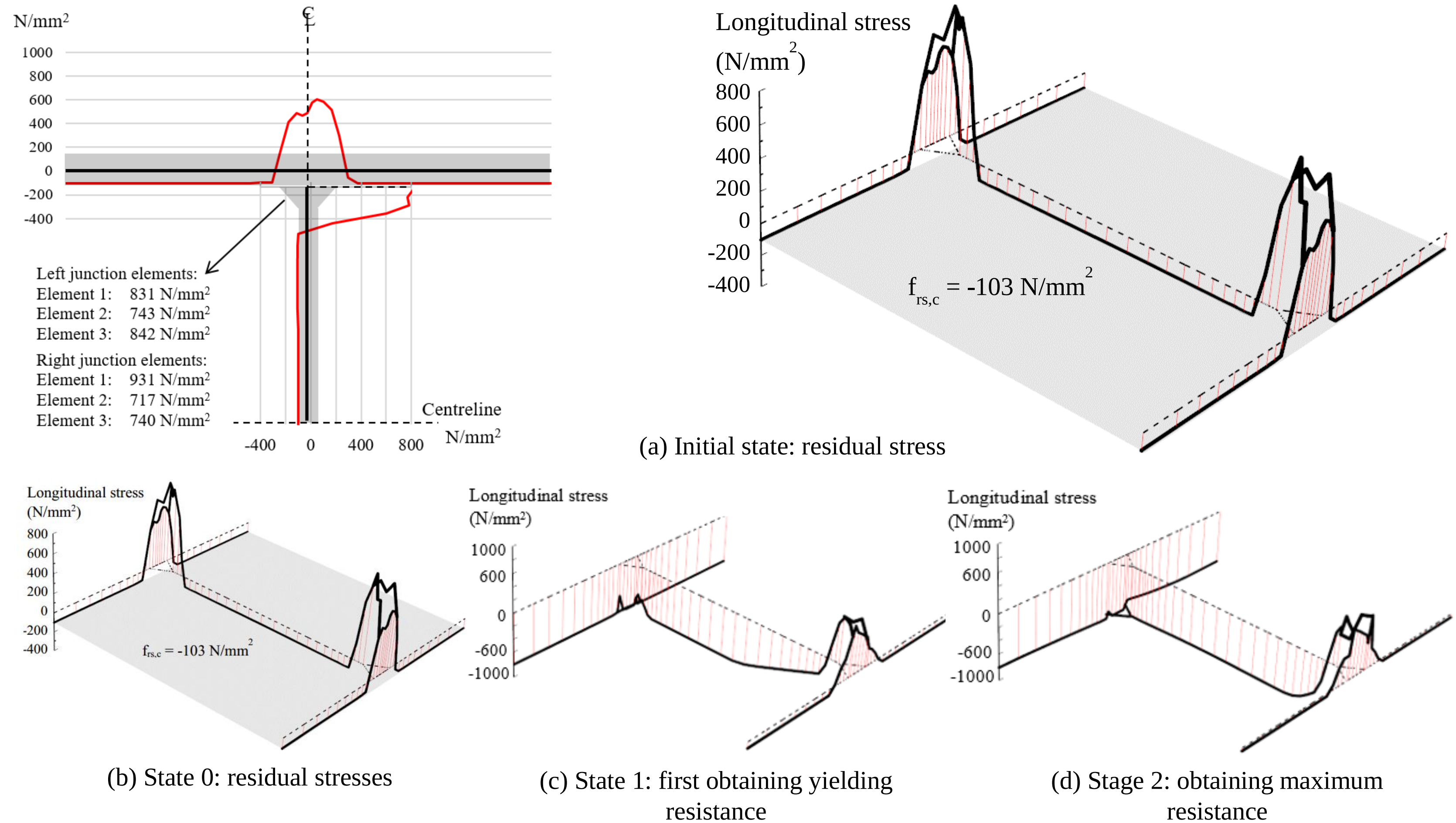

Figure 6.22: Development of longitudial stresses in Section C4SY-e

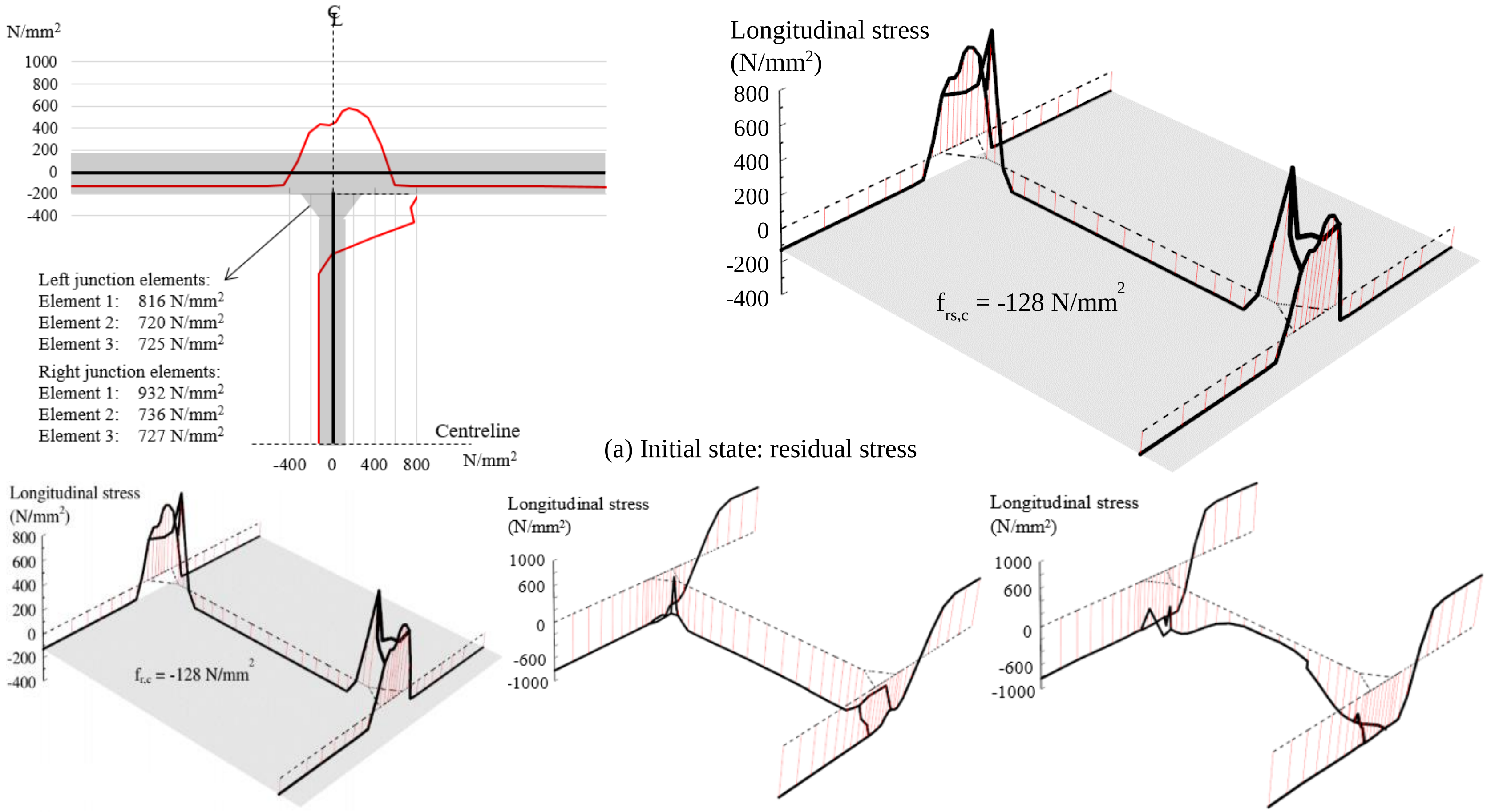

(a) Initial state: residual stress

(b) State 0: residual stresses

(c) State 1: first obtaining yielding resistance

(d) Stage 2: obtaining maximum resistance

Figure 6.23: Development of longitudial stresses in Section C3SZ-g

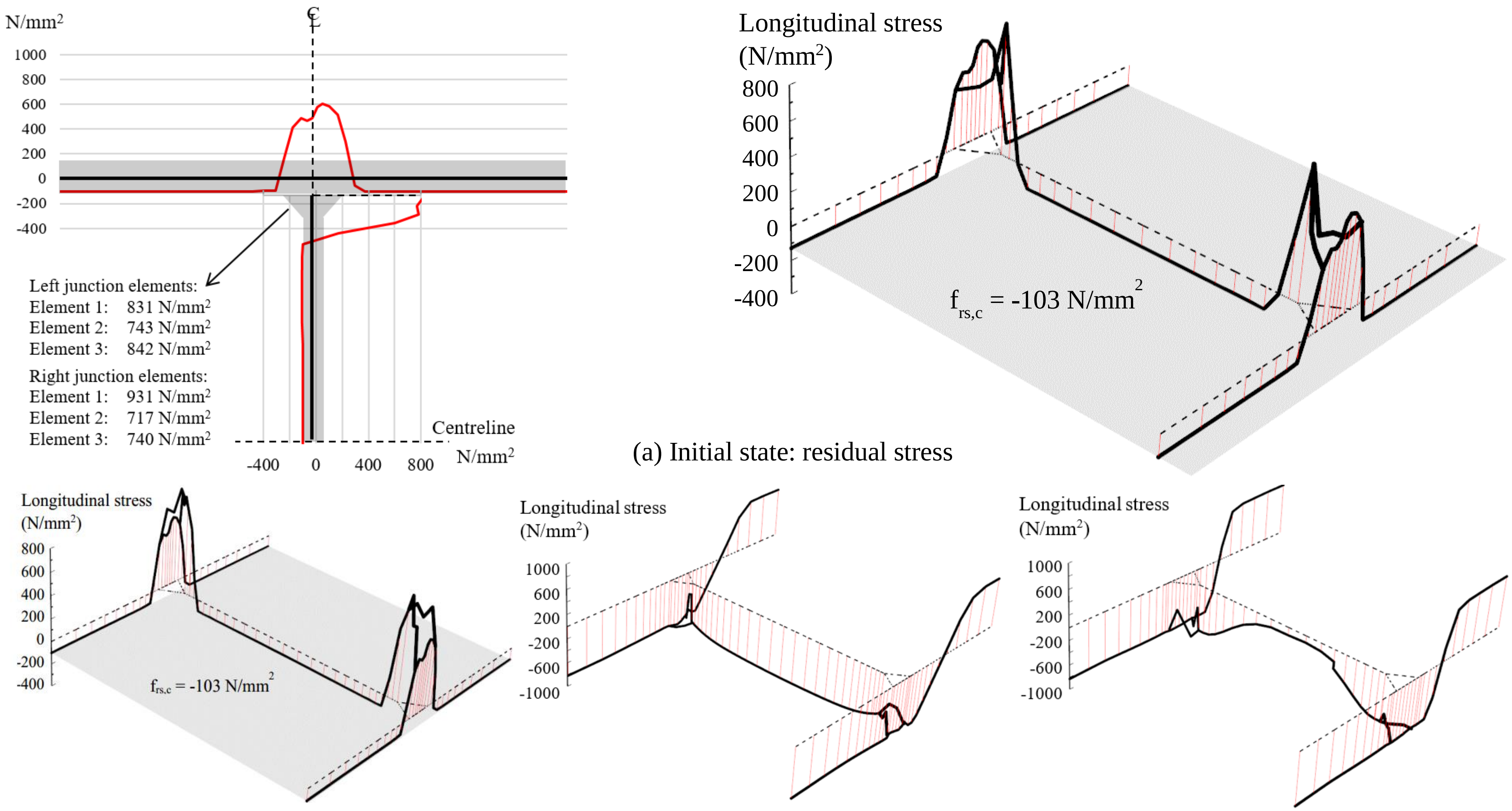

(a) Initial state: residual stress

(b) State 0: residual stresses

(c) State 1: first obtaining yielding resistance

(d) Stage 2: obtaining maximum resistance

Figure 6.24: Development of longitudial stresses in Section C4SZ-g

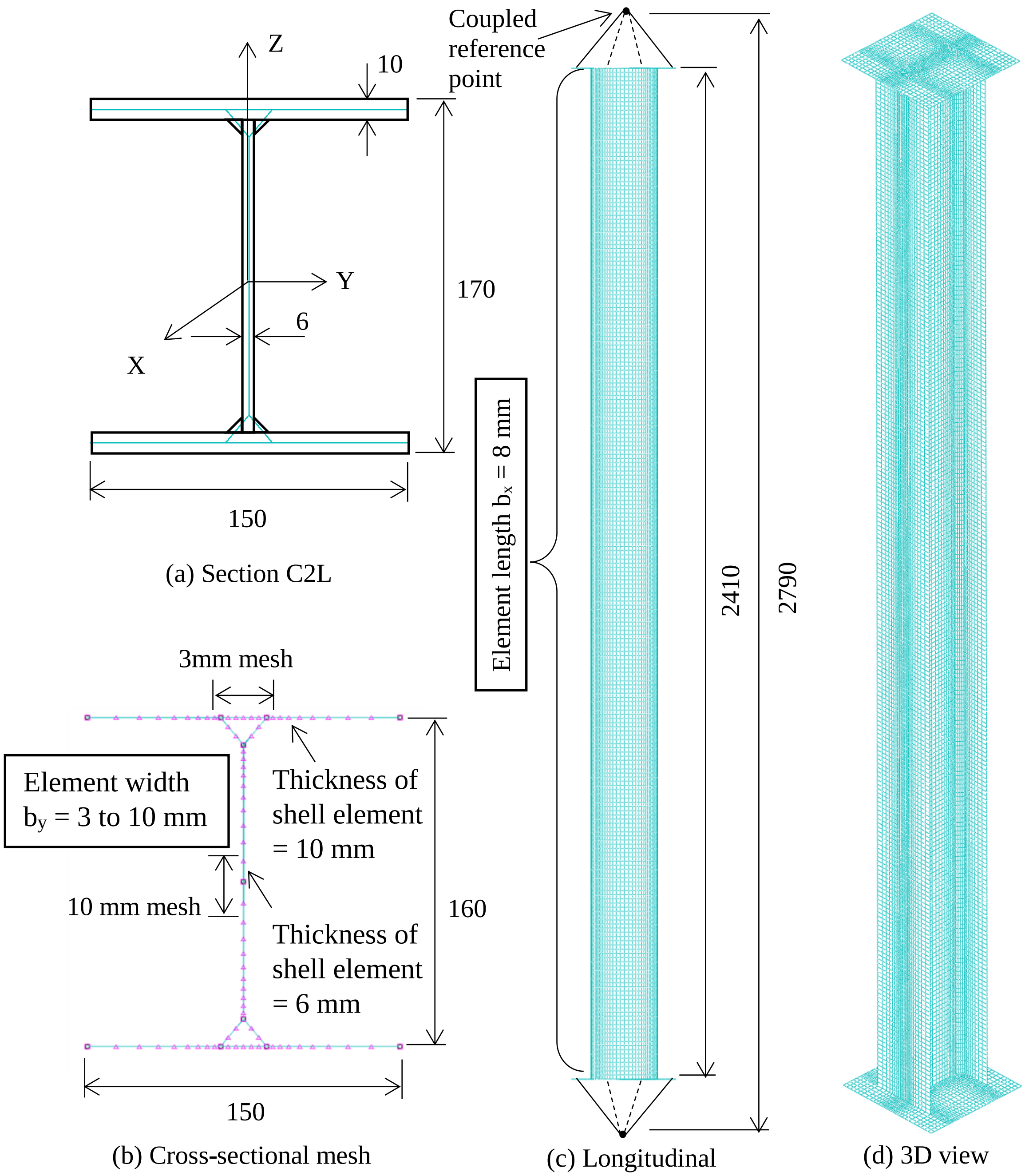

Figure 6.25: Typical mesh of slender columns of welded H-sections

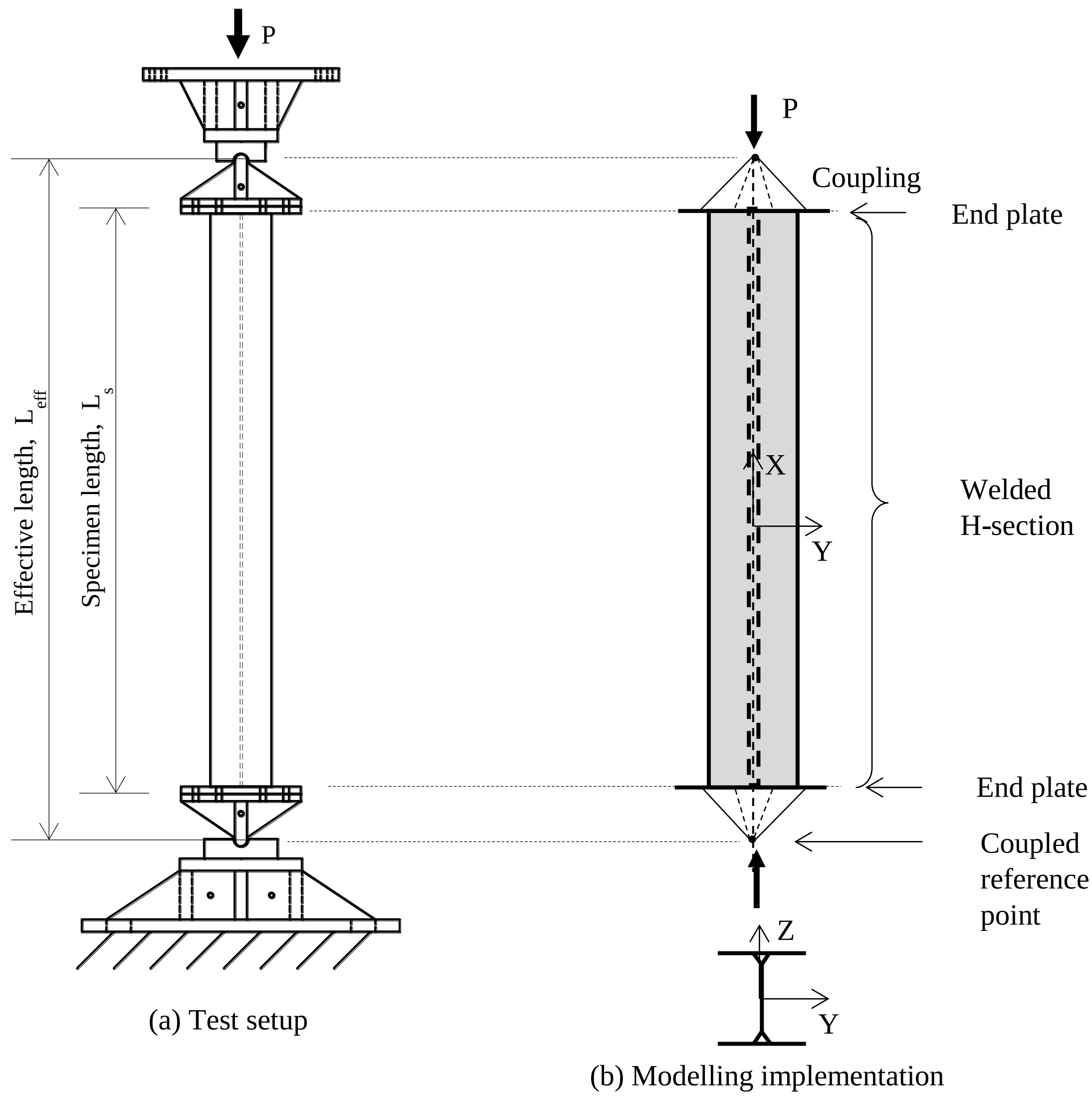

Boundary condition of reference points*:

	X	Y	Z
Translation	✓	×	×
Rotation	×	×	✓

*Note: × denotes prohibited degree of freedom; and,
✓ denotes allowed degrees of freedom.

Figure 6.25: Loading and boundary conditions for slender columns under compression

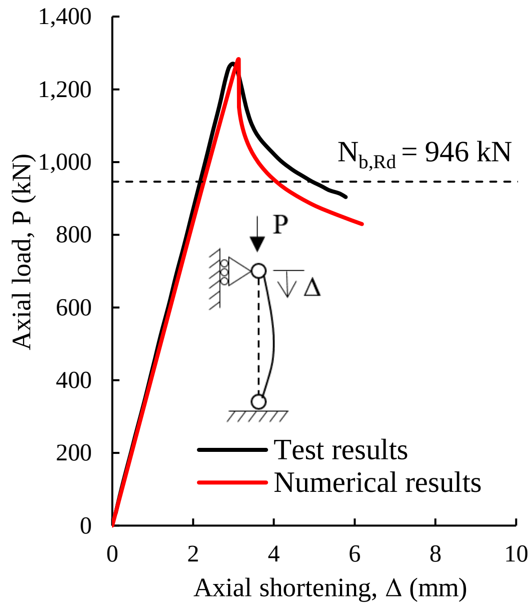

(a) Load shortening curve

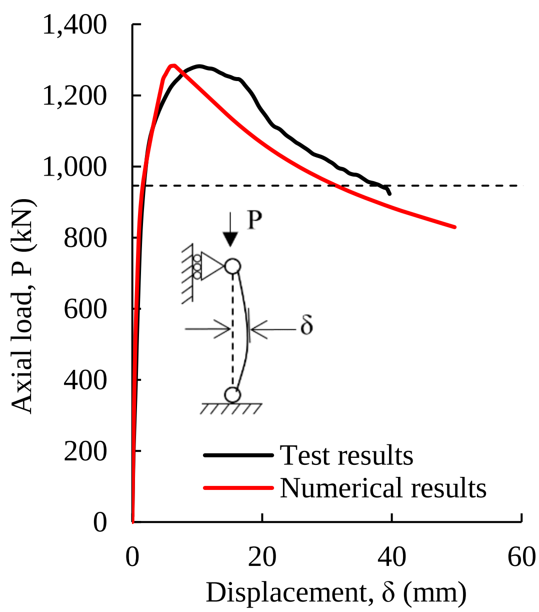

(b) Load displacement curve

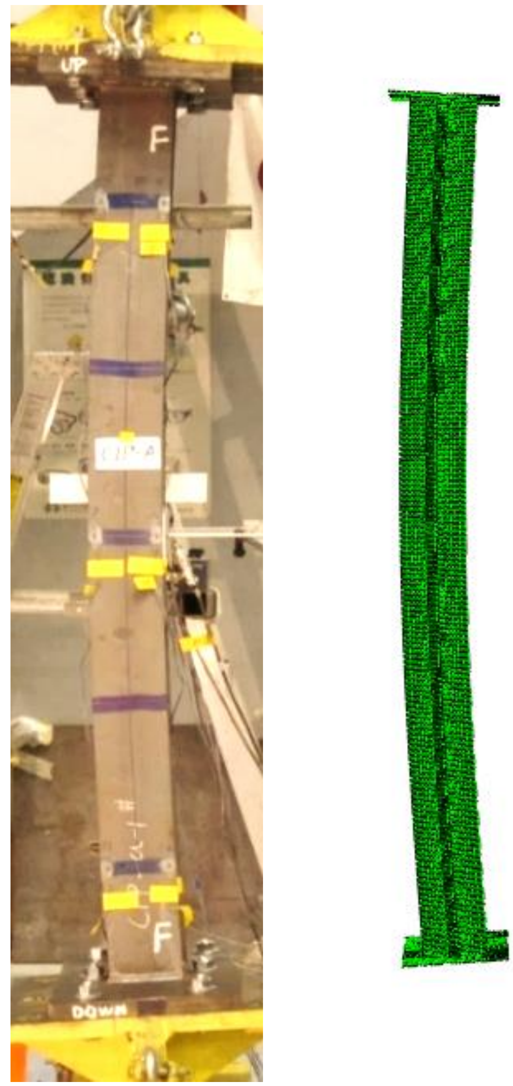

(c) Comparison of failure mode

Figure 6.26: Predicted structural behaviour of Section C1M

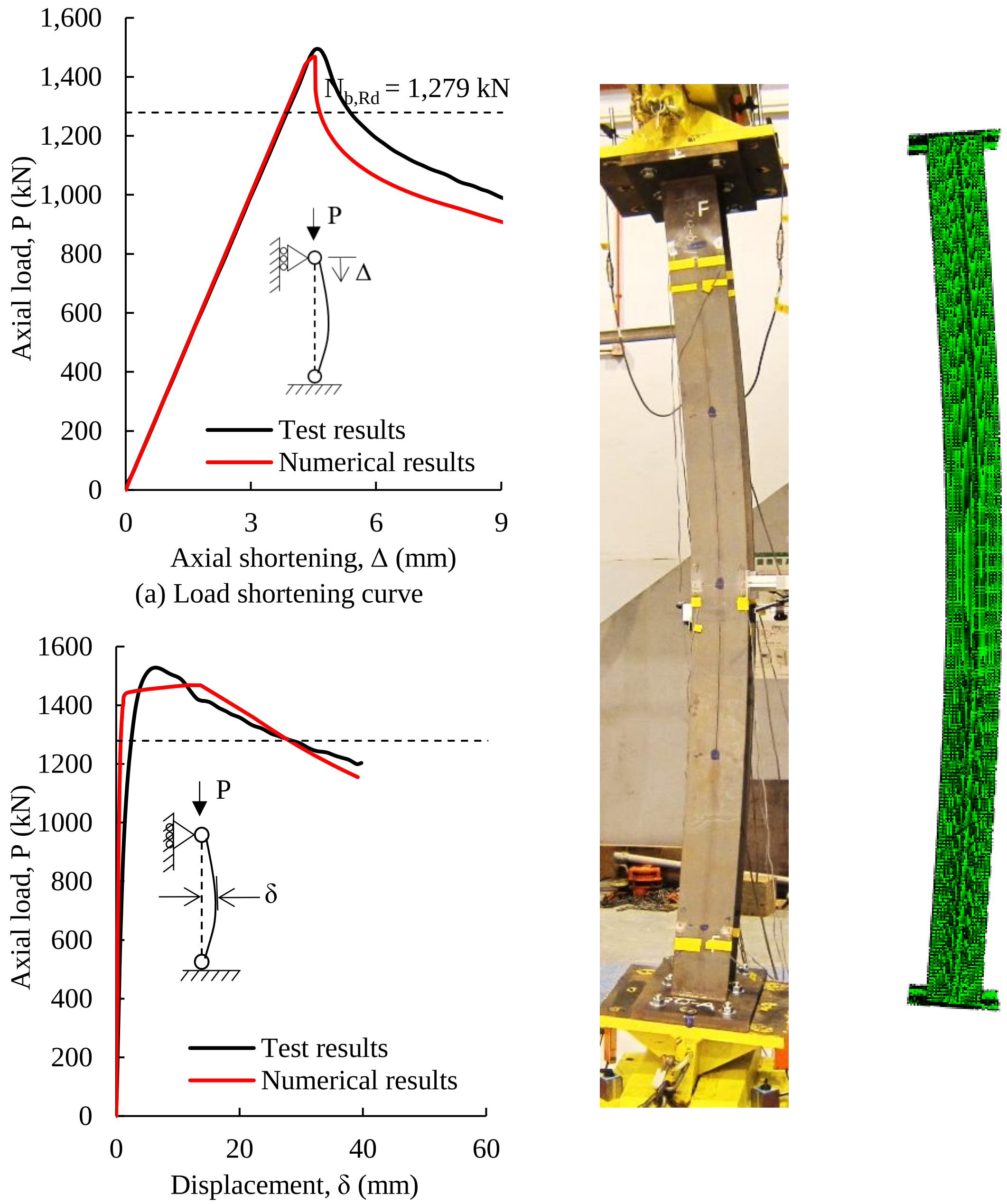

(a) Load shortening curve

(b) Load displacement curve

(c) Failure mode

Figure 6.27: Predicted structural behaviour of Section C2L

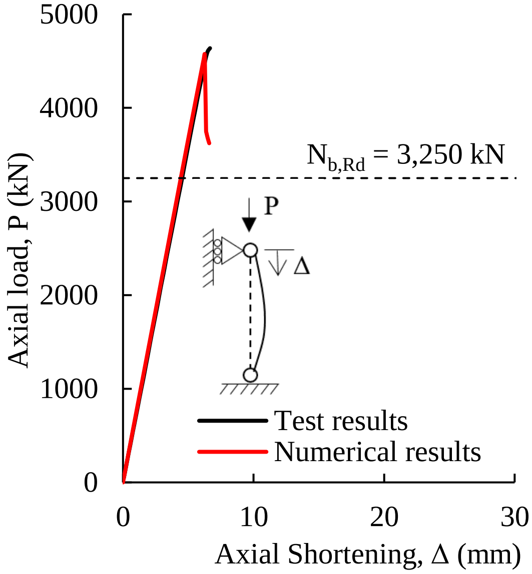

(a) Load shortening curve

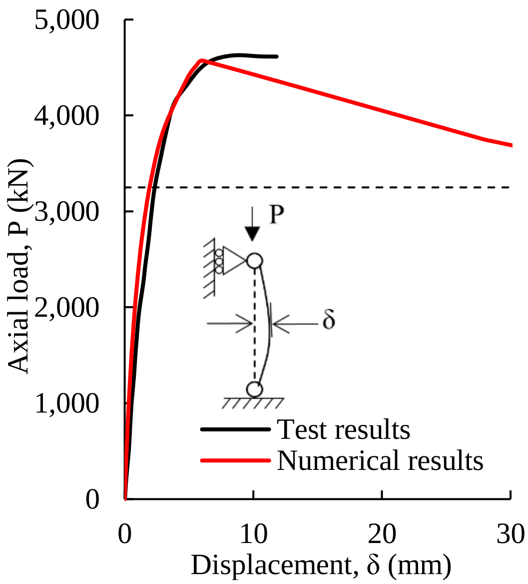

(b) Load displacement curve

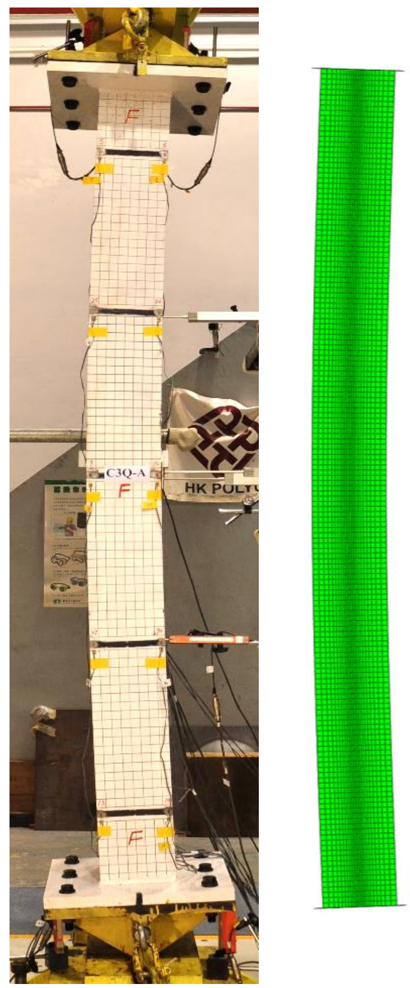

(c) Comparison of failure mode

Figure 6.28: Predicted structural behaviour of Section C1L

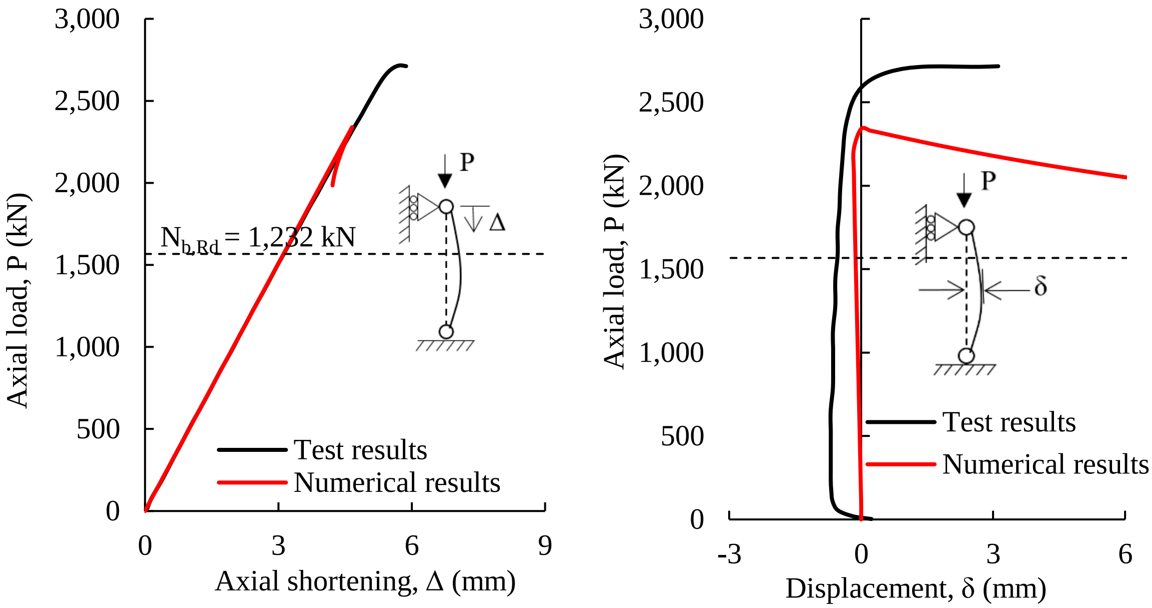

(a) Section C2M

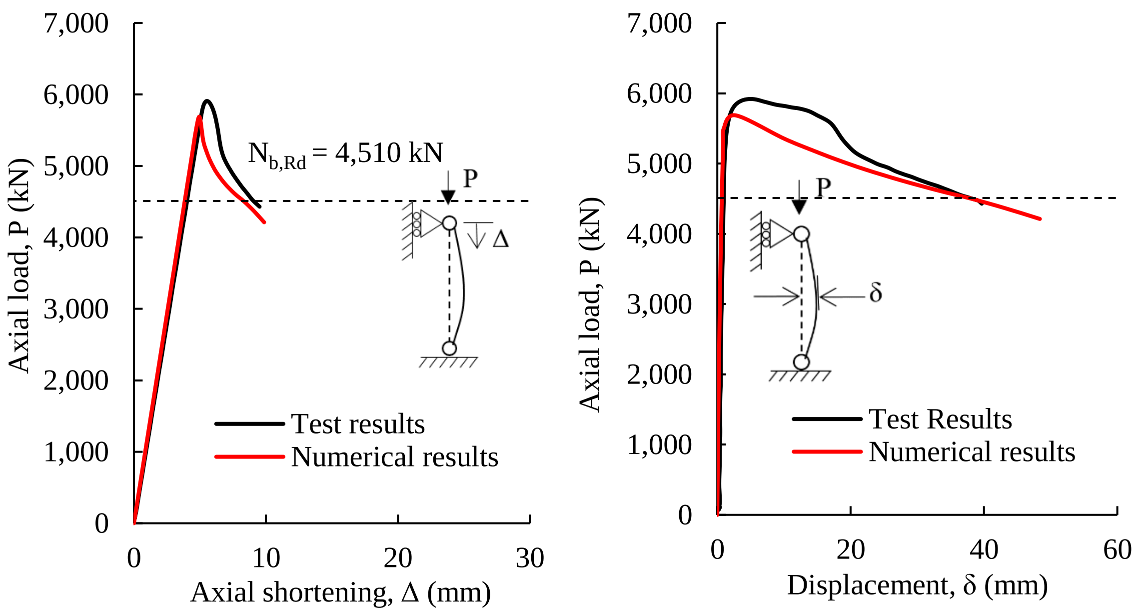

(b) Section C3M

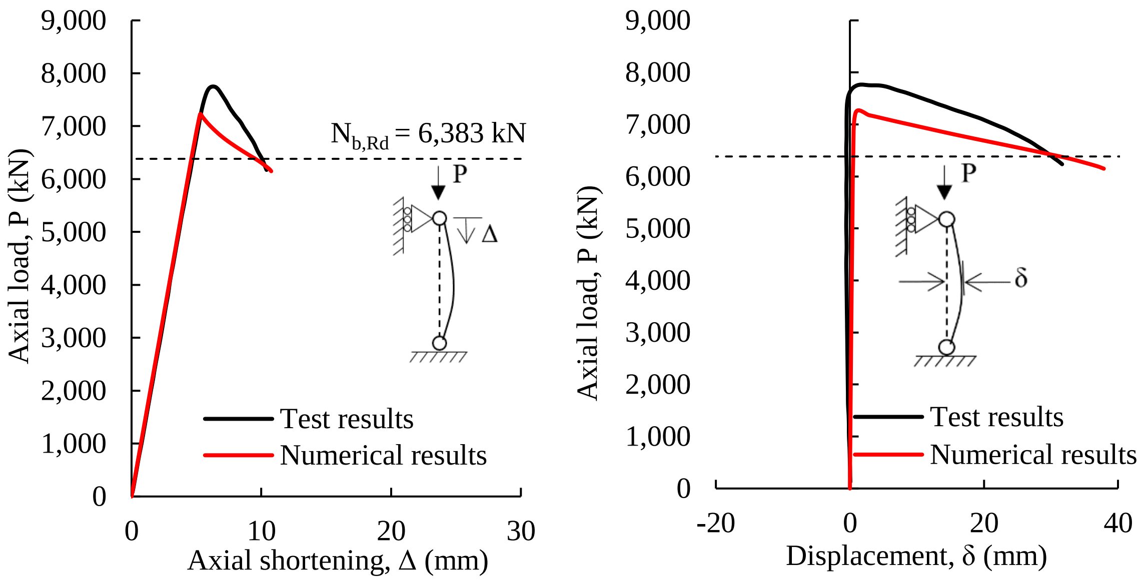

(c) Section C4M

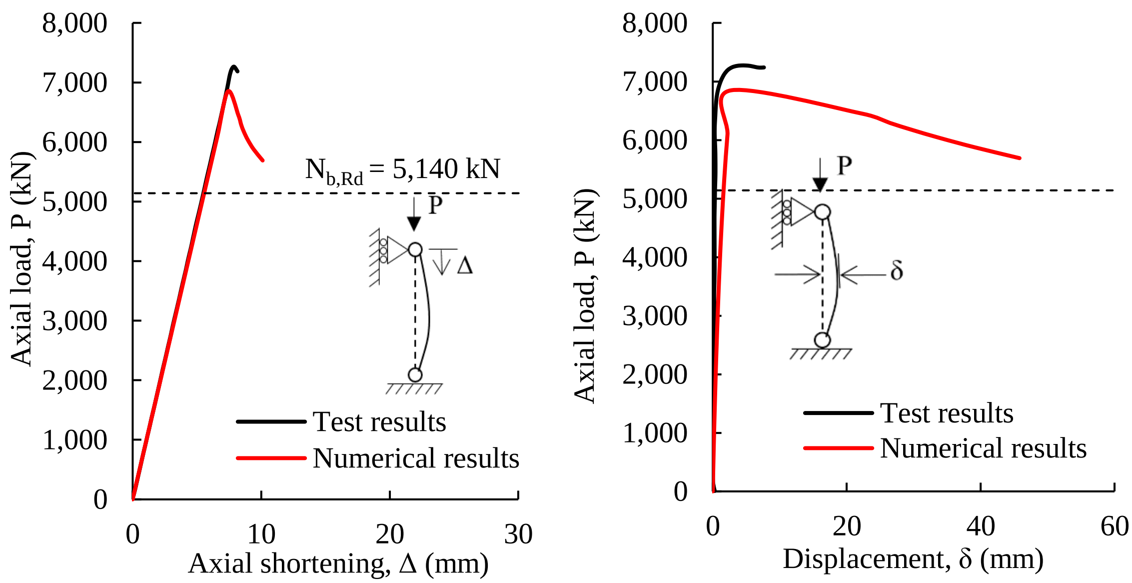

(d) Section C4L

Figure 6.29: Structural responses of Sections C2M, C3M, C4M and C4L

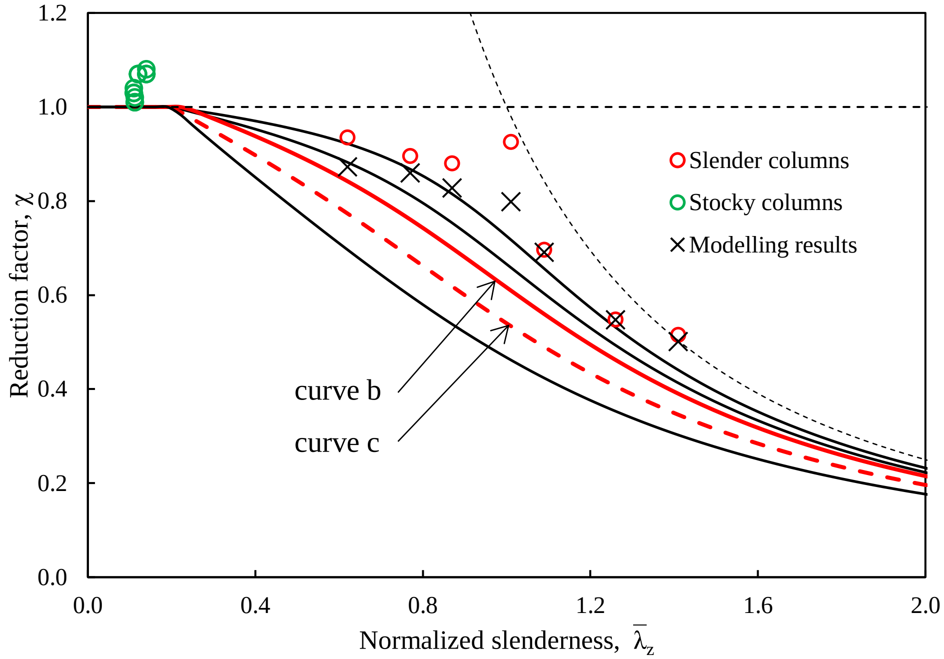

Figure 6.30: Comparison between reduction factors and column buckling curves

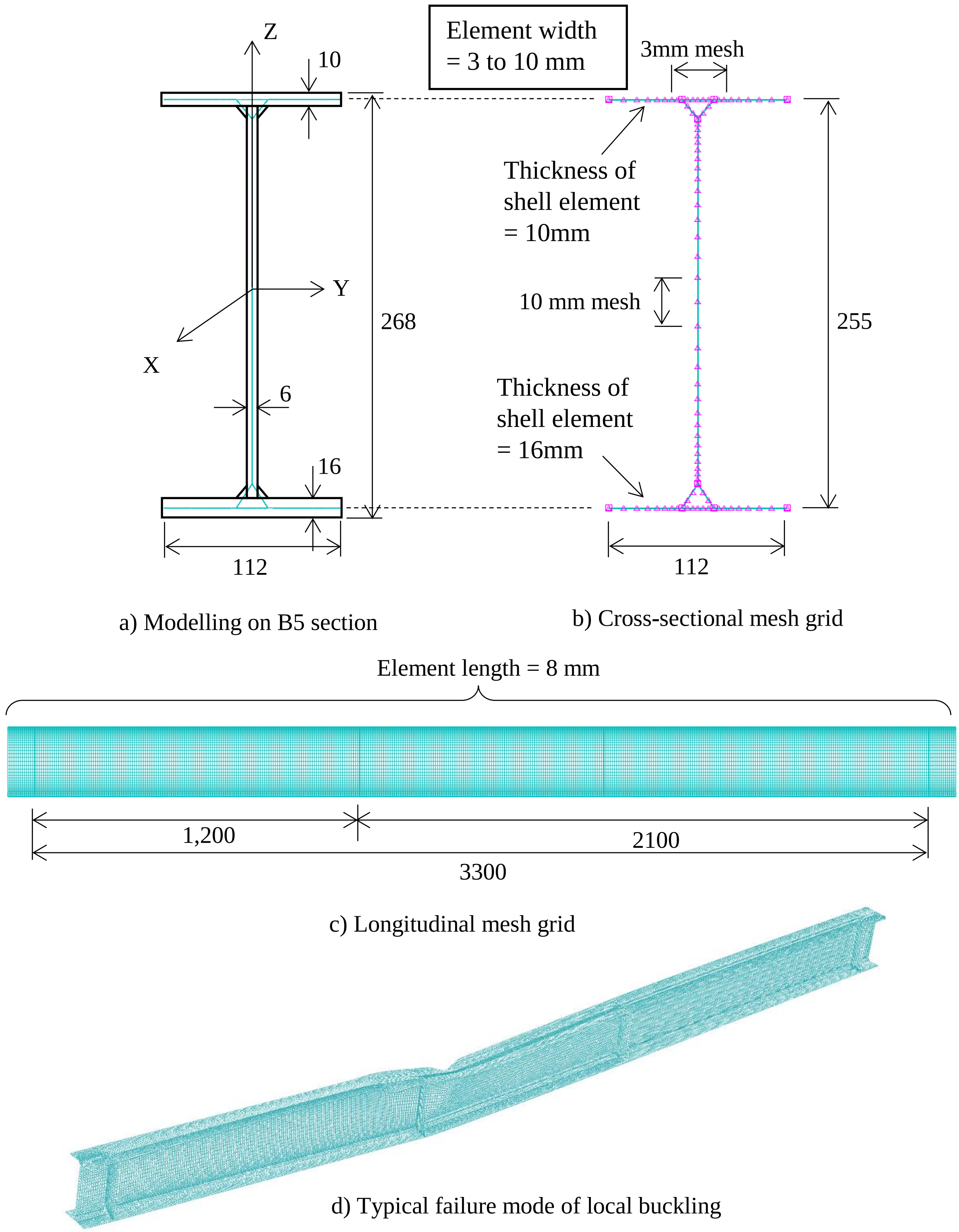

Figure 6.31: Typical mesh and failure mode of a welded I-section

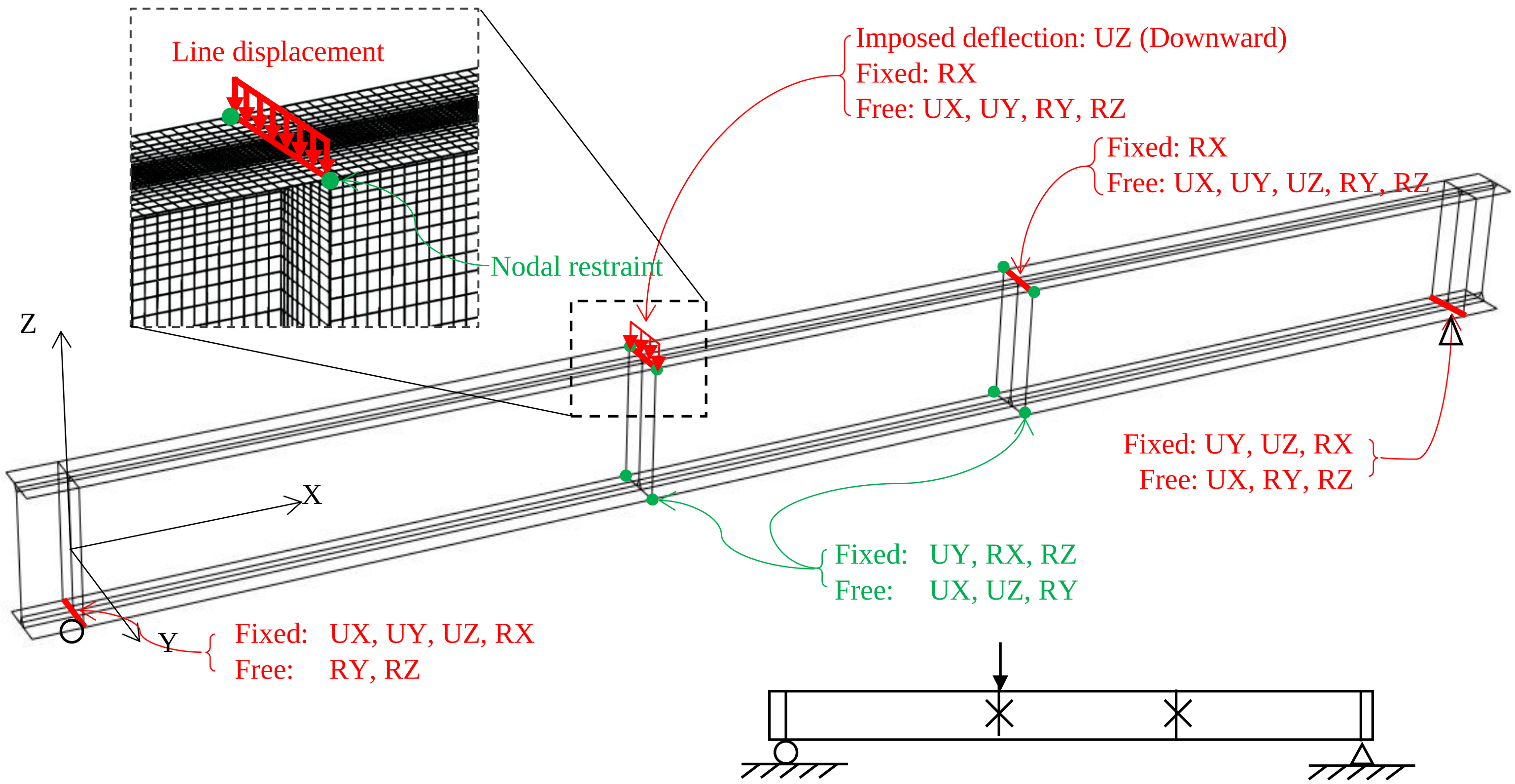

Figure 6.32: Boundary condition for fully restrained beams

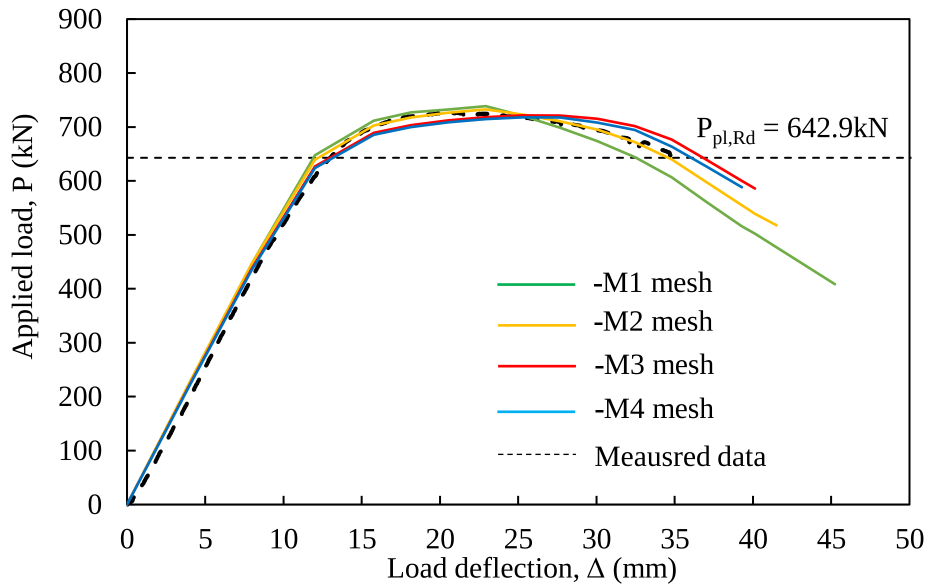

(a) Section B1 of Series LT0

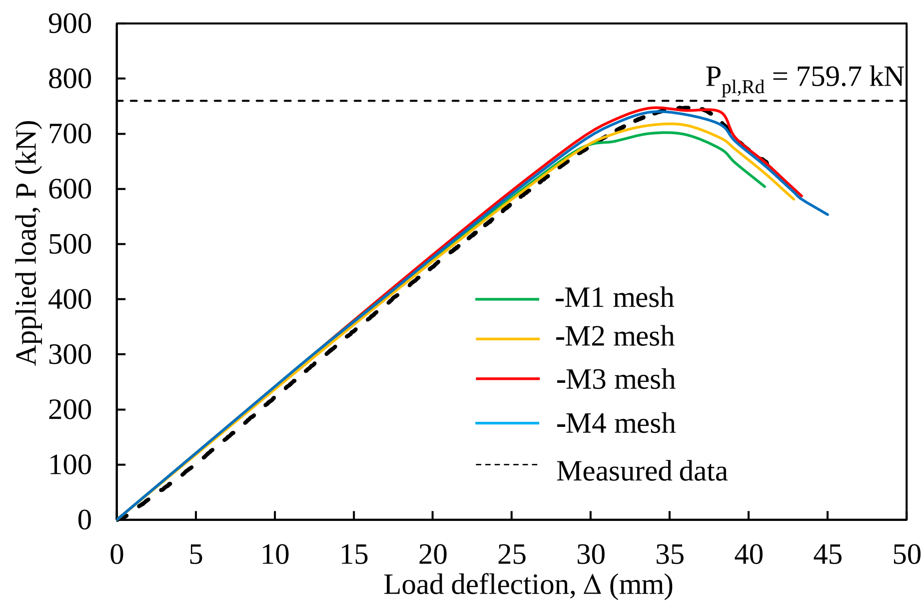

(b) Section B3 of Series LT0

Figure 6.33: Load deflection curves of fully restrained beams for convergence study

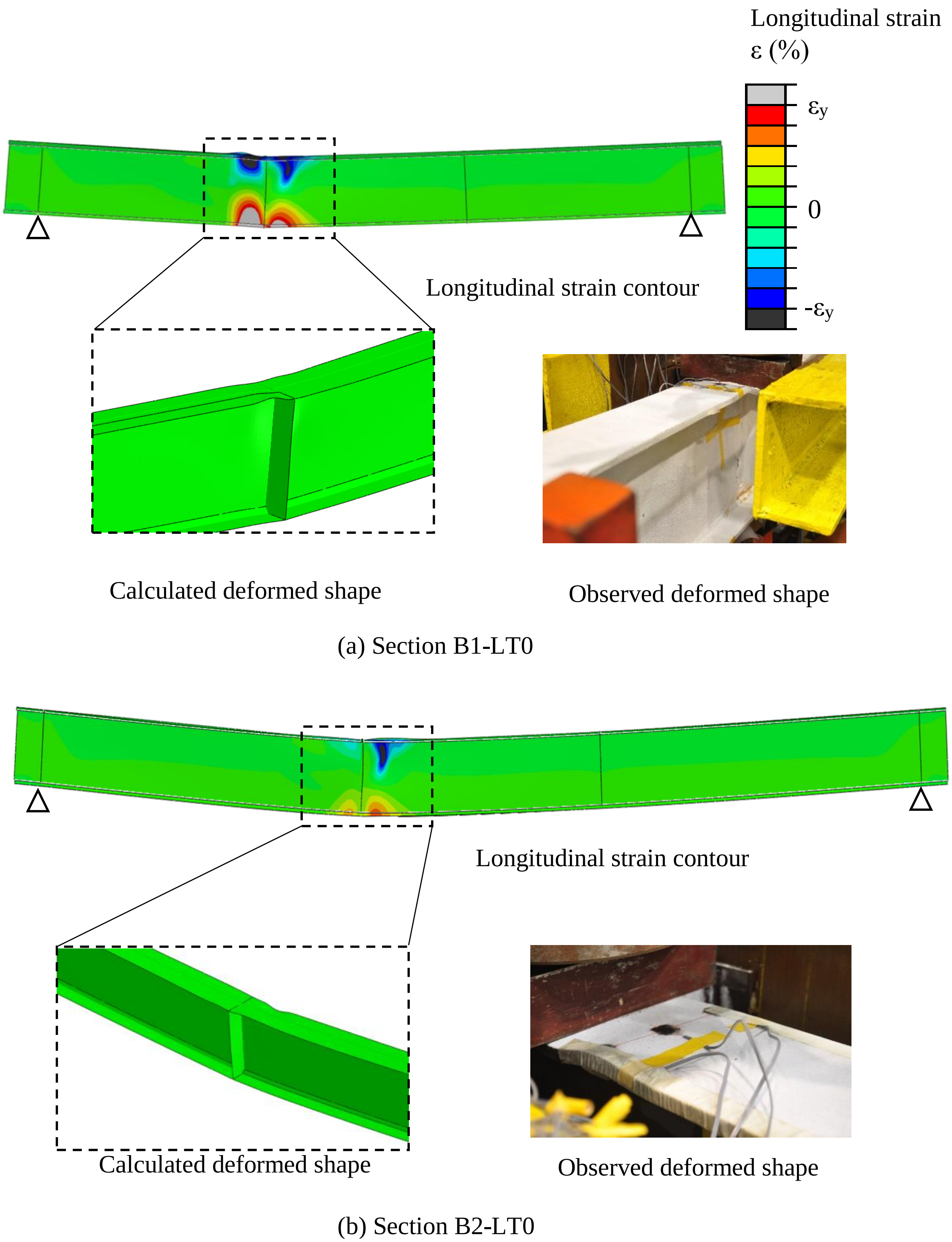

Figure 6.34: Typical failure modes and strain contour of S690 full restrained beams at maximum load

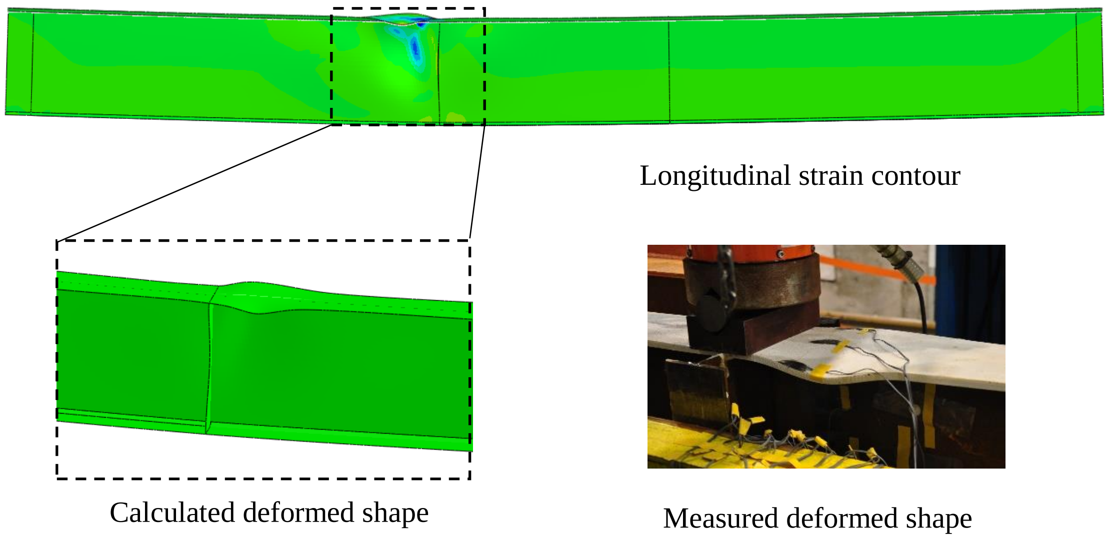

(c) Section B3-LT0

Figure 6.34: Typical failure modes and strain contour of full restrained beams at maximum load (Continued)

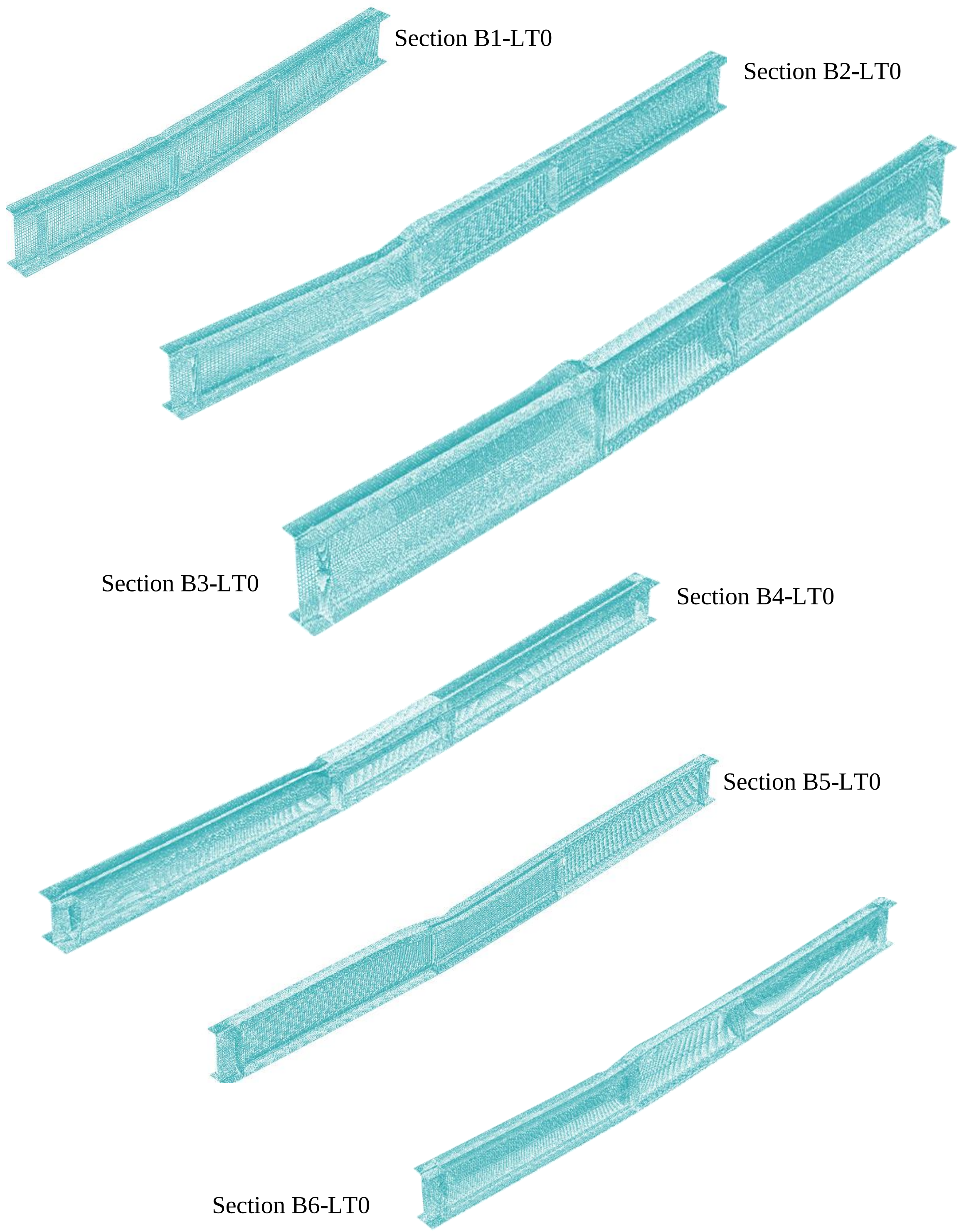

Figure 6.35: Failure modes of 6 full restrained beams of welded S690 I-sections

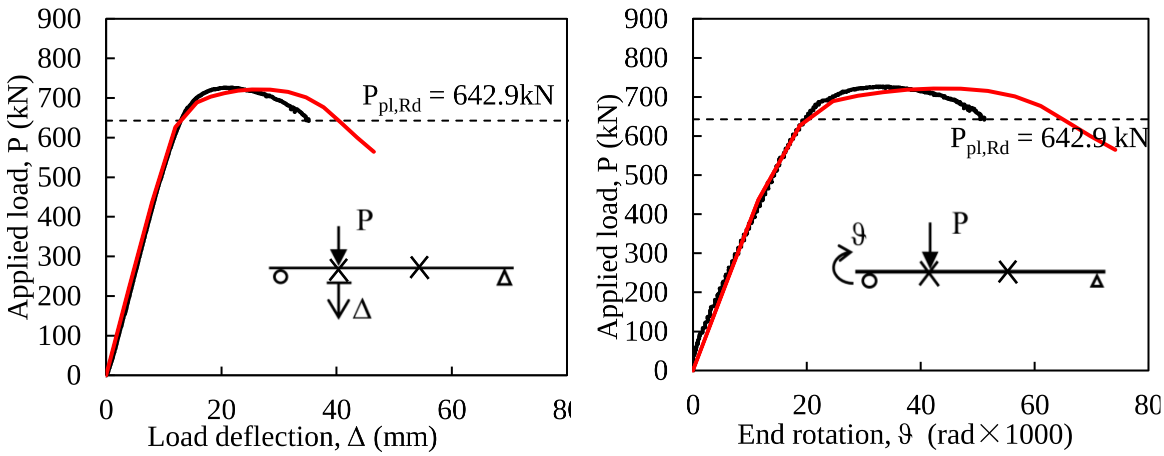

(a) Beam B1-LT0

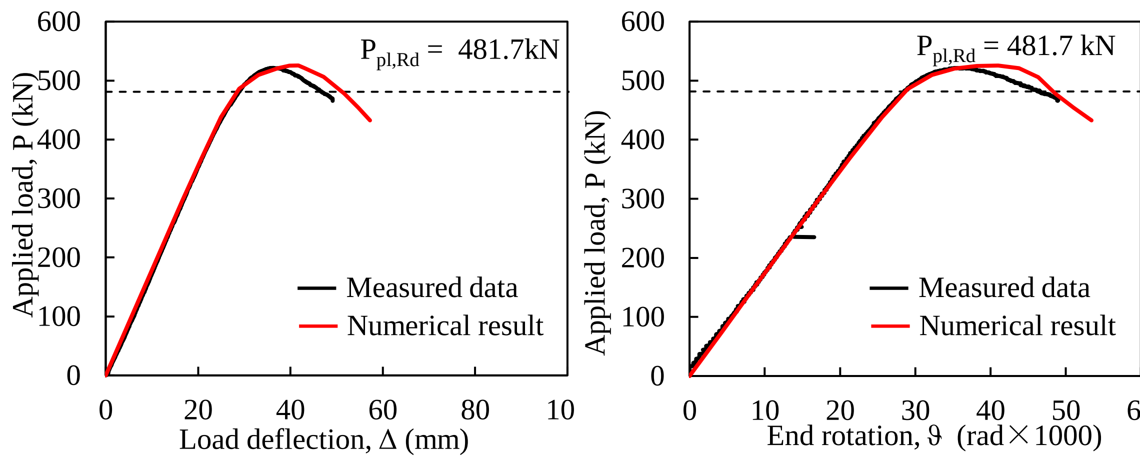

(b) Beam B2-LT0

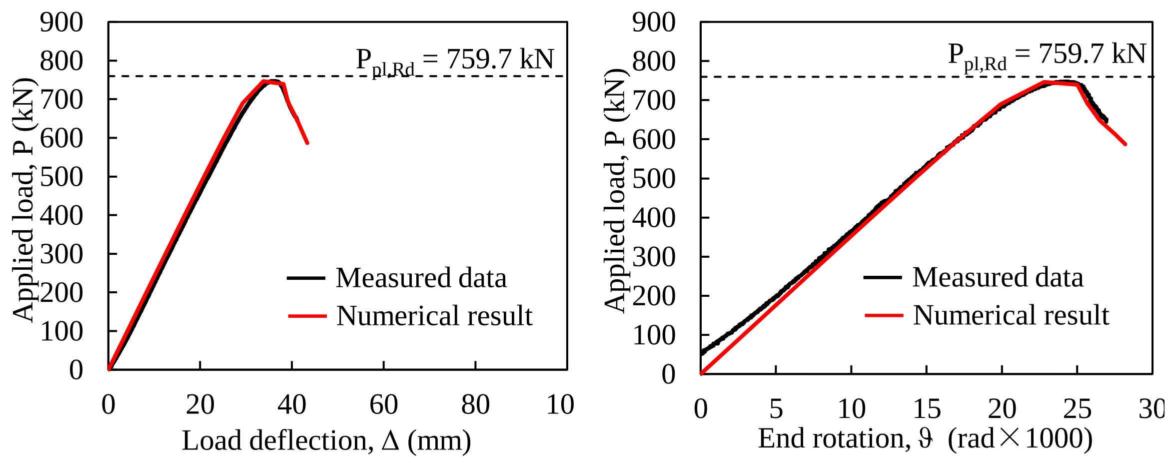

(c) Beam B3-LT0

Figure 6.36: Load deflection curves and load rotation curves of S690 fully restrained beams of Series LT0

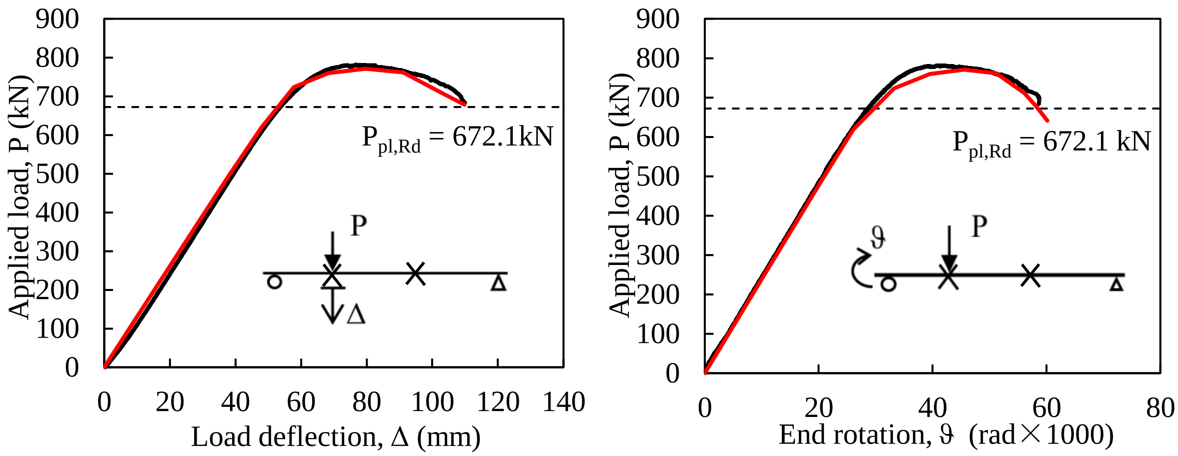

(d) Beam B4-LT0

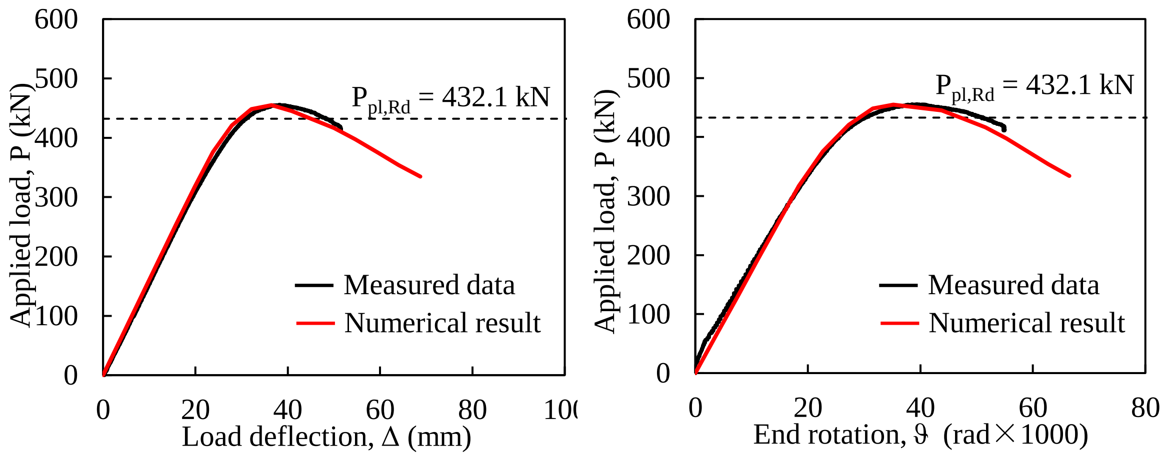

(e) Beam B5-LT0

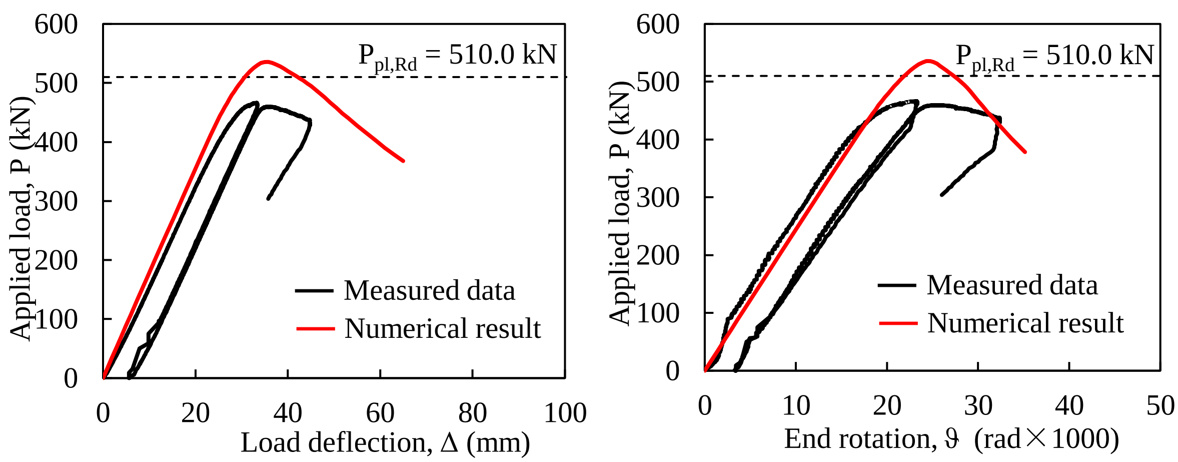

(f) Beam B6-LT0

Figure 6.36: Load deflection curves and load rotation curves of S690 fully restrained beams of Series LT0 (Continued)

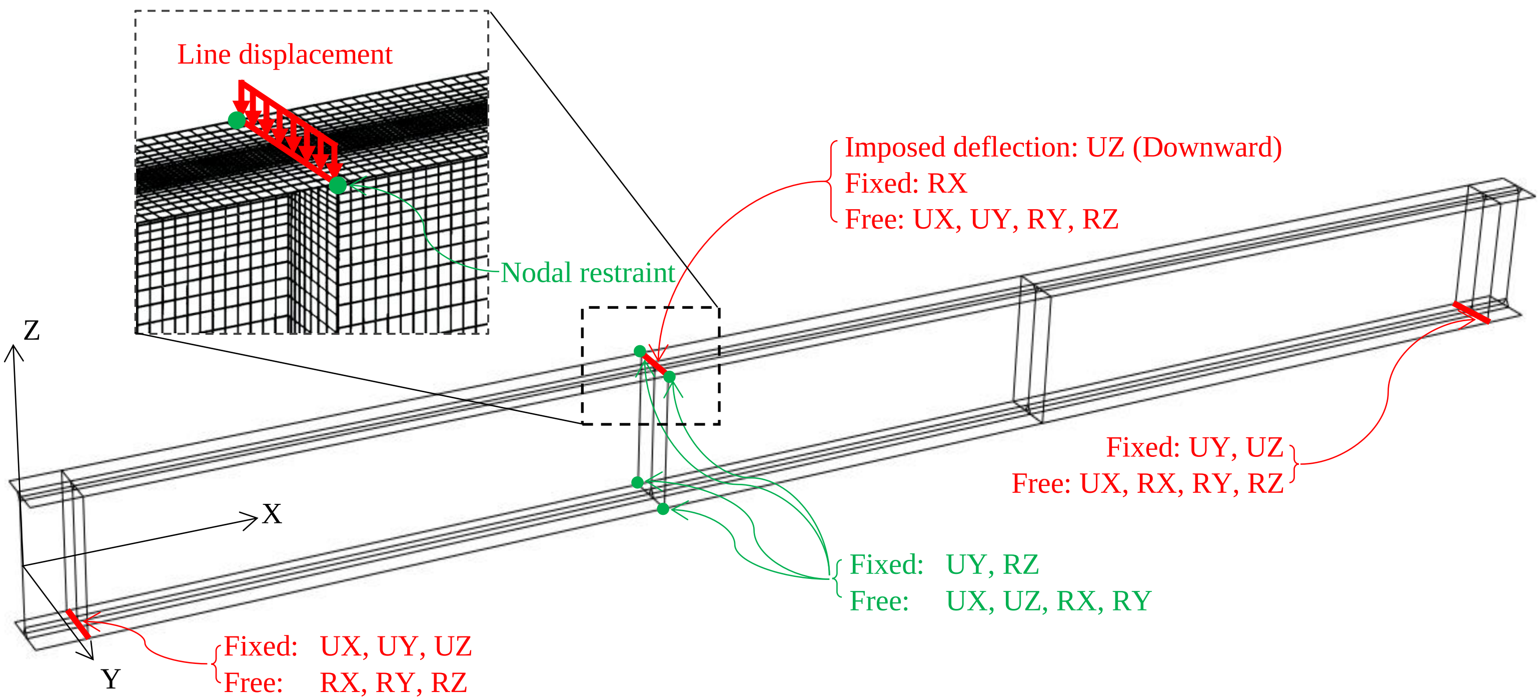

Figure 6.37: Boundary condition for partially restrained beams

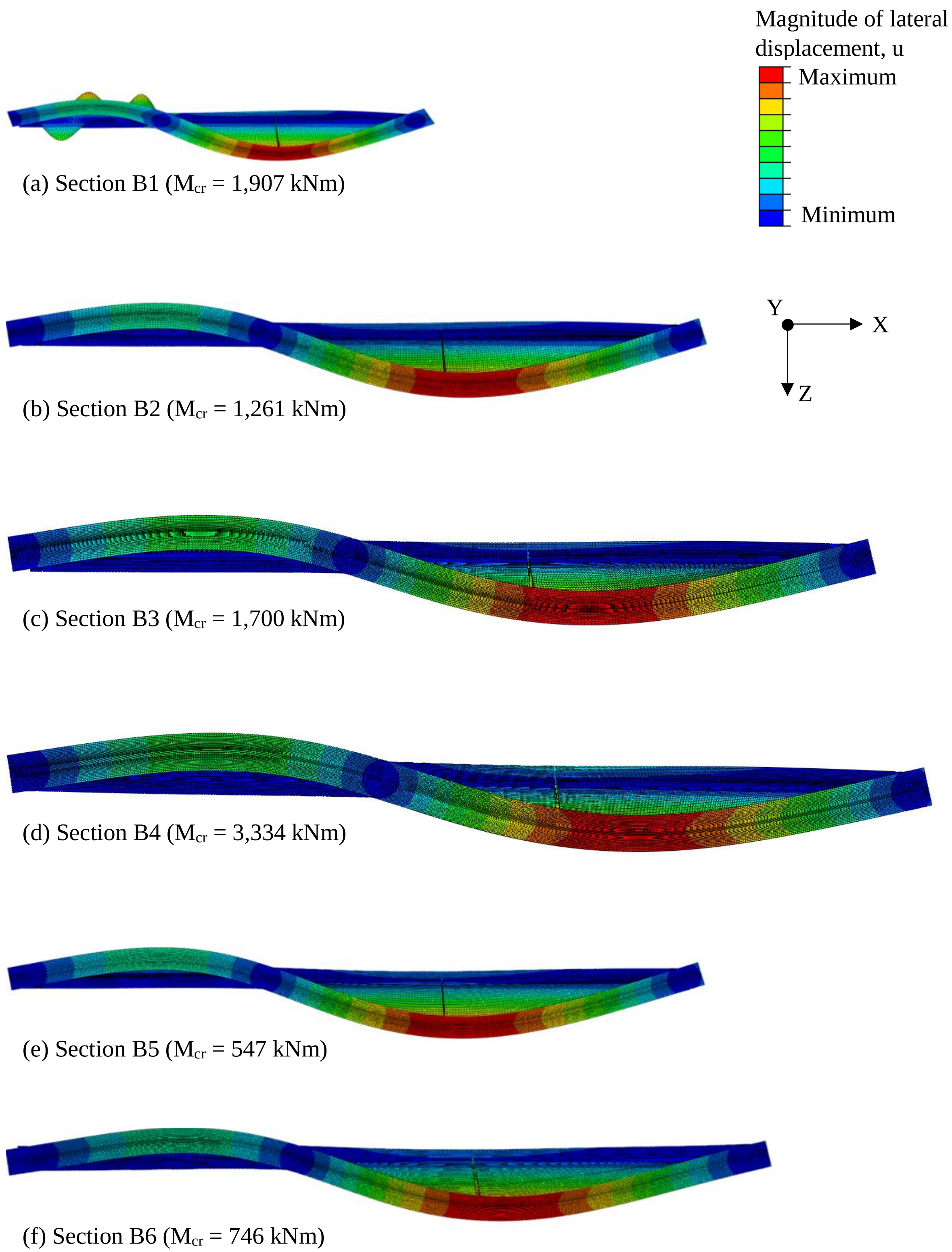

Figure 6.38 (a): Calculated eigen buckling mode of S690 partially restrained beams of Series LT1

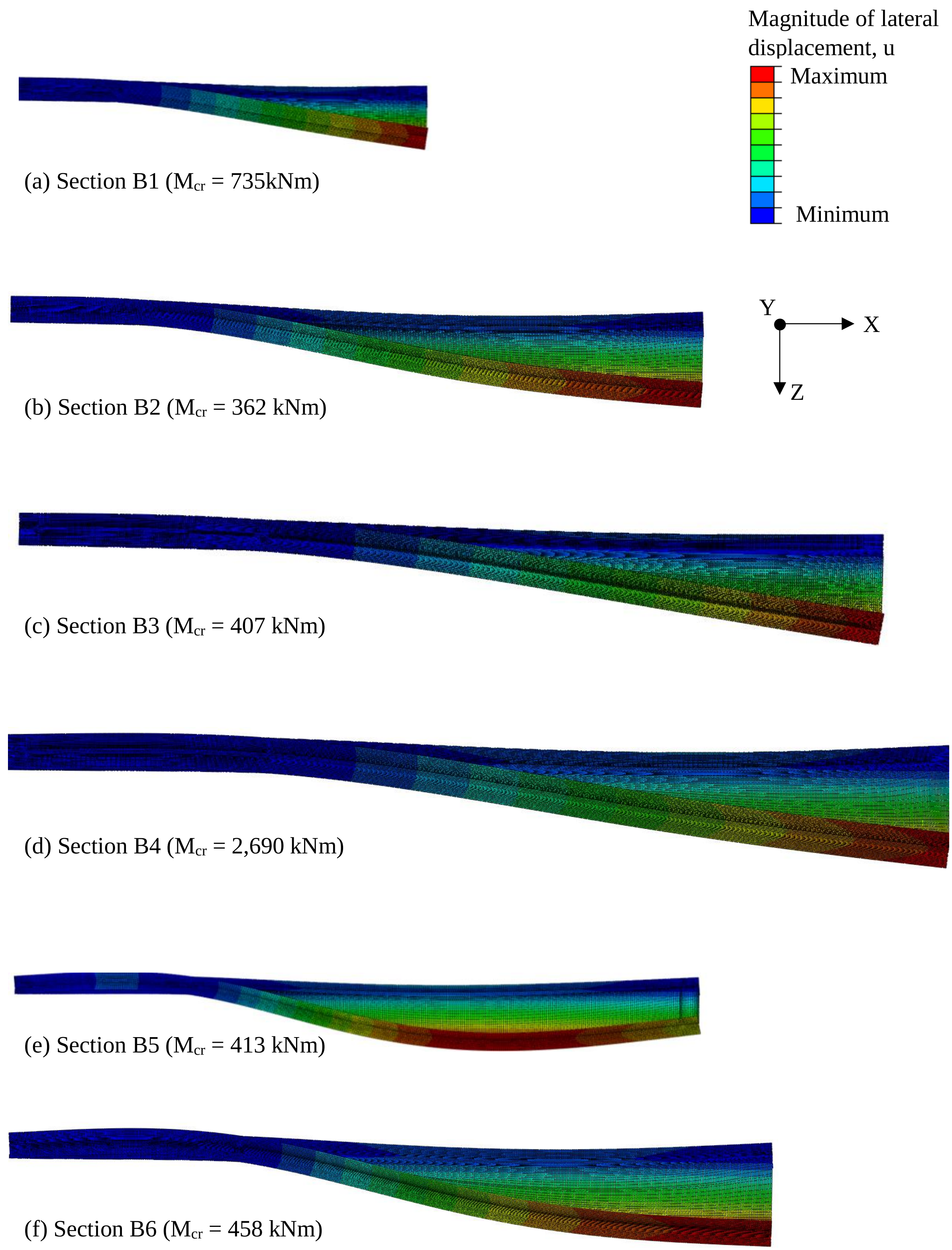

(a) Section B1 (M_{cr} = 735kNm)

(b) Section B2 (M_{cr} = 362 kNm)

(c) Section B3 (M_{cr} = 407 kNm)

(d) Section B4 (M_{cr} = 2,690 kNm)

(e) Section B5 (M_{cr} = 413 kNm)

(f) Section B6 (M_{cr} = 458 kNm)

Figure 6.38 (b): Calculated eigen buckling mode of S690 partially restrained beams of Series LT2

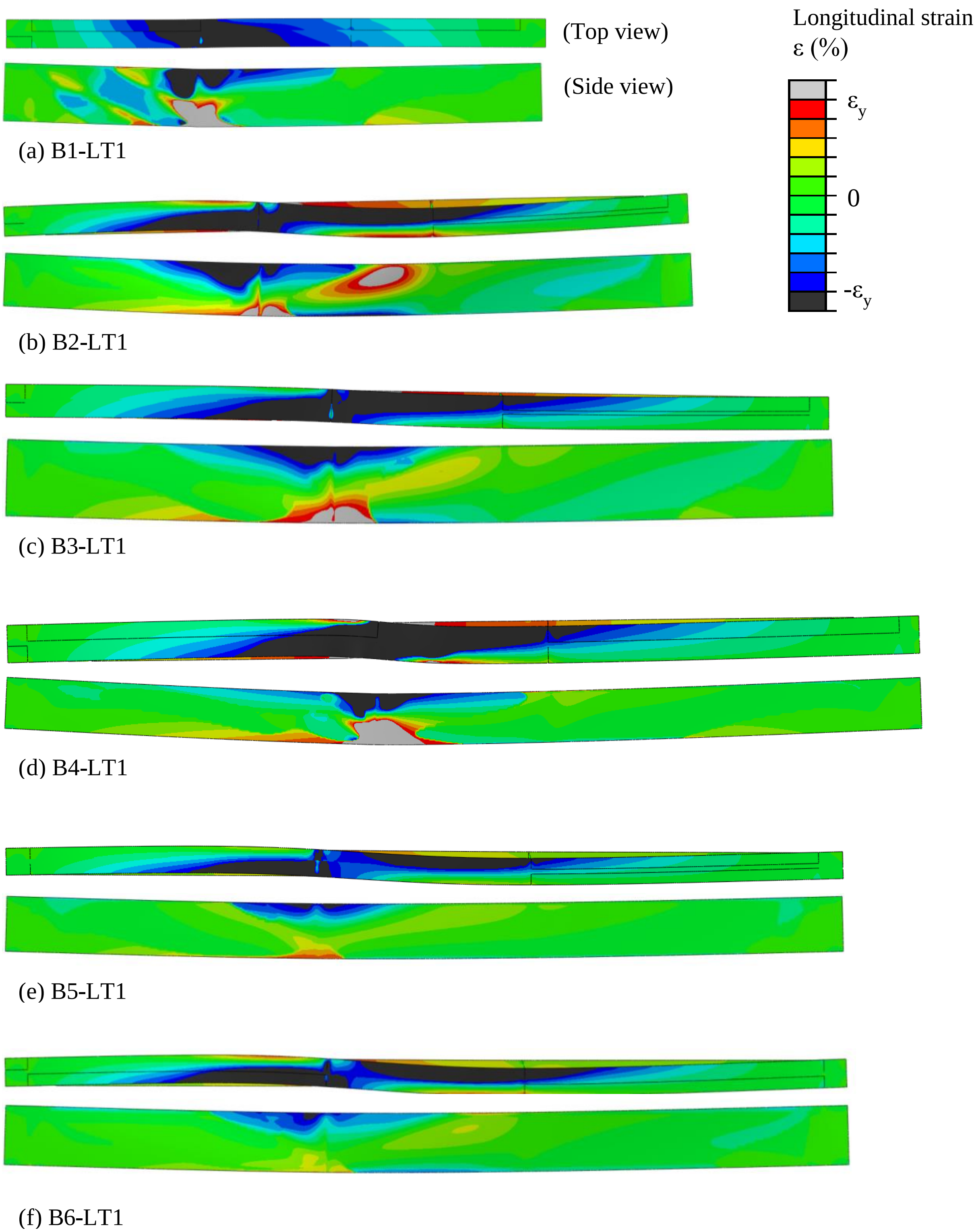

Figure 6.39: Failure modes and strain contour of S690 partially restrained beams at ULS (Series LT1)

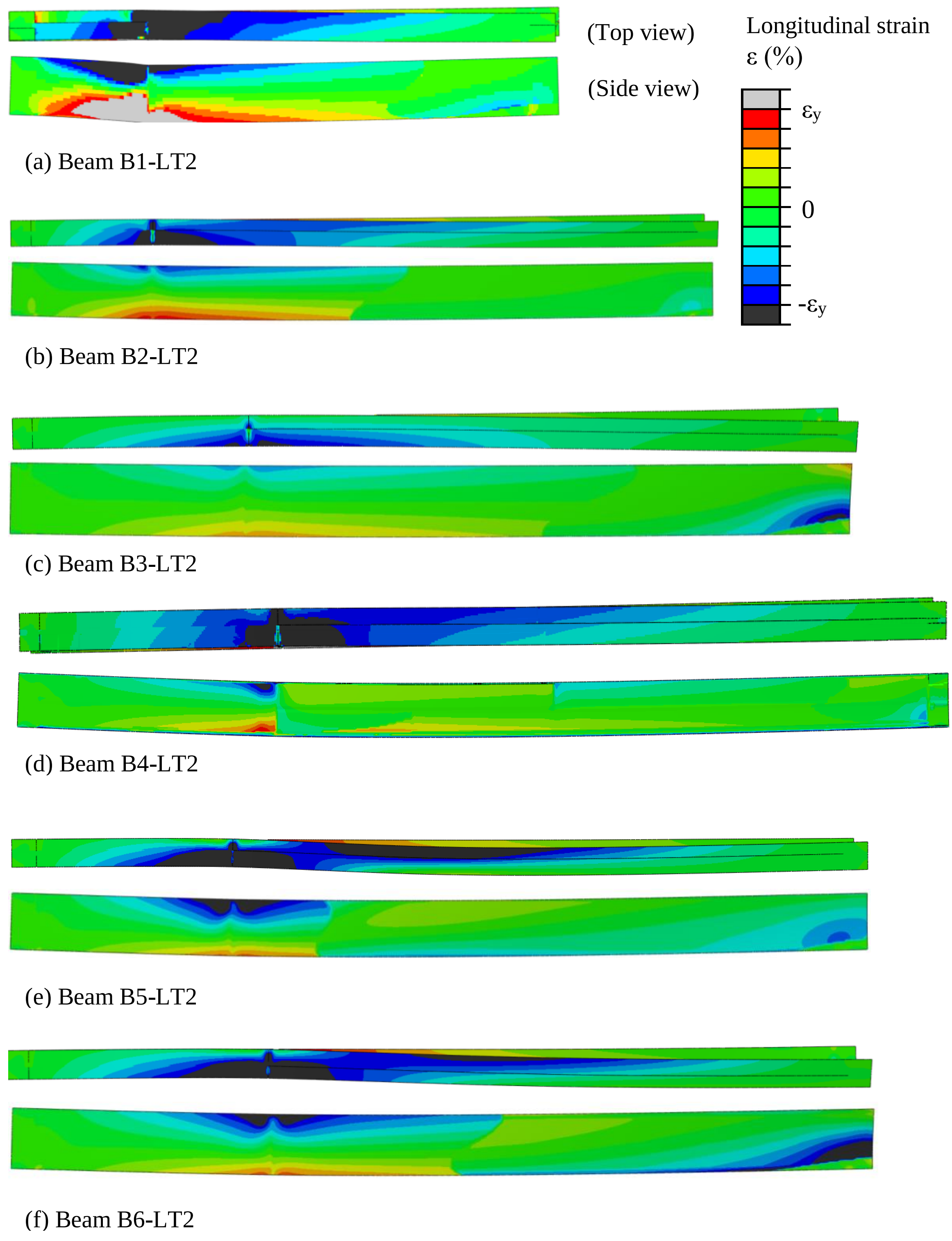

Figure 6.40: Failure modes and strain contour of S690 partially restrained beams at ULS (Series LT2)

(a) Observed local buckling in flange of Section B3 in Series LT1

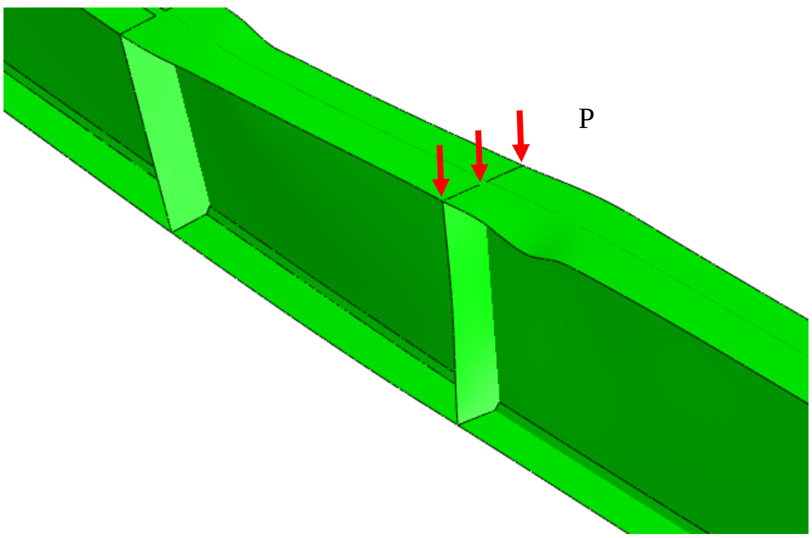

(b) Calculated local buckling in flange of Section B3 in Series LT1

Figure 6.41: Interaction of local and lateral torsional buckling in Section B3-LT1

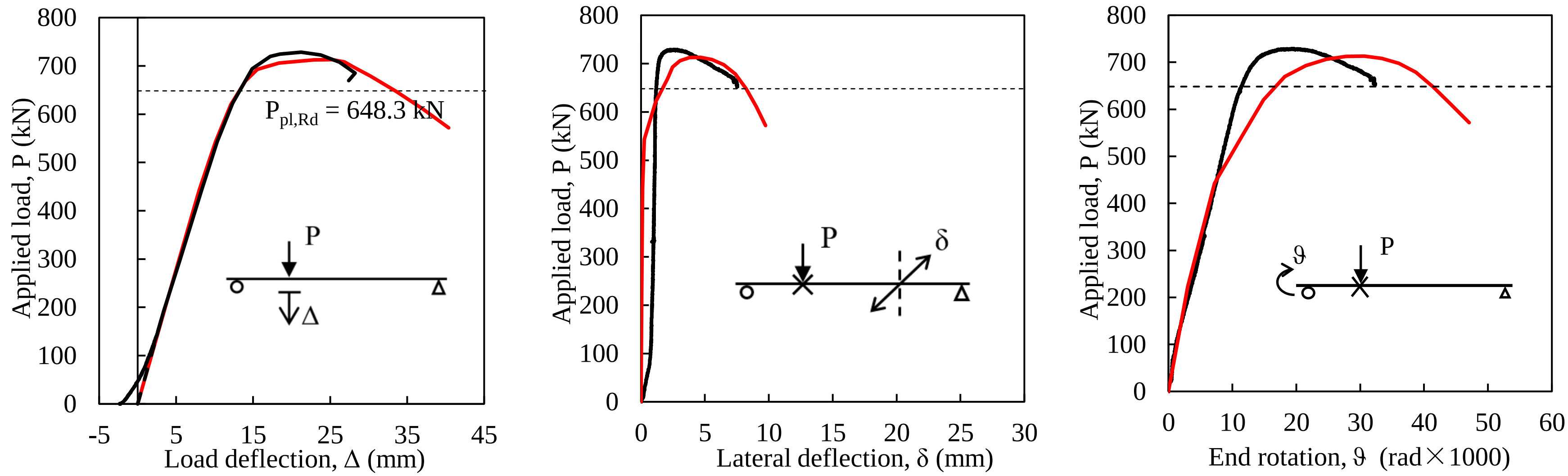

(a) Beam B1-LT1

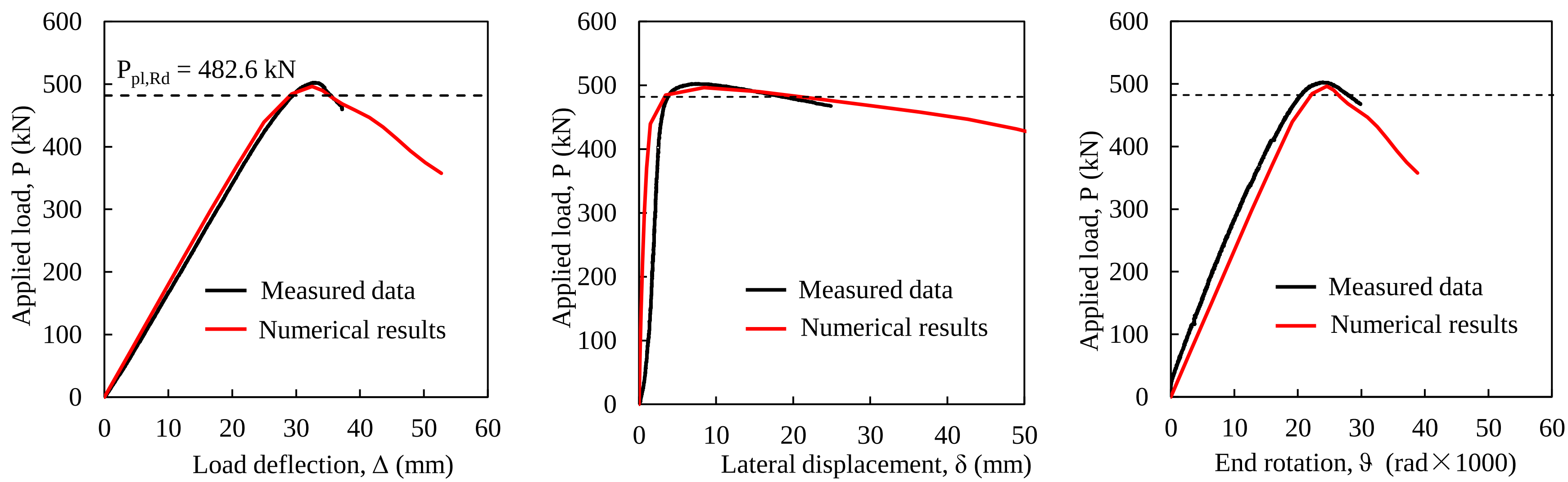

(b) Beam B2-LT1

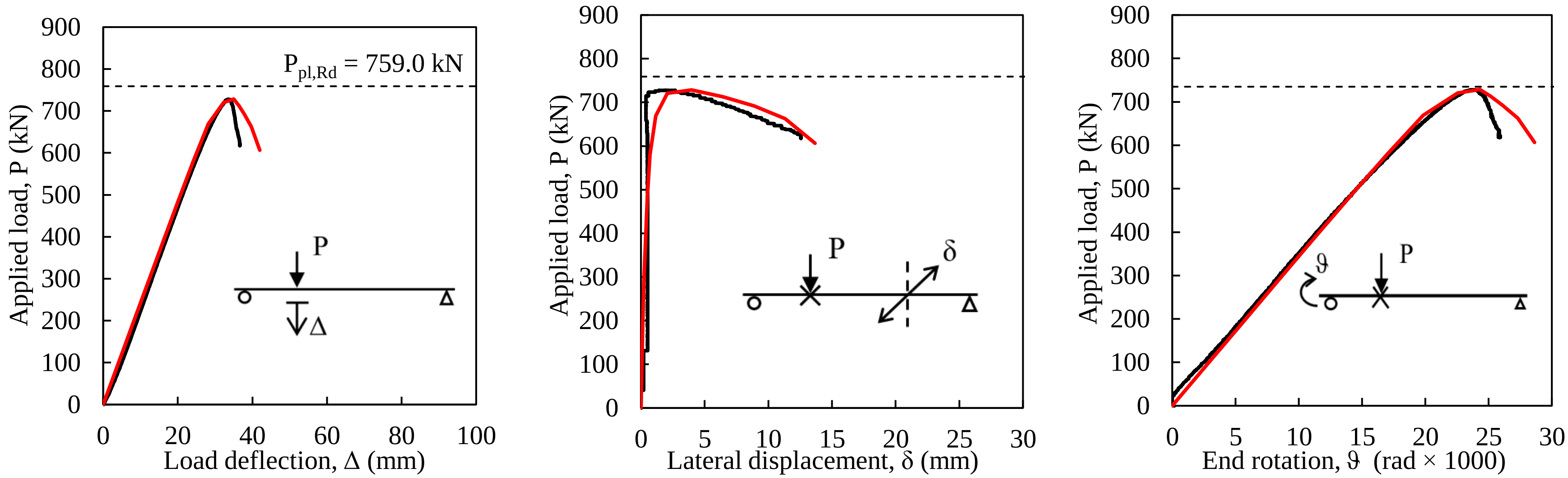

(c) Beam B3-LT1

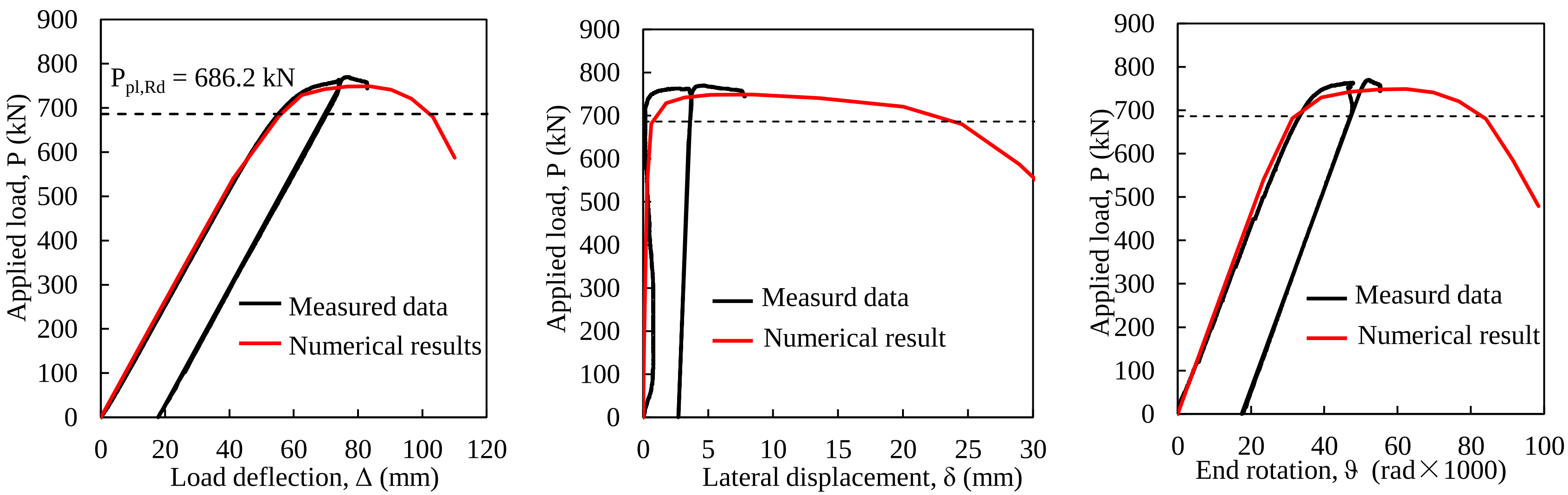

(d) Beam B4-LT1

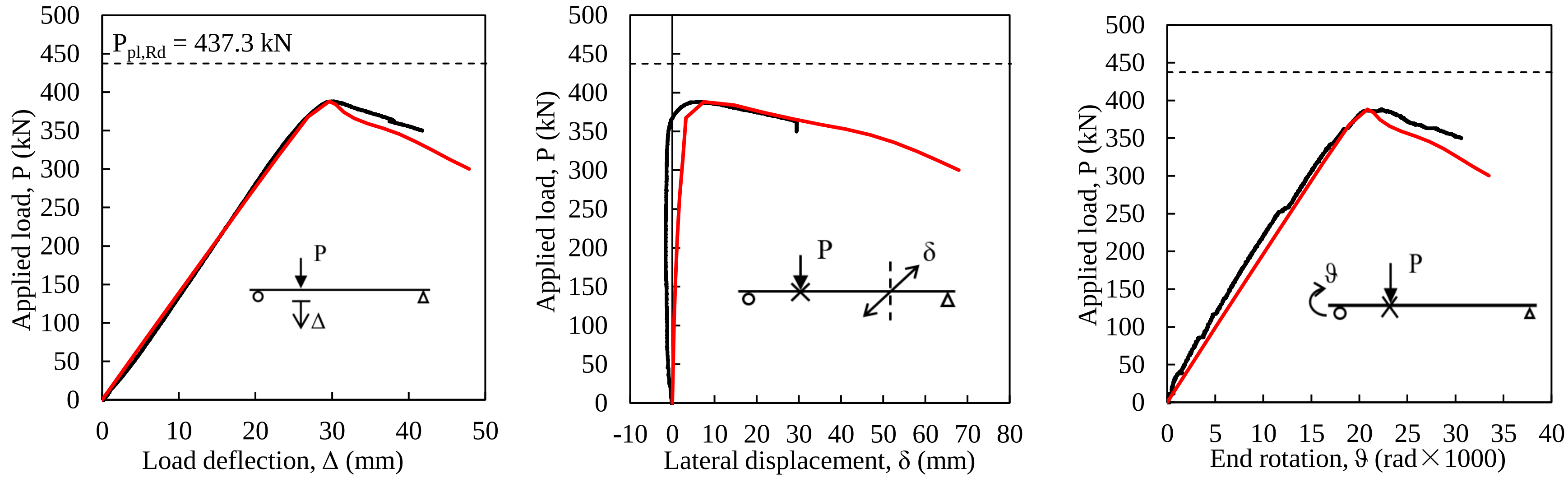

(e) Beam B5-LT1

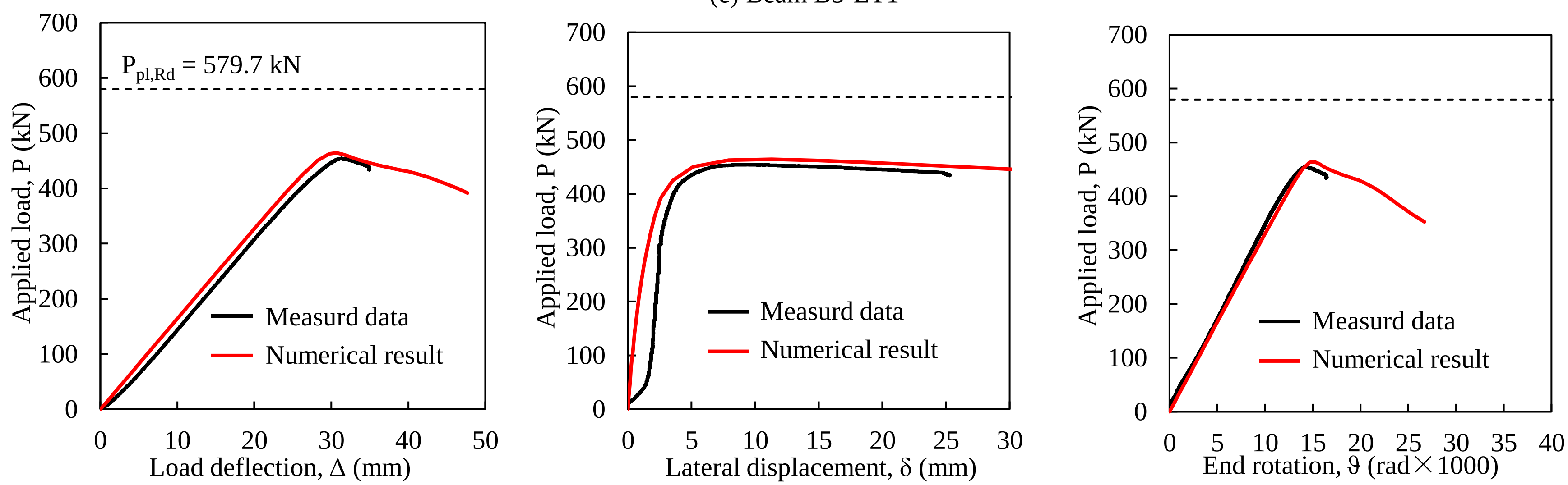

(f) Beam B6-LT1

Figure 6.42: Load deformation curves of beam sections of Series LT1

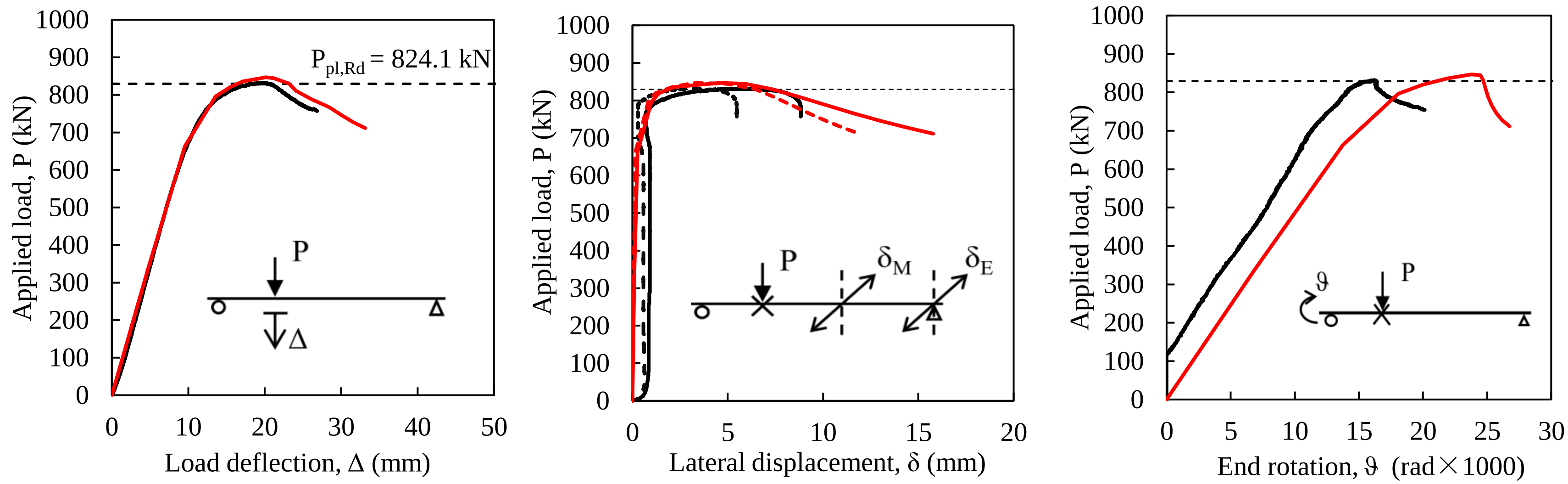

(a) Beam B1-LT2

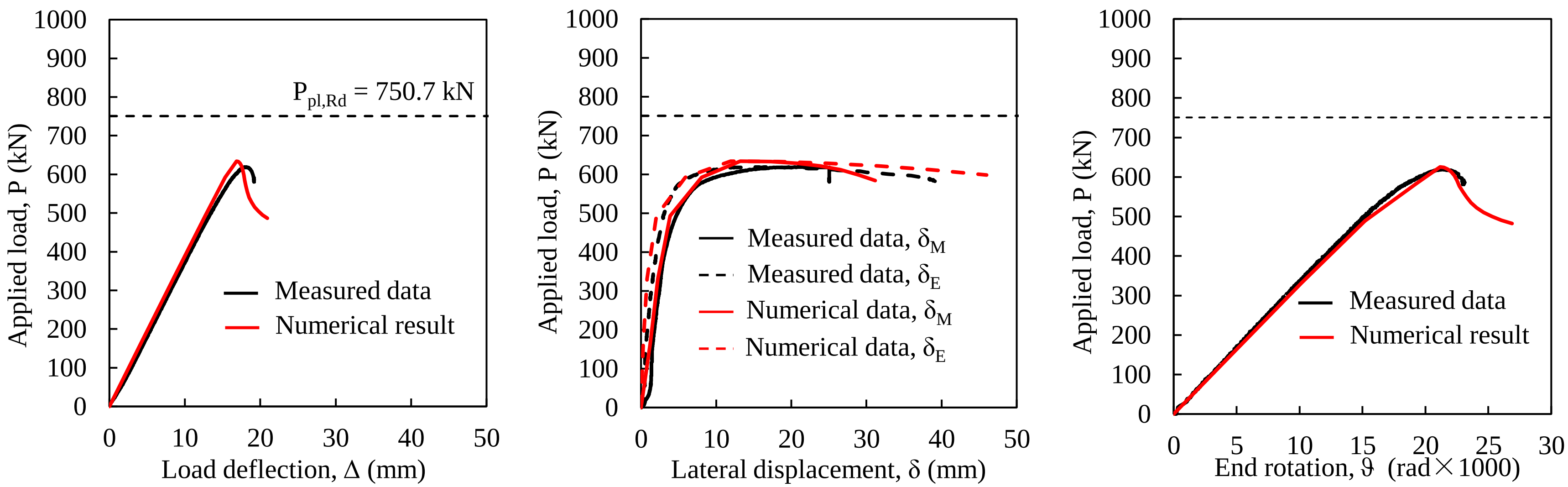

(b) Beam B2-LT2

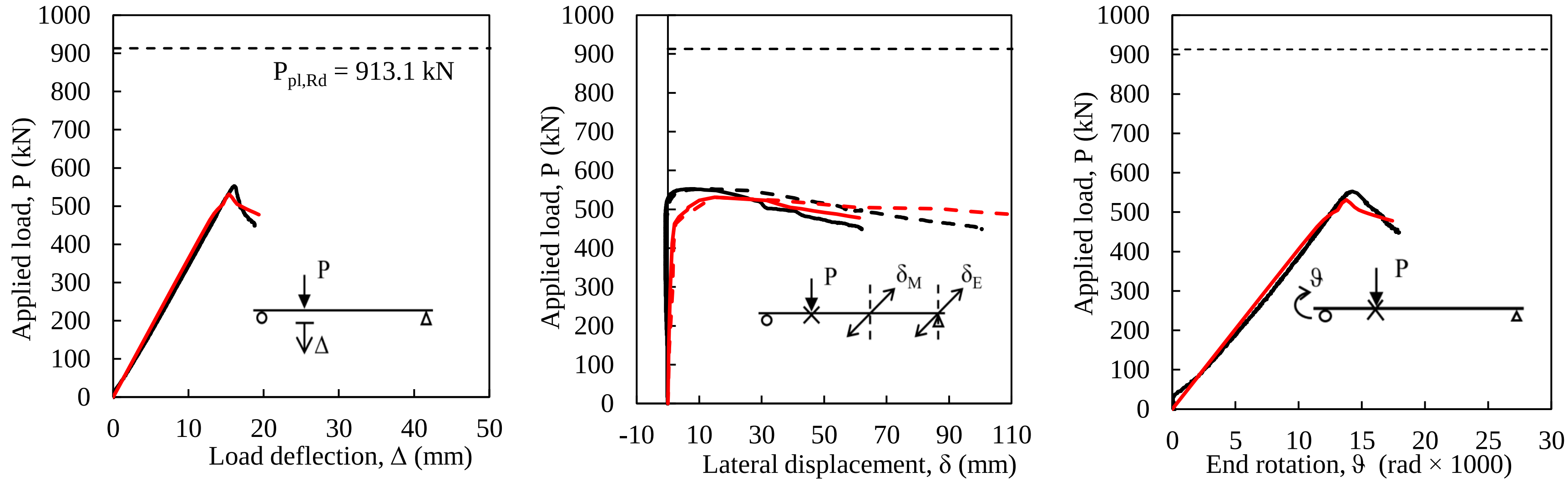

(c) Beam B3-LT2

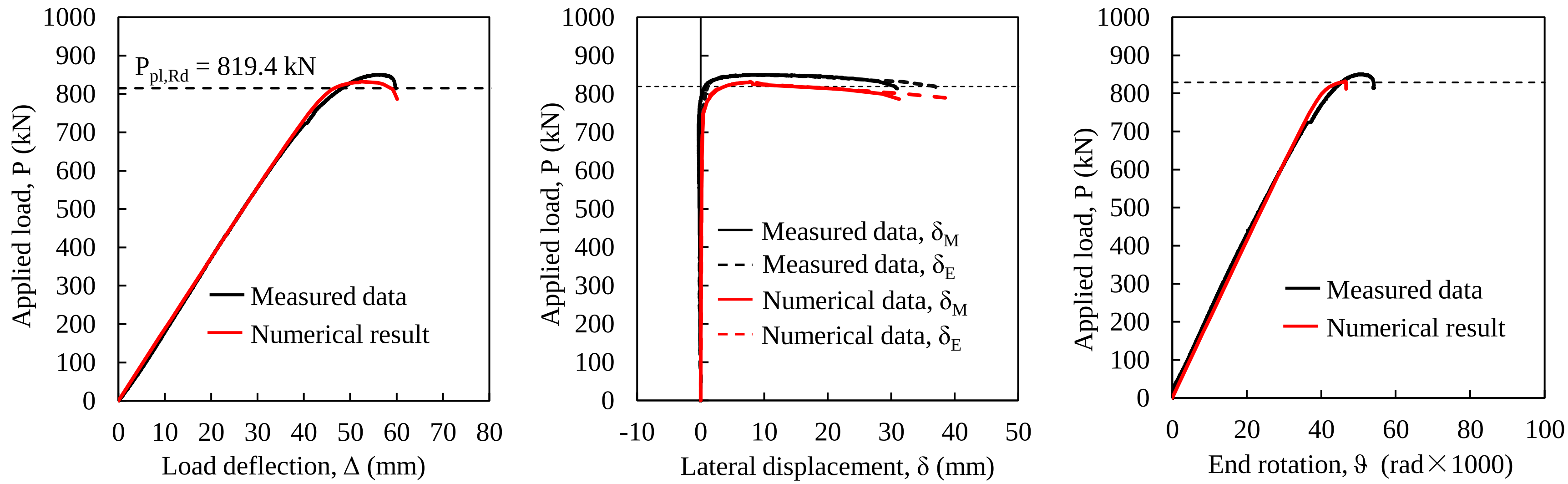

(d) Beam B4-LT2

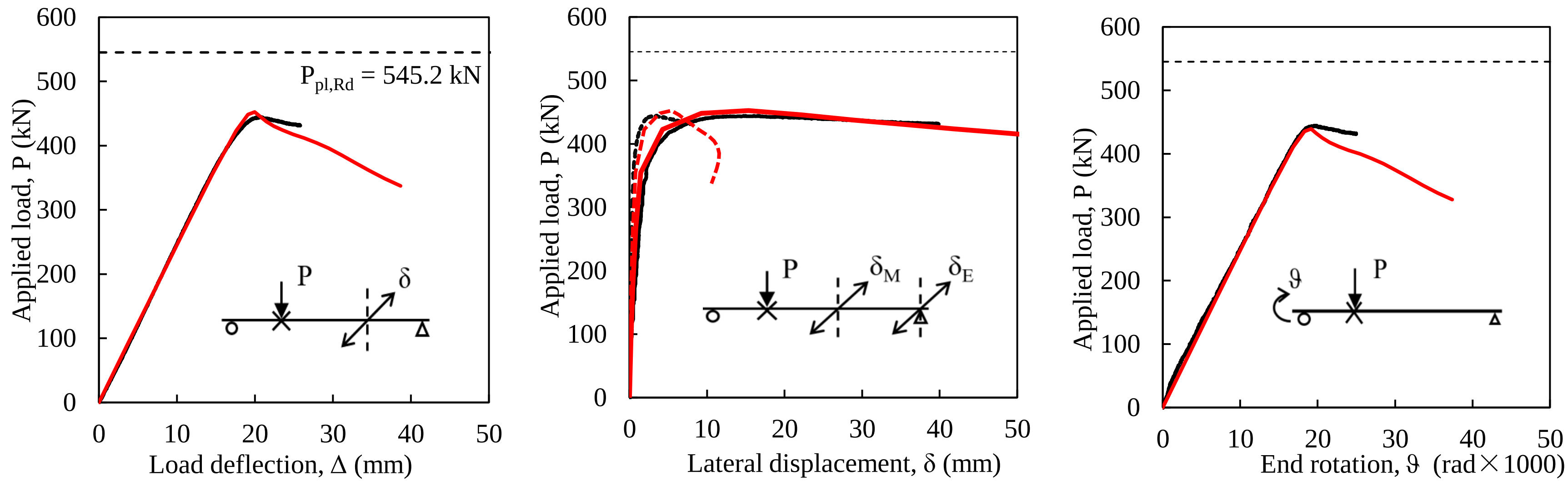

(e) Beam B5-LT2

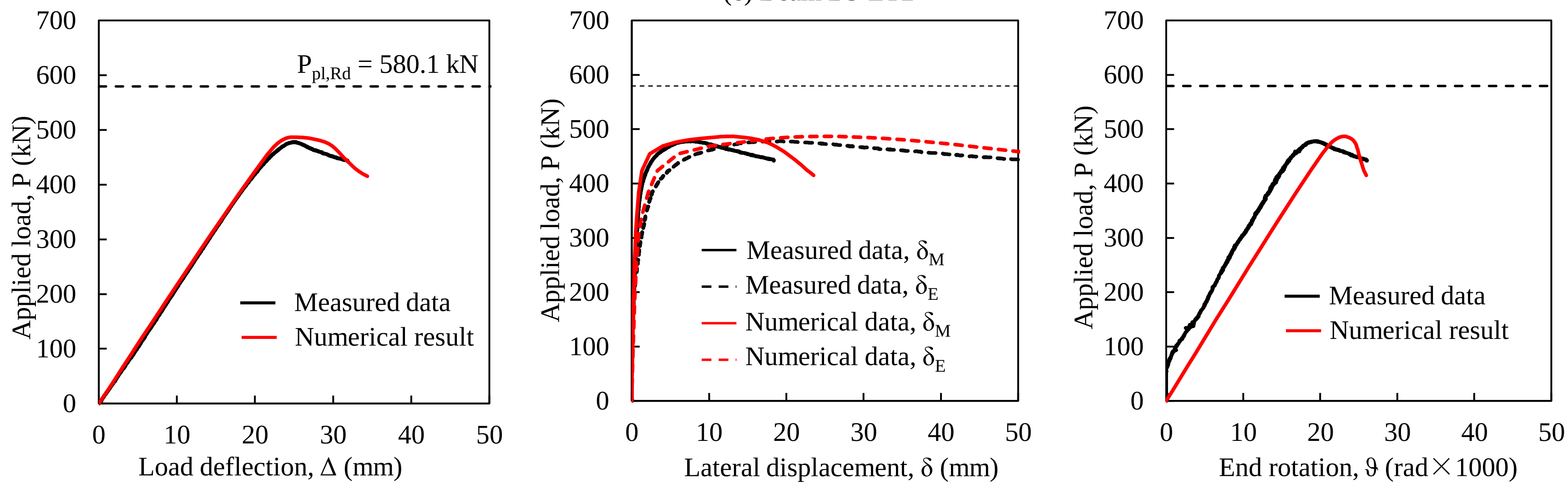

(f) Beam B6-LT2

Figure 6.43: Load deformation curves of beam sections of Series LT2

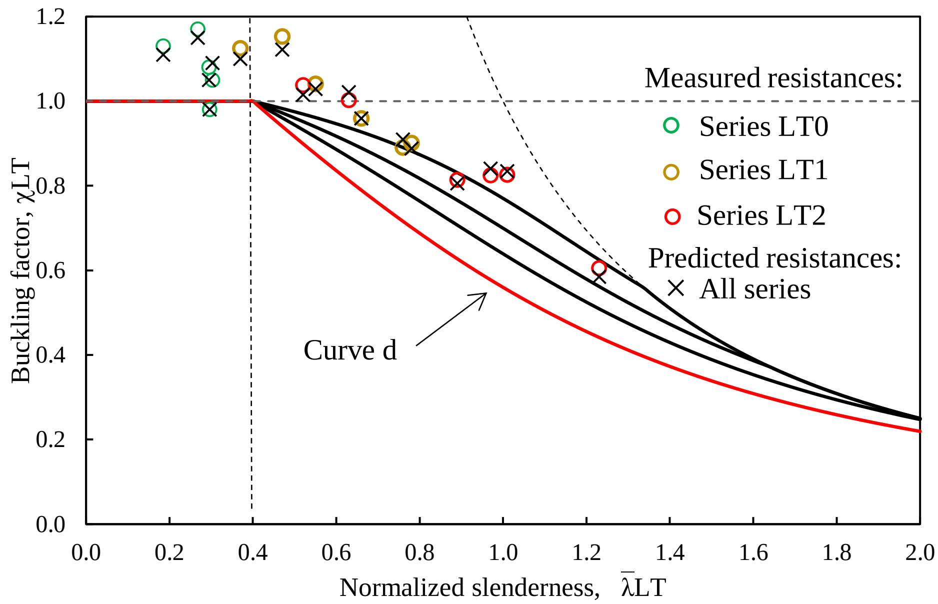

Figure 6.44: Comparison between measured and predicted resistances of S690 partially restrained beams

Table 6.1: Mechanical properties of measured high strength S690 steel plates

Steel materials		Yield strength f_y (N/mm^2)	Tensile strength f_u (N/mm^2)	Young's modulus E (kN/mm^2)	Strain corresponding to tensile strength ε_u (%)
Stocky columns under compression	**6 mm**	780	833	215	5.06
	10 mm	754	807	208	5.85
	16 mm	799	855	208	7.53
Stocky columns under combined compression and bending	**10 mm**	761	821	212	6.35
	16 mm	756	813	216	6.52
Slender columns under compression	**6 mm**	766	815	210	5.90
	10 mm	756	793	212	7.00
	16 mm	800	844	209	6.60
Fully and partially restrained beams	**6 mm#1**	723	850	207	6.31
	6 mm#2	720	843	211	6.41
	10 mm	784	874	206	7.42
	16 mm	745	832	216	6.62

Table 6.2(a): Summary of convergence studies on Section C1

	C1-M1	**C1-M2**	**C1-M3**	**C1-M4**
Cross-sectional mesh	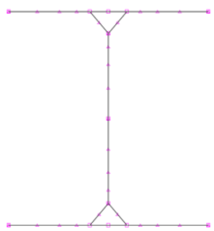	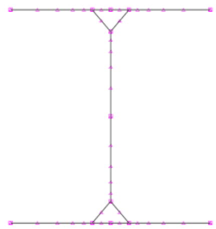	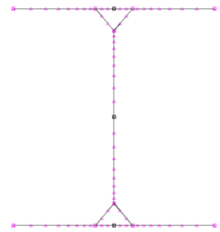	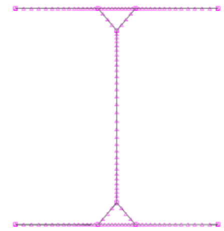
Mesh size (mm)	8 to 20 mm	5 to 15 mm	3 to 10 mm	2 to 5 mm
Longitudinal dimension (mm)	25 mm	20 mm	15 mm	8 mm
Predicted resistances (kN)	2,535	2,573	2,521	2,508
Discrepancy	1.2 %	2.7 %	0.6 %	0.1 %

Table 6.2(b): Summary of convergence studies on Section C3

	C3-M1	**C3-M2**	**C3-M3**	**C3-M4**
Cross-sectional mesh	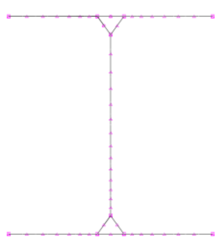	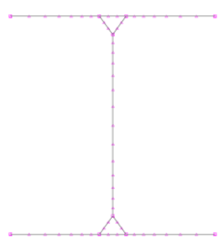	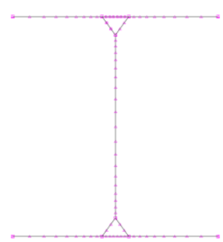	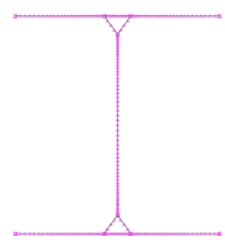
Mesh size (mm)	8 to 20 mm	5 to 15 mm	3 to 10 mm	2 to 5 mm
Longitudinal dimension (mm)	30 mm	25 mm	20 mm	15 mm
Predicted resistances (kN)	7,132	7,033	6,917	6,931
Discrepancy	0.9 %	-0.5 %	-2.1 %	-1.9 %

Table 6.3: Comparison between test and numerical results of S690 stocky columns under axial compression

Section	Section Classification	Section resistance				Resistance ratio	
		$N_{c,Rt}$ (kN)	$N_{c,FE}$ (kN)	Φ_{Rt}	$\Phi_{R,FE}$	$\frac{N_{c,Rt}}{N_{c,FE}}$	$\frac{\Phi_{Rt}}{\Phi_{R,FE}}$
C1S -a	Class 1	2,515	2,521	5.00	4.68	1.00	1.07
-b		2,495		3.74		0.99	0.80
-c		2,504		3.80		0.99	0.81
C2S -a	Class 3	2,998	3,039	--	1.51	0.99	--
-b		3,029		1.22		1.00	0.81
-c		2,994		1.46		0.99	0.97
C3S -a	Class 2	7,055	6,917	2.63	3.13	1.02	0.84
-b		7,084		2.86		1.02	0.91
-c		7,066		2.75		1.02	0.88
C4S -a	Class 3	8,384	8,377	0.76	1.25	1.00	0.61
-b		8,328		0.85		0.99	0.68
-c		8,392		0.97		1.00	0.78
Average, μ						1.00	0.83
Standard deviation, σ						0.01	0.12

Table 6.4: Comparison between test and numerical results of S690 stocky columns under combined compression and bending

Section	Section Classification	Section resistance			Resistance ratio		
		$N_{c,Rt}$ (kNm)	$N_{c,FE}$ (kNm)	$\frac{N_{c,Rt}}{N_{c,FE}}$	$N_{pl,Rd}^{*}$ (kNm)	$\frac{N_{c,Rt}}{N_{pl,Rd}}$	$\frac{N_{c,FE}}{N_{pl,Rd}}$
C3SY-d	Class 2	4,747	4,735	1.00	4,404	1.08	1.08
-e		3,690	3,684	1.00	3,400	1.09	1.08
C4SY-d	Class 3	6,222	6,175	1.01	5,849	1.06	1.06
-e		4,657	4,711	0.99	4,558	1.02	1.03
C3SZ-f	Class 2	5,948	5951	1.00	5,256	1.13	1.13
-g		3,770	3,627	1.04	3,290	1.15	1.10
C4SZ-f	Class 3	7,030	6,986	1.01	6,642	1.06	1.05
-g		4,897	4,767	1.03	4,678	1.05	1.02
Average, μ				1.01			
Standard deviation, σ				0.01			

Note: Although Section C4 is a class 3 section, plastic design resistances are listed as significant strength enhancement was observed in numerical and test results.

Table 6.5: Test programme of S690 slender columns

Section	Nominal dimensions						Section properties		
	L_s (mm)	L_{eff} (mm)	b (mm)	t_f (mm)	h (mm)	t_w (mm)	A (mm^2)	$\bar{\lambda}_z$ (--)	Section classification
C1M	1,610	1,990	120	10	140	6	3,120	1.26	Class 1
C2M	1,610	1,990	150	10	170	6	3,900	1.01	Class 3
C3M	1,610	1,990	200	16	232	10	8,400	0.77	Class 2
C4M	1,610	1,990	250	16	282	10	10,500	0.62	Class 3
C2L	2,410	2,790	150	10	170	6	3,900	1.41	Class 3
C3L	2,410	2,790	200	16	232	10	8,400	1.09	Class 2
C4L	2,410	2,790	250	16	282	10	10,500	0.87	Class 3

Table 6.6: Comparison between measured and predicted resistances of slender columns

Section	Section properties				Section resistances			
	L_{eff} (mm)	$\bar{\lambda}_z$ (--)	A (mm^2)	N_y (kN)	$N_{b,FE}$ (kN)	$N_{b,Rt}$ (kN)	$N_{b,Rd}$ (kN)	$\frac{N_{b,Rt}}{N_{b,FE}}$
C1M	1,990	1.26	3,120	2,366	1,283	1,284	946	1.00
C2M	1,990	1.01	3,900	2,957	2,340	2,714	1,232	1.16
C3M	1,990	0.77	8,400	6,632	5,687	5,924	4,510	1.04
C4M	1,990	0.62	10,500	8,290	7,222	7,739	6,383	1.07
C2L	2,790	1.41	3,900	2,957	1,468	1,510	1,279	1.02
C3L	2,790	1.09	8,400	6,632	4,571	4,605	3,250	1.01
C4L	2,790	0.87	10,500	8,290	6,852	7,284	5,140	1.06

Table 6.7(a): Summary of convergence studies on Section B1-LT0

	B1-M1	**B1-M2**	**B1-M3**	**B1-M4**
Cross-sectinoal mesh	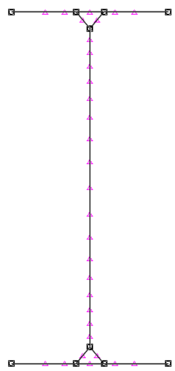	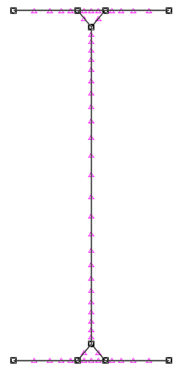	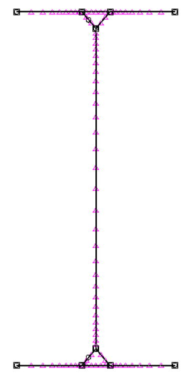	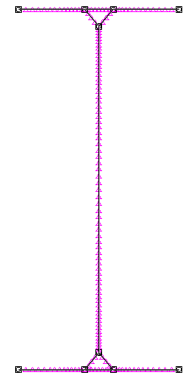
Mesh size (mm)	8 to 20 mm	5 to 15 mm	3 to 10 mm	2 to 5 mm
Longitudinal dimension (mm)	20 mm	15 mm	10 mm	5 mm
Predicted resistances (kN)	738.6	732.6	721.5	717.9
Discrepancy	1.7%	0.8%	-0.7%	-1.2%

Table 6.7(b): Summary of convergence studies on Section B3-LT0

	B3-M1	**B3-M2**	**B3-M3**	**B3-M4**
Cross-sectinoal mesh	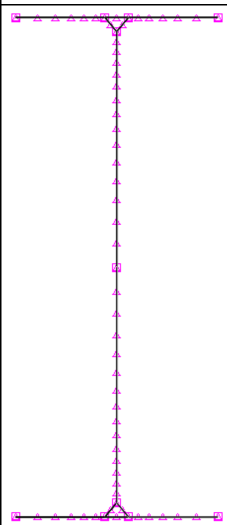	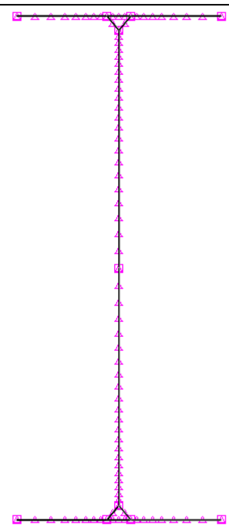	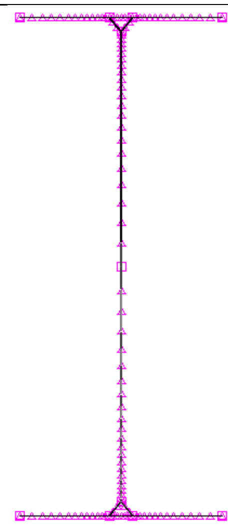	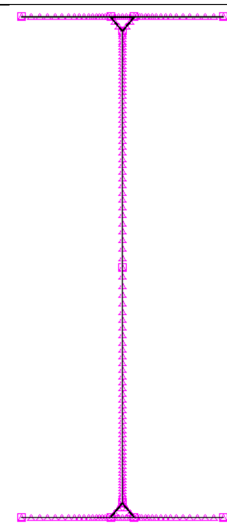
Mesh size (mm)	8 to 20 mm	5 to 15 mm	3 to 10 mm	2 to 5 mm
Longitudinal dimension (mm)	20 mm	15 mm	10 mm	5 mm
Predicted resistances (kN)	700.5	715.7	746.5	739.2
Discrepancy	-6.2%	-4.2%	0.0%	-1.0%

Table 6.8: Comparison between test measurements and numerical results from Series LT0

Section	Section classification	Moment resistance			Rotational capacity		
		Measured resistance M_{Rt} (kNm)	Predicted resistance $M_{R,FE}$ (kNm)	Ratio $\frac{M_{Rt}}{M_{R,FE}}$	Measured value Φ_{Rt} (--)	Predicted value $\Phi_{R,FE}$ (--)	Ratio $\frac{\Phi_{Rt}}{\Phi_{R,FE}}$
B1	Class 1	318.7	316.5	1.01	2.36	3.25	0.73
B2	Class 2	398.2	401.4	1.01	0.67	0.71	0.94
B3	Class 3	728.8	728.3	1.00	N.A.	N.A.	N.A.
B4	Class 2	843.3	832.6	1.01	1.02	0.97	1.05
B5	Class 2	347.9	346.5	1.00	0.99	0.91	1.09
B6	Class 2	393.0*	451.9	0.87	N.A.*	0.28	N.A.

*** Note:** Owing to unexpected failure of restraining system, values shown in gray color did not reflected resistances or rotational capacity with a correct failure mode.

Table 6.9: Comparison between test measurements and numerical results from Series LT0

Section	Section classification	Moment resistance			Compressive strain on top flanges		
		Predicted resistance $M_{R,FE}$ (kNm)	Design resistance $M_{pl,Rd}$ (kNm)	Ratio $\frac{M_{R,FE}}{M_{pl,Rd}}$	Predicted strain $\varepsilon_{tf,FE}$ (%)	Yielding strain ε_y (%)	Ratio $\frac{\varepsilon_{tf,FE}}{\varepsilon_y}$
B1	Class 1	316.5	284.4	1.11	-4.65	-0.38	12.2
B2	Class 2	401.4	368.5	1.09	-3.22	-0.38	8.5
B3	Class 3	728.3	740.5	0.98	-1.38	-0.38	3.6
B4	Class 2	832.6	721.1	1.15	-4.16	-0.38	10.9
B5	Class 2	346.5	328.9	1.05	-2.64	-0.38	6.9
B6	Class 2	451.9	430.9	1.05	-3.03	-0.38	8.0

Table 6.10: Comparison between moment resistances of S690 partially restrained beams

Section	Series LT1			Series LT2		
	Measured resistance $M_{LT,Rt}$ (kNm)	Predicted resistance $M_{LT,FE}$ (kNm)	Ratio $\frac{M_{LT,Rt}}{M_{LT,FE}}$	Measured resistance $M_{LT,Rt}$ (kNm)	Predicted resistance $M_{LT,FE}$ (kNm)	Ratio $\frac{M_{LT,Rt}}{M_{LT,FE}}$
B1	319.8	312.7	1.02	282.8	288.1	0.98
B2	383.5	379.0	1.01	303.8	307.0	0.99
B3	710.0	710.1	1.00	444.8	430.0	1.03
B4	831.4	808.7	1.03	748.4	731.9	1.02
B5	296.4	292.1	1.01	268.9	266.2	1.01
B6	383.5	391.8	0.98	355.4	362.0	0.98

Table 6.11(a): Comparison between deformation characteristics of partially restrained beams – Series LT1

Section	Deflection at maximum load			Lateral displacement at maximum load			Minor-axis curvature of top-tee sections at maximum load		
	Measured data $\Delta_{u,t}$ (mm)	Numerical data $\Delta_{u,FE}$ (mm)	Ratio $\frac{\Delta_{u,t}}{\Delta_{u,FE}}$	Measured data $\delta_{u,t}$ (mm)	Predicted data $\delta_{u,FE}$ (mm)	Ratio $\frac{\delta_{u,t}}{\delta_{u,FE}}$	Measured data $\phi_{mz,t}$ ($10^{-3}mm^{-1}$)	Predicted data $\phi_{mz,FE}$ ($10^{-3}mm^{-1}$)	Ratio $\frac{\phi_{mz,t}}{\phi_{mz,FE}}$
B1	23.7	26.2	0.90	2.6	2.9	0.90	5.4	6.7	0.81
B2	32.9	33.0	1.00	7.5	8.6	0.87	22.5	27.5	0.82
B3	33.4	35.0	0.95	1.9	3.1	0.61	26.0	24.3	1.07
B4	77.0	83.7	0.92	4.4	4.0	1.10	3.2	2.8	1.14
B5	29.9	30.3	0.99	6.7	7.9	0.85	31.6	27.6	1.14
B6	33.3	31.4	1.06	9.4	9.6	0.98	39.7	32.5	1.22

Table 6.11(b): Comparison between deformation characteristics of partially restrained beams – Series LT2

Section	Deflection at maximum load			Lateral displacement at maximum load			Minor-axis curvature of top-tee sections at maximum load		
	Measured data $\Delta_{u,t}$ (mm)	Numerical data $\Delta_{u,FE}$ (mm)	Ratio $\frac{\Delta_{u,t}}{\Delta_{u,FE}}$	Measured data (1) $\delta_{u,t}$ (mm)	Predicted data $\delta_{u,FE}$ (mm)	Ratio $\frac{\delta_{u,t}}{\delta_{u,FE}}$	Measured data $\phi_{mz,t}$ ($10^{-3}mm^{-1}$)	Predicted data $\phi_{mz,FE}$ ($10^{-3}mm^{-1}$)	Ratio $\frac{\phi_{mz,t}}{\phi_{mz,FE}}$
B1	20.4	21.1	0.97	M: 6.7	M: 4.9	1.37	13.9	15.3	0.91
B2	17.9	17.5	1.02	E: 19.6	E: 20.7	0.95	4.1	3.56	1.16
B3	16.1	14.6	1.10	E: 12.0	E: 20.6	0.58	3.3	2.77	1.18
B4	56.3	51.1	1.10	E: 10.2	E: 8.9	1.15	7.1	7.25	0.97
B5	20.6	20.0	1.03	M: 15.0	M: 15.3	0.98	43.5	55.2	0.79
B6	24.8	24.6	1.01	E: 17.6	E: 21.6	0.81	N.A. (2)	8.21	N.A.

Note:

(1): "E" represents displacement measured at section end which is larger than "M";
"M" represents displacement measured at middle of span which is larger than "E".

(2): Data was not available owing to stain gauges detached from beam specimen during the test.

CHAPTER SEVEN
PARAMETRIC STUDIES: STRUCTURAL INSTABILITY OF S690 WELDED H- AND I-SECTIONS

7.0 Introduction

In this chapter, an extensive numerical investigation into the structural behaviour of columns and beams of S690 welded H-and I-sections using advanced double Y-shaped finite element model is carried out and reported. Plate thicknesses ranging from 6 mm to 40 mm are incorporated into this study to cover a wide range of cross-sectional dimensions of the welded sections. This parametric study is composed of the following four tasks:

- Task 1: Stocky columns of S690 welded H-sections under compression

A verified numerical model is used to investigate into structural behaviour of stocky columns of S690 welded H-sections under compression. Effects of welding procedures onto residual stress patterns are discussed according to numerical results of Sections C1S to C8S which are studied in Chapter 5. Moreover, in order to determine values of limiting slenderness ratios of the plates which ensure mobilization of full section resistances, a parametric study on 40 different cross-sections is carried out. The relationship between strength enhancement and section compactness is also studied.

- Task 2: Slender columns of S690 welded H-sections under compression

The numerical model adopted in Task 1 is also used to investigate into structural behaviour of slender columns of S690 welded H-sections under compression with practical member slendernesses ranging from 0.20 to 2.00. Structural behaviour of slender columns buckling about both major axis and minor axis with Sections C1 to C8 is investigated into. And buckling resistances of 176 welded H-sections are predicted and compared with design values in EN 1993-1-1. Moreover, effects of plate thicknesses and welding procedures are examined in this numerical study. Comparison with column buckling curves given in EN

1993-1-1 leads to selection of appropriate buckling curves in existing design rules in order to achieve improved structural efficiency.

- Task 3: Restrained beams of S690 welded I-sections

In order to find out criteria on plate slendernesses in restrained beams of S690 welded I-sections, a parametric study on 51 different sections is carried out. Full restraints are introduced to the models as stipulated in EN 1993-1-1. Four different combinations of plate thicknesses and simplified residual stress patterns calibrated by Liu (2017) are incorporated into this study. Through a comparison between predicted data and current section classification rules given in EN 1993-1-1, discrepancies between these values are found out. Moreover, a more efficient design method is proposed to improve safe utilization of moment resistances.

- Task 4: Partially restrained beams of S690 welded I-sections

A parametric study onto lateral torsional buckling of partially restrained beams of S690 welded I-sections is carried out. A total of 176 sections were incorporated into this study which adopts four different combinations of plate thicknesses and eight different cross-sections. A practical range of lateral torsional slenderness ratios from 0.40 to 2.00 is introduced in this study. Effects of residual stresses onto lateral torsional buckling resistances are also examined. Based on these numerical results, a new lateral torsional buckling curve is proposed for design of partially restrained beams of S690 welded I-sections.

Both section resistances and deformation characteristics of columns and beams of high strength S690 welded sections are examined. Bilinear stress-strain curves of S690 steel materials given in Figure 7.1 is employed in the parametric studies. Effects of residual stresses are also highlighted. Detailed comparisons on the numerical results obtained from these four tasks with those of the current design rules are conducted. In order to achieve efficient use of these S690 welded sections, new design rules are proposed.

7.1 Objectives

Parametric studies are carried out to investigate the effects of various geometries of steel sections, welding parameters and boundary conditions onto structural behaviour of high strength steel S690 welded sections. Specifically, the following characteristics of S690 welded sections are incorporated, and they are examined through the following numerical studies:

- Five different plate thicknesses of 6, 10, 16, 25 and 40 mm;
- Residual stress patterns induced by high-energy and low-energy welding procedures;
- Class 1 to Class 4 cross-sections based on EN 1993-1-1;
- Member slendernesses up to 2.00; and,
- Strain hardening of S690 steel materials and strength enhancement of steel sections.

In order to quantify improvement on structural behaviour of S690 welded sections over those of conventional S355 welded sections, modification on the following design rules in EN 1993-1-1 are provided:

- To revise criteria of plate slendernesses for Class 3 and 4 sections;
- To quantify strength enhancement in plastic cross-sections, i.e. Class 1 sections;
- To select an appropriate buckling curve for slender columns of S690 welded H-sections; and,
- To select an appropriate buckling curve for partially restrained beams of S690 welded I-sections.

7.2 Parametric Study on Stocky Columns of S690 Welded H-Sections

In this parametric study on stocky columns of S690 welded H-sections, two essential factors are covered as:

- Welding procedures which are adopted in fabrication of S690 welded H-sections; and,
- Plate slendernesses of flange and web plates in S690 welded H-sections.

In this study, structural behaviour of H-sections welded using high and low heat input energy welding procedures are examined. Different structural behaviour of welded H-sections with different residual stress magnitudes are observed. It is also noted that plate slendernesses of flange and web plates have great influences on strength enhancement of stocky columns. Therefore, relationship between mobilized section resistances and plate slendernesses of flange and web plates of S690 welded H-section is examined systematically.

7.2.1 Effect of welding procedures

In order to investigate effects of different welding procedures, 8 different cross-sections, namely Sections C1 to C8, are utilized in this parametric study. The study programme is shown in Table 7.1 with various section properties. Three different series with same cross-sections are introduced as:

- Series HE: welded sections fabricated with a high-energy welding;
- Series LE: welded sections fabricated with a low-energy welding; and,
- Series 0RS: welded sections with no residual stresses as a reference.

The cross-sectional dimensions of these 8 sections are shown in Figure 5.13. Residual stresses of these welded sections introduced by two different welding procedures are calculated with these calibrated coupled thermo-mechanical models as illustrated in Figure 5.14. The residual stresses are then directly transferred to the double Y-shaped finite element models. The differences in section resistances and deformation characteristics among these three series are investigated and elaborated systematically.

7.2.1.1 Section resistances

In Table 7.2, predicted resistances of various sections of stocky columns are presented together with corresponding resistance ratios, $N_{c,FE}$ / $N_{c,Rd}$. For easy comparison, these resistance ratios are plotted against plate slendernesses of flange and web plates in Figure 7.3. It is found that full section resistances are generally attained in all 8 sections in each of the three series. Generally, section resistances in sections of Series 0RS are slightly larger than those in the other two series. And, it should be noted that the maximum variation among resistance ratios is found to be merely 2%. Therefore, the effects of residual stresses to section resistances of stocky columns are shown to be very small.

7.2.1.2 Load shortening curves

Predicted load shortening curves of 8 sections are presented in Figure 7.2. Comparing against those load shortening curves of Series 0RS, it is obvious that presence of residual stresses in welded sections always leads to an early yielding and a reduction in section rigidity. Moreover, discrepancies among these curves diminish when the applied loads reach the section resistances. Eventually, load shortening curves converge when the entire sections yield and axial shortenings become very large. This convergence usually occurs at a shortening strain between 0.7% and 1.0% which corresponds to twice the yield strain of S690 steel material. Therefore, the effect of residual stresses is shown to be small in stocky columns of S690 welded H-sections when their maximum resistances are achieved at large deformation.

Deformation capacities of stocky columns are also provided in Table 7.3. It is found that deformation capacities increase with reduced plate slendernesses of these sections. And for each section in three different series, there is only a small variation in their deformation capacities. Hence, the effect of residual stresses onto deformation capacities of stocky columns is also found to be very small.

7.2.2 Effect of plate slendernesses

In order to examine effect of plate slendernesses onto local buckling behaviour of stocky columns, a total of 40 models of S690 welded H-sections with various cross-sectional dimensions are included in this parametric study. Four series representing four different combinations of plate thicknesses from 6 mm to 40 mm are covered in this parametric study. All these H-sections are designed in such a way that their flange and web plates possess similar plate slendernesses. And the normalized plate slendernesses of these H-sections range from 0.15 to 1.05 covering Class 1 to Class 4 sections according to EN 1993-1-1. The study programme is summarized in Table 7.4.

Eigenvalue buckling mode shapes with the lowest eigenvalue are introduced as initial geometrical imperfections in the finite element models of these stocky columns. More importantly, simplified residual stress patterns devised by Liu (2017) are employed in this parametric study. It should be noted that:

i) These patterns have been successfully calibrated against measured residual stresses in S690 welded H-sections;

ii) They fully satisfy force equilibrium within cross-sections; and,

iii) They are applicable to those cross-sections in this study.

7.2.2.1 Section resistances

The resistance ratios of these finite element models against plate slendernesses are plotted in Figure 7.4. It should be noted that the trends of resistance ratios are found to follow those of the test data. Obviously, these predicted resistance ratios reduce with increasing plate slendernesses. For Class 1 sections, significant strength enhancement is observed while for Class 4 sections, full section resistances are not readily attained. However, it should be noted that differences among section resistances of those four series are somehow small.

In Figure 7.4, comparison with section classification rules in EN 1993-1-1 is also presented. It should be noted that according to the current design criteria on plate slendernesses of various section classes, design resistances are found to be appropriate to these sections as the predicted resistances are found to be very close to the full section resistances of stocky columns of S690 welded H-sections.

7.2.2.2 Deformation capacity and strength enhancement

Predicted deformation capacities of 40 stocky column are plotted against plate slendernesses in Figure 7.5. It is shown that deformation capacities decrease exponentially with increasing plate slendernesses. The design criteria of 3.0 proposed in AISC 360-10 for compact sections, i.e. Class 1 sections, are satisfied by all test and numerical results. Hence, deformation capacities over 3.0 is justified for Class 1 sections of S690 welded H-sections.

Moreover, for sections with deformation capacities over 3.0, a strength enhancement to the section resistances of Class 1 sections is observed. Based on a statistical approach on the predicted section resistances, the resistance enhancement comes from three sources:

i) Post-yielding modulus of steel material

ii) Additional section resistances owing to increased cross-sectional area

iii) Contribution from four weldments

Therefore, a total of 5% strength enhancement may be reasonably attained in stocky columns with Class 1 sections. In Figure 7.4, direct comparison between design resistance ratios with a 5% strength enhancement and corresponding numerical results are presented for easy comparison.

7.2.3 Summary

Experimental results obtained from physical tests and numerical results obtained from parametric studies on stocky columns of S690 welded H-sections show that:

- Residual stresses do not have significant effects onto section resistances and deformation capacities when full section resistances is achieved in stocky columns of S690 welded H-sections;
- Plate slenderness criteria and section resistances predicted with the use of section classification rules in EN 1993-1-1 are applicable to design stocky columns of S690 welded H-sections; and,
- In order to achieve accurate prediction of section resistances of stocky columns under compression, a 5% strength enhancement for Class 1 S690 welded H-sections should be allowed as demonstrated in both measured and numerical data.

Proposed design rules for stocky columns of S690 welded H-sections under compression are summarized in Table 7.5. They are compatible with current rules of EN 1993-1-1 for S235 to S460 welded H-sections with proposed design parameters for stocky columns.

7.3 Parametric study on Slender Columns of S690 Welded H-sections

Based on calibrated numerical models of slender columns established in Chapter 6 and predicted residual stress patterns established in Chapter 5, a parametric study on slender columns of S690 welded H-sections is conducted. A total of 352 models of slender columns with Sections C1 to C8 are modeled in four different series as:

- Series ZZ-HE: Minor-axis buckling of slender columns welded with high heat input energy;
- Series ZZ-LE: Minor-axis buckling of slender columns welded with low heat input energy;
- Series YY-HE: Major-axis buckling of slender columns welded with high heat input energy;
- Series YY-LE: Major-axis buckling of slender columns welded with low heat input energy;

In order to investigate into effects of reduced residual stresses onto overall buckling resistances of slender columns, two important factors are introduced to classify the modelling series as: i) plate thicknesses, and ii) section classification. Through a close examination into the numerical results, a revised selection table of overall buckling curves for slender columns of S690 welded H-sections is proposed. It should be noted that low residual stress ratios in slender columns of S690 welded H-sections increase their overall buckling resistances, when compared to those of S235 to S355 welded H-sections.

7.3.1 Slender columns buckling about minor axis

In this parametric study, finite element models for slender columns calibrated in Chapter 6 are employed, and the study programme is presented in Table 7.6. Two series of these models, within each including 88 sections, are established for welding with high and low heat input energy respectively. Normalized member slendernesses of these sections, i.e. $\bar{\lambda}_z$, are found to range from 0.21 to 2.00.

Numerical results of 88 sections in each series are summarized in Table 7.7. It should be noted that the numerical results are also classified according to welding procedures, flange plate thicknesses and section classifications. According to numerical studies on residual stresses in welded H-sections presented in Chapter 5, the following sections are examined: i) sections with low heat input energy; ii) sections with thick plates, and iii) sections with wide flanges and deep webs, i.e. Class 3 sections, have smaller residual stresses in these welded H-sections. Hence, an investigation into these factors is carried out, and increased overall buckling member resistances are expected.

- *Effect of welding procedure*

  A comparison of predicted buckling resistances of Series ZZ-HE and ZZ-LE, together with various buckling curves in EN 1993-1-1, is plotted in the same graph of Figure 7.6. Buckling curve c, which is suggested by EN 1993-1-1 for welded H-sections buckling about minor axis, is highlighted in Figure 7.6 for easy comparison. It should be noted that both measured and predicted minor-axis buckling resistances of Series ZZ-HE and ZZ-LE are significantly higher than buckling curve c. Therefore, buckling curve c is applicable to S690 welded H-sections over a range of member slendernesses, though it is shown to be very conservative.

  In order to increase structural efficiency, buckling curve b is proposed to design both slender columns of Series ZZ-HE and ZZ-LE, as the predicted resistances are higher than this design curve as shown in the graph. Additionally, modified buckling curve a is proposed for design of overall buckling as shown in Figure 7.6 (c). It is shown that this curve provides an improved structural efficiency.

  A direct comparison of member resistances between Series ZZ-HE and ZZ-LE shows that member resistances increase with reduced residual stresses in these sections. It should be noted that compressive residual stresses in welded sections with low heat input energy are smaller than those sections with high-heat-input energy. Hence, section rigidities of these sections with low heat input energy will be reduced under a large compression force. Discrepancies among these resistances are apparent in slender columns of normalized slendernesses ranging from 0.50 to 1.25, as the cross-sections of these slender columns are partially yielded at failure.

- *Effect of plate thickness*

A comparison of predicted overall buckling member resistances of welded H-sections with thin plates as well as with thick plates, together with various buckling curves are plotted in the same graph of Figure 7.7 for direct comparison.

It is found that welded H-sections with over 20 mm thick flanges are able to attain resistance ratios substantially higher than buckling curve a while those with flanges equal or below 20 mm thick obtain resistance ratios slightly higher than buckling curve b. Similar findings are also applicable to those slender columns of Series ZZ-HE and ZZ-LE. Hence, buckling curve a may be used to design slender columns with flanges thicker than 20 mm.

- *Effect of section classification*

A comparison of predicted overall buckling member resistances of welded H-sections with Class 3 sections together with various buckling curves are plotted in the same graph of Figure 7.8 for direct comparison.

It is found that comparison among resistance ratios of welded H-sections with Class 3 sections and those of welded H-sections with Class 1 and 2 sections is small. Most importantly, overall buckling resistances in both groups may be assessed with buckling curve b.

- *A modified buckling curve a*

In order to propose a simple buckling curve with improved structural efficiency, a modified buckling curve a is given in Figure 7.6 comparing with measured and predicted buckling resistances. With critical slenderness, $\bar{\lambda}_0$ equals 0.1, and imperfection factor, α equals 0.21, this buckling curve is found to be appropriate for all obtained data.

7.3.2 Slender columns buckling about major axis

In this parametric study, finite element models for slender columns calibrated in Chapter 6 are employed, and the study programme is presented in Table 7.8. Two series of these models, each series with 88 sections, are established for welding with high and low heat input energy respectively. Normalized slendernesses of these sections, i.e. $\bar{\lambda}_y$, are found to range from 0.22 to 2.00.

Numerical results of 88 sections in each series are summarized in Table 7.9. It should be noted that the numerical results are also classified according to welding procedures, flange plate thicknesses and section classification. According to various numerical studies on residual stresses in welded H-sections predicted in Chapter 5, the following sections are examined: i) sections welded with low-heat-input energy; ii) sections with thick plates, and iii) sections with wide flanges and deep webs, i.e. Class 3 sections. Hence, an investigation into these factors is carried out, and increased buckling resistances are expected.

- *Effect of welding procedure*

  A comparison of predicted buckling resistances of Series YY-HE and YY-LE, together with various buckling curves in EN 1993-1-1 is plotted in the same graph in Figure 7.9. Buckling curve b, which is suggested by EN 1993-1-1 for welded H-sections buckling about major axis, is highlighted in Figure 7.9 for easy comparison. It should be noted that predicted major-axis buckling resistances of Series YY-HE and YY-LE are significantly higher than buckling curve b. Therefore, this member buckling curve is applicable to S690 welded H-sections over a range of member slendernesses, though it is shown to be very conservative.

  A direct comparison of member resistances between Series YY-HE and YY-LE shows that overall member resistances increase with reduced residual stresses in these sections. It should be noted that compressive residual stresses in welded sections with low heat input energy are smaller than those with high heat input energy. Hence, section rigidities of these sections with low heat input energy will be reduced only under large compression forces. Discrepancies among these resistances are apparent in slender columns of normalized slendernesses ranging from 0.50 to 1.25, as the cross-sections of these slender columns are partially yielded at failure.

In order to increase structural efficiency, buckling curve a in EN 1993-1-1 may be employed to design slender columns of welded sections with low heat input energy.

- *Effect of plate thickness*

A comparison of predicted overall buckling member resistances of welded H-sections with thin plate as well as thick plates, together with various buckling curves are plotted in the same graph of Figure 7.10 for direct comparison.

It is found that resistance ratios of welded H-sections with at least 20 mm thick flanges are not different from those with flanges thinner than 20 mm thick. Most importantly, buckling resistances in both groups may be estimated with buckling curve b for welded sections with high heat input energy, but with buckling curve a for welded sections with low heat input energy.

- *Effect of section classification*

A comparison of predicted overall buckling member resistances of welded H-sections with Class 3 sections, together with various buckling curves are plotted in the same graph of Figure 7.11 for direct comparison.

It is found that welded H-sections with Class 3 sections attain resistance ratios higher than buckling curve a while resistances of Class 1 and 2 sections are merely higher than buckling curve b. This observation is valid to both Series YY-HE and YY-LE. Hence, buckling curve a can be used to design overall buckling of slender columns with Class 3 cross-sections.

7.3.3 Summary

In order to propose more structurally efficient design rules for slender columns of S690 welded H-sections, parametric studies are carried out. Overall buckling of slender columns about minor axis and major axis are covered in this study. Effects of residual stresses, which can be influenced by different welding procedures, plate thicknesses and section classifications of slender columns, are investigated. It is found that:

- Owing to reduced residual stress ratios in S690 welded H-sections when compared with S235 to S355 welded sections, buckling resistances of these slender columns are increased.
- Due to reduced residual stress ratios in flange and web plates of S690 welded H-sections when compared those of S235 and S355 sections, section rigidities are reduced only under large compression forces, and hence, their buckling resistance ratios are consequently increased.
- In order to increase design efficiency of slender columns of S690 welded H-sections, a higher buckling curve may be adopted, or a different critical slenderness, $\bar{\lambda}_0$, may be adopted to slender columns buckling about minor axis as shown in Table 7.10.

7.4 Parametric Study on Restrained Beams of S690 Welded I-sections

Based on calibrated numerical models of restrained beams established in in Chapter 6 and predicted residual stress patterns established in Chapter 5, a parametric study on restrained beams of S690 welded I-sections is conducted. The study programme is presented in Table 7.11. A total of 102 models of restrained beams with sections B1 to B6 are modeled in four different series as follows: i) Series I-10-6 with 10 mm thick flanges and 6 mm thick webs; ii) Series I-16-10 with 16mm thick flanges and 10mm thick webs; iii) Series I-25-16 with 25 mm thick flanges and 16 mm thick webs; and, iv) Series I-40-25 with 40 mm thick flanges and 25 mm thick webs.

In order to assess local buckling of restrained beams, a wide range of local plate slendernesses of the flange and the web plates of the welded I-sections, i.e. $\overline{\lambda}_f$ and $\overline{\lambda}_w$, ranging from 0.35 to 1.15, are introduced into this study. It should be noted that both residual stress patterns induced by welding with high and low heat input energy are considered.

7.4.1 Established finite element models

In this parametric study, finite element models for restrained beams calibrated in Chapter 6 as shown in Figure 7.12 are employed. It should be noted that transverse loads are applied at mid-span of the beams, and lateral restraints are provided at loaded points to prevent lateral torsional buckling. Stiffeners are introduced at both ends as well as at mid-span these models.

A total of 102 models of restrained beams are established for both high and low heat input energy. Normalized plate slendernesses of these sections, namely $\overline{\lambda}_f$ and $\overline{\lambda}_w$, are found to range from 0.35 to 1.14 as defined in EN 1993-1-1. A bi-linear stress strain relationship presented in Figure 7.1 is also employed. It should be noted that according to the residual stress patterns proposed for S690 welded sections, the maximum compressive residual stress is $-0.21f_y$ which is significantly smaller than $-0.41f_y$ in S355 welded sections by Liu (2017). Eigenvalue buckling mode shape is introduced as initial geometric imperfection in these beams.

7.4.2 Effect of plate slenderness

Predicted moment resistance ratios of restrained beams against plate slendernesses are plotted in Figures 7.13 and 7.14 together with section classifications given in EN 1993-1-1. These numerical results are based on welded I-sections welded with high-heat-input energy, i.e. with large residuals stress. It should be noted that these predicted resistance ratios decrease generally with an increase in plate slendernesses, and this is found to be consistent with test data.

For Class 1 and 2 sections, significant strength enhancement is observed. It is found that a strength enhancement over 5% is obtained in every single predicted and measured moment resistance. This should be attributed to large ductility ratios of S690 welded I-sections as shown in Figure 7.15. In general, section yielding is found to be developed in Class 1 sections which ductility ratios are equal to or larger than 3.

Moreover, elastic moment resistances are attained in all Class 3 sections, and even in some Class 4 sections. A significant resistance margin is observed in all Class 3 sections. Hence, it is possible to increase moment resistances, as well as their resistance ratios correspondingly. Current design criteria for Class 3 sections are obviously conservative. Hence, a modified limiting width-to-thickness ratio will be highly desirable.

Proposed section classification rules for S690 welded I-sections are given in Table 7.12. Moreover, the proposed design rules for moment resistances of welded I-sections with different classes are presented as follows:

i) Class 1 sections: $M_{Rd} = 1.05\, M_{pl,Rd}$

ii) Class 2 sections: $M_{Rd} = 1.00\, M_{pl,Rd}$

iii) Class 3 sections: $M_{Rd} = M_{el,Rd} + \eta\,(M_{pl,Rd} - M_{el,Rd})$

when, $\eta = \min\left[\frac{(14\varepsilon - c_f/t_f)}{6}, \frac{(130\varepsilon - c_w/t_w)}{47}\right]$

7.4.3 Effect of residual stress

A comparison on predicted moment resistances of restrained beams with high-heat-input energy to those with of restrained beams with low heat input energy is illustrated in Figure 7.16. It should be noted that these predicted resistance ratios of Class 3 and 4 sections fabricated with high-heat-input energy are slightly smaller than those with low-heat-input energy. This is caused by early yielding owing to presence of large compressive residual stresses induced with welding of high heat input energy. In general, differences in the moment resistance ratios of different welded sections between high and low heat-input energy are shown to be rather small. Hence, the proposed design rules are found to be valid to all welded I-sections covered in this study.

7.4.4 Summary

According to measured results from the experimental investigation and predicted data from the parametric study on restrained beams of S690 welded I-sections, it is found that:

- The proposed design rules for plate slenderness and section classification stipulated in EN 1993-1-1 are shown to be applicable to design of restrained beams of S690 welded I-sections;
- A 5% strength enhancement in Class 1 S690 welded I-sections is suggested based on demonstration with both measured and predicted results, and a revised design rule for resistance prediction of Class 3 sections is also provided;
- In general, residual stresses do not have significant effects onto section resistances of restrained beams of S690 welded I-sections.

The proposed design rules for restrained beams of S690 welded I-sections are summarized in Table 7.12.

7.5 Parametric Study on Partially Restrained Beams of S690 Welded I-sections

Based on calibrated numerical models of partially restrained beams established in Chapter 6 and predicted residual stress patterns established in Chapter 5, a parametric study on partially restrained of S690 welded I-sections is conducted. A total of 176 models of partially restrained beams with Sections B1 to B8 are modeled. The study programme is presented in Table 7.13.

In order to assess any relationships between lateral torsional buckling resistances and residual stresses in welded I-sections, sections with high-heat-input energy and low-heat-input energy are covered. Through a close examination into the numerical results, a lateral torsional buckling curve for S690 welded I-sections is proposed. It should be noted that reduced residual stress levels will increase lateral torsional buckling resistances of partially restrained beams of S690 welded I-sections, when compared with those of S235 to S355 welded sections.

7.5.1 Established numerical models

In this parametric study, finite element models for partially restrained beams calibrated in Chapter 6 as shown in Figure 7.17 are employed. It should be noted that transverse loads are applied at mid-span of the beams, and lateral restraints are provided at loaded points to prevent lateral torsional buckling. Stiffeners are introduced at both ends as well as at mid-span of these models.

A total of 176 models of partially restrained beams are established in this study. Normalized slendernesses of these sections, $\bar{\lambda}_{LT}$, are found to range from 0.37 to 1.88. A bi-linear stress strain relationship presented in Figure 7.1 is employed. It should be noted that according to the residual stress patterns proposed for S690 welded sections, the maximum compressive residual stress is $-0.21f_y$ which is significantly smaller than $-0.41f_y$ in S355 welded sections by Liu (2017). Eigenvalue buckling mode shape is introduced as initial geometric imperfection in these partially restrained beams.

7.5.2 Effect of lateral torsional slendernesses

Predicted lateral torsional buckling resistances of partially restrained beams are plotted in Figure 7.18 together with measured resistances for direct comparison. These numerical results are based on welded I-sections welded with high-heat-input energy. It should be noted that these predicted resistance ratios decrease generally with an increase in member slendernesses, and this is found to be consistent with test data.

For beams with small member slendernesses from 0.4 to 0.6, full moment resistances are readily attained. And the resistance ratios are found to be larger than 1.0 for all these beams with member slendernesses smaller than 0.5. Hence, the values of the critical slenderness should be increased from 0.4 to 0.5 so that design efficiency for partially restrained beams of S690 welded I-sections is increased.

Moreover, comparison between predicted moment resistance ratios and buckling curves are presented in this figure. It is shown that buckling curve c recommended in EN 1993-1-1 is applicable to design unrestrained beams of S690 welded I-sections. It should be noted that a significant conservatism is revealed in the graph in the region of intermediate slendernesses, i.e. $\bar{\lambda}_{LT}$ from 0.6 to 1.0. This is because of decreased compressive residual stresses in S690 welded I-sections when compared with those S235 to S355 welded sections.

In order to increase design efficiency, two different design approaches are proposed as:

i) Buckling curve b may be used instead, as shown in Figure 7.18;

ii) Modified curve b with a revised limiting slenderness 0.5, and a buckling curve with an imperfection factor equal to 0.34, as shown in Figure 7.19, may be used.

7.5.3 Effect of residual stress

A comparison of predicted moment resistances of partially restrained beams with high-heat-input energy is illustrated in Figure 7.20. It should be noted that these predicted resistances are slightly higher in those beams with intermediate slendernesses when low heat input energy welding is applied. This is caused by a relatively large section rigidity in the presence of small compressive residual stresses in welded I-sections. In general, differences in lateral torsional buckling resistances between beams with two different welding procedures are found to be rather small. Hence, the proposed design rules are found to be valid to all welded I-sections covered in this study.

7.5.4 Summary

According to measured results from the experimental investigation and predicted data from the parametric studies on partially restrained beams of S690 welded I-sections, it is found that:

- The proposed design rules for lateral torsional buckling of S690 welded I-sections with buckling curve d stipulated in EN 1993-1-1 are applicable to design of partially restrained beams of S690 welded I-sections;
- An improved design efficiency is achieved if buckling curve b or modified curve b whichever higher can be used instead;
- In general, effects of residual stresses onto lateral torsional buckling resistances of partially restrained beams are found to be smaller when compared with effects on to slender columns.

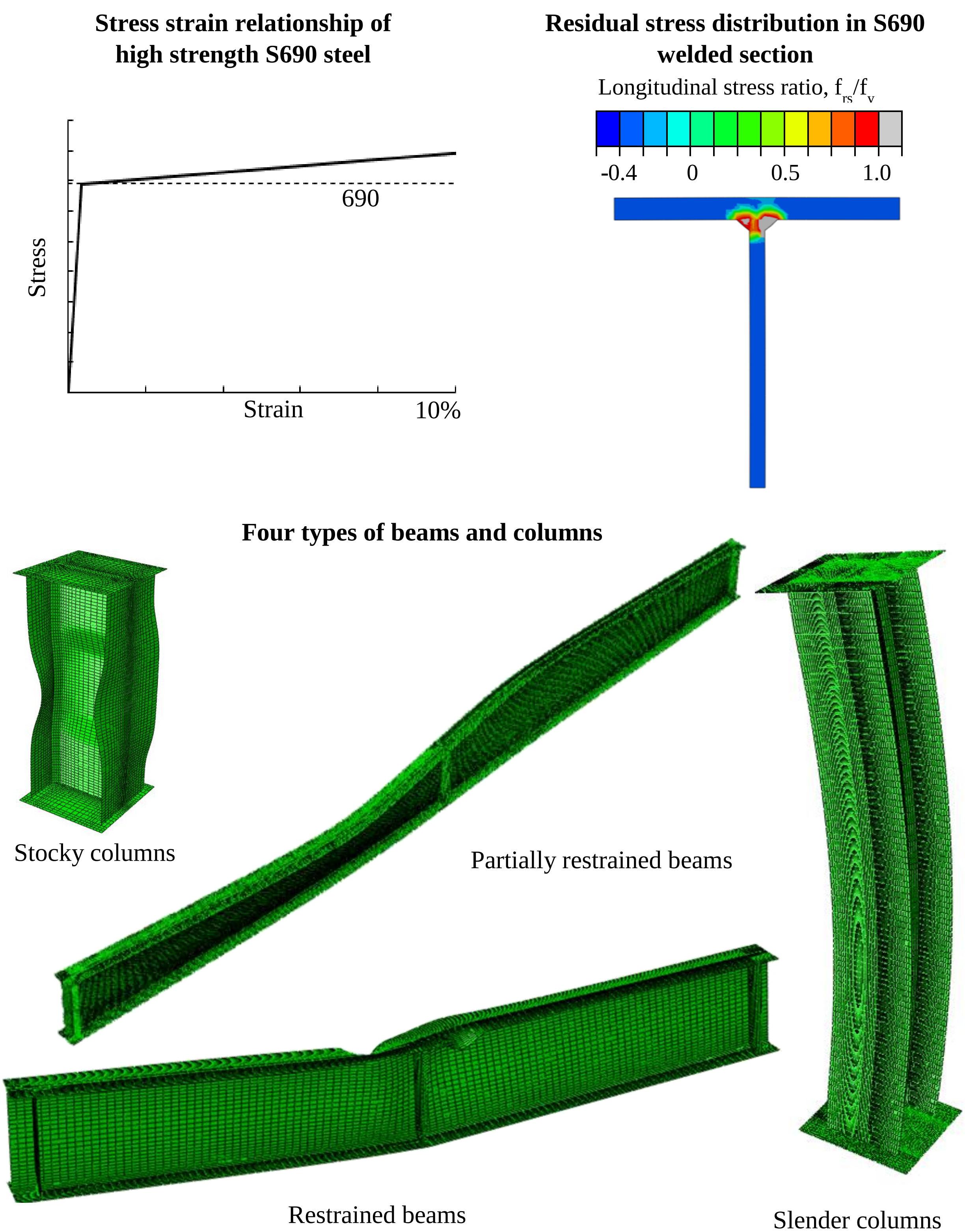

Figure 7.1: Overview of the parametric studies

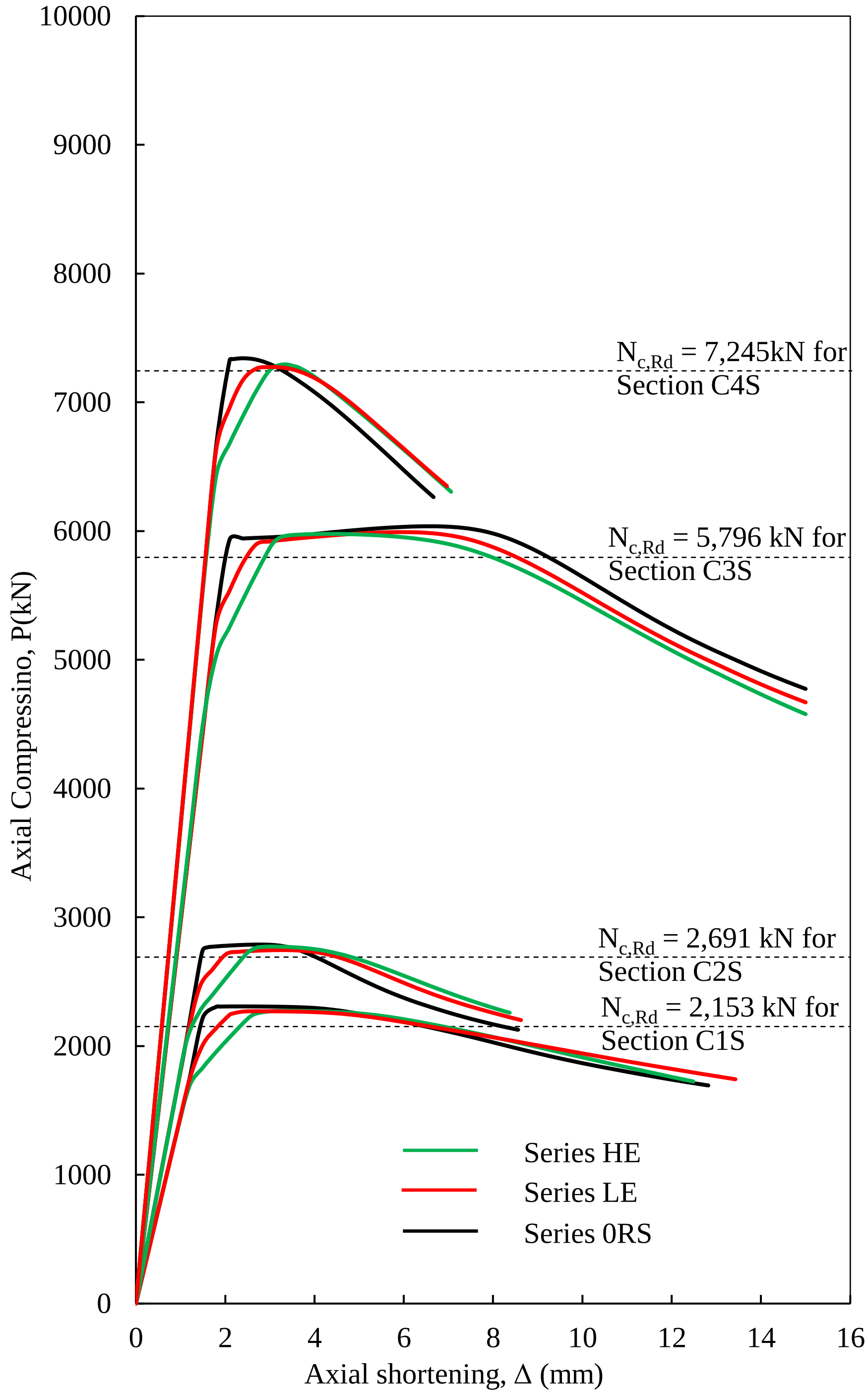

Figure 7.2 (a): Load deflection curves of S690 H-sections incorporated with different residual stress patterns (Sections C1S to C4S)

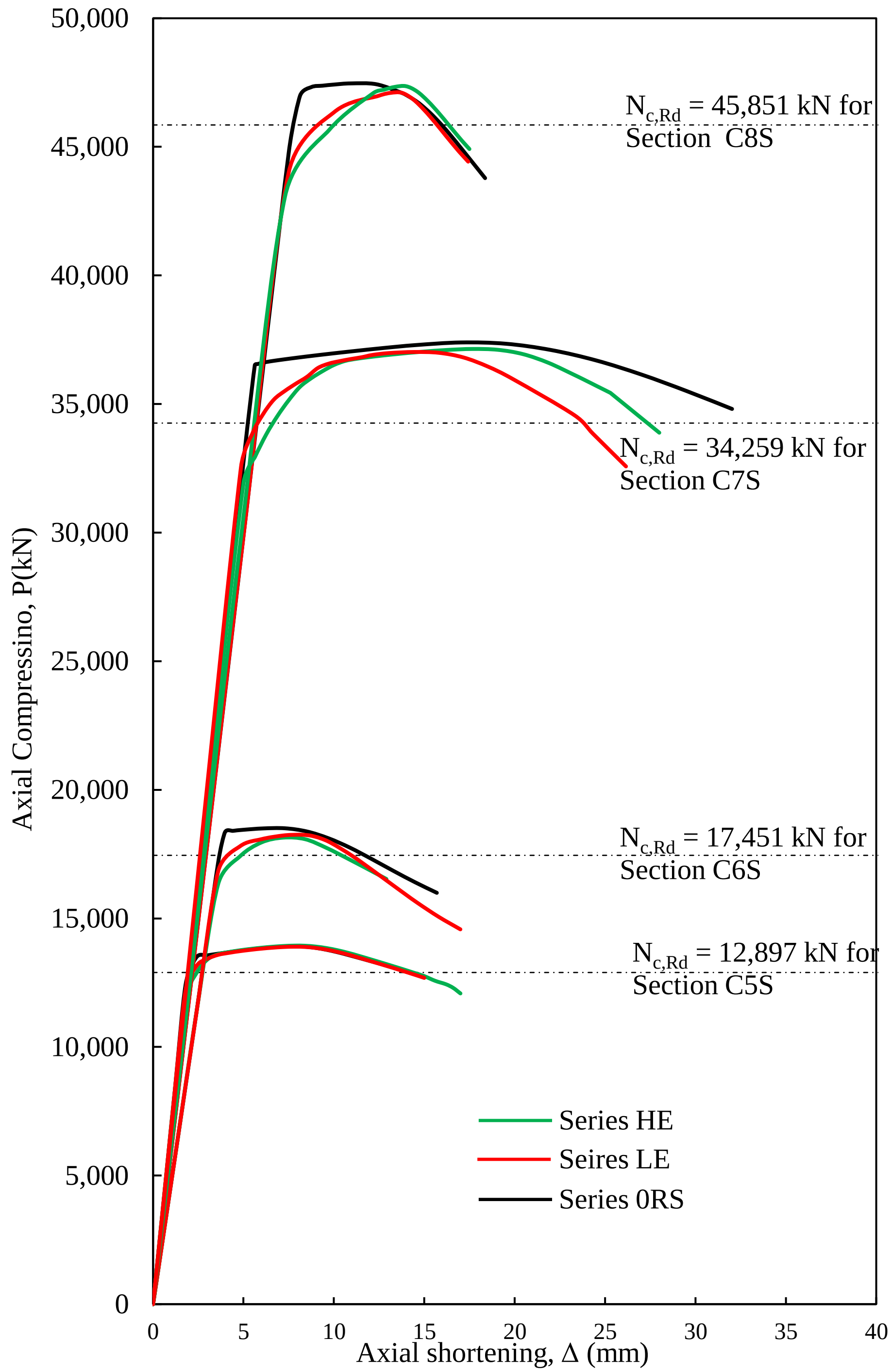

Figure 7.2 (b): Load deflection curves of S690 H-sections incorporated with different residual stress patterns (Sections C5S to C8S)

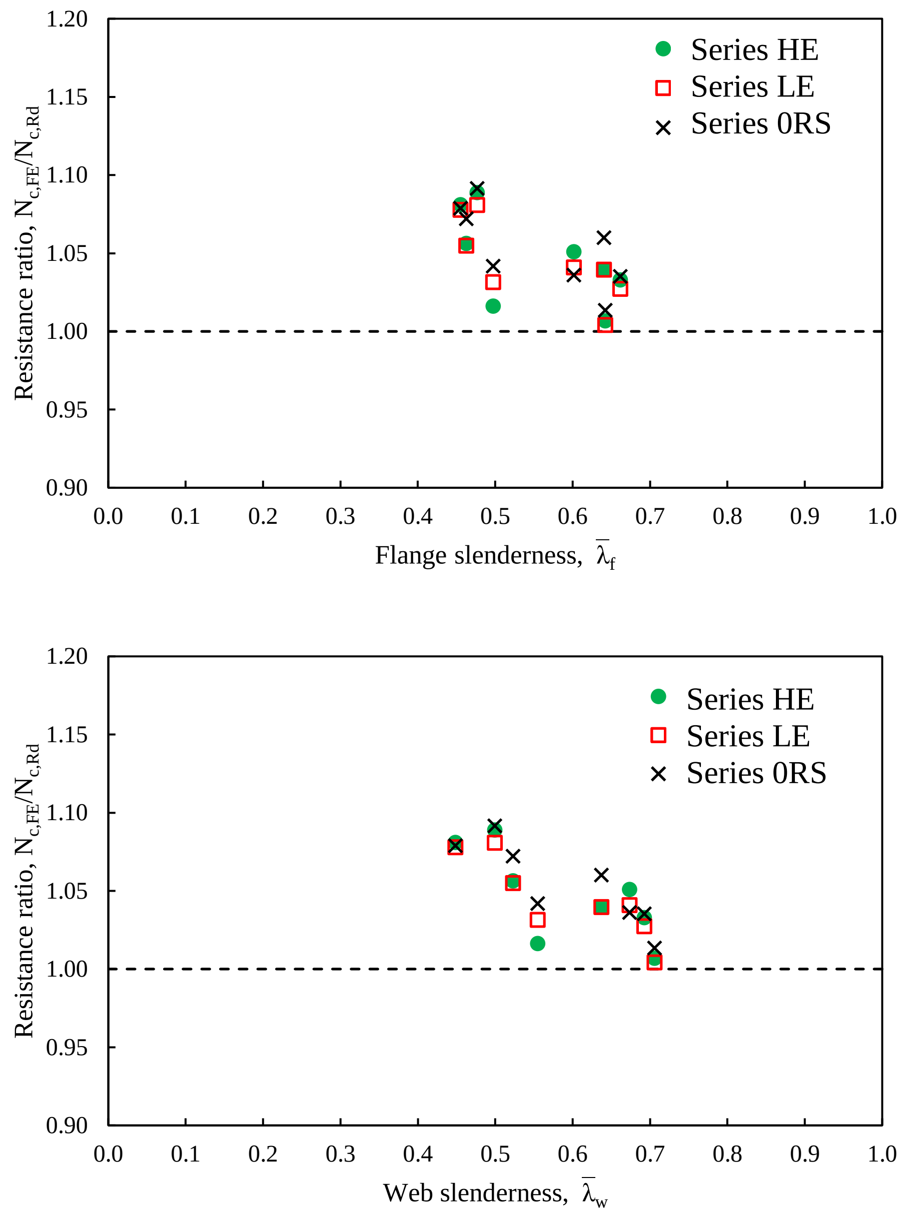

Figure 7.3: Resistance ratios of stocky columns against plate slendernesses

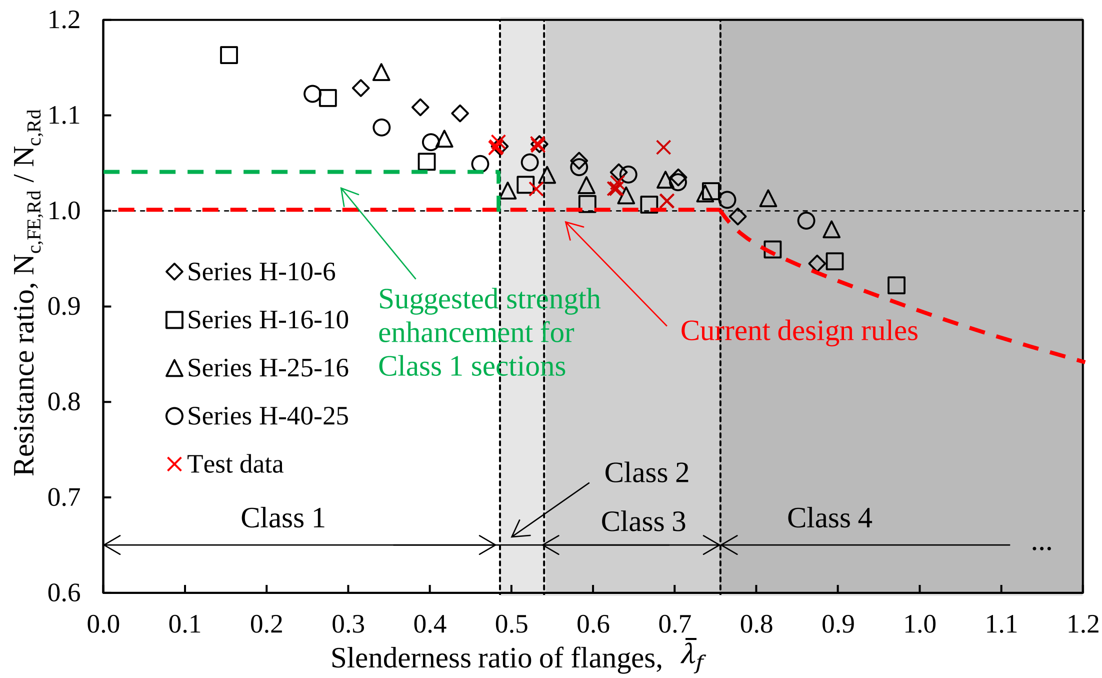

(a) Section resistances against flange slenderness

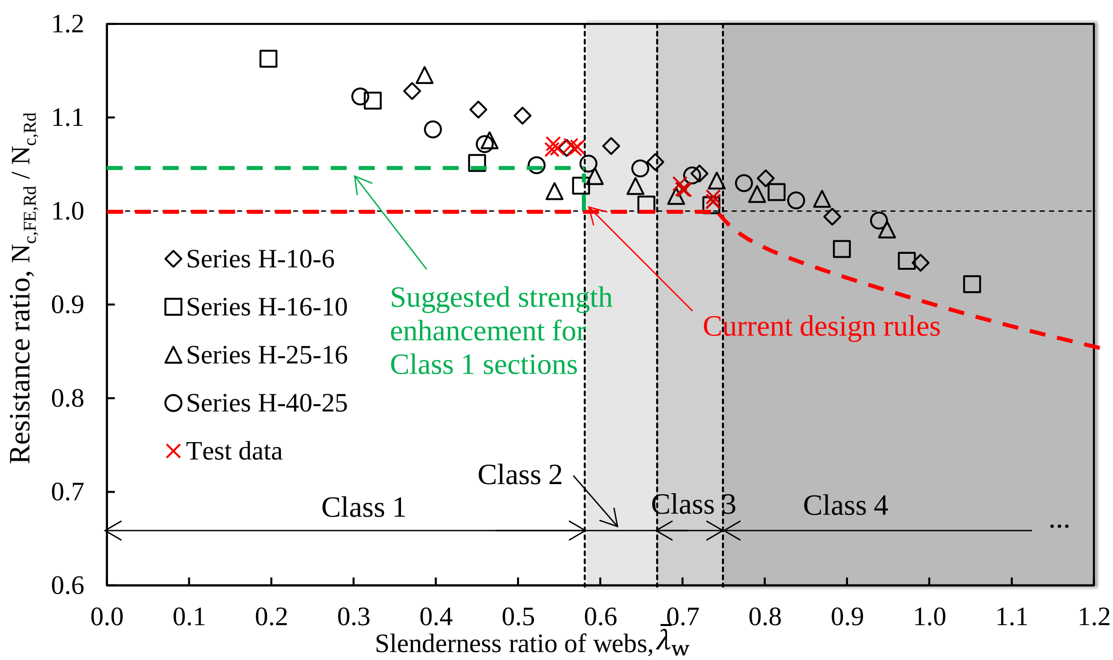

(b) Section resistances against web slenderness

Figure 7.4: Resistance ratios of finite element models comparing with current design criteria

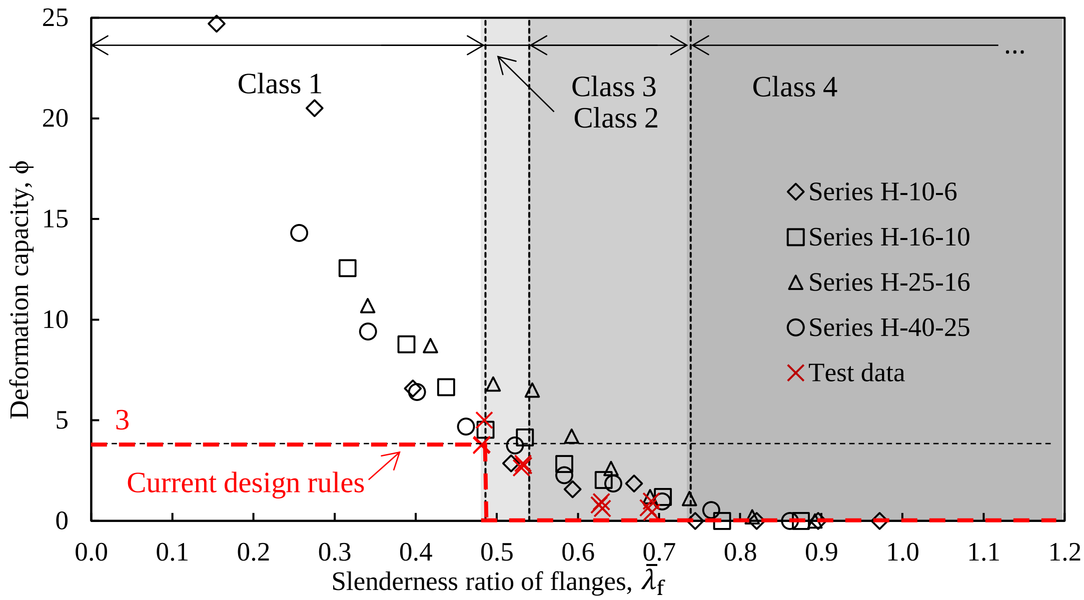

(a) Deformation capacities against flange slendernesses

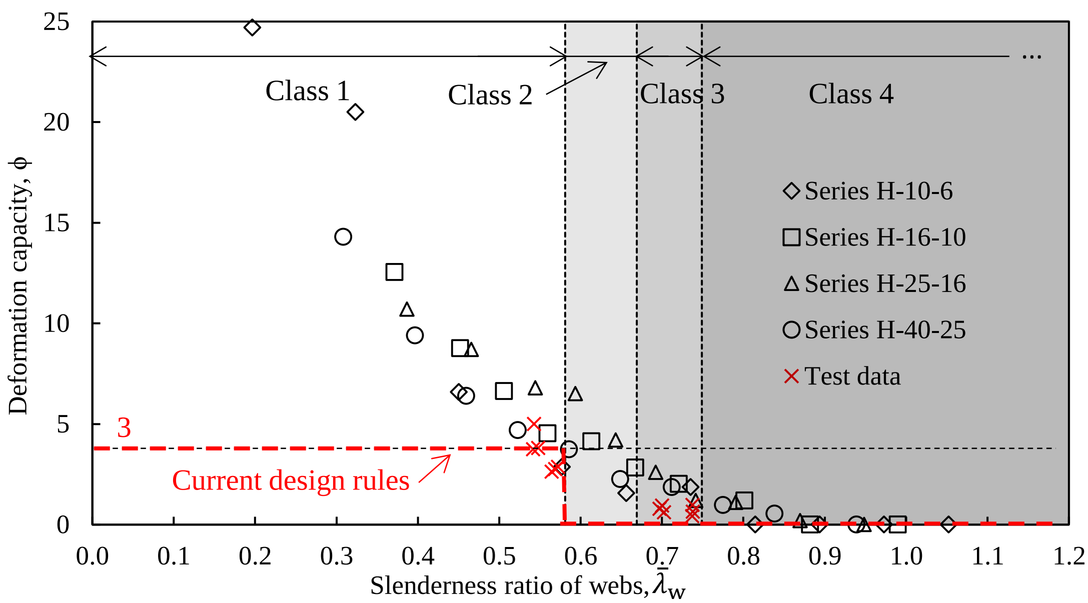

(b) Deformation capacities against web slendernesses

Figure 7.5: Predicted deformation capacities of stocky columns

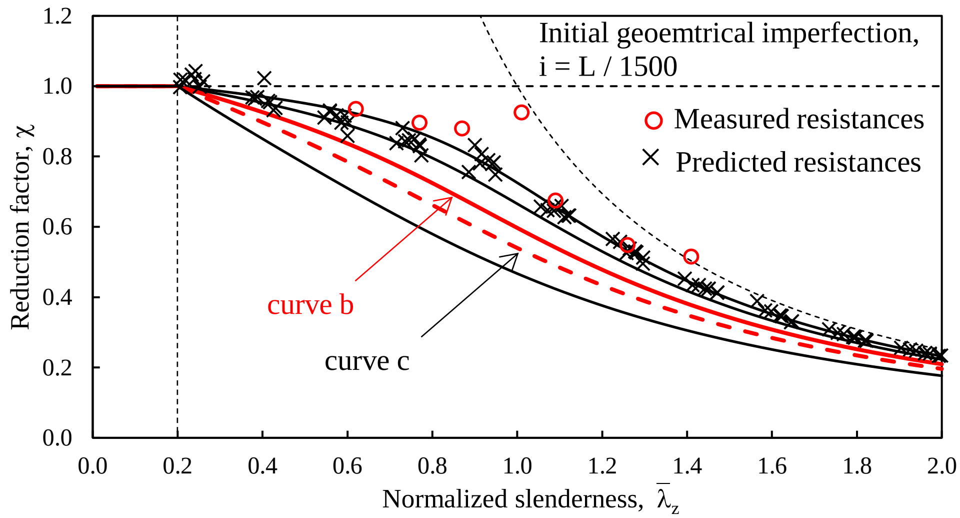

(a) Measured resistances and Series ZZ-HE

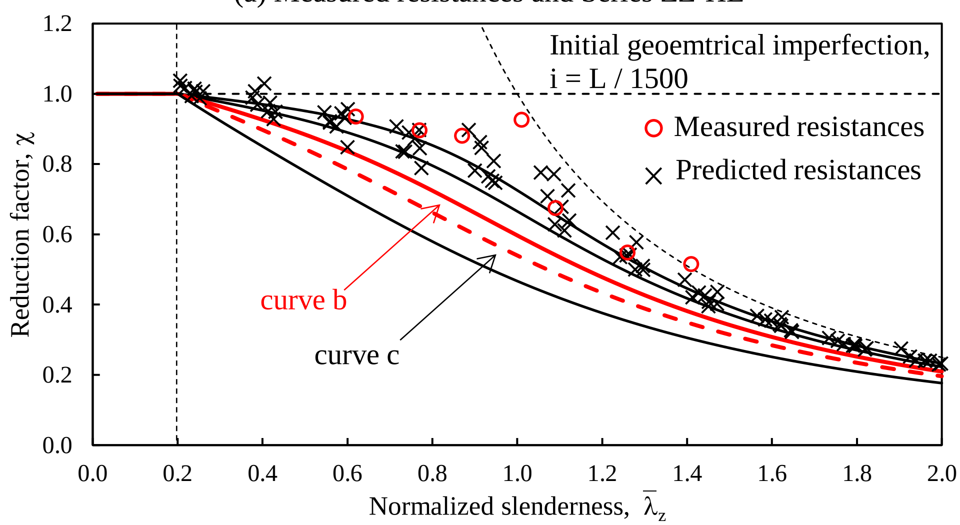

(b) Measured resistances and Series ZZ-LE

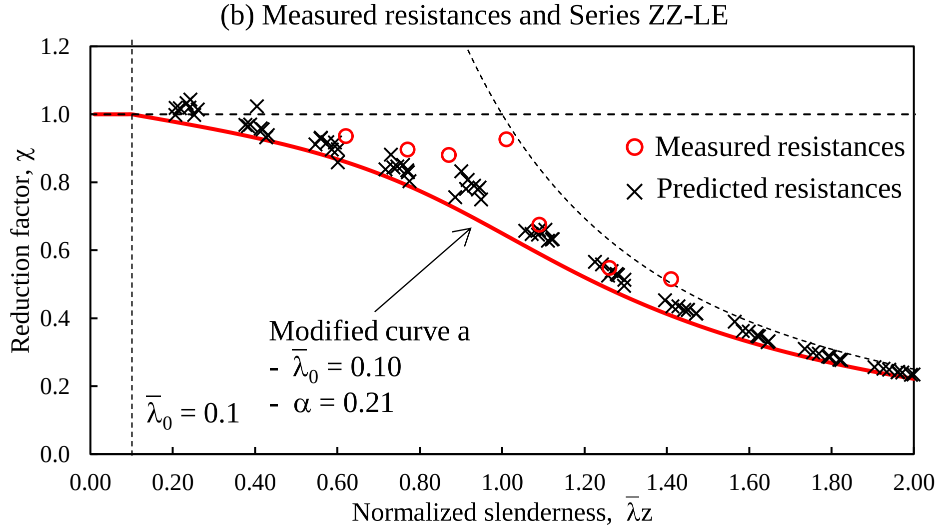

(c) Modified curve a proposed for design of minor axis buckling (Based on Series ZZ-HE)

Figure 7.6: Measured and Predicted resistances of slender columns buckling about minor axis

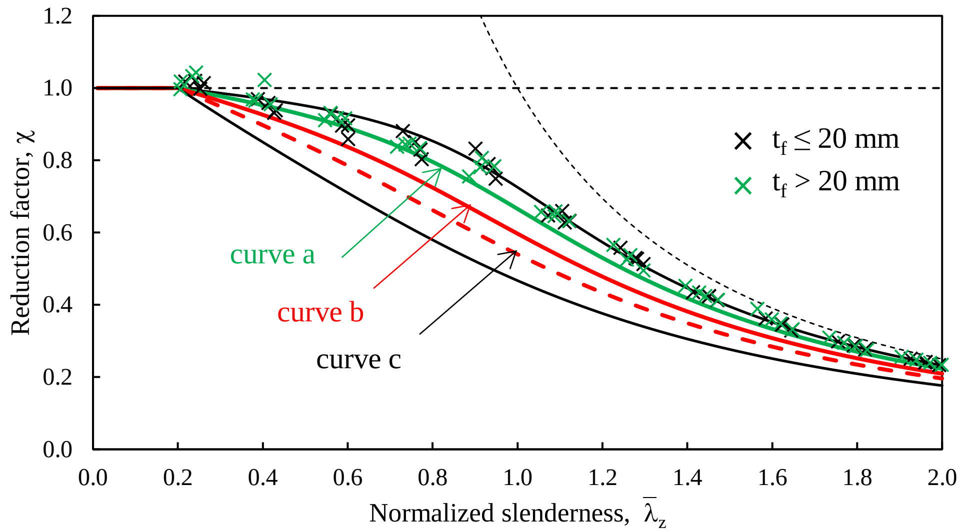

(a) Series ZZ-HE

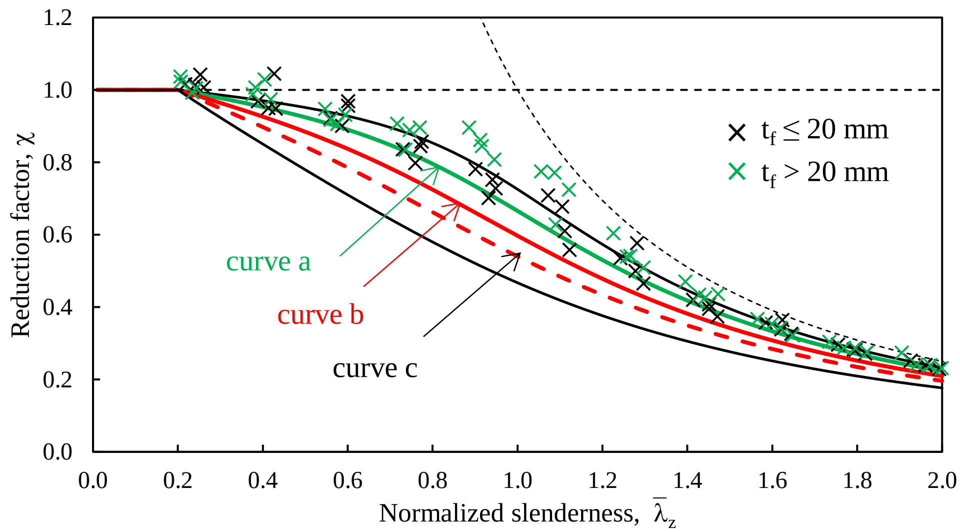

(b) Series ZZ-LE

Figure 7.7: Predicted resistances of slender columns differentiated in plate thicknesses

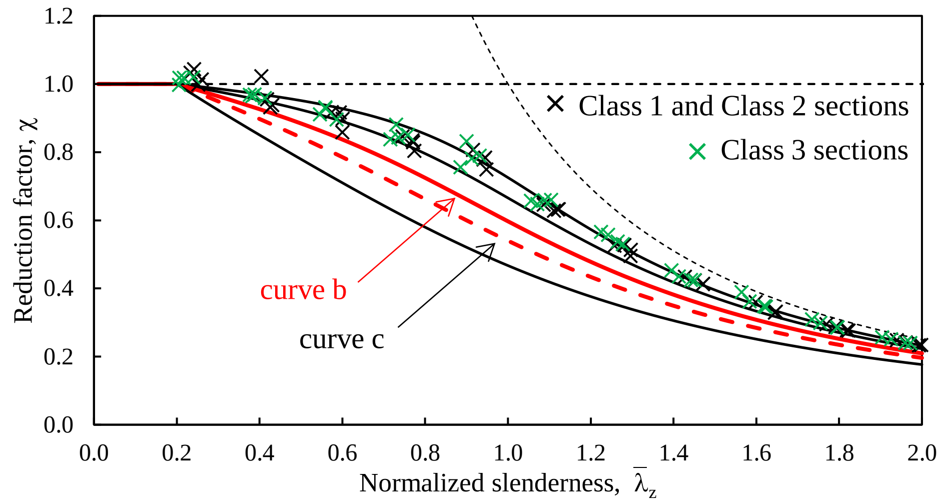

(a) Series ZZ-HE

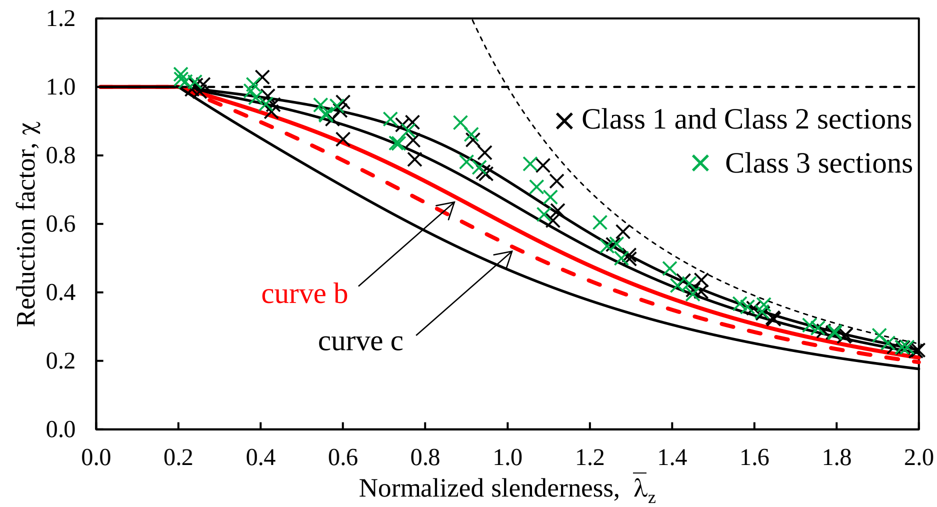

(a) Series ZZ-LE

Figure 7.8: Predicted resistances of slender columns differentiated in section classifications

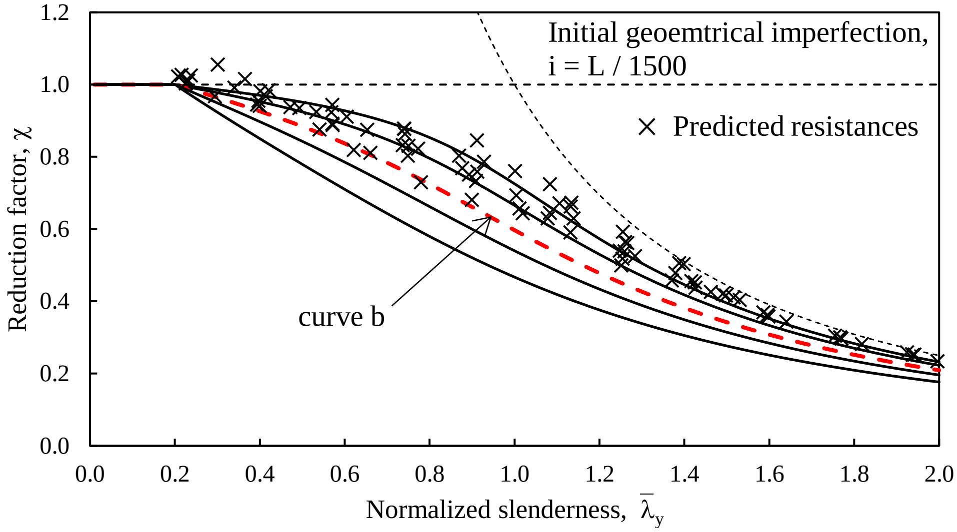

(a) Series YY-HE

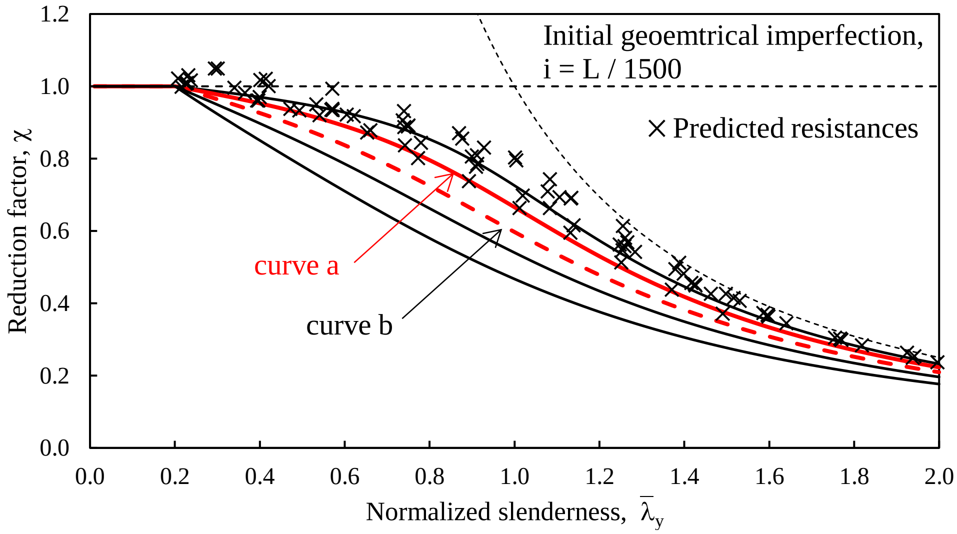

(b) Series YY-LE

Figure 7.9: Predicted resistances of slender columns buckling about major axis

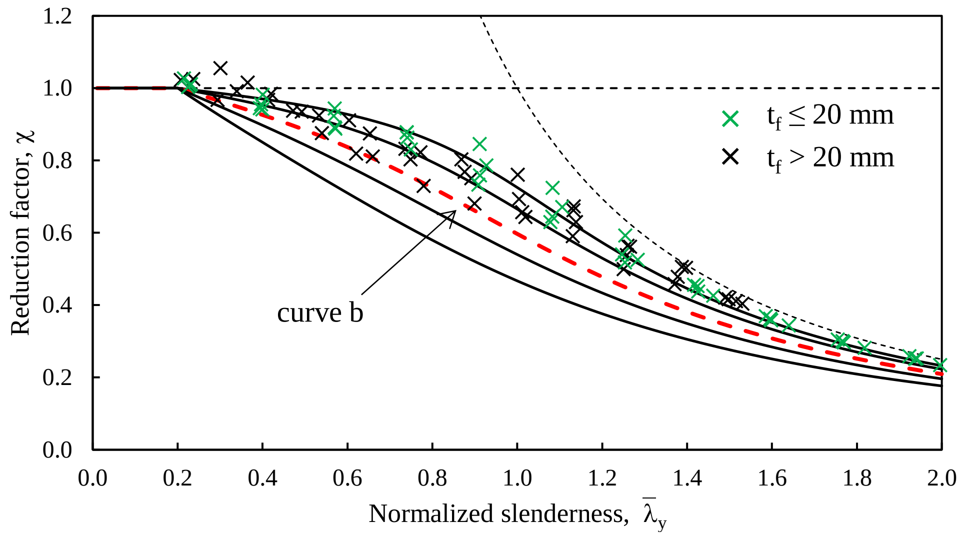

(a) Series YY-HE

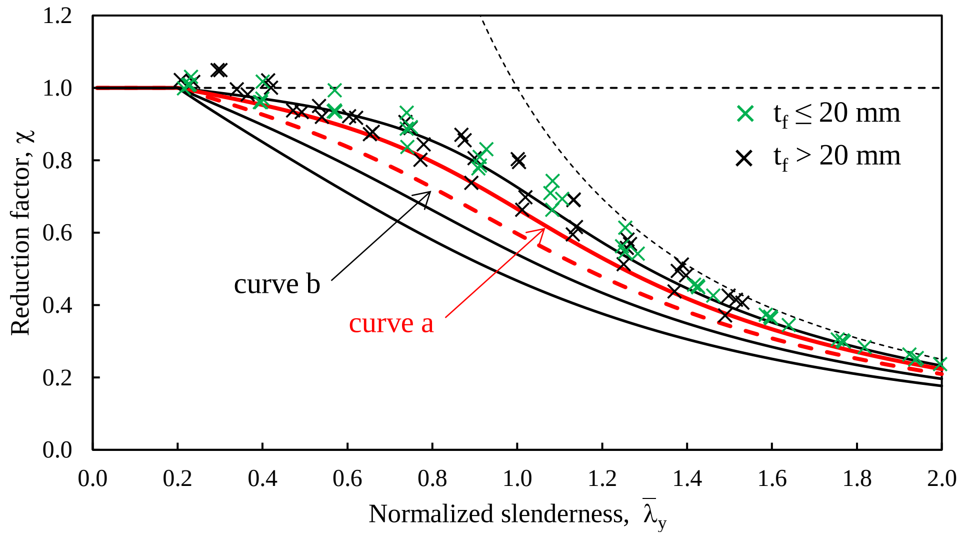

(b) Series YY-LE

Figure 7.10: Predicted resistances of slender columns differentiated in plate thicknesses

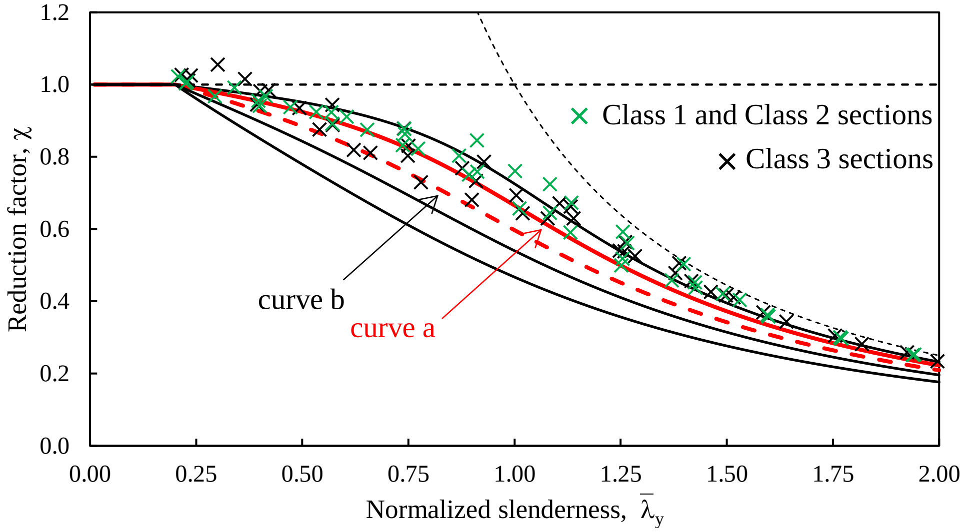

(a) Series YY-HE

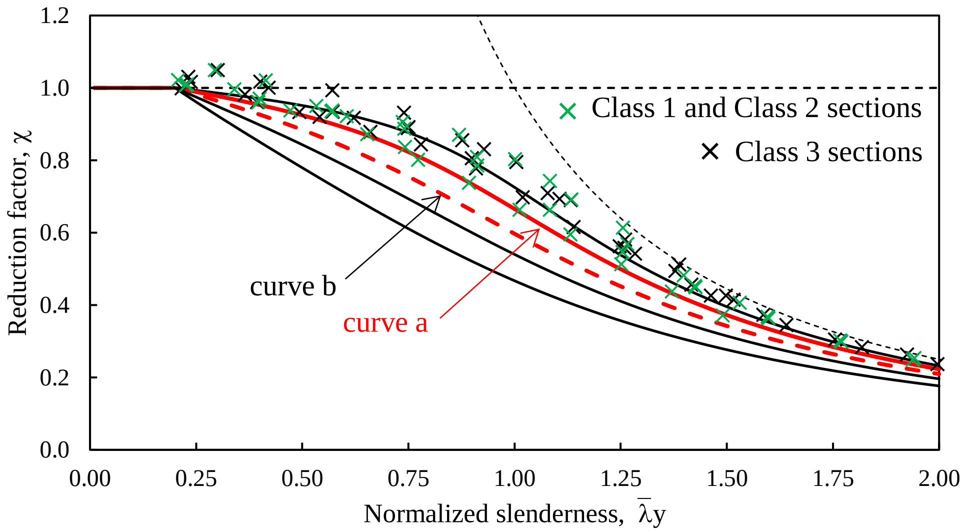

(b) Series YY-LE

Figure 7.11: Predicted resistances of slender columns differentiated in section classifications

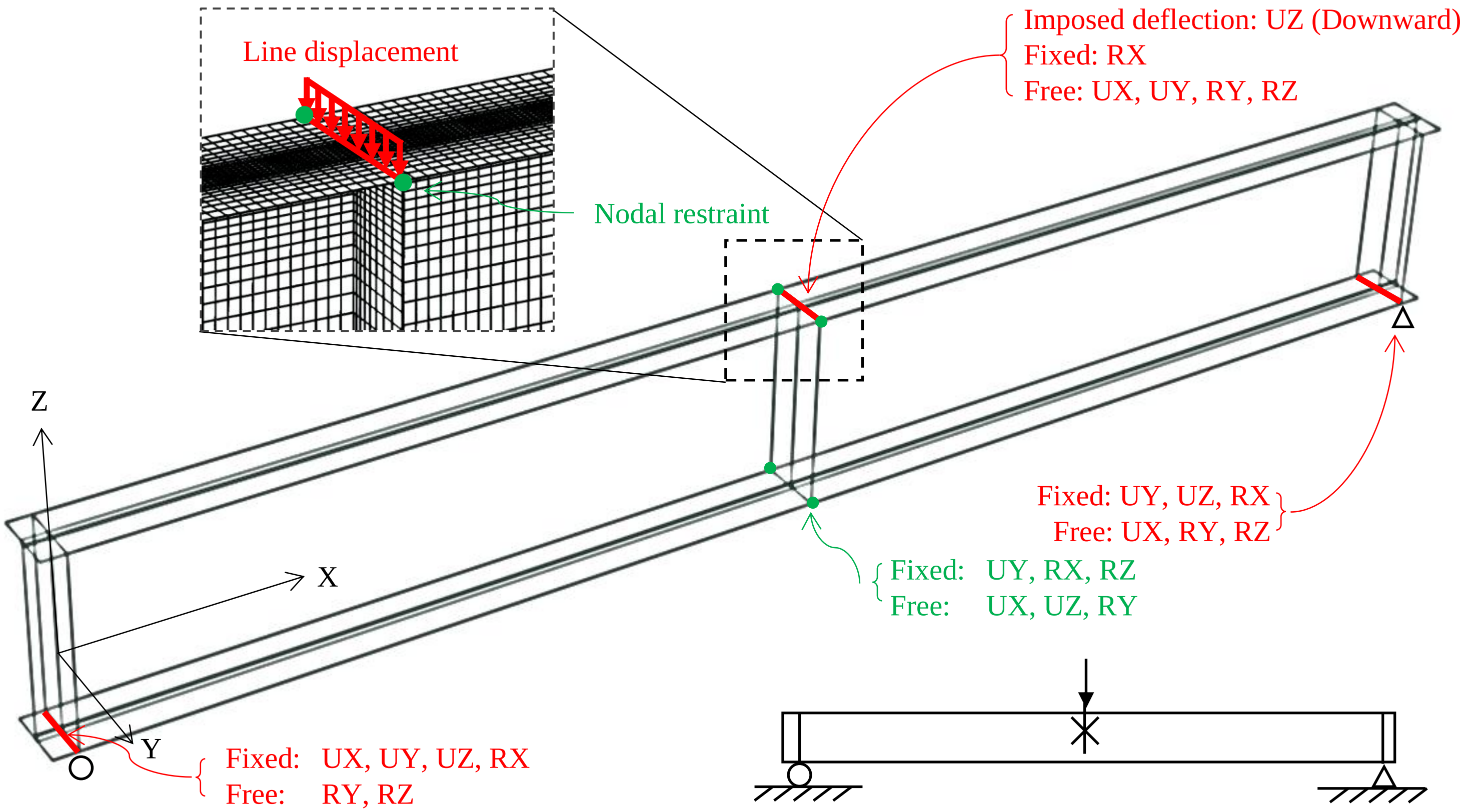

Figure 7.12: Established numerical model for restrained beams

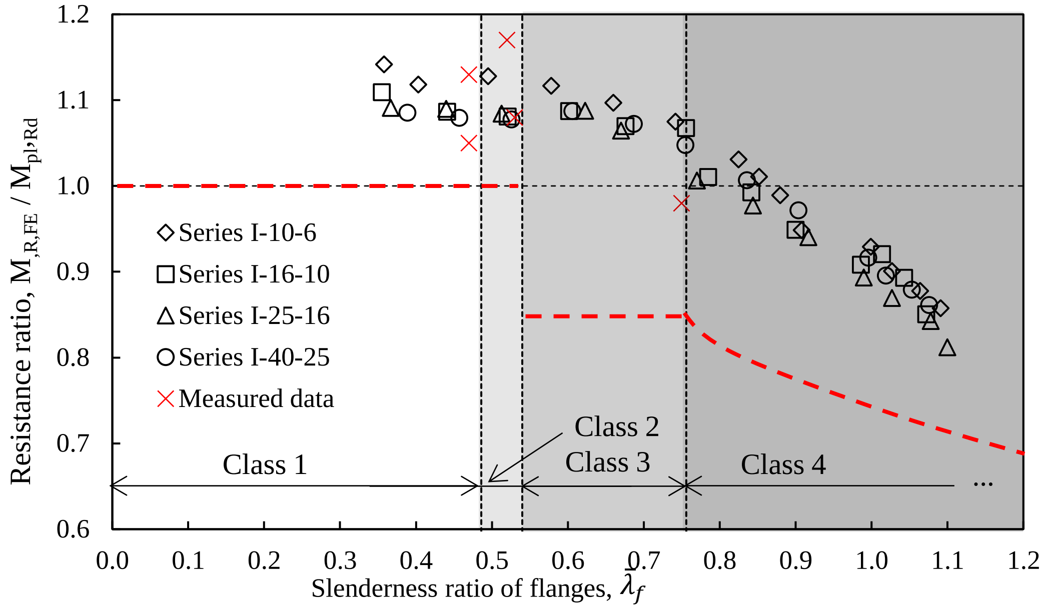

(a) Comparison with plastic moment resistances

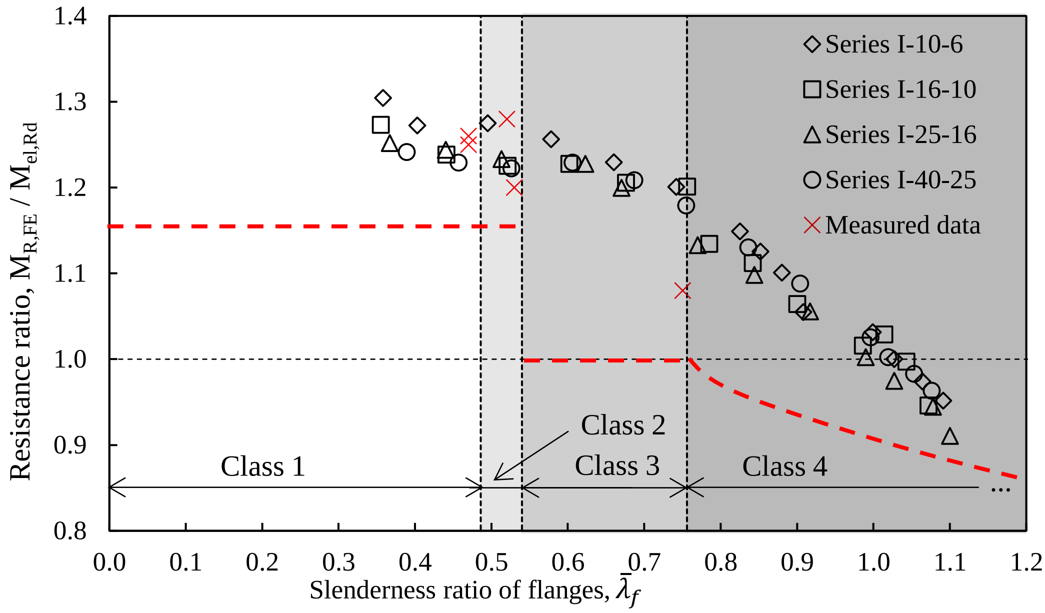

(b) Comparison with elastic moment resistances

Figure 7.13: Parametric study on moment resistances of restrained beams against flange slendernesses – with high energy welding

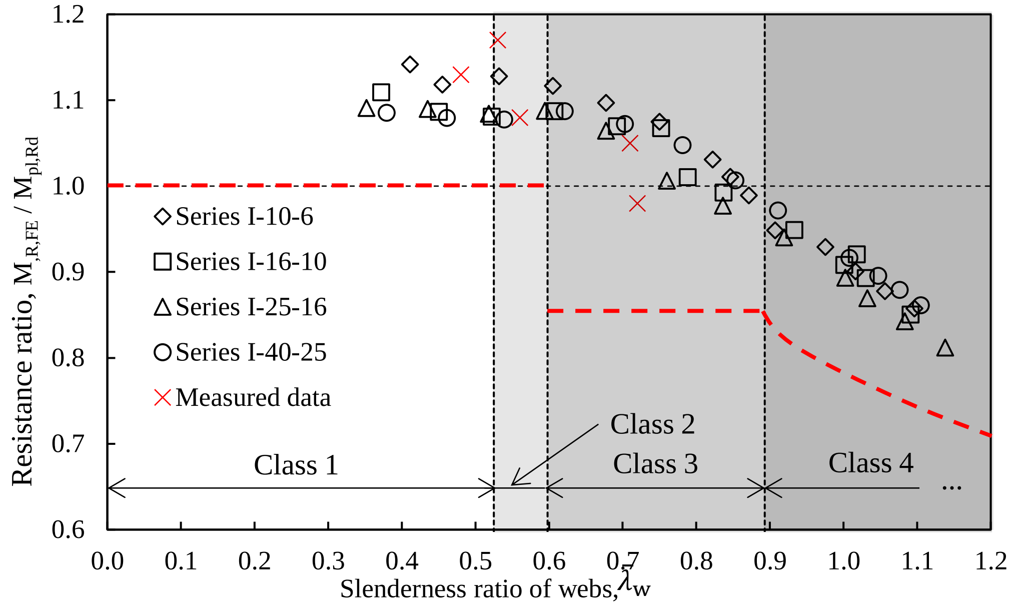

(a) Comparison with plastic moment resistances

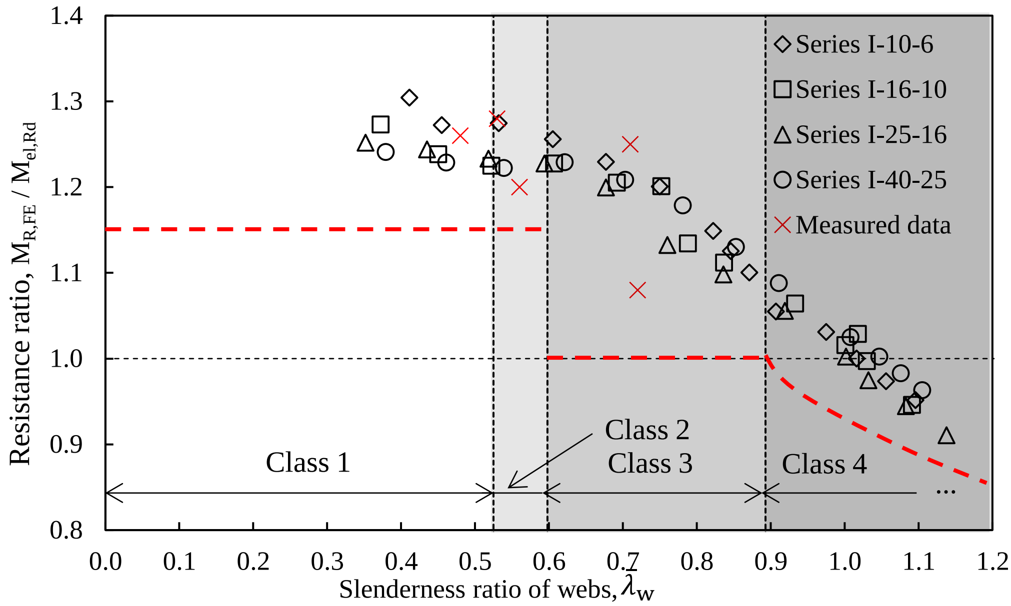

(b) Comparison with elastic moment resistances

Figure 7.14: Parametric study on moment resistances of restrained beams against web slendernesses – with high energy welding

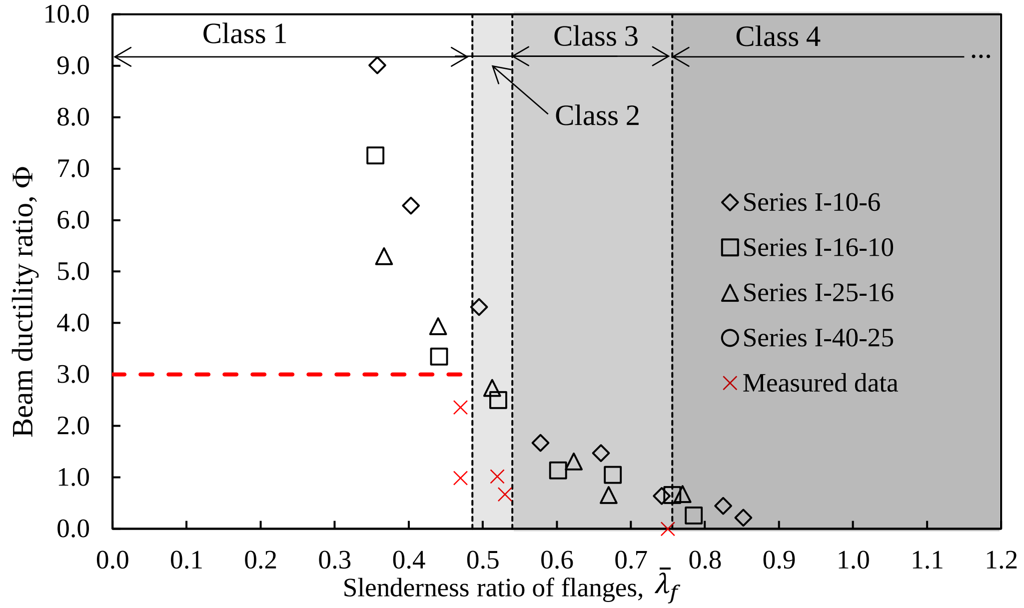

(a) Against flange slendernesses

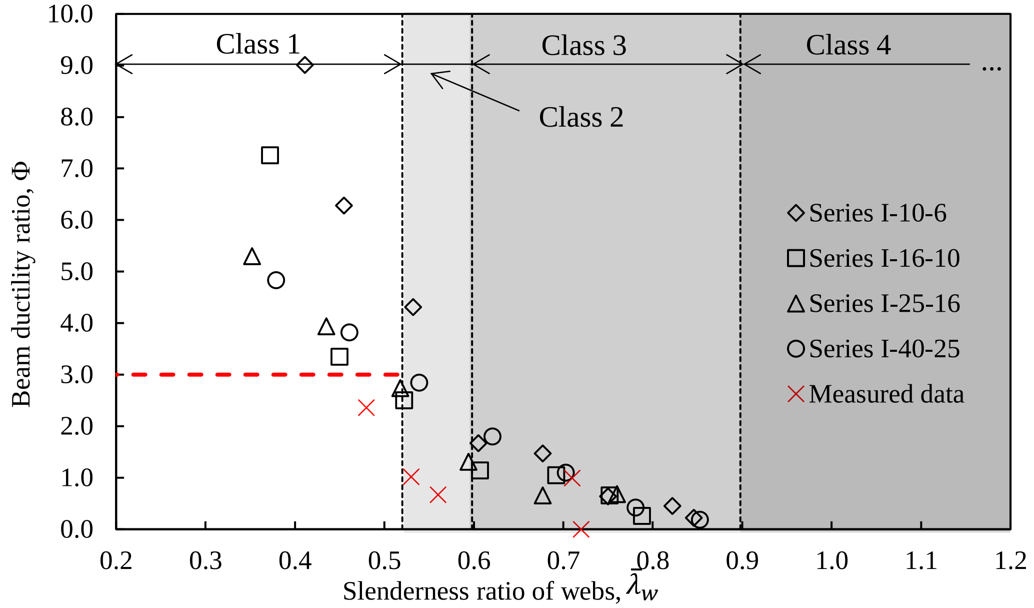

(b) Against web slendernesses

Figure 7.15: Parametric study on ductility ratios of restrained beams of S690 welded I-sections – with high energy welding

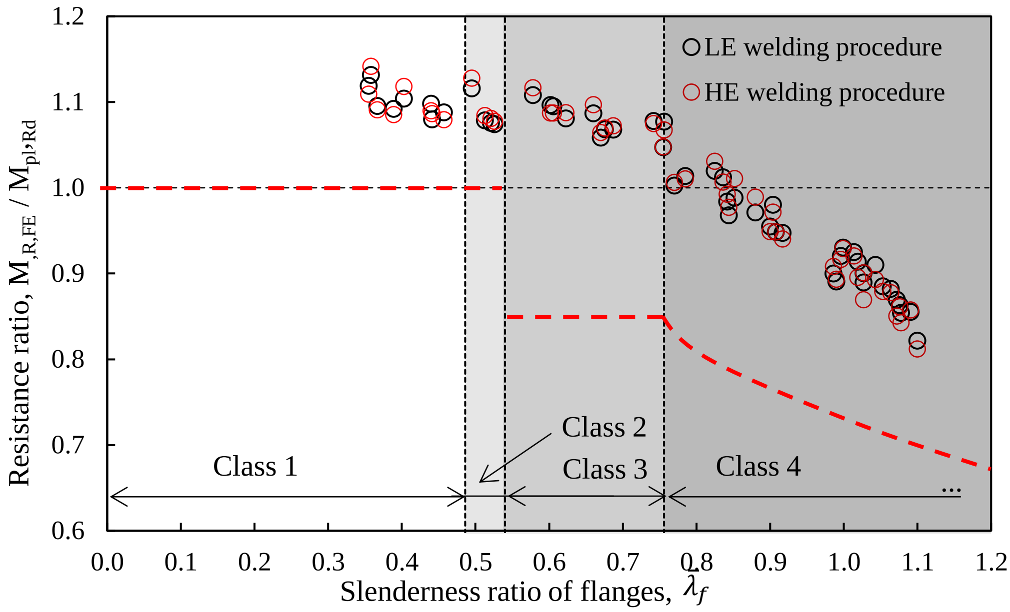

(a) Against flange slendernesses

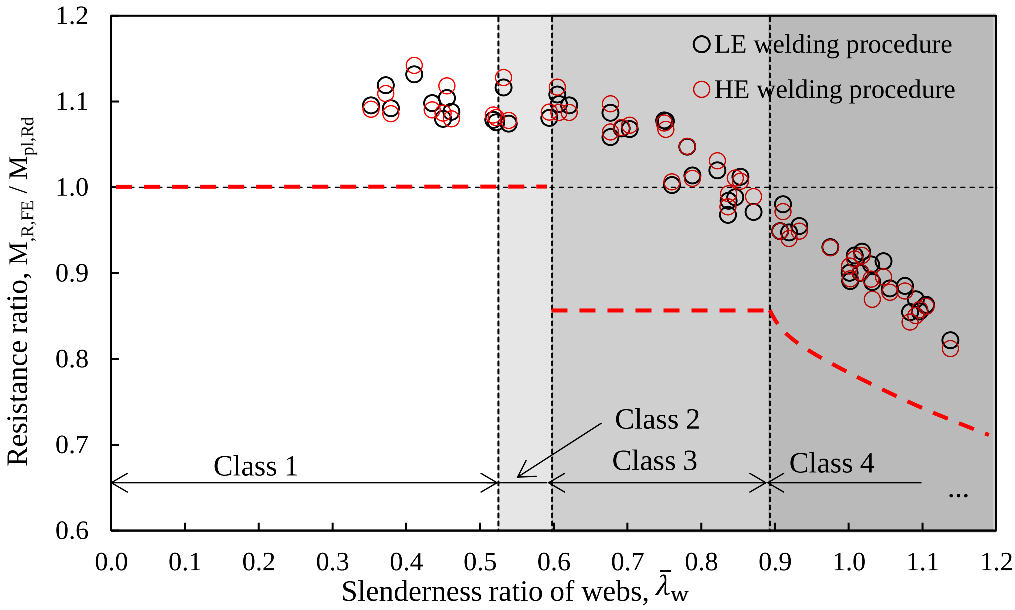

(b) Against web slendernesses

Figure 7.16: Predicted moment resistances of restrained beams fabricated with both low and high energy welding

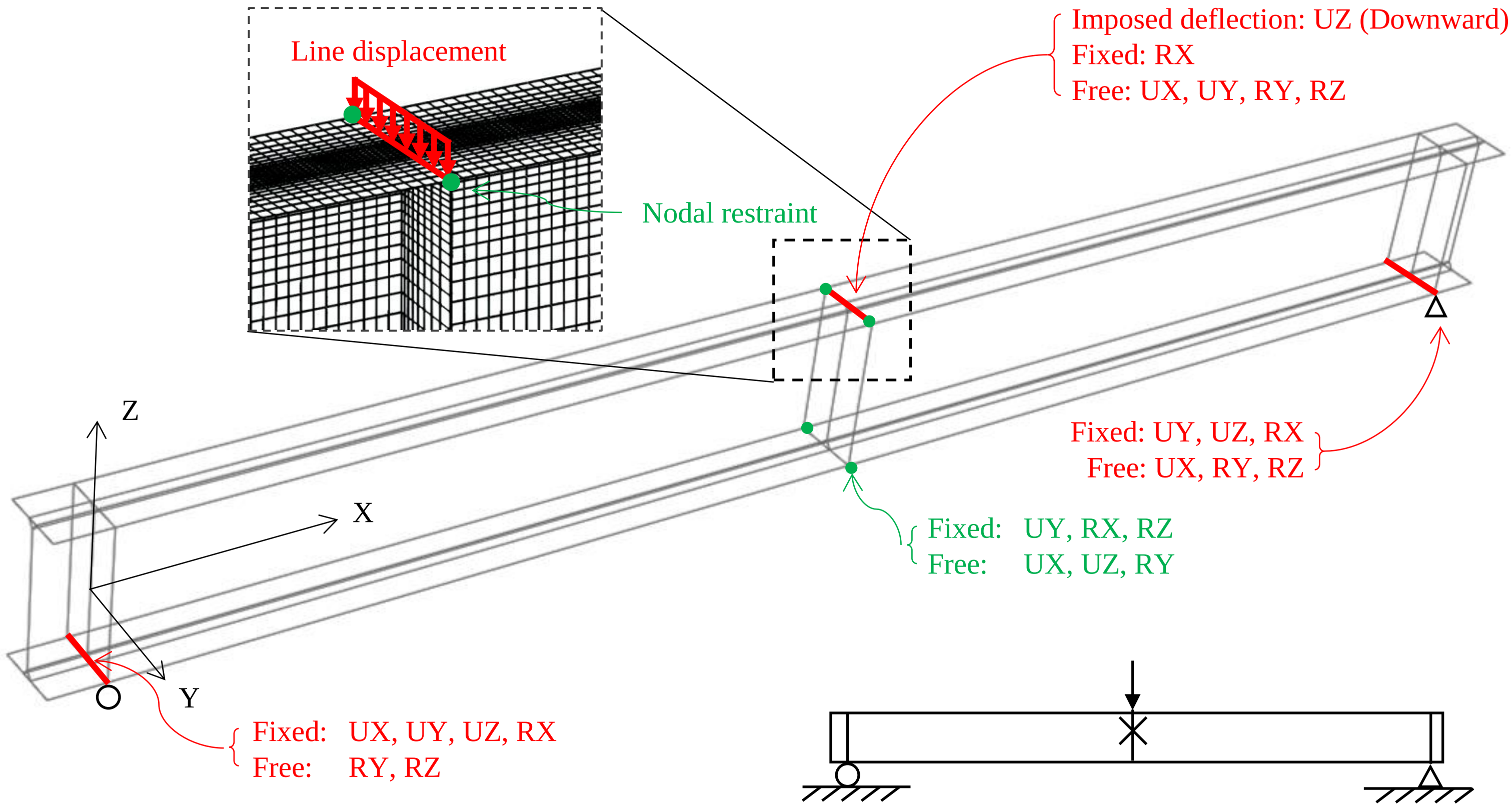

Figure 7.17: Established numerical model for partially restrained beams

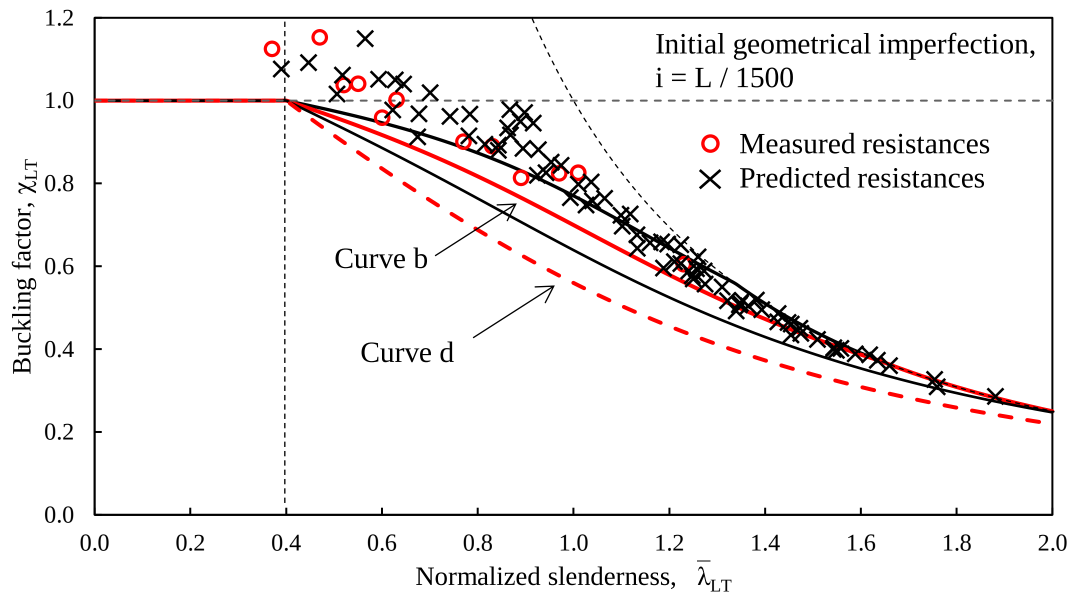

Figure 7.18: Measured and predicted resistances of partially restrained beams – with high energy welding

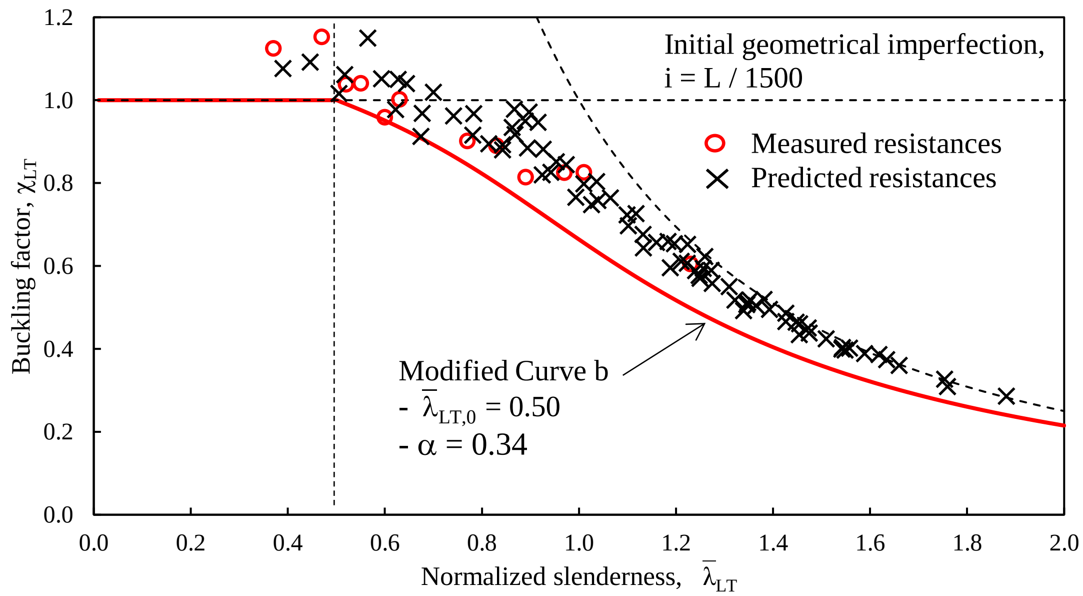

Figure 7.19: Proposed buckling curve for partially restrained beams of S690 welded sections

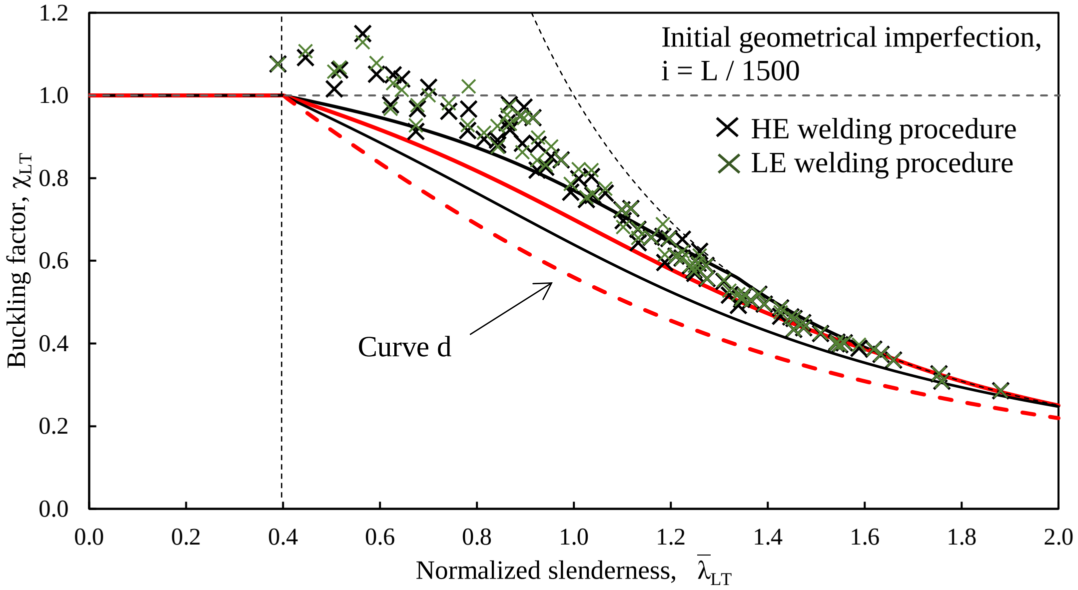

Figure 7.20: Predicted torsional buckling resistances of beams fabricated with both low and high energy welding

Table 7.1: Study programme for parametric study of stocky columns – effect of welding procedures

Section	Section Height L (mm)	Section properties			
		Plate slenderness		Section classification	Design section resistance $N_{c,Rd}$ (kN)
		$\bar{\lambda}_f$	$\bar{\lambda}_w$		
C1S	460	0.46	0.52	Class 1	2,153
C2S	460	0.60	0.67	Class 3	2,691
C3S	610	0.50	0.56	Class 2	5,796
C4S	760	0.64	0.71	Class 3	7,245
C5S	780	0.46	0.45	Class 1	12,897
C6S	1,170	0.64	0.64	Class 3	17,451
C7S	1,440	0.48	0.50	Class 1	34,259
C8S	1,920	0.66	0.69	Class 3	45,851

Table 7.2: Predicted section resistances of stocky columns

Section	Section properties			Predicted section resistances $N_{c,FE}$ (kN)			Resistance ratios $N_{c,FE}$ / $N_{c,Rd}$		
	Height L (mm)	Section classification	Design section resistance $N_{c,Rd}$ (kN)	Series HE	Series LE	Series 0RS	Series HE	Series LE	Series 0RS
C1S	460	Class 1	2,153	2,274	2,271	2,308	1.06	1.05	1.07
C2S	460	Class 3	2,691	2,828	2,801	2,788	1.03	1.04	1.04
C3S	610	Class 2	5,796	5,992	5,978	6,038	1.03	1.03	1.04
C4S	760	Class 3	7,245	7,294	7,275	7,342	1.01	1.00	1.01
C5S	780	Class 1	12,897	13,941	13,900	13,914	1.08	1.08	1.08
C6S	1,170	Class 3	17,451	18,141	18,141	18,503	1.04	1.04	1.06
C7S	1,440	Class 1	34,259	37,303	37,023	37,394	1.09	1.08	1.09
C8S	1,920	Class 3	45,851	47,359	47,102	47,467	1.03	1.03	1.04

Table 7.3: Predicted deformation capacities of stocky columns

Section	Section properties			Deformation capacity Φ_u		
	Height L (mm)	Section classification	Design section resistances $N_{c,Rd}$ (kN)	Series HE	Series LE	Series 0RS
C1S	460	Class 1	2,153	3.6	3.4	3.1
C2S	460	Class 3	2,691	1.5	1.7	1.3
C3S	610	Class 2	5,796	2.7	3.4	3.4
C4S	760	Class 3	7,245	0.8	0.9	0.7
C5S	780	Class 1	12,897	6.7	6.7	6.7
C6S	1,170	Class 3	17,451	1.7	1.8	1.9
C7S	1,440	Class 1	34,259	3.6	3.0	4.1
C8S	1,920	Class 3	45,851	0.9	0.8	0.8

Table 7.4: Study programme for parametric study of stocky columns – geometrical dimensions

Section	Section properties				
	Section classification	**h (mm)**	**b (mm)**	$\bar{\lambda}_f$	$\bar{\lambda}_w$
Series H-10-6 (10 cross-sections)	Class 1 to Class 4	105 to 220	85 to 200	0.32 to 0.87	0.37 to 0.99
Series H-16-10 (10 cross-sections)	Class 1 to Class 4	112 to 382	90 to 350	0.15 to 0.97	0.20 to 1.05
Series H-25-16 (10 cross-sections)	Class 1 to Class 4	270 to 555	220 to 505	0.34 to 0.89	0.39 to 0.99
Series H-40-25 (10 cross-sections)	Class 1 to Class 4	280 to 780	360 to 860	0.26 to 0.86	0.31 to 0.94

Table 7.5: Proposed design rules for enhanced section resistances of stocky columns

Plate elements		Section properties		
		Class 1	**Class 2**	**Class 3**
Flange plates	Width-to-thickness ratio c_f/t_f	$c_f/t_f \leq 5.3$ ($c_f/t_f \leq 9\varepsilon$)	$5.3 < c_f/t_f \leq 5.8$ ($9\varepsilon < c_f/t_f \leq 10\varepsilon$)	$5.8 < c_f/t_f \leq 8.2$ ($10\varepsilon < c_f/t_f \leq 14\varepsilon$)
	Axial resistance ratio $N_{Rd} / N_{c,rd}$	~~1.00~~ 1.05	1.00	1.00
Web plates	Width-to-thickness ratio c_w/t_w	$c_f/t_f \leq 19.3$ ($c_f/t_f \leq 33\varepsilon$)	$19.3 < c_f/t_f \leq 22.2$ ($33\varepsilon < c_f/t_f \leq 38\varepsilon$)	$22.2 < c_f/t_f \leq 24.5$ ($38\varepsilon < c_f/t_f \leq 42\varepsilon$)
	Axial resistance ratio $N_{Rd} / N_{c,rd}$	~~1.00~~ 1.05	1.00	1.00

Table 7.6: Study programme for parametric study of slender columns buckling about minor axis (88 sections)

Sections	Section properties							
	Effective length L_{eff} (mm)	h (mm)	b (mm)	t_f (mm)	t_w (mm)	r (mm)	Member slenderness $\bar{\lambda}_z$	Design section resistance $N_{c,Rd}$ (kN)
C1S	420 to 3,320	140	120	10	6	8	0.25 to 1.99	2,153
C2S	500 to 4,100	170	150	10	6	8	0.24 to 1.97	2,691
C3S	720 to 5,420	232	200	16	10	8	0.26 to 1.96	5,796
C4S	750 to 6,650	282	250	16	10	8	0.22 to 1.93	7,245
C5S	980 to 8,080	312	290	25	16	12	0.24 to 2.00	12,897
C6S	1,120 to 10,320	412	390	25	16	12	0.21 to 1.90	17,451
C7S	1,560 to 12,960	530	480	40	25	16	0.23 to 1.94	34,259
C8S	1,830 to 17,530	690	640	40	25	16	0.21 to 1.97	45,851

Table 7.7: Comparison of predicted results with buckling curves given in EN 1993-1-1

Statistics	Resistance ratio (Series YY-LE) $N_{b,FE} / N_{b,Rd}$				
	Curve a_0	Curve a	Curve b	Curve c	Curve d
Average value	1.01	1.06	1.14	1.23	1.38
Maximum value	1.17	1.27	1.42	1.57	1.81
Minimum value	0.91	0.95	1.01	1.01	1.01
Standard deviation	0.05	0.06	0.09	0.13	0.18

Statistics	Resistance ratio (Series YY-HE) $N_{b,FE} / N_{b,Rd}$				
	Curve a_0	Curve a	Curve b	Curve c	Curve d
Average value	1.00	1.05	1.13	1.21	1.36
Maximum value	1.06	1.13	1.26	1.39	1.60
Minimum value	0.93	0.96	1.00	1.00	1.00
Standard deviation	0.03	0.04	0.06	0.10	0.16

Table 7.6: Study programme for parametric study of slender columns buckling about major axis (88 sections)

Sections	Section properties							
	Effective length L_{eff} (mm)	h (mm)	b (mm)	t_f (mm)	t_w (mm)	r (mm)	Member slenderness $\bar{\lambda}_y$	Design section resistance $N_{c,Rd}$ (kN)
C1S	980 to 4,880	140	120	10	6	8	0.30 to 1.50	2,153
C2S	1,180 to 5,980	170	150	10	6	8	0.29 to 1.49	2,691
C3S	1,280 to 8,180	232	200	16	10	8	0.24 to 1.52	5,796
C4S	1,380 to 10,180	282	250	16	10	8	0.21 to 1.53	7,245
C5S	1,670 to 13,870	312	290	25	16	12	0.23 to 1.92	12,897
C6S	2,220 to 18,820	412	390	25	16	12	0.23 to 1.94	17,451
C7S	2,650 to 24,550	530	480	40	25	16	0.22 to 2.00	34,259
C8S	3,670 to 31,670	690	640	40	25	16	0.22 to 1.94	45,851

Table 7.9: Comparison of predicted results with buckling curves given in EN 1993-1-1

Statistics	Resistance ratio (Series YY-LE) $N_{b,FE} / N_{b,Rd}$				
	Curve a_0	Curve a	Curve b	Curve c	Curve d
Average value	1.03	1.08	1.17	1.26	1.41
Maximum value	1.15	1.24	1.37	1.51	1.74
Minimum value	0.92	1.00	1.01	1.01	1.01
Standard deviation	0.05	0.06	0.09	0.13	0.19

Statistics	Resistance ratio (Series YY-HE) $N_{b,FE} / N_{b,Rd}$				
	Curve a_0	Curve a	Curve b	Curve c	Curve d
Average value	1.00	1.05	1.14	1.22	1.37
Maximum value	1.12	1.20	1.33	1.47	1.70
Minimum value	0.84	0.90	1.00	1.02	1.02
Standard deviation	0.05	0.06	0.09	0.12	0.18

Table 7.10: Proposed selection table of buckling curves for S690 welded H-section

Cross sectoin	**Method 1**		
	Plate thickness	**Buckling axis**	**Buckling curve**
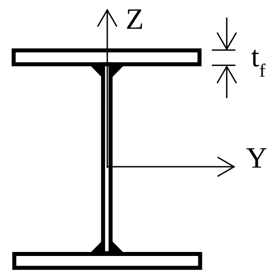	$t_f \leqslant 20$ mm	Y-Y	b
		Z-Z	~~e~~ b
	$t_f > 20$ mm	Y-Y	b (a if low-energy welding* is applied)
		Z-Z	~~e~~ a
	Method 2		
	Buckling axis	**Critical slenderness** $\bar{\lambda}_0$	**Imperfection factor** α
	Y-Y	0.2	0.34
	Z-Z	0.1	0.21

* Note:
Low-energy welding can be typically devised through multi-pass welding, or any other welding methods proved to have line heat input energy equal or below 1.0 kJ/mm.

Table 7.11: Study programme for restrained beams of S690 welded I-sections (51 sections)

Series	Section properties						
	Total span L (mm)	h (mm)	b (mm)	t_f (mm)	t_w (mm)	r (mm)	Plate slenderness $\bar{\lambda}_f$ & $\bar{\lambda}_w$
Series I-10-6	1,600 to 5,800	240 to 580	100 to 260	10	6	8	0.36 to 1.10
Series I-16-10	2,400 to 9,200	350 to 910	150 to 400	16	10	8	0.36 to 1.09
Series I-25-16	2,780 to 15,800	540 to 1,580	240 to 640	25	16	8	0.35 to 1.14
Series I-40-25	4,600 to 24,000	900 to 2,400	400 to 1,000	40	25	8	0.37 to 1.11

Table 7.12: Proposed width-to-thickness ratios of plate parts in S690 welded H- & I-section

Plate thickness	Cross section of welded H- and I-sections			
Section parts	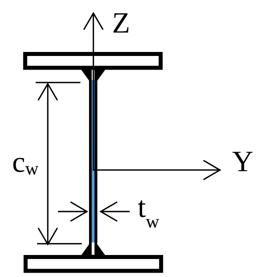		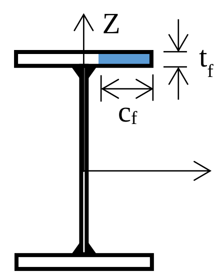	
Class	**Section under major-axis bending**	**Section under compression**	**Section under major-axis bending**	**Section under compression**
Stress distribution in parts	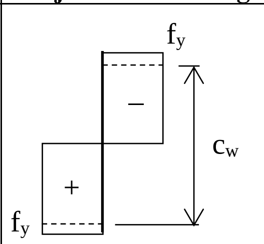	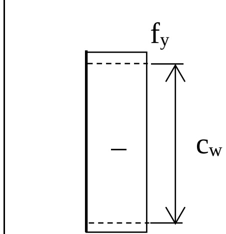	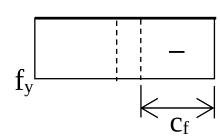	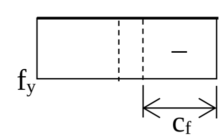
1	$c_w / t_w \leq 72\varepsilon$	$c_w / t_w \leq 33\varepsilon$	$c_f / t_f \leq 9\varepsilon$	$c_f / t_f \leq 9\varepsilon$
2	$c_w / t_w \leq 83\varepsilon$	--	$c_f / t_f \leq 10\varepsilon$	--
Stress distribution in parts	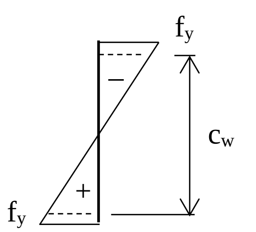	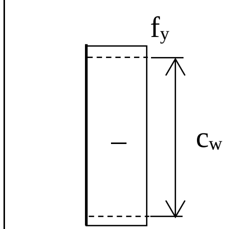	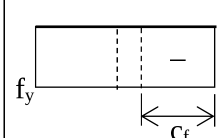	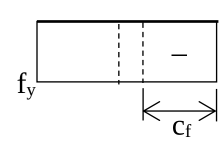
3	$\cancel{c_w / t_w \leq 124\varepsilon}$ $c_w / t_w \leq 130\varepsilon$	$c_w / t_w \leq 42\varepsilon$	$\cancel{c_f / t_f \leq 14\varepsilon}$ $c_f / t_f \leq 16\varepsilon$	$c_f / t_f \leq 14\varepsilon$

Table 7.13: Study programme for partially restrained beams of S690 welded I-sections (88 sections)

Sections	Section properties							
	Total span L (mm)	**h (mm)**	**b (mm)**	**t_f (mm)**	**t_w (mm)**	**r (mm)**	**Lateral torsional slenderness $\bar{\lambda}_{LT}$**	**Full section resistance $M_{pl,Rd}$ (kNm)**
B1	3,000 to 10,000	290	128	10	6	8	0.39 to 1.59	323
B2	4,000 to 13,000	460	180	10	6	8	0.51 to 1.43	759
B3	4,600 to 14,000	470	200	16	10	8	0.64 to 1.55	1,303
B4	6,400 to 18,000	760	280	16	10	8	0.67 to 1.76	3,214
B5	8,200 to 16,000	720	310	25	16	12	0.45 to 1.88	4,956
B6	9,600 to 22,000	1,220	440	25	16	12	0.54 to 1.54	12,848
B7	10,500 to 27,000	1,180	500	40	25	18	0.59 to 1.34	20,950
B8	15,200 to 36,000	1,920	640	40	25	18	0.68 to 1.62	51,960

CHAPTER EIGHT
CONCLUSIONS AND FURTHER RESEARCH

8.0 Introduction

In this chapter, the key research findings on the structural behaviour of columns and beams of S690 welded sections are summarized. Through the systematic experimental and numerical investigations into these welded sections, key findings are presented into three sections. Moreover, further researches are proposed.

8.1 Experimental Investigation

A comprehensive experimental investigation is carried out to understand the behaviour of columns and beams of S690 welded sections. A key significance of this experimental investigation is to control fabrication parameters during welding. Test results, such as failure modes, section resistances and deformation characteristics of S690 welded sections are clearly presented. As the experimental investigation is carried out on four different types of structural members, key findings are as following:

- *Stocky columns of S690 welded H-sections under compression*

  A total of 12 stocky columns of S690 welded H-sections under compression are found to fail in local buckling, and full section resistances are readily attained. Different levels of deformation capacities and strength enhancement are observed, depending on slenderness of plate elements of the sections. Moreover, there is a direct relationship between the deformation capacities and the strength enhancement of stocky columns of welded H-sections. It should be noted that a strength enhancement over 5% of section resistances are attained in all Class 1 and 2 sections.

- *Stocky columns of S690 welded H-sections under combined compression and bending*
  A total of 8 stocky columns of S690 welded H-sections under combined compression and bending are found to fail in local buckling, and full section resistances are attained. A wide range of deformation capacities and strength enhancement are observed, depending on slenderness of plate elements of the sections. Moreover, there is a direct relationship between the deformation capacities and the strength enhancement of stocky columns. It should be noted that a strength enhancement over 5% of section resistances are attained in all Class 1 and 2 sections.

- *Restrained beams of S690 welded I-sections – Beams of Series LT0*
  A total of 6 restrained beams of S690 welded I-sections under single-point loads are tested. Five of these sections are found to fail apparently in section failure with local buckling under large bending moment. A wide range of rotational capacities and strength enhancement are observed, depending on slenderness of plate elements of the sections. The strength enhancement of restrained beams is found to directly related to rotational capacities. And it should be noted that for Class 1 and 2 sections, plastic section resistances are attained with a significant strength enhancement at 5% above their design plastic moment resistances; and for Class 3 sections, a significant strength enhancement is achieved over the elastic section resistance.

- *Partially restrained beams of S690 welded I-sections – Beams of Series LT1 and LT2*
  A total of 12 partially restrained beams of S690 welded I-sections under single-point loads are tested. During the tests, only the loading point is carefully restrained laterally by a restraining system. All 12 partially restrained beams are found to fail in lateral torsional buckling but with different resistance levels. In general, plastic moment resistances are achieved by sections with small to intermediate member slendernesses, while their buckling resistances are found to reduce with increasing member

slendernesses. Absence of vertical stiffeners at section ends is also highlighted in this study which significantly affected effective lengths of critical span.

In addition, a direct comparison of moment resistances among Series LT0, LT1 and LT2 are carried out. Obviously, moment resistances of the beams in Series LT0 is the highest, while those in Series LT2 are the lowest. Due to the additional lateral restraints in Series LT0 comparing with Series LT1, an increase of moment resistances up to 15% is observed. Therefore, when lateral torsional slendernesses exceeds 0.5, full moment resistances may not be achieved because of lateral torsional buckling.

Through the experimental investigations, failure modes, section resistances and deformation capacities of beams and columns of S690 sections are clearly demonstrated. They are important reference data for proposed design rules as well as for verification of proposed numerical model.

8.2 Numerical Investigation

- *Residual stresses in S690 welded sections*

In order to find out residual stress distributions in S690 welded sections, a 2D thermo-mechanical coupled model is established and verified carefully against the data obtained from residual stress measurements on S690 welded I-sections. In this model, measured fabrication parameters, including welding speed, welding heat input energy and cooling history, are considered, and predicted temperature and residual stresses are successfully verified against test measurement. According to predicted numerical results, detailed residual stress distribution in cross-sections of S690 welded I-sections are illustrated.

With this verified numerical model, a number of systematic parametric studies on residual stress patterns are carried out. Welded sections of identical cross-sectional dimensions with S355 and S690 steel plates are investigated to predict residual stresses in welded sections of different yield strengths. Effects of welding procedures and plate thicknesses are also examined. It is found that residual stresses in welded H- and I-sections can be reduced for those with: i) high strength steel plates, ii) thick steel plates, and iii) low-energy welding procedures. Moreover, gradient of residual stress through plate thicknesses are revealed. In subsequent structural models, these findings will be properly incorporated.

- *Structural behaviour of beams and columns of S690 welded H- and I-sections*

A double Y-shaped structural model is established to study the structural behaviour of steel sections under various loading and boundary conditions. Both welding induced residual stresses and initial geometrical imperfection are incorporated into this model. A key significance of the proposed model is that predicted residual stress patterns in welded sections are directly input into the structural models accurately. Against reference test data, this model is successfully verified. Key parameters which govern different structural behaviour are investigated into.

In stocky columns of S690 welded H-sections, residual stresses are found to have influences on load shortening curves under large compression forces. While, their impacts onto section resistances and deformation capacities are limited. Plate slendernesses are revealed to be the most important factor to determine the load shortening behaviour of stocky columns. High deformation capacities can be achieved in stocky columns with a Class 1 cross-section, and a 5% strength enhancement can be correspondingly attained by these sections. In order to achieve higher structural efficiency, a fully verified strength enhancement may be incorporated into the design rules to increase structural efficiency.

Numerical studies on slender columns of S690 welded H-sections buckling about major and minor axis are carried out. Effects of reduced residual stresses onto overall buckling resistances are closely examined. In general, section rigidities in S690 welded sections increase under large compression forces owing to reduced compressive residual stresses in steel plates. Consequently, overall buckling factors for S690 welded H-sections are found to increase prominently, comparing with those for S235 and S355 steel sections. In order to quantify the increase of buckling resistances of S690 slender columns, a systematic parametric study is conducted. It is found that welding parameters, plate thickness and section classifications have different levels of impact onto overall buckling behaviour of slender columns. These parameters may be incorporated into the design rules to increase structural efficiency.

With test data and predicted numerical results of 102 models for restrained beams of S690 welded I-sections, structural behaviour of these beams are studied thoroughly. It is found that effects of residual stress patterns in S690 welded I-sections are not sensitive to section resistances and rotational capacities. High rotational capacities can be achieved in restrained beams of S690 sections with a Class 1 section, and a 5% strength enhancement can be correspondingly attained in these sections. For restrained beams with Class 2 and 3 sections, section resistances reduce gradually with increasing plate slendernesses. Moreover, a large portion of Class 4 sections based on EN 1993-1-1 attain their elastic moment resistances. Hence, a revised design criterion of section classifications may be proposed to increase higher structural efficiency.

According to both measured results from the experimental investigation and predicted data from the parametric studies on partially restrained beams of S690 welded I-sections, structural behaviour of these sections are closely investigated into. With full incorporation of residual stresses, relationship between increasing lateral torsional slendernesses and correspondingly reducing buckling resistances are clearly identified. In general, effects of residual stresses onto lateral torsional buckling resistances of partially restrained beams are found to be smaller, when compared with effects on to slender columns.

8.3 Design rules for S690 welded sections

In current design rules, steel materials up to Grade S460 are covered by EN 1993-1-1, and up to Grade S700 by EN 1993-1-12. In general, technical evidence supporting wide applications of high strength S690 steel structures are rather limited. Hence, applicability of current design rules onto S690 welded H- and I-sections is re-examined in this research project.

- *Material properties*

According to tensile tests of S690 steel coupons, ductility of S690 steel materials is verified. The measured ductility and strength parameters of S690 steel materials are found to be fully qualified for design to EN 1993-1-12.

- *Residual stresses in S690 welded sections*

Residual stresses measured from welded S690 I-sections and predicted for various H- and I-sections are compared with a residual stress pattern given in an ECCS recommendation. It is found that in S690 welded sections, only a limited area of the flange/web junctions are wholly yielded while in S235 or S355 sections, it is yielded in the entire junction. Moreover, compressive residual stresses in S690 sections are found to be merely half of the suggested magnitude in ECCS. Hence, impact of residual stresses onto structural behaviour of these sections with various yield strengths must be different, and verified residual stress patterns of S690 welded sections should be incorporated into structural models for accurate predictions.

- *Design of structural members*

Comparing with experimental and numerical investigations, current design rules of i) stocky columns under compression; ii) slender columns under compression; iii) restrained beams; and, iv) partially restrained beams, are reviewed. In general, current design rules are appropriate to design these members of S690 sections. However, the design rules are shown to be significantly conservative, and revision to these design rules are proposed. The proposed design rules for S690 sections are illustrated as follows:

• Section resistances of stocky columns	Table 7.5
• Bucking curves for slender columns	Table 7.10
• Section classification of welded H- and I-sections	Table 7.12
• Moment resistances of welded I-sections	Section 7.4.2
• Lateral torsional buckling of partially restrained beams	Figure 7.18, and Figure 7.19

In these cases, more efficient design rules are proposed. This is primarily attributed to reduced residual stresses in the S690 welded sections, when compared with those in S235 to S355 steel sections. More specifically, reduced compressive residual stresses in S690 welded sections lead to higher section rigidities under large loads, and buckling resistances are correspondingly increased for these sections, especially when under minor axis buckling.

8.4 Recommendations for Future Work

The following recommendations are proposed for future plan of work.

- *Experimental investigation*

In current experimental study, high strength steel sections are fabricated with: i) grade 690 steel plates with yield strength of 690 N/mm^2; ii) plate thickness up to 16 mm; and, iii) a standard welding condition.

In order to cover different section properties and configurations, the following extensive studies should be conducted with: i) grade S960 steel plates with yielding strength of 960 N/mm^2 to embrace advantages of ultra-high strength steel materials; ii) plate thicknesses up to 50 mm which are more frequently applied to main columns in high-rise buildings; and iii) steel sections possessing butt-welds which are usually found in site connections. Moreover, influences of welding heat input energy should be studied as they are not only limited to residual stresses but to welding heat input energy micro structures leading to penalty to material strengths and ductility.

- *Finite element modelling*

A highly efficient double Y-shaped structural model is established in this study, while it is possible for further improvement due to the following reasons: i) only the longitudinal residual stresses are incorporated into the model; and ii) through-thickness behaviour of steel plates is simplified, when compared with a solid element model.

In order to develop a more advanced numerical model, the following improvement may be introduced: i) to establish a numerical model which fully integrated thermo-mechanical coupled analysis and structural analysis; and ii) to establish a solid-element model with high computational efficiency. Moreover, the following studies based on verified numerical models should be considered: i) Stocky and slender columns with different loading eccentricities; ii) Parametric studies on partially restrained beams to cover various loading points, section asymmetricity and interaction from adjacent spans of beams.

REFERENCE

AISC Committee. (2010). Specification for Structural Steel Buildings (ANSI/AISC 360-10). *American Institute of Steel Construction*, Chicago-Illinois.

Ashraf, M., Gardner, L., & Nethercot, D. A. (2008). Structural stainless steel design: Resistance based on deformation capacity. *Journal of structural engineering*, *134*(3), 402-411.

ASM (1990). Materials handbook, 10th edn., Vol.1. *American Society for Metals*, USA.

Axhag, F. (1995). Plastic design of composite bridges allowing for local buckling. Technical Report, Lulea University of Technology, 09T.

AWS (2004). Welding handbook, Ninth edition, American Welding Association.

Ban, H., Shi, G., Shi, Y., & Wang, Y. (2012). Overall buckling behavior of 460MPa high strength steel columns: Experimental investigation and design method. *Journal of Constructional Steel Research*, *74*, 140-150.

Ban, H., Shi, G., Bai, Y., Shi, Y., & Wang, Y. (2013a). Residual stress of 460 MPa high strength steel welded I section: experimental investigation and modeling. *International Journal of Steel Structures*, *13*(4), 691-705.

Ban, H., Shi, G., Shi, Y., & Bradford, M. A. (2013b). Experimental investigation of the overall buckling behaviour of 960MPa high strength steel columns. *Journal of Constructional Steel Research*, *88*, 256-266.

Ban, H., Shi, G., Shi, Y., & Bradford, M. A. (2013). Experimental investigation of the overall buckling behaviour of 960MPa high strength steel columns. *Journal of Constructional Steel Research*, *88*, 256-266.

Beg, D., & Hladnik, L. (1996). Slenderness limit of class 3 I cross-sections made of high strength steel. *Journal of Constructional Steel Research*, *38*(3), 201-217.

Bischoff, M., & Ramm, E. (1997). Shear deformable shell elements for large strains and rotations. *International Journal for Numerical Methods in Engineering*, *40*(23), 4427-4449.

Bjorhovde R, Tall L. Maximum column strength and the multiple column curve concept, Fritz Laboratory Report. Lehigh University; 1971

Bose, B. (1982). The influence of torsional restraint stiffness at supports on the buckling strength of beams. *Structural Engineer. Part B*, *60*(4).

CEN. (2005). 1-1-Eurocode 3: Design of steel structures-Part 1-1: General rules and rules for buildings. *European Committee for Standardization*.

CEN. (2005). 2-1-Eurocode 3: Design of steel structures-Part 1-2: General rules – Structural fire design. *European Committee for Standardization*.

CEN. (2007). 12-1-Eurocode 3: Design of steel structures-Part 1-12: Additional rules for the extension of EN 1993 up to steel grades S700. *European Committee for Standardization*.

Chick, C. G., & Rasmussen, K. J. (1999a). Thin-walled beam-columns. I: sequential loading and moment gradient tests. *Journal of Structural Engineering*, *125*(11), 1257-1266.

Chick, C. G., & Rasmussen, K. J. (1999b). Thin-walled beam-columns. II: Proportional loading tests. *Journal of Structural Engineering*, *125*(11), 1267-1276.

Chiew, S. P., Zhao, M. S., & Lee, C. K. (2014). Mechanical properties of heat-treated high strength steel under fire/post-fire conditions. *Journal of Constructional Steel Research*, *98*, 12-19.

Chou, S. M., Chai, G. B., & Ling, L. (2000). Finite element technique for design of stub columns. *Thin-walled structures*, *37*(2), 97-112.

Chung, K. F., Li, G. Q., Wang, K., Ma, T. Y. & Liu, X. (2016). Experimental investigation into high strength steel columns of Q690 welded H-sections. Proceeding of the 11th Pacific Structural Steel Conference. Shanghai. P936-942.

Davids, A., & Hancock, G. (1991). The behaviour of thin-walled I-section columns. *Elsevier Applied Science Publishers Ltd.(UK),*, 382-395.

Davison, Buick, and Graham W. Owens, eds. *Steel designers' manual*. John Wiley & Sons, 2011.

Dawe, J. L., & Kulak, G. L. (1984a). Local buckling of W shape columns and beams. *Journal of Structural Engineering*, *110*(6), 1292-1304.

Dawe, J. L., & Kulak, G. L. (1984b). Plate instability of W shapes. *Journal of Structural Engineering*, *110*(6), 1278-1291.

Dawe, J. L., & Kulak, G. L. (1986). Local buckling behavior of beam-columns. *Journal of Structural Engineering*, *112*(11), 2447-2461.

Dawe, J. L., Kulak, G. L., & University of Alberta. Dept. of Civil Engineering. (1981). *Local buckling of W shapes used as columns, beams, and beam-columns*. Department of Civil Engineering, University of Alberta.

Dawe, J. L., & Lee, T. S. (1993). Local buckling of Class 2 beam-column flanges. *Canadian Journal of Civil Engineering*, *20*(6), 931-939.

DeLong, D. T., & Bowman, M. D. (2010). Fatigue Strength of Steel Bridge Members with Intersecting Welds. Technical Report No. FHWA/IN/JTRP-2009/19. Purdue University.

Dibley, J. E. (1969). LATERAL TORSIONAL BUCKLING OF I-SECTIONS IN GRADE 55 STEEL. *Proceedings of the Institution of Civil Engineers*, *43*(4), 599-627.

Driscoll, G. C., Beedle, L. S. (1956). *The plastic behavior of structural members and frames*. Research report (No. 205 36). Bethlehem Pa Fritz Engineering Lab, Lehigh University.

Dux, P. F., & Kitipornchai, S. (1980). Buckling approximations for laterally continuous elastic I-beams. Research report No. CE11. University of Queensland.

Dux, P. F., & Kitipomchai, S. (1982). Elastic buckling of laterally continuous I-beams. *Journal of the structural Division*, 108(ST9), 2099-2116.

Earls, C. J. (2001). Constant moment behavior of high-performance steel I-shaped beams. *Journal of Constructional Steel Research*, *57*(7), 711-728.

ECCS - Committee 8, stability. (1976). Manual on Stability of steel structures, 2nd edition. European Convention for Constructional Steelworks. Brussels.

ECCS (1976). Manual on stability of steel structures. 2nd ed. European Convention for Constructional Steelwork, June.

Galambos, T. V., & Fukumoto, Y. (1963). Inelastic lateral-torsional buckling of beam-columns. Fritz Engineering Laboratory, Lehigh University.

Galea, Y. (2005). NCCI: Elastic critical moment of cantilevers (SN006a-EN-EU). Non-Contradictory, Complimentary Information (NCCI), SCI.

Gardner, L., & Nethercot, D. A. (2004). Numerical modeling of stainless steel structural components-A consistent approach. *Journal of structural Engineering*, *130*(10), 1586-1601.

Gardner, L. (2011). Stability of steel beams and columns. The Steel Construction Institute. Publication SCI-P360. Berkshire.

Gao, L., Sun, H., Jin, F., & Fan, H. (2009). Load-carrying capacity of high-strength steel box-sections I: stub columns. *Journal of Constructional Steel Research*, *65*(4), 918-924.

Gioncu, V., & Petcu, D. (1997a). Available rotation capacity of wide-flange beams and beam-columns Part 1. Theoretical approaches. *Journal of Constructional Steel Research*, *43*(1), 161-217.

Gioncu, V., & Petcu, D. (1997b). Available rotation capacity of wide-flange beams and beam-columns Part 2. Experimental and numerical tests. *Journal of Constructional Steel Research*, *43*(1), 219-244.

Gioncu, V. (2000). Framed structures. Ductility and seismic response: General Report. *Journal of Constructional Steel Research*, *55*(1), 125-154.

Goldak, J., Chakravarti, A., & Bibby, M. (1984). A new finite element model for welding heat sources. *Metallurgical transactions B*, *15*(2), 299-305.

Green, P. S., Sause, R., & Ricles, J. M. (2002). Strength and ductility of HPS flexural members. *Journal of Constructional Steel Research*, *58*(5), 907-941.

Green, P. S., Sooi, T. K., Ricles, J. M., Sause, R., & Kelly, T. (1994). Inelastic behavior of structural members fabricated from high performance steel. *Proc. SSRC Ann. Tech. Sess., Lehigh Univ., Bethlehem, PA*, 435-56.

Hasham, A. S., & Rasmussen, K. J. (1998). Section capacity of thin-walled I-section beam-columns. *Journal of structural Engineering*, *124*(4), 351-359.

Kato, B. (1990). Deformation capacity of steel structures. *Journal of Constructional Steel Research*, *17*(1), 33-94.

Kemp, A. R. (1986). Factors affecting the rotation of plastically designed members. Structural Engineer. Part B, 64, 28-35.

Kemp, A. R. (1996). Inelastic local and lateral buckling in design codes. Journal of Structural Engineering, 122(4), 374-382.

Kim, D. K., Lee, C. H., Han, K. H., Kim, J. H., Lee, S. E., & Sim, H. B. (2014). Strength and residual stress evaluation of stub columns fabricated from 800MPa high-strength steel. *Journal of Constructional Steel Research*, *102*, 111-120.

Kubo, M., & Fukumoto, Y. (1988). Lateral-torsional buckling of thin-walled I-beams. *Journal of Structural Engineering*, 114(4), 841-855.

Kuhlmann, U. (1989). Definition of flange slenderness limits on the basis of rotation capacity values. *Journal of Constructional Steel Research*, *14*(1), 21-40.

Law, K. H., & Gardner, L. (2012). Lateral instability of elliptical hollow section beams. *Engineering Structures*, *37*, 152-166.

Lay, M. G. (1965). Flange local buckling in wide-flange shapes. Journal of the Structural Division, 91(6), 94-116.

Lay, M. G., & Gimsing, N. (1965). Experimental studies of the moment-curvature-thrust relationship, The Welding Journal, Vol. 44, Feb. 1965, Publication No. 258/65-1.

Lee, C. H., Han, K. H., Uang, C. M., Kim, D. K., Park, C. H., & Kim, J. H. (2012). Flexural strength and rotation capacity of I-shaped beams fabricated from 800-MPa steel. *Journal of Structural Engineering*, *139*(6), 1043-1058.

Li, T. J., Li, G. Q., & Wang, Y. B. (2015). Residual stress tests of welded Q690 high-strength steel box-and H-sections. *Journal of Constructional Steel Research*, *115*, 283-289.

Liew, A., & Gardner, L. (2015, February). Ultimate capacity of structural steel cross-sections under compression, bending and combined loading. In *Structures* (Vol. 1, pp. 2-11). Elsevier.

Liu, X. (2017). Structural effects of welding onto high strength S690 steel plates and welded sections. PhD dissertation. Hong Kong Polytechnic University.

Liu, X and Chung, K.F. (2016). Numerical investment into residual stresses of welded H-sections made of Q690 steel materials. Proceeding of the 11th Pacific Structural Steel Conference. Shanghai. P1205-1211.

Liu, X. (2017). Residual stresses in welded sections of high strength steel materials S690. (Doctoral dissertation, The Hong Kong Polytechnic University).

Lukey, A. F., & Adams, P. F. (1969). Rotation capacity of beams under moment gradient. Journal of the Structural Division.

Nakashima, M. (1992). Variation and prediction of deformation capacity of steel beam-columns. In *Proc, 10 th World Conference on Earthquake Engineering, Madrid, Balkama, Rotterdam* (pp. 4501-4507).

Nakashima, M. (1994). Variation of ductility capacity of steel beam-columns. *Journal of Structural Engineering*, *120*(7), 1941-1960.

Nash, D. S., & Kulak, G. L. (1976). *Web slenderness limits for non-compact beam-columns*. Department of Civil Engineering, University of Alberta.

Nethercot, D. A., & Trahair, N. S. (1976b). Inelastic lateral buckling of determinate beams. *Journal of the structural Division*, 102(ST4), 701-717.

Nethercot, D. A., & Trahair, N. S. (1977). Lateral buckling calculation for braced beams. *Civil Engineering Transactions*, CE19(2), 211-214.

Perlynn, M. J., & Kulak, G. L. (1974). *Web slenderness limits for compact beam-columns* (Master's thesis, University of Alberta).

Pépe, N., Egerland, S., Colegrove, P. A., Yapp, D., Leonhartsberger, A., & Scotti, A. (2011). Measuring the process efficiency of controlled gas metal arc welding processes. *Science and Technology of Welding and Joining*, *16*(5), 412-417.

Pi, Y. L., & Trahair, N. S. (1994). Nonlinear inelastic analysis of steel beam-columns. I: Theory. *Journal of Structural Engineering*, *120*(7), 2041-2061.

Pocock, G. (2006). High strength steel use in Australia, Japan and the US. *The Structural Engineer, 84 (21),* 27–30

Rasmussen, K. J. R., & Hancock, G. J. (1995). Tests of high strength steel columns. *Journal of Constructional Steel Research*, *34*(1), 27-52.

Remmers, J. J., Wells, G. N., & Borst, R. D. (2003). A solid‐like shell element allowing for arbitrary delaminations. *International Journal for Numerical Methods in Engineering*, *58*(13), 2013-2040.

Ricles, J. M., Sause, R., & Green, P. S. (1998). High-strength steel: implications of material and geometric characteristics on inelastic flexural behavior. *Engineering Structures*, *20*(4), 323-335.

Shi, G., Ban, H., & Bijlaard, F. S. (2012). Tests and numerical study of ultra-high strength steel columns with end restraints. *Journal of Constructional Steel Research*, *70*, 236-247.

Shi, G., Shi, Y. J., & Wang, Y. Q. (2008). Engineering application of ultra-high strength steel structures. *Progress in Steel Building Structures*, *10*(4), 32-38.

Shi, G., Zhou, W., & Lin, C. (2015). Experimental Investigation on the Local Buckling Behavior of 960 MPa High Strength Steel Welded Section Stub Columns. *Advances in Structural Engineering*, *18*(3), 423-437.

Shokouhian, M., & Shi, Y. (2014). Classification of I-section flexural members based on member ductility. *Journal of Constructional Steel Research*, 95, 198-210.

Shokouhian, M., & Shi, Y. (2015). Flexural strength of hybrid steel I-beams based on slenderness. *Engineering Structures*, *93*, 114-128.

Spadea, J. R. and Frank, K. H. (2002). Fatigue Strength of Fillet-Welded Transverse Stiffeners with Undercuts. Technical Report No. FHWA/TX-05/0-4178-1, The University of Texas at Austin.

Standard, A. (1998). AS 4100-1998 steel structures. *Sydney: Standards Australia*.

Sun, F., Xie L., Cui W., Li G., Chen S., & Wang Y.. (2013). Experimental study on material properties of Q460 high strength steel under monotonic and cyclic loading. Journal of Building Structures, 34(1), 30-35.

Systemes, D. (2009). ABAQUS 6.9 Documentation. *Providence, RI*.

Timoshenko, S. P., & Gere, J. M. (1961). Theory of elastic stability.

Trahair, N. S., Bradford, M. A., Nethercot, D., & Gardner, L. (2007). The behaviour and design of steel structures to EC3. CRC Press.

Wang, J., Afshan, S., Gkantou, M., Theofanous, M., Baniotopoulos, C., & Gardner, L. (2016). Flexural behaviour of hot-finished high strength steel square and rectangular hollow sections. *Journal of Constructional Steel Research*, *121*, 97-109.

Wang, Y. B., Li, G. Q., & Chen, S. W. (2012a). Residual stresses in welded flame-cut high strength steel H-sections. *Journal of Constructional Steel Research*, *79*, 159-165.

Wang, Y. B., Li, G. Q., Chen, S. W., & Sun, F. F. (2012b). Experimental and numerical study on the behavior of axially compressed high strength steel columns with H-section. Engineering Structures, 43, 149-159.

Wilkinson, T., & Hancock, G. J. (1998). Compact or class 1 limits for rectangular hollow sections in bending. *TUBULAR STRUCTURES-INTERNATIONAL SYMPOSIUM-* (Vol. 8, pp. 409-416). E & FN SPON.

Withers, P. J., Turski, M., Edwards, L., Bouchard, P. J. & Buttle, D. J. (2008). Recent advances in residual stress measurement. *International Journal of Pressure Vessels and Piping*, 85(3), 118-127.

Yang, D., & Hancock, G. J. (2006). Numerical simulation of high-strength steel box-shaped columns failing in local and global buckling modes. *Journal of structural engineering*, *132*(4), 541-549.